TSUNAMI HAZARD, SAMOAN ISLANDS: PALAEOTSUNAMI INVESTIGATION, NUMERICAL MODELING AND RISK IMPLICATIONS

A thesis submitted in partial fulfilment of the
requirements for the Degree of

Doctor of Philosophy in
Hazard and Disaster Management

at the
Natural Hazards Research Centre, Department of Geological Sciences
by

Shaun Paul Williams

University of Canterbury

2014

FRONTISPIECE

Serene Sunset: Virgin Cove, Sa'anapu, South Upolu. Southwest view of horizon overlying the Northern Tongan Subduction Arc (Photo: Christine Reitze 2012)

..... Emotional .....

ABSTRACT

Tsunami investigation is a fundamental component of coastal hazard mitigation and risk reduction. Recent history reveals that such hazards can influence rapid changes in global cultural dynamics through extensive loss of life (e.g. 2004 Indian Ocean Tsunami), lifeline destruction (e.g. 2011 Tohoku Tsunami) and property damage (e.g. 2014 Chile Tsunami), affecting the mobilization of regional and global humanitarian and financial resources.

The 2009 South Pacific Tsunami (2009 SPT) in the Samoan Islands, which had devastating local impacts, provided the opportunity to better understand tsunami characteristics and subsequent hazard potential in this region. Lessons were learned from the impacts of this event in the context of local and regional tsunami mitigation.

Equally a number of questions emerged. What is the long-term tsunami hazard in the Samoan region? What is the future risk of near-field events of similar or greater magnitude? What evidence is there in the geohazard chronology record? If there is evidence, what does it imply with regard to risk reduction in Samoa and the broader Pacific?

These questions formed the research basis for this thesis. Specific aims and objectives were devised to address the challenges and concerns identified. A range of inter-disciplinary techniques were used to yield innovative information to achieve them.

Proxy characteristics (e.g. loss on ignition, grain size, elemental ratio, geochronology, resonance modeling) associated with the 2009 SPT and identified 1990 and 1991 Cyclones Ofa and Val deposits, respectively, provided unique analogues for identifying and distinguishing tsunami and cyclone signatures in the deeper Samoan geologic record.

A tsunami and cyclone geochronological model spanning the last 3,000 years or so was developed. Estimation of tsunami frequency of similar or greater magnitude events than the 2009 SPT likely originating from the near-field Northern Tongan Subduction Arc (NTSA) source was also made possible. The results suggest a minimum 87 year recurrence interval of 2009 SPT-type tsunami intensities or stronger associated with a likely NTSA origin.

Assessment of the contemporaneity between identified tsunamis and cyclones in the geologic record with anomalous and/or enigmatic sequences in the ethno-archaeological, oral and indigenous records provided likely indicators of the possible extent of associated hazards. Further, the discovery and association of anthropogenically-formed charcoal contemporaneous with earliest colonization in the Samoan archipelago, with the oldest tsunami identified, likely substantiates an approximate 3,000 year hazard history.

Evidence of a landslide-generated tsunami which occurred during the Last Glacial Maximum (LGM), as well as non-related hypotheses concerning inland high-elevation calcareous deposits of cultural significance, were considered within the broader long-term tsunami hazard context. Knowledge gaps associated with landslide-generated tsunami processes and their hazard potential in this region were identified. The possibility of calcareous deposits found in a central highland location in these islands being of a potential tsunami or coastal marine origin is dismissed.

This research demonstrates that an intrinsic tsunami hazard history covering the last 3,000 years exists in the Samoan Islands. Directions for future studies that build on the findings presented here are offered. The principal research outcomes achieved provide a basis for future refinement. Nonetheless, the thesis can be used in its present form as a guide for similar investigations, as well as in long-term

coastal risk and mitigation at the local level. The techniques used and information obtained can also be developed and applied to analogous coastal environments in other countries to assist broader long-term regional and global tsunami risk reduction.

ACKNOWLEDGEMENTS

The work presented in this thesis was made possible through the generous financial support by different organisations, as well as invaluable collaborative partnership support of colleagues, family and friends.

My deepest gratitudes are given to my thesis supervisory committee; Tim Davies, James Goff, Kwok Fai Cheung, Catherine Chagué-Goff, Thomas Wilson, and Gegar Prasetya. This thesis would not have been made possible had it not been for their institutional and personal support, faith, help, and guidance in this project.

Equally, the international collaborative and co-author teams detailed in the Co-Authroship Declaration of this thesis are warmly thanked for their help and endurance of the many challenges associated with implementing research in a small island developing state.

Local University of Canterbury and Samoan Ministry of Natural Resources and Environment teams are specially acknowledged for their support in this project. There are too many colleagues to name, but their help and support is not forgotten.

My family, including friends, provided the foundation for my endurance in this research journey. Words cannot express my gratitude for their support. There are too many family members and friends to name, but special acknowledgement is given to my parents, Joan and Jim Williams.

Organizations which provided the financial means for implementing this research are acknowledged below;

- Macmillan Brown Centre for Pacific Studies, University of Canterbury.
- NZ-Fulbright Programme (IIE Grantee #15101271).
- Department of Geological Sciences and Mason Trust, University of Canterbury.
- Australian Institute for Nuclear Science and Engineering (Grant #ALNGRA12119P).
- Claude McCarthy Fellowship, Universities New Zealand.
- Building Research Capability in the Social Sciences Programme, Massey University.
- Samoa Builders' Supplies and ACE Hardware Ltd.

CO-AUTHORSHIP DECLARATION

This thesis comprises six manuscripts either published, in revision for re-submission, or in preparation for submission, in international scientific journals, peer-reviewed conference proceedings, and a book chapter.

Appendix 3 contains versions of two co-authored reports published in peer-reviewed conference proceedings. Appendix 3.1 was published in; **Malua, T.L. (ed) 2011, *Proceedings of the Samoa National Environment Forum 2010, pp 15-25.*** Appendix 3.2 was published in; **Oceans 2011, *MTS/IEEE Kona Conference Proceedings, 10p.*** Shaun Williams is first author for both papers. Appendix 3.1 co-authors are James Goff, Faigame Sale, Johnny Ah Kau, Gegar Prasetya, Tim Davies, Kwok Fai Cheung, and Thomas Wilson. Appendix 3.2 co-authors are James Goff, Gegar Prasetya, Kwok Fai Cheung, Catherine Chagué-Goff, Tim Davies, and Thomas Wilson.

Appendix 4 provides a version of a co-authored peer-reviewed report, published in; ***Science of Tsunami Hazards (2013), 32(3): 156 – 175***. Shaun Williams is first author. Co-authors include James Goff, Johnny Ah Kau, Faigame Sale, Catherine Chagué-Goff, and Tim Davies.

Chapters 3 and 4 are revised and modified versions of content in a co-authored manuscript presently in revision for re-review and publication consideration in ***Geophysical Journal International***. Shaun Williams is first author. Co-authors are Yoshiki Yamazaki, Volker Roeber, Kwok Fai Cheung, Tim Davies, Catherine Chagué-Goff, Atun Zawadzki, James Goff, Henk Heijnis, Geraldine Jacobsen, Patricia Gadd, Thomas Wilson, Gegar Prasetya, and Siosina Lui. In Chapter 4, the figures and majority of text in the methodologies, results and discussion were generated and written by Yoshiki Yamazaki.

Case Study-I in Chapter 5 is a modified version of a co-authored book chapter associated with a paper that will be presented at the World Landslide Forum 3 in Beijing, June 2014. The manuscript is presently in press in; **Sassa, K., P. Canuti, Y. Yin, (eds) 2014, *Landslide Science for a Safer Geoenvironment, Vol.3, Ch. 90, 6p***. Shaun Williams is first author. Co-authors are Tim Davies, Timothy Barrows, Matthew Jackson, Stan Hart, and Jim Cole. Laboratory analysis was conducted by Timothy Barrows. Corresponding Author is Tim Davies.

Case-Study-II in Chapter 5 is intended for journal submission. Shaun Williams is first author. Co-authors are Paul Anderson, Travis Horton, Catherine Reid, Jim Cole, Graham Leonard, Darren Gravley, and Tim Davies. Isotope determination will be conducted by Travis Horton.

Aspects of Case Study-II and Chapter 3 are intended for submission. An abstract has been accepted for oral presentation and full manuscript submission in the archaeology session at the Samoa Conference III, Apia, August 2014. The manuscript is intended for inclusion in the conference proceedings, which will be published in the ***Journal of Samoan Studies.*** Shaun Williams is author.

Case Study-III in Chapter 5 is a modified version of a co-authored manuscript presently in revision for re-review and publication consideration in the ***Journal of Island and Coastal Archaeology***. Shaun Williams is first author. Co-authors are James Goff and Tim Davies.

TABLE OF CONTENTS

List of Figures

List of Tables

Terminology

Tsunamiological and geohazard terms that are used in this thesis are defined below:

Deep earthquake: An earthquake whose focus is located more than 300 kilometers from the earth's surface. Earthquake-report.com differs from the official notification calling earthquakes with a depth of more than 100 km as "Deep". This is mainly because of the non-damaging impact of these earthquakes. (USGS terminological use: http://earthquake-report.com/2011/02/15/glossary-of-earthquake-terms-2/).

Flow depth: This refers to inundation depth (Power, 2013). See also the definition for inundation.

Flow height: This refers to flow depth calibrated against benchmarks or natural tide level indicators (Beavan et al., 2010).

Hazard: A dangerous phenomenon, substance, human activity or condition that may cause loss of life, injury or other health impacts, property damage, loss of livelihoods and services, social and economic disruption, or environmental damage (UNISDR, 2013).

Historical tsunami: A tsunami which occurred within the historic period of a given context (i.e. period in which written records began) (Goff et al., 2009). For this thesis, the historic reference year is AD 1830 [i.e. arrival of the missionary John Williams and acceptance of Christianity in Samoa (Linnekin et al., 1995)]. This differs from the use of the term Modern tsunami in this thesis, in that Modern tsunami herein refers to recent tsunamis in the historical period that have been well documented (e.g. 2009 South Pacific Tsunami).

Inundation: The depth, relative to a standard reference level, to which a particular location is covered by water (NOAA definition: http://nthmp-history.pmel.noaa.gov/terms.html).

Long-term: In the context of this thesis, Long-term refers to the entire period of human settlement and older in a given context [i.e. ~3,000 years of human settlement in Samoa and older; Petchey (2001)].

Manning coefficient: The resistance of the bed of a channel to the flow of water in it (Ocford Dictionary of Geography terminology use: http://www.answers.com/topic/manning-s-roughness-coefficient).

NTSA: Northern Tongan Subduction Arc. A term used in this thesis that refers to the northern end of the Tonga Trench, in which tectonic plate movement transitions from subduction to transform processes (Hart et al., 2004).

Nyquist period: A signal processing term that refers to the maximum frequency that can be retrieved without aliasing from an unevenly sampled time signal (Mignard, 2005).

Palaeotsunami: A tsunami which occurred prior to the historic period of a given context (i.e. period in which written records began) (Goff et al., 2009). For this thesis, the historic reference year is AD 1830 [i.e. arrival of the missionary John Williams and acceptance of Christianity in Samoa (Linnekin et al., 1995)].

Risk: The product of the probability of an event and its negative consequences (UNISDR, 2013).

MID: Refers to rapid marine inundation deposits. This is used in this thesis to refer to tsunami and cyclone deposits instead of the term CSI [catastrophic saltwater inundation by Goff et al., (2001)]. It is recognised in this thesis that not all tsunami and cyclone/storm deposits are necessarily catastrophic.

Run-up: Maximum height of the water onshore observed above a reference sea level. Usually measured at the horizontal inundation limit (NOAA definition: http://nthmp-history.pmel.noaa.gov/terms.html).

Shallow earthquake: An earthquake whose focus is located within 70 kilometers of the earth's surface. Earthquake-report.com differs from the official notification calling earthquakes with a depth up to 40 km as "Shallow". This is mainly because of the possible damaging impact of these earthquakes (USGS terminological use: http://earthquake-report.com/2011/02/15/glossary-of-earthquake-terms-2/).

Short-term: In the context of this thesis, Short-term refers to the historical period of human settlement in a given context [i.e. human settlement since AD 1830 in Samoa; see definition for Historical tsunami].

Surface elevation: Similar to amplitude (i.e. the rise above or drop below the ambient water level as read on a tide gage; NOAA definition: http://nthmp-history.pmel.noaa.gov/terms.html).

CHAPTER 1: INTRODUCTION

1.1 Rationale

The September 2009 South Pacific Tsunami (2009 SPT) in the Samoa Islands resulted in the most devastating disaster to have impacted this region since the 1918 influenza epidemic in terms of loss of life. This event resulted in recommendations to improve understanding of the medium- to long-term risks of tsunamis in these islands (Dominey-Howes and Thaman, 2009), in order to better mitigate their impacts. This research endeavours to contribute to Recommendation 4 of Dominey-Howes and Thaman (2009) (i.e. to complete a national palaeotsunami study to identify long-term-frequency-magnitudes), through an interdisciplinary pilot palaeotsunami investigation.

Firstly, the Samoan Islands, archipelago, or region as used in this thesis comprises the Independent State of Samoa (or just Samoa, formerly Western Samoa), and American Samoa, respectively. The focus of this thesis is primarily on Independent Samoa, with occasional reference to American Samoa.

Historical data beginning in 1837 indicate that the Samoan Islands archipelago has been impacted by tsunamis from all the major tsunamigenic zones within the Pacific Rim of Fire (Parraras-Carayannis and Dong, 1980) (Figure 1). Evidence of local tsunamigenic sources also exists (Cronin et al., 2006; Williams et al., 2012). This makes it an ideal location and natural laboratory for starting to understand tsunami characteristics and distribution within this region. Furthermore, the archipelago has an historical record of extreme tropical cyclones.

The overarching concept of this study is that tsunamis, like cyclones, leave distinct geological deposits within the coastal landscapes they impact. The origin of a high-energy geological deposit, be it cyclone or tsunami, can be determined by using a suite of diagnostic criteria. However, the origin of a deposit can still be ambiguous, because some of the diagnostic criteria (e.g. grain size, microfossil assemblages and characteristics) can be extremely similar for both processes. Moreover, local factors can also influence the characteristics of deposits.

This research aims to elucidate this enigma by establishing a suite of diagnostic criteria (e.g. stratigraphy, lithology, sedimentology, geochemistry, geochronology, numerical modeling, ethno-archaeology, oral and indigenous knowledge) to identify and distinguish deposits left behind by tsunamis and cyclones, in order to better understand their hazard implications in this tropical climatic regime.

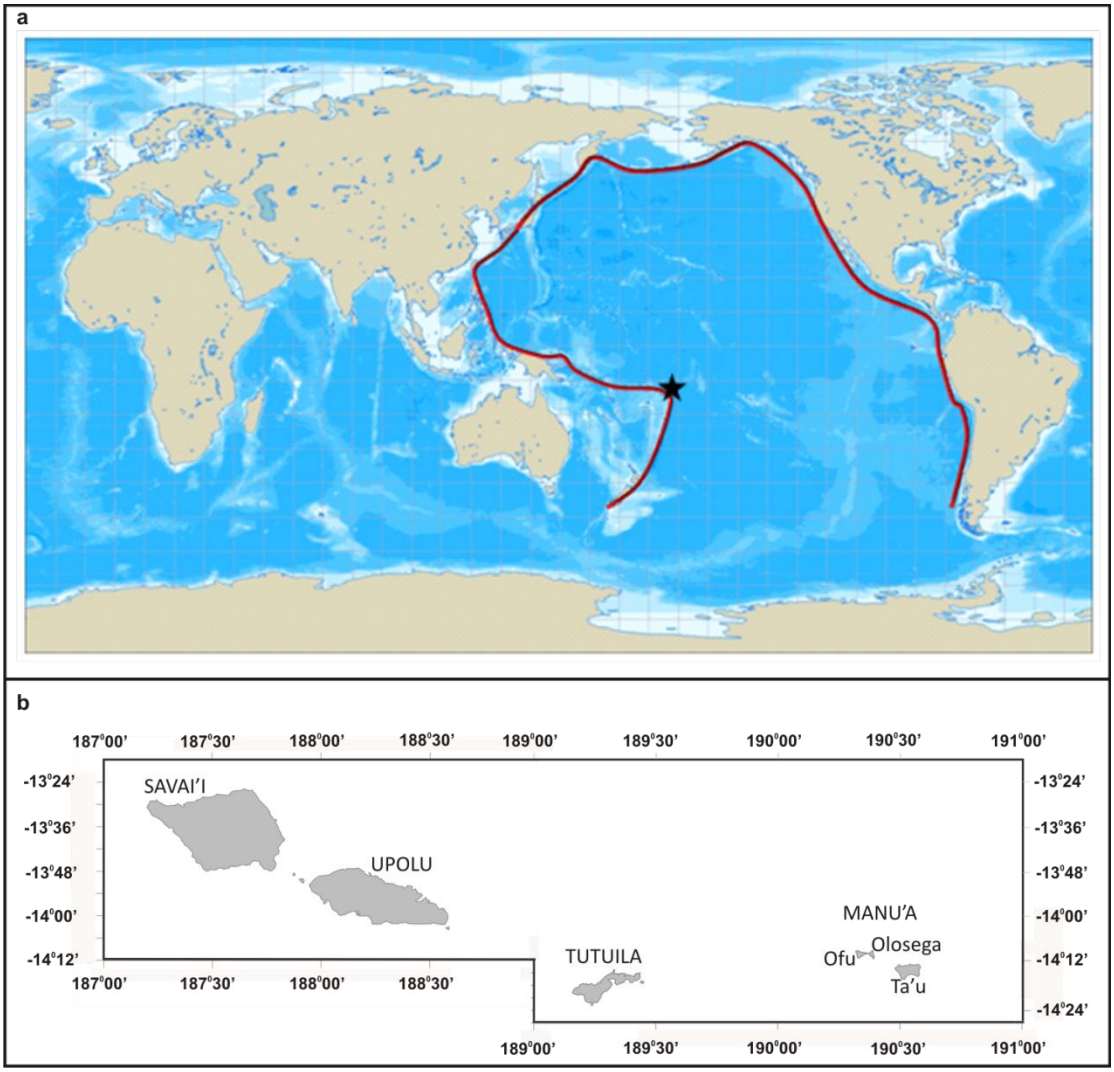

Figure 1: a) General location of the Samoan Islands (black star) relative to the Pacific Rim of Fire (red line); b) Samoan Islands chain.

1.2 Hypothetical Basis

Specific questions that formed the research basis for this investigation are:

1. What is the long-term tsunami hazard in the Samoan region?

2. What evidence is available or can be acquired to evaluate this?

3. What does the evidence suggest in terms of future tsunami threats?

These in turn provided a foundation for specifically designed thesis aims and chapter objectives that focussed on acquiring and interpreting evidence to demonstrate the long-term tsunami risk in this region.

1.3 Research Scope and Context

The work presented in this thesis represents an interdisciplinary scientific approach to tsunami hazard investigation and management applications in a tropical climatic regime. A range of geoscientific and other analytical techniques was used to address the challenges identified in Sections 1.1 and 1.2.

Primary activities took place in partnership with colleagues from the University of Canterbury NZ, The University of New South Wales, The University of Hawai'i at Manoa, the Australian Nuclear Science and Technology Organisation, the Tsunami Research Foundation – Indonesian Chapter, and the Samoan Ministry of Natural Resources and Environment.

Associated activities also took place via collaborative partnership with colleagues from Bruker Elemental Inc., Korean Institute of Geology and Mines, Applied Geoscience and Technology Division of the Secretariat of the Pacific Community, Secretariat of the Pacific Regional Environment Programme, University of Exeter, University of California Santa Barbara, Woods Hole Oceanographic Institution, Tohoku University, GNS Science NZ, Hokkaido University, NOAA American Samoa Weather Service, and local Samoan specialists at the village level.

The results and recommendations presented are specific to the Samoan Islands context. However, the research approach used can be developed and applied to similar investigation on analogous oceanic environments.

1.4 Aims and Objectives

The overarching aim of this research was designed to address the issues and hypothetical questions identified in Sections 1.1 and 1.2., provided below:

"To improve understanding of the long-term tsunami hazard in the Samoan Islands in order to contribute to tsunami mitigation and risk reduction"

This direction formed the context for establishing the primary project objectives listed below:

1. To investigate the deposit characteristics of the 2009 SPT through a marine inundation deposit investigation.

2. To establish a tsunami chronology enabling an evaluation of tsunami frequency and magnitude, including tsunamigenic source assessment and anomalous tsunami case evaluations.

3. To review tsunami risk in the Samoan region using the new information acquired, and offer recommendations to build on, and apply, the findings to long-term mitigation and risk considerations at the local and regional levels.

These objectives in turn formed the contextual frameworks for targeted chapter goals presented throughout this thesis.

1.5 Thesis Structure and Organization

The overall structure and organization of this thesis was modeled on similar hazard investigations conducted by Rahiman (2006) in the Fiji Islands, Williams (2009) in the Samoan Islands, as well as Kritikos (2013) and Wardman (2013) in New Zealand. Individual chapters have goals designed to address the aim and objectives in Section 1.4 above.

Chapter 2 provides a literature review of our current understanding of tsunami hazards known from the Samoan historical record. Aspects of tsunamigenic processes are considered with specific emphasis on local (near-field) sources. Available information concerning the challenges of identifying tsunamis from the geologic and ethno-archaeological records is reviewed. Further, a review of present tsunami risk perception in this region based on available hazard information is provided, which includes mitigation and risk reduction considerations at the local and regional levels.

Chapter 3 describes an interdisciplinary investigation of the 2009 SPT deposits formed in the coastal landscape. This includes their characterization using sedimentological, geochemical, geochronological, geomorphic and stratigraphic proxies. The 2009 SPT deposit signature is used to identify similar trends in the geologic record, emphasising the use of proxy data to distinguish between tsunamis and other inundation hazards (e.g. cyclones). A tsunami and cyclone geochronology model is developed, as well as tsunami frequency and magnitude estimates associated with the near-field NTSA (Northern Tongan Subduction Arc) source region. Ethno-archaeological records including oral and indigenous knowledge are considered in the context of long-term hazard and coastal risk. Interpretations and limitations are presented in the context of the overall thesis aim.

Resonance energy of the 2009 SPT is numerically modeled in Chapter 4. Particular attention is given to the pattern of resonance relative to the locations of associated deposits determined in Chapter 3. Implications of resonance as a proxy to assist tsunami deposit investigation are discussed, including suggested directions for future research.

Chapter 5 presents three tsunami case studies of particular relevance to long-term hazard consideration. Case Study-I evaluates the timing and hazard implications of a landslide-generated tsunami identified in the Ta'u geomorphic record. The threat of processes similar in nature is also discussed. Case Study-II determines the source of inland high-elevation calcareous deposits on central Upolu in relation to varying hypotheses concerning their origin, which includes tsunami. Case Study-III assesses the implications of a radiocarbon age of anthropogenic charcoal found in association with the oldest tsunami deposit identified in the geologic record at Fagali'i. The implications of a possible in-built

charcoal age effect on the interpretations in Chapter 3 are discussed. Its contemporaneity with earliest colonization in the Samoan Islands is also considered in the context of the overarching thesis aim.

A synthesis of the principal research outcomes is provided in Chapter 6. Conclusions and recommendations for future work that could build on the findings presented here are also provided. Finally, the application of the approach in this thesis to managing similar hazards in analogous oceanic and/or coastal environments is considered.

1.6 Introduction to Methodologies and Datasets

Interdisciplinary methods and new datasets were required to address the objectives of this research. A summary of the key analytical techniques and datasets used is given below:

1. An interdisciplinary literature review of tsunami history combined with geology, numerical modeling, ethno-archaeology, disaster management, and personal interviews was used to establish a firm information platform for understanding the investigative framework.

2. Geological field investigations involving trench analysis and core sampling at selected locations were conducted in order to establish empirical grounds for further analyses. Samples obtained provided the basis for successive laboratory analyses including sedimentological (e.g. loss on ignition and grain size), geochemical (e.g. elemental ratios), and geochronological (e.g. ^{14}C and ^{210}Pb dating). This enabled the characterization of the 2009 SPT deposits, including the identification of analogous signatures in the sampled profiles.

3. Recognizable differences in signature trends coupled with geochronological age determination enabled the identification of the 1990 and 1991 Cyclones Ofa and Val deposits, respectively. These, together with the 2009 SPT signature, formed the basis for distinguishing geologic signatures of tsunami or cyclone origin.

4. Rational inference allowed the development of a tsunami and cyclone chronology model from the geologic record. This also enabled balanced estimates to be made of the likely frequency of similar 2009 SPT-type tsunamis or stronger occurring from the NTSA source region.

5. Available bathymetry and earthquake data enabled the 2009 SPT resonance to be modeled for Upolu and Savaii Islands using NEOWAVE (Non-hydrostatic Evolution of Ocean Waves model) developed at the University of Hawai'i at Manoa. The results enabled correlations to be drawn between tsunami resonance and deposit characteristics.

6. Chlorine-36 (^{36}Cl) exposure dating of a sample collected from the Ta'u fault scarp enabled an assessment of the timing and implications of the associated flank-collapse and tsunami.

7. Field reconnaissance and literature reviews provided a means for estimating the most likely origin of the inland high-elevation calcareous deposits in central Upolu.

8. Rational assumptions concerning the age and origin of the Fagali'i charcoal demonstrated an approximate 3,000 year tsunami hazard history in this region to be demonstrated.

9. Synthesis of the datasets provided the basis for re-interpreting the long-term tsunami hazard and risk in the Samoan region.

10. Data and interpretive limitations concerning each analytical Chapter provide a basis for future research

Individual chapter objectives provide a framework for using these methods, and applying the new datasets to the context of this research. Details of these objectives are given at the beginning of each subsequent chapter.

CHAPTER 2: TSUNAMIS IN THE SAMOAN ISLANDS

2.1 Overview

This chapter presents a literature review of the tsunami hazard in the Samoan Islands. A summary of the geologic and climatic processes sets the context, followed by a review of the hazard in the historical, geologic and ethno-archaeological records.

The primary objective of this chapter is to provide an overview of the presently perceived tsunami risk in this region, and to set this thesis within the broader long-term hazard and disaster contexts at the local and regional levels.

2.2 Natural Setting: Samoan Context

2.2.1 Tectonic Context

The Samoan Islands volcanic chain is situated in a tectonic environment comprising complex interactions between mantle plume and plate subduction dynamics (Natland and Turner, 1985; Hart et al., 2000; Natland, 2003; Hart et al., 2004; Konter et al., 2004; Staudigel et al., 2004; Workman et al., 2004; Staudigel et al., 2006; Jackson et al., 2007; Koppers et al., 2008; Workman et al., 2008; Jackson et al., 2009; Jackson et al., 2010; Huang et al., 2011; Koppers et al., 2011; Konter and Jackson, 2012) (Figures 2 and 3).

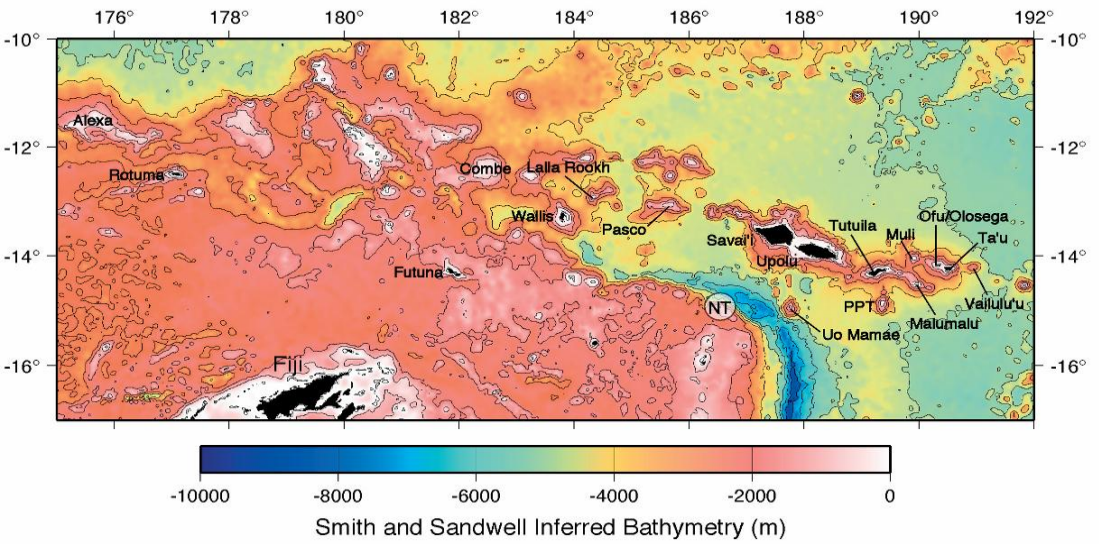

Figure 2: Samoan hotspot chain relative to the NTSA region (NT). Older seamounts include Pasco to Alexa (excluding Futuna and Rotuma). Main Samoan Islands from oldest to youngest include Savai'i, Upolu, Tutuila, Ofu, Olosega, and Ta'u. Vailulu'u seamount marks the active hotspot location. The

seamount Uo Mamae is a major long-term tsunami hazard concern due to its proximity along the NTSA subduction interface. (from Hart, 2006).

The island chain is oriented in an east-west direction along the oceanic side of the Tonga-Vitiaz tectonic pivot; termed here the Northern Tongan Subduction Arc (NTSA). The oldest island Savai'i (~ 5 Ma) is in the west and the youngest Ta'u (~0.3 Ma) is in the east (Hart et al., 2004; Koppers et al., 2008; 2011). The active seamount Vailulu'u (~0.7 Ma) which lies approximately 45 km east of Ta'u, marks the Samoan hotspot (or plume conduit) associated with the Pacific superplume and subsequent shield-building volcanism in this region (Hart et al., 2000; Staudigel et al., 2006; Huang et al., 2011; Koppers et al., 2011).

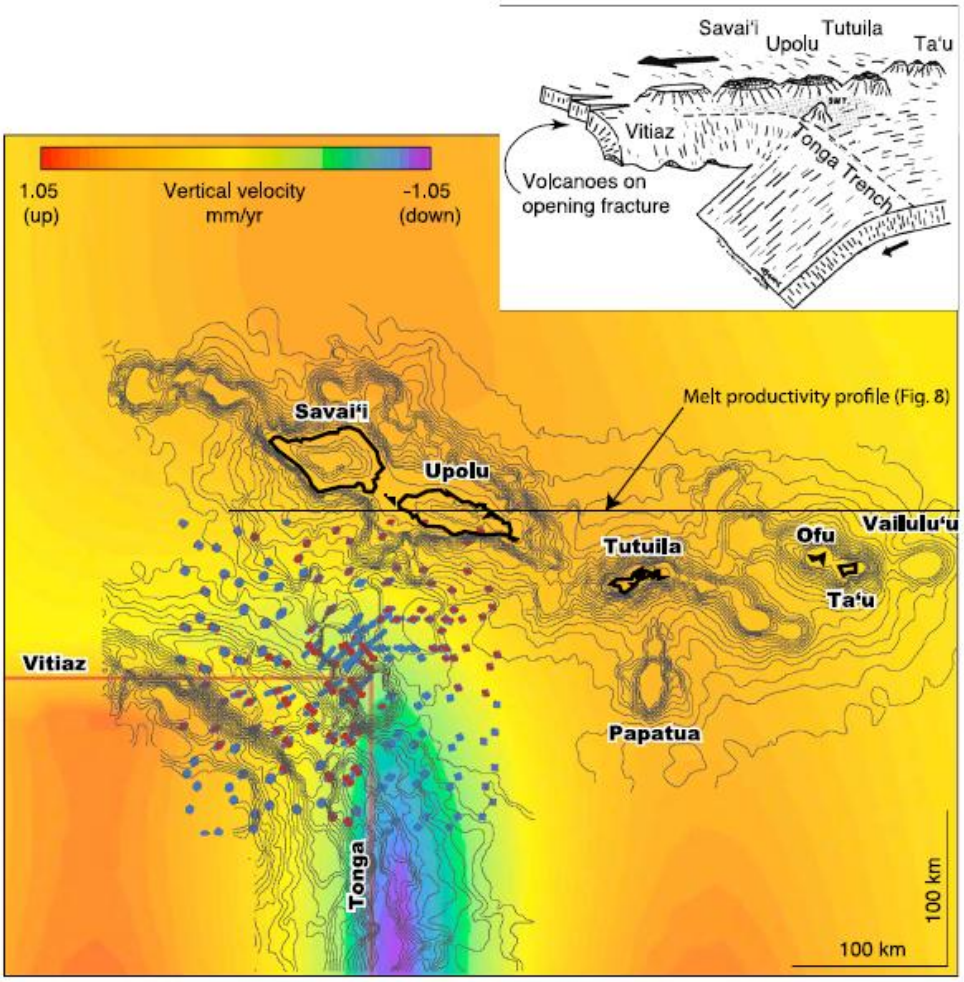

Figure 3: Schematic of lithospheric deformation around the Samoan region influencing rejuventated volcanism (from Konter and Jackson, 2011). Colour illustrates the vertical plate velocity. Blue and red dots indicate high strain rates close to the Tonga-Vitiaz pivot. Melt productivity profile is provided by Konter & Jackson, 2012.

Rejuvenated volcanism on the main islands of Savai'i, Upolu and Tutuila since 0.4 Ma is likely due to the combined effects of local tectonics, stresses, extension, flexural bending and metasomatism of the Samoan Lithosphere associated with its proximity to the eastward rollback of the NTSA boundary (Koppers et al., 2011; Konter and Jackson, 2012) (Figures 3 and 4).

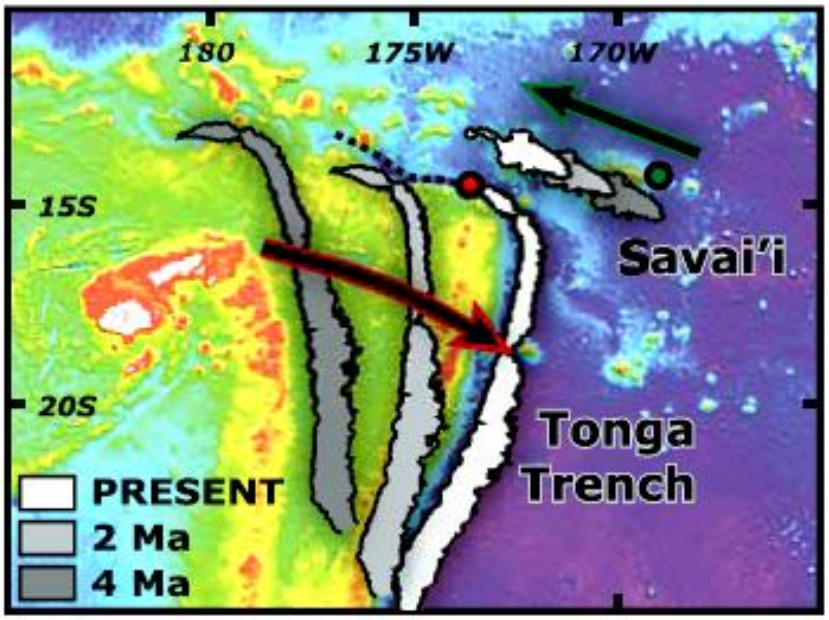

Figure 4: Eastward rollback of the Tonga Trench over the last 5 Ma. The northern portion migrated more rapidly than the southern portion, indicating more frequent geologic activity in the NTSA. Red circle = Northern termination point of this trench; Green circle = Present location of the Samoan hotspot beneath the Vailulu'u submarine volcano (from Koppers et al., 2008).

2.2.2 Geohazard Context

Located ~200 km north of the NTSA convergent tear-fault, the islands are exposed to local geohazard risk influenced by coupled NTSA-Hotspot processes. Seismicity in the region is largely influenced by faulting associated with NTSA processes (Benz et al., 2010; Okal et al., 2011) (Figure 5). Near-simultaneous fault ruptures along the outer rise of the NTSA are capable of producing earthquake intensities almost twice as strong as expected from instrument recordings (Beavan et al., 2010; Lay et al., 2010). For example, the near-simultaneous Mw 7.9 earthquake which occurred seconds after the initial Mw 8.0 earthquake on Septemeber 29, 2009, was not seismically detected because it was obscured in the seismic noise associated with the initial earthquake (Beaven et al., 2010),.

Volcanism in the east of the chain is dominated by shield-building processes associated with the active Vailulu'u seamount (Hart et al., 2000). Local seismicity associated with this seamount has also been detected (Konter et al., 2004). Recent rejuvenated volcanism in the west (e.g. 1760's, 1902, and 1905 – 1911 eruptions on Savai'i) (Cronin et al., 2006), likely manifests from flexural bending and metasomatism of the Samoan Lithosphere due to NTSA influences (Konter and Jackson, 2012). Historical eruptions in the west suggest an eastward trending eruptive recurrence every 150 years or so (Cronin et

al., 2006), meaning an eruption is possible between east Savai'i and west Upolu within the next 50 years or so (Figure 6).

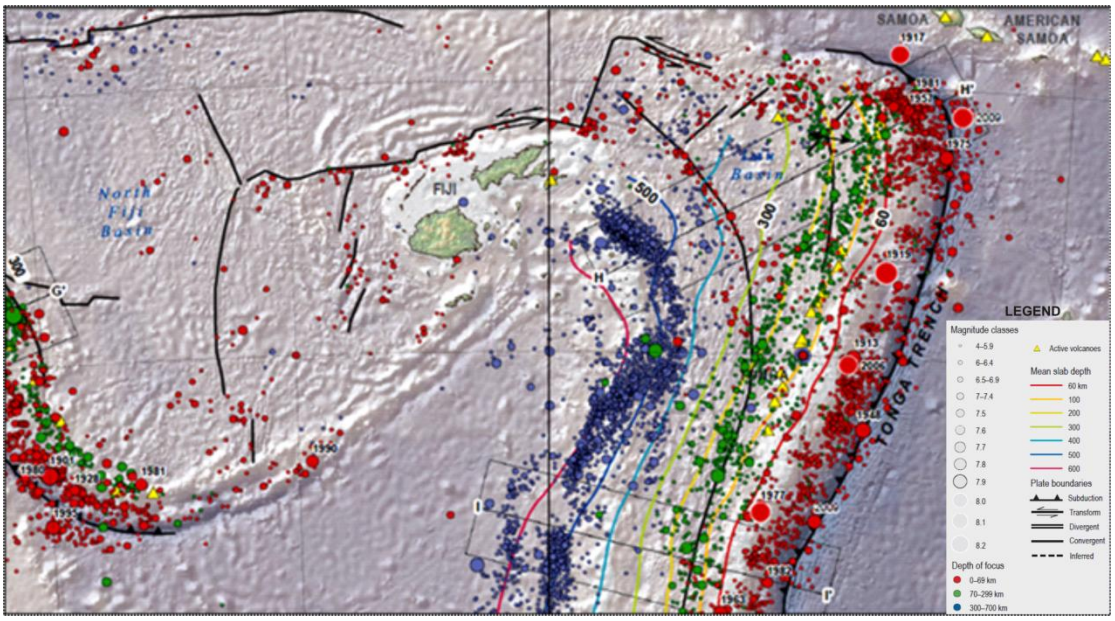

Figure 5: Seismicity in the Tonga Trench and NTSA (from Benz et al., 2010). Dated depths of focus shown are historically significant earthquakes. Profiles for I—I', H—H' and G—G' are provided by Benz et al. (2010).

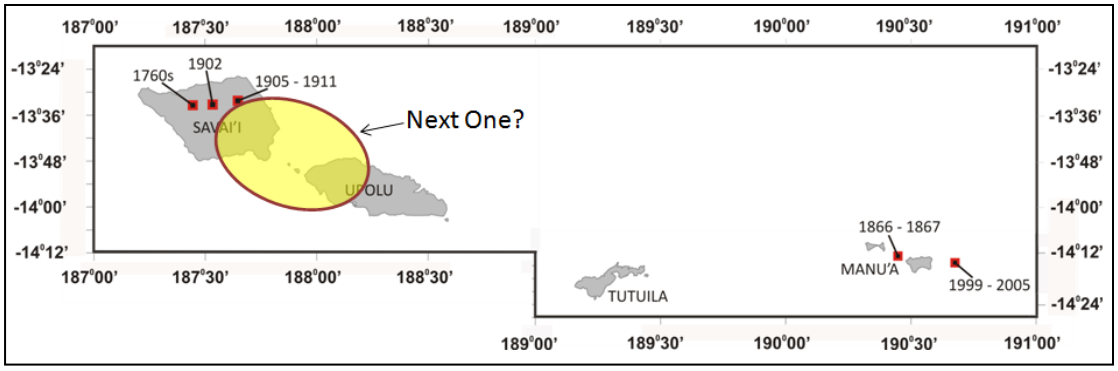

Figure 6: Distribution of historical eruptions along the Samoan volcanic chain. Red Squares = Eruption centres and timing. Eruptions in the east are plume-dominated, and rejuvenated volcanism in the west is likely due to an NTSA influence. Yellow colour depicts the likely region in which a future rejuvenated eruption may occur.

Giant landslides up to several tens of cubic kilometers are recognizable in the coastal geomorphologies of Savai'i and Ta'u (e.g. Keating et al., 2000; Cronin et al., 2006; Williams et al., 2012) (Figure 7). Such

flank collapses are possibly associated with either NTSA, hotspot, climatic, or coupled NTSA-hotspot-climatic influences on the Samoan Lithosphere.

These earthquake, volcanic and landslide processes provide individual, and/or possibly coupled, tsunamigenic sources that result in a high coastal risk to near-field tsunamis.

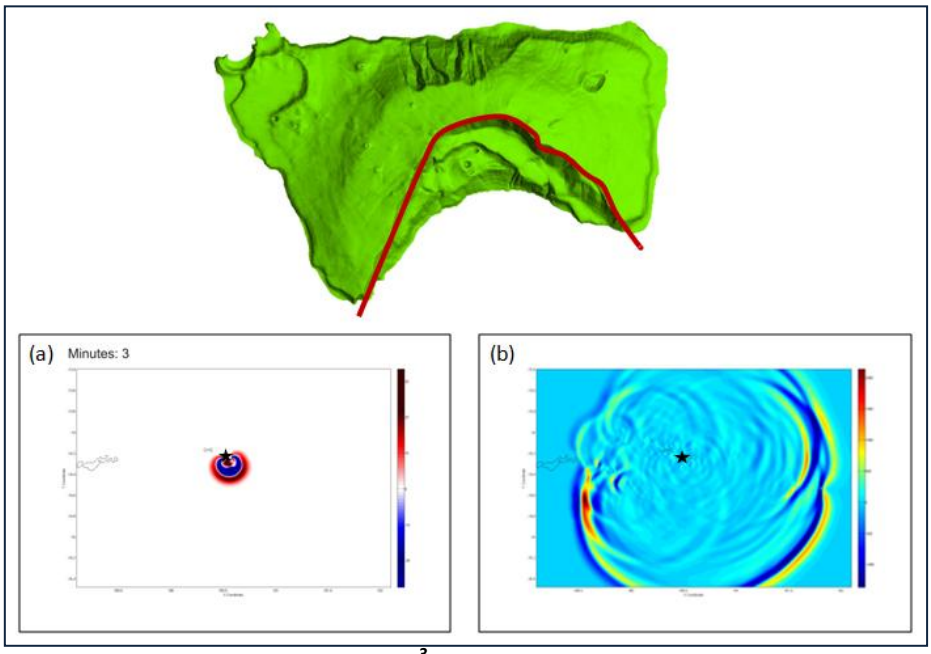

Figure 7: Southern Ta'u flank collapse ≥ 30 km^3. Red line depicts the scarp (~1 km elevation). (a) modeled landslide-tsunami propagation at 3 min; (b) modeled maximum tsunami flow direction. Black star in (a) and (b) represent Ta'u. (from Williams et al., 2012).

2.2.3 Climatic Context

The present climate range in the Samoan archipelago has largely been in place for the past 4,000 years or so (Nunn, 2012). This is generally characterized by two distinct seasons; hot and wet season from November to April, and dry and cool season from May to October (Australian Bureau of Meteorology and CSIRO, 2011). Approximately 75% of Samoa's total annual rainfall of around 3,000 mm occurs during the wet season (Figure 8), with wetter areas located in the southeast and drier areas in the northwest.

The El Niño Southern Oscillation (ENSO) which consists of three phases (El Niño, La Niña, and neutral phases, respectively), largely influences climate variability in the archipelago (Australian Bureau of Meteorology and CSIRO, 2011) (Figure 9). El Niño typically brings wet seasons that are drier than normal, and La Niña tends to bring conditions that are wetter and cooler than normal.

Tropical cyclones typically associated with the western Pacific warm pool occur during the wet season (Figure 10). Climate data over the period 1969 – 2010 suggest that cyclone occurrence is more frequent in El Niño years (Australian Bureau of Meteorology and CSIRO, 2011). Lowland and coastal flooding due to intense cyclones associated with strong La Niña events are capable of causing widespread damage (e.g. 2008 and 2011, (Australian Bureau of Meteorology and CSIRO, 2011; including the 2012 Cyclone Evan associated debris-flow-dam-burst floods in Apia) (Figure 11).

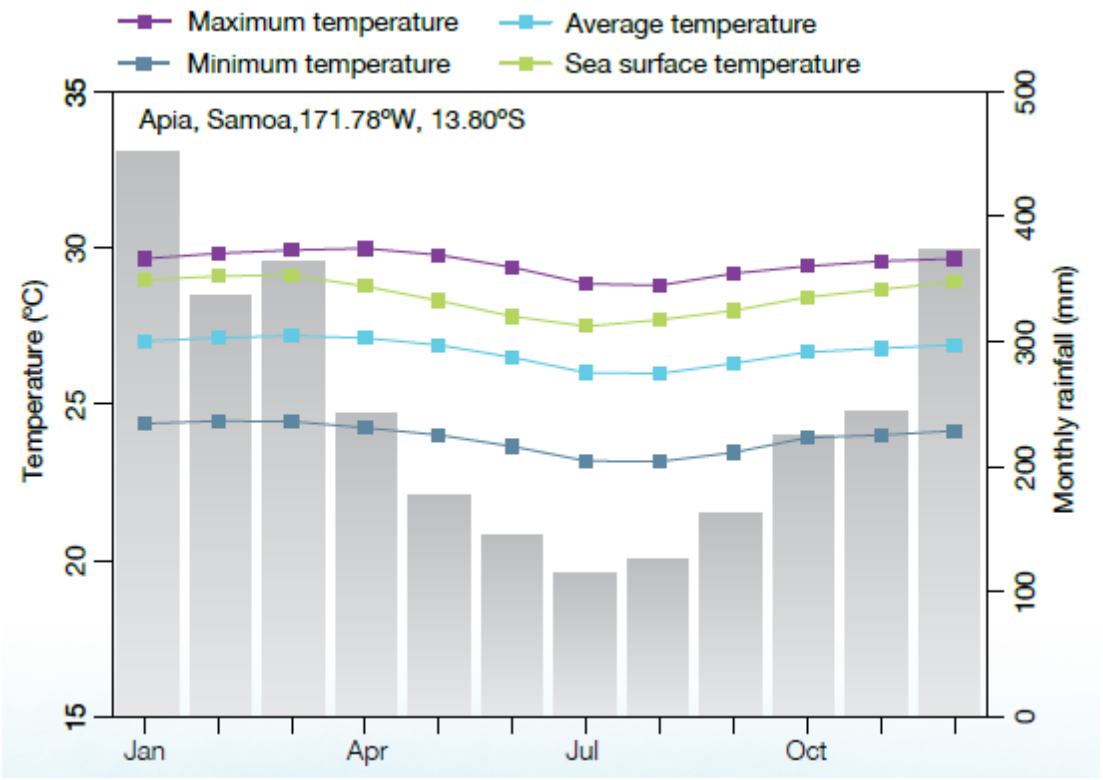

Figure 8: Annual climate distribution in Independent Samoa (from Australian Bureau of Meteorology and CSIRO, 2011).

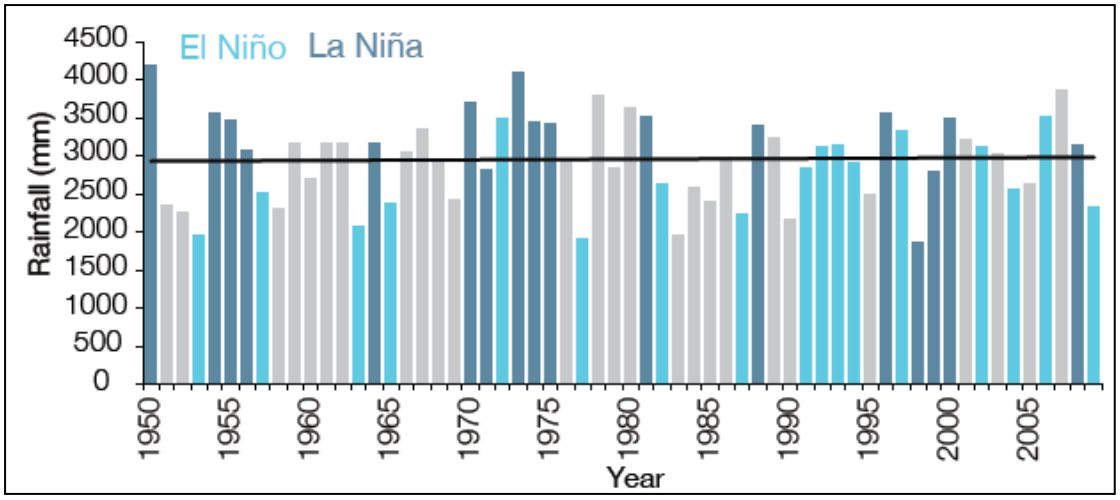

Figure 9: Rainfall distribution during El Niño and La Niña phases. (from Australian Bureau of Meteorology and CSIRO, 2011).

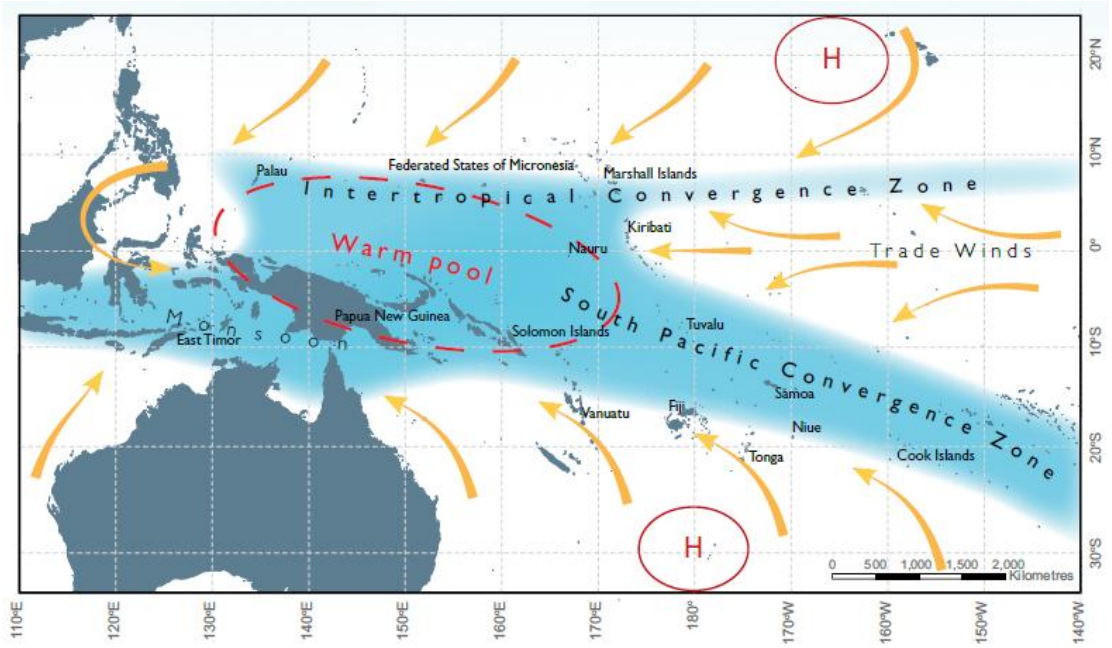

Figure 10: Average positions of major climatic features from November to April. (from Australian Bureau of Meteorology and CSIRO, 2011).

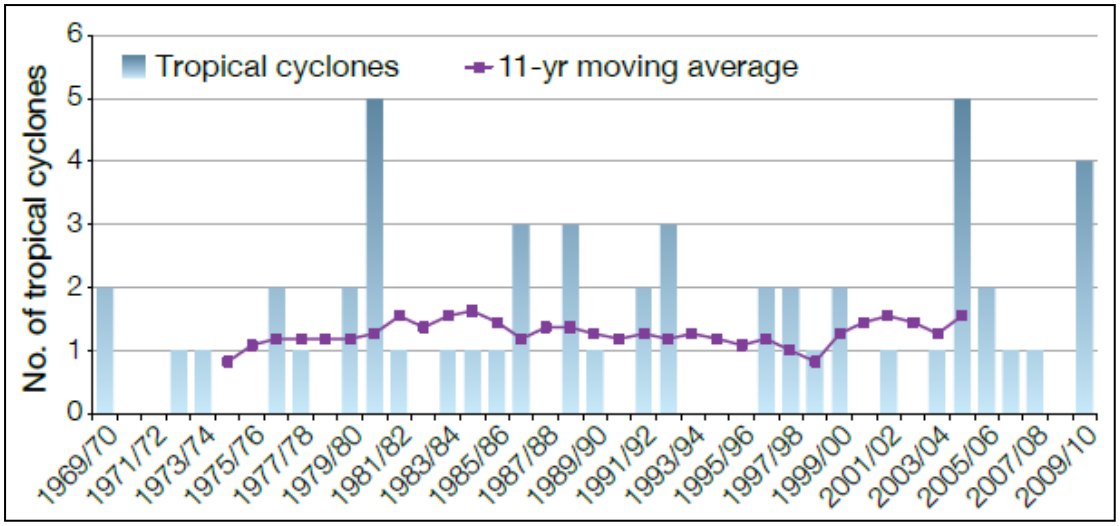

Figure 11: Tropical Cyclone frequency (from Australian Bureau of Meteorology and CSIRO, 2011).

Sea level rise near Samoa as indicated by satellite data has been approximately 4 mm/yr since 1993 (Australian Bureau of Meteorology and CSIRO, 2011)(Figure 12). Based on low, medium and high emissions scenarios (Australian Bureau of Meteorology and CSIRO, 2011), sea level near Samoa is projected to rise by 17 – 59 cm by 2090. Climatic projections for the same period and emissions scenarios suggest average annual increases in air and sea surface temperatures ranging from 0.8 – 3.3^{0}C, more frequent extreme rainfall days, less frequent but more intense tropical cyclones, and higher ocean acidification levels (Australian Bureau of Meteorology and CSIRO, 2011).

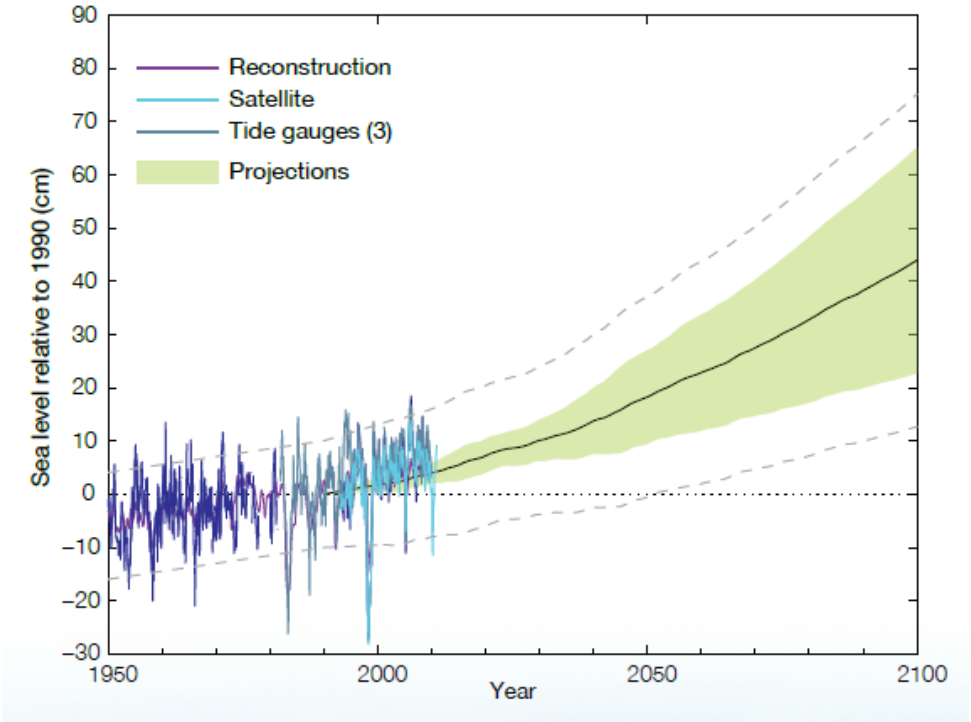

Figure 12: Observed and projected relative sea level near the Samoan region. (from Australian Bureau of Meteorology and CSIRO, 2011).

Projected sea level rise, natural climatic annual cycles and longer-term variability, as well as increasing coastal development, are expected to increase the impacts of storm surges and flooding in the Samoan Islands (Australian Bureau of Meteorology and CSIRO, 2011).

Coupled with the geohazard risk discussed in Section 2.2.2, it becomes clear that this region is vulnerable to geo-climatic processes in the short- and longer-term hazard timescales. This thesis however, focuses on tsunami hazards, with recognition that tsunami processes cannot be fully appreciated without consideration of compounding interactions within the broader geo-climatic system. Nevertheless, the investigative context in subsequent Sections and Chapters of this thesis exmpasises tsunamis.

2.3 Historical Tsunami Hazards

Parraras-Carrayanis and Dong (1980) compiled a catalogue of tsunamis in the Samoan Islands covering the period 1837 – 1980. Appendix 1 provides a summary of this catalogue. Additionally, tsunamis with damaging effects between the years 1980 – 2011 have been included.

This Section summarises the most notable of these events according to far-field or near-field sources. Far-field as used here concerns regional and distant sources that generate tsunamis with travel times of more than 1 hour (Power, 2013). Near-field refers to local sources that generate tsunamis with less than 1 hour travel time (Power, 2013).

2.3.1 Far-field Tsunamis

The 2011 Great East Japan Earthquake and Tsunami (JMA, 2013) (also known as the 2011 Tohoku Tsunami; Satake et al., 2012), caused extensive loss of life and infrastructure damage in Japan. This tsunami was recorded in Fagaloa Bay (northeast coast of Upolu) (Figure 13) at approximately 11 am – 12 pm local time, meaning it had an approximate travel time of 11 hrs (F. Nelson, pers. comm., 2014). The tsunami coincided with high-tide resulting in an approximate 1.5 m tsunami flow depth. Household members received a warning several hours before the tsunami impacted, providing ample time to evacuate (L. Lui and F. Nelson, pers. comm., 2014). Inundation flooding in this area subsided over the following few days. No injuries or loss of life were sustained.

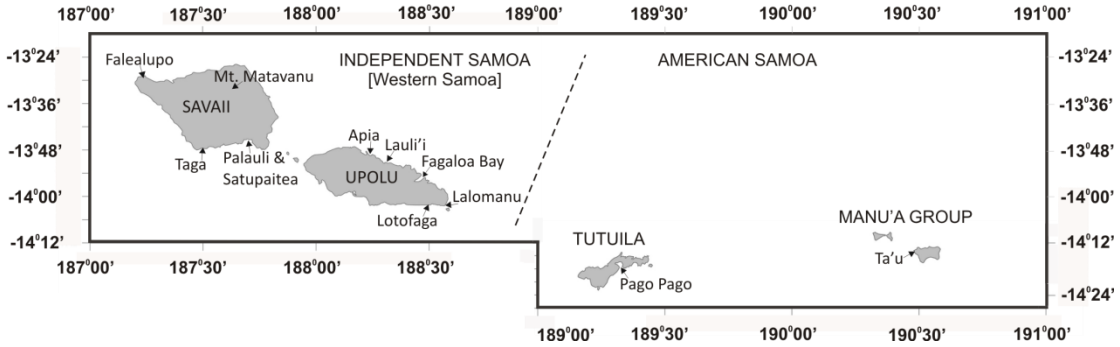

Figure 13: Location of place-names discussed in this section.

In 1960, a magnitude 9.5 earthquake in South Chile generated a Pacific-wide tsunami, which caused devastating impacts in Japan in the northwest Pacific. At Lalomanu village (east coast of Upolu Island), two fisherman in canoes near the reef were picked up by the wave and washed onto the beach by the road. At Fagaloa, the first motion was a recession of the sea beyond the reef. A few minutes later, a crest advanced 82 m through the village, where the peak water level reached the roof of one of the local Samoan houses. Fortunately, there was no loss of life recorded. In Pago Pago (Tutuila Island), damages amounted to approximately USD$50,000. One house was lifted and moved 3 m inland, and another was washed into the bay by the outgoing wave.

In 1957, a tsunami which originated from a magnitude 8.5 earthquake in the Aleutian Islands, had a travel time of approximately 9 hours. The impacts of the event were distributed relatively evenly along the north coast of Upolu, Savaii and Tutuila islands, although the most notable effects were experienced at Lauli'i and Fagaloa. Inundation inland from the high-tide mark was around 46 m at Lauli'i, and about 23 m over the lower part of Fagaloa village causing sea flooding in most of the houses in the area.

The November 1952 Kamchatka tsunami caused the destruction of a school and some Samoan houses in Fagaloa Bay, particularly Maasina, Sanamea and Taelefaga.

The 1946 Aleutian Islands tsunami caused a recession of water in the Apia harbor thus exposing the inner reef. Shortly after, six waves around 1.7 m high inundated over the next two hours; although the impacts were not documented. In Pago Pago, several huts were washed away by the tsunami.

The 1868 Peru tsunami apparently destroyed settlements in Apia (Pararas-Carayannis and Dong, 1980), although details on the extent of impacts were not available. The description of impacts caused by this event, together with the 1960 tsunami, suggest that they represent the largest far-field events to have had damaging impacts in the tsunami documented history of the Samoan Islands.

2.3.2 Near-field Tsunamis

The 2009 SPT was the most devastating tsunami disaster documented in the Samoan Islands (Dominey-Howes and Thaman, 2009; Beavan et al., 2010; Lay et al., 2010; Okal et al., 2010; Roeber et al., 2010; Chagué-Goff et al., 2011; McAdoo et al., 2010; Okal et al., 2011; Reese et al., 2011; Richmond et al., 2011a). It formed from a near-simultaneous earthquake doublet in the NTSA region (Beavan et al., 2010; Lay et al., 2010), and 149 lives were lost in Independent Samoa, 34 in American Samoa, and 9 in Niuatoputapu, northern Tonga (NGDC, 2014). Maximum flow heights of around 15 m (Beavan et al., 2010) and run-up of about 22.4 m (Okal et al., 2010) were recorded on Niuatoputapu.

Solov'ev et al. (1986) reported 1 m wave heights at the village of Taga on southern Savai'i associated with the 1981 NTSA earthquake and tsunami. No casualties or major damage was reported. Okal et al. (2010; 2011) reported that this event was around 10 times smaller than the 2009 SPT.

The June 1917 tsunami was significant in terms of the spatial distribution of impacts. A magnitude 8.3 earthquake which occurred in the NTSA region triggered the tsunami which impacted Samoa 10 minutes after the earthquake's origin time (Pararas-Carayannis and Dong, 1980). Destructive waves 3 m in height were experienced at Aleipata (east Upolu district comprising Lalomanu), and half of the village of Lotofaga was submerged and houses destroyed. A bridge was washed away at Palauli (south Savai'i) and a number of native houses destroyed. In Satupaitea (south Savai'i), a copra house was carried along the coast by the wave for about a quarter of a mile, and all native houses were demolished. In Pago Pago (American Samoa), a recession of the sea was observed a few minutes after the earthquake was felt, followed by a tsunami that destroyed many native houses, along with the partial destruction of a Catholic church in Leone, and a Mormon church in Pago Pago.

The eruption of Mt. Matavanu in Savaii from between 1905 to 1911 presented another source for local tsunami generation. A total of 7 local tsunamis were formed as a result of lava coming into contact with the ocean along the coastal area. The first of these events occurred on November 28th in 1906, and the other 6 occurred between the months of June to October, 1907. The impacts were felt along the northwest coast of Savaii, although fortunately they were small.

The March 1883 event is interesting in that the source is unknown. Apparently a storm, accompanied by an earthquake and tsunami, caused all houses within a quarter of a mile of the beach on the east end of Savaii to be swept away over a distance of about 24 km along the shore (Pararas-Carayannis and Dong, 1980). These impacts suggest a possible local tsunami influence. Further, assuming that a storm-earthquake-tsunami event did in fact occur, then the possibility of a localized coastal or submarine landslide-generated tsunami cannot be presently dismissed.

2.4 Tsunamis in the geologic record

Recent studies of modern tsunami deposits during immediate post-tsunami surveys have provided the opportunity to establish and refine diagnostic criteria associated with the deposits (Chagué-Goff et al., 2011; Etienne et al., 2011; Goto et al., 2011; Morton et al., 2011; Richmond et al., 2011a and 2011b; Chagué-Goff et al., 2012a). Many of these studies were of recent tsunamis such as the December 26, 2004, Indian Ocean tsunami (Lay et al., 2005; Titov et al., 2005), the September 29, 2009 SPT (Chagué-Goff et al., 2011; Richmond et al., 2011a), the February 27, 2010, Chile tsunami (Morton et al., 2010; 2011), and the March 11, 2011, Japan tsunami (Sugawara et al., 2011; Chagué-Goff et al., 2012a).

Understanding the characteristics of historical (or modern) tsunami deposits enables the identification of palaeotsunamis within the geologic record that have similar deposit characteristics (Nishimura and Miyaji, 1995; Goff et al., 2001). This improves understanding of the long-term risk of tsunamis to communities and underpins efforts to mitigate their impacts, including loss of life and property. Combining tsunami deposit studies with numerical modeling may provide an avenue for better understanding source characteristics (Dawson and Stewart, 2007a; 2007b; Bourgeois, 2009) (Figure 14).

While much has been written and debated about the diagnostic proxies of tsunamis (e.g. Goff et al., 2004; Dominey-Howes et al., 2006; Dawson and Stewart, 2007a; Kortekaas and Dawson, 2007; Morton et al., 2007; Bridge, 2008; Kelletat, 2008; Morton et al., 2008; Chagué-Goff, 2010; Goff and Chagué-Goff, 2009; Goff et al., 2010a; Peters and Jaffe, 2010; Richmond et al., 2011; Chagué-Goff et al., 2012; Goff et al., 2012a; 2012b; 2012c; Goff and Chagué-Goff, 2014), much work still remains to be done in the context of detailed deposit and geomorphological analyses (Chagué-Goff et al., 2011). This includes the establishment of site criteria to recognize and distinguish tsunami deposits from cyclone deposits (e.g. Goff et al., 2004; Phantuwongraj and Choowong, 2012); a challenge that remains to be fully achieved.

In the Samoan Islands (specifically Independent Samoa), tsunami research prior to the 2009 SPT was limited and focused entirely on establishing a record of historical tsunami events (Pararas-Carayannis and Dong, 1980), reviewing early warning systems (Williams and Leavasa, 2006), and limited modeling for coastal hazard planning purposes (Schmall, 2000; Williams, 2009).

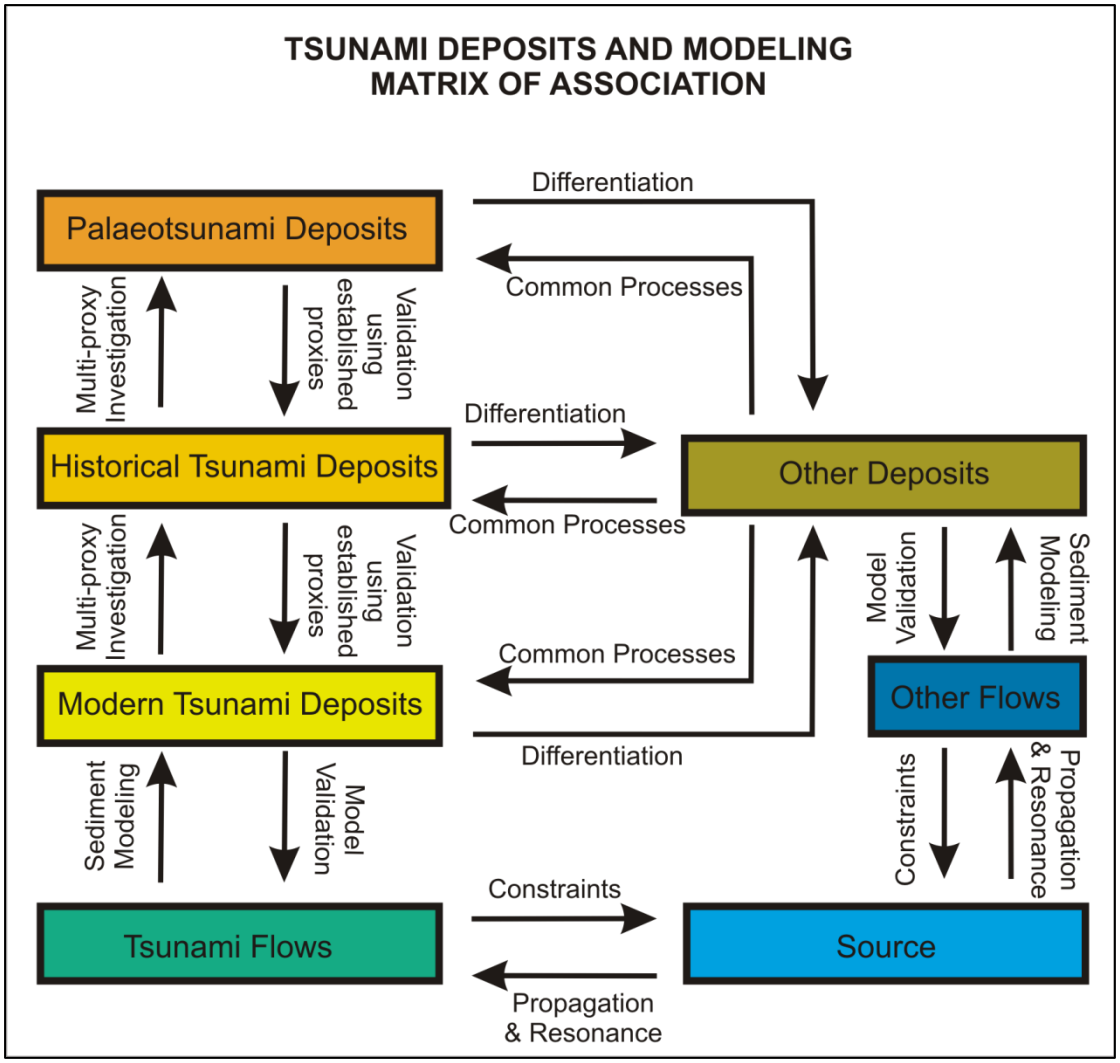

Figure 14: Tsunami deposits and modeling inter-relationships. A geoscientist generally starts with a palaeotsunami deposit and works back towards understanding the likely source (e.g. earthquake or landslide), bearing in mind other likely deposit origins (e.g. cyclone). Tsunami and cyclone deposits are generally distinguished using a suite of proxies outlined in Goff et al. (2012). A modeller generally starts at the source (either known or hypothetical) and works forward towards understanding the wave and inundation characteristics. Modeling of coastal resonance is used here as a potential tool to isolate the locations of tsunami deposits (modified from Bourgeois, 2009)

While inundation modeling and hazard mapping remain a key focus for current research, emphasis has been placed on characterising the 2009 SPT deposits as a proxy for identifying palaeotsunami deposits in the geologic record (Chagué-Goff et al., 2011; Richmond et al., 2011; this thesis). Moreover, the identification and development of criteria to distinguish tsunami from cyclone deposits is a high priority.

In summary, little is known about the prehistoric record of tsunamis in Samoa, although there is evidence for prehistoric events in the surrounding region (e.g. Goff et al., 2010b; Goff et al., 2011; Goff et al., 2012a; 2012b). A comprehensive study of the 2009 SPT analogue deposits will enable identification of their prehistoric counterparts, particularly those from the near-field NTSA source. Assessing the differences in the characteristics and ages of similar marine deposits provides an avenue

for identifying historical cyclones (e.g. 1991 Cyclone Val; Elmqvist et al., 1994) in the geologic record. Correlating identified palaeotsunamis with events that are recorded elsewhere in the Pacific (e.g. Goff et al., 2011; 2012a) will provide an indication of their broader impacts, as well as the risks they pose at the regional scale.

2.4.1 Deposit characteristics

A catastrophic saltwater inundation event (CSI) is a term to describe a deposit that is of either tsunami or cyclone origin (Goff et al., 2001); these are termed in this thesis rapid marine inundation deposits (MIDs). Typically these are identified empirically by distinct changes in sediment characteristics within the geologic record (e.g. marine sediments intercalated between soils, peat or palaeosols) (Peters and Jaffe, 2010). Distinguishing between the two requires multi-proxy characterisation (Goff et al., 2012b).

MIDs generally contain higher amounts of calcium, sulphur, magnesium, sodium, and chlorine (and other marine-derived elements) than overlying and underlying sediment layers (Goff et al., 2001; Goff et al., 2010b; Chagué-Goff et al., 2011). They can also contain much higher levels of heavier elements such as iron and/or titanium (Chagué-Goff, 2010), although iron and titanium in the Samoan Islands are predominantly of terrestrial origin. Higher calcium compositions occur due to the deposition of marine calcareous sediments (carbonates) onto pre-existing soils.

2.4.2 Tsunami and Cyclone Deposit Distinctions

There is still no clear criterion to effectively distinguish a tsunami deposit from a cyclone deposit in the geologic record without an historical event marker. Nevertheless, Goff et al. (2012b) suggest a suite of proxies which can be used to infer the most likely origin of an MID. These include geological, biological, chemical, geomorphological, archaeological, anthropological, contextual data, and numerical modeling proxies.

This thesis integrates geological, geochemical, and geochronological proxies to infer the origin of identified MIDs in the Samoan geologic record (Chapter 3). Ethno-archaeological and numerical modeling provide additional proxies to better understand the context and nature of associated deposits.

2.5 Tsunami hazard considerations

The NTSA has an important, and perhaps dominant, influence on multi-geohazard risk in the Samoan region, particularly when coupled with climatic influences (see Chapter 2.2). Further research would help contribute to developing strategies that aim to reduce the long-term vulnerability and increase resilience of the Samoan Islands to NTSA associated hazards. This thesis places particular emphasis on the local tsunami context within the broader hazard management system. A brief overview of risk reduction efforts and arrangements is now provided.

2.5.1 Tsunami Modeling

Prior to the 2009 SPT, few hypothetical tsunami modeling studies with implications on Samoa had been carried out (e.g. Schmall, 2004; Mader, 2006; Williams, 2009). Schmall (2004) conducted inundation modeling in Apia associated with the Pacific Cities regional project, which focused on the reduction of risk in central business districts. Mader (2006) modeled a hypothetical Mw 9.0+ earthquake rupture and tsunami along the Tonga-Kermadec Trench, and demonstrated that such an event would likely generate a tsunami with far-reaching impacts. Williams (2009) modeled a prehistoric landslide-generated tsunami on Ta'u, demonstrating the local tsunamigenic potential of similar processes in the future.

These studies together with the historical database, although limited in scope, provided a means to estimate the possible impact characteristics of tsunamis in view of ongoing or planned coastal developments, as well as population concentration and subsequent risk. However, they fell short of estimating the distribution of likely impacts associated with an NTSA event, particularly given the fact that exposed southern coastal areas were known to have been severely impacted by the 1917 tsunami. Hence, the threat from similar NTSA events prior to the 2009 SPT was under-estimated.

Extensive tsunami modeling has since been conducted and communicated following the 2009 SPT (e.g. Beavan et al., 2010; Lay et al., 2010; Okal et al., 2010; Roeber et al., 2010; Okal et al., 2010; 2011; Williams et al., 2012). These serve as starting points for understanding the characteristics of NTSA associated tsunamis, including hypothetical inundations and likely deposit formations (e.g. Okal et al., 2010; Roeber et al., 2010).

2.5.2 Tsunami Intensity

Similar to the Modified Mercalli Intensity Scale for earthquakes, Lekkas et al. (2012; 2013) proposed a 12-grade Integrated Tsunami Intensity Scale (ITIS) for tsunamis, covering a wide range of effects associated with different situations and environments. This scale is provided by Lekkas et al. (2013: 1498-1500). Criteria for assigning a specific intensity to a tsunami include the physical parameters of the phenomenon (from source to inundation), impacts on the human environment including loss of life, impacts on mobile objects (e.g. boats, cars) and infrastructure, geoenvironmental effects including tsunami debris and deposits, and effects on the urban environment.

Applying the ITIS to the 2009 SPT in the local Samoan context, which ignores effects on the urban Apia environment, would suggest that this event had a local tsunami intensity of [$XI_{ITIS-2012}$, Devastating].

The ITIS is mentioned in this thesis for completion purposes, primarily to reinforce that the 2009 SPT was a devastating tsunamiological event in Samoa. This in turn underlines the local need to implement geoscientific investigations to understand the long-term tsunami hazard in this region.Because the ITIS

was only recently accepted in 2013, more time and tsunami experiences are required to evaluate its usefulness and reliability in tsunami hazard and disaster management.

If it is to prove useful in coastal vulnerability mapping and/or informing operations during the response and recovery phases of a tsunami disaster, then it is important that the indicators which are used to assign a specific intensity are held in relation to the tsunami source, as well as the local context of occurrence (e.g. exposure and resilience levels). For example, the nature of urban infrastructure impacts caused by the 2009 SPT in Samoa were not as was described in the ITIS for its associated intensity (Lekkas et al. 2013:1498-1500). This is because the 2009 SPT did not impact the Apia central business district. However, there was extensive loss of life, environmental and property damage on the southeast touristic coast, thus qualifying the 2009 SPT as a devastating event.

Further, the inclusion of economic costs as an additional parameter to quantify tsunami intensity, based on the impacts criteria of the ITIS, would be useful for establishing the context of subsequent recovery and/or resilience. This would also help to place the impacts of the event into its true development context

The application of the ITIS to better understand potential palaeotsunami intensities inferred from deposits and contextual frameworks is feasible. However, it is beyond the scope of this thesis. Nevertheless, the 2009 SPT intensity represents an analogue for similar or stronger 2009 SPT-type events possibly inferred from the geologic record.

2.5.3 Local Hazard and Disaster frameworks

In Independent Samoa, the Strategy for the Development of Samoa 2012 – 2016 (SDS 2012-2016) presents the main development strategies and priority sectors for achieving Samoa's target Millennium Development Goals (MDGs) for the period 2012 – 2016 (Ministry of Finance, 2012). Climate adaptation and natural disaster risk reduction are key components of this plan, and provide the overarching directive for implementing risk reduction activities outlined in Samoa's National Disaster Management Plan 2011 – 2014 (Disaster Advisory Committee, 2011). This document identifies tsunamis as being an extreme threat to Independent Samoa.

In American Samoa, the National Tsunami Hazard Mitigation Program 2013 – 2017 Strategic Plan (NTHMP-SP 2013-2017) (Miller et al., 2013), provides the overarching framework for implementation of local tsunami mitigation and risk reduction activities. These are administered locally by the Territorial Emergency Management Coordinating Office (TEMCO) of the American Samoa Department of Homeland Security.

Deputy Vice-Chancellor's Office
Postgraduate Office

Co-Authorship Form

UNIVERSITY OF CANTERBURY
Te Whare Wānanga o Waitaha
CHRISTCHURCH NEW ZEALAND

This form is to accompany the submission of any thesis that contains research reported in co-authored work that has been published, accepted for publication, or submitted for publication. A copy of this form should be included for each co-authored work that is included in the thesis. Completed forms should be included at the front (after the thesis abstract) of each copy of the thesis submitted for examination and library deposit.

Chapter 3; Sections 3.3 – 3.7: Revised from Manuscript ID GJI-S-14-0135 entitled "Resonance: A new proxy to assist palaeotsunami investigation".

Publication status: In Revision, Geophysical Journal International.

Resubmission date: 13 July 2014.

Shaun Williams wrote the manuscript and made the revisions presented in this thesis. Development and refining of the original manuscript as well as this revised exhaustive version was conducted by co-authors stated in the Co-Authorship Declaration of this thesis.

Certification by Co-authors:
If there is more than one co-author then a single co-author can sign on behalf of all
The undersigned certifys that:

- The above statement correctly reflects the nature and extent of the PhD candidate's contribution to this co-authored work
- In cases where the candidate was the lead author of the co-authored work he or she wrote the text

Name: **Tim Davies** Signature: Date: **30 April 2014**

CHAPTER 3: TSUNAMI AND CYCLONE DEPOSIT ANALYSIS

3.1 Overview

This chapter reports and investigation of the 2009 SPT deposit characteristics. Sedimentary proxies examined are loss on ignition (LOI) and grain size. Elemental ratios were obtained using a portable X-ray fluorescence (XRF) spectrometer and ITRAX core scanner data. Application of the signature characterizing the 2009 SPT deposits provides a means for identifying similar marine inundations in the profiled geologic records.

Age data (e.g. ^{14}C and ^{210}Pb) yielded from geochronological indicators (e.g. palaeosols, plant fragments, charcoal, shells, wood) provide the means to associate identified deposits with possible historical tsunamis (e.g. 1960 Chile Tsunami) or cyclones (e.g. 1991 Cyclone Val) origin. Identification of such associations (e.g. historical cyclone deposit) enables an assessment of any differences between the 2009 SPT and cyclone deposits. It also allows correlations to be made between contemporaneously associated deposits.

This culminates in the development of a tsunami and cyclone chronology model from the geologic record, forming a basis for estimating the likely frequency of 2009 SPT-type tsunami (or stronger ones) associated with the near-field NTSA source. Cultural anomalies evident in ethno-archaeological, oral and indigenous records provide indicators of the spatial extent of contemporaneous, possibly associated, tsunami and/or cyclone hazards.

3.2 Objectives

The objectives of this Chapter are to;

1. Characterise the 2009 SPT deposits using sedimentary, geochemical, and geochronological proxies.

2. Identify and distinguish probable historical tsunami and cyclone deposits using the 2009 SPT characteristics as a baseline analogue.

3. Establish a tsunami and cyclone chronology for use in tsunami frequency and magnitude estimation.

4. Interpret the findings in the context of the overall thesis aim.

3.3 Methodologies and Data

3.3.1 Field Methods and Stratigraphic Logging

Field investigations were carried out at coastal sites shown in Figure 15. Site data and maps are provided in Appendix 2. Trench and coring techniques were used to obtain samples for laboratory analysis. Preliminary stratigraphic logging was carried out at the investigated trench sites, while the sampled cores were logged at the University of Canterbury (Appendix 3 and 4).

3.3.2 2009 South Pacific Tsunami (SPT) Analogue

In Satitoa, Vaovai and Mulivai on Upolu (Figure 15), the 2009 SPT deposits provide analogues for the identification of similar older sedimentary units preserved in the trench/core data. The 13 cm thick 2009 SPT deposit at Satitoa formed the surface layer of the trench profile located 280 m inland from the high-tide mark. This was sampled at 1 cm intervals and is characterised by a marked grain size coarsening at the contact with the underlying (pre-2009 SPT) soil (Appendix 3).

3.3.3 Sedimentary Proxy Analysis

3.3.3.1 Loss on Ignition (LOI) Analysis

LOI was carried out at the University of Canterbury following the methods of Santisteban et al. (2004), which are described by Chagué-Goff et al. (2011). LOI data is provided in Appendix 5.

3.3.3.2 Grain size Analysis

Grain size analysis was carried out using the Horiba LA-950 Particle Analyzer at the University of Canterbury, adapting the methods presented in Dinis & Castilho (2012). Grain size data is provided in Appendix 6.

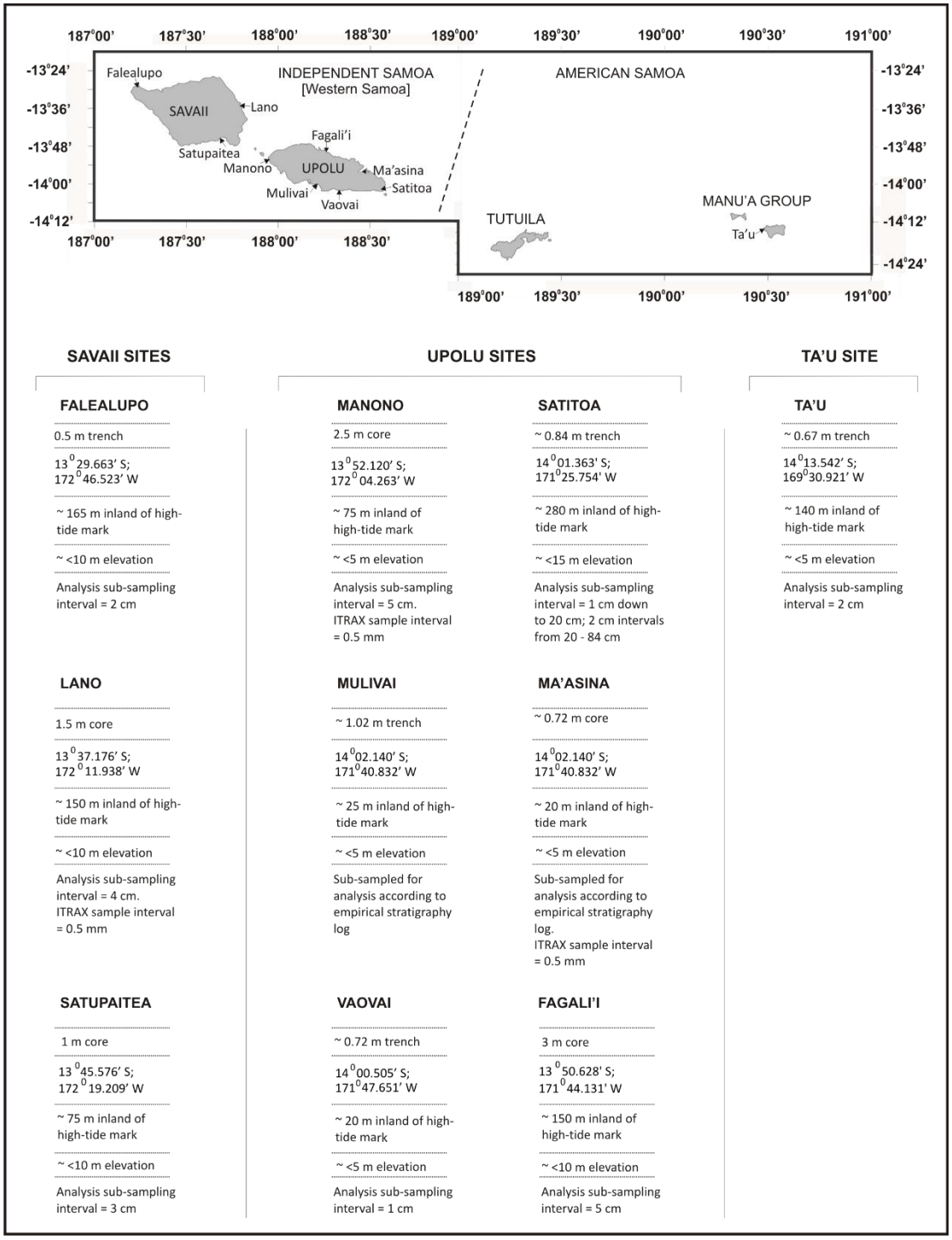

Figure 15: Site data for palaeotsunami analysis. Appendix 2 provides further site data and maps.

3.3.4 Geochemical Proxy Analysis

The geochemical composition of most sedimentary sequences was determined using a portable X-ray fluorescence spectrometer (pXRF), and was processed using the ARTAX data processing software at the University of Canterbury. In the case of the Ma'asina, Lano, and Manono sites, elemental profiles were

also obtained using the ITRAX core scanner at the Institute for Environmental Research, Australian Nuclear Science and Technology Organisation (ANSTO).

3.3.4.1 pXRF Spectroscopy Analysis

Preliminary elemental compositions were obtained for each sampled stratigraphic profile using a Tracer III portable XRF spectrometer developed by Bruker Inc. The instrument determines the relative elemental chemistry composition of a sample through the emission of photons (x-rays) onto its surface, thus exciting electrons within individual elements comprising the sample causing them to fluoresce (Bruker Inc., 2008). In this study, the samples tested were mainly soils, peat, and calcareous sands. The ARTAX software developed by Bruker Inc. was used to process the acquired data (Appendix 7).

Only three of the investigated sites contained empirical evidence of the 2009 SPT deposit (e.g. yellow/grey calcareous sand), each varying according to the nature of sediment being deposited, flow characteristics of the inundating tsunami, and geomorphology or landscape of the area (Appendix 3.1). These sites were Mulivai, Vaovai and Satitoa on the south and southeast coast of Upolu; a stretch of coastline hardest hit by the 2009 SPT.

3.3.4.2 ITRAX Core Scanner Analysis

High sampling resolution element data (0.5 mm intervals) was obtained for Ma'asina, Manono and Lano sites using the ITRAX core scanner of the Institute for Environmental Research, ANSTO, following methods described by Croudace et al. (2006) (Appendix 8). Limitations associated with ITRAX elemental data are provided by Croudace et al. (2006).

For the purposes of this study, the ITRAX data obtained adequately enabled a comparison of the results with the lower sampling resolution data obtained in the pXRF analysis. The ITRAX data permitted the identification of thinner MID layers not detected in the pXRF analysis, and/or distinction of MID signatures that were not so apparent in the pXRF analysis.

3.3.5 Geochronological Proxy Analysis

The age results obtained from standard C-14 radiocarbon and AMS dating techniques form a basis for developing the geochronology of stratigraphic profiles from investigated sites. Simple depth interpolation or extrapolation (i.e. $y = \frac{bx}{a}$; where *a* = known depth, *b* = known age, *x* = assigned depth, *y* =inferred age at *x* depth), provides estimates of the probable ages of MID's at respective sites containing only one or two geochronological reference ages (e.g. Ma'asina, Fagali'i and Lano). This assumes a constant sediment rate within the core.

3.3.5.1 Radiocarbon dating

Radiocarbon analysis of organic palaeosols, plant fragments, charcoal, wood, and carbonate shells associated with likely palaeotsunami deposits was conducted at the Radiocarbon Dating Laboratory of the University of Waikato (WK- sample code), and at ANSTO's Accelerator Mass Spectrometry Laboratory (OZP- sample code) (Appendix 9). Citations to specific radiocarbon methods used are provided in Appendix 9 and in the footnotes of Table 1.

3.3.5.2 ^{210}Pb dating

^{210}Pb dating was carried out on samples from Falealupo and Ma'asina using alpha spectrometry at ANSTO's Environmental Radioactivity Measurement Centre. Ages (N- sample code) were calculated using the CRS (constant rate of ^{210}Pb supply) model for Falealupo site and CIC (constant initial ^{210}Pb concentration) model for Ma'asina site following the methods in Appleby (2001) (Appendix 10).

The basic assumption of the CRS model is that the rate of supply of ^{210}Pb fallout to the core site is constant, reflecting the constant flux of ^{210}Pb from the atmosphere (Zawadzki and Fierro, 2012). The CIC (constant initial ^{210}Pb concentration) model assumes that sediments in the core all had the same initial unsupported ^{210}Pb concentration at the time they were deposited, regardless of differences in the sedimentation rate (Walling, et al., 2002; Zawadzki and Fierro, 2012).

In this study, the unsupported ^{210}Pb activities for the Falealupo core exhibit a decay profile with depth (Appendix 10.1), suggesting a likely constant rate of ^{210}Pb supply at this site. The unsupported ^{210}Pb activities at Ma'asina exhibit a step in the decay profile with depth (Appendix 10.2). This step in the decay profile likely suggests a change in sedimentation/deposition, thus implying that the sediments at the site all had the same initial unsupported ^{210}Pb concentration at the time they were deposited.

3.3.5.3 Ethno-archaeological proxies

Ethnohistorical and archaeological records in the literature (e.g. Stair, 1894; Davidson, 1979; Linnekin et al., 1995; Martinsson-Wallin, 2007), provide the opportunity to identify anomalous or enigmatic trends in the cultural chronology that may be associated with identified MIDs. These ethno-archaeological anomalies serve as event-markers to infer the likely hazard of associated MID-forming events identified in the geological record. Further, they facilitate an understanding of the long-term hazard context in which to interpret the possible extent of impacts concerning ethno-archaeologically related MID-forming events.

3.4 Results and Preliminary Interpretations

3.4.1 Stratigraphic logs

MIDs were detected empirically (calcareous yellow/grey sand) at Mulivai, Vaovai and Satitoa on the south coast of Upolu, at Falealupo and Lano on the west and northeast coasts of Savaii, respectively, and

at Ta'u village the northwest coast of Ta'u. Empirical stratigraphic logs for all of these sites are given in Appendix 4.

3.4.2 LOI and grain size results

A marked decrease in LOI (% organic material in the sediment) occurs in the 2009 SPT deposit analogue at Satitoa, immediately above the lower contact with the pre-event soil (Figure 16). LOI concentrations generally increase upwards to levels higher than those in the underlying soil.

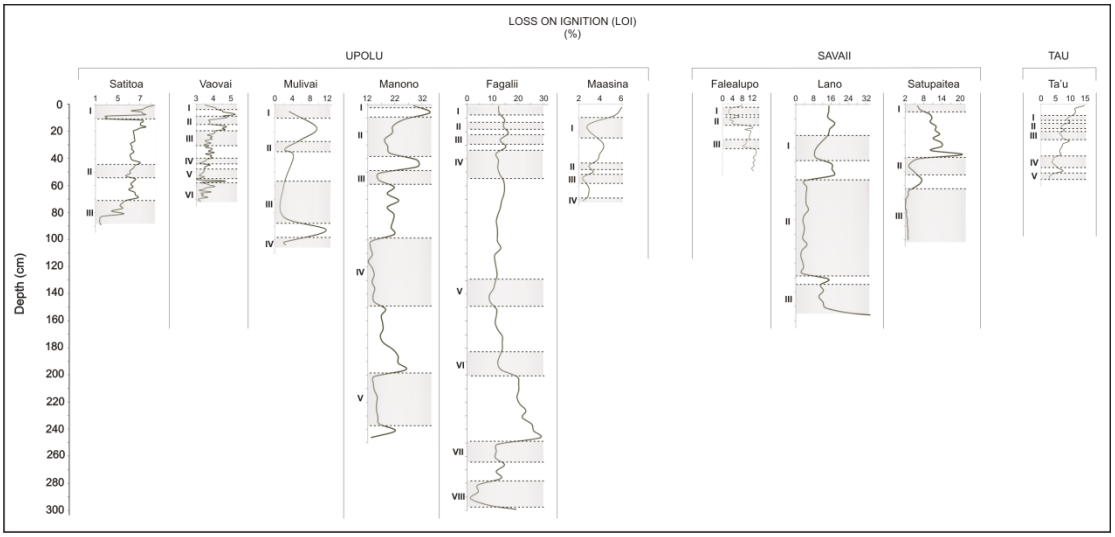

Figure 16: LOI results

In terms of grain size, the 2009 SPT deposit at Satitoa coarsens markedly relative to the pre-event soil, then fines upwards to a grain size similar to that of the pre-event soil (Figure 17).

These trends are similar to LOI and grain size characterisitics of tsunami deposits at this site studied by Chagué-Goff et al. (2011), in Japan (Chagué-Goff et al., 2012a), and in the Hawaiian Islands (Chagué-Goff et al., 2012b).

Thus, they provide a means for identifying similar LOI and grain size signatures within the stratigraphic records of all the investigated sites (Figures 16, 17, 18). In turn, they serve as proxies for identifying past MIDs of a likely similar nature to the 2009 SPT (i.e. MIDs formed due to geologically rapid deposition).

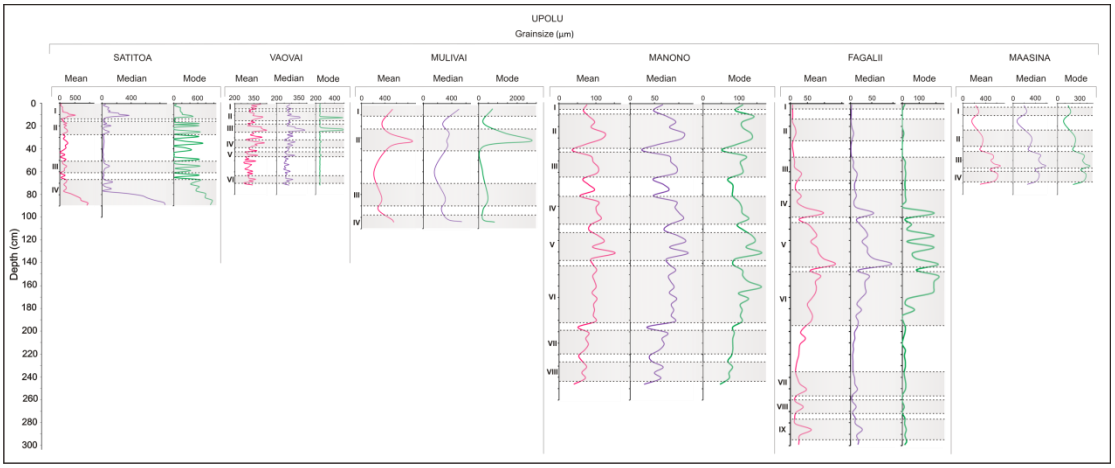

Figure 17: Grain size results for Upolu

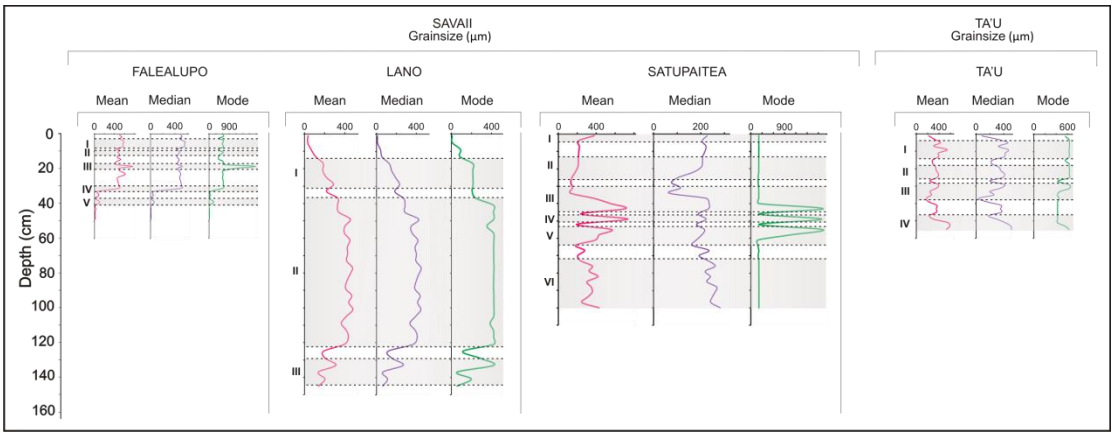

Figure 18: Grain size results for Savaii and Ta'u

3.4.3 pXRF Results

Figures 19 – 21 show the pXRF results for the investigated sites. Within the 2009 SPT deposit at Satitoa, the concentrations of the marine-derived elements calcium (Ca), strontium (Sr), and sulphur (S) increase markedly relative to the terrestrially-derived elements of iron (Fe), titanium (Ti), and manganese (Mn) immediately above the lower contact (Figure 19a). Ca/(Fe)(Ti)(Mn), ratios decrease markedly upwards, returning to pre-event levels at the surface.

These trends are consistent with similar tsunami deposit elemental trends provided by Chagué-Goff et al. (2010; 2011; 2012a; 2012b). The assumption for Fe, Ti and Mn being of terrestrial origin is supported by Ramirez-Herrera et al. (2012).

While deposits from the 2009 SPT were not empirically identified at other sites, the elemental ratio relationships for the 2009 SPT deposits at Satitoa, Vaovai and Mulivai, form a reference standard for interpreting similar relationships at other investigated sites. In Manono, weak Ca/(Fe)(Ti) and S/(Fe)(Ti) signatures are detected associated with the 2009 SPT deposit (Figure 19d).

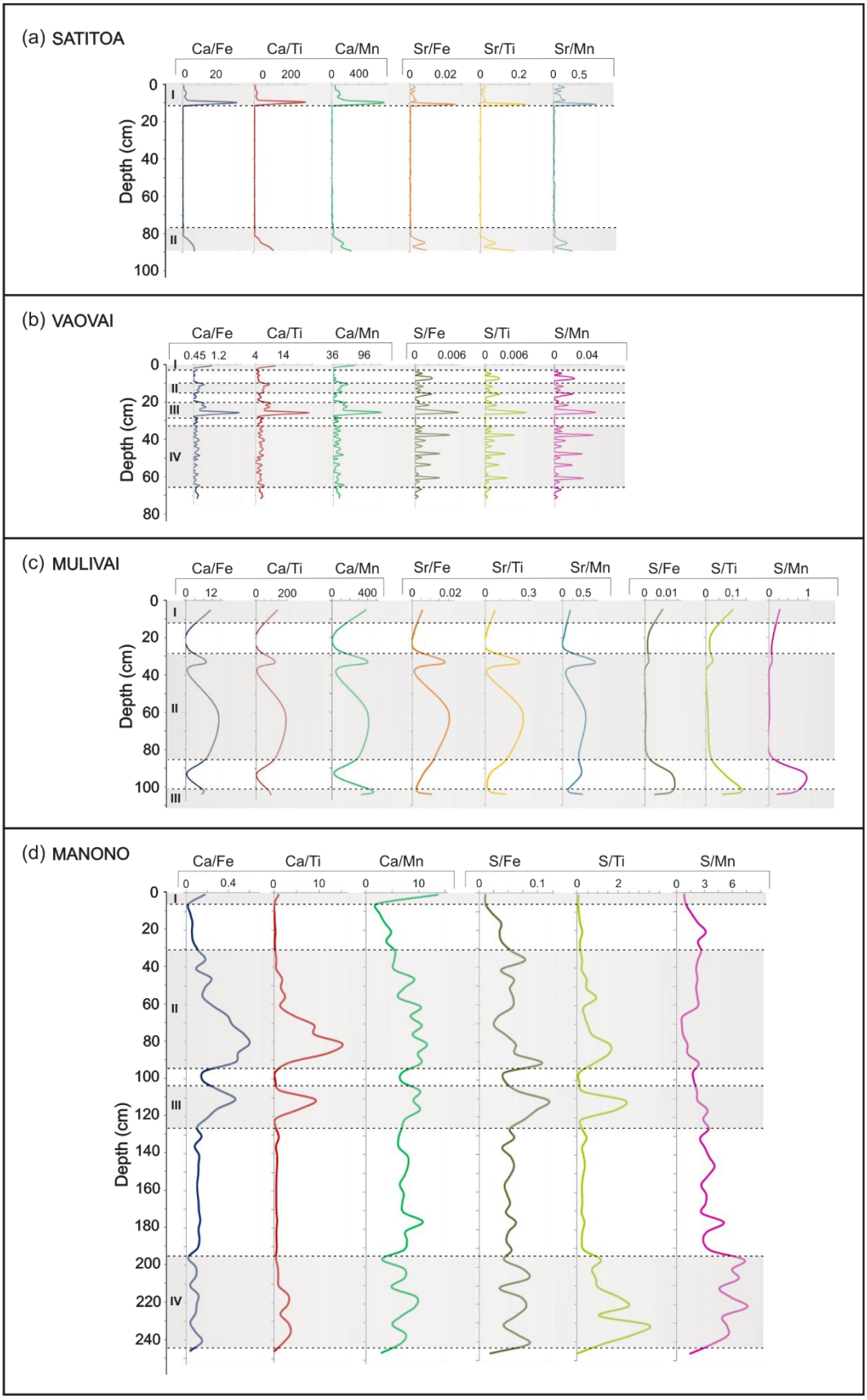

Figure 19: pXRF results for southern Upolu

The signatures detected at the Fagali'i site provide an example of inundations that do not leave an empirically recognizable MID in the landscape (Figure 20a). This further implies that while the presence of empirical deposits indicates MID deposition, their nonappearance does not mean MID absence.

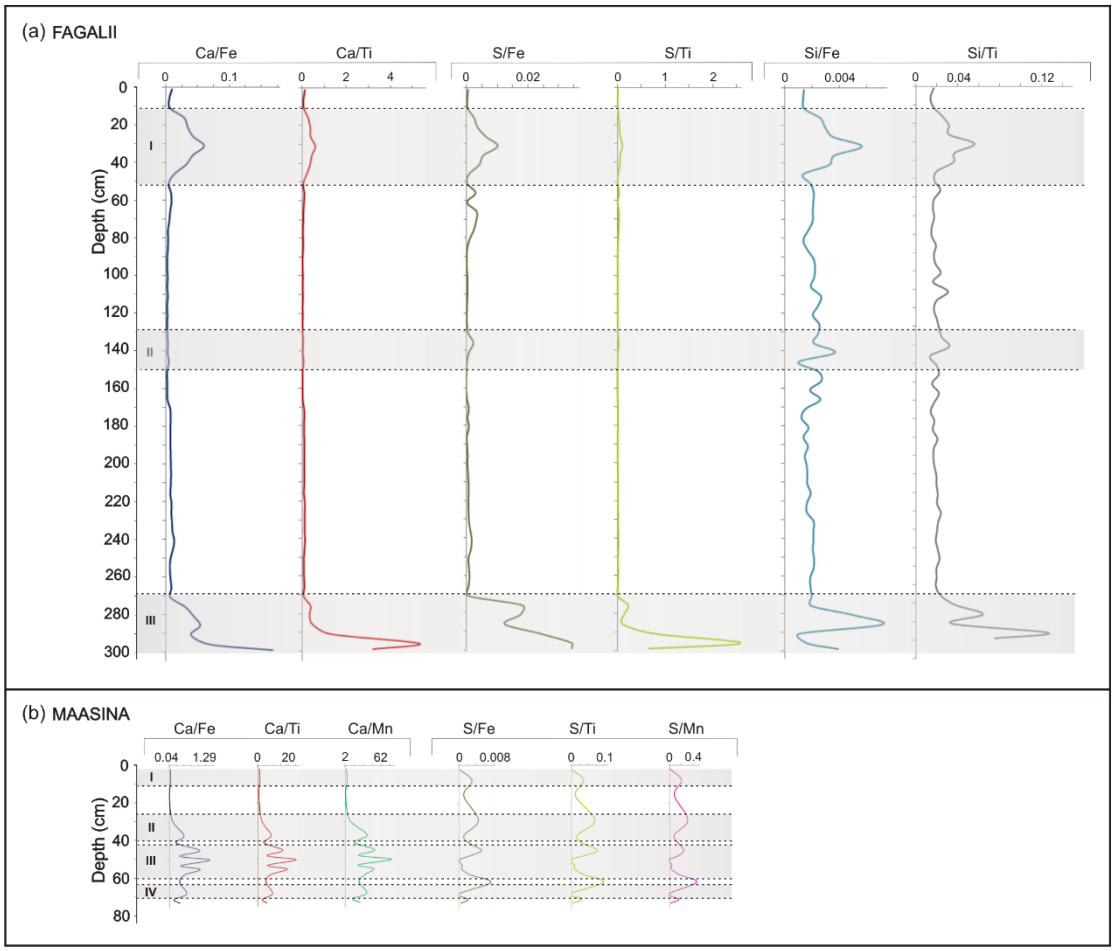

Figure 20: pXRF results for northern Upolu

In addition to Ca and/or Sr and S, the element silicon (Si) was detected at Fagali'i on north Upolu, and at sites on Savaii (Figures 21a – 21c). The Si/(Fe)(Ti)(Mn) ratios at these sites show similar patterns to either of the respective Ca, Sr and S ratios detected at these sites and others. This implies that Si at these sites is derived from an offshore source (Chagué-Goff, 2010; Chagué-Goff et al., 2011), and may also be used as a proxy for identifying rapid MID signatures. Further, it supports evidence that elemental signatures are source-dependent (e.g. Chagué-Goff, 2010).

In Ta'u, the element bromine (Br) was detected in addition to Ca, Sr, and S, and shows similarities with their ratio relationship patterns (Figure 21d). This suggests that Br ratio relationships also provide a proxy to identify MIDs, consistent with findings by Chagué-Goff et al. (2011) and Schlichting and Peterson (2006). The uppermost MID identified at this site does not record a Ca/(Fe)(Ti) signature,

indicating that the relative abundance of calcareous sand deposited by the event compared to the baseline depositional environment was limited.

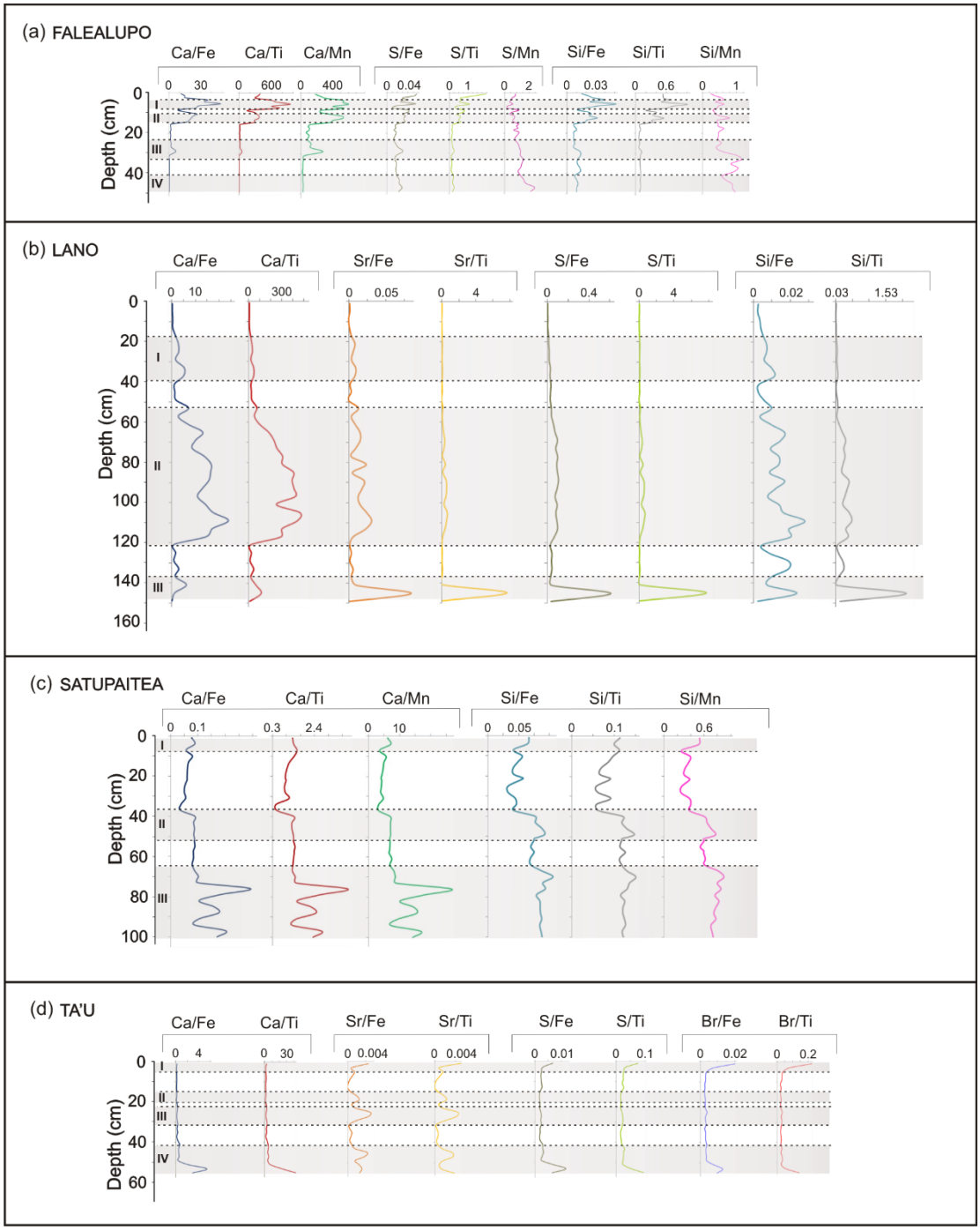

Figure 21: pXRF results for Savaii and Ta'u

In Falealupo, the elemental ratios for the uppermost two MIDs appear to differ in pattern from the 2009 SPT deposit at Satitoa (Figure 19a and 21a). Similar distinctions can be made within some of the profiles at other sites (e.g. Ma'asina) (Figure 20b). Additional to similar sedimentary contrasts discussed in

Section 3.4.2, this forms a provisional geochemical basis for starting to identify potential MIDs laid down by depositional processes different from the 2009 SPT analogue (Appendix 3.2).

3.4.4 ITRAX Results

The ITRAX results for Ma'asina, Manono and Lano show similar MID ratio relationships to the marine-derived elements identified via the pXRF analysis in Section 3.4.3 (Figure 21).

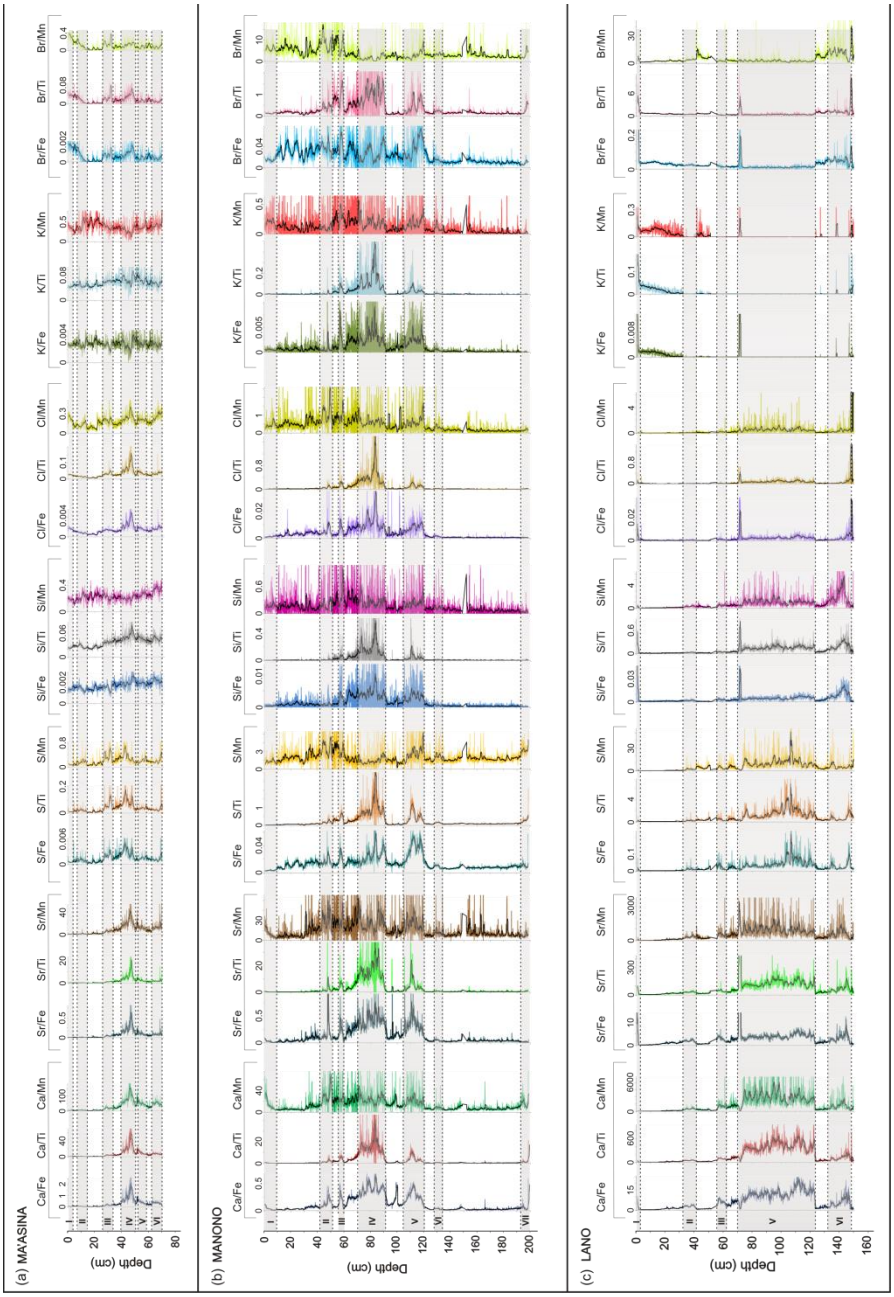

Figure 22: ITRAX elemental results for Ma'asina, Manono, and Lano sites.

In addition, the elements chlorine (Cl) and potassium (K) were also detected and have positive ratio relationships with other marine-derived elemental proxies in Figures 19 – 21. Signatures associated with the 2009 SPT are detected at the surface of each site.

The high resolution ITRAX results provide a means for recognizing differences between the signature patterns of identified MIDs within these site profiles, which were not so distinct in their corresponding pXRF characteristics. That is, distinct patterns similar to either the 2009 SPT analogue deposit at Satitoa or the uppermost two MID patterns at Falealupo can be recognized. This supports the hypothesis that the pattern differences result from differing depositional mechanisms (e.g. tsunami vs cyclone), although this cannot be substantiated without geochronological evidence from Falealupo. Such evidence enables the determination of the relative timing of sequences I and II at Falealupo (Figure 21a), providing an indication of their contemporaneity and likely association with MID-forming events in the historical record (e.g. historical tsunami or cyclones).

3.4.5 Radiocarbon Results

Radiocarbon results yielded using geochronological indicators from selected sites are given in Table 1. These data provide relative time markers to estimate the probable ages and association of identified MIDs in their respective site profiles, with MID-forming events in the historical record (Appendix 1; Section 3.4.7). They also enable an estimation of the likely timing of prehistoric events recorded in the site profiles they came from. Moreover, they provide constraints to assess the contemporaneity of individual MIDs between different sites. This enables the establishment of geological associations between MIDs at different locations that formed from the same event.

The stratigraphic profile at Satitoa yields the youngest age of 290 – 0 cal BP (i.e. AD 1660 – 1950). This date was obtained from a specimen sampled from the base of an organic soil layer directly overlying an MID. This site was located approximately 280 m inland of the present high tide water mark. Hence, a tsunami origin was assumed the most likely cause for this deposit as cyclone waves do not appear to have sufficient energy to inundate that far inland.

Appendix 3.2 provides preliminary descriptions and assumptions associated with most of the CRA ages for WK samples in Table 1.

Table 1: Radiocarbon data

Site	Laboratory No[1]	Depth (cm)	CRA[2] (^{14}C yr BP)	δ^{13}C ‰	68.2% CAR[3] (cal yr BP)	95.4% CAR[3] (cal yr BP)	Material[4]	Context[4]
Satitoa	WK30079	81	149 ± 93	-28.0 ± 0.2	290-0 (AD 1660-1950)	430-Modern (AD 1520-1950+)	Soil, Organics	Dark brown organic silty clay; sampled near the base contact.
	OZP119	82	740 ± 30	0.0	403-307 (AD 1547-1643)	445-279 (AD 1505-1671)	Shell	Unidentified shell in dark grey calcareous sand; sampled near the upper contact.
Vaovai	OZP117	23	720 ± 25	2.1 ± 0.3	382-291 (AD 1568-1659)	425-270 (AD 1525-1680)	Shell	Unidentified shell in light to dark yellow sand; sampled near the upper contact.
	WK30089	67	576 ± 33	3.1 ± 0.2	260-120 (AD 1690-1830)	280-Modern (AD 1670-1950+)	Shell	Unidentified gastropod in organic rich sand; ~8 cm from upper contact.
Mulivai	OZP114	23	Modern	-27.8 ± 0.1	Modern (1950+)	Modern (1950+)	Soil, Organics	Dark brown organic soil;~5 cm from base contact.
	OZP113	38	1125 ± 35	-25.9 ± 0.3	1050-933 (AD 900-1017)	1056-928 (AD 894-1022)	Soil, Organics	Thin olive brown soil layer sandwiched

								between calcareous sands.
	WK30084	93	528 ± 91	-25.1 ± 0.2	650-490 (AD 1300-1460)	680-320 (AD 1270-1630)	Peat	Dark brown fibrous peat; sampled from the centre of the layer.
Fagali'i[5]	Wk30087	287	3112 ± 50	-27.8 ± 0.2	3385-3265 (BC 1435-1315)	3444-3215 (BC 1494-1265)	Charcoal	Single charcoal piece ~5 cm a-axis in blackish peat; ~14 cm from upper contact.
Falealupo	WK30081	49	829 ± 28	-24.5 ± 0.2	765-690 (AD 1185-1260)	790-685 (AD 1160-1265)	Peat	Organic silty clay; sampled near the base of the core.
Lano	WK30083	139	798 ± 28	-27.8 ± 0.2	730-685 (AD 1220-1265)	765-670 (AD 1185-1280)	Plant fragments	Plant fragments in olive black silty sand; near the base contact.
	WK30082	149	1895 ± 42	-27.0 ± 0.2	1895-1740 (AD 55-210)	1930-1720 (AD 20-230)	Wood	Brown wood at the base of the core.
Ta'u	0ZP115	52	535 ± 30	-25.9 ± 0.1	534-509 (AD 1416-1441)	547-500 (AD 1403-1450)	Soil, Organics	Soil overlying visible underlying calcareous deposits.
Fale of le Fe'e[5]	WK30088	30	398 ± 73	-28.0 ± 0.2	520-320 (AD 1430-1630)	540-300 (AD 1410-1650)	Charcoal	Charcoal layer ~30cm from the surface.

1. Wk = University of Waikato, Radiocarbon Dating Laboratory (RDL); OZP = Australian Nuclear Science and Technology Organisation (ANSTO).
2. Conventional Radiocarbon Age (CRA) calculated as per Stuiver and Polach (1977).
3. Calibrated Age Range (CAR) – WK30087 age was calibrated at RDL using OxCal v.4.2.2 software © Bronk Ramsey (2013). All other WK ages were calibrated at RDL using OxCal v.4.1.7 software © Bronk Ramsey (2010) [initially developed in Bronk Ramsey (1995)]. OZP ages were calibrated in Calib 6.0 (Stuiver & Reimer 1993) using the SH Calibration dataset of McCormac et al. (2004) for sediment samples. Atmospheric and marine data for both WK and OZP samples were from Reimer et al. (2009). Ages reported in the text and Figures 22 – 25 are at 1σ to enable more robust assessment of contemporaneity.
4. Refer to Appendix 3 for descriptions of the respective core strata.
5. Samples WK30082 and WK30087 are taxonomically unidentified charcoal specimens. They could be subject to the effects of in-built age, meaning the true calendar age of the samples could be few hundred years younger (see Chapter 5.2).

3.4.6 ^{210}Pb Results

^{210}Pb ages yielded for Ma'asina and Falealupo are provided in Table 2. In Falealupo, an age of 1989 ± 5 was obtained for the soil layer separating MID sequences I and II in Figure 21a. An age of 1935 ± 9 was obtained for the soil layer separating MID sequences III and IV at this site. This indicates that the MIDs denoted by sequences I to III, and likely sequence IV, are historical, and provides a means to associate them with known MID-forming events which occurred within, or associated with, the age constraints yielded.

In Ma'asina, an age of 1957 ± 8 was obtained towards the base of MID sequence II at this site (Table 3) (Figure 20b). This indicates that sequence II was most likely formed due to a historical MID-forming event. Further, it provides a means for estimating the possible ages of other identified MIDs deeper in the Ma'asina geologic record via simple depth extrapolation. This, however, is limited by the assumption of a constant sediment type.

Nevertheless, the assumption is made here that the extrapolated depths are likely representations of the possible timing MIDs older in the geologic record. Comparison with the deposit contexts at other sites provides a means to infer potential associations.

3.4.7 Synthesized Proxy Data

MID proxy data presented in Sections 3.4.2 – 3.4.6 are synthesized in Figure 23 for south Upolu sites, Figure 24 for north Upolu sites, and Figure 25 for Savaii and Ta'u.

Cross-cutting relationships between likely MID signatures identified individually in the sedimentary and geochemical analysis provide a means to establish associations between the MID proxies at each site. This facilitates the refinement of respective site profiles from their associated empirical logs in Appendix 4.

The geochronological evidence obtained for each site provides a means to estimate the probable timing of identified MIDs within their respective stratigraphies. Moreover, they provide an avenue for associating the timing of identified MIDs with historical tsunamis or cyclones. For example, in Falealupo the ^{210}Pb ages obtained enable an association of MID sequences I and II with the 1990 (sequence II) and 1991 (sequence I) Cyclones Ofa and Val, respectively (Figure 25a). These data also enable an association between sequence III and the 1960 Great Chile Tsunami, as well as sequence IV and the 1917 Samoa Tsunami. Similar associations can be made for other sites in Figures 23c and 24b (e.g. Ma'asina, Mulivai).

Table 2 ^{210}Pb Radiochemistry data for Falealupo site cored in 2010

Site	ANSTO ID	Depth (cm)	Dry Bulk Density (g/cm^3)	Cumulative Dry Mass (g/cm^2)	Total ^{210}Pb (Bq/kg)	Supported ^{210}Pb (Bq/kg)	Unsupported ^{210}Pb (Bq/kg)[1]	Calculated CIC Ages (years)[2]	Calculated CRS Ages (years)[3]	CRS Model Mass Accumulation Rates (g/cm^2/year)
Falealupo	N574	0-1	0.98	0.5 ± 0.5	20.9 ± 0.8	0.4 ± 0.1	21.1 ± 0.9	1 ± 1	1 ± 1	0.52 ± 0.03
	N575	1-2	1.14	1.5 ± 0.5	21.1 ± 0.9	0.4 ± 0.1	21.3 ± 0.9	3 ± 1	3 ± 2	0.48 ± 0.03
	N576	2-3	0.78	2.5 ± 0.5	18.4 ± 0.7	0.3 ± 0.1	18.6 ± 0.8	5 ± 1	5 ± 2	0.52 ± 0.03
	N638	8-9	1.30	8.8 ± 0.5	15.4 ± 0.6	0.2 ± 0.1	15.8 ± 0.7	16 ± 3	19 ± 4	0.40 ± 0.03
	N577	9-10	1.03	9.9 ± 0.5	12.9 ± 0.6	0.4 ± 0.1	12.8 ± 0.6	18 ± 4	21 ± 5	0.45 ± 0.04
	N578	15-16	0.78	15.3 ± 0.5	13.9 ± 0.6	1.1 ± 0.1	13.2 ± 0.7	28 ± 6	36 ± 6	0.28 ± 0.03
	N639	18-19	0.60	17.4 ± 0.5	14.7 ± 0.6	2.9 ± 0.3	12.2 ± 0.7	32 ± 7	45 ± 7	0.23 ± 0.03
	N640	22-24	0.75	20.5 ± 0.9	11.8 ± 0.5	2.9 ± 0.3	9.2 ± 0.6	38 ± 8	59 ± 8	0.20 ± 0.03
	N579	28-30	0.59	24.5 ± 0.8	3.2 ± 0.2	0.0 ± 0.0	3.3 ± 0.2	45 ± 9	75 ± 9	0.32 ± 0.06

1. Decay corrected to 11 May 2011. Count date for N574, N575, N576, N577, N578 N579 = 17 May 2012. Count date for N638, N639, N640 = 11 July 2012.
2. CIC Model Mass Accumulation Rate = 0.54 ± 0.1 g/cm^2/y; r^2 = 0.775253.
3. CRS Ages for this site are reported in the text. All ages are reported at 2 sigma.

Table 3 ^{210}Pb Radiochemistry data for Ma'asina site cored in 2010

Site	ANSTO ID	Depth (cm)	Dry Bulk Density (g/cm^3)	Cumulative Dry Mass (g/cm^2)	Total ^{210}Pb (Bq/kg)	Supported ^{210}Pb (Bq/kg)	Unsupported ^{210}Pb (Bq/kg)[1]	Calculated CIC Ages (years)[2]	Calculated CRS Ages (years)	CRS Model Mass Accumulation Rates (g/cm^2/year)
Ma'asina	N580	0.0 – 1.5	1.20	0.9 ± 0.9	12.9 ± 0.6	3.1 ± 0.3	9.9 ± 0.7	3 ± 3	3 ± 1	0.32 ± 0.03
	N581	3.0 – 4.0	1.69	4.8 ± 0.7	10.6 ± 0.5	3.2 ± 0.3	7.4 ± 0.6	14 ± 3	16 ± 1	0.29 ± 0.04
	N583	6.0 – 7.5	2.16	11.1 ± 1.2	8.2 ± 0.4	3.1 ± 0.3	5.1 ± 0.5	33 ± 6	43 ± 4	0.18 ± 0.03
	N582	10.0 – 11.0	1.37	17.7 ± 0.8	4.8 ± 0.3	2.8 ± 0.3	2.0 ± 0.4	53 ± 8	86 ± 11	0.12 ± 0.04
	N585	16.0 – 17.5	1.93	28.0 ± 1.3	9.3 ± 0.5	3.7 ± 0.3	5.6 ± 0.6	No Result	No Result	No Result
	N584	20.0 – 22.0	1.64	35.6 ± 1.7	7.8 ± 0.4	2.8 ± 0.3	5.0 ± 0.5	No Result	No Result	No Result

1. Decay corrected to 11 May 2012. Count date = 17 May 2012.
2. CIC Model Mass Accumulation Rate = 0.334 ± 0.05 g/cm^2/y; r^2 = 0.9554. CIC Ages for this site are reported in the text. All ages are reported at 2 sigma.
3. Unsupported ^{210}Pb data from these samples were not included in the ^{210}Pb dating calculations.

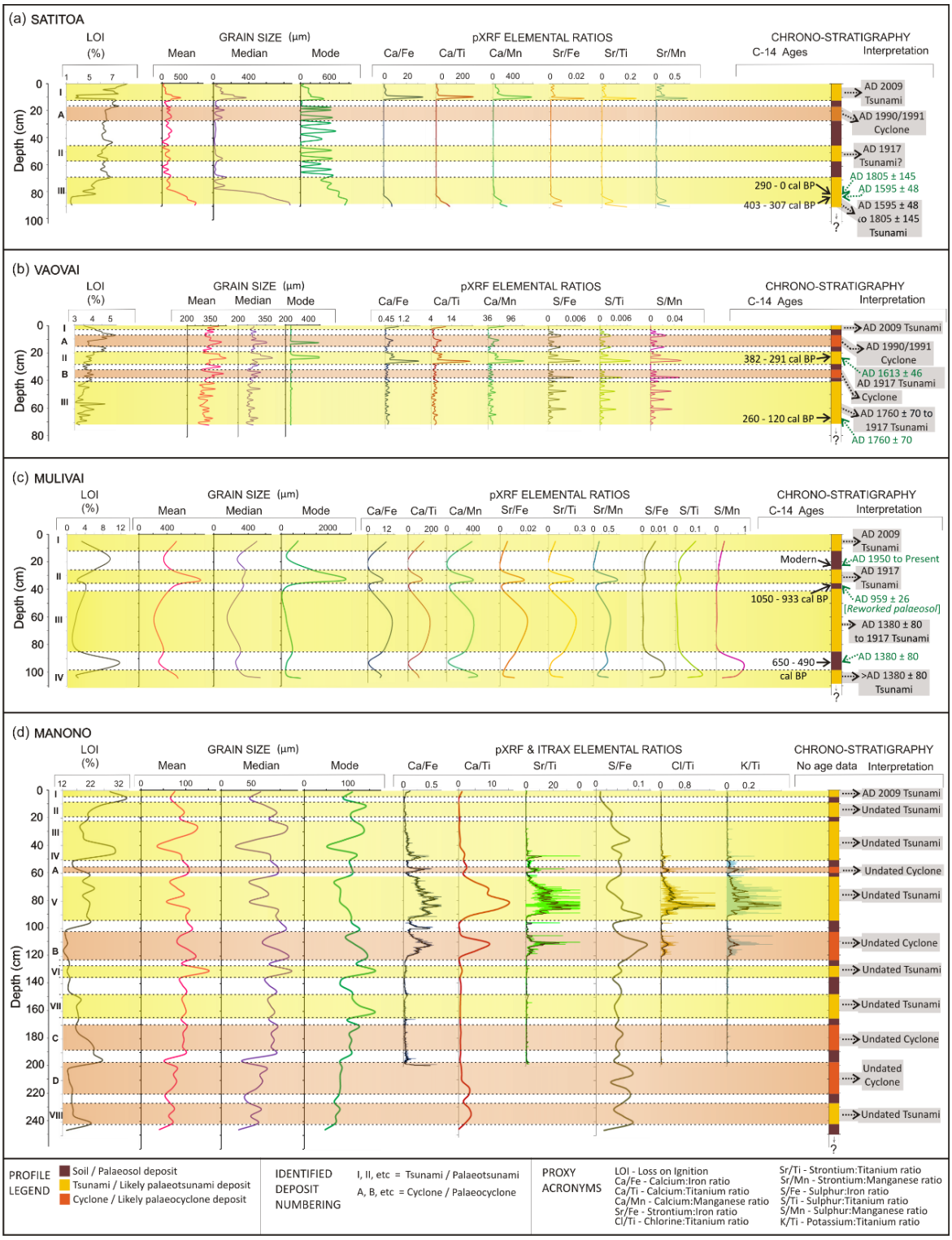

Figure 23: Synthesized proxy data for southern Upolu. Yellow shade indicates probable tsunami signatures and red shade indicates probable cyclone signatures.

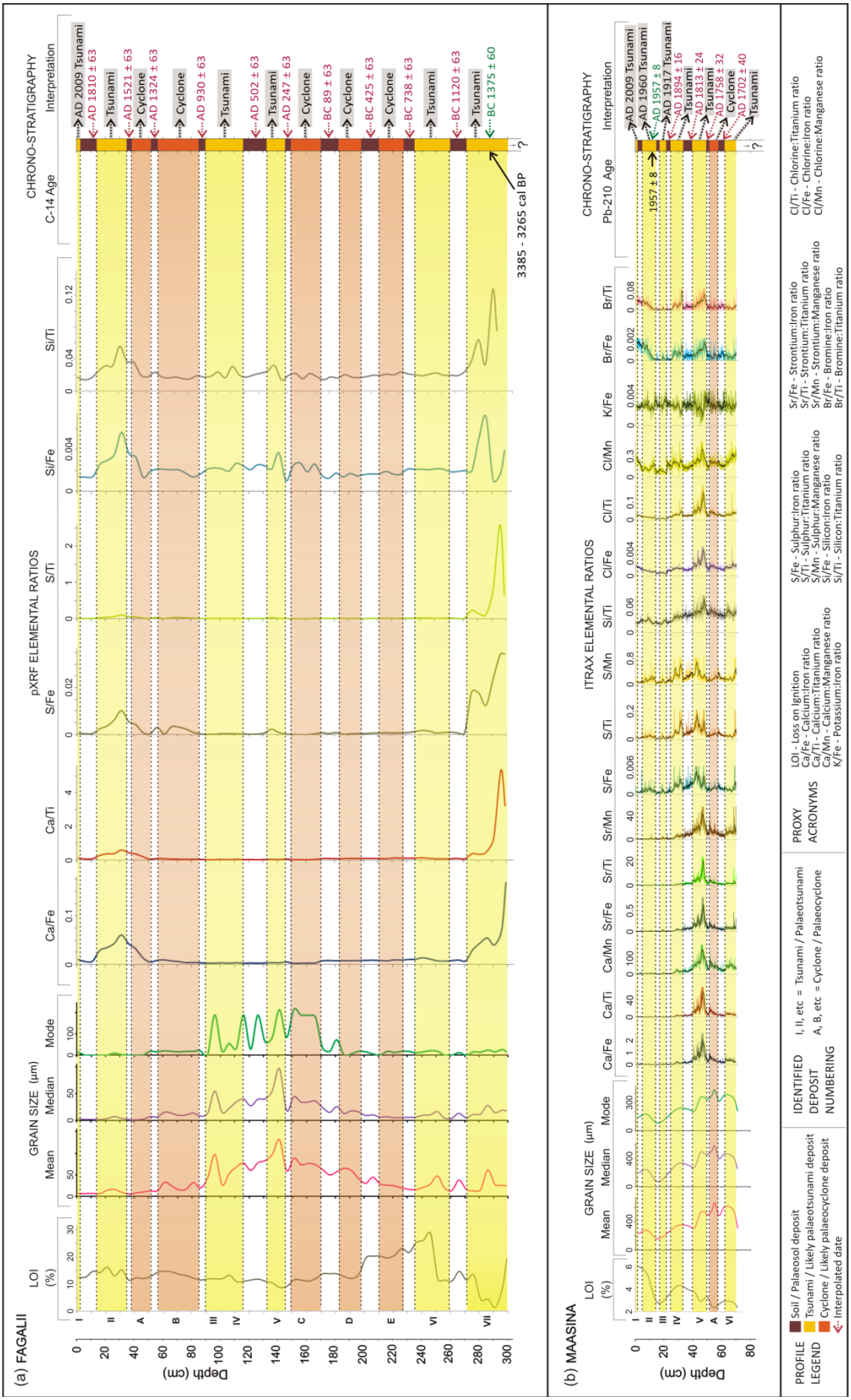

Figure 24: Synthesized proxy data for northern Upolu. Yellow shade indicates probable tsunami signatures and red shade indicates probable cyclone signatures.

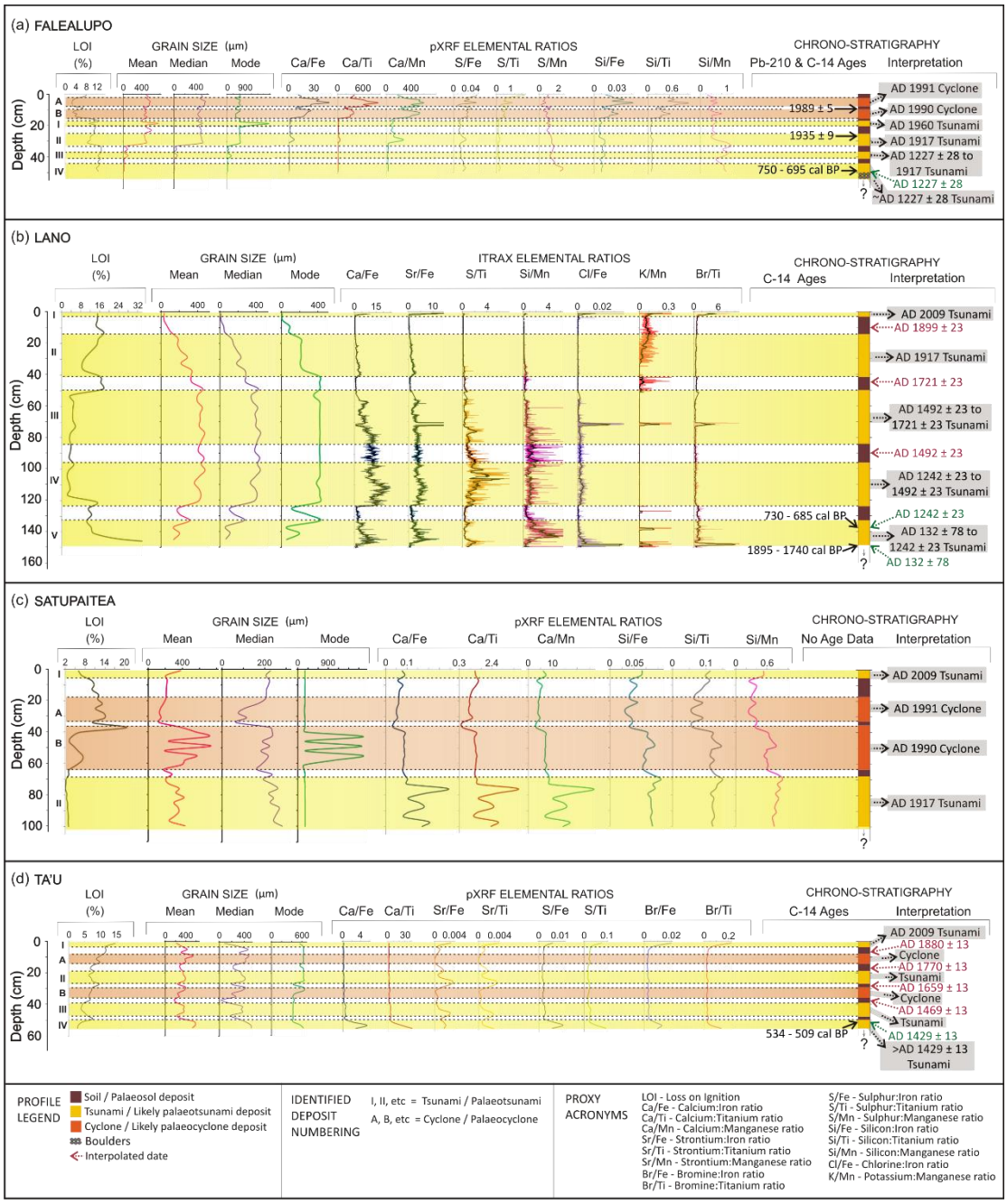

Figure 25: Synthesized proxy data for Savaii and Ta'u. Yellow shade indicates probable tsunami signatures and red shade indicates probable cyclone signatures.

Geochronological evidence presented also provides a control on assessing the pattern differences between the 2009 SPT analogue deposit at Satitoa, and the 1990/1991 Cyclone analogue deposits at Falealupo. The apparent differences in the proxy patterns between these analogues (see Sections 3.4.2 and 3.4.3), present a simple technique which can be used to determine whether identified MIDs at other sites are more likely tsunami or cyclone in origin. That is, if an MID identified at a particular site shows a similar signature pattern to the 2009 SPT analogue, then it was probably formed by a tsunami. The same

logic applies to MIDs showing similar signature patterns to the 1990/1991 Cyclone analogues. This technique was applied to determine the likely origin (i.e. tsunami or cyclone) of identified MIDs at each site (Figures 23 – 25).

Assessing the contemporaneity of determined MID origins using available geochronological data between the different sites, facilitates the establishment of associated MIDs which likely formed from the same event (Table 4) (Figure 26). This provides a means to understand the distribution of inundation locations (or impacts) associated with a single MID-forming event. Further, it enables the placement of the 2009 SPT within the context of the longer-term geological hazard for this region. In turn, this provides a relative control on interpreting the likely magnitudes of individual MID-forming events, as well as likely tsunami frequency associated with known, or inferred, tsunamigenic sources.

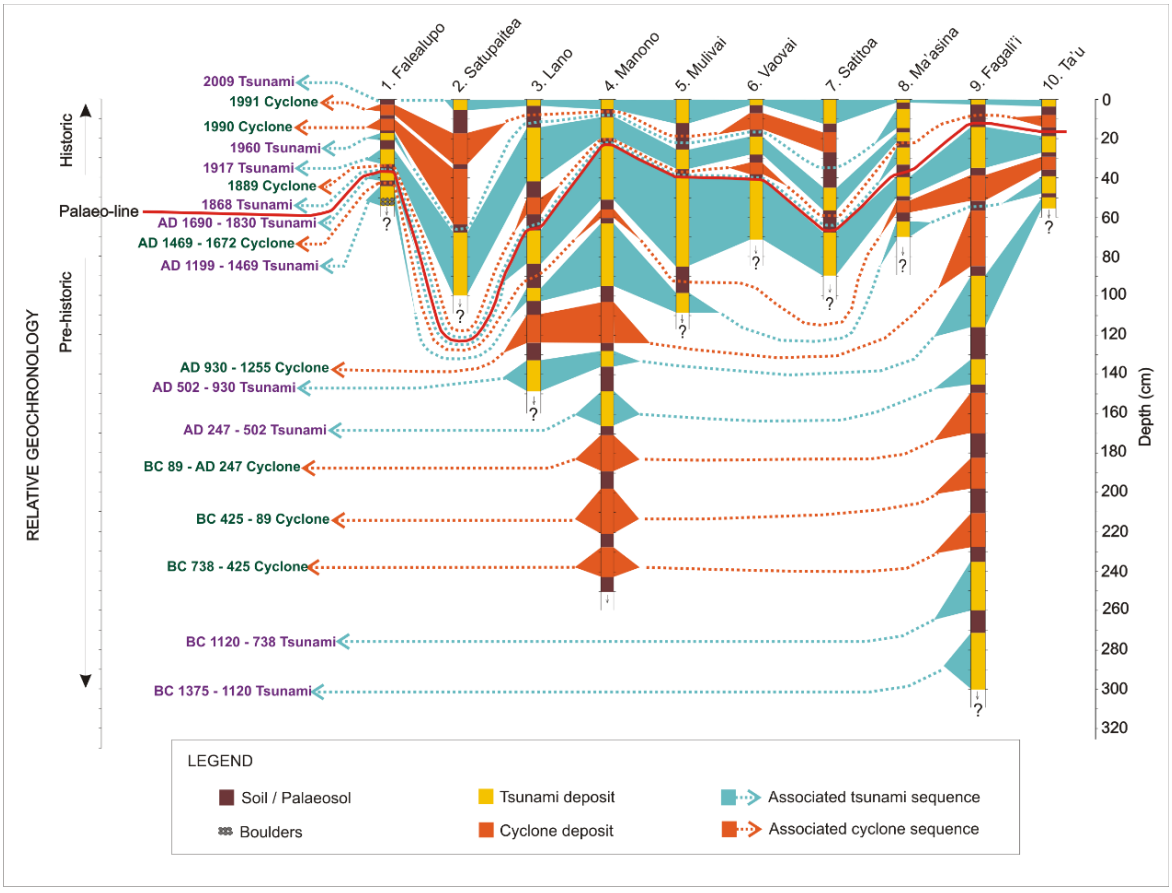

Figure 26: Tsunami and cyclone chronology in the geologic record. The Palaeo-line is an inferred isochron separating historical from prehistoric (palaeo) events.

Table 4: MID proxy associations (after Goff et al., 2012b).

MID	Falealupo	Satupiatea	Lano	Manono	Mulivai	Vaovai	Satitoa	Ma'asina	Fagali'i	Ta'u
2009 SPT		[✓;✖][✓;✖] [✓][✓;✖]	[✓][✓][✓] [✓;✖][✓] [✓][✓;✖]	[✓;✖][✓;✖] [✓;✖]	[✓;✖][✓;✖] [✓;✖][✓;✖]	[✓;✖][✓;✖] [✓;✖]	[✓][✓] [✓][✓]	[✓;✖][✓;✖]	[✓;✖][✓;✖]	[✓;✖][✓;✖] [✓;✖]
1991 Cyclone	[✓;✖][✓;✖] [✓;✖][✓;✖] [✓;✖]	[✓;✖][✓;✖]				[✓;✖][✓;✖] [✓;✖]	[✓;✖][✓;✖]			
1990 Cyclone	[✓;✖][✓;✖] [✓;✖][✓;✖] [✓;✖]	[✓;✖][✓;✖]								
1960 Tsunami	[✓][✓] [✓;✖][✓]							[✓;✖][✓][✓] [✓][✓;✖]		
1917 Tsunami	[✓][✓][✓] [✓][✓]	[✓][✓;✖]	[✓][✓][✓] [✓][✓] [✓;✖]	[✓][✓] [✓][✓]	[✓][✓][✓] [✓][✓]	[✓][✓] [✓][✓]	[✓][✓][✓]	[✓][✓][✓] [✓][✓]		
1889 Cyclone			[✓;✖][✓] [✓;✖][✓;✖] [✓;✖][✓;✖]			[✓;✖][✓]				[✓][✓;✖] [✓;✖]

1868 Tsunami							[✓][✓][✓] [✓][✓][✓][✓]	
AD 1690 – 1830 Tsunami	[✓][✓✓]	[✓][✓;✗][✓] [✓][✓][✓;✗]	[✓][✓][✓] [✓][✓]	[✓][✓] [✓][✓]	[✓]	[✓][✓] [✓][✓]	[✓][✓][✓] [✓][✓;✗] [✓][✓][✓]	[✓][✓] [✓][✓]
AD 1469 - 1672 Cyclone			[✓;✗][✓] [✓;✗][✓;✗] [✓;✗][✓;✗]				[✓][✓][✓;✗] [✓;✗][✓] [✓;✗] [✓;✗]	[✓;✗][✓] [✓;✗][✓;✗] [✓;✗]
AD 1199 - 1469 Tsunami	[✓][✓][✓]	[✓][✓][✓] [✓][✓][✓;✗] [✓;✗]	[✓][✓][✓] [✓][✓][✓]	[✓][✓] [✓][✓]			[✓;✗][✓][✓] [✓;✗][✓][✓]	
AD 930 - 1255 Cyclone		[✓;✗][✓][✓;✗] [✓;✗][✓;✗] [✓;✗][✓;✗]	[✓][✓;✗] [✓;✗][✓;✗] [✓;✗][✓;✗]					[✓][✓;✗] [✓;✗][✓;✗]
AD 502 - 930 Tsunami		[✓;✗][✓] [✓][✓][✓] [✓][✓]	[✓][✓][✓]					[✓;✗][✓]
AD 247 - 502 Tsunami			[✓;✗][✓] [✓]					[✓][✓][✓] [✓;✗] [✓]

BC 89 - AD 247 Cyclone	[✓;✖][✓;✖] [✓;✖]	[✓;✖][✓;✖] [✓;✖]
BC 425 - 89 Cyclone	[✓;✖][✓;✖] [✓][✓;✖]	[✓][✓;✖] [✓;✖]
BC 738 - 425 Cyclone	[✓;✖][✓;✖] [✓;✖][✓]	[✓;✖][✓;✖] [✓]
BC 1120 - 738 Tsunami		[✓][✓][✓;✖] [✓;✖][✓]
BC 1375 - 1120 Tsunami		[✓][✓][✓] [✓][✓]

LEGEND

TSUNAMI MID CRITERIA RELATIVE TO UNDER- AND OVER-LYING LAYERS

SEDIMENTOLOGICAL			GEOCHEMICAL		
LOI	Marked decrease relative to pre-event soil; Gradual increase to pre-event level	✓OR ✓;✖	Ca / (Fe)(Ti)(Mn)	Marked increase relative to pre-event soil; Marked decrease to pre-event level	✓OR ✓;✖

Grain size	Marked increase relative to pre-event soil; Upwards fining to pre-event level	✓OR ✓;×
Sr / (Fe)(Ti)(Mn)	Marked increase relative to pre-event soil; Marked decrease to pre-event level	✓OR ✓;×
S / (Fe)(Ti)(Mn)	Marked increase relative to pre-event soil; Marked decrease to pre-event level	✓OR ✓;×
Si / (Fe)(Ti)(Mn)	Marked increase relative to pre-event soil; Marked decrease to pre-event level	✓OR ✓;×
Br / (Fe)(Ti)(Mn)	Marked increase relative to pre-event soil; Marked decrease to pre-event level	✓OR ✓;×
Cl / (Fe)(Ti)(Mn)	Marked increase relative to pre-event soil; Marked decrease to pre-event level	✓OR ✓;×
K / (Fe)(Ti)(Mn)	Marked increase relative to pre-event soil; Gradual decrease to pre-event level	✓OR ✓;×

Note:
✓ = conditions are observed.
× = conditions are not observed.
Blank field = No data

3.5 Discussion and Interpretations

3.5.1 Satitoa 2009 SPT Analogue

The 2009 SPT unit at Satitoa provides the most comprehensive evidence of a complete, preserved, tsunami signature compared to other sites containing the 2009 SPT deposit. In turn, it can be used as the analogue for identifying similar MID signatures recorded in the geological record, and for inferring them to be of a tsunami origin.

Sediment characteristics of the 2009 SPT deposit collected at Satitoa area were also documented in Chagué-Goff et al. (2011). In addition to LOI, grain size and geochemistry which showed similar patterns to the trends presented here, Chagué-Goff et al. (2011) also presented the results of diatom and foraminifera analyses. Smaller benthic foraminifera taxa were concentrated in the finer grained upper part of the deposit, and larger taxa were concentrated in the coarser base of the deposit. Diatom assemblages showed a general upward transition from marine to brackish to mixed brackish-freshwater taxa. It was suggested that both foraminifera and diatom assemblage transitions reflected changes in flow conditions during the tsunami (Chagué-Goff et al. 2011).

The 2009 SPT deposits also formed the surface layers of the trench profiles at Vaovai and Mulivai, and its signature was noted at the surface of the core profiles at Ma'asina, Fagali'i, Manono, Satupaitea, Lano and Ta'u (Figure 23 – 25). The tsunami characteristics at these sites, however, are not as distinct as those at Satitoa and do not mimic the proxy trends at Satitoa. This possibly indicates; 1) non-complete, well-preserved, signature deposits, 2) geomorphic controls influencing deposition, and/or 3) coarse analytical data resolution compared to Satitoa. Nevertheless, similar MID trends to those observed at Satitoa exist within their profiles, forming a basis for interpreting their likely origin and association.

The criteria used here for determining an unidentified MID of tsunami origin using the proxy trends of the Satitoa 2009 SPT analogue are:

1. A marked decrease in LOI relative to the pre-event soil, then a gradual upwards increase to a level equivalent to the underlying pre-event soil.

2. A marked increase in grain size relative to the pre-event soil, then upwards fining to a grain size similar to that of the pre-event soil

3. A marked increase in the ratio compositions of the marine-derived elements Ca and Sr, relative to the terrestrially-derived elements of Fe, Ti, and Mn, at the contact with the pre-event soil. Ca and Sr decrease markedly upwards, returning to pre-event levels at the surface. The decrease in Ca and Sr is in relation to a marked increase in Fe, Ti, and Mn to pre-event levels.

4. Other elemental proxy criteria detected from other sites containing the 2009 SPT deposits, which show similar ratio trends to Ca and Sr at Satitoa, include S, Si, Br, Cl and K.

These proxies coupled with grain size and LOI can be applied to identify a tsunami origin for an MID based on signature pattern similarities with the Satitoa analogue.

3.5.2 Falealupo 1990/1991 Cyclone Analogues

Geochronological evidence in Falealupo enabled the identification of the 1990 and 1991 Cyclones Ofa and Val deposits at this coast (sequences I and II in Figure 25a). The apparent differences in the proxy trends for these sequences compared to the Satitoa 2009 SPT analogue provide a means to identify cyclone MIDs deeper in the geological record.

The criteria used here for determining an unidentified MID of cyclone origin using the proxy trends of the Falealupo 1990/1991 cyclone analogues are:

1. A gradual decrease in LOI relative to the pre-event soil, then a marked upwards increase to a level equivalent to the underlying pre-event soil.

2. A marked increase in grain size relative to the pre-event soil, then an upwards coarsening within the deposit, followed by a marked decrease to a grain size similar to that of pre-event conditions.

3. A marked increase in the ratio compositions of the marine-derived elements Ca, S, and Si, relative to the terrestrially-derived elements of Fe, Ti, and Mn, at the contact with the pre-event soil. Ca, S and Si ratios increase upwards within the deposit, before returning to pre-event levels at the surface.

4. Other elemental proxy criteria detected from sites containing MIDs which show similar ratio trends to the Falealupo 1990/1991 cyclone analogues (e.g. Lano, Manono, Ma'asina), and which are inferred to be cyclone in origin, include Br, Cl and K.

These proxies, coupled with grain size and LOI, can be applied to determine a cyclone origin for an MID based on signature pattern similarities with the Falealupo analogues.

3.5.3 Analogous deposit trends

In Satitoa, similar proxy characteristics to the 2009 SPT analogue were exhibited by a unit with an upper contact at 82 cm depth. The lower contact was beneath the base of the trench. The apparent lack of sedimentary evidence for recent cyclones at this site (e.g. 1990 Cyclone Ofa and 1991 Cyclone Val) that are known to have affected this coast (Ready & Woodcock 1992; Elmqvist et al. 1994), suggest the MID

might be of a tsunami origin. Radiocarbon dating of a sample (WK30079) taken from the overlying soil layer at 81 cm depth yielded an age of 0-290 cal BP [(68.2 % prob.) (AD 1805 ± 145)]. The ^{14}C age of an unidentified shell sample (OZP119) associated with the proposed tsunami deposit at ~82 cm depth, yielded an age of 307-403 cal BP [(68 % prob.) (AD 1595 ± 48)]. This implies that the maximum age of the likely tsunami which formed the deposit occurred between AD 1595 ± 48 to AD 1805 ± 145.

Geochronological data also enable the identification of the probable 1917 tsunami deposit at Falealupo. The overall elemental signature of this MID is weak and provides no pattern distinguishable from the upper identified cyclone deposits at this site, or the 2009 SPT analogue at Satitoa. The grain size and LOI proxy signatures for this MID, however, do resemble grain size and LOI trends of the Satitoa 2009 SPT analogue. These trends coupled with the geochronological evidence support the assumption that this MID is associated with the 1917 tsunami.

In Ma'asina on northwestern Upolu, the S, Si and Br proxy ratios, as well as grain size and LOI, show a MID signature (sequence II in Figure 19b) which is depth-associated with the yielded ^{210}Pb age of 1957 ± 8 (Figure 24b). It is likely that this signature could be associated with the 1960 Chile Tsunami which is known to have impacted this site (Pararas-Carayannis & Dong 1980). The absence of a Ca proxy signature for this MID likely indicates that the energy of this tsunami was insufficient to transport and/or deposit marine calcareous sediment at this location. Alternatively, it could also suggest that Ca was not preserved.

The signature trends associated with MID sequences A and B at Satupaitea (Figure 21c) and sequences A and B at Vaovai (Figure 19b), are closer in similarity to the Falealupo 1990/1991 cyclone analogues, suggesting they are more likely of a cyclone origin.

In general, the subtle differences between the signature trends for the cyclone MIDs at Falealupo compared to those of the 2009 SPT at Satitoa enable distinctions to be made between cyclone and tsunami MIDs in the Samoan geologic record. The pattern differences between the Satitoa and Falealupo analogues likely reflect the differing nature of depositional processes in a tsunami as opposed to a cyclone.

The detection of silica (Si) within the profiles at Fagali'i, Ma'asina and Manono on Upolu, and Falealupo and Lano on Savaii, suggest a slight difference regarding the chemical composition of sediment source at these sites.

3.5.4 Tsunami and Cyclone Deposit Chronology

The MID proxy results coupled with geomorphic and palaeo-environmental understanding indicate the existence of likely palaeotsunami and palaeocyclone deposits at all of the investigated sites. Further, the apparent differences in MID proxy trends between the Satitoa 2009 SPT and Falealupo 1990/1991

analogues permit the identification of the likely origin of MIDs deeper in the geologic record. This underlying distinction enables stratigraphic correlation of sites that have MIDs with unknown ages, to sites with chronologically dated MIDs (e.g. Manono and Satupaitea) (Figure 23d and 25c).

In Figure 26, the inferred palaeo-line is an inferred isochron that indicates the likely boundary between historic and prehistoric (palaeo) MIDs in the geologic record. The 2009 SPT deposits forms the surface layer at most sites. It is important to note that the model in Figure 26 is based on core and trench samples collected in 2010, and may not necessarily reflect the present-day surface MID in the geological record. That is, deposits associated with Cyclone Evan that recently impacted the Samoan Islands in December 2012, which were not investigated in this study, may have left signatures in the landscape. This could result in the 2012 Cyclone forming the surface MID at deposited sites. The model shown represents the tsunami and cyclone chronology as recorded in the landscape in 2010.

3.5.4.1 1991 Cyclone MIDs

In addition to Falealupo, available geochronological indicators coupled with the proxy trends suggest that the 1991 Cyclone Val deposits were also preserved at Vaovai and Satitoa (Figure 23a and b). The signature for this deposit at Satitoa is inferred based on the LOI and grain size proxies. However, the trends are not apparent using the geochemical proxies. This might suggest that wave energy during inundation was insufficient to transport and deposit marine-derived sediment at this location. Further, the appearance of a signature for this MID using only the LOI and grain size proxies may suggest that other processes (e.g. intense rainfall and subsequent flooding), may have been the dominant control during formation of this MID at Satitoa.

In Satupaitea, the MID identified for this event is inferred based on its proxy trends coupled with its likely stratigraphic correlation with the associated MIDs at Falealupo, Vaovai and Satitoa.

3.5.4.2 1990 Cyclone MIDs

Satupaitea appears to be the only site other than Falealupo to contain the 1990 Cyclone Ofa MID. The proxy trends for this MID at Satupaitea and its stratigraphic correlation with the timing of the MID at Falealupo suggest that it was formed from the same event. The absence of age data from Satupaitea prohibits a definite association with this MID at Falealupo. However, the interpretation that the two are associated is logical based on the proxy and likely associated stratigraphic criteria used.

3.5.4.3 1960 Tsunami MID

Both geochronological and proxy indicators suggest that an MID signature associated with the 1960 Chile Tsunami was preserved at Ma'asina and Falealupo. This observation is likely corroborated by the associated tsunami inundation heights of 2.4 m in the Ma'asina area, and between 1.5 – 2.7 m in the Falealupo area reported in Pararas-Carayannis and Dong (1980).

3.5.4.4 1917 Tsunami MID

Geochronological, proxy and stratigraphic correlative indicators suggest the preservation of MIDs associated with this tsunami at all of the sites except Fagali'i and Ta'u. Locations that appear to contain MID signatures for this event correlate with the source location of this tsunami relative to the 2009 SPT source (see Beavan et al., 2010; Lay et al., 2010; Okal et al., 2011). Further, it is possible that Fagali'i and Ta'u sites experienced wave activity associated with this event. However, wave activity at these locations was likely insufficient to leave a distinct signature in the landscape due to the main tsunami energy beam directed toward west Savai'i (Okal et al., 2011).

3.5.4.5 1889 Cyclone MID

This event was the deadliest cyclone experienced in Samoa's historical record (Fairburn, 1997) due to socioeconomic circumstances in Apia during this period (e.g. presence of UK, USA, and German naval and merchant ships docked in the Apia harbor). The casualties suffered in this cyclone were predominantly seamen on-board these ships at the time of the event.

Geochronological estimates and proxy trends at Ta'u, Vaovai and Lano suggest that MIDs associated with this cyclone likely formed at these locations. The absence of associated MIDs at other locations suggests that MID formation was not favoured at those sites, perhaps due to geomorphic and other characteristics of the cyclone constraining deposition.

3.5.4.6 1868 Tsunami MID

Geochronological and stratigraphic evidence suggests that this MID formed from a tsunami that occurred between 1830 and the identified 1889 cyclone MID. Pararas-Carayannis and Dong (1980) report four possible tsunamis during this period which could have formed this MID, detected only at Ma'asina. The 1837, 1868 and 1877 tsunamis associated with earthquakes along the Chile/Peru subduction source, respectively, and the 1883 supposedly local tsunami are all likely candidates. However, details of the 1883 event are ambiguous.

The 1883 event manifested from an earthquake which was apparently accompanied by a storm on March 24. The earthquake supposedly generated a tsunami and all houses within a quarter of a mile of the beach on the east end of Savaii were swept away over a distance of 24 km along the shore (Pararas-Carayannis and Dong, 1980). It was suggested that this may have been a locally generated tsunami. While the description of impacts on the east end of Savaii suggests a local tsunami wave, evidence of this at other sites in the historical record is scant, with no dated MIDs overlapping with the likely timing of this event at Ma'asina. It is possible that the impacts reported may have been associated with the storm and a related surge that may have occurred.

Interestingly, the description of the 1883 event in Pararas-Carayannis and Dong (1980) could imply that the MID at Vaovai interpreted to be associated with the 1889 cyclone, could in fact be associated with

this event. Similarly the tsunami MID identified below this event at Vaovai may in fact represent several inundations at this site as opposed to the single inundation presented in Figure 26, and that a signature for this event may exist at this site.

Present interpretation of the proxy data, however, would suggest that it is not. Further analysis at Vaovai including geochronological evidence would be needed to substantiate any associations of the possible 1883 coupled tsunami and storm event. The absence of any apparent chrono-stratigraphic sequences associated with this possible event based on available data serve as grounds to presently dismiss it as being a potential candidate for the origin of this MID at Ma'asina.

Thus, the 1837, 1868, or 1877 far-field Chile/Peru tsunamis provide alternative sources for this MID. Of these, the most plausible is the 1868 tsunami. This is based on descriptions of all three events in Pararas-Carayannis and Dong (1980), in which the 1868 tsunami is said to have destroyed settlements in Apia on north Upolu. Coupled with the understanding that Ma'asina has the tendency to preserve deposits originating from far-field tsunami sources (e.g. 1960 tsunami MID in Section 3.5.4.3), it is likely that this MID is associated with the 1868 tsunami.

3.5.4.7 AD 1690 – 1830 Tsunami MID

The timing of the AD 1690 – 1830 tsunami was inferred based on the likely geochronological deposit associations between Satitoa, Vaovai and Mulivai sites. The deposit correlations at Lano, Ma'asina and Fagali'i sites associated with this event were estimated based on the reference established ages within their profiles. Their geological depth correlation with the event deposits at Satitoa, Vaovai and Mulivai was also used to infer their possible association. In Manono and Satupaitea, the deposit associations were inferred based on their geological depth correlations with the established and inferred deposits of this event at other sites.

This tsunami was inferred based on the age of the shell sample Wk30089 which was found towards the base of the deposit associated with this event at Vaovai. The sample is assumed to be the most representative of the likely timing of the event because of; 1) its stratigraphic position within the deposit, 2) its younger age relative to other geochronological indicators for this event at other sites, and 3) its correlation with the age of the palaeosol overlying the associated event deposit at Satitoa.

It is possible that this event is associated with a local oral tradition at Lano (Appendix 4), in which calcareous boulders are believed to have been deposited several hundred metres inland due to a significant inundation.

3.5.4.8 AD 1469 – 1672 Cyclone MID

Geochronological and proxy trend associations for this cyclone MID identified at Ta'u, Ma'asina, Fagali'i and Lano coupled with their MID stratigraphic locations relative to other sequences in the broader

geologic record, suggests they are correlated. The timing of this event was deduced based on the contemporaneity of chronological age estimates inferred for this MID at these sites. The stratigraphic correlation of this event with the identified cyclone MID at Manono suggests they are associated. Further, the timing of this event overlaps with the AD 1300 event; a transitional climatic period between the Little Climatic Optimum (LCO: AD 750 – 1300) and the Little Ice Age (LIA: AD 1300 – 1800) (Nunn and Britton, 2001). This period is characterized by increased ENSO as well as tropical cyclone frequency and/or intensity.

3.5.4.9 AD 1199 – 1469 Tsunami MID

The AD 1199 – 1469 tsunami was determined based on the geochronological and proxy trend correlations for associated MID deposits at Falealupo, Lano, Mulivai, and Ta'u. In Falealupo, the existence of boulders (>20 cm in diameter) at the base of this MID points towards a high-energy wave inundation at this site. Stratigraphic correlation of this event with an associated MID at Manono provides a plausible connection of the event at this site. This event compares well with the timing of the AD 1450 Tonga-Kermadec-Trench tsunami in Goff et al. (2010; 2012). The distribution extent of this tsunami in Goff et al. (2012), coupled with the likelihood of a near-field event in the Samoan region, suggest a possible NTSA source.

3.5.4.10 AD 930 – 1255 Cyclone MID

Associated cyclone MID signatures at Fagali'i and Manono, coupled with chronological age inference at Fagali'i provide an estimate of the timing of this event. The slight overlap in the timing of this cyclone with the AD 1199 – 1469 tsunami suggests that it occurred either before AD 1199, or that the tsunami occurred after AD 1255. Nevertheless, the timing of this event possibly suggests a correlation with climatic extremes associated with the LCO to LIA transition in Nunn and Britton (2001).

3.5.4.11 AD 502 – 930 Tsunami MID

The stratigraphic correlation of tsunami MID signatures at Ta'u, Fagali'i, Manono, and Lano suggest they are associated with the same event. Geochronological data at Lano as well as inferred age estimates for associated MIDs at Fagali'i and Ta'u, coupled with stratigraphic correlations provide an indication on the timing of this event.

3.5.4.12 AD 247 – 502 Tsunami MID

The AD 247 – 502 Tsunami was inferred based on the likely stratigraphic correlations and proxy associations between Fagali'i and Manono. The age estimate provided for this event was determined through interpolative inference of its likely timing at Fagali'i (Figure 24a).

3.5.4.13 BC 89 – 247 Cyclone MID

This event was determined via the correlative stratigraphic and proxy associations at Fagali'i and Manono. The timing for this event was estimated through chronological interpolation of sample WK30087 at Fagali'i.

3.5.4.14 BC 425 – 89 Cyclone MID

Similarly, the inference of this cyclone was determined via correlative MID associations between Fagali'i and Manono.

3.5.4.15 BC 738 – 425 Cyclone MID

Similar associations as in Sections 3.5.4.14 and 3.5.4.15 above were used to infer this event.

3.5.4.16 BC 1120 – 738 Tsunami MID

This tsunami MID was identified at Fagali'i based on its tsunami proxy associations. The likely event timing was estimated based on interpolation of sample WK30087.

3.5.4.17 BC 1375 – 1120 Tsunami MID

The BC 1375 to 1120 tsunami was interpreted based on the age of 3385 to 3265 cal BP for charcoal sample WK30087 from Fagali'i, which was found in association with the identified MID. A more detailed assessment of this particular event is provided in Chapter 5, Section 5.4.

The tsunami MIDs are summarized in Table 5.

3.5.5 Tsunami Magnitude, Intensity and Frequency

The tsunami and cyclone chronology presented here provides a basis for estimating the likely frequency of tsunamis similar to, or greater in magnitude than the 2009 SPT. This tsunami had an intensity of [$XI_{IT\ IS-2012,}$ Devastating], according to the tsunami intensity scale developed in Lekkas et al. (2012; 2013). The formation of a distinct signature associated with this event in the geologic record justifies the assumption that similar distinct signatures would have formed due to comparable, perhaps local, events. Further, the thickness of the initial spike (trough-peak-trough) noted in the signature for this event at Satitoa possibly corresponds with the approximate 9 minute wave period and subsequent inundation of this tsunami (Figure 27).

These conditions provide a basis to estimate the intensity of analogous MIDs deeper in the geologic record (e.g. Luque et al., 2001). That is, MID signatures with a thicker initial signature spike would likely have formed from a tsunami with a longer wave period than the 2009 SPT. Assuming a similar NTSA source to the 2009 SPT would suggest a larger rupture at the source area, and corresponding greater earthquake and tsunami magnitudes. Similarly, MID signatures with a thinner initial signature spike would likely correspond to shorter tsunami periods and associated smaller source parameters.

Using the example in Figure 27 as a base analogy, coupled with the assumption that stratigraphically associated MIDs found in more than a few locations are associated with a local NTSA sourced tsunami, it becomes possible to estimate the likely intensity of identified MIDs using their proxy signature curves in Section 3.4.7. For example, applying the correlations at Satitoa yields a likely 8 min tsunami wave period estimate for the 1917 tsunami signature at this site. This is in good agreement with the modeled results for this event in Okal et al. (2011), and would suggest a slightly lower tsunami intensity than the 2009 SPT. Similarly, these correlations yield an approximate 14 min wave period associated with the 1960 MID at Ma'asina, which is in agreement with the periods of 8 – 20 min for this event observed in Apia (Keys, 1960). This longer period would correspond to a greater tsunami intensity at the source; in this case the Mw 9.5 earthquake and subsequent far-field tsunami.

This understanding provides a means to estimate the tsunami frequency associated with a particular source. If the assumption is made that stratigraphically associated MIDs occurring at more than several locations are due to a local, likely NTSA, source, then it becomes possible to estimate the likely magnitude and frequency of likely NTSA associated tsunami from the geologic record. For example, the magnitude of the AD 1690 – 1830 and AD 1199 – 1469 tsunamis can be estimated and assumed to be local NTSA sourced events. Both of these events would have slightly larger wave period estimates compared to the 2009 SPT using the correlation in Figure 27. This suggests slightly larger magnitude and perhaps intensity events, respectively.

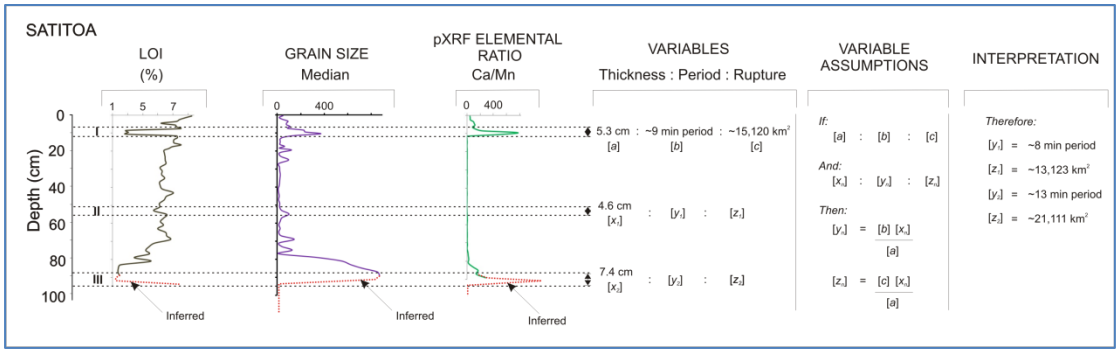

Figure 27: Relationship between the Satitoa 2009 SPT deposit thickness, mean wave period, and source rupture.

These assumptions enable a conservative baseline tsunami recurrence interval estimate of 87 – 637 years for NTSA sourced tsunami of comparable or greater magnitude to the 2009 SPT (Table 5). Similar applications could be used to estimate the likely frequency of climatic periods associated with likely intense cyclones as recorded in the geologic record.

Table 5: Age data used for frequency estimation of NTSA associated tsunami.

Millennium	Tsunami Age (Known or Inferred)	Uncertainty Distribution		Lag Interval (years)[1]	Uncertainty Lag (years)		Uncertainty Lag Range (years)[4]
		Maximum	Minimum		Maximum[2]	Minimum[3]	
3rd AD	2009	na	na				
				92	na	na	na
2nd AD	1917	na	na				
				157	227	87	140
	1760	1690	1830				
				426	631	221	410
	1334	1199	1469				
				618	967	269	698
1st AD	716	502	930				
				341	683	0	683
	375	247	502				
				1304	1622	985	637
1st BC	929	1120	738				
				319	637	0	637
2nd BC	1248	1375	1120				
			MEAN	465	795	260	534
			MEDIAN	341	660	154	506
			MEAN (Excluding Outlier)	326	629	115	514
			MEDIAN (Excluding Outlier)[5]	**330**	**637**	**87**	**550**

1. Interval from the time of last known or inferred NTSA associated tsunami occurrence.
2. Difference between minimum uncertainty, and the maximum uncertainty of last occurrence.
3. Difference between maximum uncertainty, and the minimum uncertainty of last occurrence.
4. Difference between the maximum and minimum uncertainty lag.
5. Median recurrence interval (excluding the lag outlier between 1st BC and 1st AD) is quoted in the text.

3.5.6 Ethno-archaeological Associations and Hazard Implications

The 2009 SPT not only provides the opportunity to understand tsunami signatures in the Samoan Islands, it also offers a modern analogue of the hazard associated with prehistoric events of similar and greater magnitudes. For example, families in vulnerable areas impacted by the 2009 SPT were displaced, and for the case of Saleapaga village on the southeast Upolu coast, around 90% of the entire village was abandoned in favour of the safety offered inland (F. Nelson, pers. comm., 2014). This was largely due to associated property destruction as well as the uncertainty of subsequent tsunami impacting in the immediate future. Almost five years after the 2009 SPT, many families have resettled their temporarily abandoned coastal properties. However, more than 70% of the original pre-2009 SPT inhabitants of Saleapaga remain inland (F. Nelson, pers. comm., 2014).

Interestingly, similar abandonments have been recorded in the archaeological record (e.g. Davidson, 1979). Further, the timing of some of the interpreted abandonments in investigated locations (e.g.

Davidson, 1979), appear to coincide with the timing of associated MIDs identified herein. For example, archaeological findings at Mulifanua on west Upolu led to the suggestion that settlements in the area are thought to have been abandoned in 18-C (AD 1700s). This corresponds to the AD 1690 – 1830 tsunami identified in these islands. Further, the existence of MIDs most likely associated with this event at all of the investigated sites (except Satupaitea), suggest that this tsunami may have been more intense than the 2009 SPT. The absence of evidence for this event at Satupaitea is a reflection of the geologic depth of the investigated core from this site. Present interpretations would suggest that evidence for this tsunami likely exists deeper in the geologic record at this location.

Similar archaeological enigmas associated with the AD 1690 – 1830 tsunami reported in Davidson (1979) include:

- The abundant archaeological evidence that mid 19-C (mid AD 1800s) coastal population concentration in Samoa was a response to the beginning of European contact, and the abandonment of inland areas in favour of the coast during this period was rapid (Davidson, 1979: 96).

- In Lalomanu village on southeast Upolu (south of Satitoa), 13 star mounds (settlement remains) found in the remote bush adjacent to extensive abandoned settlement areas closer to the coast (Davidson, 1979: 97). This suggests a similar pattern with the modern 2009 SPT hazard analogue at Saleapaga.

- The appearance of large earthen mounds associated with a despotic chief around 17-C (AD 1600s) at Vailele village on north Upolu (east of neighbouring Fagali'i) extending some distance inland (Davidson, 1979: 98). The coincidence in the timing of such structures could be a form of traditional tsunami mitigation, although such speculation is premature at this stage.

Other clues in the ethno-archaeological record likely associated with the AD 1690 – 1830 tsunami include evidence of inland cave dwellings (Seuao cave) around c. 240 ± 50 BP (AD 1660 – 1760) near Sa'anapu on southwest Upolu (Golson, 1969:19; Martinsson-Wallin, 2007:14). Similarly, genealogical evidence of occupation exists at the Pulemelei stone mound inland of Satupaitea around AD 1650 (Martinsson-Wallin, 2011:106). Both cases suggest a possible correlation with the pattern of abandonment at Saleapaga following the 2009 SPT.

In Fale o le Fe'e (or Temple of Fe'e, the war-god of the prehistoric A'ana province in Upolu) (Stair, 1894), radiocarbon evidence obtained in this research suggest that it was occupied or in use around AD 1430 – 1630 (Wk-30088 in Table 1). This site is situated in central Upolu approximately 8 – 10 km inland of Apia at an elevation of > 450 m above sea level. It is one of the few known prehistoric religious sites in Samoa

located in a remote highland location. The determined timing of occupation at this site is contemporaneous with the AD 1199 – 1469 tsunami and AD 1469 – 1672 cyclone (Figure 26).

It is possible that the timing of occupation at Fale o le Fe'e, based on evidence presented here, is associated with favoured inland settlement by the corresponding inhabitants. Such movements could have been an adaptive response to contemporaneous coastal hazards due to events identified in the geologic record. At present, however, these can only be treated as likely associations, because no definitive cause-effect relationships can be established between the corresponding chronological sequences.

The AD 1199 – 1469 tsunami is also contemporaneous with initial occupancy at the Pulemelei stone mound around AD 1111 – 1311 (Martinsson-Wallin 2007:105). This mound is the largest known human-built structure in prehistoric Polynesia, and lies several kilometers inland of Satupaitea. Similar to the case at Fale o le Fe'e, it is possible that initial inhabitant desire to expand or move inland from the coast during this period, is associated with a potential AD 1199 – 1469 tsunami.

The timing of this tsunami also coincides with the emergence of cannibalism in Samoa (Davidson, 1979:101), which appears to have been around AD 1130 – 1335. Evidence for this cannibalism was found at the coast of Lotofaga on southeast Upolu, and also coincided with the timing at which the area first became habitable. The reason for the area becoming habitable was interpreted by Davidson (1979:101) to be the result of shoreline changes around AD 579 – 1179. It is possible that both of these coincidences at Lotofaga are associated with a potential AD 1199 – 1469 tsunami influence (i.e. food resources and coastal erosion).

Ethno-historically, this tsunami also coincides with the emergence of the Malietoa paramount *matai* (chief) lineage around AD 1250 (Linnekin et al., 1995). This title emerged following the demise of the likely 300 year Tui-Tonga rule of parts of Samoa, which is thought to have predominantly been on southern Samoan areas. The timing of this sequence of cultural events suggests a possible correlation with an AD 1199 – 1469 tsunami influence. The predominant location of the so called Tongan occupation of southern Samoan areas, relative to the location of the NTSA, possibly suggests an NTSA source for the AD 1199 – 1469 tsunami. Further, it also implies an associated tsunami influence on the Tui-Tonga weakening, vulnerability, and subsequent defeat following a 300 year rule.

Interestingly, this tsunami is also contemporaneous with interpreted repeated coastal settlement disruptions by major coastal inundations in the Cook Islands around AD 1220 – 1440 (Allen and Wallace, 2007:1167). It is possible that one of the coastal inundations is associated with the AD 1199 – 1469 tsunami in Samoa, which would imply that this tsunami may have had far-reaching regional impacts.

The AD 930 – 1255 Cyclone and preceding AD 502 – 930 and AD 247 – 502 tsunamis, coincide with the timing of the Samoan archaeological Dark Ages around AD 500 - 1000 (Reith and Addison, 2008). The Dark Ages in Samoa refer to a period with a dearth of pottery-bearing cultural deposits. It is possible that there is some connection between this enigma and the associated contemporaneous coastal hazards identified.

Possible connections also exist between the three likely cyclone events identified between BC 738 – AD 247 and the preceding two tsunamis between BC 1375 – 738 (Figure 26), with evidence of inland settlement in Samoa by 2,000 years ago (Davidson, 1979:94). The earliest colonization of Samoa is accepted to have occurred about 2,900 – 2,600 BP (Petchey, 2001). The age of the charcoal from Fagali'i (WK30087, Table 1) found in association with the stratigraphically oldest identified tsunami MID, suggests that this tsunami was a likely hazard at the time of its occurrence. Further, WK30087 represents evidence of earliest human presence in Samoa contemporaneously with, if not slightly older than, the accepted age of initial colonization in Petchey (2001).

A more detailed consideration of the implications associated with sample WK30087 is provided in Chapter 5.4. It represents one of the two oldest tsunami hazards identified in Samoan geologic record contemporaneous with initial colonization. Further, both events coincide with the timing of a relatively quick change (1 – 2 centuries after initial colonization) in the style of pottery making in Samoa (from Lapita dentate to local variants of plainware techniques), around BC 850 – 450 (Reith and Hunt, 2008). It is possible that the associated tsunamis may have played a role in influencing such cultural changes (e.g. through sudden loss of life of pottery-making knowledge holders). However, further investigation is required to test such a correlation.

The discussions presented in this Section are possibilities on the associations between tsunamis and cyclones identified in the Samoan geological record with contemporaneous anomalies and/or enigmas in the ethno-archaeological record. If correct these would imply an approximate 3,000 year tsunami and cyclone hazard history in Samoa.

However, unlike the 2009 SPT hazard analogue at Saleapaga, local and international humanitarian aid experienced during response to and recovery from this tsunami cannot be assumed to have occurred following similar or stronger palaeo-events within the deeper Samoan history. That is, modern frameworks of centralized government, emergency deployment, and international humanitarian support including financial aid, are not comparable to prehistoric disaster recovery and mitigation arrangements. Therefore past tsunami and/or cyclones of similar or greater impact-magnitude than the 2009 SPT may have played a major role in influencing longer coastal abandonments, as well as alternative cultural settlement dynamics and manifestations (e.g. cannibalism). Such observations in the ethno-archaeological record are recognized in contemporaneity with associated identified tsunamis and cyclones identified in this thesis.

3.6 Limitations and Recommendations

Limitations of the findings and interpretations presented in this Chapter are discussed below.

The sub-sampling interval used to yield proxy data at different sites lacked consistency (Figure 15). This affects the analytical resolution of the results. That is, a larger sampling interval corresponds to a lower analytical resolution and vice versa. This in turn affects the quality of data available for interpretation of MID signature trends. The high-resolution ITRAX results relative to the corresponding lower resolution pXRF results at Ma'asina, Manono, and Lano in Sections 3.4.3 and 3.4.4 demonstrate this effect. Identified MIDs clearly visible in the ITRAX data for these sites were not as evident in the pXRF data. This has implications for the interpretations of lower resolution results yielded from sites such as Fagali'i, for example.

Nevertheless, the combined results are of adequate resolution to formulate the baseline tsunami and cyclone chronological model for Samoa presented in Figure 26. Acquisition of high resolution proxy data, including geochronological, from several more extensive core and trench profiles at each site is recommended for further research, in order to test, validate, and refine the baseline model proposed. This also has the potential to reveal the possible existence of signatures at locations which did not contain specific MIDs found only at certain sites (e.g. 1991 cyclone MIDs at Falealupo, Satupaitea, Vaovai and Satitoa).

The main premise herein, for deciding whether the identified MIDs were of a tsunami or cyclone origin, is based on the 2009 SPT analogue at Satitoa, and geological evidence supporting the 1990/1991 cyclone analogues at Falealupo. Further investigation of possible deposits left behind by the recent Cyclone Evan in December 2012 is recommended at the sites investigated herein. This would provide a means to corroborate the Falealupo cyclone analogues, and/or refine recognizable differences with the 2009 SPT analogue at Satitoa.

It is assumed herein that MIDs identified at sites where no geochronology data were obtained are stratigraphically associated with the likely timing of corresponding MIDs at other sites. However, the tsunami and cyclone chronology model in Figure 26 is based on limited geochronological indicators from each site. Acquiring more detailed chronological data from each investigated site profile is recommended for further research in order to validate the inferred MID associations in Table 4 and Figure 26. The several possibilities for the origin of the inferred historical 1868 tsunami MID at Ma'asina (discussed in Section 3.5.4.6), demonstrate the importance of this.

Profile depths at Fagali'i and Manono provide the only evidence of MIDs older than around 1,000 years ago. This demonstrates the importance of retrieving deeper profiles from other sites and subsequent

acquisition of proxy data in order to corroborate the MIDs and associated events inferred at Fagali'i and Manono.

The age obtained for charcoal sample Wk-30087 at Fagali'i could be affected by in-built age. This implies that its true calendar age, including the interpolated age estimates for the Fagali'i profile using this sample, could be a few hundred years younger. While Section 5.4 provides a more thorough consideration of this effect, present evidence permits the assumption that the model in Figure 26 is a reasonable estimate of the Samoan tsunami and cyclone chronology.

The magnitude and frequency estimations presented in Section 3.5.5 are limited by the available resolution of yielded proxy data used in their calculation. Acquisition of higher resolution and more extensive proxy data would lead to reduction of their uncertainty. Nevertheless, available evidence permits the assumption that they are likely a true indication of the characteristics of NTSA associated tsunamis of equivalent or greater magnitude than the 2009 SPT.

3.7 Summary and Conclusions

The results presented in this Chapter demonstrate the existence of distinct proxy signatures associated with the 2009 SPT deposits, particularly at Satitoa. Further, geochronological data enabled the identification of the 1990 and 1991 Cyclones Ofa and Val deposits, respectively, at Falealupo. Recognizable differences between the 2009 SPT and 1990/1991 Cyclone proxy trends provide modern signature analogues for distinguishing the origin of identified MIDs deeper within the broader Samoan historical and geologic record.

While the tsunami and cyclone chronology established in Figure 26 is based on limited proxy data, the model proposed does provide a robust baseline for future investigation, modification and refinement. More importantly, it provides evidence of long-term tsunami and cyclone occurrences in Samoa.

No definitive cause-effect hazard relationships can be presently established between the proposed tsunami and cyclone chronology with anomalous and/or enigmatic sequences in the Samoan ethno-archaeological record. The contemporaneous associations between the two chronologies, however, provide the possibility that such relationships may exist. Although further investigation is required to draw more definitive conclusions, the interpretations presented would suggest likely associations, implying that some of the identified tsunami and cyclone events in the geologic record were most likely hazardous.

Ultimately, the conclusion of this chapter is that the evidence and interpretations presented demonstrate the long-term tsunami and cyclone hazard potential in the Samoan Islands.

Deputy Vice-Chancellor's Office
Postgraduate Office

Co-Authorship Form

UNIVERSITY OF CANTERBURY
Te Whare Wānanga o Waitaha
CHRISTCHURCH NEW ZEALAND

This form is to accompany the submission of any thesis that contains research reported in co-authored work that has been published, accepted for publication, or submitted for publication. A copy of this form should be included for each co-authored work that is included in the thesis. Completed forms should be included at the front (after the thesis abstract) of each copy of the thesis submitted for examination and library deposit.

Chapter 4: Revised from Manuscript ID GJI-S-14-0135 entitled "Resonance: A new proxy to assist palaeotsunami investigation".

Publication status: In Revision, Geophysical Journal International.

Resubmission date: 13 July 2014.

Shaun Williams adapted the numerical modeling results and text of Yoshiki Yamazaki, Volker Roeber, William Templeton and Kwok Fai Cheung from the original manuscript, and expanded them into the context of this thesis. Development and refining of the original manuscript as well as this revised version was conducted by co-authors stated in the Co-Authorship Declaration of this thesis.

Certification by Co-authors:
If there is more than one co-author then a single co-author can sign on behalf of all
The undersigned certifys that:

- The above statement correctly reflects the nature and extent of the PhD candidate's contribution to this co-authored work
- In cases where the candidate was the lead author of the co-authored work he or she wrote the text

Name: **Tim Davies** Signature: Date: **30 April 2014**

CHAPTER 4: RESONANCE & TSUNAMI DEPOSITS

4.1 Overview

This Chapter presents a technical case study of the 2009 SPT resonance around Upolu and Savaii, and its relationship with the 2009 SPT deposits described in Chapter 3. Resonance of the 2009 SPT is modeled using available data, followed by an assessment of the links between the resonance energy and the locations of 2009 SPT deposits.

The effects of tsunami resonance in Pacific island regions were first documented by Munger & Cheung (2008). Resonance is the tendency of tsunami waves to oscillate due to the influence of local topography (e.g. coral reefs or embayments). This results in dominant or relative maximum wave periods for specific locations. These dominant wave periods (or resonant waves) have been found to significantly influence the variability of tsunami impacts along coasts. Understanding the nature and characteristics of resonant waves is therefore a fundamental component of tsunami hazard assessment (Munger and Cheung, 2008; Roeber et al., 2010; Yamazaki and Cheung, 2011; Cheung et al., 2013; Yamazaki et al., 2013).

In the case of the Samoa Islands (American and Independent Samoa), Roeber et al. (2010) demonstrated the effects of resonance on the impacts on Tutuila Island in American Samoa resulting from the 2009 SPT. This tsunami was generated by an outer-rise earthquake which was accompanied by a near-simultaneous rupture of the shallow interface along the northern Tongan subduction arc region (Beavan et al., 2010; Lay et al., 2010; Okal et al., 2011). The resonance focussed-energy distribution of this tsunami was due to shelf and embayment configurations. Local wave amplification was found to have resulted from the trapping of waves within the foreshore (i.e. between coral reefs and shore), as well as in narrow embayments Roeber et al. (2010). These findings demonstrated that resonance could be applied to identify areas susceptible to inundation in future tsunamis.

It could be further deduced that resonance of a given tsunami has a potential link to the locations where associated deposits form. This hypothesis is investigated herein through a comparison of the 2009 SPT resonance around Upolu and Savai'i, with the locations of 2009 SPT deposits studied in Chapter 3. This provides a means for assessing the potential use of hypothetical tsunami resonance as an indicator for identifying likely and/or potential locations for palaeotsunami deposit investigation.

Resonance of the 2009 SPT presented herein was modeled by Yoshiki Yamazaki, Volker Roeber, William Templeton, and Kwok Fai Cheung in 2013 (i.e. Yamazaki et al., University of Hawai'i at Manoa, Ocean and Resources Engineering Department), using the NEOWAVE model of Yamazaki et al. (2012). The majority of Sections 4.3 – 4.6 in this Chapter is taken from Yamazaki et al. Nearshore bathymetry data compilation and synthesis with the palaeotsunami data in Chapter 3 was conducted by Shaun Williams.

4.2 Objectives

The objectives of this Chapter are to;

1. Summarise numerical modeling of resonance of the 2009 SPT around Upolu and Savaii using available data.

2. Assess the resonance energy pattern relative to the locations of identified palaeotsunami deposit locations.

3. Interpret the findings in the context of the overall thesis aims.

4.3 Methodologies and Data

The shock-capturing dispersive wave model NEOWAVE of Yamazaki et al. (2010; 2011; 2012; 2013) is used to reproduce the 2009 SPT for resonance analysis around Upolu and Savaii Islands. NEOWAVE (Non-hydrostatic Evolution of Ocean WAVE) incorporates the spherical coordinate system and two-way grid-nesting scheme. This enables tsunami evolution processes from generation, propagation and run-up to be modeled. This staggered finite difference model builds on the nonlinear shallow-water equations with a vertical velocity term to account for wave dispersion, and a momentum conservation scheme to describe bores or hydraulic jumps.

Figure 28 shows two levels of two-way nested grids used to capture the physical processes from the open ocean to the shore. The level-1 grid extends across the south-central Pacific Ocean at 1-arcmin (~1800 m) resolution to cover DART buoys 51425, 51426 and 54401 surrounding the rupture area. The level-2 grid resolves wave transformation around the Samoan Islands at 30-arcsec (~900m) resolution for spectral analysis (Roeber et al., 2010). The digital elevation model is derived from the General Bathymetric Chart of the Oceans (GEBCO) at 30-arcsec (~900 m) resolution. A Manning coefficient of 0.035 is applied to describe the nearshore reefs and volcanic slopes around the Samoa Islands (Bretschneider et al. 1986).

The fault model of Yamazaki et al. (2012) is used, and comprises the main intraplate faulting and two subsequent thrust events as summarised in Table 6. The source parameters include the rupture initiation and rise time to reconstruct the time history of seafloor deformation through the planar fault model of Okada (1985). The NEOWAVE vertical velocity term accounts for the time history of uplift and subsidence in modeling of tsunami generation and kinetic energy transfer to the water. The computation covers 5 hours of elapsed time with time steps of 0.6 and 0.2 sec for the level-1 and -2 grids, respectively. The output time intervals are 10 sec over the computational domain for spectral analysis and 1 min at the DART buoys to match the sampling intervals of the recorded data.

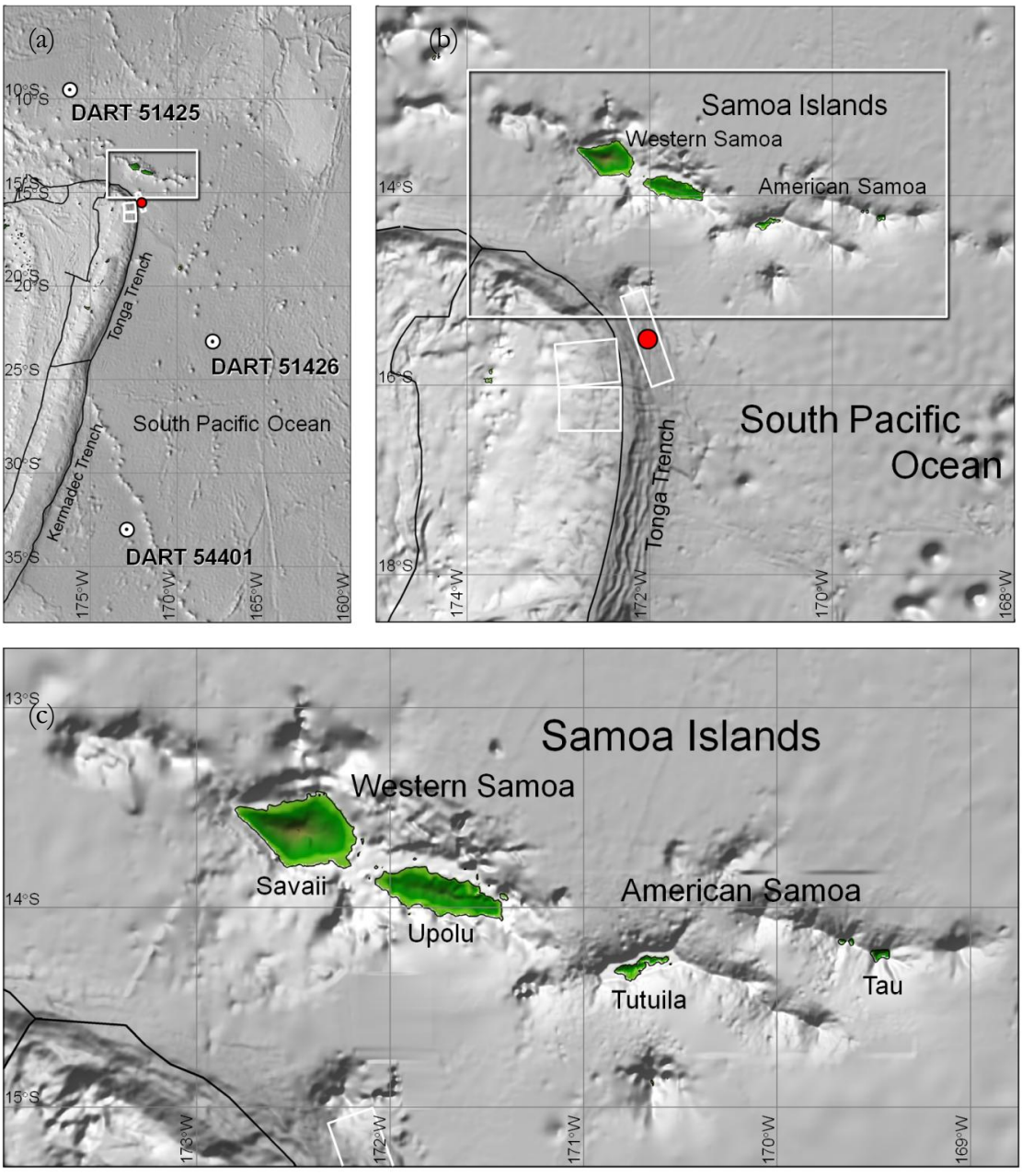

Figure 28: Bathymetry and topography in the model region for the 2009 SPT. (a) level-1 computational domain with the level-2 domain coverage (note DART buoy locations) (b) close-up view of epicenter and Samoa Islands. (c) level-2 computational domain with the level-3 domain coverage, ○ (red), epicenter; ○ (white), DART buoy water-level stations; white rectangle, nested-grid domain.

Table 6: Fault parameters for the 29 September 2009, Mw=8.1, 2009 Samoa Earthquake (after Yamazaki et al., 2012).

No	Length (km)	Width (km)	Strike angle (º)	Dip angle (º)	Rake angle (º)	Slip (m)	Depth (km)	Latitude (ºN)	Longitude (ºW)	Rise time (s)	Rupture initiation time (sec)
1	110	35	340	35	265	6.60	5.2	16.0151	171.9693	41	0
2	50	75	175	20	90	4.62	5.0	15.5260	172.3703	40	49
3	50	75	180	20	90	4.71	5.0	16.0402	172.3250	40	90

4.4 Data Limitations

No high resolution near-shore bathymetry data around Upolu and Savai'i islands is available. The highest resolution bathymetric coverage for these islands is the offshore 70 m (~3 arcsec) data archived by SOPAC (Figure 29). Near-shore (i.e. lagoonal) data are limited to surveys of eastern Savai'i, and are archived by KIGAM. Digitization of nautical charts archived by LINZ provided limited data for parts of northern Upolu and to a much lesser extent, northern Savai'i.

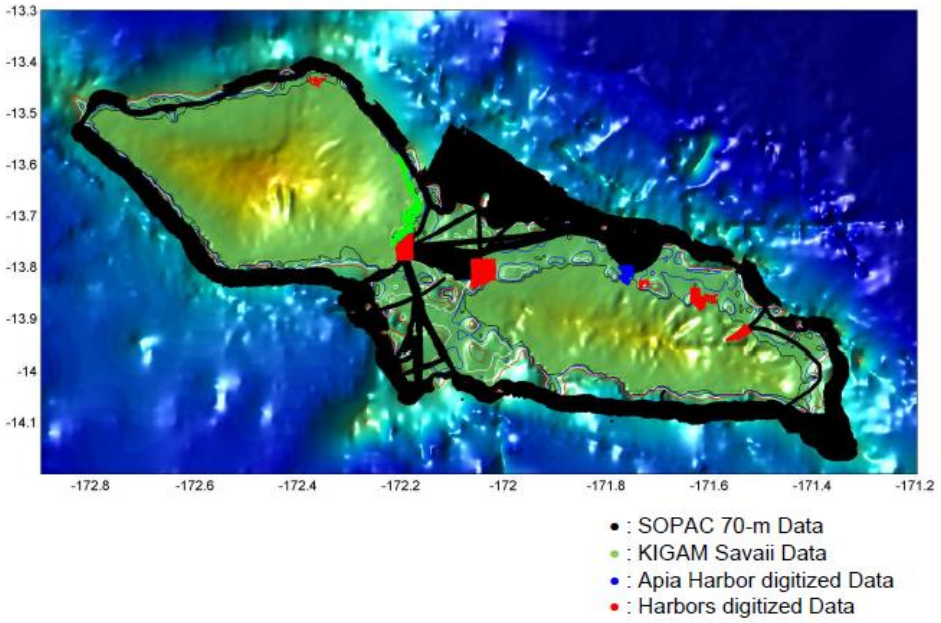

Figure 29: Bathymetry data coverage for Upolu and Savai'i Islands.

However, comparison of these merged data sets with the GEBCO 30 arcsec baseline shows several unrealistic deep water areas in near-shore lagoons (Appendix 11). Further, there are significant discrepancies between the digitized nautical charts and GEBCO data sets, making it difficult to develop sufficient DEM data for high resolution tsunami modeling.

These challenges concerning available data limited the modeling resolution provided in this Chapter, in that only coarse GEBCO 30 arcsec data was used. Current local plans to implement near-shore bathymetric and coastal LIDAR surveys in the near-future (F. Nelson, pers. comm., 2014), will provide the data necessary for high resolution tsunami modeling in these islands.

For the purposes of this thesis, the 30 arcsec resolution modeling conducted provides sufficient results to draw correlations between coastal areas of highest 2009 SPT resonance, with the distribution of associated 2009 SPT deposits (e.g. Satitoa, Vaovai, Mulivai and Manono).

4.5 Results and Interpretations

The NEOWAVE model reproduces the arrival time, amplitude and frequency content of the DART buoy measurements similar to results in Roeber et al. (2010). Figure 30 compares the computed and recorded waveforms and spectra. DART 51425 and 51426 to the northwest and southeast of the intraplate faulting are instrumental in validating the primary rupture along the Tonga Trench.

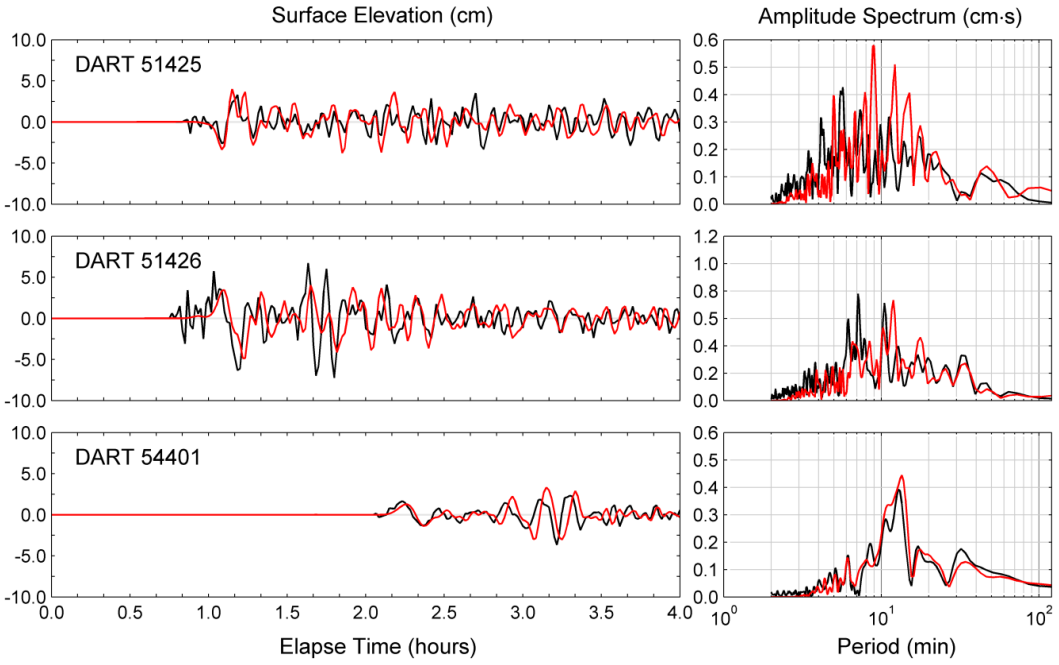

Figure 30: Time series and spectra of surface elevations at DART buoy water level stations. —— (black), recorded data; —— (red), computed data.

Figure 31 illustrates the spectral amplitude of eight oscillation modes from 7 to 31 min that extend across Savaii and Upolu with high energy. The transition from one mode to the next is smooth as the rugged coastline and varying shelf produce infinite combinations of eigenmodes (resonant frequencies). The standing waves associated with resonance have distinct nodal lines, where the amplitude is nearly zero and the phase varies rapidly by 180º.

Figure 32 plots the maximum surface elevation during the event and the integrated spectral energy across the frequency range. The maximum surface elevation provides an indication of the overall impact of the tsunami.

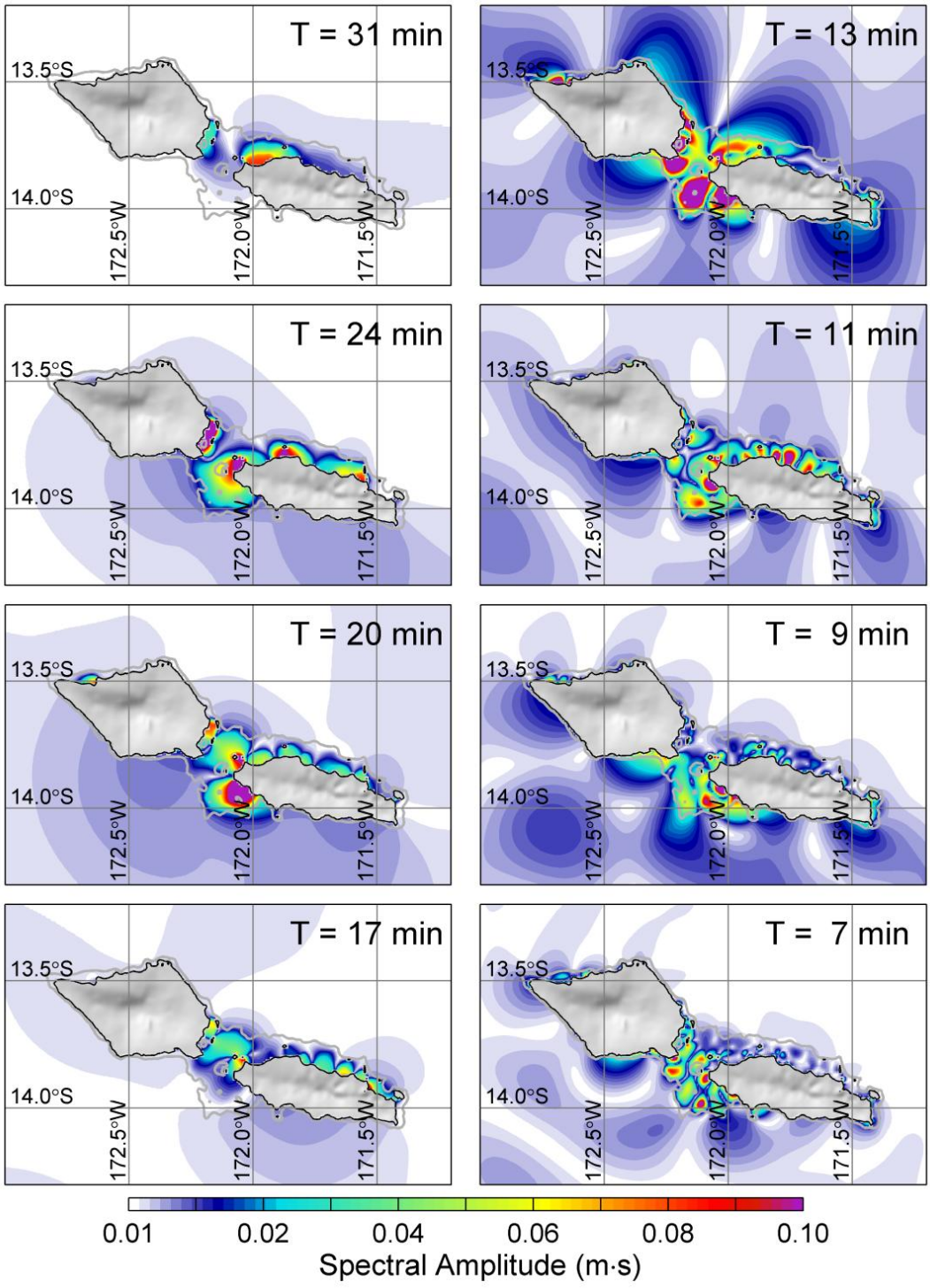

Figure 31: Spectral amplitude (m·s) of selected resonance modes. Grey lines indicate the 200-m depth contour.

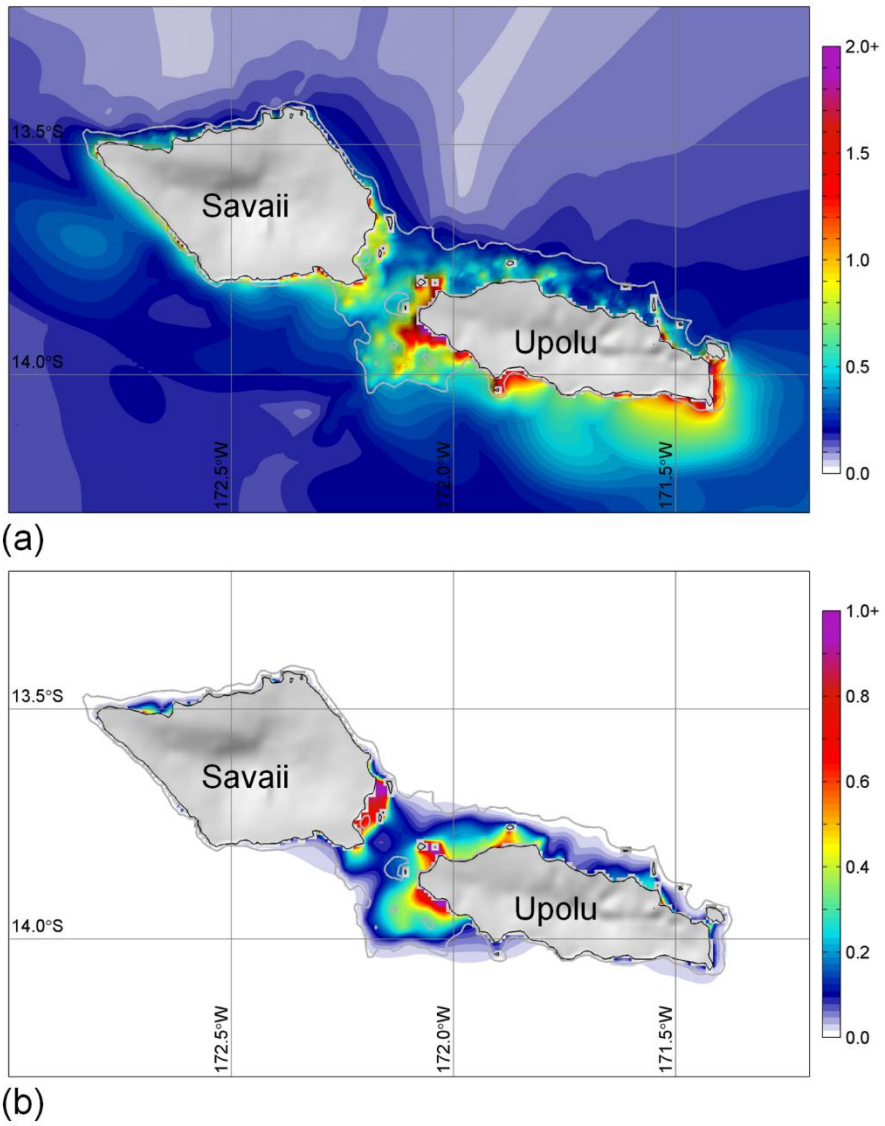

Figure 32: Maximum wave amplitude (m) and spectral energy ($m^2 \cdot s$). Grey lines indicate the 200-m depth contour.

4.6 Discussion

The results in Figure 31 illustrate that scattering along the steep trench and seamounts results in dispersive waves as short as the 2-min Nyquist period. The data at DART 54401 to the far south along an open stretch of ocean better illustrates the tsunami waveforms associated with the rupture configuration and large-scale oscillation along the Tonga trench. The good agreement of the computed and recorded initial waves in Figure 30, which originate from the thrust faults, validates the secondary source mechanism in the outer rise.

The analysis of the DART data has already demonstrated the use of a Fast Fourier Transform (FFT) algorithm to determine the amplitude spectrum over wave period and identify dominant oscillation

modes along the island chain. With the model results already validated, application of the same algorithm to the computed surface time series at all grid points defines the spatial distributions of the spectral amplitude and phase angle for visualisation of the oscillation modes. Since FFT is a linear process, the nonlinear evolution of the tsunami in time is denoted by a series of oscillation modes in the frequency domain.

The oscillations modes in Figure 31 are primarily limited to the insular shelf delineated by the 200-m contour. The insular shelf connecting the two islands is particularly susceptible to resonance. Areas of greatest resonance amplification were along the western, southern and eastern coastlines of Upolu, and corresponded to areas which sustained the greatest loss of life and damage to property (Dominey-Howes & Thaman 2009). These areas include Satitoa, Vaovai, Mulivai and Manono discussed in Chapter 3.

Similar to the oscillation modes, the maximum resonance energy in Figure 32 is primarily limited to the insular shelf delineated by the 200-m depth contour, and its distribution corresponds to locations with persistent oscillations after the initial waves (Figure 31). Constructive interference from the various oscillation modes very often accounts for belated arrival of destructive waves (e.g. Cheung et al. 2013; Yamazaki & Cheung 2011; Yamazaki et al. 2013). Since resonance modes and periods are intrinsic to the landform and independent of the excitation, the spectral energy allows identification of areas susceptible to inundation, which is useful for emergency management and palaeotsunami studies.

Resonance amplification along the southwest coast of Upolu is likely overestimated due to known artefacts associated with the local bathymetry data at 30 arcsec resolution for this area (Appendix 11). Nevertheless, this coast was inundated by the 2009 SPT with depths > 3 m (Dominey-Howes & Thaman 2009), and signatures of its deposit were detected at Manono even though a distinct sand deposit was not observed there (Chapter 3, this thesis). Other areas of coast on north Upolu and Savaii which sustained few or no observed impacts from the tsunami, nevertheless exhibit some resonance (e.g. Ma'asina, Fagali'i, Lano, Falealupo). These areas correspond to locations which comprise known and/or likely tsunami deposits in Chapter 3.

4.7 Implications and Research Directions

The tsunami geological record in Section 3.5.4 forms a basis for starting to understand the likely source(s) of these events as different coastal morphologies trigger different resonance modes. If deposits of a certain event are only found at some locations, then the respective resonance periods at those locations would likely match the tsunami wave periods. Tsunami wave periods depend on the rupture area at the source. Hence the longer the period, the larger the rupture area and probably the stronger the earthquake that generated the tsunami. This could also potentially be verified with the

(palaeo-) tsunami proxy curves, as the peak nodes observed within the known and proposed deposits likely represent wave inundation heights, therefore providing analogues of the palaeo-wave periods.

Buech et al. (2007; 2010) discussed a terrestrial analogue of similar resonance effects in mountain edifices as a result of seismic inputs. It was found that maximum seismic wave amplification (resonant waves) was reached at the crest of the mountain because of local amplification factors within the edifice. These two independently investigated situations (i.e. tsunami and mountain edifice resonances) provide an opportunity to understand the significance of resonance in multi-geohazard assessments. Exploring the likely analogies between tsunami resonance at coastal locations and seismic resonance in mountain edifices, may further enable the magnitudes of likely palaeotsunami earthquake sources to be constrained.

Evaluating the correlations between the identified palaeotsunamis identified herein and prehistoric Samoan and regional cultural patterns, significant known events, and/or gaps in cultural sequences in the archaeological and indigenous knowledge record, would aid in interpreting the data in its complete hazard context (e.g. McFadgen and Goff 2007; King and Goff 2010).

4.8 Summary and Conclusions

The findings in this Chapter suggest that tsunami resonance spatial distribution of the 2009 SPT significantly corresponds with the locations of associated 2009 SPT deposit formations in Upolu. That is, areas of highest 2009 SPT resonance on south Upolu corresponded to locations that formed distinct 2009 SPT deposits.

The findings imply that hypothetical resonance modeling (e.g. 1917 or AD 1690 – 1830 tsunamis) can potentially be used for identifying coastal locations where palaeotsunami deposits may have been preserved. Alternatively, hypothetical modeling could potentially be used to validate tsunami sources for known palaeotsunami deposits.

In the context of the aim of this thesis, applying both numerical modeling of resonance and palaeotsunami data in tsunami hazard assessment would provide a better understanding of the long-term characteristics of the NTSA near-field source. Future hypothetical NTSA-sourced tsunami resonance modeling using higher-resolution nearshore bathymetry data around Upolu and Savai'i, may enable a better understanding of the characteristics of identified palaeotsunamis in Chapter 3.

Deputy Vice-Chancellor's Office
Postgraduate Office

Co-Authorship Form

UNIVERSITY OF CANTERBURY
Te Whare Wānanga o Waitaha
CHRISTCHURCH NEW ZEALAND

This form is to accompany the submission of any thesis that contains research reported in co-authored work that has been published, accepted for publication, or submitted for publication. A copy of this form should be included for each co-authored work that is included in the thesis. Completed forms should be included at the front (after the thesis abstract) of each copy of the thesis submitted for examination and library deposit.

Chapter 5: Case Study-I: Flank collapse on Ta'u Island, Samoan Archipelago: Timing and Hazard Implications.

Publication status: In Press, Landslide Science for a Safer Geoenvironment. Vol.3, Ch.90, 6p.

Publication date: 30 June 2014.

Shaun Williams wrote the manuscript. Laboratory ^{36}Cl surface exposure dating was conducted by Timothy Barrows. Development and refining of the original manuscript was conducted by the co-authors stated in the Co-Authorship Declaration of this thesis.

Certification by Co-authors:
If there is more than one co-author then a single co-author can sign on behalf of all
The undersigned certifys that:

- The above statement correctly reflects the nature and extent of the PhD candidate's contribution to this co-authored work
- In cases where the candidate was the lead author of the co-authored work he or she wrote the text

Name: **Tim Davies** Signature: Date: **30 April 2014**

Deputy Vice-Chancellor's Office
Postgraduate Office

Co-Authorship Form

UNIVERSITY OF CANTERBURY
Te Whare Wānanga o Waitaha
CHRISTCHURCH NEW ZEALAND

This form is to accompany the submission of any thesis that contains research reported in co-authored work that has been published, accepted for publication, or submitted for publication. A copy of this form should be included for each co-authored work that is included in the thesis. Completed forms should be included at the front (after the thesis abstract) of each copy of the thesis submitted for examination and library deposit.

Chapter 5: Case Study-III: Revised from Manuscript ID UICA-2014-0012 entitled "C-14 age for newly discovered charcoal from Samoa: Evidence of either natural forest fires or human presence more than 3000 BP".

Publication status: In Revision, Journal of Island and Coastal Archaeology.

Resubmission date: 28 September 2014.

Shaun Williams wrote the manuscript. C-14 analysis data was provided by Fiona Petchey. Development and refining of the original manuscript was conducted by the co-authors stated in the Co-Authorship Declaration of this thesis.

Certification by Co-authors:
If there is more than one co-author then a single co-author can sign on behalf of all
The undersigned certifys that:

- The above statement correctly reflects the nature and extent of the PhD candidate's contribution to this co-authored work
- In cases where the candidate was the lead author of the co-authored work he or she wrote the text

Name: **Tim Davies** Signature: Date: **30 April 2014**

CHAPTER 5: TSUNAMI CASE STUDIES

5.1 Overview

This chapter presents three tsunami case studies in the Samoan archipelago. Each case study falls within a specific context that is relevant to the overarching thesis aim, and/or preceding thesis interpretations, as summarized below:

1. Case Study-I discusses the timing of a large-scale flank collapse on Ta'u and subsequent landslide-tsunami identified in Williams et al. (2012), and assesses the hazard implications of potential future occurrences of similar processes.

2. Case Study-II assesses high-elevation calcareous deposits believed to be of a marine origin located in central Upolu, approximately 10 km inland of Apia and more than 450 m above sea level. Existing hypotheses concerning the formation of the deposits, including a possible tsunami origin, are discussed.

3. Case Study-III evaluates the possible in-built age of charcoal sample Wk-30087 obtained from Fagali'i. The implications of this in-built age for the timing of certain palaeo- tsunami and cyclone events interpreted in Chapter 3 are discussed. This includes the implications of this sample in the broader context of earliest colonization and long-term tsunami hazards in the Samoan Islands. All of these Case Studies are interpreted within the context of the overarching thesis aims.

5.2 Case Study I: Flank collapse on Ta'u

5.2.1 Synopsis

A discrepancy between the cartographic depiction of Ta'u Island, Samoan archipelago, in 1849 and its present geomorphology, leads to the impression that a massive collapse involving an estimated 30 km^3 occurred on the island's southern flank less than 170 years ago. It is likely that this flank-collapse, whenever it occurred, generated a tsunami with regional impacts. Exposure dating of the remnant landslide scarp using the cosmogenic nuclide ^{36}Cl, is used to show that the flank-collapse occurred 22.4 ± 1.8 ka during the last glacial maximum (LGM).

Collapse may have been triggered due to volcanic-related processes, but it is also possible that climatic-eustatic sea-level during the LGM may have played a role in influencing failure of the flank. The initial cartographic depiction of Ta'u in 1849 is confirmed to have been in error. Further, it is deduced that this

prehistoric landslide-tsunami was not a societal hazard at the time of its occurrence, because the Samoan and surrounding Island Nations were only inhabited about 3 ka or so.

Nevertheless, it is suggested that geomorphic features similar to the Ta'u flank-collapse on islands and seamounts in the Pacific likely represent signatures of landslide-tsunamis in the past. Further, it is suggested that there is a need to identify and date other such features in the Pacific, in order to further spatial and geochronological understanding of these events. There is also a need to identify flank features that have not yet failed, and assess the likely mechanisms that could potentially trigger failure. By doing this, we can start assessing with more confidence the hazard potential of similar flank-collapses in future – a risk that is presently under-represented.

5.2.2 Introduction and Background

Ta'u is the easternmost volcanic island in the Samoan archipelago, South Pacific, and lies within the Manu'a Group of American Samoa (Figure 33a). It is the youngest island formed from the Samoan volcanic hotspot, which currently lies about 45 km to the East (Hart et al., 2000; Hart et al., 2004).

Geologically, it is in its shield-building stage of volcanism which commenced about 300 ka (Natland and Turner, 1985; Hart et al., 2004; Koppers et al., 2008; 2011). However, the nature of the 1866 – 1867 submarine eruption of Pomasame volcanic cones reported in Turner (1889), is not well understood (Williams, 2009). These cones were mapped during surveys reported in Fenner et al., (2008), and lie about 2 km NW of Ta'u along the submarine ridge connecting it to neighbouring Ofu and Olosega islands (Figure 33b).

The southern flank of Ta'u exhibits a series of down-faulted benches which are likely remnants of a large-scale flank-collapse involving an estimated 30 km^3 (Williams, 2009; Williams et al., 2012). Further, early mapping suggests that this flank-collapse could have occurred more recently than the year 1839 (Williams, 2005; 2009; Williams et al. 2012); although there was little tsunami evidence in the historical record to suggest it did (NGDC and ITIC 2010).

The possibility of a recent historical collapse stemmed from the cartographic depiction of Ta'u in Wilkes (1849) and Turner (1889) (Figure 32c and 32d). The island was depicted as having a much more symmetrical geomorphic structure than its present day planform (Williams, 2009; Williams et al., 2012) (Figure 33e and 33f). Further, the depictions were based on the initial survey data of Ta'u collected on October 8-10, 1839, and the island was described as having the form of a regular dome (Dana, 1849; Wilkes, 1849; Turner, 1889).

Geomorphic interpretations in Williams (2009) and Williams et al. (2012), suggested that the collapse occurred after the LGM sea-level low-stand, which was assumed to have been ~18 ka. The estimated

volume of material that would have collapsed based on the Ta'u depiction in Turner (1889) was about 30 km^3, and would have most likely generated a tsunami with regional impacts.

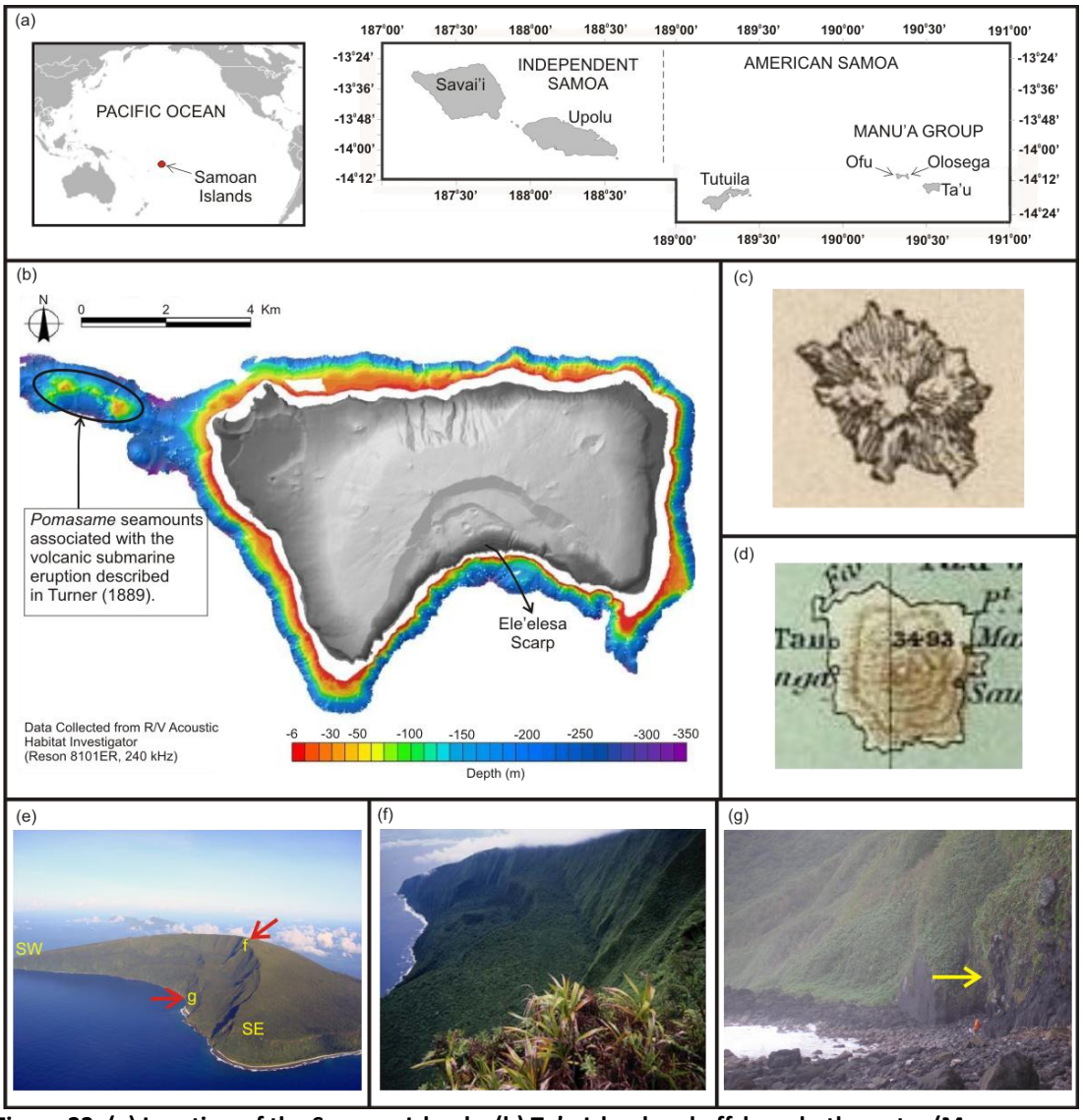

Figure 33: (a) Location of the Samoan Islands; (b) Ta'u Island and offshore bathymetry (Map source: American Samoa Department of Wildlife and Conservation); (c) Depiction of Ta'u in Wilkes (1849) based on 2 days of survey data collection in October 1839; (d) Depiction of Ta'u in Turner (1889) based on survey data of Wilkes (1849); (e) South flank of Ta'u (Photo by Michael Tenant); (f) Summit (~925 m), view looking west (Photo by Mark Rauzon); (g) Sampled outcrop in this study.

Conservative numerical modeling of the likely event in Williams et al. (2012) strengthens this landslide-tsunami hypothesis. However, it was suggested that if the event was younger than 1839, the impacts of the collapse and tsunami would not have gone unnoticed by local inhabitants. The absence of any such event occurring within recorded history (both written and oral), led to the suggestion that the event was much older than 1839, and that the depiction of Ta'u in Wilkes (1849) was incorrect.

This hypothesis is investiged further herein. ^{36}Cl cosmogenic surface exposure dating of a basalt sample is used obtained from the Ele'elesa scarp to infer the likely age of the collapse. The implications of the result with respect to the depiction of Ta'u in Wilkes (1849) is discussed, as well as to the associated geo-climatic context of collapse occurrence. The nature and implications of the event in a regional hazard and risk contexts are also considered.

5.2.3 Methodologies and Results

5.2.3.1 Field sampling

A single basalt sample was obtained from a massive outcrop on the Ele'elesa scarp (Table 7 and Figure 33g), which is the lower expression of the collapsed block mass that formed the south flank benches.

Table 7: Site data for ^{36}Cl surface exposure age determination

Sample (Field Code)	Longitude (^{0}W)	Latitude (^{0}S)	Altitude (m)	Horizon Correction	Thickness (cm)[1]
TAVI-06	169°26'50	14°14'56	8	0.50	5.5

1. ρ = 3.0 g.cm^{-3}; Λ = 160 g.cm^{-1}

5.2.3.2 ^{36}Cl cosmogenic surface exposure dating

The extraction of ^{36}Cl was undertaken at the Exeter Cosmogenic Nuclide Laboratory at the University of Exeter, UK. Total ^{36}Cl was measured on the whole rock because the fine-grained lithology prevented effective mineral separation. The concentrations of major target elements for ^{36}Cl production were determined using X-ray fluorescence. The concentrations of trace elements with large neutron capture cross sections (Gd, and Sm) and neutron-producing elements (U and Th) were measured by inductively-coupled plasma mass spectrometry. Chlorine content was determined by isotope dilution. The isotopic ratio of ^{36}Cl/Cl was measured by accelerator mass spectrometry on the 14UD accelerator at the Australian National University (Fifield et al. 2010). Major and trace element abundances and neutron capture cross sections are listed in Table 8 and Table 9.

Table 8: Major element data (wt. %)

SiO_2	Al_2O_3	Fe_2O_3	TiO_2	MgO	MnO	CaO	K_2O	Na_2O	P_2O_5
50.74 ± 0.31	13.11 ± 0.14	9.91 ± 0.09	3.69 ± 0.10	6.39 ± 0.05	0.14 ± 0.004	12.47 ± 0.12	0.78 ± 0.03	2.63 ± 0.30	0.04 ± 0.001

Table 9: Trace element data (ppm)

[B][1]	[Cl]	[Sm]	[Gd]	[Th]	[U]	cross section (10^{-3} cm^2 g^{-1})
5.0 ± 2.0	54.4 ± 1.2	7.62 ± 0.04	7.44 ± 0.07	3.23 ± 0.10	0.72 ± 0.02	7.84 ± 0.10

1. Estimated from similar rocks

The ^{36}Cl exposure age was calculated as detailed in Barrows et al. (2013) (Table 10). The production rate was scaled using the scheme of Stone (2000). All analytical errors are fully propagated, and the age in the text is reported at one standard deviation (68% prob.).

Table 10: ^{36}Cl exposure age

Field Code	Lab Code	$[^{36}Cl]_c$ $(x10^4\ g^{-1})^1$	$[^{36}Cl]_r$ $(x10^3\ g^{-1})^2$	Exposure age (ka)
TAVI-06	ANU-225-19	5.84 ± 0.435	4.88 ± 0.19	22.4 ± 1.8

Data are normalised to the GEC standard ($^{36}Cl/Cl = 444 \times 10^{-15}$).
Carrier $^{36}Cl/Cl = <1 \times 10^{-15}$. ^{36}Cl decay constant $2.3 \times 10^{-6}\ yr^{-1}$.
1. C = cosmogenic component
2. R = nucleogenic component

5.2.4 Discussion and Interpretations

5.2.4.1 Timing of collapse

The ^{36}Cl exposure age was calculated at 22.4 ± 1.8 ka and is interpreted to be indicative of the timing at which the scarp was first exposed to cosmic rays after flank collapse. This assumption is based on the location of the sample relative to the implied collapsed-mass deduced from Wilkes (1849). If the collapse was younger than 1839, then the scarp which the sample was obtained would have only recently been exposed to cosmic rays. That is, it is likely to have been less than a few hundred years old or so.

The calculated exposure age of 22.4 ± 1.8 ka is unambiguously much older than 1839. This implies that there is a 68% probability that collapse occurred between 24.2 – 20.6 ka, corroborating the suggestion in Williams et al. (2012) that the initial depiction of Ta'u in Wilkes (1849) could have been incorrect.

The proposed maximum relative collapse age of ~18 ka in Williams et al. (2012), was suggested based on geomorphic indicators. Subaerial and submarine wave-cut platforms assumed to represent the last interglacial and glacial sea-level high- and low- stands, respectively, are both absent on the southern flank. It was thus inferred that the collapse occurred after the formation of the more recent submarine wave-cut platform; which may have formed during the LGM-associated sea-level low-stand.

The timing of the collapse is also associated with the K-Ar age of a basalt sample (Sample Lab Code 82-229), collected from the densest part of the least weathered lava flow from the southwest coast at Fatatele point reported in McDougall (2010) (Figure 34). An age of 20 ± 10 ka at one standard deviation was obtained for the sample. This indicates that the island was volcanically active around that time; which was interpreted to be pre-collapse in age.

5.2.4.2 *Nature of collapse*

The association of the collapse with the timing of the LGM is interesting. The LGM is the most recent period in Earth history characterised by global ice-sheet maxima and sea-level and temperature minima (Lambeck et al., 2001; Clark et al., 2009).

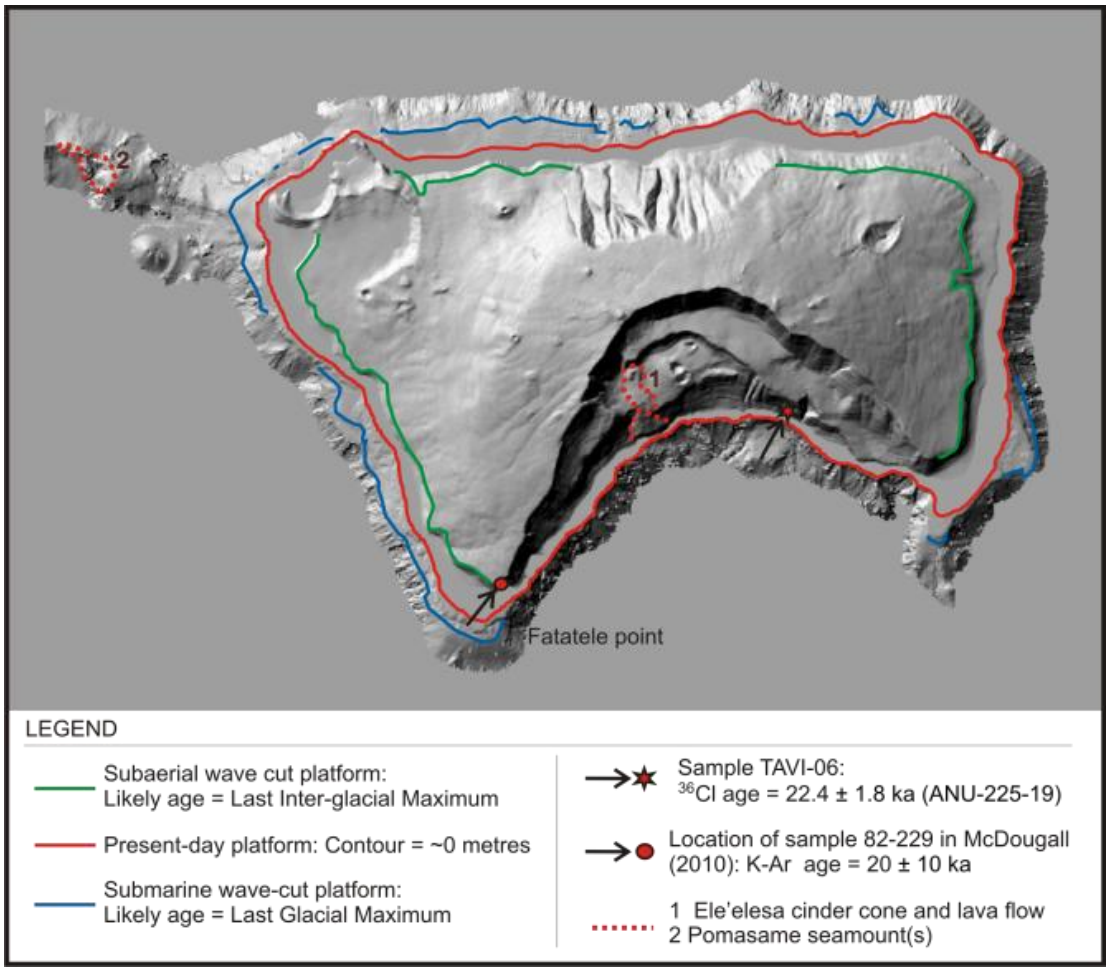

Figure 34: Digital elevation model of Ta'u showing locations of reported ages and geomorphic features (DEM data obtained from the National Park of American Samoa in 2008).

Paradoxically, it is generally accepted that large-scale volcanic flank collapses typically occurred during (or were associated with the onset of), warmer, wetter, interglacial period climates and rising sea-levels (McMurty et al. 2003; McGuire, 2012).

However, McGuire (2012) cautioned that this acceptance does not dismiss the likelihood of collapses occurring during colder, drier climates and lower (or rapidly falling) sea-levels. He suggested that a sudden reduction over a few hundred years or so of the buttressing effect as huge volumes of water were removed from the flanks of a volcano could favour collapse. Rapid changes between cold and dry to warm and wet climates, and vice-versa, were also suggested to have an effect on rapid sea-level changes which in turn would increase collapse potential. This process though is ambiguous, because

there is little evidence to suggest a distinct association between rapid climatic-eustatic sea level changes and their influence on collapse behaviour.

Nevertheless, the interpretation here that the Ta'u collapse occurred after sea-level reached its minimum at this site suggest that it occurred during the onset of warmer climes and rising sea-level; even though post-LGM sea-level rise is thought to have only commenced about 16 ka (Lambeck et al., 2001). Further investigation is needed to resolve this enigma.

The likelihood of the collapse being triggered by an earthquake was investigated in Williams (2009). It was suggested that the potential for collapse being triggered by an earthquake with similar peak ground accelerations (0.4 g) to those in Samoa's seismic history was low. However, this interpretation did not account for the long-term effects of earthquakes experienced over geologic time. Further investigation is needed to understand the likely long-term seismic influence on collapse potential.

In Williams et al. (2012), it was suggested that the lava flows from the intra-caldera cinder cone which flow over the Ele'elesa scarp were possibly indicative of an association between the eruption and the collapse. Although this could be the case, it is also likely that the eruption could be much younger. In the absence of a geochronological age for this eruption, an association between the two cannot be stated definitively.

Conversely, the collapse age is associated with the timing of likely active volcanism in the area reported in McDougall (2010). His suggestion that the timing of this volcanism was pre-collapse in age is also likely; implying that volcanic-related processes (e.g. Hart et al., 2000; van Wyk de Vries et al., 2001; Ward, 2001; Walter et al., 2005; Konter and Jackson, 2012), may have been associated with triggering the collapse. However, the large uncertainty of ± 10 ka for the age of this volcanism limits a definite association with the ^{36}Cl collapse age reported here.

5.2.5 Conclusions and Hazard Implications

The ^{36}Cl surface exposure age of 22.4 ± 1.8 ka is interpreted to be indicative of the age of the Ta'u flank collapse. Further, it is concluded that the depiction of Ta'u as a complete edifice in Wilkes (1849) was incorrect.

Currently available geochronological and geomorphic evidence in Williams (2009), McDougall (2010), Williams et al. (2012) and this study, suggests that a volcanic-related mechanism is likely to have been responsible for triggering the collapse. Dating the upper and adjacent scarps as well as the Ele'elesa cinder cone flow would clarify this.

Whilst it is recognised that climatic-eustatic conditions during the LGM may have played a role in influencing flank failure, the potential for these processes to trigger collapse is not well understood. More investigation is needed to understand, verify, or dismiss this possibility.

The landslide-tsunami associated with the collapse modelled in Williams (2009) and Williams et al. (2012), is confirmed to not have been a hazard at the time of its occurrence. This is because the Samoan and surrounding Island Nations were first inhabited about 3 ka or so (Petchey, 2001; Bedford and Sand, 2007; Reith and Hunt, 2008; this study).

Nevertheless, evidence of likely active volcanism associated with the timing of the collapse (McDougall, 2010; Williams et al., 2012), coupled with the recent eruption of the Pomasame submarine cones in 1866 – 1867 (Turner, 1889), imply that volcanism could presently be in a temporary state of quiescence. Thus there may be a present and future eruptive hazard. Coupled with the understanding that large-scale flank-collapses typically occurred (or tend to occur) during warmer, wetter, interglacial climates comparable to present and projected conditions (McGuire, 2012), the likelihood of a future collapse exists.

Further, there is a possibility that the northern flank could undergo similar large-scale collapse and generate a tsunami with likely regional impacts. More investigation is required to understand the nature, likelihood, and hazard implications of such an event occurring in future.

It is suggested that the Ta'u flank-collapse represents similar processes in comparable volcanic settings, and that analogous geomorphic features on other volcanic islands and seamounts (e.g. Terry and Goff, 2013) (Figure 35) in the Pacific likely represent forensic signatures of landslide-tsunamis in the past. There is a need to identify and date such features, in order to further spatial and temporal understanding of these processes. Identifying flank features that have not yet failed and assessing likely mechanisms that could potentially trigger failure is important. This would enable more confidence in interpreting the hazard potential of similar flank-collapses in future – a risk presently under-represented.

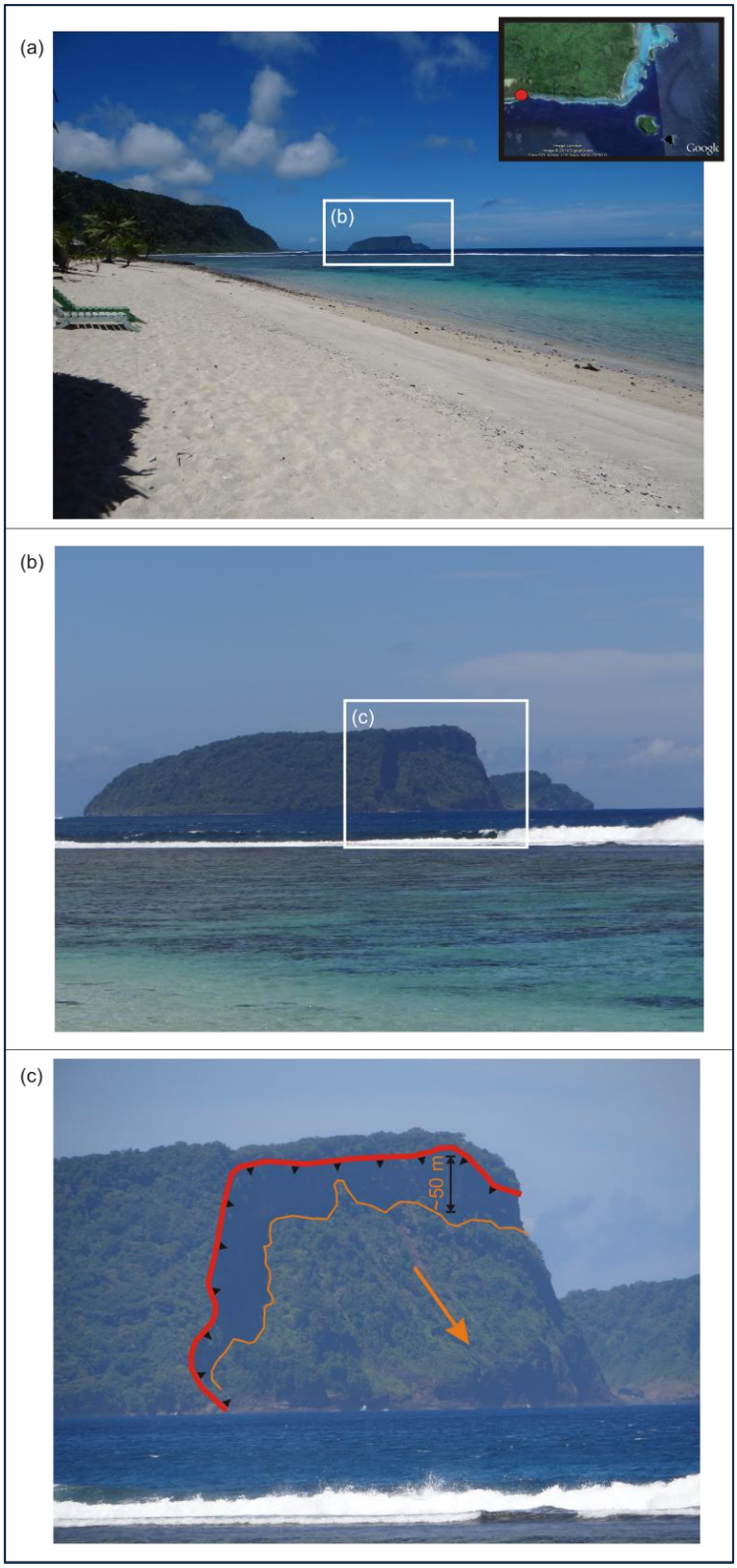

Figure 35: Potential local landslide-generated tsunami hazard off Nu'utele Island, southeast Upolu (a) View of Nu'utele Island from Faofao beach; (b) Nu'utele Island; (c) Head-scarp (red line) and potential landslide block (orange line). Red dot on inset map is Faofao beach.

5.3 Case Study II: High-elevation calcareous deposits on Central Upolu

5.3.1 Synopsis

A calcareous boulder measuring > 1 m across its longest axis and possibly weighing up to a ton was found by a local SPREP (Secretariat of the Pacific Regional Environment Programme) collaborator ~464 m elevation in the central volcanic rift zone on Upolu (Figure 36). This boulder is located at 13^0 55'10.2 S, 171^0 44'19.1 W, and is the subject of various hypotheses regarding the existence of high elevation marine limestone deposits on Upolu (i.e. human influenced, eustatic and/or uplift, meteoric, hydrothermal, tsunami).

This case study is a rapid reconnaissance review conducted to determine the most likely origin of the deposit. A likely hydrothermal or meteoric origin is suggested, which corroborates the hypothesis of Stair (1894). In the context of this thesis, this finding provides grounds to reduce the possibility of high elevation (> 460 m), extreme inland inundation (> 8 km), tsunami deposits on Upolu and in the archipelago.

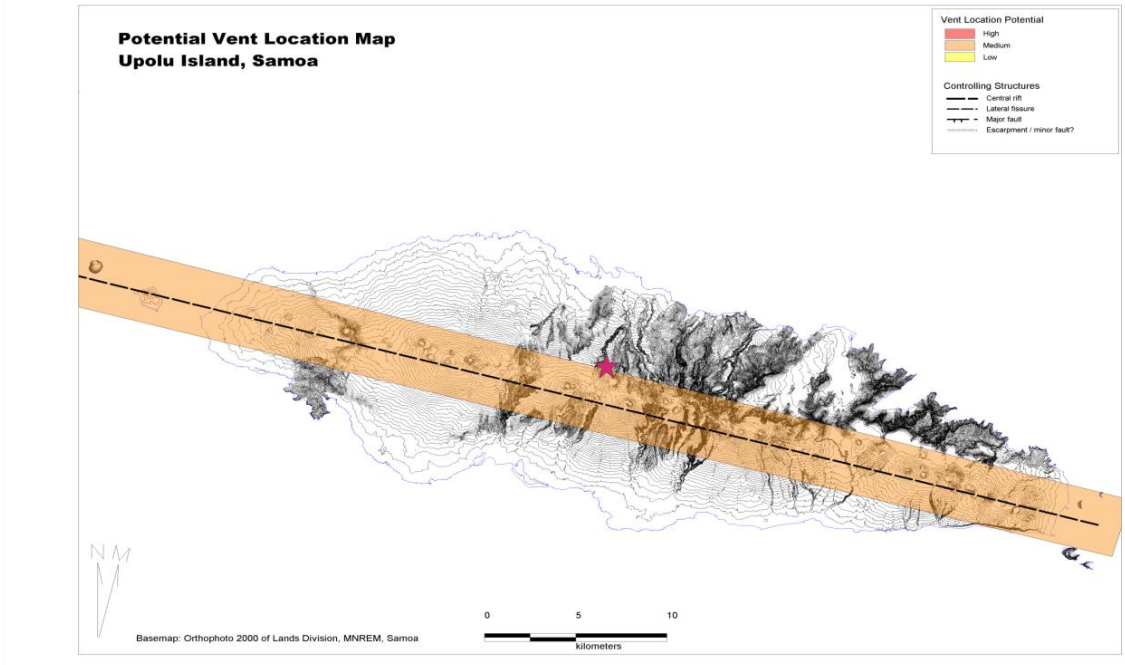

Figure 36: Location of Fale o le Fe'e (pink star) relative to the central Upolu volcanic rift (after Cronin et al., 2006).

5.3.2 Discussion Note

The deposits are located approximately 9.5 km inland of Apia, ~30 – 50 m upstream of the Fale o le Fe'e ruins (Abode of Fe'e – War God of the A'ana realm in prehistoric Samoa) (Stair, 1894). Indigenous tradition indicates that marine calcareous boulders in this area were transported by Fe'e to the site where he made his abode. Stair (1894) interpreted the presence of small calcareous specimens found in this area to have formed from terrestrial processes, and dismissed the possibility of a marine origin.

New Zealand naval explorers to this area in the 1950's reported a >10 ton calcareous boulder interpreted to be marine limestone found at ~458 m elevation (Stearns, 1955; Kear and Wood, 1959). This was suggested to be indicative of either; 1) possible transportation by humans for building purposes at the site (Kear and Wood, 1959), or, 2) large-scale emergence possibly as a result of uplift, or eustatic movements much greater than those attributed to Pleistocene glacial-interglacial cycles (Stearns, 1955; Nunn, 1998).

The possibility of high elevation marine deposits at this site, in the context of this thesis, also suggests a possible tsunami origin. A sample (WK30088) from a charcoal deposit found at 30 cm depth in a test pit adjacent to the ruins has a calibrated radiocarbon age of 520 – 320 cal BP (AD 1430 – 1630) (Table 1). This suggests that the site was inhabited along with the existence of calcareous deposits in the area during this period; which overlaps with the timing of the AD 1199 – 1469 tsunami and the AD 1469 – 1672 cyclone (Chapter 3.4.7). If WK30088 is possibly affected by in-built age, then it would have a younger age and may instead correlate with the AD 1690 – 1830 tsunami.

However, no further reports on the nature of the possible marine limestone reported in the late 1800's and 1950's exist. Thus the assumption is made that the calcareous deposit in Figure 37 is associated with the calcareous boulders discovered in this area and/or interpreted by earlier scholars and local inhabitants.

A review of the literature suggests that the deposits are most likely non-coastal in origin. For example, Stair (1894) reported that the deposits were found in the stream bed, and upon splitting a specimen said by local guides to be coral, they observed various leaves and small twigs embedded in it. Stair (1894) attributed the specimens to a substance formed in the neighbouring stream. Similarly, Stair (1894) concluded that larger deposit blocks found further upstream were calcareous spar of a more compact formation. Finally, Stair (1894) observed stalactites forming upon the surface of a rock in a nearby place that was once a large natural basin at the foot of a precipice into which the stream once fell from above, forming a small cascade.

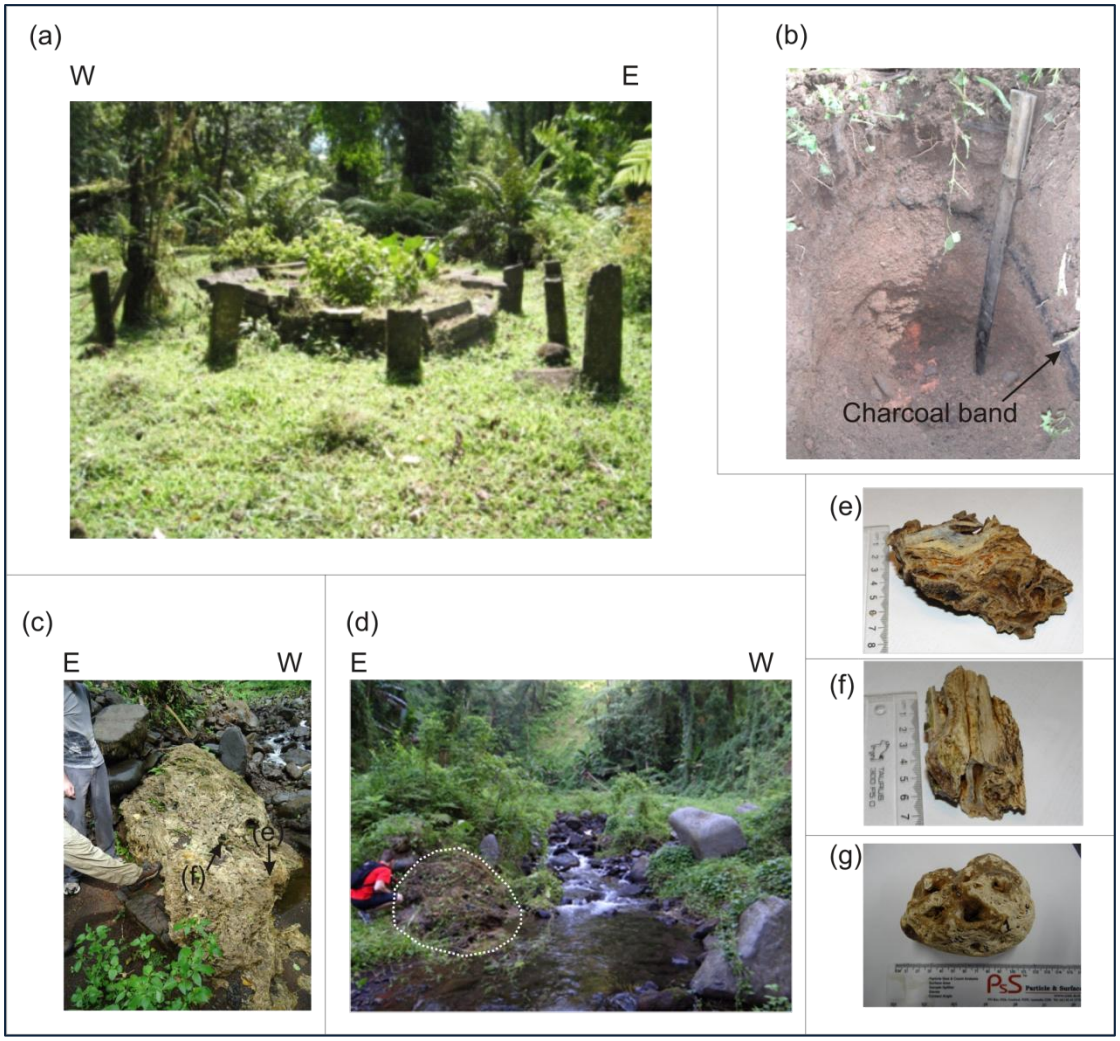

Figure 37: (a) Fale ole Fe'e ruins; (b) Charcoal layer associated with sample WK30088 which dates to 500 – 300 cal BP (Table 1); (c) Calcareous deposit ~30 – 50 m upstream of Fale o le Fe'e ruins (Photo by Paul Anderson, pre-Cyclone Evan in 2012; (d) Same deposit in (c) taken in April 2014; (e) Sample of the main deposit in (c) and (d); (f) Calcareous cast wood sampled from the main deposit in (c) and (d); (g) Calcareous cobble obtained by Paul Anderson from the river bed further down-stream.

These observations suggest in-situ formation, possibly due to either hydrothermal or cold freshwater carbonate forming processes. Further, Stearns (1955) reported that no recognizable algae were observed in sample thin sections, even though recognizable fossil coral appeared to be recrystallized in the limestone block observed in the field. This strengthens the hypothesis of Stair (1894) that the calcareous specimens found in the area were in-situ formations as opposed to having a coastal marine origin. Two unsuccessful field campaigns by Nunn (1998) to locate the calcareous specimens in the area limit any further evidence in the literature of their likely origin subsequent to the report by Stearns (1955).

Samples collected in this research together with field reconnaissance in the Fale o le Fe'e nearby stream provide preliminary evidence of transported cobbles found in the stream bed, most likely eroded from

an in-situ source (Figure 37c, 37d). The deposits most likely formed by either hydrothermal (e.g. travertine; D. Gravley and J. Cole, pers. comm., 2014) or ambient-freshwater (e.g. tufa; Pedley, 1990) carbonation.

It is difficult to determine the nature of the deposit based on available evidence as its general characteristics, including formation context, are consistent with both end-members (e.g. hydrothermal travertine or ambient-freshwater tufa). For example, the in-situ outcrop in Figure 37c has structural, textural, and contextual similarities consistent with both travertine and tufa described in comparable freshwater environments (Pedley, 1990; Viles and Goudie, 1990; Ford and Pedley, 1996; Freytat and Plet, 1996; Pedley et al., 1996; Merz-Preiß and Riding, 1999; Drysdale et al., 2003; Chen et al., 2004; Golubić et al., 2008; Shiraishi et al., 2010) (Figure 37).

The cast wood sample in Figure 37f, 38b, which appears to have been formed by either hydrothermal or ambient freshwater carbonation Ford and Pedley (1996), supports a non-coastal marine origin. Coupled with the environmental context of formation and earlier descriptions by Stair (1894), it is very likely that the deposits in the area are either travertine or tufa formations. The location of the deposit relative to the central Upolu volcanic rift (Cronin et al., 2006), as well as to the catchment headwaters, suggests that it could be travertine, tufa, or a carbonate formation between these two end-members.

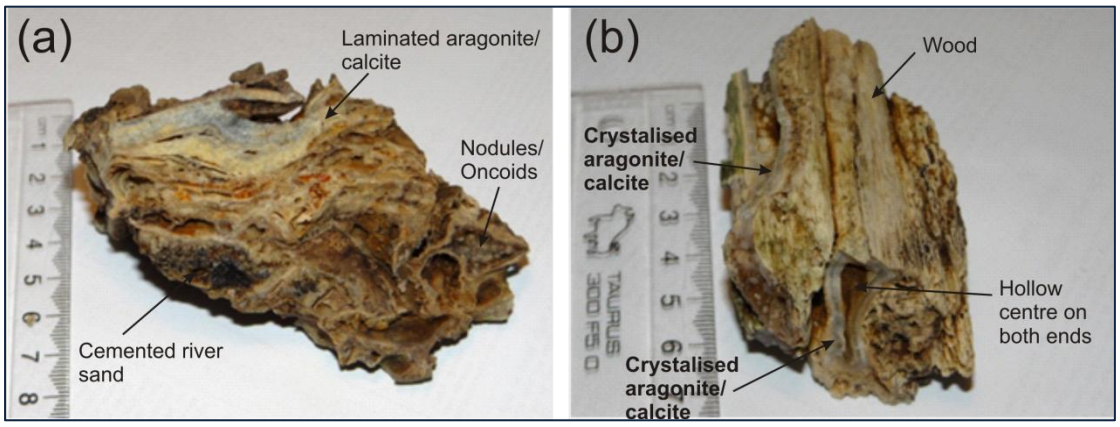

Figure 38: Outcrop samples: (a) crystallised laminations with cemented river sand and nodular/onchoidal precipitates; (b) crystalised cast wood.

It could be assumed that similar deposits are found in analogous river catchments along the Upolu rift, as well as in similar environments on other islands in the archipelago (e.g. Savai'i, Tutuila). Further, rejuvenated volcanism on this island commenced ~0.4 Ma (Koppers et al., 2011), implying that potential geothermal activity (either fossil or active), within this period may have played a role in their formation.

Based on the available evidence presented in this thesis, however, a distinction cannot be made, other than that it is most likely non-coastal marine in origin. Hence, the possibility of a >460 m elevation tsunami deposit on Upolu is reduced.

5.3.3 Conclusions

Ongoing research associated with the samples collected from this site will provide a more definitive resolution as to the origin of the deposits (e.g. isotope analysis, thin sections). Samples in Figure 39 below would provide an indication of comparative differences. Future mapping and investigation into adjacent tributaries, catchment areas, and in similar environmental contexts on other islands in the archipelago would provide an indication of the extent and characteristics of these formations.

Available evidence suggests that the deposits are non-tsunami or coastal marine deposits. Most likely they were formed by either hydrothermal, meteoric, or a combination of these processes. Determining the origin and extent of these deposits may have further implications on their environmental (e.g. tufa palaeoenvironmental indicator), or development (e.g. travertine geothermal or volcanic hazard) implications.

Figure 39: Comparative standards on known environment of formation. Calcitic column at Paia lava-tube cave, Savaii, and coral from the Ta'u AD 502 – 930 tsunami.

5.4 Case Study III: The Fagali'i charcoal

5.4.1 Synopsis

This case study explores the implications of charcoal sample WK30087 from Fagali'i (Table 1) for some of the interpretations presented in Chapter 3 of this thesis. This sample was used as a time marker to infer

the likely age of the oldest identified palaeotsunami presented in Chapter 3.4.7. Particular attention is given to its origin, as well as the possibility that the sample could be affected by an in-built age.

An anthropogenic origin for the charcoal is proposed, which substantiates an approximate 3,000 year tsunami hazard history in the Samoan region. The implications of a charcoal in-built age effect on the timing of the older palaeo- tsunami and cyclone events presented in Chapter 3.4.7 is also considered.

5.4.2 Introduction

The implications of a new ^{14}C age obtained from a charcoal specimen found towards the base of a 3 m core sampled from Fagali'i village on northern Upolu, Samoa, are examined. A calibrated mean age of 3,326 ± 60 cal BP (3,385 – 3,265 cal BP [68.2% prob.]; 3,444 – 3,215 cal BP [95.4% prob.]) was obtained for this sample. A re-calibrated result for this specimen incorporating a likely in-built age of 300 ^{14}C years produces a likely true calendar mean age of 2,914 ± 60 (2,976 – 2,852 cal BP [68% prob.] (3,065 – 2,790 cal BP [95% prob.]), prompting questions about its palaeo-environmental origin.

Did it form from a natural forest fire that may have been associated with climatic extremes during that time or was it anthropogenically formed? If the latter, then a potentially Lapita-derived cultural origin is implied. Both scenarios are discussed, and the suggestion is made that this newly-acquired date demonstrates the existence of human presence at Fagali'i contemporaneous with earliest colonization in Samoa around 3,000 cal BP.

5.4.3 Discussion

A calibrated mean ^{14}C age of 3,326 ± 60 cal BP (Wk30087: 3,385 – 3,265 cal BP [68.2% prob.]; 3,444 – 3,215 cal BP [95.4% prob.]) was obtained on a taxonomically unknown charcoal sample found on the north coast of Upolu Island, Samoa (Table 1; Figure 40). The sample was discovered during the present research, and was obtained from a blackish peat at 2.87 m depth in a 3 m core sampled from a wetland approximately 150 m inland of the Fagali'i village coastline. The taxonomy of the charcoal is not known, and the in-built age could possibly be up to 300+ ^{14}C years (Allen and Wallace, 2007; Nunn and Petchey, 2013). In this case, its recalibrated conventional radiocarbon age (CRA) could be as recent as 2,812 ± 50 BP (2,976 – 2,852 cal BP [68% prob.]; 3,065 – 2,790 cal BP [95% prob.]).

It is important to note that the data presented in Allen and Wallace (2007) demonstrate that a 300+ ^{14}C in-built age was possible in 20% of the wood charcoal samples that were not identified to originate from short-lived species. The remaining 80% had relatively shorter in-built ages. This situation is relevant to the discussion here because it is possible that sample Wk30087 originated from a short-lived species and that its in-built age is less than 300+ ^{14}C years. Nevertheless, even if an in-built age of 300 ^{14}C years is factored into the calibration, Wk30087 represents the oldest wood charcoal age ever presented from this part of the Samoan archipelago and raises questions about its origin.

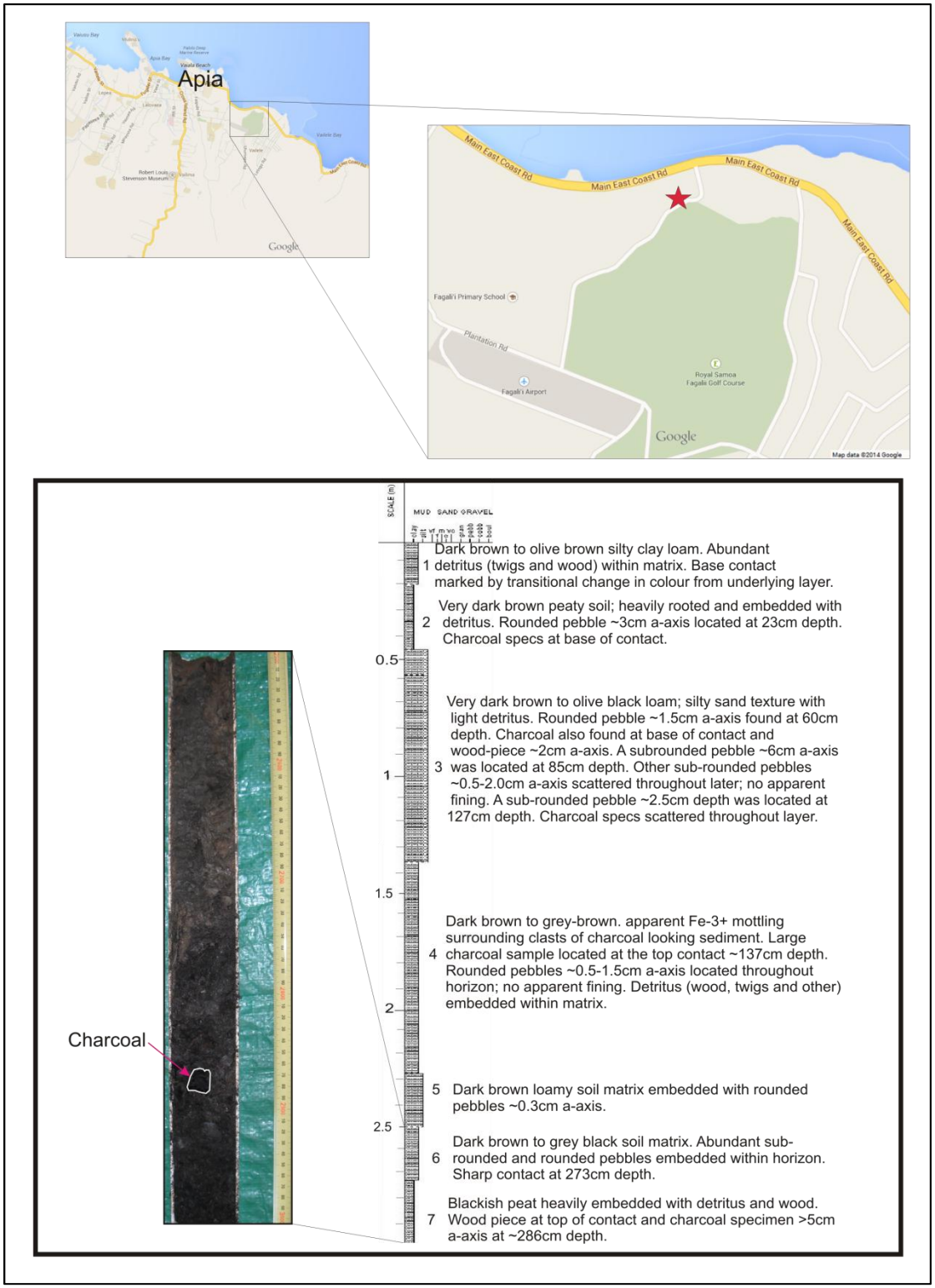

Figure 40: Location of core site of the Fagali'i core (red star), the Fagali'i core log and the strata which Wk-30087 was sampled (250 – 300 cm depth).

Firstly, it is possible that the charcoal resulted from a natural forest fire which was perhaps associated with drought conditions during an extreme climatic event (eg. El Niño Southern Oscillation). However,

Fagali'i village is not within the northwest drought-prone region of Samoa (Australian Bureau of Meteorology and CSIRO 2011) and the present climate range in the Samoan archipelago has largely been in place for the past 4,000 years or so (Nunn, 2012).

This generally sees northern and northeastern Upolu receive an average annual rainfall of around 3,000 mm and implies that the chances of natural forest fires occurring in the Fagali'i area over the last 4,000 years are low. While this cannot be presently substantiated due to the lack of palaeo-environmental studies in northern Upolu, such circumstances lead to the consideration that anthropogenic activity offers a more reasonable origin for the charcoal.

The earliest ^{14}C age related to early human settlement is 2,970 – 2,640 cal BP (NZA-5800 [95% prob.]; 2,838 – 2722 cal BP [68% prob.]) and was obtained from a turtle bone associated with a Lapita pottery deposit at Mulifanua, NW Upolu (Petchey, 2001; Rieth and Hunt, 2008) (Figure 41). The oldest taxonomically unidentified charcoal samples of potential cultural significance ever reported from the Samoan archipelago, were calibrated ^{14}C ages of 3,389 – 2,749 cal BP (Beta-48049: 95% prob.) from 'Aoa on Tutuila Island (Clark 1993), and 3,350 – 2,750 (Beta-35601: 95% prob.) from To'aga on Ofu, Manu'a Group (Kirch, 1993b; Rieth and Hunt, 2008).

However, as opposed to sample WK30087, both of the ones from 'Aoa and To'aga were obtained from deeply buried colluvial environments (Kirch, 1993a; Clark and Michlovic, 1996). This led Clark and Michlovic (1996) to reject the yielded charcoal ages due to the possibility of the charcoal having originated from old wood, or possibly being affected by an admixture with older pre-site material. These possibilities probably resulted in the calibrated age distributions spanning up to ca. 650 cal years. Such large probability distributions led Rieth and Hunt (2008) to reject the dates since they did not allow the precision necessary for identification of initial colonisation.

The very large probability distributions of both the 'Aoa and To'aga charcoal ages coupled with possible in-built age effects would have a significant impact on the reported results, leading to potentially incorrect interpretations. Therefore they cannot be considered further as being representative of the oldest specimens of cultural origin.

The ^{14}C age presented for Wk30087, which incorporates a possible in-built age of 300 ^{14}C years, overlaps at 2 sigma with the accepted age of the Lapita cultural settlement at Mulifanua, and suggests they are contemporaneous. This would yield a probable age estimate of around 2,970 – 2,790 cal BP for earliest colonization in Samoa. Further, the contemporaneity of this estimate with earliest Lapita colonisation in Vanuatu, Fiji and Tonga (e.g. Clark and Anderson 2009; Burley et al. 2012; Nunn and Petchey 2013), supports the accepted timing of initial colonisation in this region of no earlier than 3,000 cal BP (Bedford and Sand, 2007).

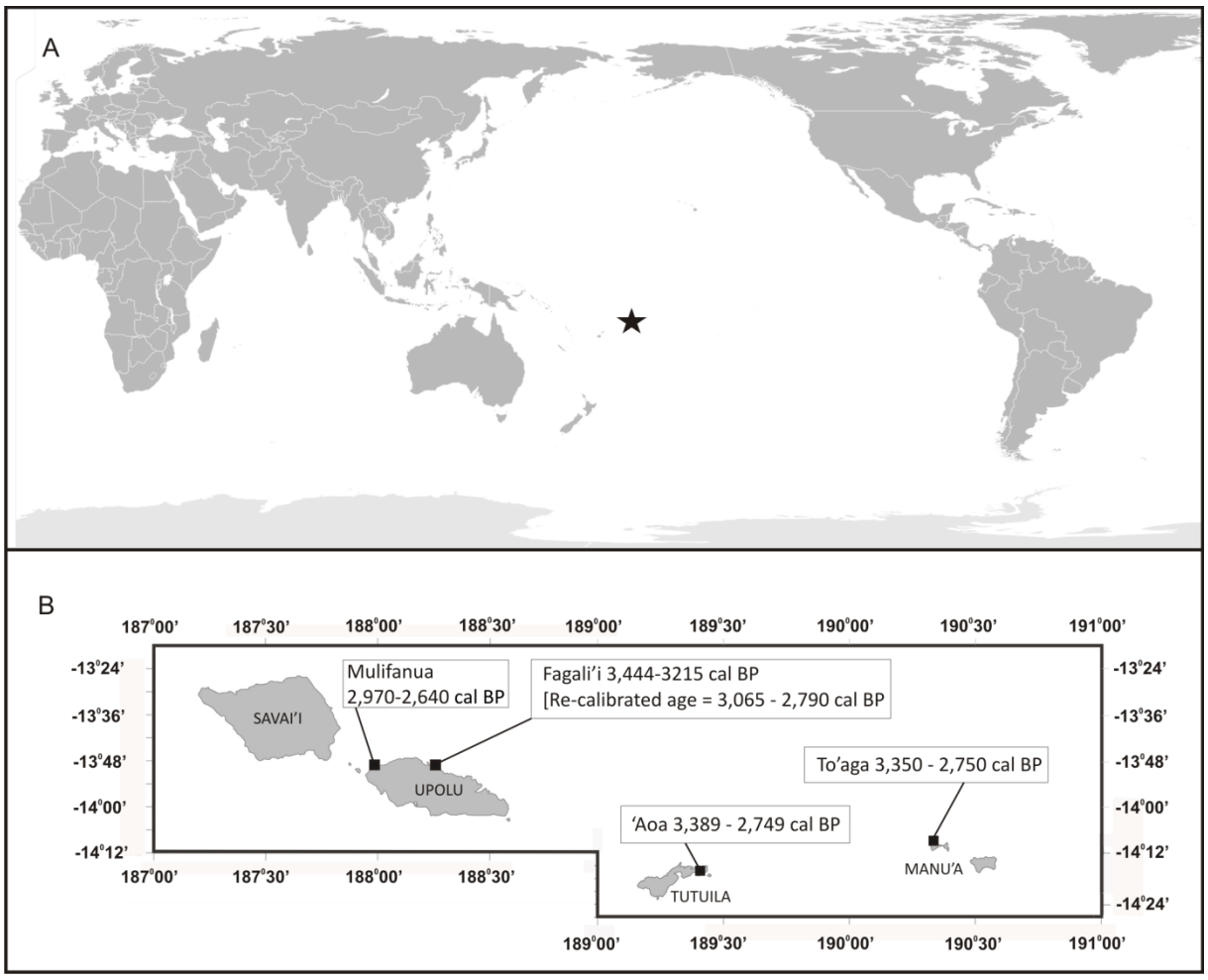

Figure 41: A) Location of the Samoan Islands (black star). B) Locations of the ^{14}C ages at Mulifanua (95% prob.) and Fagali'i (95.4% prob.) on Upolu Island, 'Aoa (95% prob.) on Tutuila Island, and To'aga (95% prob.) on Ofu Island, Manu'a. The re-calibrated age for Fagali'i incorporates a possible in-built age of 300 ^{14}C years. The ages from 'Aoa and To'aga sites are shown for reference, but are not considered indicative of earliest settlement. Base map sources: A) http://pustakalaya.org/images/maps/world_pac.png. B) http://www.ginkgomaps.com.

5.4.4 Summary

Based on past climatic conditions, it is inferred that Fagali'i on the north coast of Upolu Island was, on balance, unlikely to be vulnerable or prone to natural climate-related forest fires over the past 4,000 years or so. Further, it is suggested that the charcoal discovered at Fagali'i most likely represents evidence for human presence along this coast around 3,000 BP. This is contemporaneous with the accepted age of earliest human settlement in Samoa, and it likely corroborates the hypothesis by Green (2002) that Fagali'i might be an area containing Lapita deposits.

More palaeo-environmental, geoarchaeological and taxonomic work at this site is suggested in order to provide a better understanding of the context and true calendar age of the Fagali'i charcoal. This would

help to validate any early cultural presence at this site, and would contribute to understanding early colonisation of the Samoan Islands.

5.4.5 Implications and Conclusions

There exists a real possibility that charcoal sample WK30087 is affected by an extreme in-built age, and that its true calendar age could be up to 425 years younger than its radiocarbon age determined in Section 3.4.5. This would imply that the potential ages of identified MIDs between BC 1375 – AD 502 in Figure 26 could be overestimated, and that these events could in fact be younger, than they are depicted.

However, present evidence also implies that there is a chance that its age in Section 3.4.5 may be a true representation of its calendar age, and that the effect of in-built age on the specimen could be minimal. This then would not conflict with present interpretations of the tsunami and cyclone chronology in Chapter 3, as the inferred ages of events would represent maximum likely estimates for their timing. An appreciation of the likelihood of an extreme in-built age effect on WK30087 relative to present interpretations in this thesis is necessary for future consideration.

At the very least, sample Wk-30087 demonstrates that Fagali'i most likely contains traces of earliest colonization in the Samoan Islands. Further, the fact that it was found in association with the oldest tsunami MID identified at Fagali'i suggests that the tsunami was a hazard at the time of its occurrence. This further implies that the north coast of Upolu was (or is) likely susceptible to tsunami impacts not experienced in these areas in the 2009 SPT.

5.5 Chapter Summary

The case studies presented in this Chapter demonstrate some of the knowledge gaps and enigmas associated with understanding the long-term tsunami hazard in the Samoan Islands. Case Study-I provides an indication that landslide-tsunami processes can occur in the archipelago with possible far-reaching regional impacts.

Case Study-II underscores the importance of relevant data acquisition to enable careful interpretation, and in this case, dismissal of any likely tsunami association with high-elevation calcareous deposits in these islands.

The uncertainty surrounding the true calendar age of WK30087 in Case Study-III, does not undermine the crucial fact that its discovery in association with a tsunami MID provides evidence of an approximate 3,000 year tsunami hazard history in the Samoan region.

CHAPTER 6: SYNTHESIS & CONCLUSIONS

6.1 Overview

The overarching aim of this research was to determine the long-term tsunami hazard in the Samoan Islands, and to evaluate evidence of the likely long-term risk posed by these processes in this region. Specific challenges and limitations in addressing these aims are presented in this thesis. Data availability and subsequent interpretive limitations, coupled with time and financial constraints concerning the acquisition of new additional data were the predominant challenges encountered. Nevertheless, the research aim was achieved through carefully designed Chapter objectives that facilitated the use of available data to generate new information. Further, the application of relevant inter-disciplinary techniques to yield new data that provided alternative perspectives enabled adequate research conclusions to be drawn. A summary of key thesis outcomes is presented in this Chapter, including possible directions for further research that would build on the findings presented here.

6.2 Summary of Principal Research Outcomes

6.2.1 Tsunami deposits in the Samoan Islands

Distinct sedimentary and geochemical characteristics of the 2009 SPT deposit were identified at Satitoa on southeast Upolu. Sedimentary characteristics included apparent differences in LOI and grain size trends relative to underlying pre-2009 SPT soil. Similarly, the trend differences in elemental ratios between marine- and terrestrially- dominant elements showed similar distinctions. Ultimately, the 2009 SPT deposit at Satitoa provided the most adequate analogue in this study of a distinct tsunami signature in the Samoan geologic record.

Similar proxy characteristics including ^{210}Pb radiometric dating enabled the identification of the 1990 and 1991 Cyclones Ofa and Val deposits at Falealupo. The apparent differences in proxy trends for these deposits compared to those at Satitoa provided distinguishable cyclone analogues in the geologic record.

Comparison of these analogue tsunami and cyclone deposit trends with other MID trends deeper in the geologic record facilitated a technique for distinguishing their most likely origin. Geochronological age data coupled with stratigraphic correlations enabled likely MID associations to be made within the geological record.

The available evidence, while limited, was sufficient to develop a baseline tsunami and cyclone chronology model for the Samoan archipelago. Although subject to future refinement and reinterpretation, the model established provides an adequate foundation to better understand long-term tsunami patterns recorded in the geologic record. Coupled with known and inferred analogues of tsunami impacts over the past 3,000 years, a deeper appreciation of the hazard could be assumed. This then could be applied to prioritizing target tsunami mitigation and risk reduction indicators in long-term coastal management plans.

Similar applications using the established cyclone chronology can be applied to long-term climate mitigation plans, particularly in the context of extreme events. The association of likely cyclone MIDs with the AD 1300 event (an approximate 200 year climatic episode in Earth history characterized by cool, dry climate and intense storminess), demonstrates the long-term pattern of higher-frequency coastal hazards. That is, cyclone signatures preserved in the geologic record suggests associated Category 3 or higher cyclone intensity origins. Such events are known from the historical record to have had disastrous impacts in the Samoan region (e.g. 1991 cyclone Val). Therefore it is important to apply an all-hazard management approach within the shorter- and longer-term coastal hazard contexts to assist collective risk reduction.

Numerical modeling of the pattern of resonance energy of the 2009 SPT (although limited by available input data), and comparison of locations exhibiting high resonance amplification with areas containing preserved 2009 SPT deposits, presented an additional proxy for tsunami MID investigation. The use of hypothetical tsunami resonance data would assist in better understanding the palaeotsunami deposit characteristics in Chapter 3. Further, analogue and/or hypothetical tsunami resonance modeling in analogous coastal environments may facilitate the identification of target locations for tsunami deposit investigation.

6.2.2 Tsunami Magnitude, Intensity and Frequency

The established tsunami chronology model coupled with associated proxy signatures specific to a particular event enabled likely estimates of tsunami magnitude, intensity and frequency to be made. This was particularly so for events likely corresponding to a local NTSA source. A probable baseline tsunami recurrence interval of 87 – 637 years was calculated for NTSA sourced tsunami of likely equivalent or greater magnitude and intensity to the 2009 SPT.

Despite the limitations in yielding this estimate as well as its large uncertainty, it is held here to be a likely true indication of the long-term frequency pattern of NTSA associated tsunamis. A worst-case scenario deduced from this calculation would be an expected NTSA associated tsunami of similar or greater magnitude to the 2009 SPT in the next 90 years or so (~AD 2100). This could be used as a

baseline for long-term coastal hazard management planning and mitigation, with similar applications to climatic period frequencies associated with intense cyclones.

6.2.3 Anomalous tsunami cases

Perhaps the most anomalous tsunami in the historical record is the AD 1883 coupled cyclone and tsunami reported in Parraras-Carayannis and Dong (1980) (see Section 3.5.4.6 of this thesis). The local impacts described for this event on east Savaii suggest a tsunami association. However, this cannot be substantiated based on evidence presented in this thesis. This particular event poses an enigma within the historical tsunami and cyclone record in Samoa. Further, it provides the opportunity for further investigation into a likely unique situation in which a tsunami and cyclone impacts may have possibly coincided, without any apparent knowledge of it in the oral record.

Such instances in the Samoan historical record (c. 1830 – present), which seemingly should be common knowledge, perhaps reflect the impact of the AD 1918 influenza epidemic in Samoa (Okal et al., 2011). This disaster resulted in the loss of approximately 33% of the local Samoan population at the time, many of whom were the young and elderly. It could be assumed that many elders (traditional knowledge holders) were lost in this event. Further, it coincided with the timing of World War I and the end of the official 15-year German political administration over Samoa in 1914. This also marked the official start of New Zealand's 47-year political administration over Samoa. Such rapid changes in local cultural dynamics perhaps resulted in historical events prior to this period being lost within the local oral record.

The Fale o le Fe'e case study demonstrates the possible linkages between indigenous knowledge and interpretations, tsunamis, and the importance of acquiring adequate data to better understand enigmatic deposits in the geologic record. The contemporaneity of occupation at this highland area with identified tsunami and cyclone hazards provides a possible link. The indigenous interpretation that calcareous deposits found at the site were transported up an adjacent valley by the war-god Fe'e (cuttlefish or octopus in English), provides another clue. These calcareous deposits were preliminarily determined here to have formed by either in-situ highland hydrothermal or meteoric processes as opposed to a marine origin. Nevertheless, one might assume that corresponding inhabitants, in abandoning the coast and upon reaching the highland site, associated the presence of calcareous deposits in the area with a coastal origin based on its similar appearance to coral.

The 22.4 ± 1.8 ka landslide-tsunami event in Ta'u demonstrates the potential for similar processes occurring in the archipelago. While this particular event was determined to have not been a societal hazard at the time of its occurrence, it does demonstrate the knowledge gaps and present limitations in understanding these types of potential hazards in this region. Further investigation into these processes within the broader long-term hazard context should be considered with importance.

6.2.4 Ethno-archaeological and Indigenous Knowledge Implications

The oldest tsunami identified herein the geologic record was contemporaneous with earliest colonization in the Samoan Islands around 3,000 cal BP. The fact that cultural evidence (i.e. charcoal) was found in association with this event suggests that it was a hazard at the time of its occurrence. The contemporaneous associations suggest an alternative possibility of the processes that may have influenced the presently scant cultural evidence prior to 2,500 cal BP in these islands. Further, it offers an alternative possibility of processes that may have influenced the apparent shifts in cultural dynamics inferred from the ceramic record within the archaeological literature.

Similar interpretative syntheses were made between other identified tsunami and cyclones in the geologic record with ethno-archaeological records (Section 3.5.6). For the case of the AD 1199 – 1469 tsunami, possible evidence of this event could be identified in the Cook Islands geologic record, and would suggest a tsunami with far-reaching regional impacts. Although no definitive cause-effect correlations can be established between these processes at this stage, the contemporaneous associations provide the opportunity for designing future investigations to test, validate, or dismiss the possibilities presented here.

In the context of present and future mitigation, modern disaster arrangements at all levels are designed to ensure that the risk of such possible cultural responses to a tsunami (and cyclone), is prevented or reduced.

6.2.5 Tsunami Hazard Reviewed

The findings in this research demonstrate an intrinsic long-term tsunami hazard history in the Samoan region since earliest colonization in this archipelago around 3,000 cal BP. Evidence for both near-field and far-field tsunamis are present in the geologic record. Moreover, the likely association of near-field events with the NTSA source region suggests that events of magnitude comparable to the 2009 SPT recur with a minimum 90-year interval. Evidence of tsunamis likely sourced from this region found on northern parts of Upolu and Savaii in the geologic record suggests events of greater magnitude than the 2009 SPT have occurred in the past.

The contemporaneity of some of the past tsunamis identified in this study with palaeo-tsunami evidence in the broader Pacific (e.g. AD 1199 – 1469 with the AD 1450 TKT tsunami in Goff et al., 2012) suggests that they could be associated. This would further imply that the connected events could be related to tsunami with far-reaching regional impacts of greater magnitude than the 2009 SPT, assuming an NTSA near-field source within the Samoan context. Also, the possibility of far-field events cannot be dismissed, and requires further investigation.

Ultimately, the information provided in this thesis facilitates a deeper appreciation for tsunami (and cyclone) hazards in the Samoan region. In its current form, the information could be applied to assist local planning and prioritization of long-term coastal mitigation and risk reduction considerations. The techniques used in this research could also be applied to analogous coastal environments in other countries to assist long-term mitigation at the regional level. These techniques could be developed and used in conjunction with other techniques that fell beyond the scope of this study.

6.3 Directions for further research

While more work is needed to validate and constrain the tsunami and cyclone chronology in the geologic record presented here, the current model forms a baseline to build upon. Further, a number of subsequent questions emerged surrounding the contemporaneity of events identified in the geologic record with certain cultural dynamics in the ethno-archaeological record.

Specific recommendations for future studies and directions for building on the findings in this thesis are offered below. These are ranked, respectively, according to geoenvironmental, modeling, and socio-cultural themes.

6.3.1 Geoenvironmental research directions

1. The proxy data limitations discussed in Section 3.6, which will not be repeated here, form specific objectives in which to design and implement targeted investigations to address them. Additionally, tsunami deposit taphonomical studies at the sites investigated in this thesis would provide a better understanding of deposit changes over time (Y. Nishimura, pers.comm., 2014).

2. Further investigation into the landslide-tsunami potential, high-elevation calcareous deposits, and Fagali'i charcoal presented in Sections 5.2.5, 5.3.5, and 5.4.5, respectively, would provide a better interpretation of these situations within the broader local hazard context.

3. Investigating further the possible associations between identified tsunamis in the Samoan geologic record with contemporaneous events in the broader regional database would provide a better understanding of the extent of far-field tsunamis in the region.

4. Although not considered in this study, but nonetheless important, investigating natural coastal hazard interactions (e.g. cyclones, rainfall, landslides, floods, earthquakes, volcanoes, other) and their likely signatures in the geologic record would provide a better understanding of the broader multi-geohazard risk in the Samoan islands.

6.3.2 Modeling research directions

5. Investigating the possible correlations between tsunami resonance and deposits discussed in Section 4.7 would provide a better understanding of the likely sources associated with individual events in the geologic record.

6.3.3 Socio-cultural research directions

6. Further investigation into contemporaneous ethno-archaeological enigmas discussed in Section 3.5.6 would provide a better understanding of the likely impacts and possible influences of coastal hazards on past societies.

REFERENCES

Allen, M.S., Wallace, R., (2007). New evidence from the East Polynesian gateway: substantive and methodological results from Aitutaki, southern Cook Islands. Radiocarbon, 9: 1–17.

Annunziato, A., Franchello, G., Ulutas, E., De Grove, T., (2009). 29 September 2009 Samoa Tsunami. JRC Scientific and Technical Report. JRC 54943, EUR 24068 EN.

Appleby, P.G., (2001). Chronostratigraphic techniques in recent sediments, in: Last, W.M., Smol, J.P., (eds). Tracking environmental change using lake sediments, volume 1: Basin analysis, coring and chronological techniques, Dordrecht: Kluwer Academic Publishers. pp. 171—203.

Australian Bureau of Meteorology and CSIRO. 2011. Climate Change in the Pacific: Scientific Assessment and New Research. Volume 1: Regional Overview. Volume 2: Country Reports. Australian Bureau of Meteorology and Commonwealth Scientific and Industrial Research Organisation. ISBN: 9780643107144.

Barrows, T.T., Almond, P., Rose, R., Fifield, L.K., Mills, S., Tims, S.G., (2013). Late Pleistocene glacial stratigraphy of the Kumara-Moana region, West Coast of South Island, New Zealand. Quaternary Science Reviews, 74: 139-159.

Beavan, J., Wang, X., Holden, C., Wilson, K., Power, W., Prasetya, G., Bevis, M., Kautoke, R., (2010). Near-simultaneous great earthquakes at Tongan megathrust and outer rise in September 2009, Nature, 466, 959—963.

Bedford, S., Sand, C., (2007). Lapita and Western Pacific Settlement: Progress, prospects and persistent problems. In: Bedford, S., Sand, C., Connaughton, S.P., (eds). Oceanic Explorations: Lapita and Western Pacific Settlement, Terra Australis 26. The Australian National University E Press, Canberra. ISBN 9781921313332. pp 1—15.

Benson, L., (2004). The Tufas of Pyramid Lake, Nevada. USGS Circular 1267. 14p.

Benz, H.M., Herman, M., Tarr, A.C., Hayes, G.P., Furlong, K.P., Villasenor, A., Dart, R.L., Rhea, S., (2010). Seismicity of the Earth 1900 – 2010: Eastern Margin of the Australia Plate. USGS Open-File Report 2010-1083-1. 1p.

Bourgeois, J., (2009). Geological Effects and Records of Tsunamis, in The Sea, Volume 15: Tsunamis, pp. 53--91, eds. Robinson, A.R. & Bernard, E.N., Havard University Press.

Braun, J.J., Ngoupayou, J.R.N., Viers, J., Dupre, B., Bedimo, J.P.B., Boeglin, J.L., Robain, H., Nyeck, B., Freydier, R., Nkamdjou, L.S., Rouiller, J., and Muller, J.P. (2005) Present weathering rates in a humid tropical watershed: Nsimi, South Cameroon. Geochim. Cosmochim. Acta, 69(2): 357–387.

Bretschneider, C.L., Krock, H.J., Nakazaki, E. & Casciano, F.M., (1986). Roughness of typical Hawaiian terrain for tsunami run-up calculations: a user's manual, J.K.K. Look Laboratory Report, University of Hawaii, Honolulu.

Bridge, J., (2008). Discussion of articles in "Sedimentary features of tsunami deposits". Sedimentary Geology 211: 94.

Bronk Ramsey, C., (1995). Radiocarbon calibration and analysis of stratigraphy: The OxCal program, Radiocarbon, 37(2): 425--430.

Bronk-Ramsey, C., (2013). OxCal Program v4.2.2 Radiocarbon Accelerator Unit, University of Oxford.

Bruker Inc., (2008). Bruker AXS Handheld Tracer III-V Portable XRF Analyzer: Canadian User Manual. Bruker Inc., July 2008.

Buech, F., Davies, T.R., Pettinga, J.R., (2010). The Little Red Hill Seismic Experimental Study: Topographic Effects on Ground Motion at a Bedrock-Dominated Mountain Edifice, Bull. Seismol. Soc. Am., 100(5A), 2219--2229. doi: 10.1785/0120090345.

Buech, F., Davies, T.R., Pettinga, J.R., Finnemore, M., Berrill, J.B., (2007). The Little Hill field experiment: Seismic response of an edifice. 2007 New Zealand Society for Earthquake Engineering Conference Proceedings, 30 March – 1 April 2007, Palmerston North, New Zealand, 7p.

Burley, D., Nelson, D.E., Shutler Jr., R., (1995). Rethinking Tongan Lapita chronology in Ha'apai, Archaeology in Oceania, 30: 132—134.

Burley, D., Weisler, M.I., Zhao, J-X., (2012). High Precision U/Th Dating of First Polynesian Settlement." PLoS ONE 7(11): e48769.

Chagué-Goff, C. (2010). Chemical signatures of palaeotsunamis: a forgotten proxy?. Marine Geology, 271: 67—71.

Chague-Goff, C., Goff, J., (2009). Geochemical and sedimentological signature of catastrophic saltwater inundations (tsunami), New Zealand. Quaternary Australasia. 17: 38—48.

Chague-Goff, C., Andrew, A., Szczuciński, W., Goff, J., Nishimura, Y., (2012a). Geochemical signatures up to the maximum inundation of the 2011 Tohoku-oki tsunami – Implications for the 869 AD Jogan amd other palaeotsunamis. Sedimenary Geology, 282: 65—77.

Chagué-Goff, C., Schneider, J.-L., Goff, J.R., Dominey-Howes, D. & Strotz, L., (2011). Expanding the proxy toolkit to help identify past events: Lessons from the 2004 Indian Ocean Tsunami and the 2009 South Pacific Tsunami, Earth-Science Reviews, 107: 107—122.

Chagué-Goff, C., Goff, J., Nichol, S.L., Dudley, W., Zawadzki, A., Bennett, J.W., Mooney, S.D., Fierro, D., Heijnis, H., Dominey-Howes, D., Courtney, C. (2012b). Multi-proxy evidence for trans-Pacific tsunamis in the Hawai'ian Islands. Marine Geology, 299-302, 77-89.

Chen, J., Zhang, D.D., Wang, S., Xiao, T., Huang, R., (2004). Factors controlling tufa deposition in natural waters and waterfall sites. Sedimentary Geology, 166: 353—366.

Cheung, K.F., Bai, Y., Yamazaki, Y., (2013). Surges around the Hawaiian Islands from the 2011 Tohoku tsunami, Journal of Geophysical Research. doi: 10.1002/jgrc.20413, in press.

Cheung, K.F., Wei. Y., Yamazaki, Y., Yim, S.C.S., (2011). Modeling of 500-year tsunamis for probabilistic design of coastal infrastructure in the Pacific Northwest, Coastal Engineering, 58: 970—985.

Clark, J.T., (1993). Radiocarbon dates from American Samoa. Radiocarbon, 35 (2): 323—330.

Clark, J.T., Michlovic, M.G., (1996). An early settlement in the Polynesian homeland: Excavations at Aoa valley, Tutuila island. Journal of Field Archaeology, 23: 151—167.

Clark, P.U., Dyke, A.S., Shakun, J.D., Carlson, A.E., Clark, J., Wohlfarth, B., Mitrovica, J.X., Hostetler, S.W., McCabe, A.M., (2009). The Last Glacial Maximum. Science. 325: 710—714

Connelly, N.G., Damhus, T., Hartshorn, R.M., Hutton, A.T., (2005). Nomenclature of Inorganic Chemistry: IUPAC Recommendations 2005. The Royal Society of Chemistry. ISBN 0-85404-438-8.

Cornu, S., Lucas, Y., Lebon, E., Ambrosi, J.P., Luizao F., Rouiller, J., Bonnay, M., and Neal, C., (1999) Evidence of titanium mobility in soil profiles, Manaus, central Amazonia. Geoderma, 91(3–4), 281–295.

Cronin, S.J., Bonte-Grapentin, M., Nemeth, K., (2006). Review of Savai'i volcanic hazard map. SOPAC Technical Report, EU EDF 8 – SOPAC Project Report 59, Suva, Fiji.

Croudace, I., Rindby, A. and Rothwell, R., (2006). New techniques in sediment core analysis. Rothwell, R. (ed), pp. 51—63, Geological Society, London.

Davidson, J.M., (1979). Samoa and Tonga, in: Jennings, J.D., (ed). The Prehistory of Polynesia, pp. 82—109, Harvard University Press.

Davidson, J.M., (2012). Intrusion, integration and innovation on small and not-so-small islands with particular reference to Samoa, Archaeology in Oceania, 47: 1—13.

Dawson, A.G., Stewart, I., (2007a). Tsunami deposits in the geological record. Sedimentary Geology 200, 166-183.

Dawson, A., Stewart, I., (2007b). Tsunami Geoscience, Progress in Physical Geography, 31(6), 575--590. doi: 10.1177/0309133307087083.

de Souza, V.L.B., Rodrigues, K.R.G., Pedroza, E.H., de Melo, R.T., de Lima, V.L., Hazin, C.A., de Almeida, M.G.O., do Nascimento, R.K., 2012. Sedimentation Rate and ^{210}Pb Sediment Dating at Apipucos Reservoir, Recife, Brazil. Sustainability, 4: 2419—2429.

Dickinson, W.R., Green, R.C. (1998). Geoarchaeological Context of Holocene Subsidence at the Ferry Berth Lapita Site, Mulifanua, Upolu, Samoa. Geoarchaeology: An International Journal, 13 (3): 239–263.

Dinis, P. & Castilho, A., (2012). Integrating sieving and laser data to obtain bulk grain-size distributions, Journal of Sedimentary Research, 82, 747--754.

Disaster Advisory Committee, (2011). Samoa's National Disaster Management Plan 2011 – 2014. National Disaster Council, Government of Samoa, Apia. 78p.

Dominey-Howes, D., Thaman, R., (2009). UNESCO-IOC International Tsunami Survey Team Samoa: Interim Report of Field Survey 14th – 21st October 2009, Australian Tsunami Research Centre Miscellaneous Report No.2, October 2009.

Dominey-Howes, D., Humphreys, G., Hesse, P., (2006). Tsunami and palaeotsunami depositional signatures and their potential value in understanding the late-Holocene tsunami record. The Holocene 16: 1095-1107.

Drysdale, R., Lucas, S., Carthew, K., (2003). The influence of diurnal temperatures on the hydrochemistry of a tufa-depositing stream. Hydrological Processes, 17: 3421-3441.

Elmqvist, T., Rainey, W.E., Pierson, E.D. & Cox, P.A., 1994. Effects of tropical cyclones Ofa and Val on the structure of a Samoan lowland rain forest, Biotropica, 26(4): 384--391.

Etienne, S., Buckley, M., Paris, R., Nandasena, A.K., Clark, K., Strotz, L., Chagué-Goff, C., Goff, J., Richmond, B., (2011). The use of boulders for characterising past tsunamis: Lessons from the 2004 Indian Ocean and 2009 South Pacific tsunamis. Earth-Science Reviews, 107: 76—90.

Fairbairn, T.I.J., (1997). The economic impact of natural disasters in the South Pacific; with special reference to Fiji, Western Samoa, Niue and Papua New Guinea. IDNDR Secretariat, South Pacific Disaster Reduction Programme Report (RAS/92/360).

Fenner, D., Speicher, M., Gulick, S., and others, (2008). The State of Coral Reef Ecosystems of American Samoa. In: Waddell J E, Clarke A M (eds). The State of Coral Reef Ecosystems of the United States and Pacific Freely Associated States: 2008, NOAA Technical Memorandum NOS NCCOS 73. NOAA/NCCOS Center for Coastal Monitoring and Assessment's Biogeography team, Silver Spring, MD. pp 307—351.

Fifield, L.K., Tims, S.G., Fujioka, T., Hoo, W.T., Everett, S.E., (2010). Accelerator mass spectrometry with the 14UD accelerator at the Australian National University. Nuclear Instruments and Methods in Physics Research Section B: Beam Interactions with Materials and Atoms. 268: 858-862.

Ford, T.D., Pedley, H.M., (1996). A review of tufa and travertine deposits of the world. Earth-Science Reviews, 41: 117—175.

Freytat, P., Plet, A., (1996). Modern Freshwater Microbial Carbonates: The Phormidium Stromatolites (Tufa-Travertine) of Southeastern Burgundy (Paris Basin, France). Facies, 34: 219—238.

Gavin, D.G., (2001). Estimation of inbuilt age in radiocarbon ages of soil charcoal for fire history studies. Radiocarbon. 43(1): 27—44.

Goff, J., Chagué-Goff, C., (2014). The Australian tsunami database: A review. Progress in Physical Geography. 23p. DOI: 10.1177/0309133314522282.

Goff, J., Chagué-Goff, C., Nichol, S., (2001). Palaeotsunami deposits: A New Zealand perspective. Sedimentary Geology 143: 1—6.

Goff, J., Chagué-Goff, C., Terry, J., (2012a). The value of a Pacific-wide tsunami database to risk reduction: putting theory into practice, in:Terry, J., Goff, J., (eds). Natural Hazards in the Asia-Pacific Region: Recent Advances and Emerging Concepts. Geological Society Special Publication 361, London. pp 209—220.

Goff, J., Chagué-Goff, C., Dominey-Howes, D., McAdoo, B., Cronin, S., Bonté-Grapetin, M., Nichol, S., Horrocks, M., Cisternas, M., Lamarche, G., Pelletier, B., Jaffe, B., Dudley, W., (2011). Palaeotsunamis in the Pacific Islands, Earth-Science Reviews, 107, 141--146.

Goff, J., Chagué-Goff, C., Nichol, S.L., Jaffe, B., Dominey-Howes, D., (2012b). Progress in palaeotsunami research, Sedimentary Geology, 243-244, 70--88.

Goff, J., McFadgen, B., Chagué-Goff, C., (2004). Sedimentary differences between the 2002 Easter storm and the 15th-century Okoropunga tsunami, southeastern North Island, New Zealand. Marine Geology 204: 235—260.

Goff, J., McFadgen, B., Chagué-Goff, C., Nichol, S.L., (2012c). Palaeotsunamis and their influence on Polynesian Settlement. The Holocene, 22(9): 1067—1069.

Goff, J., Nichol, S., Kennedy, D., (2010a). Development of a palaeotsunami database for New Zealand. Nat. Hazards. DOI: 10.1007/s11069-009-9461-5.

Goff, J.R., Nichol, S.L., Chagué-Goff, C., Horrocks, M., McFadgen, B., Cisternas, M., (2010b). Predecessor to New Zealand's largest historic trans-South Pacific tsunami of 1868AD. Marine Geology 275: 155—165.

Goff, J., Pearce, S., Nichol, S.L., Chague-Goff, C., Horrocks, M., Strotz, L., (2010c). Multi-proxy records of regionally-sourced tsunamis, New Zealand. Geomorphology. 118: 369—382.

Goff, J.R., Wells, A., Chagué-Goff, C., Nichol, S.L., Devoy, R.J.N., (2004c). The elusive AD 1826tsunami, SouthWestland, NewZealand. New Zealand Geographer, 60(2): 28–39.

Golson, J. 1969a. Preliminary Research: Archaeology in Western Samoa, 1957. In: R.C. Green and J.M. Davidson (eds). Archaeology in Western Samoa. Volume I, Bulletin 6:14-20 Auckland Institute and Museum: Auckland.

Golubić, S., Violante, C., Plenković-Moraj, A., Grgasović, T., (2008). Travertines and calcareous tufa deposits: an insight into diagenesis. Geologia Croatica, 61(2-3): 363—378.

Goto, K., Chagué-Goff, C., Fujino, S., Goff, J., Jaffe, B., Nishimura, Y., Richmond, B., Suguwara, D., Szczuciński, W., Tappin, D.R.,Witter, R., Yulianto, E., (2011). New insights into tsunami risk from the 2011 Tohoku-oki event, Marine Geology, 290, 46—50.

Green, R.C., (2002). A Retrospective View of Settlement Pattern Studies in Samoa. In: Pacific Landscapes: Archaeological Approaches (T.N. Ladefoged, and M.W. Graves, eds.): 125-152. Easter Island Foundation Press. Los Osos, California.

Greenwood, N.N., Earnshaw, A., (1997). Chemistry of the Elements, 2nd ed. Butterworth-Heinemann, Oxford, UK.

Grimm, E.C., (2011). High-resolution age model based on AMS radiocarbon ages for Kettle Lake, North Dakota, USA. Radiocarbon, 53(1): 39–53.

Hart, S.R., (2006). CSEDI Research Proposal. Woods Hole Oceanographic Institution, Massachusetts. Unpublished Document.

Hart, S.R., Coetzee, M., Workman, R.K., Blusztajn, J., Johnson, K.T.M., Sinton, J.M., Steinberger, B., Hawkins, J.W., (2004). Genesis of the Western Samoa seamount province: age, geochemical fingerprint and tectonics. Earth and Planetary Science Letters. 227: 37—56.

Hart, S.R., Staudigel, H., Koppers, A.P., Blusztajin, J., Baker, E.T., Workman, R., Jackson, M., Hauri, E., Kurz, M., Sims, K., Fornari, D., Saal, A., Lyons, S., (2000). Vailulu'u undersea volcano: The New Samoa. Geochemistry Geophysics Geosystems. 1(2000GC000108). 13p.

Higman, B., Jaffe, B., (2005). A comparison of grading in deposits from five tsunamis: Does tsunami wave duration affect grading patterns?. Eos Trans. AGU, 86(52). Fall Meet. Suppl. Abstract T11A-0362.

Huang, S., Hall, P.S., Jackson, M.G., (2011). Geochemical zoning of volcanic chains associated with Pacific hotspots. Nature Geoscience, 5p. DOI: 10.1038/NGEO1263.

Jackson, M.G., Kurz, M.D., Hart, S.R., (2009). Helium and neon isotopes is phenocrysts from Samoan lavas: Evidencce for heterogeneity in the terrestrial high $^{3}He/^{4}He$ mantle. Earth and Planetary Science Letters, 10p. DOI: 10.1016/j.espl.2009.08.039.

Jackson, M.G., Carlson, R.W., Kurz, M., Kempton, P.D., Francis, D., Blusztajn, J.,(2010). Evidence for the survival of the oldest terrestrial mantle reservoir. Nature, 7p. DOI: 10.1038/nature09287.

Jackson, M.G., Hart, S.R., Koppers, A.A.P., Staudigel, H., Konter, J., Blusztajn, J., Kurz, M., Russell, J.A., (2007). The return of subducted continental crust in Samoan lavas. Nature, 448. 29p. DOI: 10.1038/nature06048.

JMA, (2013)., Lessons learned from the tsunami disaster caused by the 2011 Great East Japan earthquake and improvements in JMA's tsunami warning system. Japan Meteorological Agency, October 2013, 13p.

Jopling, T.W., (2014). Samoa: A Geologic History, A Visitor's Guide. Samoa Tourism Authority, Apia. 27p.

Kear, D., Wood, B.L., (1959). The Geology and Hydrology of Western Samoa. New Zealand Geological Survey Bulletin (No.63).

Keating, B.H., Helesley, C.E., Karogodina, I., (2000). Sonar studies of submarine mass wasting and volcanic structures off Savaii Island, Samoa. Pure and Appl. Geophys. 157: 1285—1313.

Kelletat, D., (2008). Comments to Dawson, A.G. Stewart, I. (2007), Tsunami deposits in the geological record [Sedimentary Geology 200, 166-183]. Sedimentary Geology 211, 87-91.

King, D., Goff, J., (2010). Benefitting from differences in knowledge, practice and belief: Māori oral traditions and natural hazards science, Natural Hazards and Earth System Sciences, 10, 1927—1940.

Kirch, P.V., (1993a). Ofu island and the To'aga site: dynamics of the natural and cultural environment. In: The To'aga Site: Three Millennia of Polynesian Occupation in the Manu'a Islands, American Samoa (P.V. Kirch, and T.L. Hunt, eds.): 9—22. Contributions of the University of California Archaeological Research Facility 51, University of California at Berkeley.

Kirch, P.V., (1993b). Radiocarbon Chronology of the To'aga Site. In: The To'aga Site: Three Millennia of Polynesian Occupation in the Manu'a Islands, American Samoa (P.V. Kirch, and T. L. Hunt, eds.): 85-92. Contributions of the University of California Archaeological Research Facility 51, University of California at Berkeley.

Konter, J.G., Staudigel, H., Hart, S.R., Shearer, P.M., (2004). Seafloor seismic monitoring of an active submarine volcano: Local seismicity at Vailulu'u seamount, Samoa. Geochemistry Geophysics Geosystems, 5(6). 15p. DOI: 10.1029/2004GC000702.

Konter, J.G., Jackson, M.G., (2012). Large volumes of rejuvenated volcanism in Samoa: Evidence supporting a tectonic influence on late-stage volcanism. Geochemistry Geophysics Geosystems, 13(1). 23p. Q0AM04, DOI: 10.1029/2011GC003974.

Koppers, A.A.P., Russell, J.A., Jackson, M., Staudigel, H., Konter, J., Hart, S.R., (2008). Samoa reinstated as a primary hotspot trail. Geology. 36(6): 435-438.

Koppers, A.A.P., Russell, J.A., Roberts, J., Jackson, M.G., Konter, J.G., Wright, D.J., Staudigel, H., Hart, S.R., (2011). Age systematics of two young en echelon Samoan volcanic trails, Geochemistry Geophysics Geosystems, 12, Q07025, DOI:10.1029/2010GC003438.

Kortekaas, S., Dawson, A.G., (2007). Distinguishing tsunami and storm deposits: An example from Martinhal, SW Portugal. Sedimentary Geology 200, 208-221.

Kritikos, T., (2013). Geomorphic Hazard Analyses in Tectonically-Active Mountains: Applications to the Western Southern Alps, New Zealand. PhD Thesis, Department of Geological Sciences, University of Canterbury, UC Library Repositry, 299p.

Lambeck, K., Yokoyama, Y., Purcell, T., (2001). Into and out of the Last Glacial Maximum: sea-level change during Oxygen Isotope Stages 3 and 2. Quaternary Science Reviews. 21 (2002): 343-360.

Lay, T., Kanamori, H., Ammon, C.J., Nettles, M., Ward, S.N., Aster, R.C., Beck, S. L., Bilek, S. L., Brudzinski, M.R., Butler, R., DeShon, H.R., Ekström, G., Satake, K., and Sipkin, S., (2005), The great Sumatra-Andaman earthquake of 26 December 2004. Science, 308: 1127–1133.

Lay, T., Ammon, C.J., Kanamori, H., Rivera, L. & Koper, K.D., (2010). The 2009 Samoa-Tonga great earthquake triggered doublet. Nature, 466, 964--968, doi:10.1038/nature09214.

Lekkas, E.L., Andreadakis, E., Kostaki, I., Kapourani, E., (2012). A New Tsunami Intensity Scale proposed after the Tsunamis of 11 Mar. 2011, Japan & 26 Dec. 24, Indian Ocean. 15 WCEE, Lisboa, 2012. 9p.

Lekkas, E.L., Andreadakis, E., Kostaki, I., Kapourani, E., (2013). A Proposal for a New Integrated Tsunami Intensity Scale (ITIS-2012). Bulletin of the Seismological Society of America, 103(2B): 1493—1502.

Linnekin, J., Hunt, T., Lang, L., McCormick, T., (1995). Ethnographic Assessment and Overview: The National Park of American Samoa. Department of Anthropology, University of Hawaii.

Luque, L., Lario, J., Zazo, C., Goy, J.L., Dabrio, C.J., Silva, P.G., (2001). Tsunami deposits as palaeoseismic indicators: examples from the Spanish coast. Acta Geologica Hispanica, 36(3-4): 197—211.

Ma, J-. L., Wei, G-. J., Xu, Y-. G., Long, W-. G., Sun, W-. D., (2007). Mobilization and redistribution of major and trace elements during extreme weathering of basalt in Hainan Island, South China. Geochimica, Cosmochimica Acta 71 (2007) 3223–3237.

Mader C., (2006). A Mag 9+Tsunami Generated in the Tongan Trench. Mader Consulting Co. 7p.

Marra, J.J., Kari, U.S., Sabbatelli, T.A., (2008). Anatomies of historical storm events in the Pacific. Proceedings of the Solutions to Coastal Disasters Congress, 2008, 312: 222-228.

Martinsson-Wallin, H., (2007). Samoan Archaeology: A review of research history, Archaeology in Oceania, 42(Supplement), 11--27.

Martinsson-Wallin, H., (2011). The complexity of an archaeological site in Samoa: The past in the present. Terra Australis 35, pp 101—114.

Matter, J.M., Takahashi, T., (2007). Experimental evaluation of in-situ CO_2-water-rock reactions during CO_2 injection in basaltic rocks: Implications for geological CO_2 sequestration. Geochemistry Geophysics Geosystems, 8 (2): 19 pp.

McAdoo, B.G., Ah-Leong, J.S., Bell, L., Ifopo, P., Ward, J., Lovell, E., Skelton, P., (2010). Coral reefs as buffers during the 2009 South Pacific Tsunami, Upolu Island, Samoa. Earth-Sciencce Reviews, 107: 147—155.

McCormac, F.G., Hogg, A.G., Blackwell, P.G., Buck, C.E., Higham, T.F.G. & Reimer, P.J., (2004). SHCal04 Southern Hemisphere Calibration 0 - 11.0 cal kyr BP, Radiocarbon, 46, 1087--1092.

McDougall, I., (2010). Age of volcanism and its migration in the Samoa Islands. Geological Magazine. 147(5): 705-717.

McFadgen, B.G., Goff, J., (2007). Tsunamis in the archaeological record of New Zealand, Sedimentary Geology, 200, 263--274.

McGuire, B., (2012). Waking the Giant: How a changing climate triggers earthquakes, tsunamis, and volcanoes. Oxford University Press, Oxford. ISBN 9780199592265. 318p.

McMurtry, G.M., Watts, P., Fryer, G.J., Smith, J.R., Imamura, F., (2003). Giant landslides, mega tsunamis, and paleo-sea level in the Hawaiian Islands. Marine Geology. 203(2004): 219-233. doi:10.1016/S0025-3227(03)00306-2.

Merz-Preiß, M., Riding, R., (1999). Cyanobacterial tufa calcification in two freshwater streams: ambient environment, chemical thresholds and biological processes. Sedimentary Geology, 126: 103-124.

Mignard, F., (2005). About the Nyquist Frequency. Observatoire de la Côte d'Azur, Dpt. Cassiopée. GAIA FM 022. 15p.

Miller, K., Rizzo, A., Togiai, L., Walsh, T., Whitmore, P., Williams, C. (compilers), (2013). National Tsunami Hazard Mitigation Program 2013 – 2017 Strategic Plan. NOAA. 32p.

Ministry of Finance, (2012). Strategy for the Develoment of Samoa 2012 – 2016. Economic Policy and Planning Division, Ministry of Finance, Government of Samoa, Apia. 79p.

Morse, J.W., Arvidson, R.S., Lüttge, A., (2007). Calcium Carbonate Formation and Dissolution. Chemical Reviews, 107: 342 – 381.

Morton, R.A., Gelfenbaum, G., Jaffe, B.E., (2007). Physical criteria for distinguishing sandy tsunami and storm deposits using modern examples. Sedimentary Geology 200: 184-207.

Morton, R.A., Goff, J.R., Nichol, S.L., 2008. Hydrodynamic implications of textural trends in sand deposits of the 2004 tsunami in Sri Lanka. Sedimentary Geology 207: 59-64.

Morton, R.A. and others, (2010). Geological impacts and sedimentary record of the February 27, 2010, Chile tsunami; La Trinchera to Concepcion: U.S. Geological Survey Open-File Report 2010-1116, 22 p.

Morton, R.A., Gelfenbaum, G., Buckley, M.L., Richmond, B.M., (2011). Geological effects and implications of the 2010 tsunami along the central coast of Chile. Sedimentary Geology 242: 34–51.

Munger, S. & Cheung, K.F., (2008). Resonance in Hawaii waters from the 2006 Kuril Islands Tsunami, Geophysical Research Letters, 35(L07605), 7p. doi:10.1029/2007GL032843.

Natland, J.H., (2003). The Samoan Chain: A Shallow Lithospheric Fracture System. MantlePlumes.org. 10p.

Natland J. H., Turner, D.L., (1985). Age progression and petrological development of Samoan shield volcanoes: Evidence from K-Ar ages, lava compositions and mineral studies. In: Brocker T M (ed) Geological investigations of the northern Melanesian borderland: Houston, Texas, Council for Energy and Mineral Resources, Circum-Pacific Council for Energy and Mineral Resources Earth Science Series. 3: 139-172.

Nesbitt H. W., Markovics G., (1997). Weathering of granodioritic crust, long-term storage of elements in weathering profiles, and petrogenesis of siliciclastic sediments. Geochim. Cosmochim. Acta 61(8), 1653–1670.

NGDC and ITIC, (2010). TsuDig WDC-MGG Historical Tsunami GIS version 0.5 beta, March 2010. National Geophysical Data Center and The International Tsunami Information Center, A UNESCO/IOC – NOAA Partnership. CD ROM.

Nichol, S.L., Chagué-Goff, C., Goff, J.R., Horrocks, M., McFadgen, B.M., Strotz, L.C., (2010). Geomorphology and accommodation space as limiting factors on tsunami deposition: Chatham Island, southwest Pacific Ocean. Sedimentary Geology 229: 41-52.

Nishimura, Y., Miyaji, N., (1995). Tsunami Deposits from the 1993 Southwest Hokkaido Earthquake and the 1640 Hokkaido Komagatake Eruption, Northern Japan. Pure and Applied Geophysics, 144(2/3): 719—732.

Nunn, P.D., (1998). Pacific Island Landscapes: Landscape and Geological Development of Southwest Pacific Islands, especially Fiji, Samoa and Tonga. Institute of Pacific Studies, The University of the South Pacific, Fiji. pp 161—193.

Nunn, P.D., (2012). Climate Change and Pacific Island Countries. Asia-Pacific Human Development Report Background Papers Series 2012/07, Commissioned by the Human Development Report Unit, United Nations Development Program. 97p.

Nunn, P.D., Britton, J.M.R., (2001). Human-Environment Relationships in the Pacific Islands around A.D. 1300. Environment and History, 7(1): 3—22.

Nunn, P.D., Petchey, F. (2013). Bayesian Re-evaluation of Lapita Settlement in Fiji: Radiocarbon analysis of the Lapita occupation at Bourewa and nearby sites on the Rove Peninsula, Viti Levu Island. Journal of Pacific Archaeology, 4 (2): 14 pp.

Okada, Y., (1985). Surface deformation due to shear and tensile faults in a half space, Bull. Seismol. Soc. Am., 75(4): 1135--1154.

Okal, E., Borrero, J., Chagué-Goff, C., (2011). Tsunamigenic predecessors to the 2009 Samoa earthquake, Earth-Science Reviews, 107, 127--140.

Okal, E.A., Fritz, H.M., Synolakis, C.E., Borrero, J.C., Weiss, R., Lynett, P.J., Titov, V.V., Foteinis, S., Jaffe, B.E., Liu, P.L.-F., Chan, I-chi., (2010). Field Survey of the Samoa Tsunami of 29 September 2009. Seismological Research Letters, 81(4): 577—591.

Oliva P., Viers J., Dupre B., Fortune J. P., Martin F., Braun J. J., Nahon D., Robain H., (1999) The effect of organic matter on chemical weathering: study of a small tropical watershed: Nsimi-Zoetele site, Cameroon. Geochim. Cosmochim. Acta 63(23–24), 4013–4035.

Pararas-Carayannis, G., Dong, B., (1980). Catalog of Tsunamis in the Samoan Islands, International Tsunami Information Center, Honolulu, 75p.

Patino L. C., Velbel M. A., Price J. R., Wade J. A., (2003). Trace element mobility during spheroidal weathering of basalts and andesites in Hawaii and Guatemala. Chem. Geol. 202(3–4), 343–364.

Patino L. C., Velbel M. A., Price J. R., Wade J. A. (2005). Element redistribution during weathering of volcanic rocks in sedentary landscapes. Geochim. Cosmochim. Acta 69(10), A683.

Pedley, H.M., (1990). Classification and environmental models of cool freshwater tufa. Sedimentary Geology, 68: 143—154.

Pedley, M., Andrews, J., Ordonez, S., Garcia del Cura, M.A., Martin, J-A. G., Taylor, D., (1996). Does climate control the morphological fabric of freshwater carbonates? A comparative study of Holocene barrage tufas from Spain and Britian. Palaeogeography Palaeoclimatology Palaeoecology, 121: 239-257.

Petchey, F.J., (2001). Radiocarbon determinations from the Mulifanua Lapita site, Upolu, Western Samoa. Radiocarbon, 43 (1): 63 – 68.

Petchey F., Anderson, A., Zondervan, A., Ulm, S., Hogg, A., (2008). New marine ΔR values for the South Pacific subtropical gyre region. Radiocarbon 50(3):373-397.

Peters, R., Jaffe, B.E., (2010). Identification of tsunami deposits in the geologic record; developing criteria using recent tsunami deposits, U.S. Geological Survey Open-File Report 2010-1239, 39p.

Phantuwongraj, S., Choowong, M., (2012). Tsunami versus storm deposits from Thailand. Natural Hazards, 63: 31—50.

Phelan, M.B., (1999). A ΔR correction value for Samoa from known-age marine shells, Radiocarbon, 41:99—101.

Power, W.L. (compiler), (2013). Review of Tsunami Hazard in New Zealand (2013 Update). GNS Science Consultancy Report 2013/131. 222p.

Rahiman, T., (2006). Neotectonics, Seismic and Tsunami Hazards, Viti Levu, Fiji. PhD Thesis, Dept. of Geological Sciences, University of Canterbury, NZ. UC Library Repositry, 326p.

Ramírez-Herrera, M.-T., Lagos, M., Hutchinson, I., Kostoglodov, V., Machain, M.L., Caballero, M., Goguitchaichvili, A., Aguilar, B., Chagué-Goff, C., Goff, J., Ruiz-Fernández, A.-C., Ortiz, M., Nava, H., Bautista, F., Lopez, G.I. and Quintana, P., (2012). Extreme wave deposits on the Pacific coast of Mexico: Tsunamis or storms? — A multi-proxy approach. Geomorphology, 139-140, 360—371.

Ready, S. & Woodcock, F., (1992). The South Pacific and southeast Indian Ocean tropical cyclone season 1989-1990, Australian Meteorological Magazine, 40(2), 111--121.

Reese, S., Bradley, B.A., Bind, J., et al., (2011). Empirical building fragilities from observed damage in the 2009 South Pacific tsunami. Earth-Science Reviews, 107: 156–173.

Reimer, P.J., Baillie, M.G.L., Bard, E., Bayliss, A., Beck, J.W., Blackwell, P.G., Bronk Ramsey, C., Buck, C.E., Burr, G.S., Edwards, R.L., Friedrich, M., Grootes, P.M., Guilderson, T.P., Hajdas, I., Heaton, T.J., Hogg, A.G., Hughen, K.A., Kaiser, K.F., Kromer, B., McCormac, F.G., Manning, S.W., Reimer, R.W., Richards, D.A., Southon, J.R., Talamo, S., Turney, C.S.M., van der Plicht, J. & Weyhenmeyer, C.E., (2009). IntCal09 and Marine09 radiocarbon age calibration curves, 0-50,000 years cal BP, Radiocarbon, 51(4): 1111—1150.

Richmond, B.M., Buckley, M., Etienne, S., Chagué-Goff, C., Clark, K., Goff, J., Dominey-Howes, D., Strotz, L., (2011a). Deposits, flow characteristics, and landscape change resulting from the September 2009 South Pacific tsunami in the Samoan islands, Earth-Science Reviews, 107: 38—51.

Richmond, B.M., Watt, S., Buckley, M., Jaffe, B.E., Gelfenbaum, G., Morton, R.A., (2011b). Recent storm and tsunami coarse-clast deposit characteristics, southeast Hawai'i. Marine Geology, 283 (1-4): 79-89.

Reith, T., Addison, D.J., (2008). How Dark Are They? The Sāmoan Dark Ages, ~1500—1000 BP. In: Adddison, D.J., Sand, C. (eds). Recent Advances in the Archaeology of the Fiji/West-Polynesia Region. University of Otago Studies in Prehistoric Anthropology, No.21. Department of Anthropology, University of Otago, NZ. pp 87—96.

Rieth, T.M., Hunt, T.L., (2008). A radiocarbon chronology for Samoan prehistory. Journal of Archaeological Science, 35 (7): 1901—1927.

Roeber, V., Yamazaki, Y., Cheung, K.F., (2010). Resonancce and impact of the 2009 Samoa tsunami arounnd Tutuila, Geophysical Research Letters, 37(L21604), 8p. doi:10.1029/2010GL044419.

Rothwell, R.G., (2006). New Techniques in Sediment Core Analysis. Geological Society, London, Special Publications, 267p.

Satake, K., Rabinovich, A.B., Dominey-Howes, D., Borrero, J.C., (2012). Introduction to “Historical and Recent Catastrophic Tsunamis in the World: Volume I. The 2011 Tohoku Tsunami”. Pure and Applied Geophysics, 170: 955—961.

Schlichting, R. and Peterson, C., (2006). Mapped overland distance of paleotsunami: high-velocity inundation in back-barrier wetlands of the central Cascadia margin, U.S.A. The Journal of Geology 114, 577-592.

Schmall, S., (2000). The end-users of ‘Pacific Cities II’ hazard, vulnerability and risk assessment information. Final Report, September 1999 – March 2000. SOPAC Miscellaneous Report 384.

Shiraishi, F., Okumura, T., Takahashi, Y., Kano, A., (2010). Influence of microbial photosynthesis on tufa stromatolite formation and ambient water chemistry, SW Japan. Geochimica et Cosmochimica Acta, 74: 5289-5304.

Stair, J.B., (1894). "O le Fale o le Fe'e": or, ruins of an old Samoan temple. The Journal of the Polynesian Society, 3 (4): 239-244.

Staudigel, H., Hart, S.R., Koppers A.A.P., Constable, C., Workman R., Kurz M., Baker E. T., (2004). Hydrothermal venting at Vailulu'u Seamount: The smoking end of the Samoan chain. American Geophysical Union 5(2).

Staudigel, H., S.R. Hart, A. Pile, B.E. Bailey, E.T. Baker, S. Brooke, D.P. Connelly, L. Haucke, C.R. German, I. Hudson, D. Jones, A.A.P. Koppers, R.L.J. Konter, T.W. Pietsch, B.M. Tebo, A.S. Templeton, R. Zierenberg, and C.M. Young, (2006). Vailulu'u Seamount, Samoa: Life and death on an active submarine volcano. PNAS 103(17): 6448-6453.

Stearns, H.T., (1955). High-level fossiliferous limestone on Upolu Island, Samoan archipelago. Abstracts for papers submitted for meeting in Laramie, Wyoming, May 6-7, 1955, Rocky Mountain Section, Geological Society of America. p1681.

Stice, G.D., McCoy, F.W., (1968). The geology of the Manu'a Islands, Samoa. Pacific Sci. 22: 427-457.

Stone, J.O., (2000). Air pressure and cosmogenic isotope production. Journal of Geophysical Research. 105: 23753-23759.

Stuiver, M., Polach, H.A., (1977). Discussion: Reporting of ^{14}C data, Radiocarbon, 19(3): 355--363.

Stuiver, M., Reimer, P.J., (1993). Extended ^{14}C data base and revised CALIB 3.0 ^{14}C age calibration program, Radiocarbon, 35: 215--230.

Sugawara, D., Goto, K., Chagué-Goff, C., Fujino, S., Goff, J., Jaffe, B., Nishimura, Y., Richmond, B., Szczuciński, W., Tappin, D.R., Witter, R., Yuliento, E., (2011). Initial field survey report of the 2011 East Japan Tsunami in Sendai, Natori and Iwanuma Cities. UNESCO-IOC International Tsunami Survey Team. Report to UNESCO, 16 pp.

Terry, J.P., Goff, J., (2012). One hundred and thirty years since Darwin: 'Reshaping' the theory of atoll formation. The Holocene, 23(4): 615—619.

Titov, V., Rabinovich, A.B., Mofjeld, H.O., Thomson, R.E., and Gonzalez, F.I., (2005), The global reach of the 26 December 2004 Sumatra tsunami: Science, v. 309, no. 5743, p. 2045-2048.

Turner, G.A. (1889). Samoa. Scottish Geographical Magazine. 5: 235-256.

Uchida, J-I., Fugiwara, O., Hasegawa, S. & Kamataki, T., 2010. Sources and depositional processes of tsunami deposits: Analysis using foraminifera tests and hydrodynamic verification, Island Arc, 19, 427--442.

UNISDR, (2013). From Shared Risk to Shared Value –The Business Case for Disaster Risk Reduction. Global Assessment Report on Disaster Risk Reduction. Geneva, Switzerland: United Nations Office for Disaster Risk Reduction (UNISDR).

U.S.G.S. Pacific Coastal and Marine Science Centre, (2009). Preliminary Analysis of the September 29, 2009 Samoa Tsunami, Southwest Pacific Ocean. [Online at: http://walrus.wr.usgs.gov/tsunami/samoa09/]

van Wyk de Vries, B., Self, S., Francis, P.W., and Keszthelyi, L., (2001), A gravitational spreading origin for the Socompa debris avalanche. Journal of Volcanology and Geothermal Research, 105: 225–247, doi:10.1016/S0377-0273(00)00252-3.

Viles, H., Goudie, A.S., (1990). Tufas, travertines and allied carbonate deposits. Progress in Physical Geography, 14: 19-41.

Walling, D.E., He, Q. and Appleby, P.G., (2002). Conversion models for use in soil-erosion, soil-redistribution and sedimentation investigations. In: Zapata, F. Handbook for the assessment of soil erosion and sediment using environmental radionuclides. Kluwer Academic Publishers, 111-164.

Walters, R.A., Goff, J., (2006). Assessing Tsunami Hazard along the New Zealand Coast, Science of Tsunami Hazards 21(3): 137-153. DOI: 10.1177/030913339001400102.

Walter, T.R., Troll, V.R., Caileau, B., Belousov, A., Schimincke, H.U., Amelung, F., Bpgaard, P.v.d., (2004). Rift zone reorganization through flank instability in ocean island volcanoes: an example from Tenerife, Canary Islands. Bulletin of Volcanology, 67: 281—291.

Ward, S.N., (2001). Landslide Tsunami. Journal of Geophysical Research, 106(6): 11201—11215.

Wardman, J.B., (2013). Vulnerability of Electric Power Systems to Volcanic Ashfall Hazards. PhD Thesis, Natural Hazards Research Centre, University of Canterbury, UC Library Repository, 265p.

Wassmer, P., J.-L. Schneider, A.-V. Fonfrege, F. Lavigne, R. Paris, C. Gomez., (2010). Use of Anisotropy of Magnetic Susceptibility (AMS) in the study of tsunami deposits: Application to the 2004 deposits on the eastern coast of Banda Aceh, North Sumatra, Indonesia. Marine Geology, doi:10.1016/j.margeo.2010.06.007.

Workman, R.K., Eiler, J.M., Hart, S.R., Jackson, M.G., (2008). Oxygen isotopes in Samoan lavas: Confirmation of continent recycling. Geology, 36(7): 551—554.

Workman, R.K., Hart, S.R., Jackson, M.G., Regelous, M., Farley, K.A., Blusztajn, J., Kurz, M., Staudigel, H., (2004). Recycled metasomatised lithosphere as the origin of the Enriched Mantle II (EM2) end-member: Evidence from the Samoan Volcanic Chain. Geochemistry Geophysics Geosystems, 5(4). 44p. Q04008, doi:10.1029/2003GC000623.

Wessel, P., Smith, W.H.F., (1991). Free software helps map and display data, Eos Trans., AGU 72(41), 445--446.

Wilkes, C., (1849). Narrative of the United States Exploring Expedition during the years 1838-1842, Vol I. United States Navy, Philadelphia, USA.

Williams, S., (2005). Ta'u through the Hourglass: An alternative look. Enduring Resources Earth Science Education, Earthref.org. [URL: http://earthref.org/ERESE/projects/ALIA/reports/report-tau-morphology.htm. [(Last accessed: 21/08/2013)].

Williams, S., (2009). Ocean-island flank collapse on the south of Ta'u, Manu'a Group, Samoa Islands: implications for risk management. MSc thesis, University of Canterbury Library Repository. 129p + 3 digital appendices.

Williams, S.P., Leavasa, A.F.M., (2006). Exploring the status of tsunami early warning systems in Samoa. In: Taulealo, T., (ed), Proceedings of the Samoa National Environment Forum 2005. pp. 52-58.

Williams, S., Davies, T., Cole, J., (2012). Catastrophic flank collapse on Ta'u Island and subsequent tsunami: Has this occurred during the last 170 years. Science of Tsunami Hazards. 31(3): 178-198.

Yamazaki, Y., Cheung, K.F., (2011). Shelf resonance and impact of near-field tsunami generated by the 2010 Chile earthquake, Geophysical Research Letters, 38(L12605), 8p. doi:10.1029/2011GL047508.

Yamazaki, Y., Cheung, K.F., Kowalik, Z., (2010). Depth-integrated, non-hydrostatic model with grid nesting for tsunami generation, propagation, and run-up. Int. J. Numer. Meth. Fluids (2010), 27p. doi: 10.1002/fld.2485.

Yamazaki, Y., Cheung, K.F., Kowalik, Z., Pawlak, G., Lay T., (2012). NEOWAVE, Proceedings and Results of the 2011 National Tsunami Hazard Mitigation Program (NTHMP) Model Benchmarking Workshop, Boulder, pp. 239--302, U.S. Department of Commerce/NOAA/NTHMP; NOAA Special Report.

Yamazaki, Y., Cheung, K.F., Lay, T., (2013). Modeling of the 2011 Tohoku Near-Field Tsunami from Finite-Fault Inversion of Seismic Waves, Bull. Seismol. Soc. Am., 103(2B), 1444--1455. doi: 10.1785/0120120103.

Yamazaki, Y., Kowalik, Z., Cheung, K.F., (2009). Depth-integrated, non-hydrostatic model for wave breaking and run-up, Int. J. Numer. Meth. Fluids, 61, 473--497.

Zawadzki, A., Fierro, D., (2012). 15 samples analysed for Pb-210 dating by alpha – Report for Project Name: Using Pb-210, C-14 and ITRAX to reconstruct the palaeosunami and palaeostorm record on the Samoan Islands. Environmental Radioactivity Measurement Centre Certificate of Analysis, Project Number 2012rc0035ab,36a, AINSE Grant No. AINGRA12119P, ANSTO.

.

APPENDICES

APPENDIX 1: HISTORICAL TSUNAMI DATA

Historical tsunami data compiled by Pararas-Carayannis and Dong (1980) for the period 1837 – 1980 is summarized in Appendix Table 1.1 below. Citations to specific events are provided by Pararas-Carayannis and Dong (1980).

Also included in Table 1.1 are tsunami events of particular hazard concern during the period 1980 – 2011. These include the 1981 tsunami and 2009 SPT near-field events, and the far-field 2011 Great Earthquake and Tsunami in Japan.

Specific events discussed in the thesis text are highlighted in red font.

Appendix Table 1.1: Historical tsunami for the period AD 1837 – 2011.

DATE	EARTHQUAKE DATA				TSUNAMI DATA			
	Origin Time (Local Samoan Time)	Location	Latitude / Longitude	Magnitude	Place of Observation	Maximum Wave Height (metres)	Travel Time (Hours)	Observations and Remarks
1837 Nov 7	1:51 a.m.	South Chile	36-38 S, 72-74 W		Tutuila Island			A large earthquake in South Chile generated a tsunami wave which caused major loss of life and property damage in Hawaii. Details of the impacts on Tutuila island were not available, although the tsunami was recorded by Rev. W. Mills (Capt. Charles Wilkes obtained a copy of the observations).
1868 Aug 14	5:45 a.m.	North Chile	18.5 S, 71.0 W		Apia, Upolu Is.		16.0	The great Peru earthquake and tsunami destroyed settlements in Apia according to the Preliminary Catalog of Pacific Tsunamis. Details on the extent of damage caused was not available.
1877 May 10	1:59 p.m.	Chile	21.5 S, 71.0 W		Apia, Upolu Is.	2.0 - 4.0	15.0	The great Chilean earthquake and tsunami caused devastating damages throughout the Pacific. Details on the extent of damage noted in Apia was not available.

1883 Mar 24		Samoa Islands?			Savaii Island			Captain Pearson, who commanded the Wachusett reported that a storm was accompanied by an earthquake on the night of March 24. He reported that all houses within a quarter of a mile of the beach on the east end of Savaii were swept away from a tsunami for a distance of 15 miles along the shore. This may have been a locally generated tsunami.
1896 Jun 15	11:33 a.m.	Sanriku, Japan	39.6 N, 144.2 E	7.6	Savaii Island	1.7		Several villages along the north coast of Savaii noted an unusual surge in the water level during low tide of about 1 foot higher than the normal high tide mark; approximately 5 1/2 feet higher than it should have been. Details on any impacts were not available.
1906 Nov 28		North coast of Savaii			Matautu, Savaii Is.	0.5		Lava flows from the Mt. Matavanu volcanic eruption from 1905 - 1911 occasionally generated small tsunamis as a result of avalanching materail into the adjacent ocean. Sea flooding was the main impact noted during these tsunamis. The first of these small tsunamis occurred at 5:30 PM on November 28 1906.
1907 Jun 8		North coast of Savaii			Matautu, Savaii Is.	0.5		The second tsunami to have occurred as a result of the Mt. Matavanu volcanic eruptive influences was at 12:00 PM on June 8 1907.
1907 Jun 19		North coast of Savaii			Matautu, Savaii Is.	0.5		The third tsunami to have occurred as a result of the Mt. Matavanu volcanic eruptive influences was at 3:00 AM on June 19 1907.
1907 Jun 27		North coast of Savaii			Matautu, Savaii Is.	0.5		The fourth tsunami to have occurred as a result of the Mt. Matavanu volcanic eruptive influences was between 6:00 - 7:00 PM on July 9 1907.

1907 Jul 9		North coast of Savaii			Matautu, Savaii Is.	0.5		The fifth tsunami to have occurred as a result of the Mt. Matavanu volcanic eruptive influences was at 6:45 PM on July 9 1907.
1907 Jul 25		North coast of Savaii			Matautu, Savaii Is.	0.5		The sixth tsunami to have occurred as a result of the Mt. Matavanu volcanic eruptive influences was at 11:00 AM on July 25 1907.
1907 Oct 6		North coast of Savaii			Matautu - Savaii Is. Apia - Upolu Is;	3.0 - 3.6 (Matautu) 0.3 - 0.6 (Apia)		The largest and most important tsunami formed from the Matavanu eruption was at 5:30 PM on October 6 1907. At Matautu, Savaii, several boats were damaged and a 400-gallon tank of water was lifted bodily from its foundation and carried across the road. The height of the wave observed in Apia may not have been hazardous, hence resulting in no damages to property and infrastructure.
1915 Feb 11		Samoa Islands?			Manua Is.			The New YorK Times (13 Feb. 1915) reported that hurricane and an earthquake followed by a 'tidal wave' swept the Manua Islands. The impacts that resulted were the loss of three lives, as well as more than 75% destruction of respective village infrastructure and plantation crops. No seismic activities were recorded for that period.
1917 May 1	7:26 a.m.	Kermadec Is.	29.0S, 177.0 W	8.0	Apia, Upolu Is.			This tsunami probably generated from the magnitude 8.0 earthquake in the Kermadec Island area, although the wave height of the tsunami documented may have been confused with the June 25 1917 tsunami, thus resulting in error. A 12-metre wave was reported in the existing literature, although no mention of impacts was made. The actual magnitude of the tsunami generated is therefore not known.

1917 Jun 25	6:50 p.m.	Samoa Islands	15.5 S, 173.0 W	8.3	Apia, Aleipata, Lotofaga - Upolu Is. Palauli, Satupaitea - Savaii Is. Pago Pago - Tutuila Is.	0.8 (Apia) 3.0 (Aleipata, Lotofaga, Palauli, Satupaitea) 2.4 (Pago Pago)	0.9	The tsunami wave was noted in Apia at about 6:55 pm. Reports indicate that destructive waves were experienced at Aleipata, and for the case of Lotofaga, half of the village was submerged and houses destroyed. A bridge was washed away at Palauli and a number of native houses destroyed. In Satupaitea, a copra house was carried down the coast by the wave for about a quarter of a mile, and all native houses demolished. In Pago Pago, a recession of ocean water was observed a few minutes after the earthquake was felt. Many native houses were destroyed, including partial destruction of a Catholic church in Leone, and a Mormon church in Pago Pago.
1918 Sep 7	6:16 a.m.	South Kuril Islands	45.5 N, 151.5 E	8.25	Apia, Sogi - Upolu Is. Safune - Savaii Is.	0.4 (Apia) 0.3 (Sogi) 0.3 (Safune)	9.7 (Apia) 12.7 (Sogi)	No damage was reported in Apia from the initial wave which arrived a few minutes before 3:00 pm on September 8. At Sogi and Safune, 3 hours folowing the wave in Apia, a recession was noted, followed by a wave of about 0.3 metres.
1919 Apr 30	8:17 p.m.	Tonga Islands	19.0 S, 172.5 W	8.3	Apia - Upolu Island Pago, Pago - Tutuila Is.	0.37 (Apia) 1.8 - 2.4 (Tutuila)	0.9	The tsunami wave was noted in Apia at 9:12 pm. No details on any impacts were documented. In Tutuila (most probably Pago Pago harbour), a recession of about 2 metres was observed. A 1.8 - 2.4 metre wave returned a few minutes after the recession. No details however on the impacts in Tutuila have been documented.

1920 Aug -		Samoa Islands			Apia, Upolu Is.			Although early scholars noted that an earthquake and tsunami occurred in the month of August 1920, those reports were probably in error, as recent seismic studies have shown that no earthquake was registered in the area during this period. It is therefore concluded that this event is erroneously reported
1920 Sep 20	3:39 a.m.	New Hebrides	20.0 S, 168.0 E	8.0	Apia, Upolu Is.		4.4	Reports indicate that the first wave reached Apia at 8:04 am. No information regarding the impacts of this event as well as the wave height experienced could be located.
1922 Nov 11					Apia, Upolu Is. Pago Pago, Tutuila Is.			It is reported that the first wave reached Apia at 6:36 pm. Slight damage was reported in Pago Pago.
1923 Feb 3					Apia, Upolu Is.			The first wave was reported to have reached Samoa at 2:42 pm, although the change in water level was considered to be small.
1928 Jun 17					Apia, Upolu Is.			Records indicate that the first tsunami wave was recorded at 4:50 am. However, no other information on the details of this event was located.
1932 Jun 3					Apia, Upolu Is.	0.06		The Apia Observatory tide gauge recorded this event at about 10:45 am. No other details of this event were recorded. The tsunami was insignificant in causing any damages.
1933 Mar 2					Apia, Upolu Is.			Reports indicate that this event was recorded at Apia, although the details of it could not be located.

1944 Dec 7					Apia, Upolu Is.	0.05		A weak event was recorded at Apia, although the tsunami was insignificant in causing any damages.
1946 Apr 1		Aleutian Is.		7.1	Apia, Upolu Is. Pago Pago, Tutuila Is.	1.7		A recession of water in the Apia harbour was first noticed at 10:30 am, leaving the inner reef quite exposed. This was followed shortly after by an inrush of waves about 1.7 metres high. Six of these waves were noticed in 2 hours. The impacts caused were not documented. In Pago Pago village, officers of the MV Honda Knot reported that several huts were washed away by the tsunami wave.
1948 Sep 8		Tonga Islands	21.0 S, 174.0 W	7.8	Pago Pago, Tutuila Is.	0.1		It was noted that a small tsunami formed as a result of the magnitude 7.8 earthquake in Tonga. The wave was probably too small to cause any notable impacts. No other details of this event were available.
1952 Mar 4		Tokachi, Japan			Pago Pago, Tutuila Is.			A minor trace of the tsunami generated from the earthquake in Tokachi was recorded at the Pago Pago tide gauge. The wave was probably too small to cause any notable impacts.
1952 Mar 10		South East of Hokkaido, Japan		7.1	Pago Pago, Tutuila Is.			A monir trace of the tsunami generated was recorded at the Pago Pago tide gauge. Again, the wave was probably too small to cause any notable impacts.
1952 Mar 17		Hawaii			Pago Pago, Tutuila Is.			A minor trace of the tsunami generated was recorded at the Pago Pago tide gauge. The tsunami formed as a result of an earthquake which occurred off the coast of Hawaii. The wave was probably too small to cause any notable impacts.

1952 Mar 19		Mindanao, Phillipines		7.8	Pago Pago, Tutuila Is.			A minor trace of the tsunami generated from this earthquake was recorded at the Pago Pago tide gauge. The tsunami was too small to cause any damages, or even be noticed as a tsunami to the general observer.
1952 May 13		Costa Rica			Pago Pago, Tutuila Is.			A minor trace of the tsunami generated from this earthquake was recorded at the Pago Pago tide gauge. The tsunami was too small to cause any damages, or even be noticed as a tsunami to the general observer.
1952 Jul 13		New Hebrides			Pago Pago, Tutuila Is.			A minor trace of the tsunami generated from this earthquake was recorded at the Pago Pago tide gauge. The tsunami was too small to cause any damages, or even be noticed as a tsunami to the general observer.
1952 Nov 4		Kamchatka	52.8 N, 159.5 E	9.0	Apia, Mulinuu, Laulii, Fagaloa - Upolu Is. Safai - Savaii Is.	1.3 (Apia) 0.6 (Mulinuu) 1.8 (Laulii) 1.8 (Fagaloa) 2.0 (Safai)		The first signs of a disturbance were noticed in Apia at 3:45 pm, where water in the harbour was drained to below low-tide level exposing all the inner reef, and filled to over highest tide level upon the return of water. Land around the the Custom House in Apia was flooded to a depth of a few inches. At Mulinuu, the wave was perhaps too small to cause any damages. At Laulii, the water penetrated up to the road, which was about 3 feet above low tide level. In Fagaloa, particularly Maasina, Samamea and Taelefaga, a school and some Samoan houses were completely destroyed. In Safai, it is reported that the wave was much higher than the March 1957 tsunami, although no reports of any damages were located.

1953 Sep 13	1:27 p.m.	Kandaru Passage, Fiji	18.5 S, 178.5 E	6.75	Pago Pago, Tutuila Is.	0.2		No details were on any impacts were noted for the Samoan Islands. Waves of 1.5 metres at Beqa Island and 3 metres at Suva (Viti Levu) in Fiji were reported. The wave however was probably too small in Samoa to cause any significant impacts.
1957 Mar 9	3:22 a.m.	Andreanof Is., Aleutian Islands	51.3 N, 175.8 W	8.5	Faleolo, Vaiusu, Mulinuu, Apia, Laulii, Saoluafata, Fagaloa (Taelefaga & Maasina) - Upolu Is. Safai - Savaii Is. Pago Pago, Fagasa - Tutuila Is.	0.3 (Faleolo) 0.3 (Mulinuu) 0.3 (Apia) 0.9 (Laulii) 0.9 (Saoluafata) 1.5 (Fagaloa - Taelefaga) 1.05 (Fagaloa - Maasina) 1.8 (Safai) 1.2 (Pago Pago) 1.5 (Fagasa)	9.0 (Apia)	At Faleolo, the water level rose by about 1 foot but only once. At Vaiusu Bay, the water current was strong enough to damage a wire-netting fish trap in the bay, but no inundation reports were received. At Laulii, inundation amounted to about 50 yards (45.7 metres) inland from the high water mark. At Saoluafata, the first motion noticed was a small recession of the sea exposing the reef at approximately 11:00 am - 12:00 pm, followed by a small advance. The next advance washed over a gently sloping sandy bank, carrying light vegetation debris, and flowed under some Samoan houses on the inland side. At Fagaloa Bay (Taelefaga), inundation over the lower lying part of the village was about 25 yards (23 metres); the sea washing into huts and depositing a canoe with a boy inside a Samoan house. At Safai, the waves had sufficient force to demolish a stone causeway used by the villagers to cross the adjacent creek to their plantation area. In Pago Pago and Fagasa harbour, a maximum of 1.5 metre waves were experienced, although the extent of damages (if any) were not reported.
1958 Nov 6	11:58 a.m.	Iturup, South Kuril Islands	44.5 N, 148.5 E	8.25	Pago Pago, Tutuila Is.	0.1	9.9	The waves experienced at Pago Pago were probably too small to cause any significant effects, or even be noticed as a tsunami to the lay observer.

1960 May 22 1960 May 23	8:11 a.m.	South Chile	39.5 S, 74.5 W	8.5	Apia, Lalomanu, Fagaloa Bay, Malaela - Upolu Is. Falelima, Neiafu, Tufutafoe, Tuasivi, Sasina - Savaii Is. Pago Pago - Tutuila Is.	1.5 (Apia) 1.8 (Lalomanu) 2.4 (Fagaloa Bay) 2.7 (Falelima) 2.1 (Tufutafoe) 1.5 (Tuasivi) 3.6 (Pago Pago) 0.75 (Fagaalua) 1.8 (Malaela) 1.5 (Sasina)	12.4	This tsunami was undoutedly one of the largest that has been recorded in the Samoan group. No impacts were noted in Apia. At Lalomanu, two fisherman in canoes near the reef had been picked up by the wave and washed onto the beach by the road. At Fagaloa, the first motion was a recession of the sea beyond the reef at about 11:45 pm . A few minutes later, a crest advanced 90 yards (82 metres) through the village. The peak water level reached the roof of one of the local Samoan houses. Debris was scattered about the village, although there were no loss of lives. There were no reports of any damages in the other areas listed in both Upolu and Savaii. For the case of Malaela and Sasina, the wave was noticed in the early morning of the next day as both areas enclosed bay entrances as a result of the offshore reef. at Pago Pago, damages amounted to USD$50,000. One house was lifted and moved 10 feet (3 metres) inland, and another was washed into the bay by the outgoing wave.
1963 Feb 13	9:50 p.m.	North Taiwan	24.5 N, 7.25 E	7.25	Pago Pago, Tutuila Is.			A minor trace of the tsunami was recorded at the tide gauge, although the wave was probably too small to cause any significant effects.
1963 Mar 30		Dixon Entrance			Pago Pago, Tutuila Is.			A minor trace of a tsunami was recorded at the Pago Pago tide gauge, although no earthquake data could be found.
1963 Oct 13	6:18 p.m.	South Kuril Islands	44.7 N, 150.7 E	8.25	Pago Pago, Tutuila Is.	0.1	9.6	This tsunami was probably too small to cause any significant effects.
1963 Oct 20	1:00 p.m.	South Kuril Islands	44.7 N, 150.7 E	6.75	Pago Pago, Tutuila Is.	0.1	9.8	This tsunami was probably too small to cause any significant effects.
1964 Mar 27	4:36 p.m.	Gulf Of Alaska	61.1 N, 147.7 W	8.4	Apia, Upolu Is. Pago Pago, Tutuila Is.	0.39	10.3	The great Alaska earthquake. No reports of any damages in the Samoan Islands.

1964 Jun 16	5.02 PM	Niigata Yamagata	38.3 N, 139.2 E	7.5	Pago Pago, Tutuila Is.			A minor trace of the tsunami was recorded at the tide gauge, although it was probably too small to cause any significant effects.
1965 Jan 24	1:11 p.m.	Indonesia Mollucas Sanana Is.	2.4 S, 126.0 E	7.5	Pago Pago, Tutuila Is.			A minor trace of the tsunami was recorded at the tide gauge, although it was probably too small to cause any significant effects.
1965 Feb 4	6:01 p.m.	Rat Is., Alleutin Is.	51.3 S, 178.6 E	7.75	Pago Pago, Tutuila Is.			A minor trace of the tsunami was recorded at the tide gauge, although it was probably too small to cause any significant effects.
1965 Mar 29	3:27 p.m.	Aleutian Is.	50.6 N, 177.9 E	7.3	Pago Pago, Tutuila Is.			A minor trace of the tsunami was recorded at the tide gauge, although it was probably too small to cause any significant effects.
1965 Jul 2	9:59 a.m.	Near Unalaska, Aleutian Is.	53.1 N, 167.6 W	6.9	Pago Pago, Tutuila Is.			A minor trace of the tsunami was recorded at the tide gauge, although it was probably too small to cause any significant effects.
1965 Aug 12	11:32 a.m.	New Hebrides	15.8 S, 167.2 E	6.4	Pago Pago, Tutuila Is.			A minor trace of the tsunami was recorded at the tide gauge, although it was probably too small to cause any significant effects.
1966 Oct 17	10:42 a.m.	New Coast of Peru	10.7 S, 78.7 W	7.5	Pago Pago, Tutuila Is.	0.1		A minor trace of the tsunami was recorded at the tide gauge, although it was probably too small to cause any significant effects.
1966 Dec 28	9:18 p.m.	New Coast Of Northern Chile	25.5 S, 70.7 W	7.75	Pago Pago, Tutuila Is.	0.2		A minor trace of the tsunami was recorded at the tide gauge, although it was probably too small to cause any significant effects.
1966 Dec 31	7:23 a.m.	Santa Cruz Is.	11.8 S, 166.5 E	7.5	Pago Pago, Tutuila Is.	0.1		A minor trace of the tsunami was recorded at the tide gauge, although it was probably too small to cause any significant effects.
1968 Mar 31	1:42 p.m.		32.5 N, 132.2 E	6.2	Pago Pago, Tutuila Is.			A minor trace of the tsunami was recorded at the tide gauge, although it was probably too small to cause any significant effects.
1969 Nov 22	12:09 p.m.	East Coast Of Kamchatka	57.8 N, 163.5E	7.1	Pago Pago, Tutuila Is.			A minor trace of the tsunami was recorded at the tide gauge, although it was probably too small to cause any significant effects.

1971 Jul 14	7:11 p.m.	New Ireland	5.5 S, 153.9 E	7.7	Pago Pago, Tutuila Is.	0.06		A minor trace of the tsunami was recorded at the tide gauge, although it was probably too small to cause any significant effects.
1973 Jan 30	10:01 a.m.	Near Coast of Michoacan, Mexico	18.5 N, 103.0 W	7.3	Pago Pago, Tutuila Is, Apia.	0.22 (Pago Pago) 0.09 (Apia)		A minor trace of the tsunami was recorded at the tide gauge, although it was probably too small to cause any significant effects.
1973 Jun 17	4:55 p.m.	Hokkaido, Japan	43.2 N, 145.8 E	7.7	Pago Pago, Tutuila Is.	0.09		A minor trace of the tsunami was recorded at the tide gauge, although it was probably too small to cause any significant effects.
1974 Oct 3	3:21 a.m.	Near Coast of Peru	12.3 S, 77.8 W	7.5	Pago Pago, Tutuila Is.	0.31		A minor trace of the tsunami was recorded at the tide gauge, although it was probably too small to cause any significant effects.
1975 Nov 29	3:47 a.m.	Hawaii, Near Kiluaea Crater.	19.33 N, 155.01 W	7.2	Pago Pago, Tutuila Is	0.21		A minor trace of the tsunami was recorded at the tide gauge, although it was probably too small to cause any significant effects.
1975 Dec 26	4:56 a.m.	Tongan Trench	16.3 S, 172.5 W	7.6	Pago Pago, Apia	0.75 (Pago Pago) 0.15 (Apia)		A minor trace of the tsunami was recorded at the tide gauge, although it was probably too small to cause any significant effects.
1976 Jan 14		Kermadec Is.	28.4 S, 177.7W	8.0	Apia, Upolu Is.	0.14		A minor trace of the tsunami was recorded at the tide gauge, although it was probably too small to cause any significant effects.
1977 Apr 2	8:15 p.m.	Tonga Trench.	16.2 S, 171.6 W	7.2	Pago Pago, Tutuila Is, Apia, Upolu Is.	0.15 (Pago Pago) 0.07 (Apia)	0.6 0.5	A minor trace of the tsunami was recorded at the tide gauge, although it was probably too small to cause any significant effects.
1977 Apr 20	12:13 p.m.	Solomon Is.	9.5 S, 160.4 E	6.5	Apia, Upolu Isl .	0.04	6.5	A minor trace of the tsunami was recorded at the tide gauge, although it was probably too small to cause any significant effects.
1977 Apr 21	5:24 p.m.	Solomon Is.	11.1 S, 160.7 E	7.5	Apia, Upolu Is.	0.03	6.8	A minor trace of the tsunami was recorded at the tide gauge, although it was probably too small to cause any significant effects.
1977 Jun 22	1:08 a.m.	Tonga Trench	20.9 S, 177.4 W	7.0	Pago Pago, Tutuila Is.	0.13	1.2	A minor trace of the tsunami was recorded at the tide gauge, although it was probably too small to cause any significant effects.

1977 Oct 10	12:54 p.m.	Tonga Trench	26.1 S, 175.3 W	6.9	Pago Pago, Tutuila Is.	0.02	0.9	A minor trace of the tsunami was recorded at the tide gauge, although it was probably too small to cause any significant effects.
1979 Mar 14	12:07 p.m.	Pacific Coast Of Japan	17.82 N, 101.26 W		Pago Pago, Tutuila Is	0.1		A minor trace of the tsunami was recorded at the tide gauge, although it was probably too small to cause any significant effects.
1981 Sep 1	See Okal et al.(2010; 2011)	Tonga Trench	14.96 S, 173.09 W		Taga, Savai'i	1.0		Wave height of 1m was reported, although there were no casualties.
2009 Sep 29	Dominey-Howes and Thaman (2009)	Tonga Trench	Dominey-Howes and Thaman (2009)	Dominey-Howes and Thaman (2009)	See Dominey-Howes and Thaman (2009)	Dominey-Howes and Thaman (2009)	Dominey-Howes and Thaman (2009)	Impacts for this tsunami are provided by Dominey-Howes and Thaman (2009); Beavan et al. (2010); Lay et al. (2010); Okal et al. (2010); Roeber et al. (2010); Chagué-Goff et al. (2011); McAdoo et al. (2011); Okal et al. (2011); Reese et al. (2011); Richmond et al. (2011).
2011 Mar 11	See Satake et al. (2012)	Tohoku, Japan	See Satake et al. (2012)	See Satake et al. (2012)	Fagaloa Bay	~1.5	See Satake et al. (2012)	See Satake et al. (2012)

APPENDIX 2: SITE DATA

OVERVIEW

This Appendix contains site data for the investigated sites.

Appendix Table 2.1 provides the locations, GPS spot heights and inland distances at each site.

Appendix Figures 2.1—2.10 are site maps corresponding to Appendix Table 2.1, as well as the general site locations shown in Figure 15 of the main thesis text. Observation dates are also provided in these maps, respectively.

Appendix Table 2.1: Investigated site data.

Site	Coordinate Location	Distance inland of high tide mark (m)	Elevation above mean sea level (m)	Stratigraph depths (m)
Fagalii	$13^0$50.628' S; $171^0$44.131' W	150	12	3
Falealupo	$13^0$29.663' S; $172^0$46.523' W	165	10	0.5
Fale o le Fee	$13^0$55.134' S; $171^0$44.285' W	7,500	475	0.6
Lano	$13^0$37.176' S; $172^0$11.938' W	150	8	1.5
Maasina	$13^0$56.607' S; $171^0$33.585' W	40	8	0.7
Manono	$13^0$52.120' S; $172^0$04.263' W	75	3	2.5
Mulivai	$14^0$00.505' S; $171^0$47.651' W	25	3	1.02
Satitoa	$14^0$01.363' S; $171^0$25.754' W	280	16	0.84
Satupaitea	$13^0$45.576' S; $172^0$19.209' W	75	10	1
Tau	$14^0$13.542' S; $169^0$30.921' W	140	5	0.67
Vaovai	$14^0$02.140' S; $171^0$40.832' W	20	3	0.72

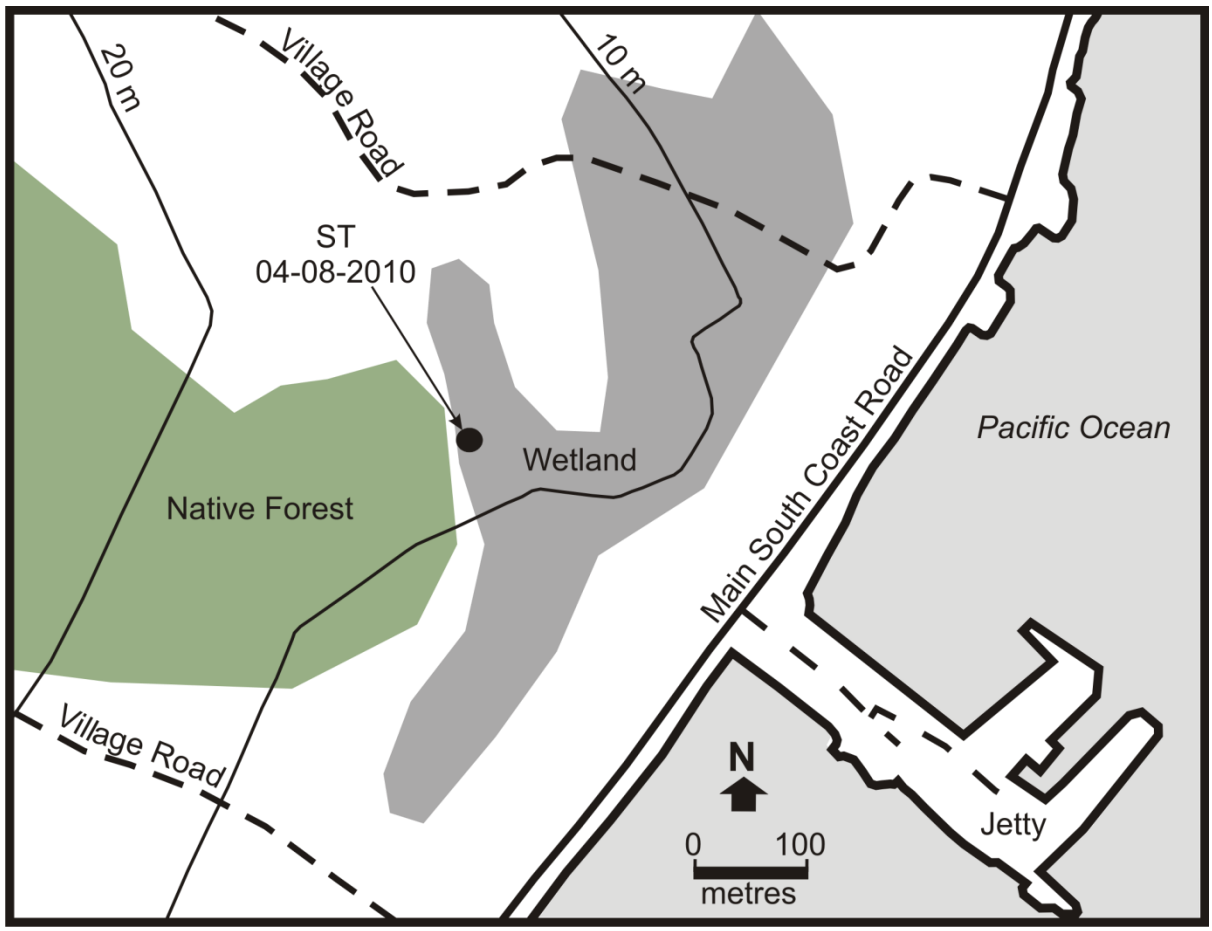

Appendix Figure 2.1: Satitoa site map. ST = Satitoa trench site. 04-08-2010 = Observation date. The 10 m and 20 m contour lines are shown.

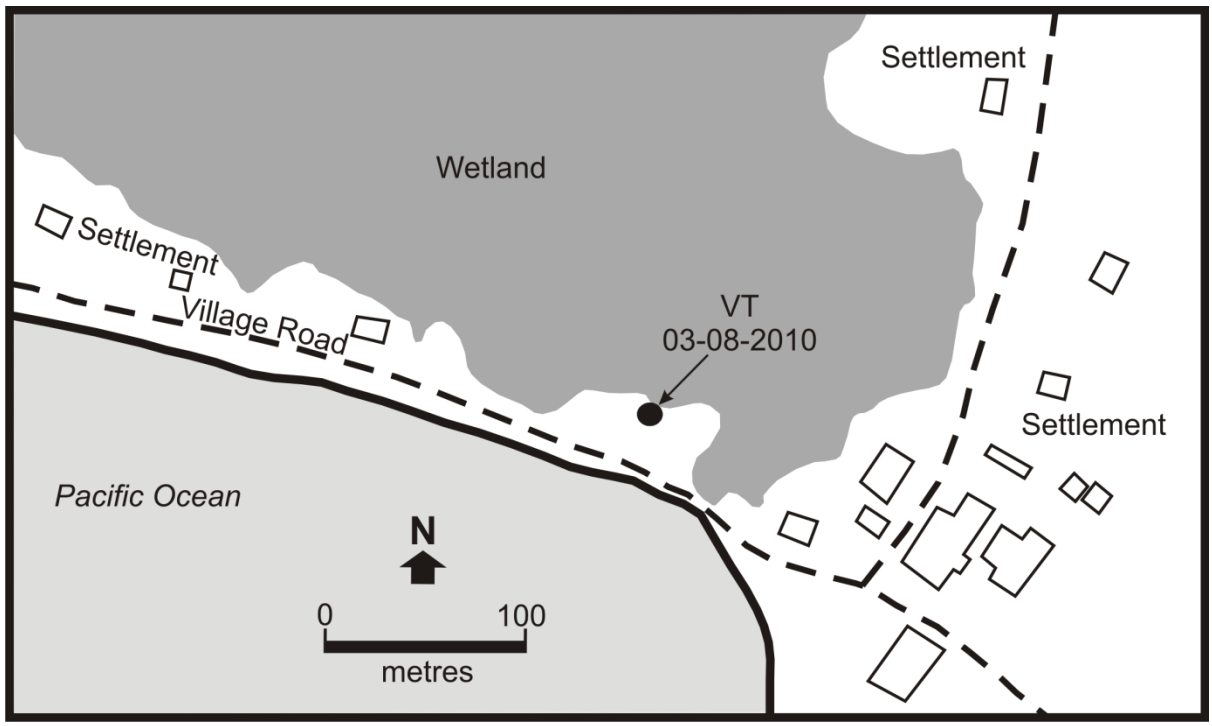

Appendix Figure 2.2: Vaovai site map. VT = Vaovai trench site. 03-08-2010 = Observation date.

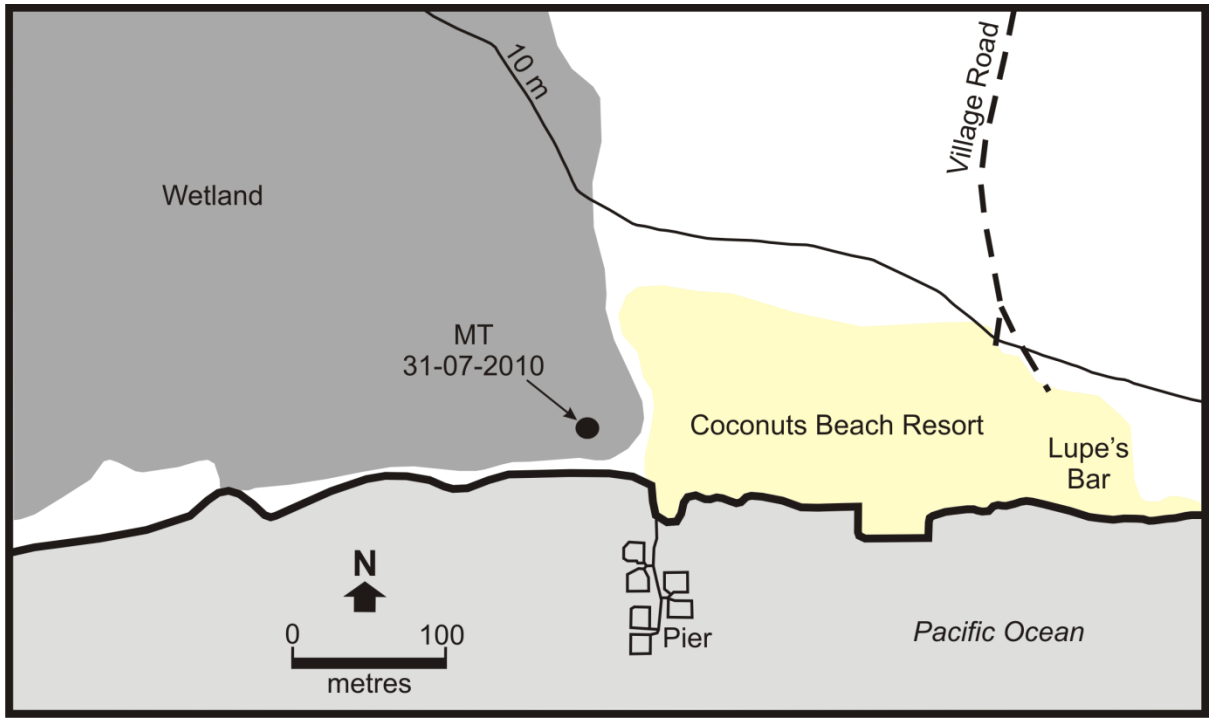

Appendix Figure 2.3: Mulivai site map. MT = Mulivai trench site. 31-07-2010 = Observation date. The 10 m contour line is shown.

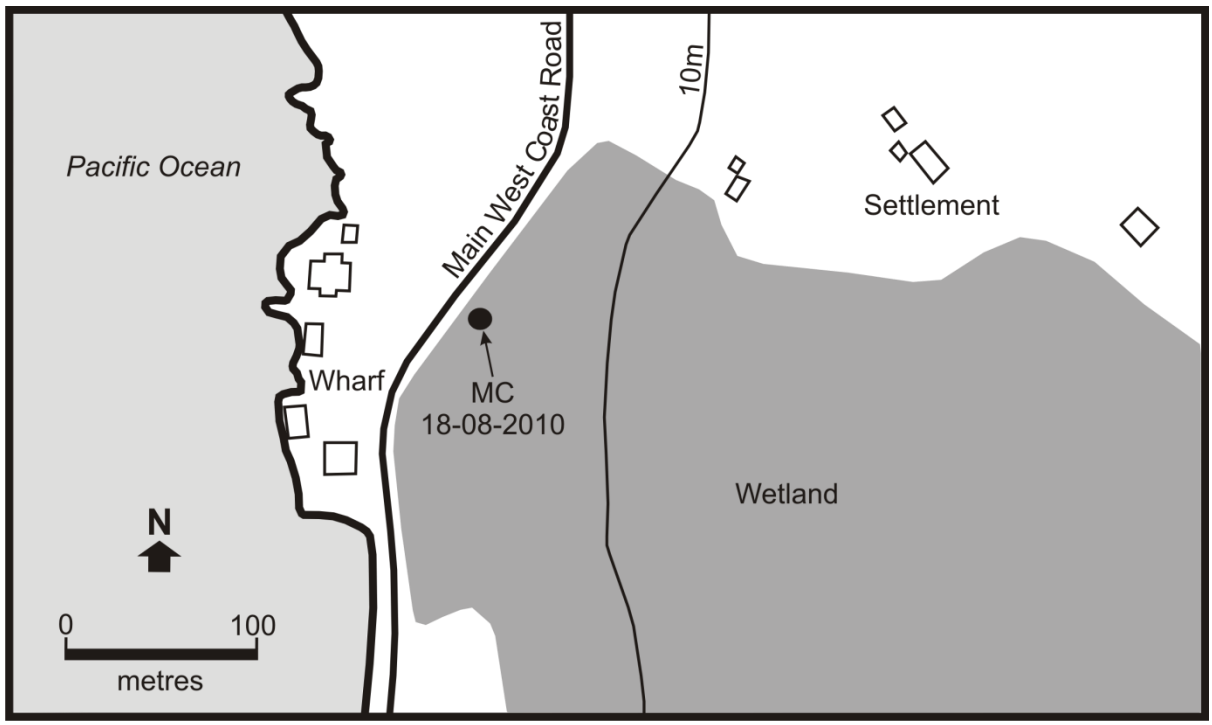

Appendix Figure 2.4: Manono site map. MC = Manono core site. 18-08-2010 = Observation date. The 10 m contour line is shown.

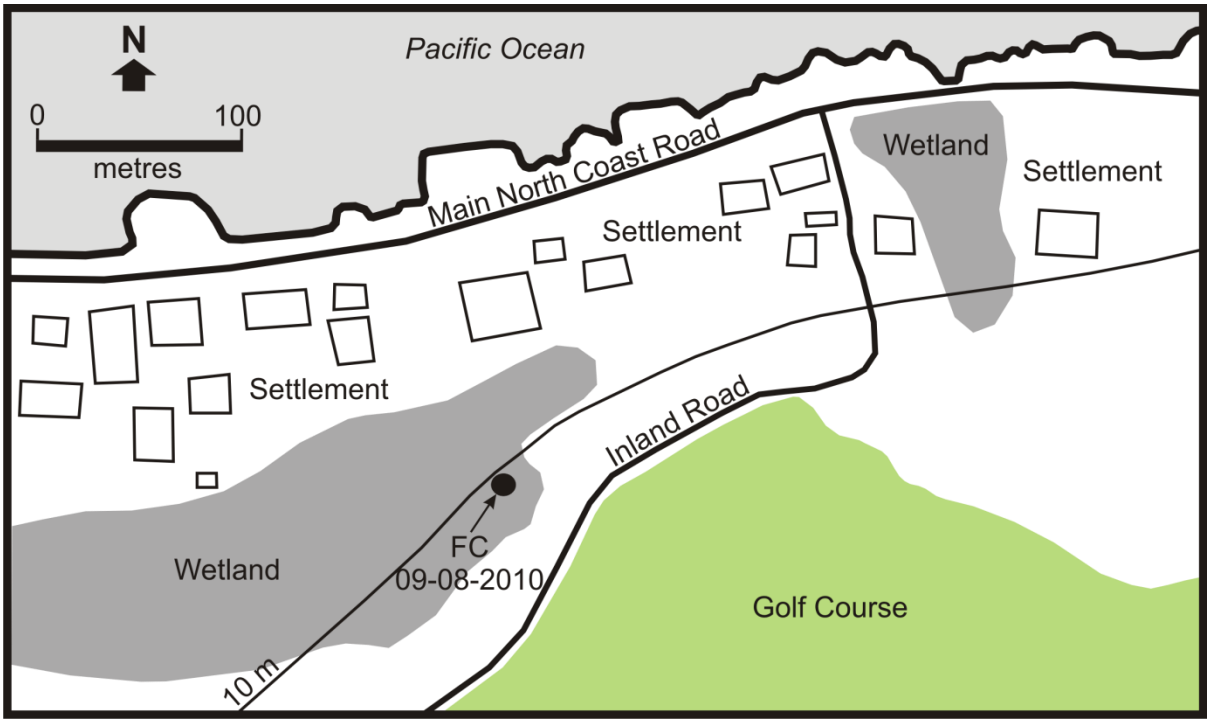

Appendix Figure 2.5: Fagali'i site map. FC = Fagali'i core site. 09-08-2010 = Observation date. The 10 m contour line is shown.

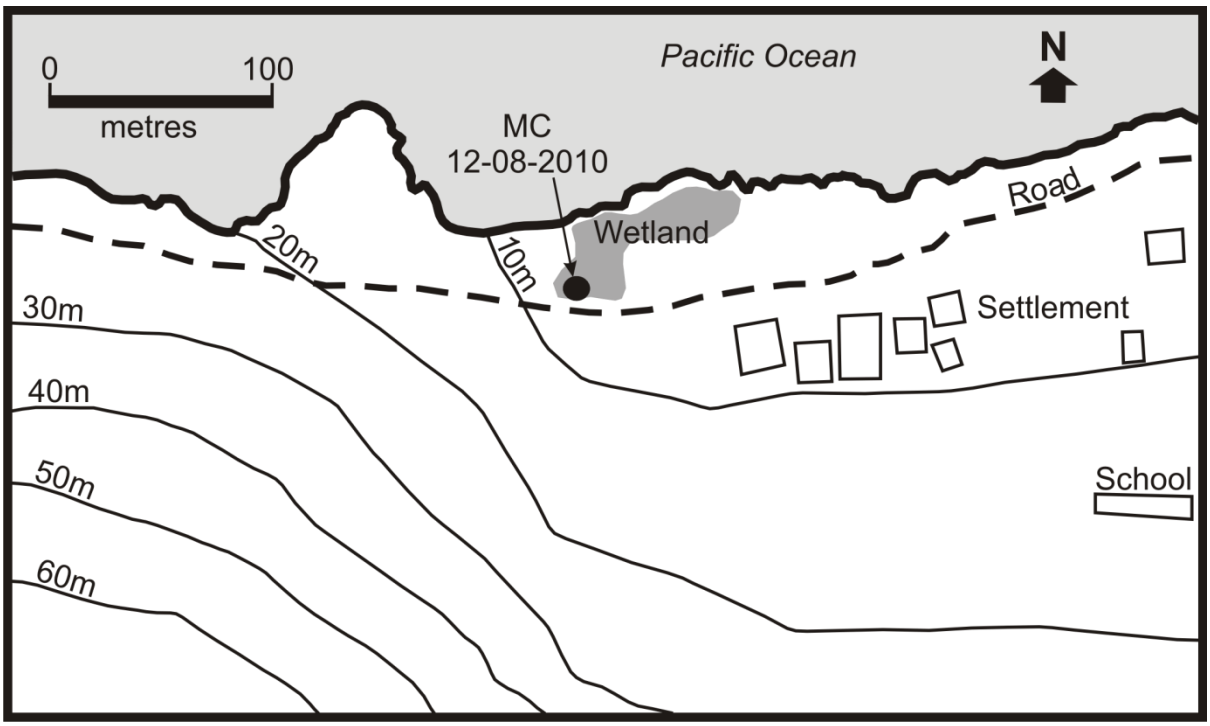

Appendix Figure 2.6: Ma'asina site map. MC = Ma'asina core site. 12-08-2010 = Observation date. The 10 m—60 m contour lines are shown.

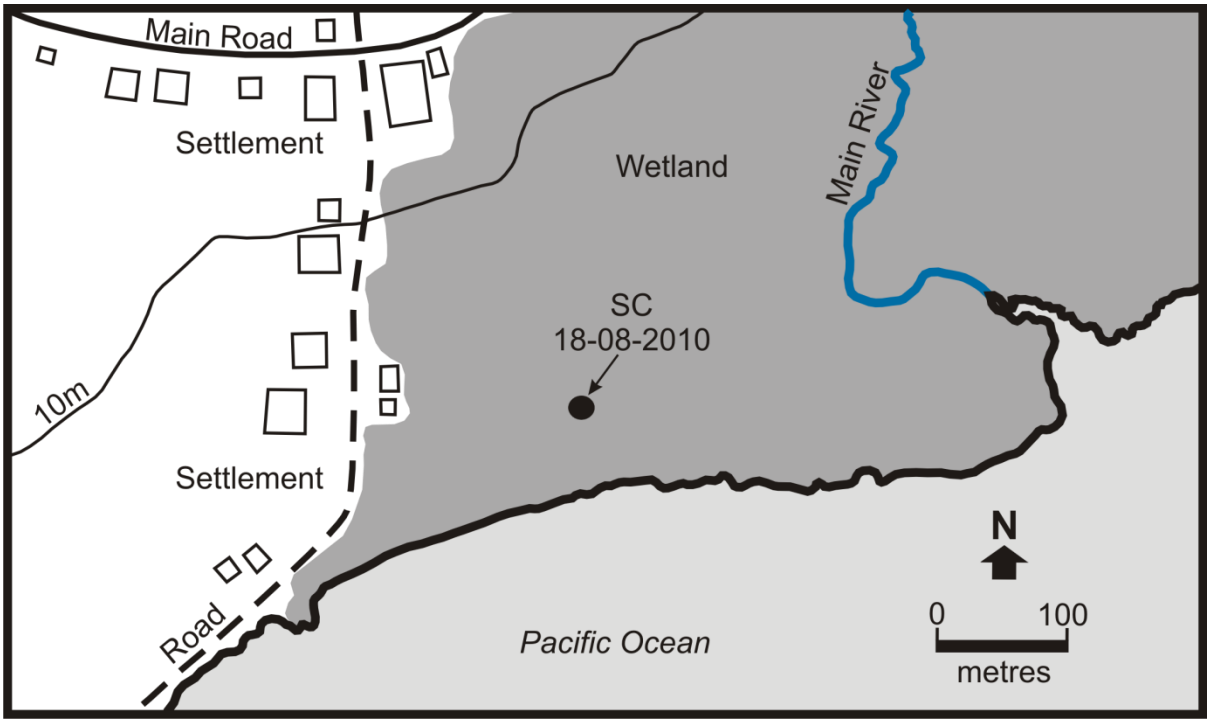

Appendix Figure 2.7: Satupaitea site map. SC = Satupaitea core site. 18-08-2010 = Observation date. The 10 m contour line is shown.

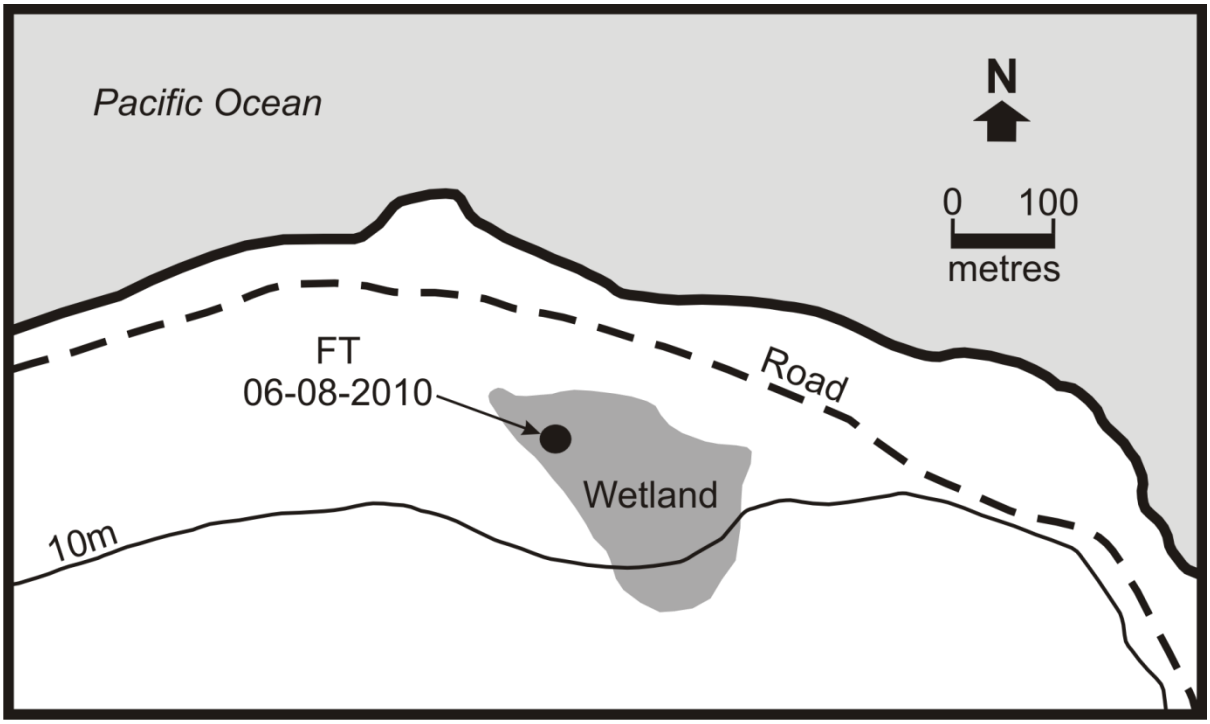

Appendix Figure 2.8: Falealupo site map. FT = Falealupo trench site. 06-08-2010 = Observation date. The 10 m contour line is shown.

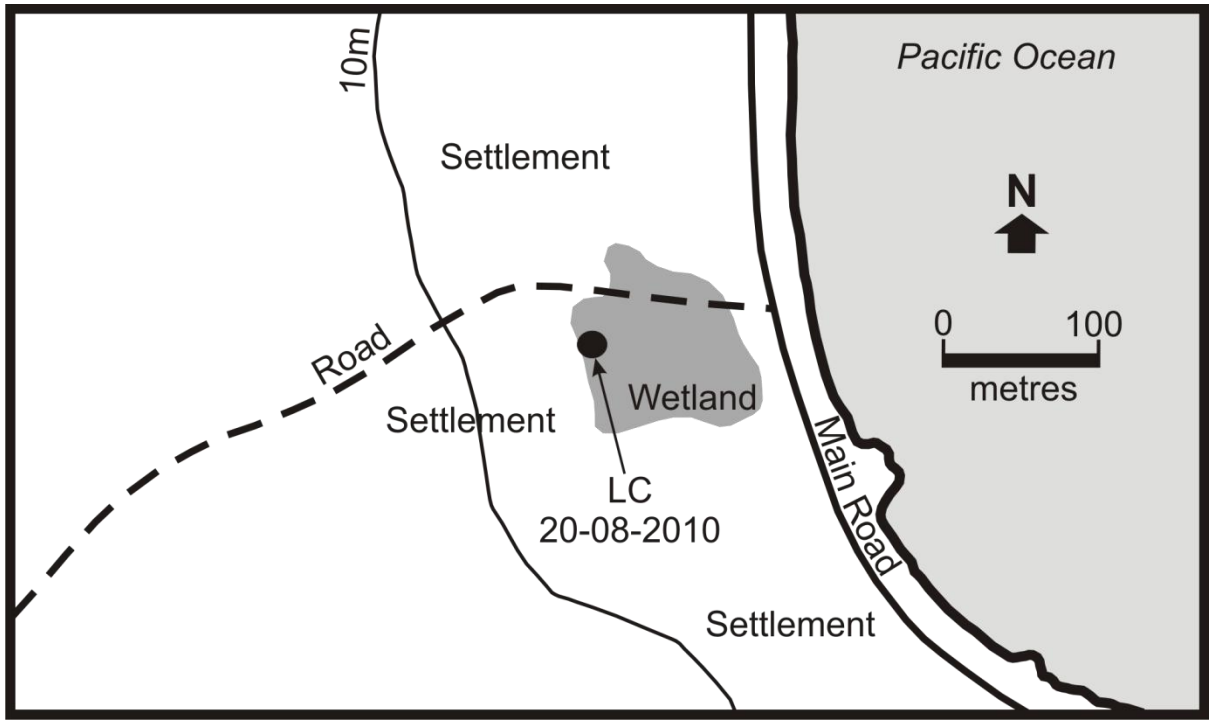

Appendix Figure 2.9: Lano site map. LC = Lano core site. 20-08-2010 = Observation date. The 10 m contour line is shown.

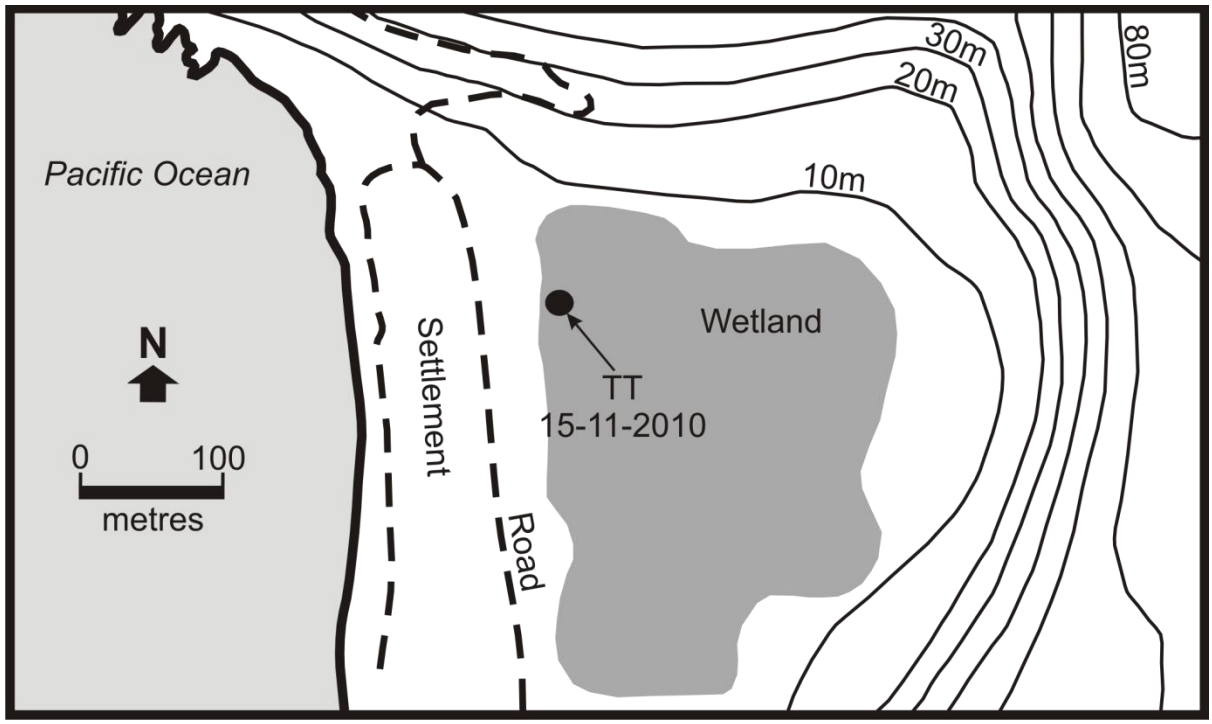

Appendix Figure 2.10: Ta'u site map. TT = Ta'u trench site. 15-11-2010 = Observation date. The 10 m—80 m contour lines are shown.

Deputy Vice-Chancellor's Office
Postgraduate Office

Co-Authorship Form

UNIVERSITY OF CANTERBURY
Te Whare Wānanga o Waitaha
CHRISTCHURCH NEW ZEALAND

This form is to accompany the submission of any thesis that contains research reported in co-authored work that has been published, accepted for publication, or submitted for publication. A copy of this form should be included for each co-authored work that is included in the thesis. Completed forms should be included at the front (after the thesis abstract) of each copy of the thesis submitted for examination and library deposit.

Appendix 3.1: Sands of Time: Evidence for palaeotsunamis and/or palaeostorms in Samoa, and what this means for tsunami risk reduction.

Publication status: 2011. In; Malua, T.L. (ed). Proceedings of the Samoa National Environment Forum 2010.

Shaun Williams wrote the manuscript. Development and refining of the original manuscript was conducted by the co-authors stated in the Co-Authorship Declaration of this thesis.

Certification by Co-authors:
If there is more than one co-author then a single co-author can sign on behalf of all
The undersigned certifys that:

- The above statement correctly reflects the nature and extent of the PhD candidate's contribution to this co-authored work
- In cases where the candidate was the lead author of the co-authored work he or she wrote the text

Name: **Tim Davies** Signature: Date: **30 April 2014**

Deputy Vice-Chancellor's Office
Postgraduate Office

Co-Authorship Form

UNIVERSITY OF CANTERBURY
Te Whare Wānanga o Waitaha
CHRISTCHURCH NEW ZEALAND

This form is to accompany the submission of any thesis that contains research reported in co-authored work that has been published, accepted for publication, or submitted for publication. A copy of this form should be included for each co-authored work that is included in the thesis. Completed forms should be included at the front (after the thesis abstract) of each copy of the thesis submitted for examination and library deposit.

Appendix 3.2: Characterising diagnostic proxies for identifying palaeotsunamis in a tropical climatic regime, Samoan Islands.

Publication status: 2011. In; Oceans 2011, MTS/IEEE Kona Conference Proceedings.

Shaun Williams wrote the manuscript. Development and refining of the original manuscript was conducted by the co-authors stated in the Co-Authorship Declaration of this thesis.

Certification by Co-authors:
If there is more than one co-author then a single co-author can sign on behalf of all
The undersigned certifys that:

- The above statement correctly reflects the nature and extent of the PhD candidate's contribution to this co-authored work
- In cases where the candidate was the lead author of the co-authored work he or she wrote the text

Name: **Tim Davies** Signature: Date: **30 April 2014**

APPENDIX 3: PRELIMINARY THESIS REPORTS

OVERVIEW

This Appendix is subdivided into Appendices 3.1 and 3.2.

Appendix 3.1 is a version of a co-authored conference proceeding report published in; **Malua, T.L. (ed) 2011, *Proceedings of the Samoa National Environment Forum 2010, pp 15-25.***The published report is entitled 'Sands of Time: Evidence of palaeotsunamis and/or palaeostorms in Samoa, and what this means for tsunami risk reduction'.

Appendix 3.2 is a version of a co-authored conference proceeding report published in; **Oceans 2011, *MTS/IEEE Kona Conference Proceedings, 10p.***The published report is entitled 'Characterising diagnostic proxies for identifying palaeotsunamis in a tropical climatic regime, Samoan Islands'.

Shaun Williams was first author for both reports. Appendix 3.1 co-authors include James Goff, Faigame Sale, Johnny Ah Kau, Gegar Prasetya, Tim Davies, Kwok Fai Cheung, and Thomas Wilson. Appendix 3.2 co-authors include James Goff, Gegar Prasetya, Kwok Fai Cheung, Catherine Chagué-Goff, Tim Davies, and Thomas Wilson.

These Appendices provide an overview of preliminary interpretations of this thesis. Citations in both Appendices are provided in the thesis References.

Appendix 3.1: Preliminary Report 1

Contents

3.1.1 Report Abstract

Following the 29th September 2009 tsunami in the Samoan Islands, there has been an increased demand to improve understanding of the medium- to long-term risks posed by tsunamis in order to better mitigate their impacts. The historical tsunami database for Samoa, which extends back to 1837, indicates that these islands have been impacted from all the major source regions of the Pacific Ring of Fire. Given that there is virtually no specific reference to tsunamis in Samoa's prehistory (i.e. the ~3000 years prior to the arrival of the first official missionaries) it is difficult to ascertain the long-term frequency and consequent risk posed by these hazards to the people of Samoa.

This research aims to address this issue through an interdisciplinary palaeotsunami investigation. The overarching concept is that tsunamis, like cyclones and storms, leave a distinct sedimentary deposit within the coastal landscapes they impact. Distinguishing palaeotsunami from palaeostorm deposits is challenging, although detailed field and laboratory analyses of diagnostic proxies can be used to distinguish between the two processes.

This provides an avenue for understanding the likelihood of future tsunamis from various source regions, as well as the risks they pose. This paper discusses preliminary geochemical characteristics of sediment samples collected from various coastal locations on Upolu and Savaii islands during field surveys in August 2010. Specific emphasis is made on the challenges associated with distinguishing palaeotsunami from palaeostorm deposits, as well as the overall implications of this research for tsunami risk reduction in Samoa.

3.1.2 Introduction

Samoa is highly vulnerable to tsunamis, as evidenced by the 29th September 2009 South Pacific tsunami (2009 SPT) disaster in which 180 people lost their lives. Historically, Samoa has been impacted by tsunamis from all the major source regions in the Pacific Ring of Fire; some of them thousands of kilometres away (e.g. Chile/Peru and Alaska). Unfortunately, the historical database only extends back as far as 1837 (Pararas-Carayannis and Dong, 1980; Williams and Leavasa, 2006), and as such is extremely limiting for our long-term understanding of these events in terms of distribution, frequency, and magnitude. Similarly, there has not yet been any nation-wide effort to collect anecdotal evidence of historical (or pre-historic) tsunamis in Samoa. This makes it difficult to determine the long-term risk and distribution of tsunami impacts prior to 1837 (Williams, 2009).

The work discussed in this paper represents part of ongoing research that aims to determine long-term risk through an interdisciplinary palaeotsunami investigation involving a range of different analytical techniques. These include geological field investigations and empirical stratigraphic analysis, laboratory analysis involving chemical proxies, micropalaeontology, radiometric dating, sediment grainsize and distribution analysis, as well as numerical sediment and tsunami modelling.

The 2009 SPT that impacted the Samoan Islands left a distinct sedimentary deposit in much of the coastal landscapes it impacted (Annunziato et al., 2009; Dominey-Howes and Thaman, 2009). It affected much of the southeastern and eastern coastlines of Upolu island and the southern harboured landscapes on Tutuila island in American Samoa (eg. Pago Pago harbour). Most of these deposits were well preserved in coastal marshes or swamps adjacent to impacted areas where the bulk of the wave energy was absorbed thus enabling transported sediments to settle out of suspension. This was particularly evident in some areas where stagnated water remained in the landscape for several hours to days following the main tsunami.

Deposits associated with the 2009 SPT in different areas provide a reference standard for similar tsunami deposits within the geologic record specific to that area. Moreover, distinct similarities may represent similar-type events originating from the same source area. This at least holds true for areas in which a distinct sediment deposit was left behind by the 2009 SPT. In areas that were not impacted by the 2009 SPT or in which a deposit was not left behind, (palaeo-) tsunami deposits are identified and characterized by a distinct change in the stratigraphic sequence for that particular site. For example, a calcareous sand deposit may be found lying between two soil or peat layers at depth, and display distinct sedimentary and elemental composition change from the overlying and underlying soil layers. In such cases however, distinguishing whether the deposit was caused by a tsunami or a cyclone is challenging, and is normally resolved following detailed laboratory analysis using a collation of results from different analytical techniques; some of which have been mentioned above (Goff et al., 2001; Goff

et al., 2004a and 2004b; Higman and Jaffe, 2005; Goff et al. 2009; Chague-Goff and Goff, 2009; Yamazaki et al., 2009; Chague-Goff et al., 2010; Goff et al., 2010; Peters and Jaffe, 2010; Wassmer et al., 2010).

This paper discusses the initial findings of geochemical analyses of potential tsunami or cyclone deposits at different coastal sites on Upolu and Savaii islands. We present how this type of information can be used as a semi-quantitative tool for identifying palaeotsunamis and/or palaeocyclones at different sites. We also discuss how these results complement empirical stratigraphic observations of the deposits made during field investigations at various sites. In some cases these data can also help identify potential saltwater inundation events (palaeotsunamis and/or palaeostorms) that did not necessarily leave a distinct deposit in the landscapes they impacted. These geochemical results represent the first semi-quantitative findings associated with the overarching aims of this research, and will be used in the later synthesis of the broader analytical findings associated with characterizing and developing a palaeotsunami database for the Samoan Islands.

The overarching intention of this work is to improve long-term understanding of the frequency and magnitude distributions of tsunamis within the Samoa Islands. This in turn enables more informed decisions to be made when prioritizing mitigation and preparedness work for potentially vulnerable areas.

3.1.3 Investigative Analysis

Geological field investigations were carried out at thirteen sites around Upolu and Savaii islands. Mulivai (Safata), Vaovai, Vaiula, Satitoa, Salimu and Maasina (Fagaloa), Fagalii, and Manono-uta were investigated on Upolu. Satupaitea, Lano and Falealupo-tai were investigated on Savaii (Appendix Figure 3.1.1 and Table 3.1.1).

Investigated sites along the southern and eastern coastline of Upolu were all impacted by the 2009 SPT and as a working hypothesis were assumed to have preserved evidence of (pre-) historic tsunamis originating from a similar source area. That is a source area along the outer-rise region of the inter-plate thrust fault separating the Pacific and Indo-Australian tectonic plates at the northern terminus of the Tonga trench/subduction boundary (Annunziato et al. 2009; USGS, 2009).

Fagalii and Salimu and Maasina in Fagaloa Bay were studied to see whether any significant saltwater inundation events have impacted the northern coastline. It is known that Fagaloa harbour has been historically impacted by several tsunamis which originated within the Chile/Peru subduction region thousands of kilometres to the east east. In 1868 AD, settlements in Apia were apparently destroyed by a tsunami which originated from northern Chile, although details of the extent of the damage were not reported (Pararas-Carayannis and Dong, 1980). Similarly, sites on Savaii were selected to provide a

representative distribution of potentially impacted coastlines along the southern and northern parts of the island.

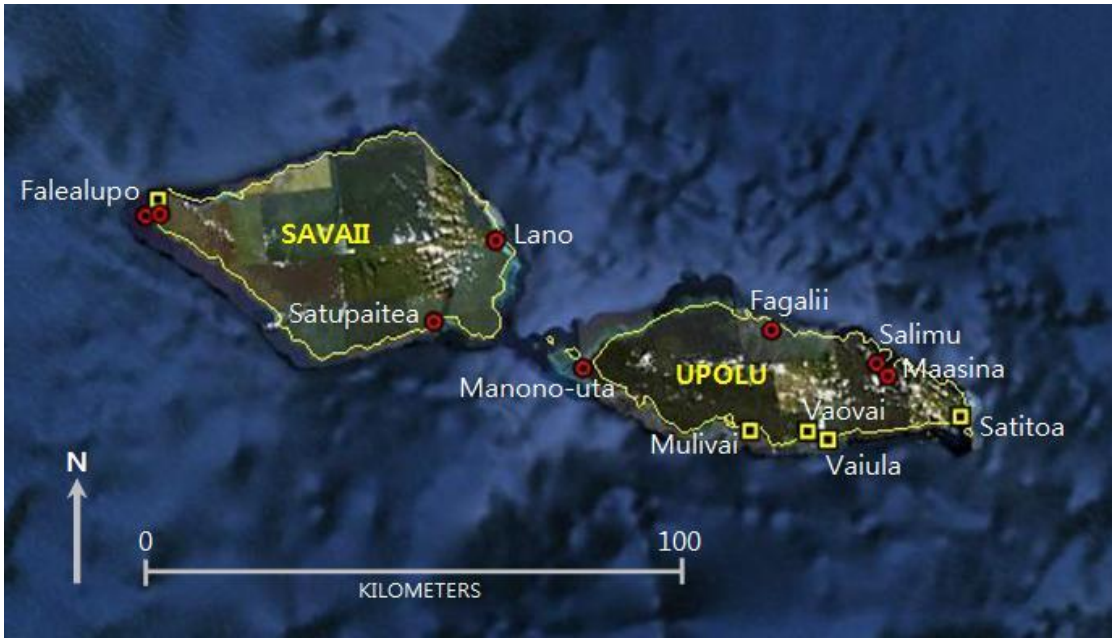

Appendix Figure 3.1.1: Map of Savaii and Upolu showing the sites investigated. Yellow squares represent trench-sites, red circles represent core-sites.

Empirical stratigraphic observations were made at each site, and sediment samples were collected for more detailed laboratory analysis using coring and trenching techniques. The first laboratory work was the elemental stratigraphic analysis carried out on samples from each site using a Tracer III portable x-ray fluorescence spectrometer (pXRF) developed by Bruker Inc. The instrument determines the relative elemental chemistry composition of a sample through the emission of photons (x-rays) onto its surface, thus exciting electrons within individual elements comprising the sample causing them to fluoresce (Bruker, 2008). In this study, the samples tested were mainly soils, peat, and calcareous sands.

3.1.3.1 Elemental Stratigraphic Analysis

Stratigraphies based on relative changes in elemental composition down the stratigraphic column at each site, provide a semi-quantitative method for analysing and interpreting empirical data collected in the field (Rothwell, 2006). Catastrophic saltwater inundation events (CSIs) is a generic term encompassing tsunamis and cyclones, and is used to label a deposit upon which it is unknown whether it was formed from tsunami or cyclone deposition (Chagué-Goff and Goff, 1999). CSIs are identified empirically through marked changes in sediment characteristics down a straitgraphic column. They are most often comprised of marine sediments sandwiched between soil or peat layers.

Appendix Table 3.1.1: Summary of sites investigated listing the number of identified catastrophic saltwater inundations based on empirical observations compared to the calcium-iron relationship technique.

Site	Coordinates	Stratigraphic Depth (m)	Distance inland from high-tide mark (m)	Likely Number of CSI deposits identified empirically	Likely Numer of CSIs identified using calcium-iron ratio technique
Mulivai	14°00.505' S; 171°47.651' W	> 1.02	25	4 at (0-10cm; 24-36cm; 38-85cm; >102cm depths)	4 at (5cm; 26cm-33cm; 60cm; 104cm depths)
Vaiula	14°02.361' S; 171°39.631' W	> 0.7	100	3 at (0-16cm; 16-40cm; >40cm depths)	5 at (5cm; 21cm; 34cm; 43cm; 46->69cm depths)
Vaovai	14°02.140' S; 171°40.832' W	> 0.72	20	3 at (0-1cm; 7-27cm; 57-72cm depths)	3 at (0-1cm; 10-11cm; 25-27cm depths).
Satitoa	14°01.363' S; 171°25.754' W	> 0.84	280	7 at (0-8cm; 8-11cm; 18-22cm; 28-30cm; 59-75; 75-84; >84cm depths)	2 at (0-11cm; >80cm depths)
Falelupo (Trench)	13°29.663' S; 172°46.523' W	>0.5	165	5 at (3-8cm; 10-15cm; 15-27cm; 27-32cm; 45-50cm)	3 at (0-15cm; 15-28cm; 28-32cm)
Falelupo (Core 1)	13°30.064' S; 172°47.161' W	1	220	0	4 at (1-21cm; 41-46cm; 61-66cm; 76-90cm)
Falelupo (Core 2)	13°29.670' S; 172°46.521' W	1	160	2 at (0-5cm; 6-27cm)	4 at (1-22cm; 30-33cm; 48-53cm; 78-83cm)
Fagalii	13°50.628' S; 171°44.131' W	3	150	0	3 at (16-46cm; 231-246cm; 276-299cm)
Salimu - Fagaloa	13°55.904' S; 171°33.614' W	0.5	12	1 at (36-46cm)	3 at (5-13cm; 19-22cm; 37-41cm)
Maasina - Fagaloa	13°56.607' S; 171°33.585' W	0.8	40	5 at (5-12cm; 35-39cm; 47-51cm; 54-56cm; 65-73cm)	6 at (29-40cm; 43-47cm; 49-51cm; 54-57cm; 64-68cm; 72-73cm)
Manono-uta.	13°52.120' S; 172°04.263' W	2.5	75	0	9 at (1-5cm; 28-38cm; 48-51cm; 58-91cm; 106-119cm; 130-134cm; 201-206cm; 216-224cm; 236-243cm)
Satupaitea	13°45.576' S; 172°19.209' W	1	75	3 at (39-60cm; 65-71cm; 76-100cm)	6 at (1-16cm; 31-34cm; 40-70cm; 75-81; 84-89cm; 96-100cm)
Lano	13°37.176' S; 172°11.938' W	1.5	150	3 at (13-69; 70-119cm; 119-139cm)	4 at (15-39cm; 43-119cm; 123-127cm; 131-145cm)

Distinguishing whether an unknown CSI was formed from tsunami or cyclone deposition requires mutli-proxy characterization using, but not limited to, the analytical techniques mentioned earlier. In terms of the chemical results discussed here, they represent a method for quantifying the identification of empirically identified CSI deposits at each investigated site.

CSI deposits generally contain higher amounts of calcium, sulphur, magnesium, sodium, and chlorine (and other elements) relative to overlying and underlying sediment layers (Goff et al, 2001; 2009; Chagué-Goff, 2010). They can also contain much higher levels of heavier elements such as iron and/or titanium. Higher CSI calcium compositions occur due to the deposition of marine calcareous sediments (carbonates) on pre-existing soils.

Out of the thirteen sites investigated in this study, three of them (Mulivai, Vaovai and Satitoa), contained the 2009 SPT deposit, each varying according to the nature of offshore sediment being deposited as well as the geomorphology of the area. These deposits provide a solid reference standard for identifying similar deposits formed from tsunamis that may have originated from similar sources within the geological record at these sites. Other sites investigated did not necessarily contain the 2009 SPT deposit, either because they were not impacted by the event, or the waves had insufficient energy to leave behind a deposit, or the environment was not conducive to sediment deposition.

3.1.3.2 Elemental Results and Preliminary Interpretations

The 2009 SPT deposits at Mulivai, Satitoa, and Vaovai consistently contained distinctly higher concentrations of calcium (Ca) and lower iron (Fe) and titanium (Ti) concentrations relative to underlying (pre-2009 SPT event) soils at each site. The lower titanium and iron values are problematic, as both elements require higher energy to transport them since they are denser. Because of this they are typically found in CSI deposits (Chagué-Goff, 2010; Chagué-Goff et. al., 2010). It is likely that most of the Ti in particular is sourced from terrestrial sources and is therefore common in soils. When the 2009 SPT inundated, it introduced calcareous (shell and coral) material and most probably some heavy minerals such as Ti and Fe, but these were most likely (relatively) diluted because of all the calcium in the deposit. It is possible that heavier minerals get washed out through river channels beyond the coral reefs and become relatively inaccessible to storm waves and hence there is less of them in the nearshore zone than one would expect. This is an important indicator and potentially offers a way to differentiate between a storm and tsunami; i.e., a storm/cyclone comes with rain which would wash more Ti down to the coast resulting in higher Ti concentration in the deposit, so if there is less Ti in a deposit, it becomes more likely that it is a tsunami (J. Goff, pers.comm., 2010).

The high Ca concentrations are largely explained by the deposition of marine calcareous sands high in calcium bearing minerals on top of pre-existing soils (Peters and Jaffe, 2010). Geologically, soils on Upolu and Savaii islands are derived from heavy mineral bearing terrestrial rock sources; basalt and gabbro (Kear and Wood, 1959). There are no reported limestone outcrops on these islands, so high Ca contents found near the coast are attributed to deposition from a nearby marine source.

Sulphur exists in varying concentrations relative to adjacent soil layers, showing no distinct comparable patterns between the sites. For example, the 2009 SPT deposit at Satitoa contains slightly more sulphur than the underlying soil layer, whereas the deposit at Mulivai from the same event contains less sulphur than the underlying soil layer. It is likely that sulphur in this case has been leached to the underlying soil layer causing a relative increase in its sulphur composition. Alternatively, it is also likely that there was initially more sulphur in the underlying soil due to decomposition of pre-existing organic detritus within the soil sequence (Oliva et. al., 1999; Ma et. al., 2010).

The elements sodium, chlorine and magnesium were not present in any of the 2009 SPT deposits at Mulivai, Satitoa, and Vaovai. It is likely that the high mobility of these elements coupled with tropical climatic conditions do not favour their long-term preservation within the deposits (Greenwood and Earnshaw, 1997; Nesbitt and Markovics, 1997; Patino et. al., 2003 and 2005; Braun et. al., 2005; Connelly et. al. 2005; Ma et. al. 2010). Minor concentrations of phosphorus and silicon existed in corresponding pre-event soils, which are not present in their overlying tsunami deposits.

The only elemental relationship showing distinct correlations between the 2009 SPT deposits and corresponding underlying soils are the calcium-iron and calcium-titanium ratio differences at each site. That is, each of the deposits consistently show distinct higher calcium concentrations and lower iron and

titanium concentrations than adjacent underlying (pre-2009 SPT event) soils. For example, Appendix Figures 3.1.2B and 3.1.3B show the relative calcium and iron concentrations for their corresponding stratigraphic sequences (Appendix Figures 3.1.2A and 3.1.3A) at Mulivai and Satitoa sites, respectively. For the case of Mulivai, the first straitgraphic sequence in Appendix Figure 3.1.2A shows a high calcium concentration and low iron concentration (Appendix Figure 3.1.2B) relative to the underlying second stratigraphic sequence; the pre-2009 SPT event soil. This sequence shows a reverse Ca-Fe correlation in that there is significantly less calcium and higher iron than the overlying 2009 SPT event deposit.

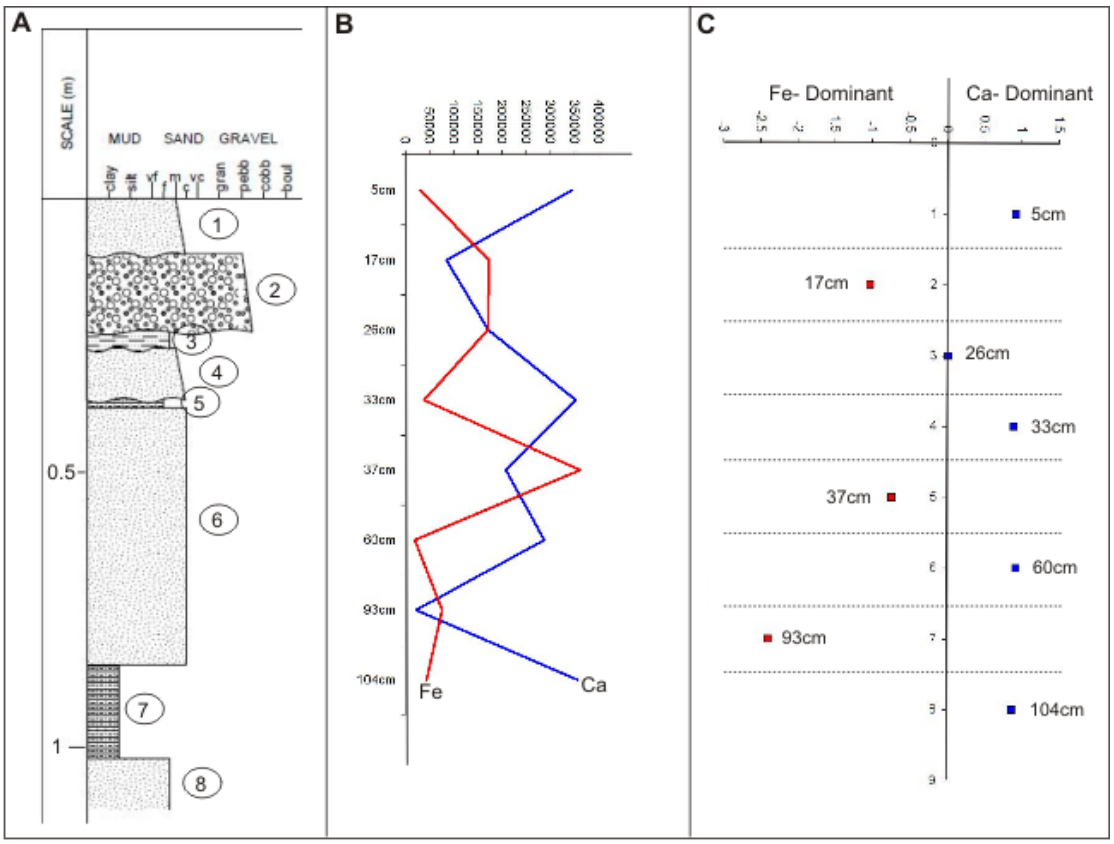

Appendix Figure 3.1.2: A) Empirical stratigraphic column at Mulivai site showing 8 stratigraphic sequences. Sequence 1 is the 29/09 tsunami deposit, and sequences 3, 4, 6 and 8 all have higher calcium content relative to iron than in respective adjacent soil sequences 2, 5 and 7; B) Relative calcium (blue) and iron (red) concentration curves for samples obtained from each sequence; C) Calcium-iron difference as a function of calcium [(Ca-Fe)/Ca] for each sample. Positive values indicate more calcium than iron for that particular sample, and vice versa for negative values.

Appendix Figure 3.1.2C shows the calcium-iron difference represented as a function of calcium at Mulivai site; i.e., [(Ca-Fe)/Ca]. This provides a representation of the total amount of calcium relative to iron within each sample from each sampled sequence down the stratigraphic column. A positive value indicates more calcium present in the sample, and a negative value indicates more iron. A value of 0 indicates that the ratio between calcium and iron present in the sample is 1:1. As seen, the specimen from 5cm depth which was sampled from the 2009 SPT deposit contains higher amounts of calcium relative to iron. The specimen from 17cm depth which was sampled from the underlying pre-2009 SPT event soil contains higher amounts of iron relative to calcium.

Similar calcium-iron ratio trends are observed at Satitoa. The 2009 SPT deposit for this site is comprised of sequences 1 and 2 in Appendix Figure 3.1.3A, with corresponding calcium-iron trends in Appendix Figure 3.1.3B, and difference ratios in Appendix Figure 3.1.3C. Sequence 1 in Appendix Figure 3.1.3A is a thin (3cm) surface mud deposit formed during the temporary resonance surge immediately following the main tsunami waves. This explains why there is slightly more iron in this deposit than in the underlying sand. The underlying second sequence corresponds to calcareous marine sands deposited from the tsunami, and contains a higher calcium concentration than the underlying pre-2009 SPT event soil (Appendix Figure 3.1.3C).

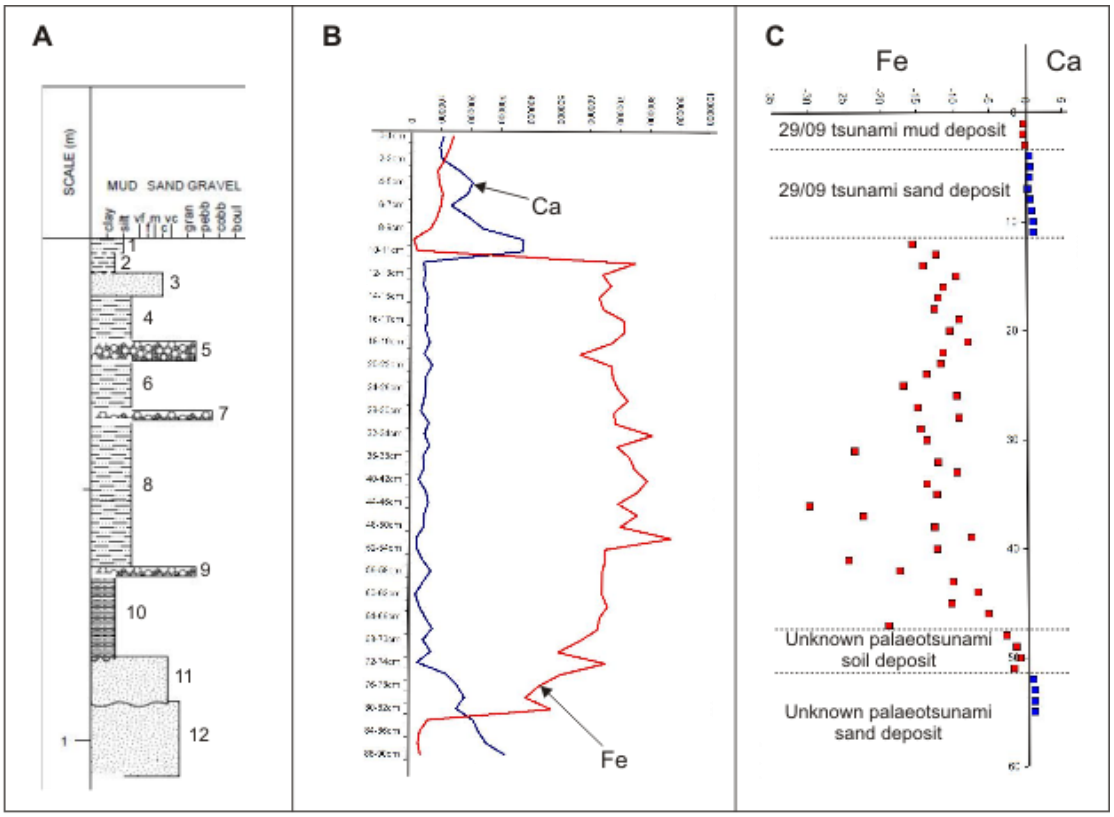

Appendix Figure 3.1.3: A) Empirical stratigraphic column at Satitoa site showing 12 stratigraphic sequences. Sequences 1, 2, and 3 at the top are the 29/09 tsunami deposit, and the last three sequences down to the base of the column show distinct elemental similarities with those deposits; B) Relative calcium (blue) and iron (red) concentration curves for samples obtained at 1cm intervals down to a depth of 20cm, then 2cm intervals down to the base of the column; C) Calcium-iron difference as a function of calcium [(Ca-Fe)/Ca] for each sample. Positive values indicate more calcium than iron for that particular sample, and vice versa for negative values.

The 2009 SPT deposit at Vaovai also displays similar calcium-iron characteristics to those at Satitoa, in that there is a marked increase in calcium concentration relative to the underlying pre-existing soil.

This relationship between calcium and iron in the 2009 SPT deposits from the three sites provides a potential diagnostic tool for identifying similar deposits in their corresponding stratigraphic columns. Equally, similar elemental characteristics may help in the identification of the nature of an extreme

event; i.e., a tsunami or cyclone. A more definitive interpretation of the CSI event however, requires more detailed multi-proxy analysis and data synthesis.

At Mulivai, three (possibly four) other deposits have been identified within the stratigraphic column. These all show distinct increases in calcium relative to iron when compared with overlying and underlying soil layers. In Appendix Figure 3.1.2C, these are represented by units at 26cm, 33cm, 60cm, and 104cm depth. Similarly, for Satitoa site in Appendix Figure 3.1.3C, a significant increase in calcium from the overlying soil occurs at approximately 82cm depth. Interestingly, this deposit has a similar elemental composition to the 2009 SPT deposit. There is a similar trend in iron content in the ~3-4 cm mud layer directly above the calcareous sands at 82cm depth. It is plausible that this deposit could have been laid down by a tsunami similar to the 2009 SPT, although more detailed multi-proxy analysis is needed to be more than tentative in this interpretation.

The pebble layers in Figure 3.1.3A correspond to the high iron concentrations shown in Figures 3.1.3A and 3.1.3C. Based on the absence of calcium bearing calcareous minerals within the associated deposits however, it is difficult to ascertain elementally whether these pebbly deposits were formed from saltwater inundation. More work is needed to clarify this.

The calcium-iron relationship established for CSI deposits at Mulivai, Satitoa and Vaovai can be applied to identify deposits that show similar calcium-iron stratigraphy relationships at other sites. This identification however, largely depends on the deposition of marine calcareous sediments within the stratigraphic column. The deposition of distinct calcareous sands from a tsunami or cyclone depends largely on the energy of the depositing wave coupled with favourable deposition conditions (eg. geomorphology). However, lower energy waves that are inadequate for transporting and depositing distinct calcareous sediments may still cause saltwater inundation, which in turn may cause an increase in the calcium content of the inundated soil due to deposition of marine muds or microscopic calcareous organisms. These types of cases may not necessarily resemble a catastrophic saltwater inundation process based on the calcium-iron relationship, as there will always be more iron present in the soil than calcium, and a negative value will always be obtained.

This was particularly the case for samples obtained from Fagalii site on the north coast of Upolu, and Manono-uta on the southwest. The stratigraphic column for Fagalii was 3m deep, and for Manono-uta it was 2.5m. No calcareous sand deposits were observed in the stratigraphies of either site, although distinct increases in calcium content in some sequences relative to baseline calcium in overlying and underlying soils were still observed. They were however insufficient for yielding positive calcium-iron difference ratios. It is likely that these higher calcium layers are due to saltwater inundation events that had insufficient wave energies to transport and deposit distinct marine sands, and are assumed to contain marine muds or microscopic organisms. Although, more research into the microbiological content of these deposits is needed to verify this assumption.

Appendix Table 3.1.1 summarizes the number and depths of inferred catastrophic saltwater inundations (and likely non-catastrophic events) identified at each site based on the calcium-iron difference ratios between investigated stratigraphic sequences. Events labelled as likely saltwater saturations (non-catastrophic) are based on deposits that show marked calcium increases from overlying and underlying sequences, although the calcium content is insufficient for generating a positive value on the difference ratio chart.

2.1.4 Conclusions

In summary, it is proposed here that the calcium-iron ratios between stratigraphic sequences at the investigated sites should be considered as a possible diagnostic tool for identifying catastrophic (or non-catastrophic) saltwater inundation events specific to individual sites. The data gathered can be synthesized with other analytical results (eg. micropalaeontology, grainsize distribution, radiocarbon dating) to form a solid basis for developing multi-proxy tsunami diagnostic characteristics for the Samoa Islands. It should be noted however that relationships presented here depend on the formation of calcareous deposits directly associated with the catastrophic saltwater inundation. In some instances, empirically identified saltwater inundations do no necessarily yield distinctive calcium-iron ratios due to heterogeneities within the matrix of the deposit.

Other expected saltwater inundation elements such as sodium, magnesium and chlorine were not present in any of the saltwater inundation deposits investigated. It is likely that their high mobility coupled with Samoa's tropical climatic conditions limits their retention within saltwater inundation deposits. It is also likely that the investigated sites did not necessarily undergo saltwater ponding and subsequent salt precipitation, hence their absence in the studied deposits. The element sulphur appears to have high variability between sites, and is likely the result of its mobility in tropical climatic conditions where leaching possibly causes disorder of any distinct distribution patterns between saltwater inundation deposits and adjacent soils. It needs to be stressed however that these findings are specific to Samoa and have yet to be fully interpreted in the context of broader factors. It is yet to be established whether these observations are relatively consistent throughout similar tropical island settings which have coral reefs and nearby calcareous sources.

Collating the data obtained from this research with future work will form a platform for identifying tsunamis within Samoa's recent geological past, and will enable the existing historical tsunami database to be extended beyond 1830 AD. This not only provides a more informed understanding of the long-term recurrence and impact of tsunamis at different coastlines, it also enables a more informed understanding of coastal vulnerability and distribution of tsunami risk. Ultimately, the information yielded may be used to strengthen mitigation efforts and help reduce tsunami risk through mainstreaming into local hazard and disaster management plans.

Appendix 3.2: Preliminary Report 2

Contents

3.2.1 Report Abstract

The September 2009 South Pacific Tsunami (2009 SPT) in the Samoa Islands resulted in local public and national calls to improve understanding of the medium- to long-term risks of tsunamis in these islands in order to further mitigate their impacts. This research addresses some of these calls through an interdisciplinary palaeotsunami investigation. Historical data beginning in 1837 indicate that the Samoan Islands have been impacted by tsunamis from all the major tsunamigenic zones within the Pacific Rim of Fire, making it an ideal location for starting to understand tsunami frequency and distribution within this region. Furthermore, the region has an historical record of extreme tropical cyclones.

The overarching concept of this study is that tsunamis, like cyclones, leave a distinct geological deposit within coastal landscapes they impact. The origin of a high-energy geological deposit, be it storm or

tsunami, can be determined by using a suite of diagnostic criteria. However, the origin of a deposit can still be ambiguous, because some of the diagnostic criteria (e.g. grain size, microfossil assemblages and characteristics) can be extremely similar for both processes. Moreover, local factors can also influence the characteristics of deposits.

This project aims to elucidate this enigma by establishing a suite of diagnostic criteria (e.g., stratigraphy, lithology, macro- and micro-palaeontology, geomorphology, grain size characteristics, geochemistry, anthropology, archaeology, numerical modelling) to distinguish between tsunamis and cyclones in this tropical climatic regime. Preliminary studies show that a geological record of historical /palaeotsunamis and storms/palaeostorms is preserved on the south and south east coast of Upolu, west and northeast coast of Savai'i (Independent State of Samoa), and northwest coast of Ta'u in the Manu'a Group (American Samoa). We present preliminary X-ray fluorescence spectroscopy (XRF) and geochronological results (C-14 radiocarbon dates) conducted on samples (sands and paleosols) collected from various sites on Upolu, Savaii, and Ta'u islands.

These serve as a starting point for developing a suite of diagnostic proxies for identifying and distinguishing tsunami from storm deposits in the Samoan Islands, and establishing the geochronology of identified events. Numerical modelling of wave resonance around these islands, as well as identified palaotsunamis will form an additional proxy for interpreting the palaeotsunami data. Further, it forms a basis for starting to understand the likely sources of these events, forming a basis for refining the frequency and (likely) magnitude distributions associated with these events.

Planned Pb-210, Cs-137 and C-14 dating will enable a detailed interpretation of the chronology of specific events identified in the geologic record. Furthermore, they will enable a correlation of deposits with known historical events, providing a control on distinguishing recent tsunami from storm deposits (subsequent to 1837 AD), and enabling palaeo-events to be identified. This will form a basis for identifying similar events within the geologic record in similar environmental regimes. Ultimately, this work will significantly improve understanding of the nature and risks of coastal hazards in Samoa, thereby improving local capability to mitigate their medium- to long-term impacts. It will also contribute to tsunami hazard mitigation efforts within the broader SW Pacific through a strengthened tsunami database in the region.

2.2.2 Introduction

Investigating tsunami deposits has become a key component in tsunami hazard assessments worldwide, and is recognized as essential in efforts to mitigate tsunami risk to communities (Peters and Jaffe, 2010; Chagué-Goff et al., 2011). Recent studies of modern tsunami deposits during immediate post-tsunami surveys have provided the opportunity to characterise, establish, and refine diagnostic criteria associated with the deposits (Chagué-Goff et al., 2011; Morton et al., 2007). Much of these studies were

enabled through recent tsunamis such as the December 26, 2004, Indian Ocean tsunami (Lay et al., 2005; Titov et al., 2005), the September 29, 2009, South Pacific tsunami (2009 SPT) (Lay et al., 2010), the February 27, 2010, Chile tsunami (Morton et al., 2010), and the March 11, 2011, Japan tsunami Sugawarra et al., 2011). Understanding the characteristics of historical (or modern) tsunami deposits enables the identification of palaeotsunamis within the geologic record that have similar deposit characteristics (Goff et al., 2001). This improves understanding of the long-term risk of tsunamis to communities and underpins efforts to mitigate their impacts, including loss of life and property.

While much has been written and debated about the diagnostic proxies of tsunamis (Goff et al., 2004; Dawson and Stewart, 2007; Kortekaas and Dawson, 2007; Morton et al., 2007; Bridge, 2008; Kelletat, 2008; Morton et al., 2008; Chagué-Goff, 2010; Peters and Jaffe, 2010; Dominey-Howes et al., 2011; Richmond et al., 2011), much work still remains to be done in the context of detailed deposit and geomorphological analyses (Chagué-Goff et al., 2011).

In the Samoa Islands, tsunami research prior to the 2009 SPT was extremely limited and focussed entirely on establishing a record of historical tsunami events (Pararas-Carayannis and Dong, 1980), reviewing early warning systems (Williams and Leavasa, 2006), and limited modelling for coastal hazard planning purposes (Schmall, 2000; Williams, 2009). While inundation modelling and hazard mapping remain a key focus for current research, significant emphasis has been made on characterising the 2009 SPT deposits as a proxy for identifying palaeotsunami deposits in the geologic record (Chagué-Goff et al., 2011; Richmond et al., 2011; Appendix 3.1, this thesis).

The results and interpretations we present in this paper are preliminary, and form part of an ongoing project to characterise and establish tsunami deposit criteria specific to the Samoan Islands in the context of hazard assessment. Major emphasis is made on identifying palaeotsunami deposits using the established criteria or proxies, and establishing their age constraints through datable material either within the deposits or within adjacent sediment horizons.

In terms of the overall project, field investigations were conducted at thirteen coastal sites distributed along the islands of Upolu and Savaii in Independent State of Samoa, and Ta'u in American Samoa (Appendix Figure 3.2.1). Trench and core samples ranging between 0.5–3.0 m were collected from sedimentary sequences containing a number of sand layers. Included in these layers were deposits from the 2009 SPT at the surface, as well as previous high-energy events at depth (storms or tsunamis), intercalated with palaeosols, on the south coast (Mulivai, Coconut Beach Resort near Maninoa, Vaovai, Vaiula) and south east coast (Satitoa) of Upolu, the west (Falealupo) and northeast (Lano) coasts of Savaii, and the northwest coast (Ta'u village) of Ta'u. These samples were collected during the 2009 UNESCO-IOC Post Tsunami Survey of the 2009 SPT and during follow up studies in August and November 2010 (Dominey-Howes and Thaman, 2009).

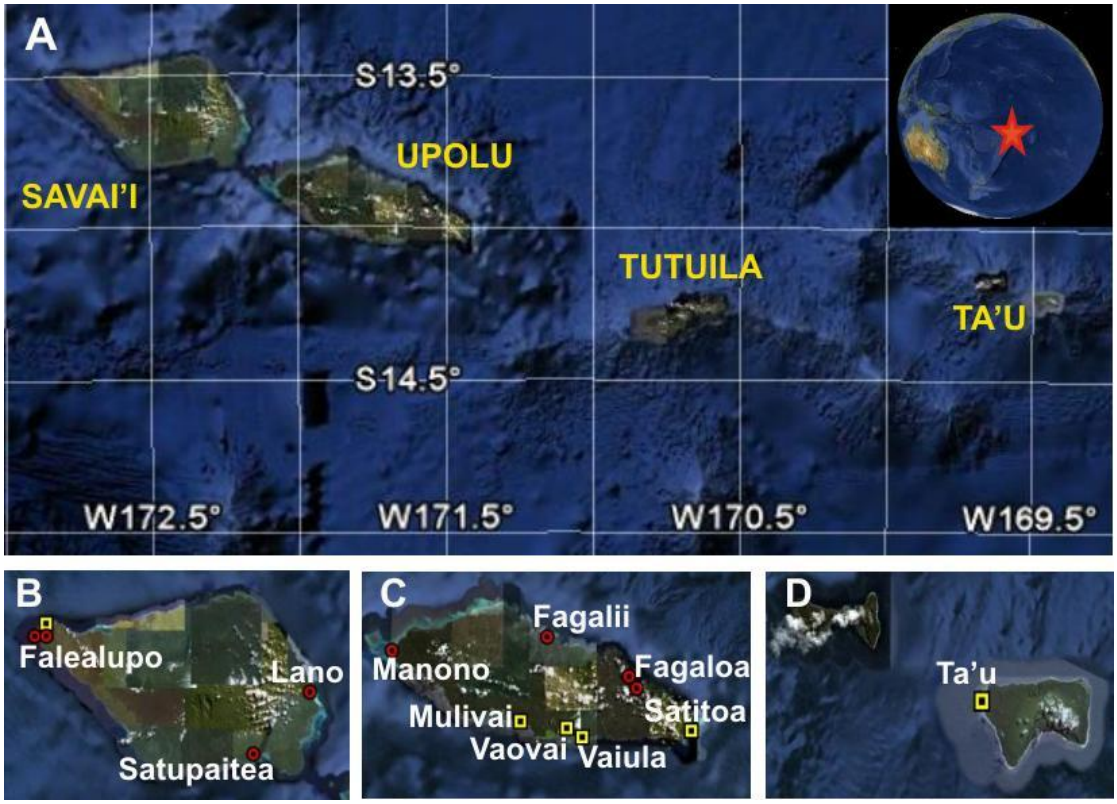

Appendix Figure 3.2.1: A) Location map of the Samoa Islands chain; B - D) Investigated sites on Savai'i (B), Upolu (C), and Ta'u (D). Investigated trench sites are depicted by the yellow squares, and core sites by the red circles. Map source: Google Earth.

Semi-quantitative geochemical profiles (elemental compositions) of the stratigraphic sequences were obtained using a portable X-ray fluorescence (XRF) spectrometer (Appendix 3.1, this thesis). The results provide an initial interpretation of elemental proxies for the 2009 SPT. Moreover, they form a semi-quantitative basis for identifying deposits with similar geochemical characteristics in each sequence that may have formed from similar high-energy deposition processes for more detailed analysis, including geochronological.

Initial C-14 analysis was conducted on samples from the bases of seven priority core/trench sites in order to obtain maximum age limits for their profiles. These sites were identified using the preliminary geochemical data obtained, and included Mulivai, Vaovai, and Satitoa on the south and SE coast of Upolu, Fagalii on the north coast of Upolu, Falealupo and Lano on the west and NE coasts of Savai'i, and Ta'u village on NW Ta'u in American Samoa. Geochemical results from Falealupo, Lano and Ta'u are presented here, and are discussed in the context of the initial geochronology results obtained. Ultimately, these will contribute towards forming the underpinning data required for long-term hazard mitigation in these islands.

2.2.3 Preliminary geochemical analysis

2.2.3.1 Background

Preliminary elemental compositions were obtained for each sampled stratigraphic profile using a portable XRF spectrometer developed by Bruker Inc. The instrument determines the relative elemental chemistry composition of a sample through the emission of photons (x-rays) onto its surface, thus exciting electrons within individual elements comprising the sample causing them to fluoresce (Bruker Inc., 2008). In this study, the samples tested were mainly soils, peat, and calcareous sands. Only three of the investigated sites contained the 2009 SPT deposit, each varying according to the nature of sediment being deposited, flow characteristics of the inundating tsunami, and geomorphology or landscape of the area (Appendix 3.1, this thesis). These sites included Mulivai, Vaovai and Satitoa on the south and southeast coast of Upolu; a stretch of coastline hardest hit by the 2009 SPT.

These deposits provide a reference standard for identifying similar deposits formed from tsunamis that may have originated from similar sources within the geological record (Chagué-Goff, 2010). The 2009 SPT deposit was not contained in other investigated sites (e.g. Falealupo, Lano, and Ta'u) either because they were not impacted by the event, the waves did not have sufficient energy to leave behind a deposit, or the landscape was not conducive to sediment deposition (Chagué-Goff et al., 2011; Richmond et al., 2011).

2.2.3.3 Elemental Proxies

A catastrophic saltwater inundation event (CSI) is a term to describe a deposit that is not known whether it is of tsunami or cyclone origin (Goff et al., 2001). Typically they are identified empirically by distinct changes in sediment characteristics within the geologic record (e.g. marine sediments intercalated between soils, peat or palaeosols) (Peters and Jaffe, 2010). Distinguishing between the two requires multi-proxy characterisation (Chagué-Goff et al., 2011; Goff et al., 2010), and is beyond the scope of this paper.

CSI deposits generally contain higher amounts of calcium, sulphur, magnesium, sodium, and chlorine (and other elements) relative to overlying and underlying sediment layers (Chagué-Goff et al., 2011; Goff et al., 2001; 2010). They can also contain much higher levels of heavier elements such as iron and/or titanium. Higher CSI calcium compositions occur due to the deposition of marine calcareous sediments (carbonates) on pre-existing soils.

Preliminary interpretations on the elemental characteristics of the 2009 SPT deposit at Mulivai, Vaovai and Satitoa were discussed in Appendix 3.1. The results showed a relationship between the calcium-iron ratios between stratigraphic sequences at the investigated sites, and it was suggested that these observations be considered as a possible diagnostic tool for identifying catastrophic (or non-catastrophic) saltwater inundation events specific to individual sites. The analysed deposits consistently contained higher concentrations of calcium (Ca), and lower iron (Fe) and titanium (Ti) concentrations relative to underlying (pre-2009 SPT) soils at each site. The lower titanium and iron values were

problematic as both elements require higher energy to transport them due to their higher density. Hence, they are typically found in CSI deposits (Chagué-Goff, 2010; Chagué-Goff et al., 2011). It was suggested that these heavier elements, (Ti in particular), were sourced from terrestrial sources and is therefore common in soils. Inundation of the 2009 SPT introduced calcareous material and some Ti and Fe, but these were relatively diluted because of the calcium in the deposit. It was assumed that Fe and Ti get transported through river channels to the coast, and are likely deposited beyond the coral reefs. This renders them relatively inaccessible to surface waves and hence there is less of them in the nearshore zone than one might expect.

The high Ca concentrations were explained by the deposition of marine calcareous sands high in calcium bearing minerals on top of pre-existing soils (Peters and Jaffe, 2010). There are no reported limestone outcrops on these islands (Kear and Wood, 1959; Stice and McCoy, 1968), so high Ca found near the coast is attributed to deposition from a nearby marine source.

Other expected saltwater inundation elements such as sodium, magnesium and chlorine were not present in any of the saltwater inundation deposits investigated. It was suggested that their high mobility coupled with Samoa's tropical climatic conditions limits their retention within saltwater inundation deposits. It was also likely that the investigated sites did not necessarily undergo saltwater ponding and subsequent salt precipitation, hence their absence in the studied deposits. The element sulphur appeared to have high variability between sites, and was assumed to be the result of its mobility in tropical climatic conditions where leaching influences elemental distribution patterns between saltwater inundation deposits and adjacent soils.

These observations, while yet to be fully interpreted in the context of broader factors, form the basis for tentative elemental interpretations at Falealupo, Lano, and Ta'u discussed below.

2.2.4 Elemental results

While deposits from the 2009 SPT were not formed at Falealupo, Lano and Ta'u, the preliminary Ca-Fe ratio relationship for the 2009 SPT deposits at Mulivai, Vaovai and Satitoa form a reference standard for interpreting similar relationships at Falealupo, Lano, and Ta'u sites.

2.2.4.1 Falealupo Site

Appendix Figure 3.2.2 depicts the stratigraphy and Ca-Fe relationships for samples from Falealupo. The trench at Falealupo was located at 13^{0}29.663' S; 172^{0}46.523' W, approximately 165 m inland from the present high-tide water mark. A 3.5 m storm berm (resembling a sand-dune) was located at the coastline; approximately 5 m wide at its base. A depth of greater than 0.5 m was logged at the trench site, with detailed 1 cm sampling down to 20 cm depth, followed by 2 cm sampling down to the base of the trench.

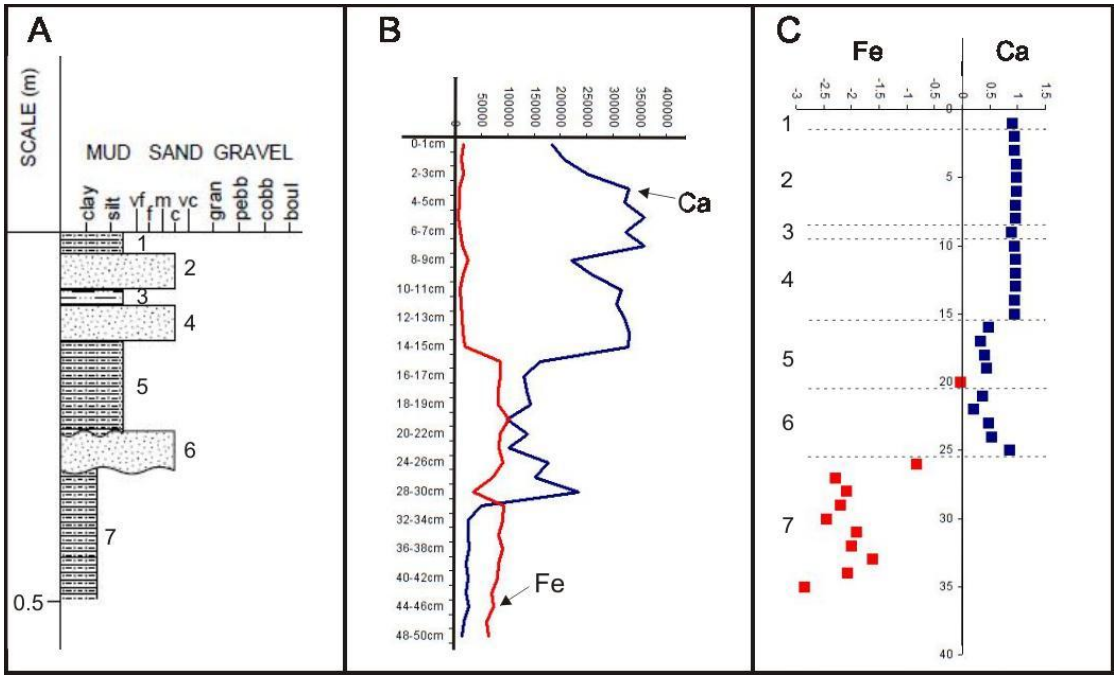

Appendix Figure 3.2.2: A) Empirical stratigraphic column at Falealupo site showing 7 stratigraphic sequences. Sequences 4 and 6 are assumed to be of tsunami origin; B) Relative calcium (blue) and iron (red) concentration curves for samples obtained from each sequence; C) Calcium-iron difference as a function of calcium [(Ca-Fe)/Ca] for each sample in (B). Positive values indicate more calcium than iron for that particular sample, and vice versa for negative values.

Seven sequences were identified empirically based on changes in sediment characteristics between adjacent sequences. Sequences 2 and 3 in (Figure 3.2.2A) are assumed to represent the December 7 – 10, 1991, Cyclone Val, and the February 1 – 4 1990, Cyclone Ofa deposits, respectively. These deposits are empirically characterised by poorly sorted, coarse yellow calcareous sand. Cyclones Ofa and Val collectively were the worst category 5 cyclones ever recorded in Samoa within the last 100 years in terms of their socioeconomic impacts (Faiburn, 1997).

Sequence 4 shown is empirically characterised by coarse greyish-yellow sand comprising organic laminae at approximately 12.5 and 13.5 cm depths. Coral cobbles approximately 4 – 6 cm at their longest axis were also comprised within the deposit matrix. This deposit required higher wave energy to transport these coarser sediments 165 m inland, and is likely to represent the June 25, 1917 tsunami which impacted the Samoa Islands. This tsunami originated approximately 130 km northwest along the same tear-fault region that the 2009 SPT originated (Lay et al., 2010; Beavan et al., 2010), and its inundation impacts are believed to have been more geographically widespread across southern and parts of northern Upolu and Savai'I (Pararas-Carayannis and Dong, 1980).

Sequence 6 represents another saltwater inundation and is empirically characterised by coarse yellow-grey sand deposited between two organic soil layers both comprising sub-angular to sub-rounded boulders 10 – 30 cm at their longest axis. It is assumed that Sequence 6 likely represents a palaeotsunami deposit based on its empirical sedimentary characteristics relative to adjacent palaeosols.

While the sequence deposits discussed have been tentatively identified through empirical means, the distinction between stratigraphic sequences is not so apparent using the Ca-Fe relationship technique. The assumed palaeotsunami identified in stratigraphic sequence 6 shows a very similar Ca-Fe trend to those of the 2009 SPT deposits at Mulivai, Vaovai and Satitoa, hence strengthening the likelihood of a tsunami origin for this deposit (Figure 3.2.2B and C).

The Ca-Fe trend for the deposit at stratigraphic sequence 4, which is tentatively assumed to represent the June 25, 1917 tsunami, does not show a similar trend to the reference 2009 SPT deposit trends. This makes it difficult to use the Ca-Fe relationship in this case as an indicator for the likelihood of a tsunami origin for this deposit. More multi-proxy analysis coupled with geochronological analysis will help elucidate this enigma.

2.2.4.2 Lano Site

Six stratigraphic sequences were identified empirically at Lano (Appendix Figure 3.2.3). The 1.5 m core sampled from Lano was located at 13^{0}37.176' S; 172^{0}11.938' W, approximately 150 m inland of the present high tide water mark.

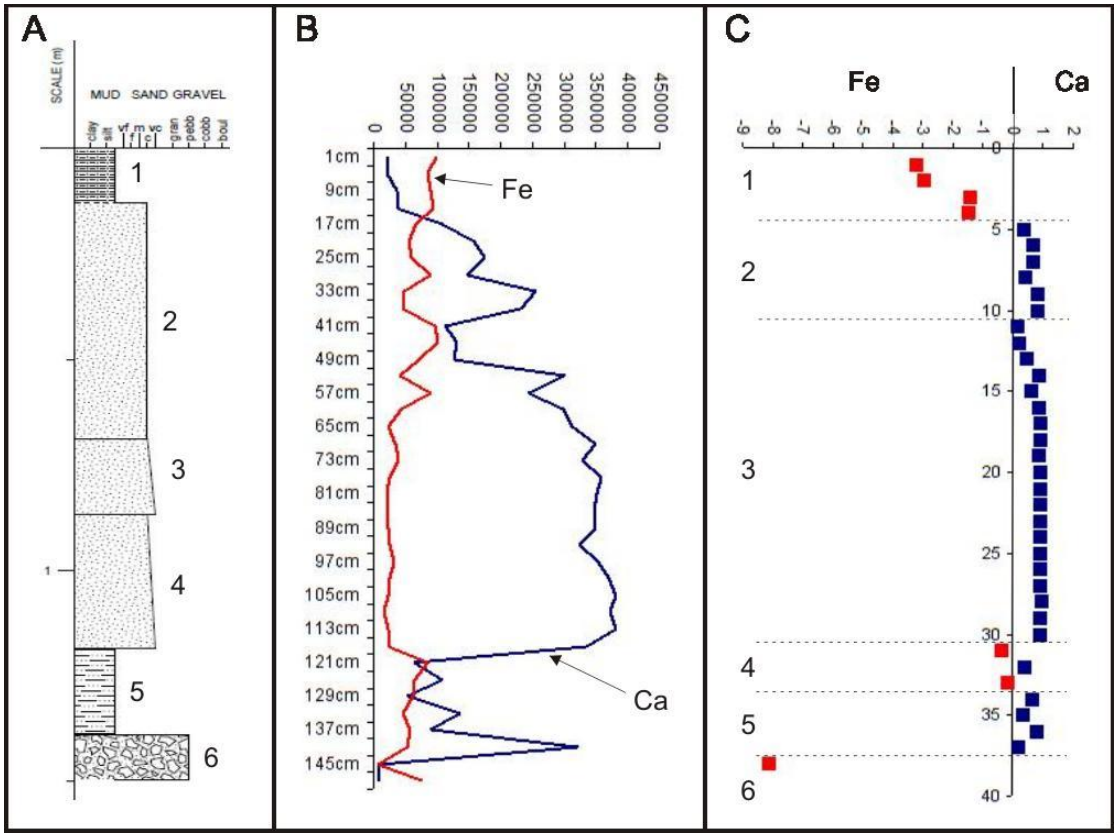

Appendix Figure 3.2.3 A) Empirical stratigraphic column at Lano site showing 6 stratigraphic sequences. Sequence 5 shown is assumed to be of a tsunami origin; B) Relative calcium (blue) and iron (red) concentration curves for samples obtained from each sequence; C) Calcium-iron difference as a function of calcium [(Ca-Fe)/Ca] for each sample in (B). Positive values indicate more calcium than iron for that particular sample, and vice versa for negative values.

Stratigraphic sequence 1 (Figure 3.2.3A) represents the present soil layer, and sequences 2, 3 and 4 are likely associated with deposits from Cyclones Ofa and Val based on their empirical sedimentary characteristics, although further geochronological evidence is required to strengthen this assumption.

Stratigraphic sequences 4 and 5 (Figure 3.2.3C) likely represents a single deposit from a high energy wave event, and shows a very similar Ca-Fe trend to the reference 2009 SPT deposit trends at Mulivai, Vaovai and Satitoa. Sequence 4 yields a very similar Ca-Fe relationship to the surface mud layers of the reference 2009 SPT deposits. Sequence 5 is assumed to be the calcareous base of the deposit overlain by a surface mud layer as the transportation mechanism lost energy; a very similar characteristic to the reference 2009 SPT deposits. It is likely that this deposit was formed from a tsunami origin, but more multi-proxy evidence is required to elucidate this.

2.2.4.3 Ta'u Site

The 0.67 m trench at Ta'u was located at 14^{0}13.542' S; 169^{0}30.921' W, approximately 140 m inland of the present high tide water mark. Only two distinct sequences were observed in the stratigraphy (Appendix Figure 3.2.4A). A sharp contact at approximately 51 cm depth separates the overlying organic soil horizon from the underlying very coarse, grayish-yellow calcareous sand deposit. This deposit also comprised of coral cobbles (branching and brain corals), gastropod and other unidentified shells, as well as rounded basalt cobbles towards the base of the deposit matrix.

Recent category 5 cyclones which have impacted this island had insufficient wave energy to inundate 140 m inland, and hence there is no apparent deposit associated with recent cyclone activity at the site. Sequence 2 likely represents a high wave energy deposition source sufficient to transport the denser coral and basalt cobbles observed within the matrix. It is empirically assumed that this deposit is likely associated with a tsunami origin.

The Ca-Fe relationship for sequence 2 in (Figure 3.2.4C) also shows a very similar trend to the reference 2009 SPT deposit trends. Sequence 2a likely represents the surface mud layer similar to the reference 2009 SPT deposits formed as tsunami energy dissipated. This overlies coarser marine sediment deposited during higher energy wave inundation associated with the same deposition event. However, more multi-proxy analysis is required for a more definitive interpretation.

3.2.5 Preliminary Geochronology Results

Standard C-14 radiocarbon analysis and anisotropy of mass spectrometry (AMS) analysis was conducted at the Waikato Radiocarbon Dating Laboratory (WRDL) on palaesols and other organic material (e.g. plant fragments, wood and coral), from the stratigraphic bases of seven investigated sites. These sites included Mulivai, Vaovai, and Satitoa on the south and SE coast of Upolu, Fagalii on the north coast of Upolu, Falealupo and Lano on the west and NE coasts of Savai'i, and Ta'u village on NW Ta'u in American

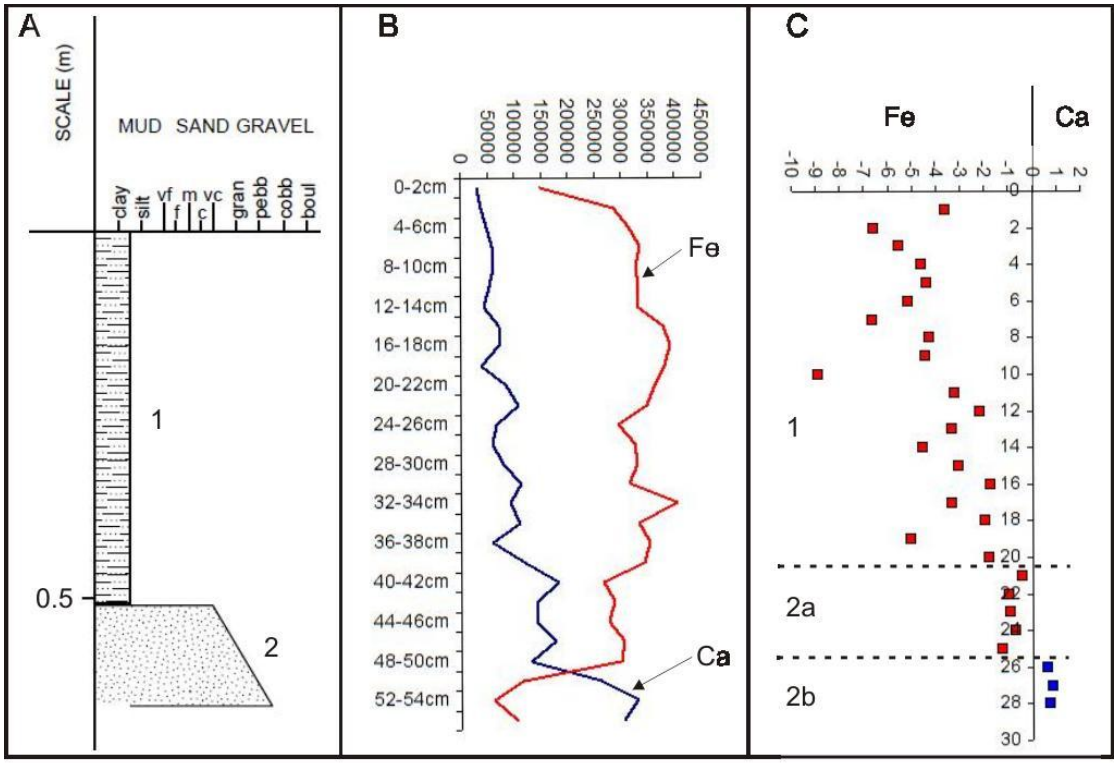

Appendix Figure 3.2.4: A) Empirical stratigraphic column at Ta'u site showing 2 stratigraphic sequences. Sequence 2 shown is assumed to be a palaeotsunami deposit, and has a higher calcium content relative to iron than the overlying sequence 1; B) Relative calcium (blue) and iron (red) concentration curves for samples obtained from each sequence; C) Calcium-iron difference as a function of calcium [(Ca-Fe)/Ca] for each sample in (B). Positive values indicate more calcium than iron for that particular sample, and vice versa for negative values.

Samoa. The sites were selected for initial C-14 analysis using limited funding based on the likely saltwater inundation deposits identified empirically, and through their Ca-Fe elemental relationships down their respective stratigraphies. This dating analysis was carried out in order to establish maximum age limits on the sampled profiles from these sites.

Appendix Table 3.2.1 summarizes the results from this analysis, with the resulting ages and estimated errors presented in years before present (BP). The stratigraphic profile at Satitoa yields the youngest age of 149 +/- 93 BP (i.e. 1862 AD +/- 93 years). This date was obtained from a specimen sampled from the base of an organic soil layer directly overlying an assumed palaeotsunami deposit.

The site at Satitoa was located approximately 280 m inland of the present high tide water mark. Hence, a tsunami origin was assumed the most likely cause for this deposit as cyclone waves do not have sufficient energy to inundate that far inland.

Due to the high uncertainties in the estimated age from this site, it is difficult to narrow down an association with a known tsunami origin. It is likely that this deposit may have formed from the June 25, 1917 Samoa tsunami discussed earlier. The geographical extent of inundation on Upolu and Savaii from this tsunami is believed to have been more widespread than the 2009 SPT. Other likely documented tsunami sources include the August 14, 1868, great Peru earthquake and tsunami which apparently

destroyed settlements in Apia, north Upolu. Details on the extent of damage on other parts of the islands were not documented.

Appendix Table 3.2.1: Conventional radiocarbon age results for the standard C-14 and AMS analysis

	Site	Location	Sample Material	Sample depth (m)	Result
Standard C-14					
	Satitoa	Coastal marsh	Soil, organics	0.81	149 +/- 93 BP
	Falealupo (core)	Swamp	Peat	0.99	3953 +/- 104 BP
	Lano	Marsh	Unidentified Wood	1.49	1895 +/- 43 BP
	Mulivai	Marsh	Peat	0.92	528 +/- 91 BP
	Ta'u	Marsh	Unidentified Coral	0.65	3661 +/- 41 BP
	Fagalii	Back-swamp	Charcoal	2.86	3112 +/- 51 BP
	Fale o le Fee	Fluvial valley	Charcoal	0.30	398 +/- 73 BP
	Vaovai	Swamp	Unidentified Gastropod	0.67	576 +/- 33 BP
AMS					
	Falealupo (trench)	Marshy swamp	Peat	0.49	829 +/- 28 BP
	Lano	Marsh	Plant fragments	1.39	798 +/- 28 BP

Similarly, the May 10, 1877, great Chile earthquake and tsunami may also be a likely source. This tsunami caused devastating damages across the Pacific, although details on the extent of impacts in the Samoa Islands were not recorded.

The standard C-14 age results given for Falealupo in Table 3.2.1 were yielded from the base of a 1.0 m core sampled from a swamp approximately 1.2 km southwest of the trench site which the Ca-Fe elemental results discussed earlier were obtained from. This site was located approximately 220 m inland of the present high tide water mark. The AMS results obtained for Falealupo were yielded from the base of the organic soil layer depicted by sequence 7 in Figure 3.2.2. Further C-14 dating will help elucidate the age limits of the assumed palaeotsunami deposit depicted by sequence 6 in Figure 3.2.2. Pb-210 and Cs-137 dating on the assumed 1990 and 1991 Cyclones Ofa and Val deposits, respectively, will aid in elucidating whether those deposits were indeed formed by those events. The standard C-14 age result yielded for Lano was obtained from an unidentified wood specimen located at the base of stratigraphic sequence 6 in Figure 3.2.3.

However, due to in-built age uncertainties associated with unidentified wood samples (Gavin, 2001; Grimm, 2011), it is likely that the result obtained is not a true depiction of the age of the stratigraphic profile at this site. This assumption is supported by the AMS age result yielded from plant fragments sampled from within the assumed palaeotsunami deposit depicted by sequences 4 and 5 (Figure 3.2.3C), and is held to represent the lower age limit of the deposit. As seen in Table 3.2.1, there is an approximate 1000 year age difference between the dated samples from the adjacent stratigraphic sequences 6 and 7 in (Figure 3.2.2A). This further strengthens the likelihood of in-built age uncertainties associated with the standard C-14 result yielded from the unidentified wood specimen.

The standard C-14 result yielded for Mulivai in Table 3.2.1 was obtained peat specimen sampled from the centre of a 16 cm peat layer towards the base of the stratigraphic profile from this site. This layer has been tentatively interpreted as a palaeosol overlying an assumed palaeotsunami deposit identified and discussed in Appendix 3.1. A similar C-14 age result to that obtained from Mulivai was yielded from an unidentified gastropod sampled from a layer assumed to be associated with a palaeotsunami origin. Based on the proximity of these two sites to each other on the south coast of Upolu, it is possible that their age results represent the approximate timing of a palaeotsunami that impacted them around 528 – 576 BP.

Age results for Fagalii and Fale o le Fee sites given in Table 3.2.1 are not directly associated with the objectives of this paper, and are hence not discussed any further. They are listed here for completion purposes.

The age result of 3,661 +/- 41 BP yielded for Ta'u was obtained from an unidentified coral specimen sampled from the base of the stratigraphic sequence (Figure 3.2.4A). It was initially assumed empirically that this deposit may have represented a relatively recent palaeo-landslide generated tsunami origin (i.e. < 500 BP), associated with the large-scale ocean-island flank collapse on Ta'u island discussed in (Williams, 2009). While there is still a possibility that this deposit may be associated with the event investigated in (Williams, 2009), this cannot be stated definitively based on the results obtained. Dating a specimen from the base of the organic soil horizon depicted by sequence 1 (Figure 3.2.4A) will aid significantly in elucidating this enigma.

2.2.6 Summary and Directions for Future Work

The Ca-Fe elemental relationship technique presented in Appendix 3.1, for the 2009 SPT deposits at Mulivai, Vaovai and Satitoa proved useful in identifying deposits with similar Ca-Fe elemental characteristics at Falealupo, Lano, and Ta'u. More multi-proxy analytical evidence, including geochronology data, is required to state definitively that the tentatively assumed palaeotsunami deposits identified at the sites discussed in this paper are indeed of a tsunami origin. This is because the preliminary Ca-Fe elemental proxy is incapable of distinguishing between a tsunami or cyclone origin for an identified CSI deposit. Further, while the Ca-Fe elemental relationship for the 2009 SPT deposits are assumed to be a preliminary standard for similar deposits with similar origins, this assumption does not hold true for all coastal areas across the islands due to the differing nature of offshore and onshore geomorphologies. These factors, coupled with wave energy and flow characteristics, determine the nature of material deposited at a particular location. They also influence the extent of inundation inland at a particular coastal location, as well as influence whether a deposit is formed at all from a particular tsunami or cyclone event.

The Ca-Fe elemental proxy does have useful applications in the identification of likely CSI deposits. But, only coupled with a suite of diagnostic proxies can identified CSI deposits begin to be fully interpreted in the context of their origin and likely source and wave characteristics.

Samples from distinct stratigraphic units will be analysed in due course for organic matter content by loss on ignition (LOI), and grain size by laser diffraction using a particle multisizer. Selected sub samples will also be processed for pollen and micropalaeontological (diatoms and foraminifera) analysis. Planned computational modelling using the NEOWAVE numerical tsunami model (Roeber et al., 2010; Yamazaki et al., 2010), will provide an additional proxy for interpreting the palaeotsunami data. It will also provide the opportunity for beginning to understand the likely source and wave characteristics associated with identified palaeotsunami deposits. These studies will significantly broaden the diagnostic toolkit for identifying tsunami and cyclone deposits in these islands.

The age results obtained from standard C-14 radiocarbon and AMS dating techniques form a basis for developing the geochronology of stratigraphic profiles from investigated sites. While far from complete, these initial results help provide a semi-quantitative estimation of the lower age limits of the profiles selected for dating. Further C-14 radiocarbon dating is planned for implementation in due course. This will largely complement the initial age results discussed here in that specific age controls will be established for individual tsunami/storm events identified in the investigated stratigraphic sequences.

Further, Pb-210 backup up by Cs-137 dating is also planned for implementation on deposits assumed to be of recent unknown origin (e.g. the assumed cyclone deposits at Falealupo). This will provide a good control on identifying the deposits with known historical events, thus allowing us to refine the diagnostic criteria for distinguishing cyclone and tsunami deposits in a tropical volcanic island setting.

In summary, little is known about the prehistoric record of storms and tsunamis in Samoa, although there is evidence for previous events (Goff et al., 2010). A comprehensive study of historically documented deposits will enable us to identify their prehistoric counterparts. Correlating them with events that are recorded elsewhere in the Pacific, such as New Zealand (Nichol et al., 2010), will provide an indication of their broader regional impacts, as well as the risks they pose at the regional Pacific scale. C-14 dating is thus a crucial part of this study, as it will provide the dating control allowing a correlation with known events, and the identification of unknown events. Furthermore, it will be instrumental for determining the extent of the deposits on these Islands. Pb-210 and Cs-137 dating will enable a correlation of deposits with known historical events, providing a control on distinguishing recent tsunami from storm deposits.

Ultimately, this work will significantly improve understanding of the nature and risks of coastal hazards in Samoa, thereby improving local capability to mitigate their medium- to long-term impacts. It will also

contribute to tsunami hazard mitigation efforts at the broader regional scale through a strengthened tsunami database in the region.

Deputy Vice-Chancellor's Office
Postgraduate Office

Co-Authorship Form

UNIVERSITY OF CANTERBURY
Te Whare Wānanga o Waitaha
CHRISTCHURCH NEW ZEALAND

This form is to accompany the submission of any thesis that contains research reported in co-authored work that has been published, accepted for publication, or submitted for publication. A copy of this form should be included for each co-authored work that is included in the thesis. Completed forms should be included at the front (after the thesis abstract) of each copy of the thesis submitted for examination and library deposit.

Appendix 4: Geological investigation of palaeotsunamis in the Samoan Islands: Interim report and research directions.

Publication status: 2013. In; Science of Tsunami Hazards. Vol.32, No.3, pp.156—175.

Shaun Williams wrote the manuscript. Development and refining of the original manuscript was conducted by the co-authors stated in the Co-Authorship Declaration of this thesis.

Certification by Co-authors:
If there is more than one co-author then a single co-author can sign on behalf of all
The undersigned certifys that:

- The above statement correctly reflects the nature and extent of the PhD candidate's contribution to this co-authored work
- In cases where the candidate was the lead author of the co-authored work he or she wrote the text

Name: **Tim Davies** Signature: Date: **30 April 2014**

APPENDIX 4: INTERIM THESIS REPORT

Overview

This Appendix provides a version of a co-authored peer-reviewed report, published in; ***Science of Tsunami Hazards, 32(3): 156 – 175***. The report is entitled 'Geological Investigation of Palaeotsunamis in the Samoan Islands: Interim Report and Research Directions'. Shaun Williams is first author, and co-authors include James Goff, Johnny Ah Kau, Faigame Sale, Catherine Chagué-Goff, and Tim Davies.

Contents

4.1 Report Abstract

The September 29, 2009 Samoa Tsunami provided the opportunity to sample the sediments deposited in the Samoan Islands landscape by the tsunami. Analysing the characteristics of the sediment deposits using an established suite of diagnostic criteria, and assessing how they differ from cyclone deposits enables the identification and dating of similar events in the geologic record. This helps to better understand the long-term frequency and likely magnitude of these events. Here we report on a pilot palaeotsunami field-sampling investigation carried out in 2010 at selected sites on Upolu and Savaii Islands in the Independent State of Samoa, and on Ta'u Island in American Samoa. We present empirical stratigraphic data for the investigated sites, and we demonstrate the existence of high energy marine inundation deposits at some of these sites which were laid down by past tsunamis and/or cyclones. We review and discuss the analytical outcomes, as well as summarise the overarching directions of this research. We propose that there is a need for this study to continue and for

such studies to be carried out in other islands in the Pacific. By doing this, we can build on the sparse palaeotsunami database in the region, thereby helping to improve our understanding of the long-term frequency, impact distribution, and likely magnitude of these events. Further, we can start assessing their likely sources and the long-term risk these hazards pose to coastal cities and communities in the Pacific.

4.2 Introduction

Following the September 29th 2009 tsunami in the Samoan Islands, public and national calls were made to improve our understanding of the medium- to long-term risks of tsunamis in the archipelago in order to mitigate their impacts. The historical database of tsunamis in Samoa, which extends back to 1837, indicates that these islands have been impacted from all the major source regions within the Pacific Rim of Fire (Pararas-Carayannis and Dong, 1980: Williams and Leavasa, 2006). Given that there is virtually no specific reference to tsunamis in Samoa's prehistory (i.e. the approximate 3000 years prior to the arrival of the first official missionaries in 1830), it is difficult to ascertain the long-term frequency and subsequent risk of these hazards to the people of Samoa (Williams 2009; Williams et al., 2012).

This study aims to improve our long-term understanding of the frequency and magnitude distributions of tsunamis within the Samoan Islands through an interdisciplinary palaeotsunami investigation. Future modelling of potential sources attributed to the identified palaeotsunamis will improve our understanding of the frequency and potential magnitude distributions associated with individual source regions. This information can then be used to re-evaluate the medium- to long-term risk of tsunamis in Samoa.

This work builds on the recommendation made in the United Nations Educational, Scientific and Cultural Organization – Intergovernmental Oceanographic Commission International Tsunami Survey Team (UNESCO-IOC ITST) Interim Field Report of October 2009 for a national palaeotsunami study (Dominey-Howes and Thaman, 2009). Preliminary discussions with the Assistant Chief Executive Officer - Meteorology Division of the Ministry of Natural Resources and Environment in February 2010 resulted in the implementation of this collaborative field investigation.

A summary of the provisional observations, local interviews, current analytical outcomes and deductions to date as well as directions for future work is presented.

4.3 Field Objectives and Methods

The overarching concept behind this study is that tsunamis, like cyclones, leave distinct sedimentary evidence in the coastal landscapes they impact (Goff et al, 2001; Goff et al, 2009). Many of these deposits are preserved in wetland environments, although they are not limited to these environment types.

Tsunami and cyclone deposits are generally known as catastrophic saltwater inundation (CSI) events, and distinguishing the two in the field remains a challenge. Recent characteristic and analytical advancements within

the global tsunami community have proven successful in distinguishing these events based upon detailed laboratory analysis (e.g. Chagué-Goff et al., 2011).

This field study involved geological investigations at targeted sites in Upolu, Savaii and Ta'u Islands in order to identify CSIs. These sites are listed in Appendix Table 4.1 and shown in Figure 4.1. Trenches were dug at the sites shown in order to record the subsurface sediment stratigraphy and to identify CSI deposits. Sampling of sediment within the trenches was conducted for detailed laboratory analysis of their physical and geochemical characteristics. Core samples were also obtained from the sites shown, which were subsequently logged at the University of Canterbury in New Zealand.

Appendix Table 4.1: Summary of investigated sites.

Site	Coordinate Location	Approximate Distance inland from high tide mark (m)	Approximate elevation (m)	Stratigraphic depths (m)
Fagalii	13^{0}50.628' S; 171^{0}44.131' W	150	< 10	3
Falealupo	13^{0}29.663' S; 172^{0}46.523' W	165	< 10	0.5
Fale o le Fee	13^{0}55.134' S; 171^{0}44.285' W	750	475	0.6
Lano	13^{0}37.176' S; 172^{0}11.938' W	150	< 10	1.5
Ma'asina	13^{0}56.607' S; 171^{0}33.585' W	40	< 10	0.7
Manono	13^{0}52.120' S; 172^{0}04.263' W	75	< 5	2.5
Mulivai	14^{0}00.505' S; 171^{0}47.651' W	25	< 5	1.02
Satitoa	14^{0}01.363' S; 171^{0}25.754' W	280	<15	0.84
Satupaitea	13^{0}45.576' S; 172^{0}19.209' W	75	< 10	1
Tau	14^{0}13.542' S; 169^{0}30.921' W	140	< 5	0.67
Vaovai	14^{0}02.140' S; 171^{0}40.832' W	20	< 5	0.72
Vaiula	14^{0}02.361' S; 171^{0}39.631' W	100	< 10	0.7

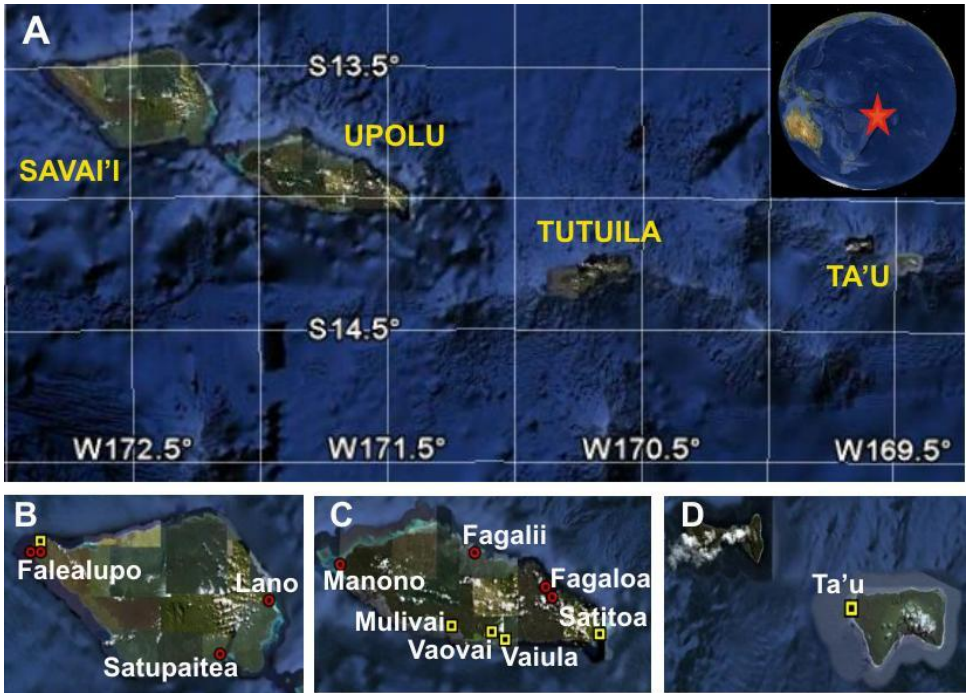

Appendix Figure 4.1: A) Location map of the Samoan Islands; Investigated palaeotsunami sites on B) Savai'i Island; C) Upolu Island; D) Ta'u Island. Yellow squares represent trench-sites and red circles represent core-sites (from Williams et al., 2011a). Note that Ma'asina is located at Fagaloa on NE Upolu.

Personal interviews were also conducted at Salimu (Fagaloa) and Vaovai on Upolu, and Lano and Falealupo-tai on Savaii.

Fault scarp sampling of the SE Upolu, Fagaloa and SW Savaii faults was conducted with the long-term objective of cosmogenically dating past landslide activity. These data would help establish an understanding of the timing of catastrophic coastal landslides (and subsequent tsunamis) which resulted in the exposed escarpments. The assumption for such events occurring in these islands is based on the Ta'u catastrophic landslide scenario presented in Williams et al (2012). Reconnaissance of the Ologogo fault in NW Savaii, the largest fault in Samoa, was also conducted, although sampling was not undertaken due to the lack of accessible scarp outcrops.

4.3.1 Study Sites

Satellite images and field reconnaissance observations were used to select the study sites. Coastal areas with wetland or swamp depositional environments were chosen, followed by field reconnaissance to explore them in terms of their geomorphology and likelihood of preserving CSIs. Most of the areas visited had either been impacted by the 2009 tsunami, or had been impacted by an earlier event.

4.3.1.1 Trench and core sites

Trench studies were conducted at Mulivai near Coconuts Beach Resort, Vaiula and Vaovai, Satitoa, Falealupo, and Ta'u (Appendix Figure 4.1). A pit trench was also dug at Fale o le Fee to investigate possible calcareous deposits

within the area. The Dwarfs Cave (Paia lava tube cave) in Savaii was also visited to investigate whether preserved sand deposits could be found.

Hand-drilled core samples were obtained from Maasina, Fagalii, and Manono-uta on Upolu. On Savaii, they were obtained from Satupaitea, Falealupo-tai, and Lano (Appendix Figure 4.1).

An erosional scour along the coastline at Mulivai (Safata), near the old Hideaway Resort, was also logged, although sampling at this site was not carried out. The stratigraphic log for this site is not presented in this report.

4.3.1.2 Fault scarps

One rock sample was obtained from the Fagaloa fault scarp on NE Upolu. Another rock sample was obtained from the SE Upolu fault scarp, as well as two rock samples from the SW fault scarp on Savaii. Attempts were made to obtain rock samples from the Ologogo fault on NW Savaii, although this was not completed due to the lack of sufficient scarp outcrops for sampling.

The faults mentioned are assumed to have undergone catastrophic ocean-island flank collapses (landsliding) in the past, with the potential to generate local tsunamis (e.g. Williams et al, 2012). It is planned to date these samples cosmogenically in order to constrain the likely ages of the respective collapses.

4.4 Results and Outcomes

Below are preliminary results associated with the investigated sites, based on field work observations. Hence, they should be treated as such. Detailed results will be reported in the future following laboratory analysis of the collected samples.

4.4.1 Trench logs

The subsurface stratigraphy associated with each trench was logged empirically. These serve as a benchmark for comparison with the (pending) detailed laboratory analysis of samples associated with each trench.

4.4.1.1 Mulivai trench (near Coconuts Beach Resort)

The trench at Mulivai was located at 14000.505' S; 171047.651' W, approximately 25 m inland from the high-tide water mark. A depth of 1.02m comprising six horizons was logged (Appendix Figures 4.2 and 4.3), with bulk samples obtained from individual beds. Approximately 3 to 4 CSIs were identified empirically; the 2009 tsunami deposit at the surface, possibly the 1990 Cyclone Ofa (Ready and Woodcock, 1992) and the1991 Cyclone Val (Elmqvist et al., 1994), and a CSI beneath the fibrous peat layer at > 1m depth.

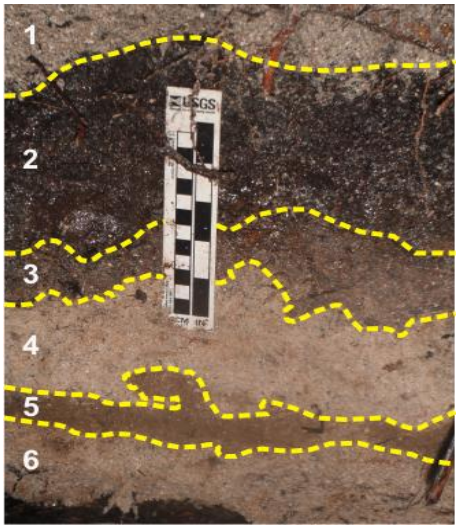

Appendix Figure 4.2: Stratigraphy of Mulivai trench showing six layered deposits. Layer 1 represents the 2009 tsunami deposit. Two more layers below Layer 6 are shown in Figure 3 below - not visible in this photograph due to obscuring from groundwater at Layer 6.

14C dating of the organic peat (sample number Wk30084) at ~1m depth (Layer 7 in Appendix Figure 4.3), yielded an upper-radiocarbon age limit of 528 ± 91 BP for the identified CSI at the base of the log (Appendix 3.2).

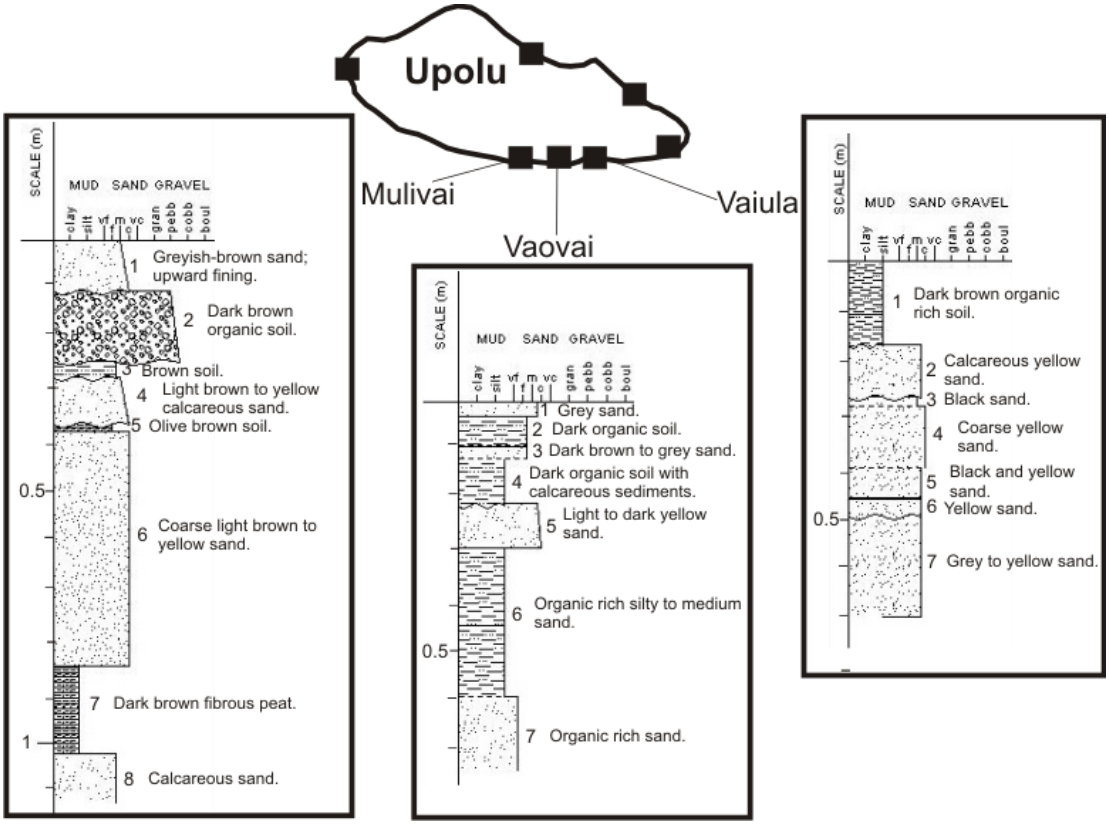

Appendix Figure 4.3: Empirical stratigraphic logs from Mulivai, Vaovai, and Vaiula trench sites on the south of Upolu Island. Stratigraphic depths shown are in metres. Sand particle sizes shown are; vc – very coarse; c – coarse; m – medium; f – fine; vf – very fine.

4.4.1.2 Vaiula trench

The trench at Vaiula was located at 14^{0}02.361' S; 171^{0}39.631' W, approximately 100 m inland from the high-tide water mark. A depth of 0.7 m comprising seven horizons was logged (Appendix Figures 4.3 and 4.4), with bulk sampling obtained from individual beds.

The 2009 tsunami is represented by a thin silty-sand deposit on the surface overlying a soil. A sequence of 6 layers was noted below this soil layer, and it is difficult to ascertain at this point whether this represents a series of different CSI events, or a combination of 1 or 2, with the layers representing different wave energies associated with a single event.

Appendix Figure 4.4: Photograph of Vaiula L-shaped trench taken from (a) south and (b) east end of trench. (c) Northeast corner of trench which was logged (see Figure 3.5) and sampled.

4.4.1.3 Vaovai Trench

The trench at Vaovai was located at 14^{0}02.140' S; 171^{0}40.832' W, approximately 20 m inland from the present-day high-tide water mark. A depth of 0.72 m was logged, with detailed 1 cm sampling down to the base of the trench.

Approximately 3 to 4 CSIs were identified empirically; the 2009 tsunami deposit at the surface. It is possible that the CSI identified in layer 5 of the stratigraphic log (Appendix Figure 4.3) may be associated with the 1990 and 1991 cyclones.

A local matai (chief), Leleimalefao Ionatana, was interviewed and reported that his grandfather had told him a story of a strong earthquake and subsequent tsunami he had experienced while a child. The wave had swept

through their village at night, although minimal damaged was experienced. Leleimalefao was born in 1957, meaning it is highly likely the story his grandfather told him refers to the 1917 tsunami; assuming two generations (50 years) in the past. The 1917 tsunami originated from an MPAS 8.7 earthquake at the northern Tongan Subduction bend (Okal et al., 2011), about 200 km south of Falealupo and 120 km west of the 29/09 earthquake epicentre and 2009 Tsunami source. The earthquake occurred at 6:50 pm on June 25th 1917. However, there is no report in the tsunami catalogue (Pararas-Carrayanis-and Dong, 1980) of an inundation time. The fact that a strong earthquake was felt prior to the tsunami means it was local, suggesting it was most likely to be the 1917 event. Also, the fact that the wave was experienced at night further strengthens this argument since the 1917 earthquake occurred at 6:50 pm (night time) on a dry-season day. The tsunami would have inundated the Samoan islands several minutes after the earthquake; similar to the 2009 Tsunami impact time (Dominey-Howes and Thaman, 2009; Okal et al., 2011).

14C-dating of an unidentified gastropod (sample number Wk30089) obtained from layer 7 in Appendix Figure 4.3 yielded a radiocarbon age of 576 ± 33 BP (Williams et al., 2011a). The dated gastropod is assumed to represent the age of the deposit.

3.4.1.4 Satitoa trench

The trench at Satitoa was located at 14^{0}01.363' S; 171^{0}25.754' W, approximately 280 m inland from the present-day high-tide water mark. A depth of 0.84 m was logged (Appendix Figure 4.5), with detailed 1 cm sampling down to 20 cm depth, followed by 2 cm sampling down to the base of the trench.

Approximately 5 to 7 CSIs were identified empirically with the 2009 tsunami deposit at the surface. There was equivocal evidence of deposits that may have been associated with the 1990 and 1991 Cyclones Ofa and Val suggesting that either these events did not impact far inland, that they did not leave any deposits, or the deposits were not preserved.

Interestingly, three pebbly layers were found within a silty-clay soil layer intermixed with calcareous sands, and two distinct calcareous sand deposits towards the base of the trench. It is likely that these are tsunami deposits; and the upper-age of the event directly below the organic layer at ~0.7 m depth can be constrained by ^{14}C-dating of the overlying organics.

3.4.1.5 Falealupo trench

The trench at Falealupo was located at 13^{0}29.663' S; 172^{0}46.523' W, approximately 165 m inland from the present-day high-tide water mark. A 3.5 m high and 5 m wide storm berm (resembling a sand-dune) was present at the coastline. A depth of 0.5 m was logged at the trench site (Appendix Figure 4.6), with sampling in 1 cm intervals down to 20 cm depth, followed by 2 cm sampling down to the base of the trench.

This site presents an interesting case as the primary goal was to investigate the 1990 and 1991 cyclones Ofa and Val deposits, which would serve as a baseline for distinguishing cyclone from tsunami deposits within this area. These events are most likely represented by the fine sand deposit directly beneath the surface soil layer.

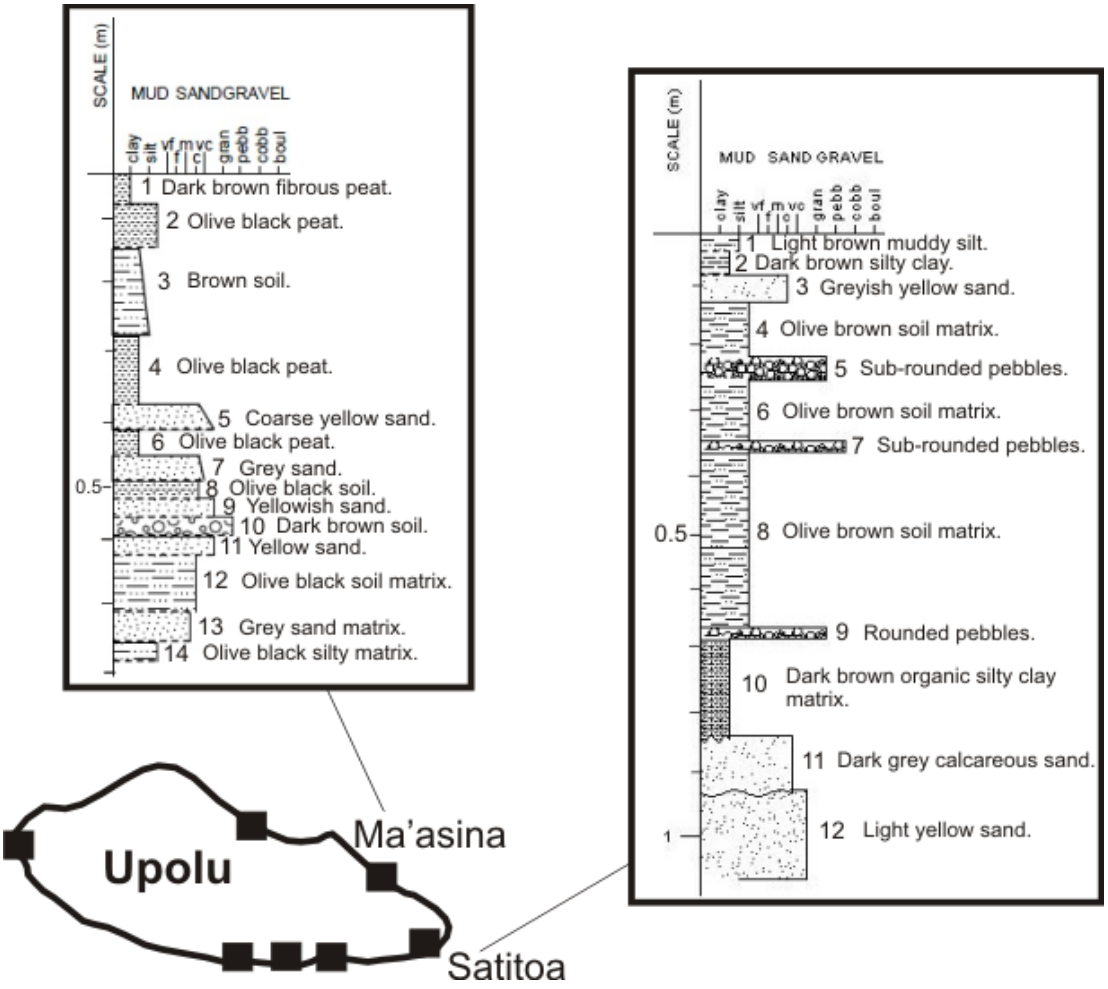

Appendix Figure 4.5: Empirical stratigraphic logs at Satitoa trench site on SE Upolu Island, and Ma'asina core site on NE Upolu. Stratigraphic depths shown are in metres.

The third sequence shown in Figure 4.6 likely represents the pre-1990 soil, while the coarse sand layer beneath that may have been deposited by an historical tsunami, possibly the 1917 tsunami. A local Falealupo resident, Mrs. Siuli Togia, reported that her father, born in 1886, told her a story of a large wave which swept through their village when he was a child. Apparently, he was returning to the coast from their inland plantation when he saw a large wave sweep through their property, taking with it his parents. Fortunately he was able to swim out and rescue them using a log as a raft to haul them back to shore. It is very likely that this narrative is an account of the 1917 tsunami which impacted the Samoan islands.

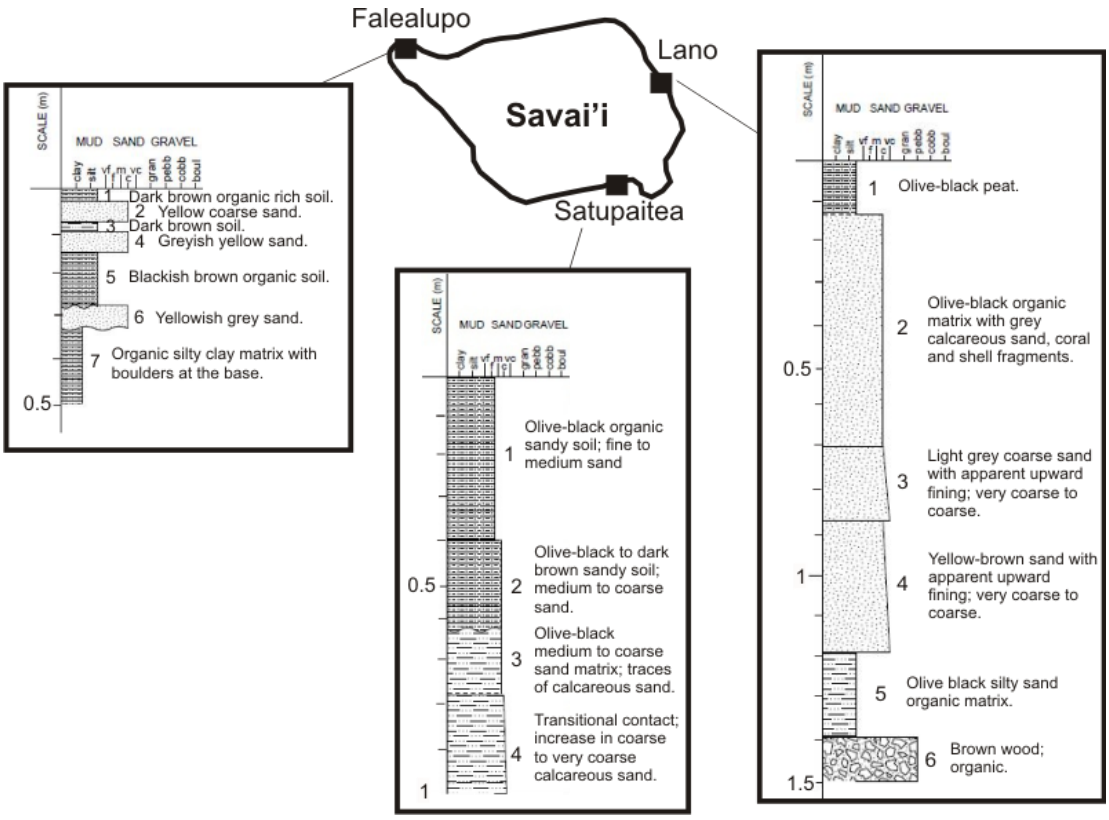

Appendix Figure 4.6: Empirical stratigraphic logs at Falealupo trench site on west Savai'i Island, and Lano and Satupaitea core sites on NE and SE Savai'i, respectively. Stratigraphic depths shown are in metres.

The yellowish coarse sand deposit sandwiched between the two organic layers possibly represents an earlier tsunami. The 1990 Ofa and 1991 Val Cyclones are assumed to have laid down very-fine to fine sand deposits (layer 2 and 4, respectively, in Appendix Figure 4.6).

In this instance, a coarser sand deposit most likely indicates higher wave energy penetrating into the coastal environment. Also, boulders up to 30 cm a-axis were noted within the organic silty layers which sandwich the lower calcareous sand deposit, indicating that they were deposited by high wave energy events.

4.4.1.6 Ta'u trench

The 0.67 m trench at Ta'u was located at 14^{0}13.542' S; 169^{0}30.921' W, approximately 140 m inland of the present high tide water mark. Only two distinct sequences were observed in the stratigraphy (Appendix Figure 4.7). A sharp contact at approximately 51 cm depth separates the overlying organic soil horizon from the underlying very coarse, greying yellow calcareous sand deposit. This deposit also comprised coral cobbles (branching and brain corals), gastropod and other unidentified shells, as well as rounded basalt cobbles towards the base of the deposit matrix (Appendix 3.2).

Recent Category 5 cyclones (eg. Cyclones Ofa in 1990 and Val in 1991 and Cyclone Heta in 2004 (Marra et al., 2008) which have impacted this island had insufficient wave energy to inundate 140 m inland, and hence there is no evidence of deposits associated with recent cyclone activity at the site. Sequence 2 likely represents a high

wave energy deposition source sufficient to transport the denser coral and basalt cobbles observed within the matrix. It is empirically assumed that this deposit is likely associated with a tsunami origin (Appendix 3.2), although further research is required to ascertain this.

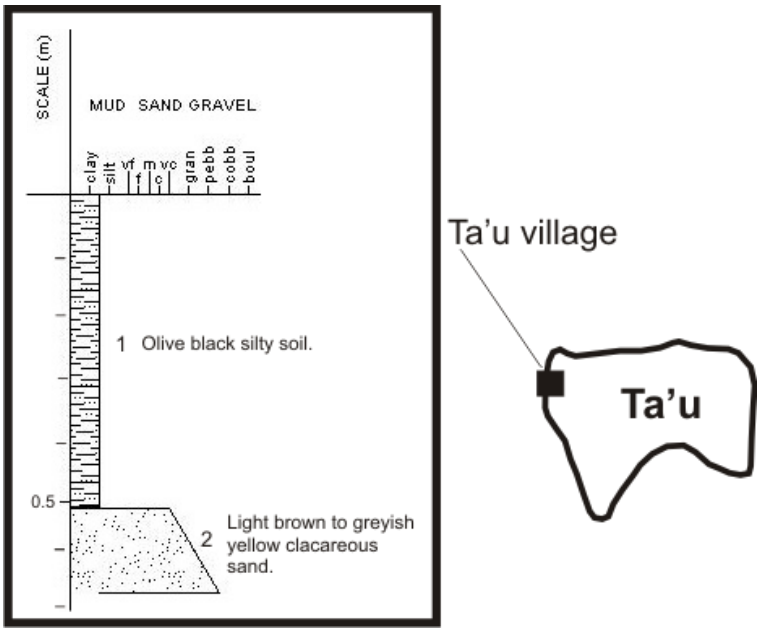

Appendix Figure 4.7: Empirical stratigraphic log at Ta'u trench site on NW Ta'u Island. Stratigraphic depth shown is in metres.

4.4.1.7 Fale o le Fe'e reconnaissance pit-trench

Reconnaissance to Fale o le Fe'e was conducted in order to investigate the local belief that calcareous coastal deposits are present at the site. The site is ~7.5 km inland (south) of Apia and 475 m in elevation (Appendix Figure 4.8). The site is culturally significant in that it is the residence of the ancient war God of A'ana, the God Fe'e. It was visited to investigate whether coastal deposits are found this far inland, and what processes might have been involved in their deposition.

Reverend J.B. Stair visited the site in 1845 and concluded that the (believed) limestone pillars and house remnants were basalts mined from a nearby outcrop (Stair, 1894). He also concluded that (believed) corals on the nearby stream bed were actually stalagmites and calcareous spar which formed on the surface of outcrops, in association with the nearby stream.

Field observations made during this reconnaissance confirmed the former. Dense olivine basalt outcrops associated with the Salani volcanics (Kear and Wood, 1959), appear to have been where the house pillars and associated building (rock) material were mined. The basalts appear to have a calcitic skin on their surface giving it a light grey colour, which likely formed as a result of secondary mineralisation of Mg/Fe olivines as they interact with CO2 in air and water. The basalts also fracture prismatically and appear to resemble limestone at first glance.

However, upon examining a few samples, visible olivine crystals ~1-3 mm along their a-axis can be seen embedded within a mafic matrix.

The (assumed) coral deposits further upstream of the site were not observed. A small calcitic pillar, including small stalactites and stalagmites were observed (during this study) in the Dwarf's lava-tube cave at Paia on Savaii; also located on olivine basalts. It is highly likely that Stair's conclusions of the calcitic like material he observed at Fale o le Fe'e formed in a similar way to that observed in the Dwarf's cave, and that they are not coastal calcareous deposits.

Calcite ($CaCO_3$) minerals formed at the coast are mainly derived from the fossils of calcareous marine organisms (Morse et al., 2007), whereas calcite formed within basalts is due to secondary mineralisation (a weathering process) involving CO_2-water-rock interactions (Matter and Takahashi, 2007).

A pit-trench was also dug in order to rule out the possibility of a distinct sand deposit at depth (Appendix Figure 4.8). Interestingly, a well-preserved charcoal layer was observed at ~0.35 m depth, and is assumed to be anthropogenic. C14 dating of a sample (sample number Wk30088) of this charcoal presented in Appendix 3.2 showed this deposit to have a radiocarbon age of 398 ± 73 BP; provisionally suggesting that likely worshipers of Fe'e occupied or used the site around this time.

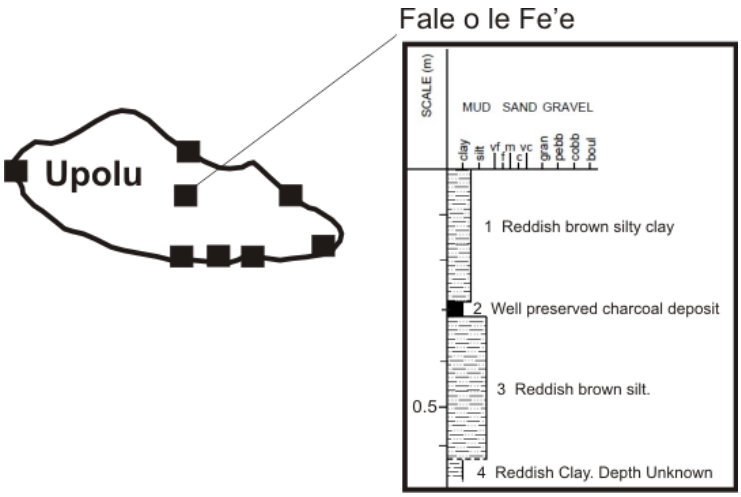

Appendix Figure 4.8: Empirical stratigraphic log at Fale o le Fe'e trench site on Upolu Island. Stratigraphic depth shown is in metres.

4.4.2 Core samples

Core samples were obtained from the locations shown in Appendix Figure 4.1. The cores were not logged in the field due to time constraints. Logging and detailed laboratory analysis of the samples will be conducted in due course.

4.4.2.1 Ma'asina core sample

A 0.7 m core was obtained from Ma'asina village (Fagaloa Bay) in a small coastal marsh ~40 m inland of the high-tide mark A sand deposit was observed at approximately 0.4 – 0.8 m depth (Appendix Figure 4.5).

The historical database indicates that Fagaloa Bay has been impacted by tsunamis causing destructive damages in 1952, 1957, and 1960. The 1952 (1.8 m wave) and 1960 (2.4 m wave) tsunamis originated from major earthquakes in the Chile/Peru region. The 1957 (1.5 m wave) tsunami originated from an 8.5 magnitude earthquake in the Aleutian Islands (Pararas-Carayannis and Dong, 1980).

4.4.2.2 Fagalii core sample

A 3 m core was obtained from a swamp at Fagalii village located at $13^0$50.628' S; $171^0$44.131' W, within the 8 km radius of Apia Township. The site was located ~150 m inland of the high-tide water mark, and directly behind the current Minister of Communication and Information Technology's residence.

No apparent CSI deposits were observed (Appendix Figure 4.9), although detailed laboratory analysis will clarify this. Interestingly, a charcoal deposit was observed at ~2.9 m depth which is likely to be anthropogenic. If the sample is found to be anthropogenic and older than 2800 BP, this finding could represent evidence for initial human settlement in Upolu older than the currently accepted ~2800 BP (Dickinson and Green, 2008). 14C-dating of this sample (sample number Wk30087) yielded a radiocarbon age of 3,112 ± 50 BP (Appendix 3.2), but further study is required to ascertain its origin.

Historically, the most destructive tsunami to have impacted the Apia region was on 14 August 1868, which originated from a major earthquake in the Peru/Chile region (Pararas-Carayannis and Dong, 1980). It was reported that the tsunami destroyed buildings in Apia, although there were no detailed accounts on the geographic extent and magnitude of damage, nor on loss of life.

4.4.2.2 Manono core sample

A 2.5 m core was obtained from the Manono-uta marsh located at $13^0$52.120' S; $172^0$04.263' W, ~75 m inland of the high-tide water mark. No apparent CSI deposits were observed (Appendix Figure 4.9), although detailed laboratory analysis will clarify this. The site was chosen to identify CSIs which may have impacted east Upolu.

4.4.2.3 Lano core sample

A 1.5 m core was obtained from a swamp at Lano village, located at $13^0$37.176' S; $172^0$11.938' W; ~150 m inland of the high-tide mark. A distinct CSI deposit was observed at ~1 m depth (layer 4 in Appendix Figure 4.6). 14C-dating of plant fragments (sample number Wk30083) obtained from layer 5 at 1.4 m depth yielded a radiocarbon age of ~798 ± 28 BP (Appendix 3.2). Detailed laboratory analysis of organics above and below the deposit will help to establish its age. This site was chosen to identify events along NE Savaii.

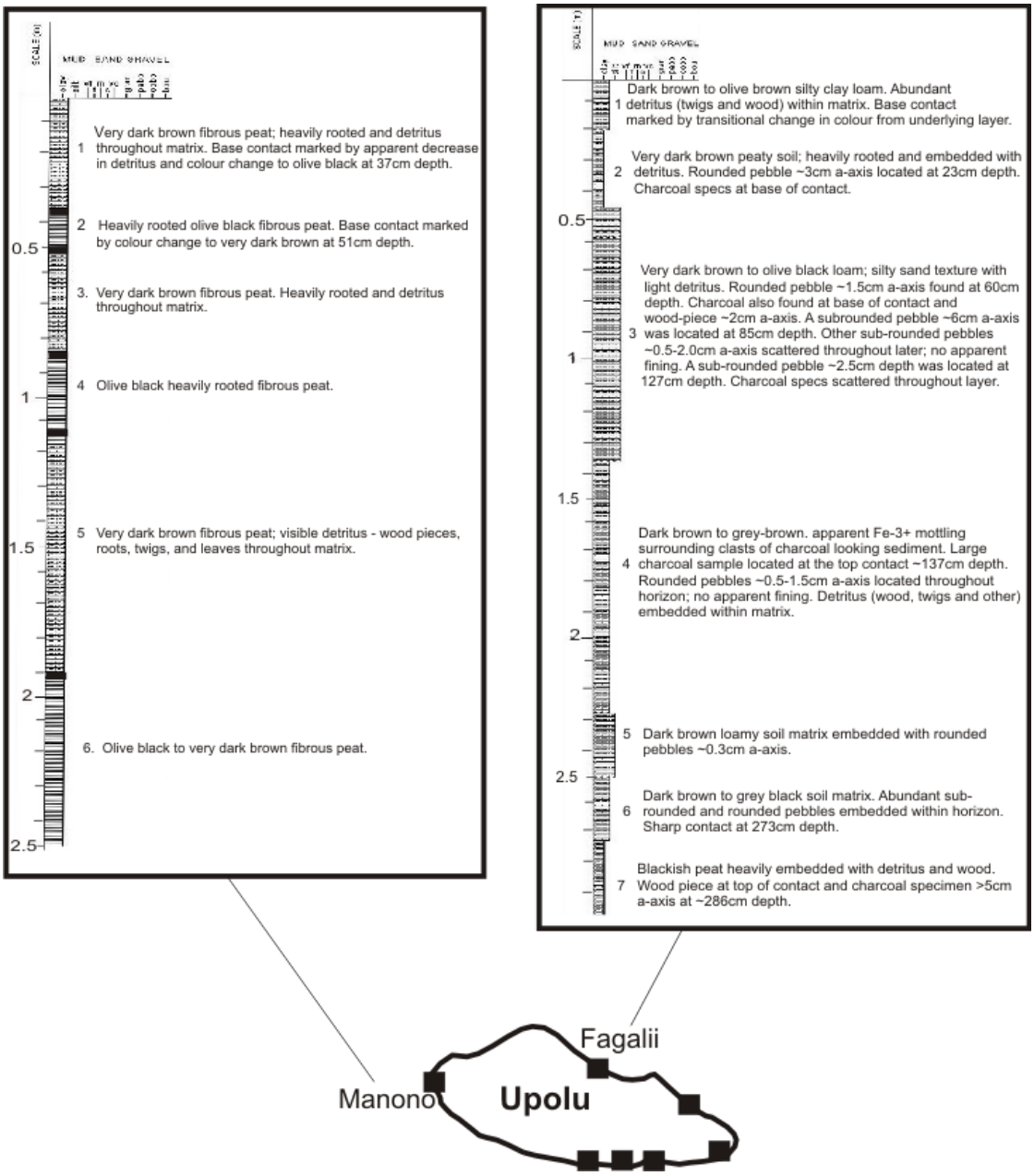

Appendix Figure 4.9: Empirical stratigraphic logs at Fagali'i and Manono core sites on north and west Upolu Island, respectively. Stratigraphic depths shown are in metres.

4.4.2.4 Falealupo core samples

Two core samples were obtained from two separate swamps at Falealupo. Falealupo Core-1 (FC-01) was located at $13^0$30.064' S; $172^0$47.161' W ~220 m inland of the high-tide water mark. Falealupo Core-2 (FC-02) was located at $13^0$29.670' S; $172^0$46.521' W ~160 m Inland of the high tide water mark. Both cores reached 1 m in depth, and FC-02 appeared to have 2 or 3 CSIs within them. These cores were subsequently not selected for analysis as the samples obtained from Falealupo trench (see Section 4.1.5) were sufficient for the purposes of this study.

4.4.2.5 Satupaitea core sample

A 1 m core sample was obtained from a swamp located at $13^0$45.576' S; $172^0$19.209' W, ~75 m inland of the high-tide water mark. The Satupaitea coastal area comprised mainly black sandy sediments derived from inland basalts that have been transported to the coast by a network of streams and rivers, and some re-deposited by waves. Two distinct calcareous deposits were observed at 0.8 m and 0.95 m depths (Appendix Figure 4.6), indicating two separate CSI events. This area was chosen to identify events which may have impacted SE Savaii.

4.4.3 Personal Interviews

Four interviews were carried out at Salimu (Fagaloa Bay) and Vaovai on Upolu, as well as Lano and Falealupo on Savaii. One individual from each village was interviewed. Questions asked centred on any local stories related to tsunamis or unusual wave activity which were either experienced by the individuals or were told by older generations.

4.4.3.1 Salimu-Fagaloa interview

A 67 year old local matai from Salimu (Fagaloa), Limu Filifilia, stated that he had known of two unusual waves to have impacted his village while he was a teenager. The first one had slightly inundated Salimu, but had transported the local medical barge across the other side of the harbour and deposited it on the reef adjacent to Ma'asina (Fagaloa). Several years later, another wave struck which brought the barge back to its present day location (Appendix Figure 4.10).

The events he described are most likely the 1957 and 1960 tsunamis which impacted Fagaloa harbour. The 1957 tsunami originated from an 8.5 earthquake in the Aleutian Islands which ruptured at 3:22 am (local Samoan time) on March 9th. It had a 9 hour travel time, meaning it would have impacted Fagaloa bay at approximately 12:22 pm. 1.5 m and 1.05 m waves were reported at Taelefaga and Maasina villages, respectively (Pararas-Carayannis and Dong, 1980).

The 1960 tsunami originated from an Mw 9.5 earthquake in the south Chile region which ruptured at 8:11am (local Samoan time) on May 22nd (Pararas-Carayannis and Dong, 1980). The tsunami had a travel time 12.4 hours, meaning it would have impacted Fagaloa at approximately 9:00pm. 2.4 m waves reportedly inundated villages at Fagaloa, causing damage and flooding to local huts.

4.4.3.2 Vaovai interview

Refer to Section 4.4.1.3 for an account of the story told by Leleimalefao Ionatana (local matai of Vaovai village).

Appendix Figure 4.10: Fagaloa harbour showing the present-day barge location relative to Salimu and Ma'asina villages. Photograph is taken facing north, and the straight-line distance from Salimu to Ma'asina is ~1.3km (standing are J. Ah Kau – left; and F. Sale – right).

4.4.3.3 Lano interview

The late sa'o (head matai) of Lano village, afioga Vui Vaea (82 years of age in 2010), told of calcareous boulders which were deposited about 70 m inland from the core site. A local Lano story passed down to him while he was a child stated that the boulders were deposited by a large wave ages before. He viewed these coralline boulders when he was young and stated that they had average a-axes greater than 20 cm. There is no mention as to the timing of the event, and he did not indicate that it occurred during his parents or grandparents' generation. These boulders have since been removed due to recent development in the area, but it is likely they were deposited by a palaeotsunami. Further detailed geological studies in the area would be useful to clarify the nature and extent of this event.

4.4.3.4 Falealupo interview

Refer to Section 4.4.1.5 for an account of the story told by Mrs. Siuli Togia (local Falealupo-tai resident).

4.5 Review of Preliminary Analytical Outcomes

The samples collected were processed using a set of multi-proxy diagnostic criteria in relevant laboratories at the Universities of Canterbury and Waikato in New Zealand, and at the Australian Nuclear Science and Technology Organisation in Australia. The diagnostic proxy criteria used included sedimentological (stratigraphic logging, loss on ignition and grain size distributions), geochemical (elemental profiles), and geochronological (^{14}C and ^{210}Pb dating) techniques.

While the data are currently being analysed and will be communicated in due course, preliminary geochemical and geochronological aspects of the project were presented (Appendix 3). Using elemental data collected with a portable X-Ray fluorescence spectrometer; it was found that the Ca/Fe and Ca/Ti ratio-relationships for the 2009 Samoa Tsunami deposits at investigated impact sites could be used to identify similar high energy deposits in their respective geologic records. However it was acknowledged that elemental proxies alone were insufficient in distinguishing between a tsunami and a cyclone deposit (Appendix 3).

In some cases (eg. Satitoa and Ta'u), high energy deposits identified were provisionally assumed to be of a tsunami origin due to their relative locations inland from mean sea level. Moreover, we observed no evidence of any deposits at these sites which might have formed from recent cyclones over the past several decades, such as from Cyclones Ofa in 1990 and Val in 1991 (Ready and Woodcock, 1992; Elmqvist et al., 1994), and Cyclone Heta in 2004 (Marra et al., 2008).

In the case of Satitoa, a ^{14}C radiocarbon age obtained from the soil horizon (~0.81 m stratigraphic depth), overlying the assumed tsunami deposit provisionally suggests that the deposit may have been laid down by the 1917 Samoa Tsunami.

At Mulivai (near Coconuts Beach Resort) and Vaovai sites, high energy deposits with radiocarbon ages of ~437 – 619 BP (see Sections 4.1.1 and 4.1.3) were identified at both sites, respectively. Although it was assumed the respective deposits were formed by the same event, it was uncertain whether the deposits were of a tsunami or cyclone origin.

4.6 Summary and directions for future work

While the outcomes to date provide a provisional basis for starting to understand the long-term impacts of tsunamis at the investigated sites, much work remains to be carried out in order to allow us to draw conclusive evidence to distinguish between deposits of tsunami or cyclone origin. Only coupled with a suite of multi-proxy criteria (e.g. Goff et al., 2001; 2004; 2011; 2012; Morton et al., 2007; Chagué-Goff et al., 2011; Richmond et al., 2011), and assessed in the broader regional geochronological context can we develop more robust conclusions.

Further palaeotsunami studies on other islands and nations in the Pacific are required, as they can serve as point-sources of potential palaeotsunami information. This would contribute to the existing, but sparse, palaeotsunami database for the region, and would contribute to our geochronological and spatial understanding of long-term tsunami impacts. By doing this, we can start to better understand the long-term risk of coastal communities to tsunami hazards in the Pacific.

APPENDIX 5: LOI DATA

Overview

Loss on Ignition (LOI) was carried out at the University of Canterbury following methods in Santisteban et al. (2004) and Chagué-Goff et al. (2011).

LOI data for each site is provided.

Contents

Appendix 5.1: Satitoa LOI Data

Appendix Table 5.1: Satitoa LOI Data

Sub-sample	Depth	Loss on Ignition at 550^0 : $100(DW_{105} - DW_{550})/WS$	Sub-sample	Depth	Loss on Ignition at 550^0 : $100(DW_{105} - DW_{550})/WS$
ST001	0.5	11	ST029	37	7
ST002	1.5	11	ST030	39	7
ST003	2.5	10	ST031	41	8
ST004	3.5	9	ST032	43	9
ST005	4.5	7	ST033	45	8
ST006	5.5	9	ST034	47	8
ST007	6.5	9	ST035	49	7
ST008	7.5	10	ST036	51	7
ST009	8.5	3	ST037	53	6
ST010	9.5	3	ST038	55	8
ST011	10.5	3	ST039	57	8
ST012	11.5	9	ST040	59	7
ST013	12.5	10	ST041	61	8
ST014	13.5	9	ST042	63	7
ST015	14.5	9	ST043	65	8
ST016	15.5	9	ST044	67	8
ST017	16.5	10	ST045	69	9
ST018	17.5	9	ST046	71	7
ST019	18.5	8	ST047	73	6
ST020	19.5	8	ST048	75	5
ST021	21	8	ST049	77	6
ST022	23	8	ST050	79	4
ST023	25	8	ST051	81	6
ST024	27	8	ST052	83	2
ST025	29	7	ST053	85	2
ST026	31	8	ST054	87	2
ST027	33	7	ST055	89	2
ST028	35	8			

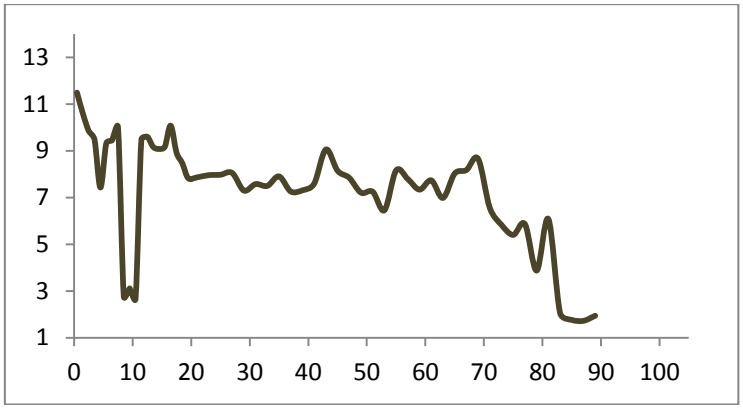

Appendix Figure 5.1: Satitoa LOI curve (x axis = depth in cm; y = LOI in %)

Appendix Table 5.1.1: Satitoa LOI data calculations obtained using method in Santisteban et al., 2004.

Sub-sample ID	Crucible/Beaker weight (g)	Crucible + wet weight of sub-sample (g)	Crucible + dry weight (g) (105^0C for 12 - 24 hours)	Crucible + dry (ash) weight (g) (550^0C for 4 hours)	Wet Sample Weight (WS) (g)	Dry Sample Weight (DW_{105}) (g)	Burned Sample Weight (DW_{550}) (g)	Loss on Ignition at 105^0 : 100(WS-DW_{105})/WS	Loss on Ignition at 550^0 : 100(DW_{105} - DW_{550})/WS
ST001	11.909	15.556	13.114	12.695	3.647	1.205	0.786	66.9591	11.4889
ST002	14.668	18.387	15.702	15.308	3.719	1.034	0.64	72.1968	10.5942
ST003	15.558	20.614	16.904	16.406	5.056	1.346	0.848	73.3782	9.8497
ST004	15.241	19.382	16.526	16.134	4.141	1.285	0.893	68.9688	9.4663
ST005	17.625	22.287	19.625	19.279	4.662	2	1.654	57.1000	7.4217
ST006	15.369	20.188	16.918	16.469	4.819	1.549	1.1	67.8564	9.3173
ST007	11.806	16.782	13.503	13.033	4.976	1.697	1.227	65.8963	9.4453
ST008	14.593	18.948	15.866	15.43	4.355	1.273	0.837	70.7692	10.0115
ST009	15.142	22.49	20.654	20.452	7.348	5.512	5.31	24.9864	2.7490
ST010	15.094	21.656	20.398	20.194	6.562	5.304	5.1	19.1710	3.1088
ST011	15.468	20.172	19.079	18.954	4.704	3.611	3.486	23.2355	2.6573
ST012	15.532	20.458	18.117	17.65	4.926	2.585	2.118	47.5233	9.4803
ST013	11.908	17.656	15.074	14.522	5.748	3.166	2.614	44.9200	9.6033
ST014	15.558	22.43	19.664	19.034	6.872	4.106	3.476	40.2503	9.1676
ST015	15.241	22.799	19.468	18.782	7.558	4.227	3.541	44.0725	9.0765
ST016	17.625	22.031	20.09	19.686	4.406	2.465	2.061	44.0536	9.1693
ST017	15.37	19.538	17.901	17.481	4.168	2.531	2.111	39.2754	10.0768
ST018	14.669	19.872	17.559	17.095	5.203	2.89	2.426	44.4551	8.9179
ST019	11.803	15.857	14.175	13.832	4.054	2.372	2.029	41.4899	8.4608
ST020	14.593	19.924	17.859	17.442	5.331	3.266	2.849	38.7357	7.8222
ST021	15.094	20.653	18.349	17.912	5.559	3.255	2.818	41.4463	7.8611
ST022	15.532	21.968	19.12	18.608	6.436	3.588	3.076	44.2511	7.9553
ST023	15.142	20.36	18.022	17.606	5.218	2.88	2.464	44.8064	7.9724
ST024	15.467	19.79	17.805	17.457	4.323	2.338	1.99	45.9172	8.0500
ST025	11.906	16.539	14.794	14.456	4.633	2.888	2.55	37.6646	7.2955

ST026	17.625	22.59	20.676	20.3	4.965	3.051	2.675	38.5498	7.5730
ST027	15.369	19.865	18.064	17.727	4.496	2.695	2.358	40.0578	7.4956
ST028	14.668	20.957	18.6	18.103	6.289	3.932	3.435	37.4781	7.9027
ST029	15.241	21.029	18.882	18.462	5.788	3.641	3.221	37.0940	7.2564
ST030	15.558	21.142	18.921	18.513	5.584	3.363	2.955	39.7744	7.3066
ST031	11.801	17.058	14.706	14.307	5.257	2.905	2.506	44.7403	7.5899
ST032	14.593	20.271	17.984	17.47	5.678	3.391	2.877	40.2783	9.0525
ST033	15.094	23.627	19.873	19.178	8.533	4.779	4.084	43.9939	8.1448
ST034	15.532	22.548	19.798	19.248	7.016	4.266	3.716	39.1961	7.8392
ST035	15.467	21.574	18.802	18.362	6.107	3.335	2.895	45.3905	7.2048
ST036	15.142	20.29	17.933	17.56	5.148	2.791	2.418	45.7848	7.2455
ST037	11.357	18.332	15.094	14.644	6.975	3.737	3.287	46.4229	6.4516
ST038	11.904	16.99	14.251	13.836	5.086	2.347	1.932	53.8537	8.1597
ST039	15.37	21.983	18.52	18.005	6.613	3.15	2.635	52.3666	7.7877
ST040	14.67	22.877	18.641	18.039	8.207	3.971	3.369	51.6145	7.3352
ST041	15.242	22.69	18.461	17.885	7.448	3.219	2.643	56.7803	7.7336
ST042	17.626	27.812	23.096	22.385	10.186	5.47	4.759	46.2988	6.9802
ST043	11.796	15.809	13.72	13.398	4.013	1.924	1.602	52.0558	8.0239
ST044	15.532	21.025	18.266	17.817	5.493	2.734	2.285	50.2276	8.1740
ST045	15.094	22.338	18.167	17.54	7.244	3.073	2.446	57.5787	8.6554
ST046	15.142	25.523	21.285	20.605	10.381	6.143	5.463	40.8246	6.5504
ST047	15.468	19.933	17.36	17.1	4.465	1.892	1.632	57.6260	5.8231
ST048	14.593	22.43	19.817	19.394	7.837	5.224	4.801	33.3418	5.3975
ST049	11.913	17.427	15.356	15.033	5.514	3.443	3.12	37.5589	5.8578
ST050	11.367	20.128	17.48	17.141	8.761	6.113	5.774	30.2249	3.8694
ST051	17.64	24.387	21.673	21.263	6.747	4.033	3.623	40.2253	6.0768
ST052	15.254	23.351	20.498	20.332	8.097	5.244	5.078	35.2353	2.0501
ST053	15.382	23.511	20.697	20.554	8.129	5.315	5.172	34.6168	1.7591
ST054	14.681	22.878	20.501	20.36	8.197	5.82	5.679	28.9984	1.7201
ST055	11.801	18.977	16.793	16.654	7.176	4.992	4.853	30.4348	1.9370

Appendix 5.2: Vaovai LOI Data

Appendix Table 5.2: Vaovai LOI Data

Sub-Sample	Depth (cm)	Loss on Ignition at 550^0 : $100(DW_{105} - DW_{550})/WS$	Sub-Sample	Depth (cm)	Loss on Ignition at 550^0 : $100(DW_{105} - DW_{550})/WS$	Sub-Sample	Depth (cm)	Loss on Ignition at 550^0 : $100(DW_{105} - DW_{550})/WS$
VV001	0.5	3	VV025	24.5	3	VV049	48.5	3
VV002	1.5	3	VV026	25.5	4	VV050	49.5	3
VV003	2.5	4	VV027	26.5	3	VV051	50.5	3
VV004	3.5	4	VV028	27.5	3	VV052	51.5	3
VV005	4.5	4	VV029	28.5	3	VV053	52.5	3
VV006	5.5	4	VV030	29.5	3	VV054	53.5	3
VV007	6.5	5	VV031	30.5	3	VV055	54.5	3
VV008	7.5	5	VV032	31.5	3	VV056	55.5	3
VV009	8.5	4	VV033	32.5	4	VV057	56.5	4
VV010	9.5	4	VV034	33.5	3	VV058	57.5	3
VV011	10.5	4	VV035	34.5	3	VV059	58.5	3
VV012	11.5	3	VV036	35.5	4	VV060	59.5	3
VV013	12.5	3	VV037	36.5	3	VV061	60.5	4
VV014	13.5	3	VV038	37.5	3	VV062	61.5	3
VV015	14.5	3	VV039	38.5	3	VV063	62.5	3
VV016	15.5	4	VV040	39.5	4	VV064	63.5	3
VV017	16.5	4	VV041	40.5	3	VV065	64.5	3
VV018	17.5	4	VV042	41.5	3	VV066	65.5	3
VV019	18.5	4	VV043	42.5	3	VV067	66.5	3
VV020	19.5	4	VV044	43.5	3	VV068	67.5	3
VV021	20.5	4	VV045	44.5	3	VV069	68.5	3
VV022	21.5	4	VV046	45.5	3	VV070	69.5	3
VV023	22.5	3	VV047	46.5	3	VV071	70.5	3
VV024	23.5	4	VV048	47.5	3	VV072	71.5	3

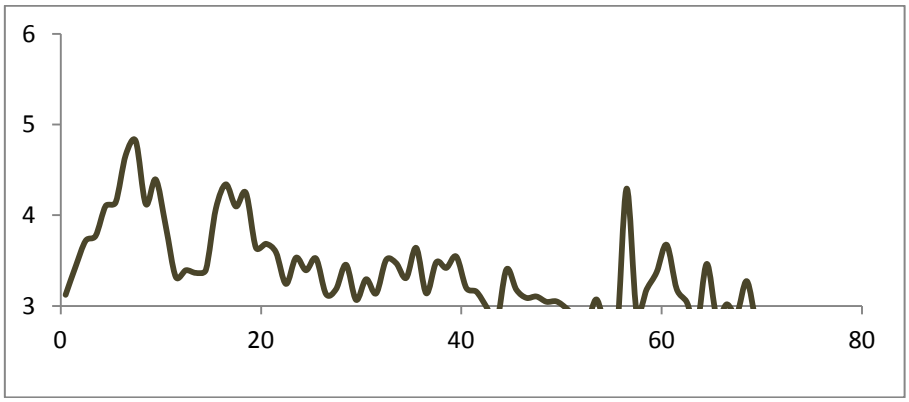

Appendix Figure 5.2: Vaovai LOI Curve (x axis = depth in cm; y = LOI in %)

Appendix Table 5.2.1: Vaovai LOI data calculations obtained using method in Santisteban et al., 2004.

Sub-sample ID	Crucible/Beaker weight (g)	Crucible + wet weight of sub-sample (g)	Crucible + dry weight (g) (105^0C for 12-24 hours)	Crucible + dry (ash) weight (g) (550^0C for 4 hours)	Wet Sample Weight (WS) (g)	Dry Sample Weight (DW_{105}) (g)	Burned Sample Weight (DW_{550}) (g)	Loss on Ignition at 105^0 : 100(WS-DW_{105})/WS	Loss on Ignition at 550^0 : 100(DW_{105} - DW_{550})/WS
VV001	15.478	21.214	20.698	20.519	5.736	5.22	5.041	8.9958	3.1206
VV002	15.152	20.366	19.598	19.419	5.214	4.446	4.267	14.7296	3.4331
VV003	15.543	21.273	20.434	20.221	5.73	4.891	4.678	14.6422	3.7173
VV004	15.106	19.639	18.932	18.761	4.533	3.826	3.655	15.5967	3.7723
VV005	14.603	18.772	18.143	17.972	4.169	3.54	3.369	15.0876	4.1017
VV006	11.35	15.914	15.203	15.014	4.564	3.853	3.664	15.5784	4.1411
VV007	11.912	16.459	15.657	15.445	4.547	3.745	3.533	17.6380	4.6624
VV008	17.637	22.203	21.323	21.103	4.566	3.686	3.466	19.2729	4.8182
VV009	15.252	20.539	19.458	19.24	5.287	4.206	3.988	20.4464	4.1233
VV010	15.38	20.115	18.982	18.774	4.735	3.602	3.394	23.9282	4.3928
VV011	14.679	18.985	18.12	17.953	4.306	3.441	3.274	20.0882	3.8783
VV012	11.802	15.962	15.335	15.197	4.16	3.533	3.395	15.0721	3.3173
VV013	15.153	20.106	19.406	19.238	4.953	4.253	4.085	14.1328	3.3919
VV014	15.543	20.777	19.949	19.773	5.234	4.406	4.23	15.8196	3.3626
VV015	14.603	18.697	17.956	17.817	4.094	3.353	3.214	18.0997	3.3952
VV016	15.478	21.84	20.182	19.923	6.362	4.704	4.445	26.0610	4.0710
VV017	15.104	20.173	18.935	18.715	5.069	3.831	3.611	24.4230	4.3401
VV018	11.911	15.915	14.844	14.68	4.004	2.933	2.769	26.7483	4.0959
VV019	11.34	16.594	15.142	14.919	5.254	3.802	3.579	27.6361	4.2444
VV020	15.381	21.012	19.846	19.641	5.631	4.465	4.26	20.7068	3.6406
VV021	17.639	22.634	21.36	21.176	4.995	3.721	3.537	25.5055	3.6837
VV022	15.543	19.499	18.574	18.432	3.956	3.031	2.889	23.3822	3.5895
VV023	15.253	20.406	19.368	19.201	5.153	4.115	3.948	20.1436	3.2408
VV024	11.8	16.899	15.884	15.704	5.099	4.084	3.904	19.9059	3.5301
VV025	15.154	19.842	18.79	18.631	4.688	3.636	3.477	22.4403	3.3916

VV026	14.603	19.546	18.387	18.213	4.943	3.784	3.61	23.4473	3.5201
VV027	15.479	19.954	19.147	19.007	4.475	3.668	3.528	18.0335	3.1285
VV028	15.105	20.602	19.39	19.215	5.497	4.285	4.11	22.0484	3.1836
VV029	15.543	19.656	18.676	18.534	4.113	3.133	2.991	23.8269	3.4525
VV030	11.91	16.609	15.477	15.333	4.699	3.567	3.423	24.0902	3.0645
VV031	11.338	17.23	15.702	15.508	5.892	4.364	4.17	25.9335	3.2926
VV032	14.679	20.928	19.268	19.072	6.249	4.589	4.393	26.5643	3.1365
VV033	17.637	22.97	21.515	21.328	5.333	3.878	3.691	27.2830	3.5065
VV034	15.38	21.951	20.228	20	6.571	4.848	4.62	26.2213	3.4698
VV035	15.251	19.968	18.653	18.497	4.717	3.402	3.246	27.8779	3.3072
VV036	11.799	16.966	15.536	15.348	5.167	3.737	3.549	27.6756	3.6385
VV037	15.105	20.3	18.841	18.678	5.195	3.736	3.573	28.0847	3.1376
VV038	15.479	19.445	18.266	18.128	3.966	2.787	2.649	29.7277	3.4796
VV039	15.152	18.78	17.729	17.605	3.628	2.577	2.453	28.9691	3.4179
VV040	15.543	21.499	19.878	19.667	5.956	4.335	4.124	27.2163	3.5426
VV041	14.603	20.203	18.481	18.302	5.6	3.878	3.699	30.7500	3.1964
VV042	11.335	16.405	15.084	14.924	5.07	3.749	3.589	26.0552	3.1558
VV043	11.91	18.466	16.536	16.34	6.556	4.626	4.43	29.4387	2.9896
VV044	14.679	20.02	18.523	18.373	5.341	3.844	3.694	28.0285	2.8085
VV045	15.252	20.606	19.066	18.884	5.354	3.814	3.632	28.7635	3.3993
VV046	15.381	20.827	19.278	19.105	5.446	3.897	3.724	28.4429	3.1766
VV047	17.637	22.334	21.075	20.93	4.697	3.438	3.293	26.8043	3.0871
VV048	11.798	18.406	16.622	16.417	6.608	4.824	4.619	26.9976	3.1023
VV049	15.153	20.212	18.759	18.605	5.059	3.606	3.452	28.7211	3.0441
VV050	15.543	21.022	19.387	19.22	5.479	3.844	3.677	29.8412	3.0480
VV051	15.479	19.822	18.738	18.609	4.343	3.259	3.13	24.9597	2.9703
VV052	15.105	19.274	18.203	18.084	4.169	3.098	2.979	25.6896	2.8544
VV053	14.603	19.612	18.29	18.15	5.009	3.687	3.547	26.3925	2.7950
VV054	11.908	18.195	16.35	16.157	6.287	4.442	4.249	29.3463	3.0698
VV055	11.332	17.236	15.636	15.476	5.904	4.304	4.144	27.1003	2.7100
VV056	14.68	19.683	18.336	18.203	5.003	3.656	3.523	26.9238	2.6584

VV057	15.252	19.236	17.802	17.631	3.984	2.55	2.379	35.9940	4.2922
VV058	17.637	21.765	20.685	20.564	4.128	3.048	2.927	26.1628	2.9312
VV059	15.38	20.851	19.453	19.279	5.471	4.073	3.899	25.5529	3.1804
VV060	11.798	16.812	15.553	15.384	5.014	3.755	3.586	25.1097	3.3706
VV061	15.543	22.132	20.411	20.169	6.589	4.868	4.626	26.1193	3.6728
VV062	15.152	21.149	19.395	19.204	5.997	4.243	4.052	29.2480	3.1849
VV063	14.603	21.276	19.398	19.195	6.673	4.795	4.592	28.1433	3.0421
VV064	15.479	21.214	19.532	19.373	5.735	4.053	3.894	29.3287	2.7724
VV065	15.105	22.067	19.948	19.707	6.962	4.843	4.602	30.4367	3.4616
VV066	11.326	19.08	16.771	16.548	7.754	5.445	5.222	29.7782	2.8759
VV067	11.908	19.401	16.962	16.736	7.493	5.054	4.828	32.5504	3.0161
VV068	15.381	22.969	20.768	20.547	7.588	5.387	5.166	29.0063	2.9125
VV069	17.637	26.868	24	23.698	9.231	6.363	6.061	31.0692	3.2716
VV070	15.251	21.403	19.771	19.599	6.152	4.52	4.348	26.5280	2.7958
VV071	14.68	19.955	18.483	18.34	5.275	3.803	3.66	27.9052	2.7109
VV072	15.104	21.7	19.73	19.541	6.596	4.626	4.437	29.8666	2.8654

Appendix 5.3: Mulivai LOI Data

Appendix Table 5.3: Mulivai LOI Data

Sub-Sample	Depth (cm	Loss on Ignition at 550^0 : $100(DW_{105} - DW_{550})/WS$
MU001	5	3
MU002	17	10
MU003	26	6
MU004	33	2
MU005	38	4
MU006	60	2
MU007	83	2
MU008	93	12
MU009	102	2
MU010	104	3

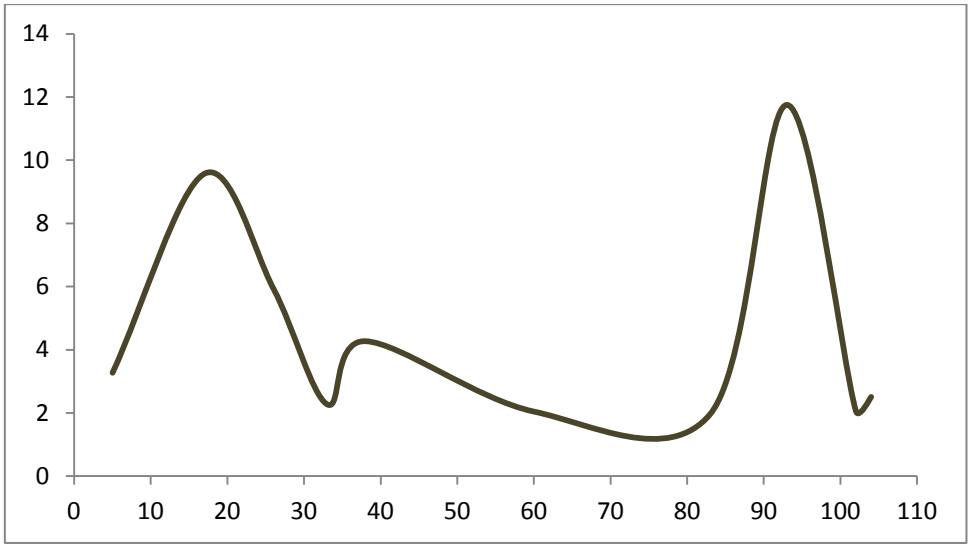

Appendix Figure 5.3: Mulivai LOI Curve (x axis = depth in cm; y = LOI in %)

Appendix Table 5.3.1: Mulivai LOI data calculations obtained using method in Santisteban et al., 2004.

Sub-sample ID	Crucible/Beaker weight (g)	Crucible + wet weight of sub-sample (g)	Crucible + dry weight (g) (105^0C for 12-24 hours)	Crucible + dry (ash) weight (g) (550^0C for 4 hours)	Wet Sample Weight (WS) (g)	Dry Sample Weight (DW_{105}) (g)	Burned Sample Weight (DW_{550}) (g)	Loss on Ignition at 105^0 : $100(WS-DW_{105})/WS$	Loss on Ignition at 550^0 : $100(DW_{105}-DW_{550})/WS$
MU001	15.531	17.887	17.478	17.401	2.356	1.947	1.87	17.3599	3.2683
MU002	15.369	18.388	16.467	16.178	3.019	1.098	0.809	63.6303	9.5727
MU003	15.468	18.47	17.151	16.973	3.002	1.683	1.505	43.9374	5.9294
MU004	14.669	18.989	17.933	17.835	4.32	3.264	3.166	24.4444	2.2685
MU005	14.593	18.904	17.602	17.418	4.311	3.009	2.825	30.2018	4.2682
MU006	17.625	25.029	23.06	22.909	7.404	5.435	5.284	26.5937	2.0394
MU007	15.242	23.956	21.545	21.374	8.714	6.303	6.132	27.6681	1.9624
MU008	15.559	21.226	16.596	15.93	5.667	1.037	0.371	81.7011	11.7522
MU009	15.094	21.012	19.36	19.238	5.918	4.266	4.144	27.9148	2.0615
MU010	15.142	21.172	20.462	20.311	6.03	5.32	5.169	11.7745	2.5041

Appendix 5.4: Manono LOI Data

Appendix Table 5.4: Manono LOI Data

Sub-Sample	Depth (cm)	Loss on Ignition at 550^0 : $100(DW_{105} - DW_{550})/WS$	Sub-Sample	Depth (cm)	Loss on Ignition at 550^0 : $100(DW_{105} - DW_{550})/WS$
MN001	1	29	MN026	126	14
MN002	6	35	MN027	131	14
MN003	11	26	MN028	136	15
MN004	16	21	MN029	141	14
MN005	21	21	MN030	146	15
MN006	26	18	MN031	151	19
MN007	31	19	MN032	156	17
MN008	36	20	MN033	161	18
MN009	41	30	MN034	166	18
MN010	46	30	MN035	171	17
MN011	51	16	MN036	176	18
MN012	56	16	MN037	181	21
MN013	61	22	MN038	186	23
MN014	66	19	MN039	191	23
MN015	71	23	MN040	196	26
MN016	76	19	MN041	201	14
MN017	81	22	MN042	206	14
MN018	86	21	MN043	211	15
MN019	91	21	MN044	216	16
MN020	96	22	MN045	221	15
MN021	101	13	MN046	226	15
MN022	106	13	MN047	231	16
MN023	111	14	MN048	236	16
MN024	116	12	MN049	241	22
MN025	121	14	MN050	246	13

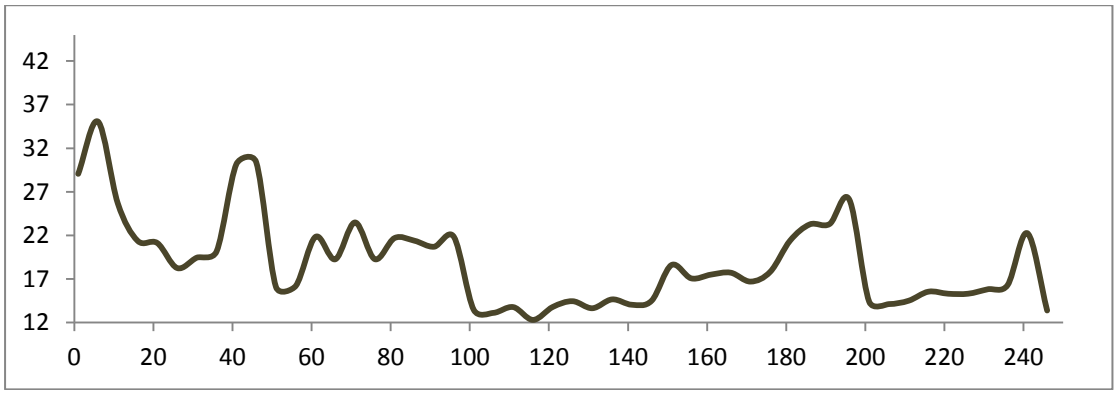

Appendix Figure 5.4: Manono LOI Curve (x axis = depth in cm; y = LOI in %)

Appendix Table 5.4.1: Manono LOI data calculations obtained using method in Santisteban et al. (2004).

Sub-sample ID	Crucible/Beaker weight (g)	Crucible + wet weight of sub-sample (g)	Crucible + dry weight (g) (105^0C for 12-24 hours)	Crucible + dry (ash) weight (g) (550^0C for 4 hours)	Wet Sample Weight (WS) (g)	Dry Sample Weight (DW_{105}) (g)	Burned Sample Weight (DW_{550}) (g)	LOI at 105^0: 100(WS-DW_{105})/WS	Loss on Ignition at 550^0 : 100(DW_{105} - DW_{550})/WS
MN001	11.319	14.182	12.363	11.531	2.863	1.044	0.212	63.5	29.1
MN002	11.908	14.829	13.104	12.08	2.921	1.196	0.172	59.1	35.1
MN003	17.637	20.506	18.474	17.737	2.869	0.837	0.1	70.8	25.7
MN004	15.251	18.074	15.922	15.318	2.823	0.671	0.067	76.2	21.4
MN005	15.151	18.596	15.969	15.241	3.445	0.818	0.09	76.3	21.1
MN006	14.603	18.052	15.298	14.668	3.449	0.695	0.065	79.8	18.3
MN007	11.797	14.562	12.398	11.86	2.765	0.601	0.063	78.3	19.5
MN008	14.679	17.533	15.31	14.734	2.854	0.631	0.055	77.9	20.2
MN009	15.542	18.597	16.564	15.642	3.055	1.022	0.1	66.5	30.2
MN010	15.104	18.541	16.255	15.21	3.437	1.151	0.106	66.5	30.4
MN011	15.478	19.409	16.177	15.544	3.931	0.699	0.066	82.2	16.1
MN012	15.38	19.119	16.043	15.437	3.739	0.663	0.057	82.3	16.2
MN013	11.906	14.337	12.498	11.967	2.431	0.592	0.061	75.6	21.8
MN014	11.318	14.261	11.935	11.368	2.943	0.617	0.05	79.0	19.3
MN015	15.152	18.438	15.969	15.197	3.286	0.817	0.045	75.1	23.5
MN016	14.603	18.021	15.296	14.637	3.418	0.693	0.034	79.7	19.3
MN017	17.637	20.885	18.38	17.675	3.248	0.743	0.038	77.1	21.7
MN018	15.251	17.882	15.853	15.29	2.631	0.602	0.039	77.1	21.4
MN019	11.796	15.215	12.574	11.866	3.419	0.778	0.07	77.2	20.7
MN020	15.477	18.486	16.24	15.583	3.009	0.763	0.106	74.6	21.8
MN021	15.542	18.961	16.068	15.607	3.419	0.526	0.065	84.6	13.5
MN022	15.381	19.761	16.02	15.445	4.38	0.639	0.064	85.4	13.1
MN023	15.104	18.593	15.627	15.146	3.489	0.523	0.042	85.0	13.8
MN024	14.679	17.942	15.108	14.706	3.263	0.429	0.027	86.9	12.3
MN025	11.906	16.288	12.587	11.982	4.382	0.681	0.076	84.5	13.8

MN026	11.317	14.829	11.905	11.397	3.512	0.588	0.08	83.3	14.5
MN027	17.637	21.181	18.181	17.697	3.544	0.544	0.06	84.7	13.7
MN028	14.603	18.74	15.327	14.72	4.137	0.724	0.117	82.5	14.7
MN029	15.153	19.834	15.946	15.288	4.681	0.793	0.135	83.1	14.1
MN030	15.251	19.438	16.001	15.393	4.187	0.75	0.142	82.1	14.5
MN031	11.796	15.472	12.627	11.943	3.676	0.831	0.147	77.4	18.6
MN032	14.678	20.432	15.865	14.882	5.754	1.187	0.204	79.4	17.1
MN033	15.379	21.415	16.653	15.596	6.036	1.274	0.217	78.9	17.5
MN034	15.477	19.966	16.438	15.642	4.489	0.961	0.165	78.6	17.7
MN035	15.104	18.766	15.851	15.239	3.662	0.747	0.135	79.6	16.7
MN036	15.541	20.809	16.679	15.739	5.268	1.138	0.198	78.4	17.8
MN037	11.906	17.044	13.241	12.141	5.138	1.335	0.235	74.0	21.4
MN038	11.313	15.718	12.578	11.553	4.405	1.265	0.24	71.3	23.3
MN039	15.152	19.523	16.465	15.446	4.371	1.313	0.294	70.0	23.3
MN040	17.636	20.745	18.662	17.851	3.109	1.026	0.215	67.0	26.1
MN041	15.25	20.225	16.118	15.401	4.975	0.868	0.151	82.6	14.4
MN042	14.601	20.693	15.635	14.774	6.092	1.034	0.173	83.0	14.1
MN043	11.795	16.182	12.577	11.94	4.387	0.782	0.145	82.2	14.5
MN044	15.106	20.37	16.102	15.283	5.264	0.996	0.177	81.1	15.6
MN045	15.48	19.723	16.263	15.613	4.243	0.783	0.133	81.5	15.3
MN046	15.379	19.987	16.239	15.533	4.608	0.86	0.154	81.3	15.3
MN047	15.542	19.603	16.33	15.687	4.061	0.788	0.145	80.6	15.8
MN048	14.679	19.181	15.596	14.862	4.502	0.917	0.183	79.6	16.3
MN049	17.635	20.079	18.325	17.781	2.444	0.69	0.146	71.8	22.3
MN050	15.152	20.475	16.872	16.159	5.323	1.72	1.007	67.7	13.4

Appendix 5.5: Fagali'i LOI Data.

Appendix Table 5.5: Fagali'i LOI Data

Sub-Sample	Depth (cm)	Loss on Ignition at 550^0 : $100(DW_{105} - DW_{550})/WS$	Sub-Sample	Depth (cm)	Loss on Ignition at 550^0 : $100(DW_{105} - DW_{550})/WS$	Sub-Sample	Depth (cm)	Loss on Ignition at 550^0 : $100(DW_{105} - DW_{550})/WS$
FG001	1	12	FG022	106	13	FG042	206	20
FG002	6	13	FG023	111	11	FG043	211	20
FG003	11	15	FG024	116	11	FG044	216	20
FG004	16	14	FG025	121	12	FG045	221	21
FG005	21	16	FG026	126	12	FG046	226	23
FG006	26	13	FG027	131	11	FG047	231	22
FG007	31	15	FG028	136	10	FG048	236	25
FG008	36	11	FG029	141	9	FG049	241	26
FG009	41	12	FG030	146	9	FG050	246	29
FG010	46	12	FG031	151	12	FG051	251	12
FG011	51	13	FG032	156	11	FG052	256	12
FG012	56	14	FG033	161	11	FG053	261	11
FG013	61	15	FG034	166	12	FG054	266	15
FG014	66	14	FG035	171	14	FG055	271	11
FG015	71	14	FG036	176	14	FG056	276	13
FG016	76	13	FG037	181	14	FG057	281	4
FG017	81	12	FG038	186	13	FG058	286	4
FG018	86	12	FG039	191	12	FG059	291	1
FG019	91	12	FG040	196	14	FG060	296	9
FG020	96	12	FG041	201	20	FG061	299	19
FG021	101	12						

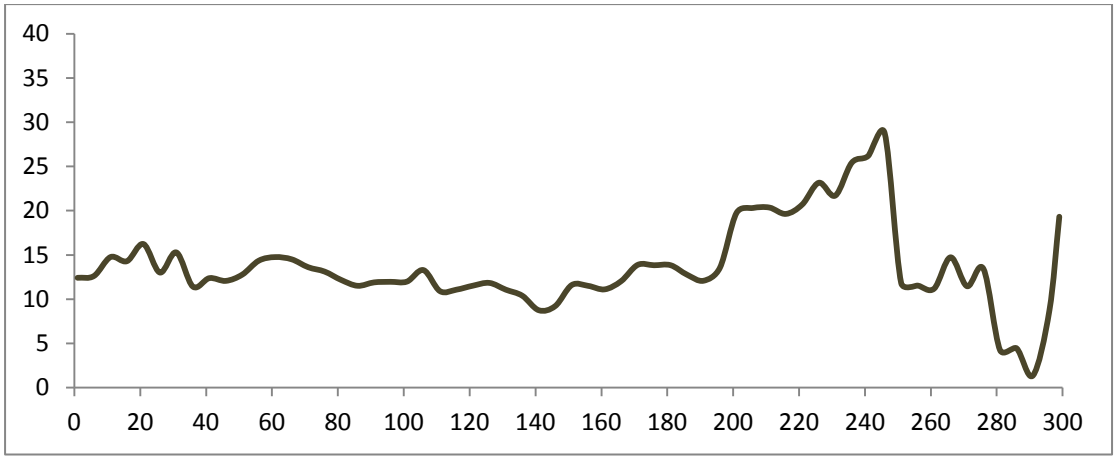

Appendix Figure 5.5: Fagali'i LOI Curve (x axis = depth in cm; y = LOI in %)

Appendix Table 5.5.1: Fagali'i LOI data calculations obtained using method in Santisteban et al. (2004).

Sub-sample ID	Crucible/Beaker weight (g)	Crucible + wet weight of sub-sample (g)	Crucible + dry weight (g) (105^0C for 12-24 hours)	Crucible + dry (ash) weight (g) (550^0C for 4 hours)	Wet Sample Weight (WS) (g)	Dry Sample Weight (DW_{105}) (g)	Burned Sample Weight (DW_{550}) (g)	LOI at 105^0: 100(WS-DW_{105})/WS	LOI at 550^0 : 100(DW_{105} - DW_{550})/WS
FG001	16.332	20.183	17.539	17.061	3.851	1.207	0.729	68.7	12.4
FG002	14.406	18.906	15.824	15.256	4.5	1.418	0.85	68.5	12.6
FG003	17.637	21.711	18.932	18.331	4.074	1.295	0.694	68.2	14.8
FG004	14.916	19.5	15.887	15.232	4.584	0.971	0.316	78.8	14.3
FG005	15.151	18.695	15.857	15.282	3.544	0.706	0.131	80.1	16.2
FG006	14.602	18.186	15.197	14.731	3.584	0.595	0.129	83.4	13.0
FG007	15.541	18.723	16.108	15.622	3.182	0.567	0.081	82.2	15.3
FG008	15.378	18.891	15.934	15.533	3.513	0.556	0.155	84.2	11.4
FG009	13.97	18.843	14.923	14.32	4.873	0.953	0.35	80.4	12.4
FG010	14.842	20.114	16.781	16.145	5.272	1.939	1.303	63.2	12.1
FG011	15.102	20.331	17.824	17.156	5.229	2.722	2.054	47.9	12.8
FG012	15.148	20.286	17.524	16.787	5.138	2.376	1.639	53.8	14.3
FG013	15.476	21.259	18.377	17.524	5.783	2.901	2.048	49.8	14.8
FG014	16.334	22.011	18.831	18.008	5.677	2.497	1.674	56.0	14.5
FG015	15.25	20.688	17.992	17.252	5.438	2.742	2.002	49.6	13.6
FG016	14.406	20.698	17.87	17.045	6.292	3.464	2.639	44.9	13.1
FG017	14.601	21.839	18.674	17.793	7.238	4.073	3.192	43.7	12.2
FG018	14.915	22.58	19.896	19.014	7.665	4.981	4.099	35.0	11.5
FG019	11.793	18.343	16.258	15.479	6.55	4.465	3.686	31.8	11.9
FG020	19.675	26.508	24.271	23.454	6.833	4.596	3.779	32.7	12.0
FG021	17.636	24.336	22.297	21.494	6.7	4.661	3.858	30.4	12.0

FG022	15.149	22.273	20.165	19.219	7.124	5.016	4.07	29.6	13.3
FG023	13.675	21.112	18.872	18.061	7.437	5.197	4.386	30.1	10.9
FG024	15.103	21.769	19.783	19.045	6.666	4.68	3.942	29.8	11.1
FG025	15.076	21.933	19.888	19.098	6.857	4.812	4.022	29.8	11.5
FG026	14.676	20.786	18.997	18.274	6.11	4.321	3.598	29.3	11.8
FG027	11.905	18.112	16.345	15.658	6.207	4.44	3.753	28.5	11.1
FG028	15.378	21.696	19.824	19.168	6.318	4.446	3.79	29.6	10.4
FG029	15.102	20.612	19.106	18.624	5.51	4.004	3.522	27.3	8.7
FG030	15.541	21.137	19.514	18.998	5.596	3.973	3.457	29.0	9.2
FG031	13.97	19.267	17.783	17.169	5.297	3.813	3.199	28.0	11.6
FG032	14.842	20.991	19.223	18.516	6.149	4.381	3.674	28.8	11.5
FG033	15.148	21.551	19.658	18.947	6.403	4.51	3.799	29.6	11.1
FG034	11.309	16.536	14.734	14.105	5.227	3.425	2.796	34.5	12.0
FG035	14.405	20.059	17.953	17.169	5.654	3.548	2.764	37.2	13.9
FG036	15.248	20.093	18.291	17.621	4.845	3.043	2.373	37.2	13.8
FG037	15.475	20.427	18.628	17.943	4.952	3.153	2.468	36.3	13.8
FG038	14.601	19.71	18.088	17.436	5.109	3.487	2.835	31.7	12.8
FG039	14.915	20.189	18.512	17.875	5.274	3.597	2.96	31.8	12.1
FG040	16.333	21.333	19.695	19.017	5	3.362	2.684	32.8	13.6
FG041	19.677	22.805	22.532	21.915	3.128	2.855	2.238	8.7	19.7
FG042	15.476	19.191	18.885	18.131	3.715	3.409	2.655	8.2	20.3
FG043	14.6	18.37	18.074	17.307	3.77	3.474	2.707	7.9	20.3
FG044	14.404	18.103	17.813	17.087	3.699	3.409	2.683	7.8	19.6
FG045	16.333	19.758	19.486	18.777	3.425	3.153	2.444	7.9	20.7
FG046	14.915	18.436	18.146	17.331	3.521	3.231	2.416	8.2	23.1
FG047	15.25	18.781	18.501	17.735	3.531	3.251	2.485	7.9	21.7

FG048	19.676	22.506	22.267	21.548	2.83	2.591	1.872	8.4	25.4
FG049	15.104	18.347	18.075	17.226	3.243	2.971	2.122	8.4	26.2
FG050	14.678	17.98	17.704	16.755	3.302	3.026	2.077	8.4	28.7
FG051	13.676	19.524	16.591	15.9	5.848	2.915	2.224	50.2	11.8
FG052	15.075	20.866	17.969	17.301	5.791	2.894	2.226	50.0	11.5
FG053	17.635	23.696	20.741	20.063	6.061	3.106	2.428	48.8	11.2
FG054	15.15	21.377	17.884	16.967	6.227	2.734	1.817	56.1	14.7
FG055	11.905	18.513	15.203	14.446	6.608	3.298	2.541	50.1	11.5
FG056	15.384	19.331	16.397	15.868	3.947	1.013	0.484	74.3	13.4
FG057	13.971	18.799	15.269	15.064	4.828	1.298	1.093	73.1	4.2
FG058	15.54	21.462	16.893	16.629	5.922	1.353	1.089	77.2	4.5
FG059	15.149	19.736	16.251	16.188	4.587	1.102	1.039	76.0	1.4
FG060	14.843	19.254	15.857	15.472	4.411	1.014	0.629	77.0	8.7
FG061	15.104	19.698	16.238	15.351	4.594	1.134	0.247	75.3	19.3

Appendix 5.6: Ma'asina LOI Data

Appendix Table 5.6: Ma'asina LOI Data

Sub-Sample	Depth (cm)	Loss on Ignition at 550^0 : $100(DW_{105} - DW_{550})/WS$
MS001	2	6
MS002	8	5
MS003	16	3
MS004	29	4
MS005	37	4
MS006	41	4
MS007	45	3
MS008	48	3
MS009	50	3
MS010	53	2
MS011	55	2
MS012	58	3
MS013	62	3
MS014	68	3
MS015	71	2

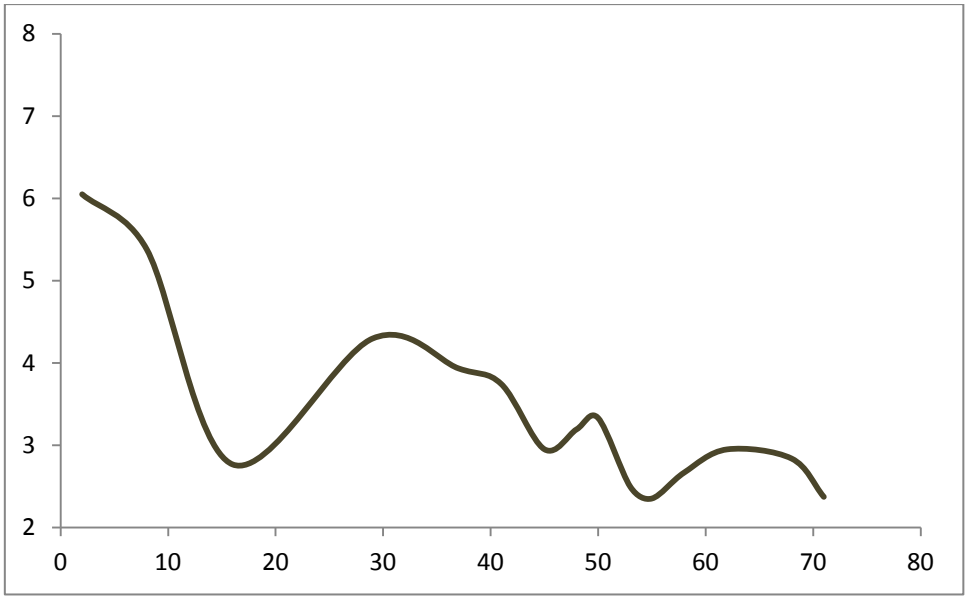

Appendix Figure 5.6: Ma'asina LOI Curve (x axis = depth in cm; y = LOI in %)

Appendix Table 5.6.1: Mulivai LOI data calculations obtained using method in Santisteban et al. (2004).

Sub-sample ID	Crucible/Beaker weight (g)	Crucible + wet weight of sub-sample (g)	Crucible + dry weight (g) (105^0C for 12-24 hours)	Crucible + dry (ash) weight (g) (550^0C for 4 hours)	Wet Sample Weight (WS) (g)	Dry Sample Weight (DW_{105}) (g)	Burned Sample Weight (DW_{550}) (g)	LOI at 105^0: 100(WS-DW_{105})/WS	Loss on Ignition at 550^0 : 100(DW_{105} - DW_{550})/WS
MS001	11.797	16.21	14.95	14.683	4.413	3.153	2.886	28.5520	6.0503
MS002	11.324	15.188	14.179	13.971	3.864	2.855	2.647	26.1128	5.3830
MS003	14.68	22.271	20.915	20.705	7.591	6.235	6.025	17.8633	2.7664
MS004	15.478	19.319	18.435	18.27	3.841	2.957	2.792	23.0148	4.2958
MS005	15.379	20.208	19.127	18.937	4.829	3.748	3.558	22.3856	3.9346
MS006	17.636	22.071	21.21	21.044	4.435	3.574	3.408	19.4138	3.7430
MS007	11.907	16.278	16.001	15.872	4.371	4.094	3.965	6.3372	2.9513
MS008	14.602	18.83	18.541	18.406	4.228	3.939	3.804	6.8354	3.1930
MS009	15.152	20.826	19.573	19.384	5.674	4.421	4.232	22.0832	3.3310
MS010	15.103	20.475	19.628	19.494	5.372	4.525	4.391	15.7669	2.4944
MS011	15.252	19.886	19.24	19.131	4.634	3.988	3.879	13.9404	2.3522
MS012	15.542	20.304	19.596	19.469	4.762	4.054	3.927	14.8677	2.6669
MS013	15.38	21.585	20.778	20.595	6.205	5.398	5.215	13.0056	2.9492
MS014	15.478	20.446	19.815	19.674	4.968	4.337	4.196	12.7013	2.8382
MS015	14.678	21.886	21.104	20.933	7.208	6.426	6.255	10.8491	2.3724

Appendix 5.7: Falealupo LOI Data

Appendix Table 5.7: Falealupo LOI Data

Sub-Sample	Depth (cm)	Loss on Ignition at 550^0 : $100(DW_{105} - DW_{550})/WS$	Sub-Sample	Depth (cm)	Loss on Ignition at 550^0 : $100(DW_{105} - DW_{550})/WS$
FT001	0.5	8	FT019	18.5	9
FT002	1.5	7	FT020	19.5	11
FT003	2.5	4	FT021	21	11
FT004	3.5	3	FT022	23	11
FT005	4.5	3	FT023	25	11
FT006	5.5	3	FT024	27	9
FT007	6.5	3	FT025	29	9
FT008	7.5	3	FT026	31	8
FT009	8.5	7	FT027	33	13
FT010	9.5	6	FT028	35	14
FT011	10.5	4	FT029	37	13
FT012	11.5	3	FT030	39	12
FT013	12.5	4	FT031	41	13
FT014	13.5	4	FT032	43	12
FT015	14.5	5	FT033	45	13
FT016	15.5	9	FT034	47	12
FT017	16.5	12	FT035	49	12
FT018	17.5	12			

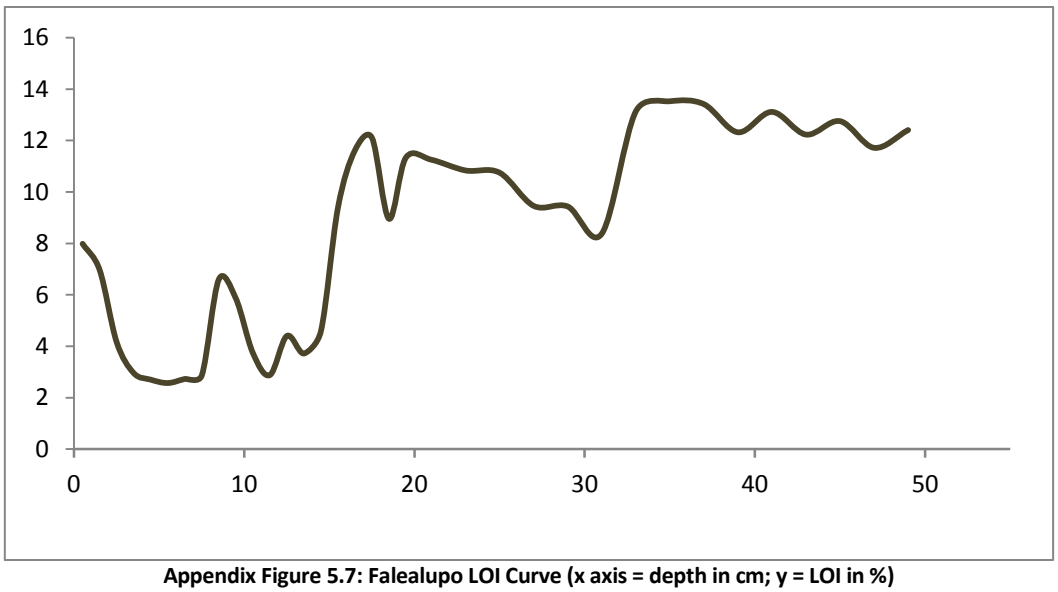

Appendix Figure 5.7: Falealupo LOI Curve (x axis = depth in cm; y = LOI in %)

Appendix Table 5.7.1: Falealupo LOI data calculations obtained using method in Santisteban et al. (2004).

Sub-sample ID	Crucible/Beaker weight (g)	Crucible + wet weight of sub-sample (g)	Crucible + dry weight (g) (105^0C)	Crucible + dry (ash) weight (g) (550^0C for 4 hours)	Wet Sample Weight (WS) (g)	Dry Sample Weight (DW_{105}) (g)	Burned Sample Weight (DW_{550}) (g)	Loss on Ignition at 105^0 : $100(WS-DW_{105})/WS$	Loss on Ignition at 550^0 : $100(DW_{105}-DW_{550})/WS$
FT001	11.847	15.003	13.541	13.289	3.156	1.694	1.442	46.3245	7.9848
FT002	14.669	17.797	16.109	15.891	3.128	1.44	1.222	53.9642	6.9693
FT003	15.369	20.27	18.392	18.188	4.901	3.023	2.819	38.3187	4.1624
FT004	15.468	20.633	19.334	19.181	5.165	3.866	3.713	25.1500	2.9622
FT005	15.531	21.075	19.63	19.48	5.544	4.099	3.949	26.0642	2.7056
FT006	17.625	22.987	22.179	22.041	5.362	4.554	4.416	15.0690	2.5737
FT007	11.92	16.276	15.731	15.612	4.356	3.811	3.692	12.5115	2.7319
FT008	14.592	21.15	19.92	19.732	6.558	5.328	5.14	18.7557	2.8667
FT009	15.094	20.261	17.863	17.522	5.167	2.769	2.428	46.4099	6.5996
FT010	15.558	20.247	18.527	18.252	4.689	2.969	2.694	36.6816	5.8648
FT011	15.241	20.473	18.791	18.595	5.232	3.55	3.354	32.1483	3.7462
FT012	15.142	19.584	18.57	18.442	4.442	3.428	3.3	22.8276	2.8816
FT013	11.839	16.311	14.908	14.711	4.472	3.069	2.872	31.3730	4.4052
FT014	15.532	21.391	19.778	19.56	5.859	4.246	4.028	27.5303	3.7208
FT015	15.468	19.457	18.746	18.563	3.989	3.278	3.095	17.8240	4.5876
FT016	14.669	19.132	16.923	16.504	4.463	2.254	1.835	49.4959	9.3883
FT017	15.37	21.015	17.749	17.093	5.645	2.379	1.723	57.8565	11.6209
FT018	17.625	21.467	19.19	18.725	3.842	1.565	1.1	59.2660	12.1031
FT019	11.92	16.743	14.441	14.009	4.823	2.521	2.089	47.7296	8.9571
FT020	15.241	19.755	17.193	16.681	4.514	1.952	1.44	56.7568	11.3425
FT021	15.558	20.82	17.767	17.175	5.262	2.209	1.617	58.0198	11.2505
FT022	15.142	19.849	17.121	16.611	4.707	1.979	1.469	57.9562	10.8349
FT023	14.593	19.85	16.976	16.411	5.257	2.383	1.818	54.6700	10.7476
FT024	15.094	21.004	18.001	17.442	5.91	2.907	2.348	50.8122	9.4585
FT025	11.832	16.665	14.091	13.635	4.833	2.259	1.803	53.2588	9.4351

FT026	15.532	24.641	20.165	19.402	9.109	4.633	3.87	49.1382	8.3763
FT027	17.625	22.027	18.924	18.346	4.402	1.299	0.721	70.4907	13.1304
FT028	14.668	20.509	16.1	15.31	5.841	1.432	0.642	75.4837	13.5251
FT029	15.467	21.29	16.85	16.069	5.823	1.383	0.602	76.2494	13.4123
FT030	15.37	20.971	16.625	15.935	5.601	1.255	0.565	77.5933	12.3192
FT031	11.92	17.93	13.211	12.423	6.01	1.291	0.503	78.5191	13.1115
FT032	15.092	22.737	16.672	15.737	7.645	1.58	0.645	79.3329	12.2302
FT033	15.142	20.71	16.242	15.532	5.568	1.1	0.39	80.2443	12.7514
FT034	15.559	21.628	16.716	16.005	6.069	1.157	0.446	80.9359	11.7153
FT035	14.593	19.292	15.563	14.98	4.699	0.97	0.387	79.3573	12.4069

Appendix 5.8: Lano LOI Data

Appendix Table 5.8: Lano LOI Data

Sub-Sample	Depth (cm)	Loss on Ignition at 550^0 : $100(DW_{105} - DW_{550})/WS$	Sub-Sample	Depth (cm)	Loss on Ignition at 550^0 : $100(DW_{105} - DW_{550})/WS$
LN001	1	15	LN020	77	4
LN002	5	15	LN021	81	3
LN003	9	15	LN022	85	4
LN004	13	18	LN023	89	4
LN005	17	16	LN024	93	3
LN006	21	15	LN025	97	5
LN007	25	12	LN026	101	3
LN008	29	10	LN027	105	2
LN009	33	9	LN028	109	3
LN010	37	9	LN029	113	4
LN011	41	16	LN030	117	3
LN012	45	17	LN031	121	15
LN013	49	17	LN032	125	11
LN014	53	4	LN033	129	13
LN015	57	5	LN034	133	11
LN016	61	5	LN035	137	12
LN017	65	5	LN036	141	14
LN018	69	5	LN037	145	28
LN019	73	6	LN038	149	69

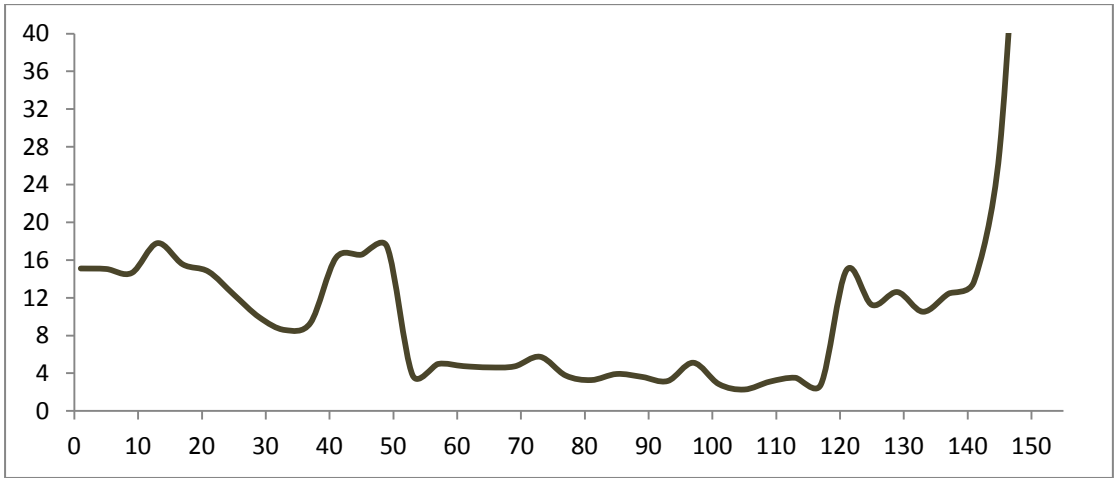

Appendix Figure 5.8: Lano LOI Curve (x axis = depth in cm; y = LOI in %)

Appendix Table 5.8.1: Lano LOI data calculations obtained using method in Santisteban et al. (2004).

Sub-sample ID	Crucible/Beaker weight (g)	Crucible + wet weight of sub-sample (g)	Crucible + dry weight (g) (105^0C for 12-24 hours)	Crucible + dry (ash) weight (g) (550^0C for 4 hours)	Wet Sample Weight (WS) (g)	Dry Sample Weight (DW_{105}) (g)	Burned Sample Weight (DW_{550}) (g)	LOI at 105^0: 100(WS-DW_{105})/WS	Loss on Ignition at 550^0 : 100(DW_{105} - DW_{550})/WS
LN001	15.541	18.658	16.173	15.702	3.117	0.632	0.161	79.7	15.1
LN002	14.679	18.279	15.432	14.89	3.6	0.753	0.211	79.1	15.1
LN003	15.104	19.317	16.175	15.558	4.213	1.071	0.454	74.6	14.6
LN004	17.635	20.692	18.621	18.077	3.057	0.986	0.442	67.7	17.8
LN005	15.152	18.446	16.467	15.955	3.294	1.315	0.803	60.1	15.5
LN006	14.603	17.728	15.864	15.402	3.125	1.261	0.799	59.6	14.8
LN007	14.678	18.96	16.955	16.427	4.282	2.277	1.749	46.8	12.3
LN008	15.103	20.07	18.082	17.589	4.967	2.979	2.486	40.0	9.9
LN009	15.541	20.583	18.776	18.343	5.042	3.235	2.802	35.8	8.6
LN010	15.151	19.069	17.699	17.333	3.918	2.548	2.182	35.0	9.3
LN011	14.602	18.141	16.231	15.656	3.539	1.629	1.054	54.0	16.2
LN012	17.636	20.61	19.239	18.746	2.974	1.603	1.11	46.1	16.6
LN013	15.54	18.622	17.611	17.074	3.082	2.071	1.534	32.8	17.4
LN014	15.104	20.07	18.676	18.487	4.966	3.572	3.383	28.1	3.8
LN015	14.678	20.671	18.487	18.188	5.993	3.809	3.51	36.4	5.0
LN016	14.601	20.276	18.903	18.633	5.675	4.302	4.032	24.2	4.8
LN017	15.152	21.745	20.186	19.881	6.593	5.034	4.729	23.6	4.6
LN018	17.637	24.625	22.764	22.433	6.988	5.127	4.796	26.6	4.7
LN019	15.541	21.226	20.178	19.851	5.685	4.637	4.31	18.4	5.8
LN020	15.104	21.079	20.505	20.28	5.975	5.401	5.176	9.6	3.8
LN021	14.679	21.197	20.663	20.449	6.518	5.984	5.77	8.2	3.3
LN022	17.635	23.868	23.671	23.426	6.233	6.036	5.791	3.2	3.9
LN023	15.152	22.066	21.9	21.65	6.914	6.748	6.498	2.4	3.6
LN024	14.603	20.566	20.431	20.241	5.963	5.828	5.638	2.3	3.2
LN025	15.541	20.677	20.574	20.311	5.136	5.033	4.77	2.0	5.1

LN026	15.104	20.526	19.629	19.474	5.422	4.525	4.37	16.5	2.9
LN027	14.679	21.3	20.376	20.225	6.621	5.697	5.546	14.0	2.3
LN028	17.636	24.408	23.993	23.782	6.772	6.357	6.146	6.1	3.1
LN029	15.151	20.709	20.212	20.016	5.558	5.061	4.865	8.9	3.5
LN030	14.603	20.301	19.851	19.691	5.698	5.248	5.088	7.9	2.8
LN031	15.542	19.295	17.493	16.933	3.753	1.951	1.391	48.0	14.9
LN032	14.678	18.802	16.781	16.317	4.124	2.103	1.639	49.0	11.3
LN033	15.105	19.046	16.774	16.277	3.941	1.669	1.172	57.7	12.6
LN034	14.602	18.232	16.684	16.302	3.63	2.082	1.7	42.6	10.5
LN035	15.153	19.262	18.11	17.599	4.109	2.957	2.446	28.0	12.4
LN036	17.636	20.785	19.868	19.436	3.149	2.232	1.8	29.1	13.7
LN037	15.542	17.388	16.221	15.713	1.846	0.679	0.171	63.2	27.5
LN038	15.105	16.269	16.073	15.273	1.164	0.968	0.168	16.8	68.7

Appendix 5.9: Satupaitea LOI Data

Appendix Table 5.9: Satupaitea LOI Data

Sub-Sample	Depth (cm)	Loss on Ignition at 550^0 : $100(DW_{105} - DW_{550})/WS$	Sub-Sample	Depth (cm)	Loss on Ignition at 550^0 : $100(DW_{105} - DW_{550})/WS$
SP001	1	6	SP018	52	6
SP002	4	7	SP019	55	7
SP003	7	10	SP020	58	7
SP004	10	11	SP021	61	5
SP005	13	10	SP022	64	3
SP006	16	12	SP023	67	3
SP007	19	12	SP024	70	2
SP008	22	13	SP025	73	2
SP009	25	11	SP026	76	2
SP010	28	14	SP027	79	2
SP011	31	14	SP028	82	2
SP012	34	10	SP029	85	3
SP013	37	21	SP030	88	3
SP014	40	7	SP031	91	3
SP015	43	4	SP032	94	3
SP016	46	3	SP033	97	3
SP017	49	5	SP034	100	3

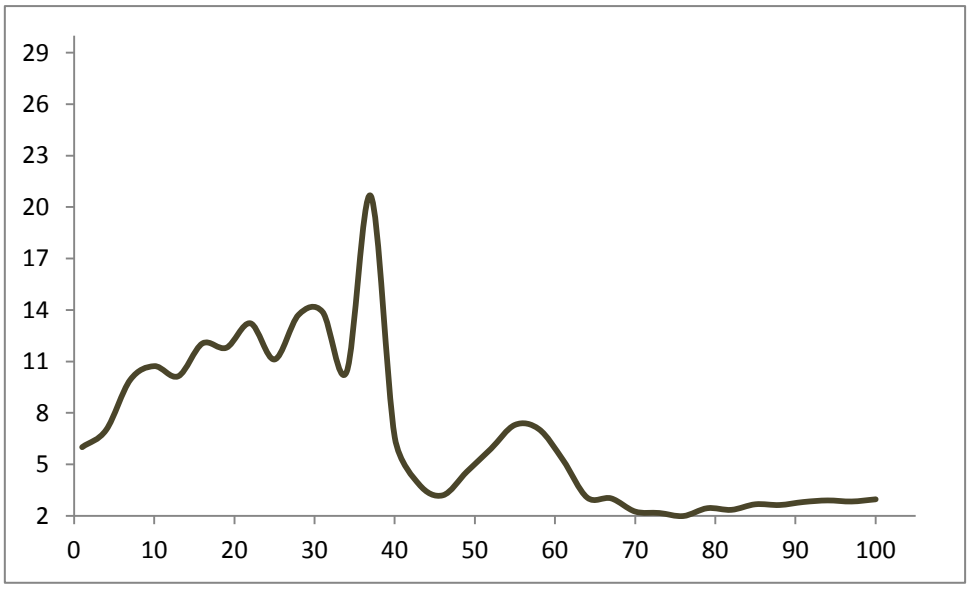

Appendix Figure 5.9: Satupaitea LOI Curve (x axis = depth in cm; y = LOI in %)

Appendix Table 5.9.1: Satupaitea LOI data calculations obtained using method in Santisteban et al. (2004).

Sub-sample ID	Crucible/Beaker weight (g)	Crucible + wet weight of sub-sample (g)	Crucible + dry weight (g) (105^0C f0r 12-24 hours)	Crucible + dry (ash) weight (g) (550^0C for 4 hours)	Wet Sample Weight (WS) (g)	Dry Sample Weight (DW_{105}) (g)	Burned Sample Weight (DW_{550}) (g)	LOI at 105^0: 100(WS-DW_{105})/WS	Loss on Ignition at 550^0 : 100(DW_{105} - DW_{550})/WS
SP001	14.602	18.87	17.395	17.139	4.268	2.793	2.537	34.6	6.0
SP002	17.637	21.832	20.244	19.95	4.195	2.607	2.313	37.9	7.0
SP003	15.152	18.889	16.869	16.498	3.737	1.717	1.346	54.1	9.9
SP004	15.541	18.338	16.847	16.547	2.797	1.306	1.006	53.3	10.7
SP005	14.679	18.102	16.245	15.898	3.423	1.566	1.219	54.3	10.1
SP006	15.477	18.374	16.601	16.252	2.897	1.124	0.775	61.2	12.0
SP007	17.635	21.406	19.216	18.771	3.771	1.581	1.136	58.1	11.8
SP008	15.153	18.768	16.382	15.904	3.615	1.229	0.751	66.0	13.2
SP009	14.603	17.968	15.869	15.495	3.365	1.266	0.892	62.4	11.1
SP010	14.677	17.075	15.716	15.387	2.398	1.039	0.71	56.7	13.7
SP011	15.542	18.027	16.61	16.265	2.485	1.068	0.723	57.0	13.9
SP012	15.476	18.833	16.924	16.575	3.357	1.448	1.099	56.9	10.4
SP013	17.635	19.363	19.029	18.672	1.728	1.394	1.037	19.3	20.7
SP014	15.151	18.938	18.719	18.47	3.787	3.568	3.319	5.8	6.6
SP015	14.602	19.121	18.914	18.74	4.519	4.312	4.138	4.6	3.9
SP016	14.678	18.184	18.048	17.936	3.506	3.37	3.258	3.9	3.2
SP017	15.542	18.955	18.81	18.654	3.413	3.268	3.112	4.2	4.6
SP018	15.476	19.761	18.388	18.135	4.285	2.912	2.659	32.0	5.9
SP019	17.636	21.883	20.577	20.267	4.247	2.941	2.631	30.8	7.3
SP020	15.152	19.268	18.026	17.736	4.116	2.874	2.584	30.2	7.0
SP021	14.602	19.35	18.209	17.96	4.748	3.607	3.358	24.0	5.2
SP022	14.677	19.511	19.163	19.015	4.834	4.486	4.338	7.2	3.1
SP023	15.478	20.887	20.59	20.427	5.409	5.112	4.949	5.5	3.0
SP024	15.542	22.183	21.996	21.847	6.641	6.454	6.305	2.8	2.2

SP025	17.636	23.56	23.412	23.284	5.924	5.776	5.648	2.5	2.2
SP026	14.602	19.442	19.319	19.223	4.84	4.717	4.621	2.5	2.0
SP027	15.15	21.787	21.546	21.384	6.637	6.396	6.234	3.6	2.4
SP028	14.677	19.794	19.625	19.505	5.117	4.948	4.828	3.3	2.3
SP029	15.541	21.31	21.102	20.948	5.769	5.561	5.407	3.6	2.7
SP030	15.477	21.189	20.986	20.836	5.712	5.509	5.359	3.6	2.6
SP031	15.151	21.361	21.207	21.033	6.21	6.056	5.882	2.5	2.8
SP032	14.603	19.717	19.589	19.441	5.114	4.986	4.838	2.5	2.9
SP033	17.636	23.711	23.571	23.399	6.075	5.935	5.763	2.3	2.8
SP034	14.678	19.984	19.834	19.677	5.306	5.156	4.999	2.8	3.0

Appendix 5.10: Ta'u LOI Data

Appendix Table 5.10: Ta'u LOI Data

Sub-Sample	Depth (cm)	Loss on Ignition at 550^0 : $100(DW_{105} - DW_{550})/WS$	Sub-Sample	Depth (cm)	Loss on Ignition at 550^0 : $100(DW_{105} - DW_{550})/WS$
TA001	1	15	TA015	29	8
TA002	3	12	TA016	31	7
TA003	5	12	TA017	33	7
TA004	7	11	TA018	35	6
TA005	9	10	TA019	37	7
TA006	11	9	TA020	39	5
TA007	13	10	TA021	41	4
TA008	15	8	TA022	43	4
TA009	17	7	TA023	45	5
TA010	19	8	TA024	47	6
TA011	21	6	TA025	49	8
TA012	23	7	TA026	51	4
TA013	25	8	TA027	53	3
TA014	27	10	TA028	55	3

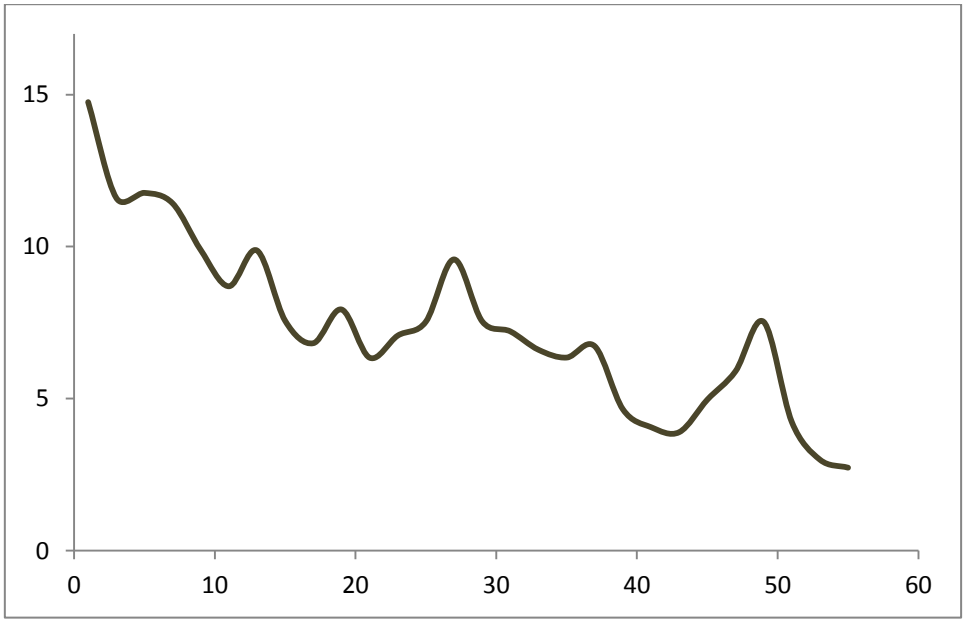

Appendix Figure 5.10: Ta'u LOI Curve (x axis = depth in cm; y = LOI in %)

Appendix Table 5.10.1: Ta'u LOI data calculations obtained using method in Santisteban et al. (2004).

Sub-sample ID	Crucible/Beaker weight (g)	Crucible + wet weight of sub-sample (g)	Crucible + dry weight (g) (105^0C)	Crucible + dry (ash) weight (g) (550^0C for 4 hours)	Wet Sample Weight (WS) (g)	Dry Sample Weight (DW_{105}) (g)	Burned Sample Weight (DW_{550}) (g)	Loss on Ignition at 105^0 : 100(WS-DW_{105})/WS	Loss on Ignition at 550^0 : 100(DW_{105} - DW_{550})/WS
TA001	11.825	15.418	13.324	12.794	3.593	1.499	0.969	58.2800	14.7509
TA002	14.669	18.402	16.24	15.807	3.733	1.571	1.138	57.9159	11.5992
TA003	17.627	23.644	20.382	19.674	6.017	2.755	2.047	54.2131	11.7667
TA004	15.531	19.952	17.307	16.802	4.421	1.776	1.271	59.8281	11.4228
TA005	15.369	21.74	18.095	17.465	6.371	2.726	2.096	57.2124	9.8886
TA006	15.467	21.643	18.251	17.714	6.176	2.784	2.247	54.9223	8.6949
TA007	11.92	17.897	14.303	13.713	5.977	2.383	1.793	60.1305	9.8712
TA008	15.094	20.478	17.511	17.104	5.384	2.417	2.01	55.1077	7.5594
TA009	15.558	21.317	18.551	18.158	5.759	2.993	2.6	48.0292	6.8241
TA010	15.142	22.743	18.231	17.628	7.601	3.089	2.486	59.3606	7.9332
TA011	14.593	22.233	18.198	17.713	7.64	3.605	3.12	52.8141	6.3482
TA012	15.241	21.476	18.057	17.616	6.235	2.816	2.375	54.8356	7.0730
TA013	11.814	16.129	13.824	13.499	4.315	2.01	1.685	53.4183	7.5319
TA014	14.668	18.687	16.885	16.5	4.019	2.217	1.832	44.8370	9.5795
TA015	17.625	21.789	19.64	19.326	4.164	2.015	1.701	51.6090	7.5408
TA016	15.532	20.843	17.688	17.305	5.311	2.156	1.773	59.4050	7.2114
TA017	15.369	19.743	17.399	17.11	4.374	2.03	1.741	53.5894	6.6072
TA018	15.467	20.647	17.957	17.628	5.18	2.49	2.161	51.9305	6.3514
TA019	11.915	18.28	14.792	14.364	6.365	2.877	2.449	54.7997	6.7243
TA020	15.093	24.406	20.697	20.264	9.313	5.604	5.171	39.8260	4.6494
TA021	15.142	21.321	19.278	19.027	6.179	4.136	3.885	33.0636	4.0621
TA022	15.558	21.484	19.233	19.002	5.926	3.675	3.444	37.9852	3.8981
TA023	14.593	21.78	19.327	18.97	7.187	4.734	4.377	34.1311	4.9673
TA024	15.241	22.53	19.047	18.617	7.289	3.806	3.376	47.7843	5.8993
TA025	15.369	16.671	16.612	16.514	1.302	1.243	1.145	4.5315	7.5269

TA026	14.668	19.414	17.931	17.73	4.746	3.263	3.062	31.2474	4.2351
TA027	17.625	21.265	20.532	20.423	3.64	2.907	2.798	20.1374	2.9945
TA028	15.531	19.706	18.938	18.824	4.175	3.407	3.293	18.3952	2.7305

APPENDIX 6: GRAIN SIZE DATA

Overview

Grain size analysis was carried out at the University of Canterbury using the Horiba LA-950 Particle Analyser (laser diffraction), adapting the methods described by Dinis and Castilho (2012).

Mean, median and mode grain size data for each site is provided. Grain size thresh-holds used in this analysis are 0.03 – 2000 microns (0.00003 – 2.0 mm)

Contents

Data CD Contents for Appendix 6

Appendix 6.11: Satitoa grain size distribution data, which is provided as an example in the Data CD of this thesis (Digital Appendix 6.11) of the type of grain size data obtained for each site. Grain size distribution data for all the sites are housed at the University of Canterbury, Geological Sciences Department database.

Appendix 6.1: Satitoa grain size data.

Appendix Table 6.1.1: Satitoa grain size data obtained using methods described by Dinis and Castilho (2012).

Sub-sample	Depth (cm)	Mean			Average	Median			Average	Mode			Average
		ST - .1	ST - .2	ST - .3		ST - .1	ST - .2	ST - .3		ST - .1	ST - .2	ST - .3	
ST001	0-1cm	64.51949	52.88293	52.37865	56.59369	54.26862	44.96532	44.20271	47.812217	71.6556	63.0537	63.0327	65.914
ST002	1-2cm	44.24505	34.01195	30.34719	36.201397	28.64145	13.04555	8.19897	16.628657	55.1426	0.4108	0.3659	18.639767
ST003	2-3cm	56.90842	53.0782	50.01049	53.33237	48.4576	44.10793	40.01365	44.19306	72.1489	71.7597	71.652	71.853533
ST004	3-4cm	101.36991	99.97276	96.71749	99.353387	91.84905	90.44298	88.44653	90.246187	163.6469	163.451	163.0915	163.39647
ST005	4-5cm	93.58796	93.54606	92.95268	93.362233	79.63705	79.73615	79.37746	79.583553	163.1908	163.0928	163.1089	163.13083
ST006	5-6cm	93.13927	94.15604	93.10844	93.467917	77.09398	78.71591	77.86355	77.891147	163.2606	163.2996	163.1982	163.2528
ST007	6-7cm	115.56067	115.46027	114.88371	115.30155	108.16267	108.59116	109.01246	108.58876	164.3468	164.4705	164.4228	164.41337
ST008	7-8cm	105.04718	103.94825	103.98898	104.32814	88.98508	86.98013	86.85986	87.608357	184.3368	184.2683	184.3185	184.30787
ST009	8-9cm	268.11362	264.03177	264.58691	265.57743	225.82278	224.24205	224.43329	224.83271	213.9172	213.9064	213.8657	213.89643
ST010	9-10cm	282.03427	319.19162	313.56424	304.93004	238.5755	234.67725	234.90782	236.05352	215.0001	214.5549	214.6678	214.74093
ST011	10-11cm	507.70288	517.79504	538.09283	521.19692	375.97537	368.32678	365.42868	369.91028	420.3748	419.9674	419.7899	420.04403
ST012	11-12cm	304.15237	254.78555	251.90256	270.28016	235.42648	102.78614	101.42278	146.54513	635.9462	421.5145	368.226	475.2289
ST013	12-13cm	252.49109	242.35849	224.07838	239.64265	63.13629	43.36496	34.73006	47.077103	24.3782	24.3414	24.3112	24.3436
ST014	13-14cm	86.42342	80.86372	79.60232	82.296487	23.59897	23.17233	22.43967	23.070323	27.8039	27.784	27.725	27.770967
ST015	14-15cm	112.21626	92.16072	67.77892	90.718633	26.10695	24.76985	23.21335	24.696717	27.793	27.7466	27.6415	27.727033
ST016	15-16cm	134.383	127.46863	106.87006	122.90723	25.56982	24.61277	21.72367	23.968753	18.6263	18.6225	18.5621	18.603633
ST017	16-17cm	132.02425	116.69273	142.7937	130.50356	23.82364	22.49723	22.73494	23.018603	21.4434	21.4211	21.4001	21.421533
ST018	17-18cm	259.30212	222.96132	235.00262	239.08869	120.91917	32.80491	31.48572	61.7366	640.942	631.2059	639.5075	637.21847
ST019	18-19cm	156.90739	117.64148	131.86044	135.46977	19.35814	17.43504	17.50228	18.098487	18.5206	18.4873	18.4661	18.491333
ST020	19-20cm	236.38849	227.9249	218.04359	227.45233	142.32712	120.16644	98.64307	120.37888	629.9797	629.7753	626.0586	628.60453
ST021	20-22cm	153.50325	172.991	131.49496	152.66307	21.94983	21.13567	19.16549	20.75033	18.6607	18.5994	18.5754	18.611833
ST022	22-24cm	248.40932	257.55316	211.62344	239.19531	31.357	29.39902	24.87804	28.544687	21.4183	21.353	21.2917	21.354333
ST023	24-26cm	265.10776	248.92419	254.60439	256.21211	119.2995	88.78246	81.21513	96.432363	712.1896	640.9334	634.3124	662.47847
ST024	26-28cm	117.39547	103.43117	107.96474	109.59713	12.94452	11.98256	12.0618	12.329627	14.1578	14.129	14.1205	14.135767
ST025	28-30cm	178.37001	168.56651	194.79355	180.57669	20.71039	18.501	19.00972	19.407037	618.5022	620.6929	637.3534	625.51617
ST026	30-32cm	140.05284	128.54752	112.00565	126.86867	21.82667	20.51806	19.64952	20.66475	18.746	18.718	18.7048	18.722933

ST027	32-34cm	226.01355	195.73291	232.52637	218.09094	27.71715	23.06878	25.76193	25.515953	18.6588	18.6102	703.4559	246.9083
ST028	34-36cm	281.24564	288.13068	247.90227	272.4262	27.06511	23.97487	17.57181	22.870597	725.73	731.5545	725.3215	727.53533
ST029	36-38cm	184.67465	193.35431	187.92896	188.65264	20.88788	19.82726	19.15239	19.955843	16.3401	16.3267	16.323	16.329933
ST030	38-40cm	228.47296	264.51788	144.54478	212.51187	18.95327	18.0335	14.17878	17.055183	16.2383	845.5406	16.1352	292.63803
ST031	40-42cm	96.57001	137.20206	131.78571	121.85259	8.66276	8.18904	7.20498	8.0189267	16.0692	645.3514	639.5583	433.65963
ST032	42-44cm	14.2281	24.26879	14.83875	17.778547	11.08829	11.00799	10.34744	10.814573	14.2537	14.2423	14.2159	14.2373
ST033	44-46cm	198.60318	168.558	153.7422	173.63446	18.61919	15.69151	14.81543	16.375377	14.321	14.2228	14.206	14.249933
ST034	46-48cm	35.97062	34.30447	32.1353	34.136797	11.44515	10.8651	10.43599	10.915413	14.1024	14.0708	14.0554	14.0762
ST035	48-50cm	212.94524	212.3627	207.58797	210.9653	23.04576	19.28231	18.79785	20.375307	630.1311	644.4573	647.5647	640.7177
ST036	50-52cm	114.83026	91.48057	101.78927	102.70003	20.08713	19.36782	19.46235	19.6391	21.1625	21.1455	21.1369	21.1483
ST037	52-54cm	136.02223	111.29632	100.04897	115.78917	39.97608	37.34977	34.98917	37.43834	36.5118	36.4823	36.4379	36.477333
ST038	54-56cm	237.52708	232.12346	235.46776	235.03943	131.30367	85.32041	83.05112	99.891733	626.5697	635.7921	710.1379	657.4999
ST039	56-58cm	169.56407	157.80392	149.85248	159.07349	42.61241	39.96842	37.75158	40.110803	36.262	36.1831	32.3942	34.946433
ST040	58-60cm	167.93694	159.05545	134.51923	153.83721	27.81819	25.75669	21.62403	25.066303	626.2741	619.8406	21.3856	422.5001
ST041	60-62cm	23.19369	20.33023	16.8454	20.123107	13.73309	13.08953	12.69247	13.171697	18.6446	18.568	18.5435	18.585367
ST042	62-64cm	219.16481	163.90036	161.37523	181.48013	30.39247	22.09762	20.14978	24.21329	647.0461	624.3318	640.3274	637.2351
ST043	64-66cm	93.25217	44.38385	21.14614	52.927387	13.94852	12.21342	10.84573	12.33589	16.305	16.2845	16.294	16.2945
ST044	66-68cm	216.32446	234.67621	237.15575	229.38547	30.87052	35.05152	28.62514	31.515727	639.641	700.9398	644.1253	661.5687
ST045	68-70cm	255.90533	211.28639	191.47218	219.55463	192.40616	136.69499	101.65312	143.58476	627.8079	550.2269	427.4526	535.16247
ST046	70-72cm	154.45581	143.85327	129.0098	142.43963	18.88881	14.99804	13.6777	15.85485	635.2627	637.9755	0.2131	424.48377
ST047	72-74cm	243.84818	198.4621	194.89146	212.40058	82.05726	21.85096	14.4031	39.437107	625.1678	637.183	637.6103	633.32037
ST048	74-76cm	245.29765	197.72775	193.78789	212.2711	189.0724	94.52296	93.48214	125.6925	623.4928	544.8206	549.8257	572.71303
ST049	76-78cm	144.29514	125.20159	144.10303	137.86659	16.10991	10.47287	9.61707	12.066617	545.7752	539.9009	611.4784	565.71817
ST050	78-80cm	353.58554	340.73709	397.79404	364.03889	310.58041	319.53726	364.47406	331.53058	803.191	733.9558	828.2516	788.46613
ST051	80-82cm	518.39734	579.10162	514.28436	537.26111	534.39636	573.34644	532.08905	546.61062	829.0257	729.9536	827.647	795.5421
ST052	82-84cm	737.71466	586.05585	746.12653	689.96568	698.02979	556.4201	614.11017	622.85335	1099.672	639.5626	640.1766	793.13707
ST053	84-86cm	737.30481	766.16669	666.18048	723.21733	768.36145	698.64233	697.96692	721.6569	956.8333	834.0275	1084.0796	958.31347
ST054	86-88cm	848.80585	994.46948	964.4386	935.90464	849.95331	856.08911	843.58942	849.87728	955.8949	944.4855	947.2796	949.22
ST055	88-90cm	872.69543	887.07605	982.09583	913.95577	868.01697	854.54846	887.83832	870.13458	839.1645	833.6974	1082.2822	918.38137

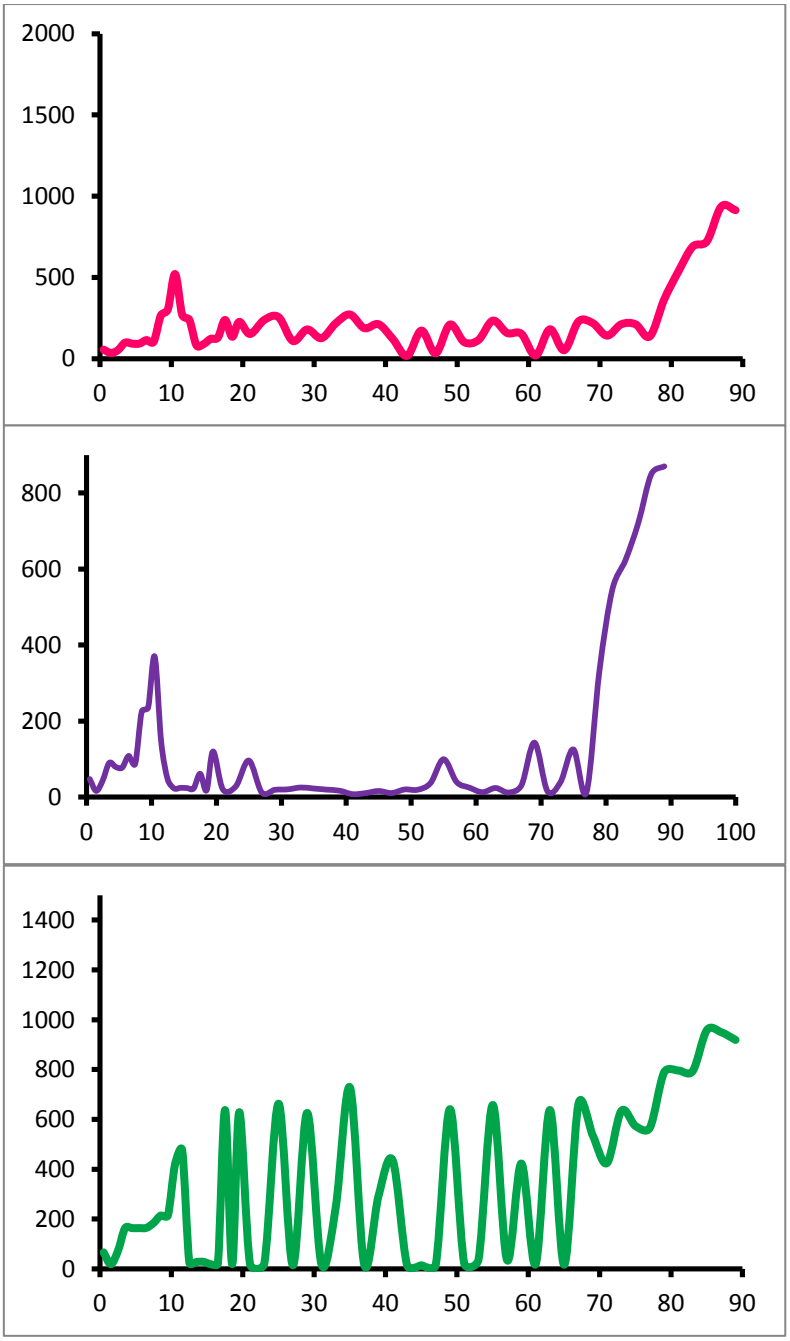

Appendix Figure 6.1: Satitoa grain size curves: a) mean; b) median; c) mode.

Appendix 6.2: Vaovai grain size data.

Appendix Table 6.2.1: vaovai grain size data obtained using methods described by Dinis and Castilho (2012).

Sub-sample	Depth (cm)	Mean			Average	Median			Average	Mode			Average
		VV - .1	VV - .2	VV - .3		VV - .1	VV - .2	VV - .3		VV - .1	VV - .2	VV - .3	
VV001	0.5	327.07806	412.61404	469.17368	402.95526	285.92484	289.61258	279.90097	285.14613	246.3198	246.8834	245.9171	246.37343
VV002	1.5	328.39948	337.35965	329.90335	331.88749	282.76999	285.47574	283.69604	283.98059	245.2198	245.6019	245.6485	245.49007
VV003	2.5	308.11954	302.9006	514.66064	375.22693	260.0929	263.00253	279.14127	267.41223	243.5365	244.0874	244.388	244.00397
VV004	3.5	302.49365	380.9834	300.37299	327.95001	269.92871	275.48175	269.73737	271.71594	245.9371	245.895	246.1453	245.99247
VV005	4.5	324.46021	455.71606	330.61731	370.26453	293.50797	306.77222	294.98642	298.4222	247.2442	247.5893	247.6357	247.48973
VV006	5.5	354.72928	297.2218	295.31625	315.75578	278.52591	269.29568	266.81918	271.54692	245.5995	245.5907	245.5587	245.58297
VV007	6.5	327.95755	323.72736	323.40598	325.0303	279.13788	279.22351	278.38013	278.91384	245.2569	245.4821	245.5056	245.41487
VV008	7.5	320.42746	322.93274	303.12854	315.49625	279.14984	278.77017	269.92896	275.94966	246.0436	246.0181	245.6205	245.89407
VV009	8.5	328.01517	314.93005	411.85733	351.60085	283.53781	277.66428	281.29425	280.83211	246.3392	246.5686	246.4547	246.45417
VV010	9.5	352.71622	352.03491	343.00806	349.25306	302.29123	297.44019	294.81082	298.18075	246.1516	245.8094	245.9918	245.98427
VV011	10.5	349.2471	347.43698	336.83807	344.50738	277.60312	273.78314	270.37643	273.9209	243.6404	243.7352	243.6929	243.6895
VV012	11.5	421.55368	408.99014	425.78955	418.77779	355.44568	344.8862	347.98532	349.43907	246.9816	247.1581	247.2	247.11323
VV013	12.5	393.37988	413.25055	405.3678	403.99941	355.87341	356.05521	355.59412	355.84091	629.4839	419.8435	421.8663	490.3979
VV014	13.5	363.96436	368.28568	356.23676	362.82893	296.78799	294.52567	286.78436	292.69934	244.7139	244.3725	244.312	244.46613
VV015	14.5	332.63675	336.6532	341.3381	336.87602	279.93814	281.19241	283.69778	281.60944	244.533	244.7551	244.1887	244.49227
VV016	15.5	358.08069	318.88593	306.53766	327.83476	296.32648	277.38312	270.54041	281.41667	245.0208	244.9614	244.9445	244.97557
VV017	16.5	365.54883	365.63776	337.77969	356.32209	296.07074	293.33749	284.98563	291.46462	245.3287	245.3574	245.556	245.41403
VV018	17.5	318.13727	314.50473	276.89404	303.17868	279.70486	276.77393	259.86221	272.11367	246.0629	246.3394	245.6647	246.02233
VV019	18.5	341.26978	323.83887	309.98221	325.03029	285.85519	276.23932	274.01581	278.70344	245.4937	245.4211	245.369	245.42793
VV020	19.5	307.22003	301.34286	302.82477	303.79589	271.08154	270.24335	269.1759	270.16693	244.3255	244.522	244.7321	244.52653
VV021	20.5	405.90613	428.84439	390.82809	408.5262	325.25067	319.40173	317.25092	320.63444	245.5832	245.6346	245.4708	245.56287

VV022	21.5	420.65866	367.76791	435.93015	408.11891	322.93491	318.21283	327.86679	323.00484	247.4727	279.8113	279.7206	269.00153
VV023	22.5	433.0206	416.30853	419.06729	422.79881	377.46429	370.40167	369.89081	372.58559	420.8587	420.9319	628.1058	489.96547
VV024	23.5	436.76776	434.41153	473.53513	448.23814	396.36557	394.00403	367.7717	386.0471	422.6907	629.0405	421.8644	491.19853
VV025	24.5	330.37897	326.84454	379.07364	345.43238	278.51828	278.43823	279.16812	278.70821	244.3015	244.4868	244.5325	244.44027
VV026	25.5	346.43845	337.32584	346.26785	343.34405	289.09122	289.8587	289.21939	289.38977	244.3644	244.871	244.5257	244.58703
VV027	26.5	353.00473	354.65158	336.26462	347.97364	309.20935	308.9227	296.89603	305.00936	245.9954	246.1127	245.8641	245.99073
VV028	27.5	331.97269	324.46848	311.86835	322.76984	276.63358	272.14474	266.94724	271.90852	243.8128	244.0999	243.9268	243.9465
VV029	28.5	365.46271	358.80692	352.73801	359.00255	310.02298	308.5997	306.6622	308.42829	246.8608	247.1019	246.878	246.9469
VV030	29.5	330.97058	440.61679	474.12723	415.2382	278.27411	282.68866	280.06342	280.34206	245.4193	245.3108	244.4468	245.05897
VV031	30.5	336.28076	328.6904	376.46368	347.14495	278.09219	275.44455	273.69861	275.74512	245.0272	244.8994	244.835	244.92053
VV032	31.5	305.21289	292.33643	277.51489	291.68807	261.04929	254.57634	248.1288	254.58481	244.3361	244.1252	243.9386	244.1333
VV033	32.5	355.90497	293.62347	276.86407	308.7975	261.62668	252.40671	246.2229	253.41876	243.4871	243.599	243.3036	243.46323
VV034	33.5	375.39072	356.60852	368.06635	366.68853	327.03128	318.74576	319.96429	321.91378	247.7101	247.7711	279.8926	258.45793
VV035	34.5	487.83917	482.09152	331.21332	433.71467	311.86957	298.11072	278.65662	296.2123	245.9931	246.0266	246.2312	246.08363
VV036	35.5	409.49585	375.62354	298.4722	361.1972	280.62885	275.56345	261.51611	272.56947	244.6869	244.6251	244.5243	244.6121
VV037	36.5	419.82031	369.61523	339.71194	376.38249	315.04581	308.42484	298.07785	307.18283	247.2083	247.0112	246.8489	247.0228
VV038	37.5	339.68045	346.71265	319.2645	335.2192	283.64575	281.02383	271.68005	278.78321	245.8119	245.6015	245.2161	245.54317
VV039	38.5	353.88248	304.30206	304.39499	320.85984	266.97229	262.51682	262.0809	263.85667	244.4766	244.6894	244.4495	244.5385
VV040	39.5	326.80347	307.52899	303.67184	312.6681	284.50818	277.41327	275.37341	279.09829	246.7313	246.6332	246.6071	246.6572
VV041	40.5	326.82428	326.82788	307.97498	320.54238	283.55417	280.29199	271.55029	278.46548	246.3904	246.0346	246.1501	246.1917
VV042	41.5	326.19046	404.99301	392.80054	374.66134	271.68723	275.24075	268.40649	271.77816	244.7906	244.8308	244.9856	244.869
VV043	42.5	286.67673	282.55771	272.80319	280.67921	255.52521	253.43912	250.82977	253.2647	244.26	244.4243	244.64	244.44143
VV044	43.5	308.79865	292.71091	297.61569	299.70842	266.87256	258.97659	258.26111	261.37009	244.7795	244.5735	244.5501	244.63437
VV045	44.5	310.80518	294.33542	293.8317	299.65743	272.12018	265.39334	265.29602	267.60318	245.994	245.4822	245.523	245.6664
VV046	45.5	393.58679	381.53494	369.29901	381.47358	327.70535	320.21933	315.08304	321.00257	247.5887	279.4741	247.4111	258.15797
VV047	46.5	277.27301	333.80975	274.56284	295.2152	250.11565	251.59279	247.32768	249.67871	244.0557	243.9239	243.8583	243.94597

VV048	47.5	294.28931	291.33282	276.3472	287.32311	260.36472	257.8855	254.03305	257.42776	245.0671	244.9965	244.9701	245.01123
VV049	48.5	313.33939	314.77274	301.05612	309.72275	278.09677	278.80402	272.40839	276.43639	246.9194	247.1581	246.6287	246.90207
VV050	49.5	280.20615	282.32016	280.89923	281.14185	257.58923	258.45349	257.48169	257.84147	245.6735	245.8236	245.9229	245.80667
VV051	50.5	290.70956	415.83737	390.09488	365.54727	260.77402	266.53394	264.62109	263.97635	245.1027	245.0374	245.3351	245.1584
VV052	51.5	275.31747	271.81244	266.95801	271.36264	252.86829	251.95309	251.22433	252.01524	244.902	244.9662	244.8623	244.91017
VV053	52.5	282.0658	273.94263	276.79358	277.60067	253.86349	251.59146	251.10835	252.18777	244.5345	244.658	244.528	244.5735
VV054	53.5	337.82861	327.32074	327.5585	330.90262	284.15005	280.45871	280.92996	281.84624	245.9757	245.8615	246.0138	245.95033
VV055	54.5	298.84723	384.21133	280.10806	321.05554	259.58405	259.19382	251.84103	256.87297	244.8669	244.6268	244.5703	244.688
VV056	55.5	277.99634	310.04034	343.51544	310.51737	253.08192	250.9346	251.66429	251.8936	244.5795	244.2465	244.2042	244.3434
VV057	56.5	302.88959	302.85873	289.15634	298.30155	265.1709	262.30554	257.16306	261.5465	245.1198	244.8534	244.6223	244.86517
VV058	57.5	291.58051	277.35034	268.74725	279.22603	251.63527	246.8407	243.00926	247.16174	243.5745	243.5111	243.3547	243.4801
VV059	58.5	321.98999	311.22141	304.27252	312.49464	272.40353	268.79239	264.87549	268.69047	245.3065	244.9983	244.8015	245.03543
VV060	59.5	342.85406	350.42255	329.17557	340.81739	294.36035	291.03326	285.56686	290.32016	246.4346	246.4326	246.1686	246.34527
VV061	60.5	299.70212	300.5358	297.1825	299.14014	259.44025	258.29095	254.62575	257.45232	243.8805	243.8316	243.5443	243.75213
VV062	61.5	335.66571	368.94724	316.46024	340.35773	273.28363	269.82455	265.15988	269.42269	244.0923	244.073	243.6945	243.95327
VV063	62.5	307.65417	301.26981	303.5257	304.14989	265.64868	261.86829	263.09146	263.53614	245.0838	244.982	244.9646	245.01013
VV064	63.5	300.16138	299.32095	300.10757	299.8633	258.11591	258.23798	257.69928	258.01772	244.4954	244.5717	244.3875	244.48487
VV065	64.5	322.87833	307.88855	299.09818	309.95502	268.40945	262.2489	259.81363	263.49066	244.5456	244.2751	244.3497	244.39013
VV066	65.5	315.37106	301.19879	313.41336	309.9944	263.42111	257.84494	260.84015	260.70207	243.9011	243.8447	243.9079	243.88457
VV067	66.5	365.37524	368.84332	359.45432	364.55763	311.06561	308.56677	305.62143	308.41794	246.8211	246.9704	246.6578	246.81643
VV068	67.5	315.93661	308.62146	309.60486	311.38764	268.51965	265.5592	265.02176	266.36687	244.721	244.6866	244.6379	244.68183
VV069	68.5	332.96207	323.09161	378.76361	344.9391	287.60941	281.73679	283.27026	284.20549	246.582	246.1851	246.0942	246.2871
VV070	69.5	278.2066	272.41992	265.44409	272.02354	248.13779	245.87358	243.96501	245.99213	243.6638	243.6118	243.4274	243.56767
VV071	70.5	288.35202	280.76401	275.11691	281.41098	253.34381	251.15569	249.80437	251.43462	243.8577	244.0119	243.8278	243.89913
VV072	71.5	340.03256	339.75259	338.1084	339.29785	282.83047	282.06805	279.60809	281.5022	245.5252	245.6181	245.2814	245.4749

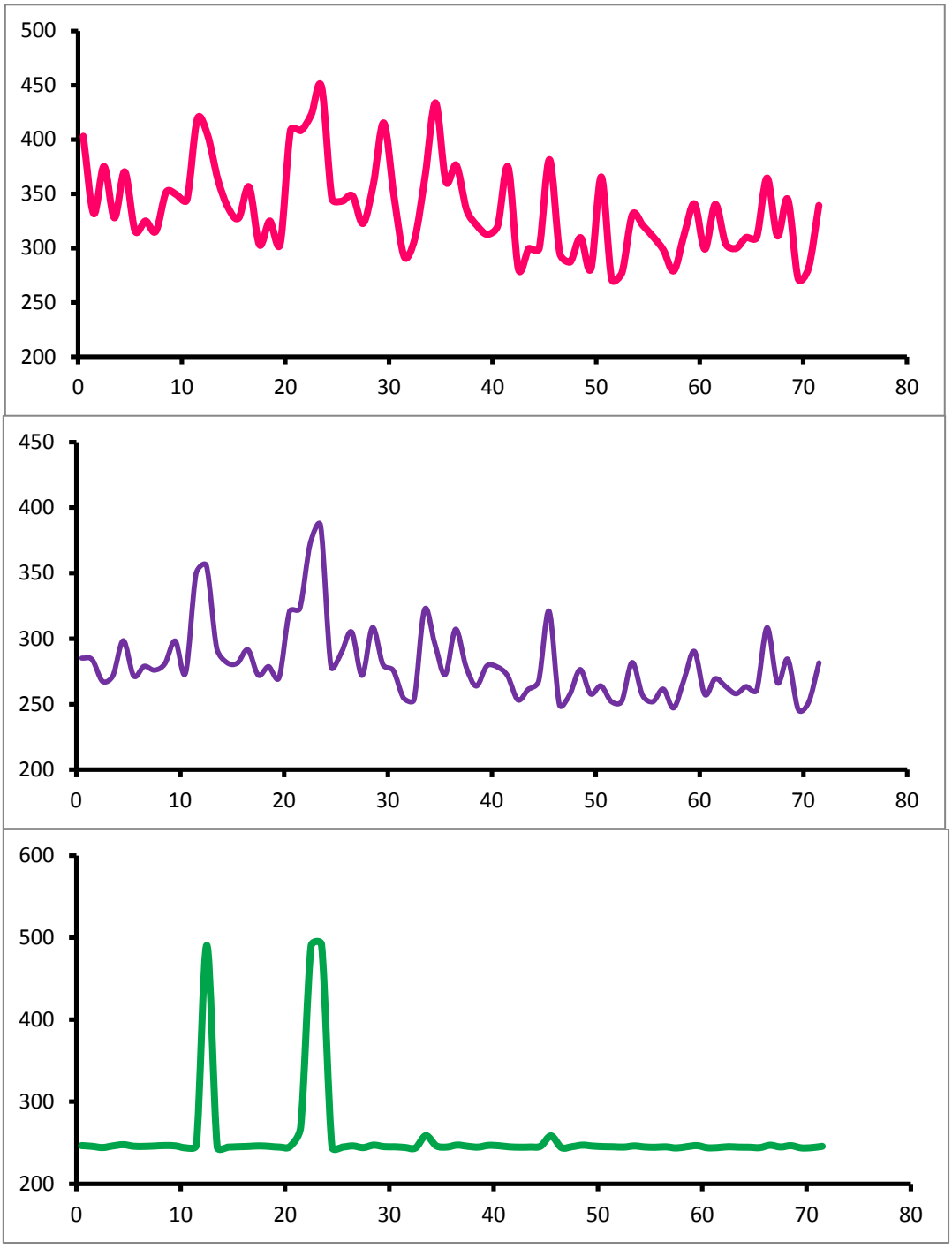

Appendix Figure 6.2: Vaovai grain size curves: a) mean; b) median; c) mode.

Appendix 6.3: Mulivai grain size data.

Appendix Table 6.3.1: Mulivai grain size data obtained using methods described by Dinis and Castilho (2012).

Sub-sample	Depth (cm)	Mean			Average	Median			Average	Mode			Average
		UPS - .1	UPS - .2	UPS - .3		UPS - .1	UPS - .2	UPS - .3		UPS - .1	UPS - .2	UPS - .3	
UPS01	5	558.8	539.6	498.5	532.3	521.6	509.1	469.4	500.0	726.4	724.8	725.4	725.5
UPS02	17	395.0	331.2	327.9	351.4	312.0	259.6	255.6	275.8	244.0	243.3	243.2	243.5
UPS03	26	455.9	588.8	394.8	479.8	389.9	367.6	332.8	363.4	635.2	2774.7	638.1	1349.3
UPS04	33	836.8	811.6	988.4	878.9	317.8	297.1	368.8	327.9	2742.7	2779.6	2751.1	2757.8
UPS05	38	443.8	423.8	578.2	482.0	356.9	317.1	348.1	340.7	244.2	243.5	243.8	243.8
UPS06	60	213.0	192.8	232.8	212.9	146.5	147.2	169.9	154.5	215.2	213.0	214.8	214.3
UPS07	83	368.0	331.3	346.7	348.7	318.1	291.9	315.5	308.5	631.3	426.1	427.7	495.0
UPS08	93	278.1	299.1	279.6	285.6	245.2	262.2	253.5	253.6	243.7	244.1	243.9	243.9
UPS09	102	527.9	507.7	542.2	525.9	380.5	317.9	332.0	343.5	245.0	243.3	243.3	243.8
UPS10	104	571.5	539.2	551.4	554.0	554.6	525.4	540.0	540.0	828.1	824.8	832.1	828.3

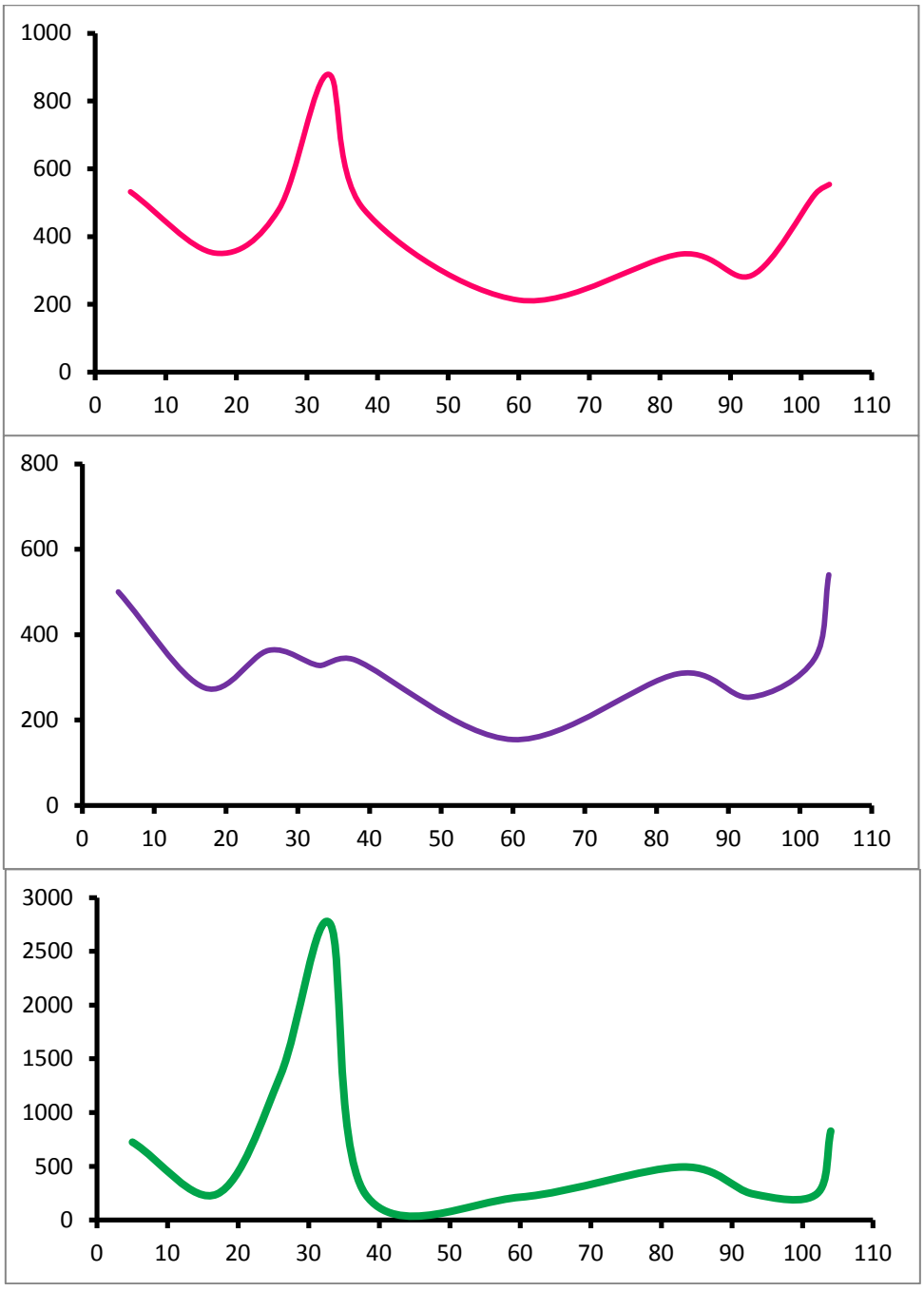

Appendix Figure 6.3: Mulivai grain size curves: a) mean; b) median; c) mode.

Appendix 6.4: Manono grain size data.

Appendix Table 6.4.1: Manono grain size data obtained using methods described by Dinis and Castilho (2012).

Sub-sample	Depth (cm)	Mean			Average	Median			Average	Mode			Average
		MN - .1	MN - .2	MN - .3		MN - .1	MN - .2	MN - .3		MN - .1	MN - .2	MN - .3	
MN001	1	76.4	75.4	74.8	75.5	61.7	68.3	69.6	66.5	142.0	94.6	94.8	110.5
MN002	6	62.5	67.9	67.8	66.1	41.7	50.3	51.4	47.8	83.0	94.2	94.2	90.5
MN003	11	83.3	81.5	77.9	80.9	71.3	76.9	75.2	74.5	143.2	142.0	141.8	142.3
MN004	16	99.3	96.8	94.2	96.8	93.7	94.5	93.1	93.8	109.9	109.1	108.9	109.3
MN005	21	85.4	88.1	89.7	87.7	75.6	82.8	84.6	81.0	142.3	95.1	95.0	110.8
MN006	26	127.1	125.4	123.3	125.3	115.0	110.0	108.8	111.3	184.9	108.9	108.9	134.2
MN007	31	116.4	115.4	114.0	115.3	103.7	104.6	104.4	104.2	185.1	109.3	109.2	134.5
MN008	36	66.5	68.8	71.5	69.0	48.3	57.3	61.4	55.7	83.1	94.4	94.6	90.7
MN009	41	35.8	33.2	38.9	36.0	24.8	23.4	24.3	24.2	55.1	55.0	48.1	52.7
MN010	46	83.5	87.5	87.7	86.2	72.2	83.6	84.8	80.2	142.0	108.4	108.7	119.7
MN011	51	91.3	93.6	92.8	92.6	79.1	84.8	86.1	83.4	94.9	108.8	109.0	104.2
MN012	56	109.7	107.1	103.4	106.8	97.6	96.1	94.3	96.0	109.3	108.9	108.6	108.9
MN013	61	103.5	101.7	102.5	102.6	91.2	93.4	94.8	93.1	109.4	109.3	109.1	109.3
MN014	66	68.2	64.8	62.1	65.0	46.0	47.8	47.5	47.1	63.2	72.4	72.3	69.3
MN015	71	77.7	81.3	81.5	80.2	65.3	70.2	70.6	68.7	82.6	82.6	82.8	82.7
MN016	76	97.0	94.1	96.8	96.0	80.2	78.2	79.1	79.1	83.0	82.9	82.8	82.9
MN017	81	59.2	56.7	54.9	56.9	47.1	47.3	48.0	47.5	82.5	82.4	82.8	82.6
MN018	86	112.2	105.3	103.3	106.9	99.4	93.7	92.1	95.1	108.8	107.8	83.5	100.0
MN019	91	102.9	100.0	98.1	100.3	93.3	91.6	91.3	92.1	108.4	108.0	107.9	108.1
MN020	96	100.4	104.9	105.8	103.7	96.0	102.5	103.9	100.8	109.5	109.4	109.4	109.4
MN021	101	115.3	114.4	114.0	114.6	108.7	109.5	109.7	109.3	162.9	109.7	109.6	127.4

MN022	106	85.0	87.6	87.3	86.6	76.8	82.7	83.2	80.9	94.7	95.1	95.4	95.1
MN023	111	80.0	82.3	82.4	81.6	62.8	72.7	74.1	69.8	124.1	108.3	108.9	113.7
MN024	116	111.3	107.5	103.5	107.4	100.2	99.8	97.3	99.1	162.4	142.3	109.1	137.9
MN025	121	124.2	122.3	121.3	122.6	114.8	113.2	113.3	113.7	163.2	162.2	109.6	145.0
MN026	126	92.4	91.0	90.6	91.3	79.0	81.5	82.2	80.9	142.6	108.9	108.8	120.1
MN027	131	198.8	130.0	128.5	152.4	131.4	113.7	112.5	119.2	164.4	163.5	163.1	163.7
MN028	136	87.3	88.7	88.8	88.3	70.3	76.8	78.0	75.1	82.9	94.8	94.7	90.8
MN029	141	93.1	91.9	91.1	92.0	79.1	80.7	80.1	80.0	83.0	83.2	83.2	83.1
MN030	146	102.4	102.1	102.2	102.2	92.0	94.1	94.7	93.6	109.7	109.4	109.5	109.5
MN031	151	90.9	92.1	91.7	91.5	76.1	80.0	80.0	78.7	142.8	95.0	95.0	110.9
MN032	156	95.9	97.6	96.8	96.8	80.9	84.4	84.5	83.3	162.6	108.9	108.8	126.8
MN033	161	101.5	100.8	99.3	100.5	90.5	90.7	89.4	90.2	163.1	162.5	162.3	162.6
MN034	166	87.7	89.9	91.3	89.7	76.4	81.3	83.1	80.3	94.7	94.7	108.4	99.3
MN035	171	103.3	102.6	103.3	103.1	94.2	95.8	96.8	95.6	161.8	109.5	109.5	126.9
MN036	176	93.6	93.7	94.5	93.9	81.7	85.0	86.1	84.2	94.6	108.7	108.7	104.0
MN037	181	97.4	94.9	96.6	96.3	86.6	90.1	91.5	89.4	109.0	109.2	109.0	109.1
MN038	186	91.7	93.4	93.7	92.9	79.5	85.8	86.9	84.1	94.7	108.6	108.7	104.0
MN039	191	99.5	99.8	99.8	99.7	90.4	92.8	93.5	92.2	109.2	108.8	108.7	108.9
MN040	196	50.7	51.5	52.5	51.6	32.9	34.3	35.4	34.2	82.5	82.7	82.8	82.7
MN041	201	79.2	81.3	82.2	80.9	74.4	77.4	78.2	76.7	94.2	83.5	83.5	87.1
MN042	206	71.5	73.5	72.6	72.5	63.8	65.7	66.1	65.2	82.8	82.7	82.9	82.8
MN043	211	81.5	78.8	78.6	79.6	69.5	69.6	69.8	69.7	82.7	82.9	82.9	82.9
MN044	216	66.7	70.9	71.8	69.8	52.7	62.1	64.2	59.7	82.4	83.2	83.2	83.0
MN045	221	51.6	55.1	54.3	53.7	36.8	41.0	42.1	40.0	72.2	82.7	82.7	79.2
MN046	226	66.2	62.1	60.6	63.0	45.1	44.2	44.4	44.5	63.2	72.0	72.1	69.1
MN047	231	76.0	75.1	73.5	74.9	67.7	68.0	67.4	67.7	82.3	82.4	82.3	82.3

MN048	236	62.9	62.8	59.8	61.8	48.2	50.7	50.0	49.6	72.1	72.4	72.4	72.3
MN049	241	71.1	71.4	71.5	71.3	60.4	63.4	63.9	62.6	72.2	72.7	72.8	72.6
MN050	246	40.5	40.4	41.4	40.8	29.4	29.0	28.9	29.1	48.2	48.2	48.2	48.2

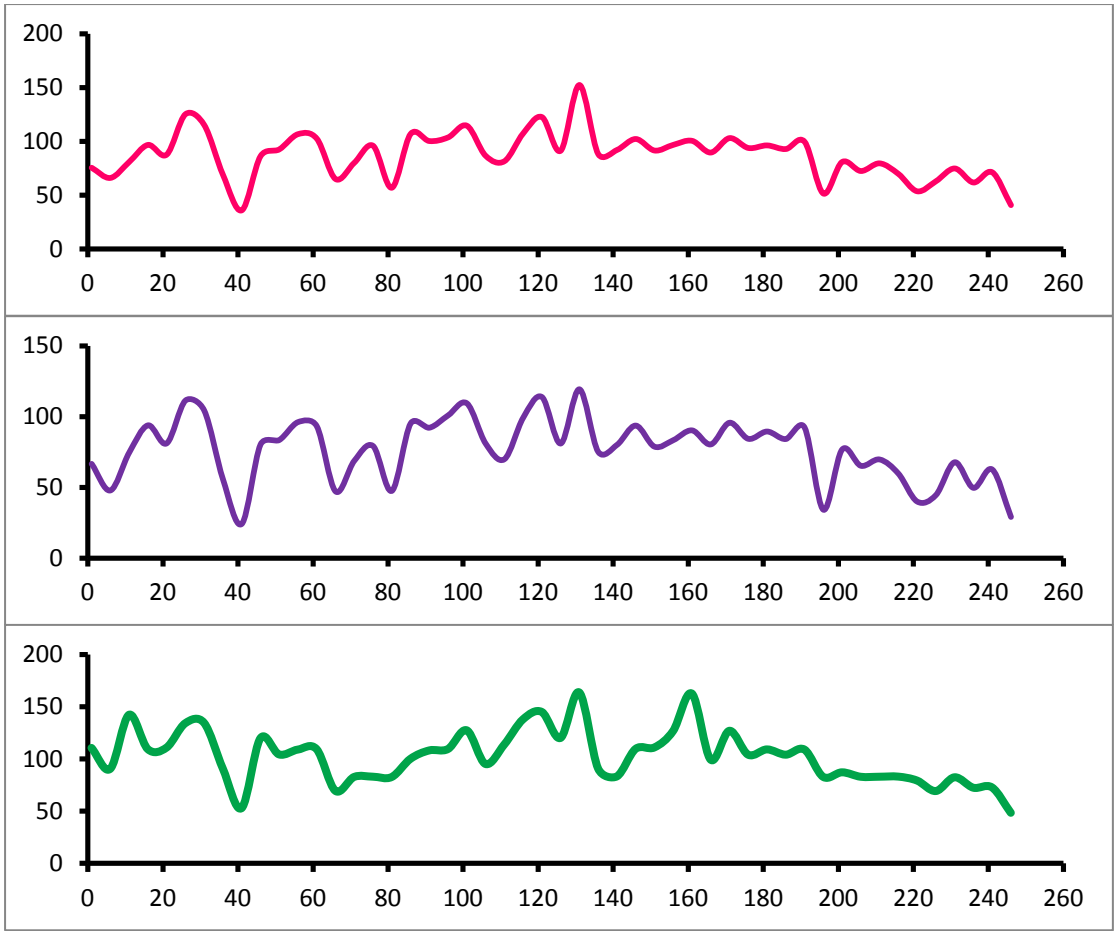

Appendix Figure 6.4: Manono grain size curves: a) mean; b) median; c) mode.

Appendix 6.5: Fagali'i grain size data.

Appendix Table 6.5.1: Fagali'i grain size data obtained using methods described by Dinis and Castilho (2012).

Sub-sample	Depth (cm)	Mean			Average	Median			Average	Mode			Average
		FG - .1	FG - .2	FG - .3		FG - .1	FG - .2	FG - .3		FG - .1	FG - .2	FG - .3	
FG001	1	9.5	6.2	6.3	7.3	3.8	2.8	2.8	3.1	16.2	14.2	16.1	15.5
FG002	6	8.4	7.2	6.3	7.3	2.3	2.2	2.1	2.2	0.3	0.3	0.3	0.3
FG003	11	7.2	8.4	7.0	7.6	2.3	2.2	2.0	2.2	0.3	0.3	0.3	0.3
FG004	16	7.5	6.8	6.6	7.0	2.1	2.0	2.0	2.0	0.3	0.3	0.3	0.3
FG005	21	16.1	15.3	12.8	14.7	4.2	3.9	3.6	3.9	0.2	0.2	0.2	0.2
FG006	26	21.6	16.4	12.4	16.8	9.0	7.6	6.6	7.7	10.8	9.5	9.4	9.9
FG007	31	11.5	10.1	9.1	10.2	4.8	4.4	4.2	4.5	3.2	3.2	3.2	3.2
FG008	36	7.7	5.8	5.3	6.3	1.9	1.8	1.8	1.9	0.2	0.2	0.2	0.2
FG009	41	11.4	7.8	6.3	8.5	1.7	1.5	1.4	1.5	0.2	0.2	0.2	0.2
FG010	46	11.7	11.2	9.1	10.7	2.7	2.6	2.5	2.6	0.2	0.2	0.2	0.2
FG011	51	13.9	13.3	12.3	13.2	8.2	7.6	7.0	7.6	18.6	18.6	18.6	18.6
FG012	56	14.4	13.5	12.4	13.4	7.6	6.9	6.4	7.0	16.2	16.2	16.3	16.2
FG013	61	27.5	30.6	40.9	33.0	16.1	15.7	15.8	15.9	21.3	21.2	21.2	21.2
FG014	66	27.5	22.2	23.7	24.5	14.4	13.6	13.5	13.8	18.5	18.6	18.5	18.5
FG015	71	15.7	16.3	15.3	15.8	10.1	9.7	9.3	9.7	16.3	16.3	16.3	16.3
FG016	76	18.5	15.7	17.0	17.1	11.3	10.5	10.5	10.7	18.5	18.5	18.5	18.5
FG017	81	34.8	32.8	29.6	32.4	15.2	14.2	13.3	14.2	18.6	18.6	18.6	18.6
FG018	86	22.0	19.8	18.4	20.1	9.6	8.3	7.5	8.5	21.3	21.3	21.3	21.3
FG019	91	35.3	66.4	27.4	43.0	14.2	16.2	10.5	13.6	0.3	0.3	0.3	0.3
FG020	96	92.9	103.6	95.0	97.2	55.8	56.9	51.9	54.9	188.3	187.9	187.9	188.0
FG021	101	30.6	26.5	24.6	27.2	17.4	15.7	14.7	15.9	21.4	21.3	21.3	21.3

FG022	106	58.0	55.4	46.6	53.4	25.8	23.4	19.8	23.0	82.8	82.7	0.3	55.2
FG023	111	69.8	67.8	67.6	68.4	36.7	34.7	33.4	34.9	32.1	32.1	32.0	32.1
FG024	116	79.4	77.0	75.6	77.3	42.6	39.9	38.6	40.4	187.4	187.2	186.9	187.2
FG025	121	62.5	59.9	58.4	60.2	29.1	27.2	26.5	27.6	27.9	27.9	27.9	27.9
FG026	126	82.8	76.3	75.2	78.1	43.9	38.6	37.1	39.9	186.8	186.5	186.3	186.5
FG027	131	112.4	68.5	68.2	83.0	49.9	36.7	35.5	40.7	63.1	63.0	63.0	63.0
FG028	136	110.4	73.1	108.5	97.3	60.7	48.7	56.3	55.3	82.5	82.4	82.4	82.4
FG029	141	131.3	133.5	128.6	131.1	97.2	99.6	93.5	96.8	211.9	212.0	211.4	211.8
FG030	146	64.0	63.4	51.5	59.6	21.1	19.3	16.7	19.0	211.8	18.6	18.6	83.0
FG031	151	90.3	87.5	88.9	88.9	48.0	43.0	43.0	44.7	211.9	211.8	212.7	212.1
FG032	156	76.5	72.7	71.3	73.5	37.5	33.9	32.7	34.7	187.5	187.7	187.4	187.6
FG033	161	79.6	75.5	73.9	76.4	38.0	33.8	32.0	34.6	185.4	185.7	185.5	185.5
FG034	166	77.5	74.6	68.4	73.5	41.6	36.2	31.8	36.5	185.4	185.5	163.6	178.2
FG035	171	69.0	59.7	58.8	62.5	28.5	22.8	22.5	24.6	82.7	0.3	21.1	34.7
FG036	176	56.5	48.0	45.9	50.1	17.0	15.0	14.4	15.5	18.5	18.5	18.5	18.5
FG037	181	61.5	54.6	56.3	57.5	28.9	25.0	24.7	26.2	72.3	72.2	72.2	72.2
FG038	186	79.1	85.9	30.0	65.0	17.2	15.7	7.5	13.5	0.2	0.2	0.2	0.2
FG039	191	62.8	60.7	57.6	60.4	19.6	18.3	17.4	18.4	18.8	0.3	0.2	6.4
FG040	196	45.6	41.0	39.5	42.0	17.9	16.2	15.6	16.6	18.8	18.8	18.8	18.8
FG041	201	33.2	28.4	30.5	30.7	10.7	9.3	9.1	9.7	16.3	16.3	16.3	16.3
FG042	206	35.8	29.7	68.8	44.8	10.5	8.5	13.6	10.9	0.3	0.3	18.7	6.4
FG043	211	33.4	31.0	23.4	29.3	7.9	6.6	5.4	6.6	0.3	0.2	0.3	0.3
FG044	216	28.3	25.3	25.4	26.3	8.3	7.1	6.7	7.4	18.6	18.6	18.7	18.6
FG045	221	25.2	23.9	25.7	24.9	6.1	5.3	4.9	5.4	21.2	18.6	0.3	13.4
FG046	226	23.1	20.4	16.9	20.2	7.2	6.0	5.2	6.1	18.6	18.6	18.5	18.6
FG047	231	18.1	15.6	17.4	17.0	6.9	5.9	5.8	6.2	18.6	18.6	18.6	18.6

FG048	236	16.5	16.2	15.3	16.0	7.2	6.6	6.2	6.7	16.2	9.5	9.4	11.7
FG049	241	24.2	21.1	19.2	21.5	11.2	9.9	9.3	10.2	16.2	16.2	16.2	16.2
FG050	246	29.9	28.5	27.4	28.6	11.7	10.6	9.9	10.7	48.2	16.2	0.3	21.6
FG051	251	49.5	48.0	45.3	47.6	16.3	17.4	16.4	16.7	18.5	18.8	18.7	18.7
FG052	256	22.2	18.2	17.9	19.4	5.7	4.4	4.2	4.8	0.2	0.2	0.2	0.2
FG053	261	15.2	14.3	12.9	14.1	5.0	4.3	3.9	4.4	0.2	0.2	0.2	0.2
FG054	266	41.0	37.3	36.2	38.1	15.4	13.5	12.4	13.8	18.7	18.7	0.2	12.5
FG055	271	18.6	17.0	15.9	17.2	6.0	5.2	4.7	5.3	0.2	0.2	0.2	0.2
FG056	276	15.3	12.9	12.2	13.5	12.8	11.4	10.8	11.7	16.3	16.3	16.3	16.3
FG057	281	17.3	15.8	14.6	15.9	12.7	11.9	11.5	12.0	16.2	14.2	14.2	14.9
FG058	286	63.9	62.3	58.6	61.6	29.6	28.2	26.9	28.2	24.4	24.4	24.4	24.4
FG059	291	31.7	28.1	25.6	28.4	16.4	14.9	14.1	15.1	16.3	16.3	16.3	16.3
FG060	296	27.7	26.0	24.8	26.2	20.5	19.4	18.6	19.5	47.9	16.3	16.2	26.8
FG061	299	26.4	24.6	24.0	25.0	18.6	17.8	17.5	18.0	16.2	16.2	16.2	16.2

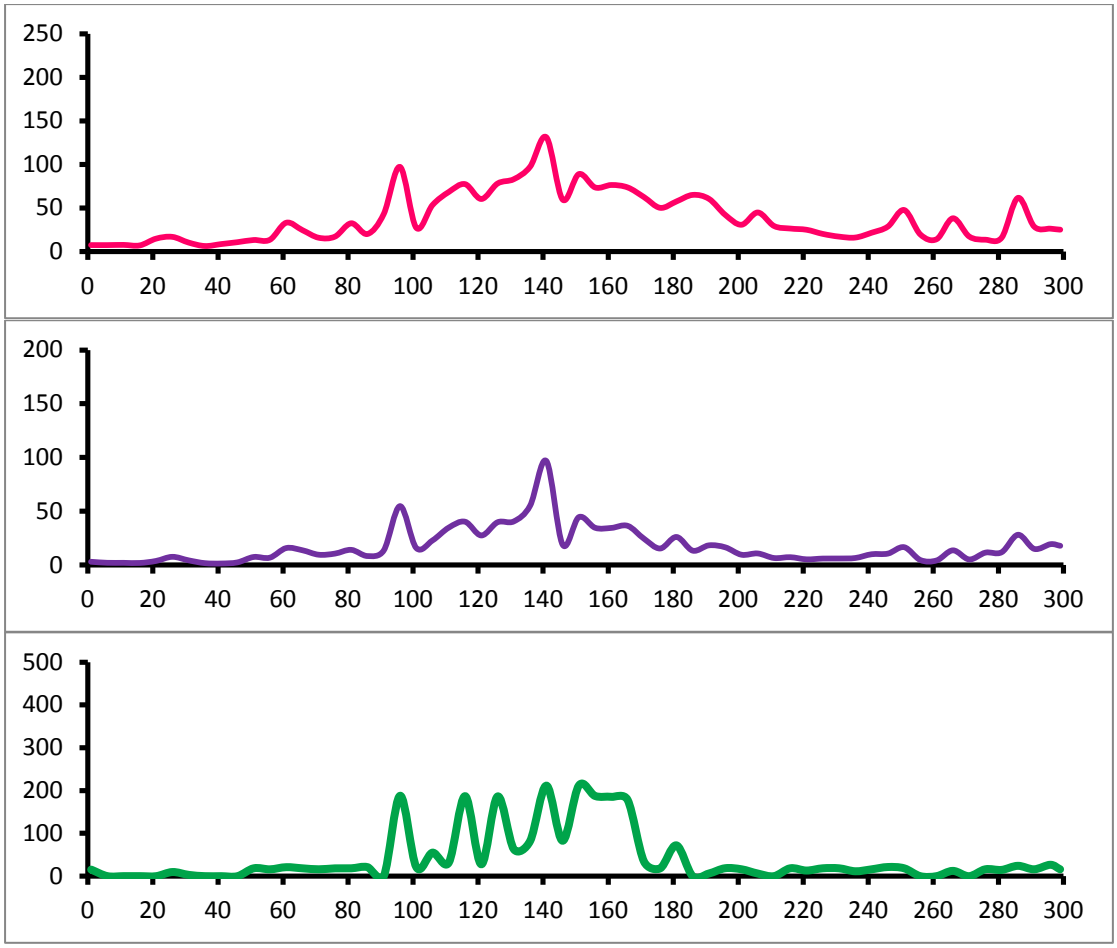

Appendix Figure 6.5: Fagali'i grain size curves: a) mean; b) median; c) mode.

Appendix 6.6: Ma'asina grain size data.

Appendix Table 6.6.1: Ma'asina grain size data obtained using methods described by Dinis and Castilho (2012).

Sub-sample	Depth (cm)	Mean			Average	Median			Average	Mode			Average
		MS - .1	MS - .2	MS - .3		MS - .1	MS - .2	MS - .3		MS - .1	MS - .2	MS - .3	
MS001	2	233.5	228.5	222.9	228.3	205.4	202.1	197.3	201.6	245.0	245.0	245.1	245.0
MS002	8	279.2	273.6	279.4	277.4	242.7	236.9	239.2	239.6	244.5	244.6	244.7	244.6
MS003	16	175.2	152.4	142.2	156.6	82.2	69.8	62.4	71.5	214.1	214.0	213.1	213.7
MS004	29	359.1	337.9	330.2	342.4	335.4	324.7	319.5	326.5	418.2	417.7	417.8	417.9
MS005	37	342.8	341.1	328.0	337.3	303.7	312.5	297.9	304.7	421.6	421.6	422.4	421.9
MS006	41	293.3	322.7	309.1	308.4	266.4	288.4	286.6	280.5	422.8	422.7	422.4	422.6
MS007	45	537.6	509.3	528.1	525.0	509.5	475.2	492.0	492.2	636.9	633.8	635.8	635.5
MS008	48	528.8	523.7	572.7	541.7	481.4	468.0	460.6	470.0	633.7	633.9	634.6	634.1
MS009	50	548.7	486.2	457.6	497.5	516.6	441.8	425.5	461.3	633.5	630.6	631.0	631.7
MS010	53	578.0	557.3	529.1	554.8	522.3	512.2	498.8	511.1	633.9	633.4	829.5	698.9
MS011	55	654.7	605.7	730.5	663.6	600.9	573.2	590.5	588.2	640.1	824.8	726.2	730.4
MS012	58	476.8	568.2	415.4	486.8	406.8	438.7	355.1	400.2	424.8	425.0	423.3	424.3
MS013	62	645.3	624.8	570.4	613.5	497.5	465.0	454.3	472.3	426.0	424.4	425.9	425.5
MS014	68	567.6	537.4	577.6	560.9	432.0	419.2	422.5	424.6	423.1	422.0	422.3	422.5
MS015	71	307.6	293.6	320.0	307.1	259.0	253.4	261.0	257.8	244.3	244.5	244.3	244.4

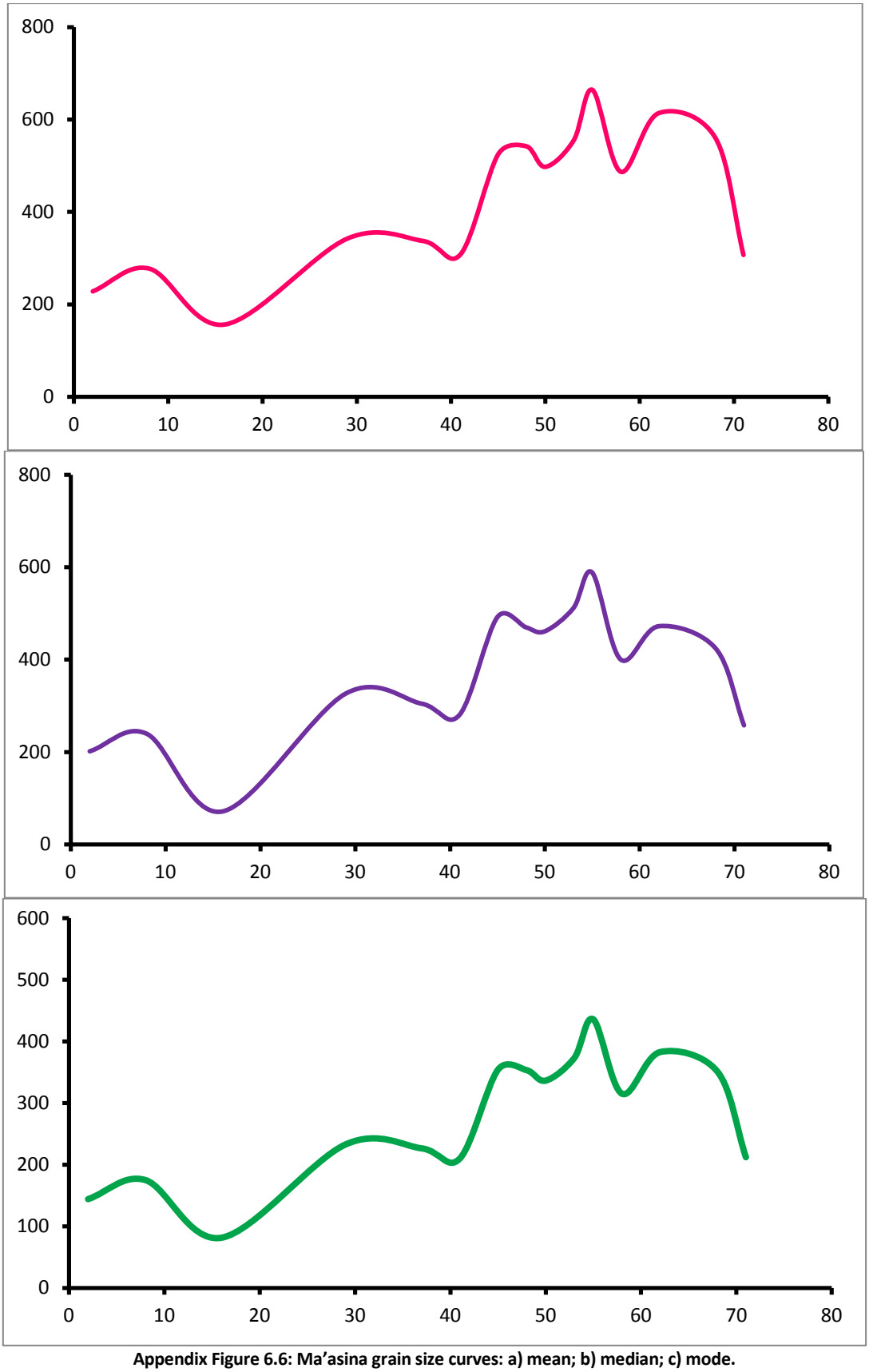

Appendix Figure 6.6: Ma'asina grain size curves: a) mean; b) median; c) mode.

Appendix 6.7: Falealupo grain size data.

Appendix Table 6.7.1: Falealupo grain size data obtained using methods described by Dinis and Castilho (2012).

Sub-sample	Depth (cm)	Mean			Average	Median			Average	Mode			Average
		FT - .1	FT - .2	FT - .3		FT - .1	FT - .2	FT - .3		FT - .1	FT - .2	FT - .3	
FT001	0.5	509.1	506.0	496.1	503.7	501.2	493.9	494.3	496.5	630.9	629.0	632.7	630.9
FT002	1.5	532.6	517.9	601.5	550.7	521.6	510.4	515.0	515.6	629.9	629.3	628.2	629.1
FT003	2.5	502.3	499.7	555.1	519.0	474.8	472.8	475.0	474.2	427.7	427.8	428.1	427.8
FT004	3.5	543.6	525.4	598.9	555.9	518.7	507.4	512.8	513.0	626.9	627.0	625.8	626.6
FT005	4.5	595.6	591.4	598.7	595.3	573.6	568.4	571.9	571.3	632.0	632.6	631.0	631.9
FT006	5.5	588.6	570.7	550.1	569.8	569.0	554.6	541.4	555.0	632.0	557.8	558.1	582.6
FT007	6.5	606.9	554.5	564.0	575.1	580.0	546.2	553.5	559.9	630.5	628.1	630.5	629.7
FT008	7.5	564.8	550.0	546.2	553.7	539.1	527.4	523.1	529.8	627.8	629.8	628.4	628.7
FT009	8.5	497.2	415.0	413.2	441.8	444.7	416.5	414.8	425.3	425.3	424.9	423.5	424.6
FT010	9.5	487.1	472.0	555.3	504.8	472.3	464.9	458.1	465.1	483.2	482.9	427.6	464.5
FT011	10.5	477.6	478.6	452.2	469.4	487.9	484.7	453.1	475.2	632.4	635.1	633.0	633.5
FT012	11.5	481.4	463.3	571.4	505.3	469.4	448.7	445.4	454.5	624.8	553.1	421.3	533.1
FT013	12.5	446.4	430.6	533.4	470.1	437.9	427.6	434.7	433.4	425.2	423.5	423.8	424.2
FT014	13.5	484.4	452.1	447.1	461.2	456.9	437.9	427.7	440.9	426.7	424.3	424.9	425.3
FT015	14.5	508.9	488.8	590.4	529.4	482.7	450.7	474.6	469.3	427.3	426.8	426.8	427.0
FT016	15.5	475.2	462.1	438.2	458.5	467.7	457.3	441.6	455.5	628.0	554.0	632.4	604.8
FT017	16.5	449.7	420.7	376.2	415.5	474.0	450.0	413.8	445.9	632.3	627.8	622.8	627.6
FT018	17.5	436.4	422.4	419.6	426.1	457.5	444.0	443.4	448.3	629.0	629.2	628.8	629.0
FT019	18.5	583.9	833.7	890.5	769.4	502.2	525.2	537.1	521.5	627.3	2764.3	2764.5	2052.0
FT020	19.5	435.8	394.8	668.1	499.6	457.2	427.7	463.1	449.3	629.4	553.5	2787.3	1323.4
FT021	21	459.0	516.9	542.7	506.2	475.1	463.8	465.9	468.3	630.1	624.4	624.4	626.3

FT022	23	752.9	560.5	544.1	619.2	526.9	485.8	472.0	494.9	628.9	626.8	626.1	627.2
FT023	25	472.7	465.0	453.1	463.6	479.0	477.2	470.7	475.6	627.2	630.6	553.5	603.7
FT024	27	534.2	433.3	449.1	472.2	540.6	468.6	471.6	493.6	634.5	630.8	632.7	632.6
FT025	29	493.3	482.8	472.7	482.9	514.0	500.7	499.8	504.8	633.9	630.8	631.9	632.2
FT026	31	521.0	491.3	500.2	504.1	532.7	511.3	498.5	514.2	636.5	632.8	627.6	632.3
FT027	33	71.5	63.0	55.2	63.2	48.5	40.8	36.1	41.8	55.2	54.9	48.2	52.8
FT028	35	129.1	74.0	66.3	89.8	65.7	44.3	39.1	49.7	63.0	55.1	48.2	55.4
FT029	37	15.9	13.2	12.5	13.8	9.6	8.4	7.7	8.6	9.5	9.4	9.4	9.4
FT030	39	125.3	96.9	87.6	103.3	74.0	62.5	56.6	64.3	212.7	211.5	187.7	204.0
FT031	41	14.8	11.9	11.6	12.8	10.1	8.2	8.0	8.8	10.8	9.4	9.4	9.9
FT032	43	23.6	25.9	19.9	23.1	9.1	8.6	8.3	8.7	9.4	9.4	9.4	9.4
FT033	45	12.3	11.0	10.4	11.2	8.2	7.9	7.7	7.9	9.4	9.4	9.4	9.4
FT034	47	17.4	14.5	13.8	15.2	10.1	9.5	9.3	9.6	9.4	9.4	9.4	9.4
FT035	49	16.5	11.3	10.3	12.7	7.8	7.0	6.8	7.2	8.2	8.2	7.2	7.9

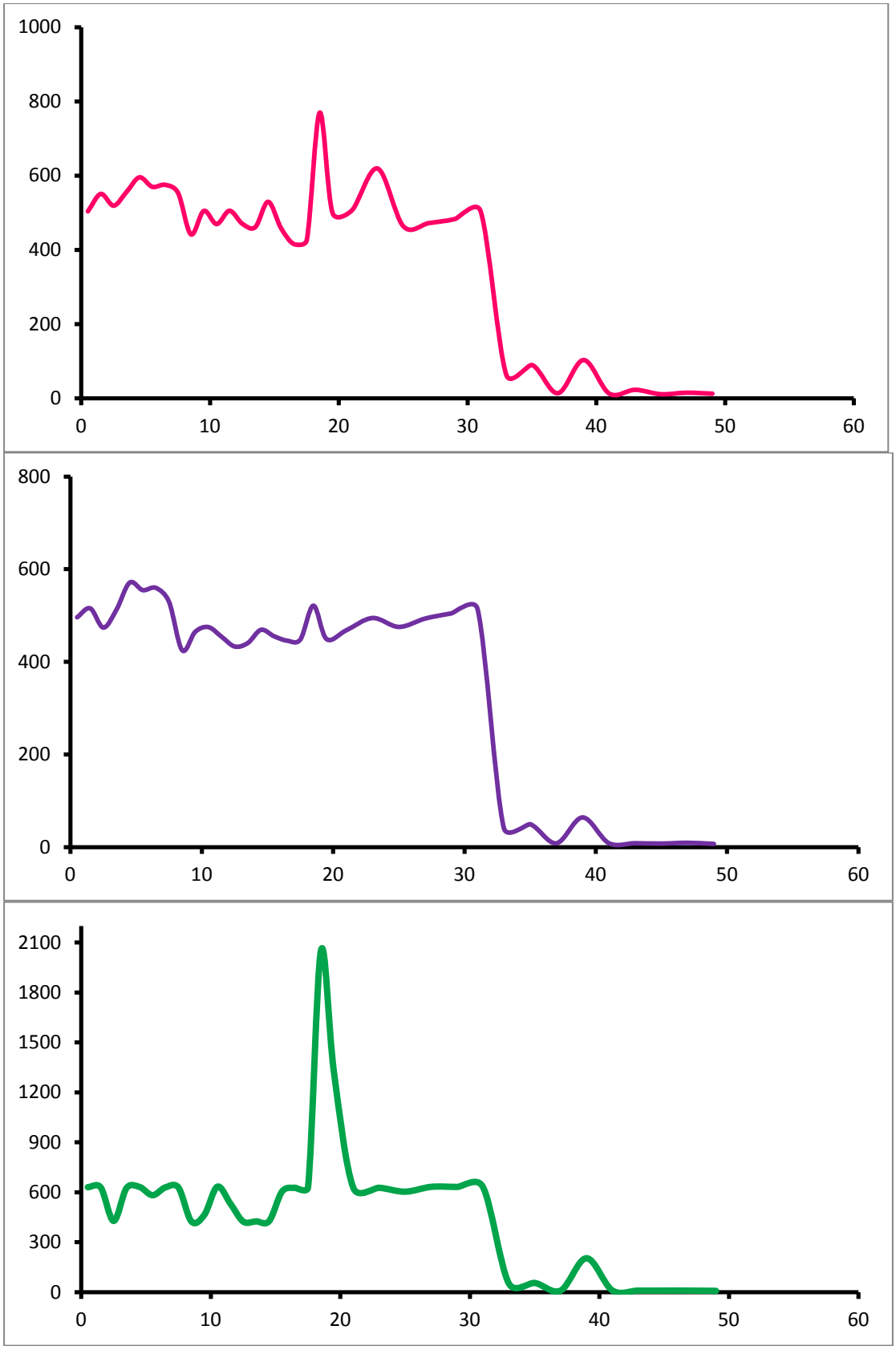

Appendix Figure 6.7: Falealupo grain size curves: a) mean; b) median; c) mode.

Appendix 6.8: Lano grain size data.

Appendix Table 6.8.1: Lano grain size data obtained using methods described by Dinis and Castilho (2012).

Sub-sample	Depth (cm)	Mean			Average	Median			Average	Mode			Average
		LN - .1	LN - .2	LN - .3		LN - .1	LN - .2	LN - .3		LN - .1	LN - .2	LN - .3	
LN001	1	34.9	35.9	36.6	35.8	12.3	11.9	11.3	11.8	7.2	7.2	7.2	7.2
LN002	5	32.8	31.8	31.9	32.2	12.1	11.2	10.7	11.3	8.2	7.2	7.2	7.5
LN003	9	68.5	65.2	67.5	67.1	41.0	42.4	43.5	42.3	82.5	94.4	94.4	90.5
LN004	13	111.0	111.0	107.5	109.8	53.4	57.1	57.8	56.1	82.7	82.8	82.8	82.7
LN005	17	189.2	177.9	192.0	186.4	125.6	127.9	137.8	130.4	212.7	212.5	213.0	212.7
LN006	21	177.7	185.5	182.3	181.8	149.9	154.9	155.3	153.4	212.0	212.5	212.7	212.4
LN007	25	217.6	220.4	217.3	218.4	192.4	194.9	192.3	193.2	214.1	214.1	213.7	214.0
LN008	29	290.1	292.7	283.3	288.7	231.8	235.2	232.1	233.0	215.4	215.0	215.0	215.2
LN009	33	301.8	179.2	176.0	219.0	248.4	153.1	152.0	184.5	243.5	186.8	187.5	205.9
LN010	37	330.2	336.1	330.2	332.2	273.8	275.1	274.3	274.4	244.2	244.1	244.2	244.2
LN011	41	336.5	328.4	319.7	328.2	298.0	285.1	278.2	287.1	419.9	419.4	419.9	419.7
LN012	45	345.6	332.0	341.2	339.6	294.6	287.6	283.7	288.6	418.1	419.7	418.4	418.7
LN013	49	463.6	448.7	454.2	455.5	430.1	419.7	423.1	424.3	422.6	422.2	422.9	422.6
LN014	53	432.3	501.0	273.0	402.1	400.0	401.5	243.1	348.2	422.1	420.9	216.3	353.1
LN015	57	401.8	395.4	391.5	396.2	366.2	356.0	354.9	359.0	420.2	419.0	419.0	419.4
LN016	61	455.4	466.6	432.2	451.4	419.4	424.8	405.3	416.5	422.8	423.5	422.7	423.0
LN017	65	444.7	421.0	410.9	425.5	397.3	384.9	382.2	388.1	419.8	420.1	421.2	420.4
LN018	69	427.9	430.2	425.1	427.8	402.1	403.3	399.6	401.7	421.2	421.7	421.2	421.4
LN019	73	421.9	419.2	415.0	418.7	399.6	397.5	394.6	397.2	421.4	421.4	421.4	421.4
LN020	77	480.1	473.7	477.9	477.2	452.0	446.8	449.5	449.4	424.5	424.3	424.5	424.4
LN021	81	458.5	450.5	441.5	450.2	428.1	422.4	416.1	422.2	421.7	421.4	421.1	421.4

LN022	85	417.7	421.4	417.6	418.9	397.1	399.0	395.7	397.3	420.6	420.8	419.9	420.5
LN023	89	411.7	409.7	404.3	408.6	388.7	387.0	381.9	385.9	419.7	419.6	418.6	419.3
LN024	93	468.2	475.4	468.2	470.6	438.8	441.2	436.6	438.8	423.4	423.7	423.6	423.6
LN025	97	442.4	445.5	429.9	439.2	416.5	416.0	408.0	413.5	422.1	421.6	422.0	421.9
LN026	101	479.9	486.2	477.7	481.3	446.0	447.2	445.2	446.2	424.0	424.2	424.5	424.2
LN027	105	418.3	413.6	410.9	414.3	394.7	393.3	389.3	392.4	421.7	421.6	421.2	421.5
LN028	109	371.7	369.0	355.8	365.5	339.2	338.0	329.9	335.7	369.7	416.6	369.7	385.3
LN029	113	421.4	414.5	413.9	416.6	393.4	389.6	389.5	390.8	418.3	418.8	419.1	418.7
LN030	117	442.5	429.1	436.8	436.1	413.3	407.6	408.6	409.8	420.8	422.2	421.0	421.4
LN031	121	399.2	392.8	395.7	395.9	371.3	369.3	367.3	369.3	420.5	420.7	420.5	420.6
LN032	125	187.2	193.5	184.9	188.5	109.1	124.6	115.9	116.5	62.8	213.6	62.9	113.1
LN033	129	211.8	196.6	207.7	205.4	155.1	150.6	158.8	154.8	215.1	214.7	424.4	284.7
LN034	133	314.0	309.6	314.9	312.9	269.1	267.2	274.0	270.1	424.3	424.3	424.5	424.4
LN035	137	150.1	131.6	131.5	137.7	65.6	64.3	64.9	64.9	55.1	55.0	54.9	55.0
LN036	141	205.9	211.0	192.9	203.3	105.2	126.1	104.9	112.0	55.2	483.4	55.0	197.9
LN037	145	129.5	145.6	142.3	139.2	64.2	67.4	67.2	66.3	55.4	55.3	55.2	55.3

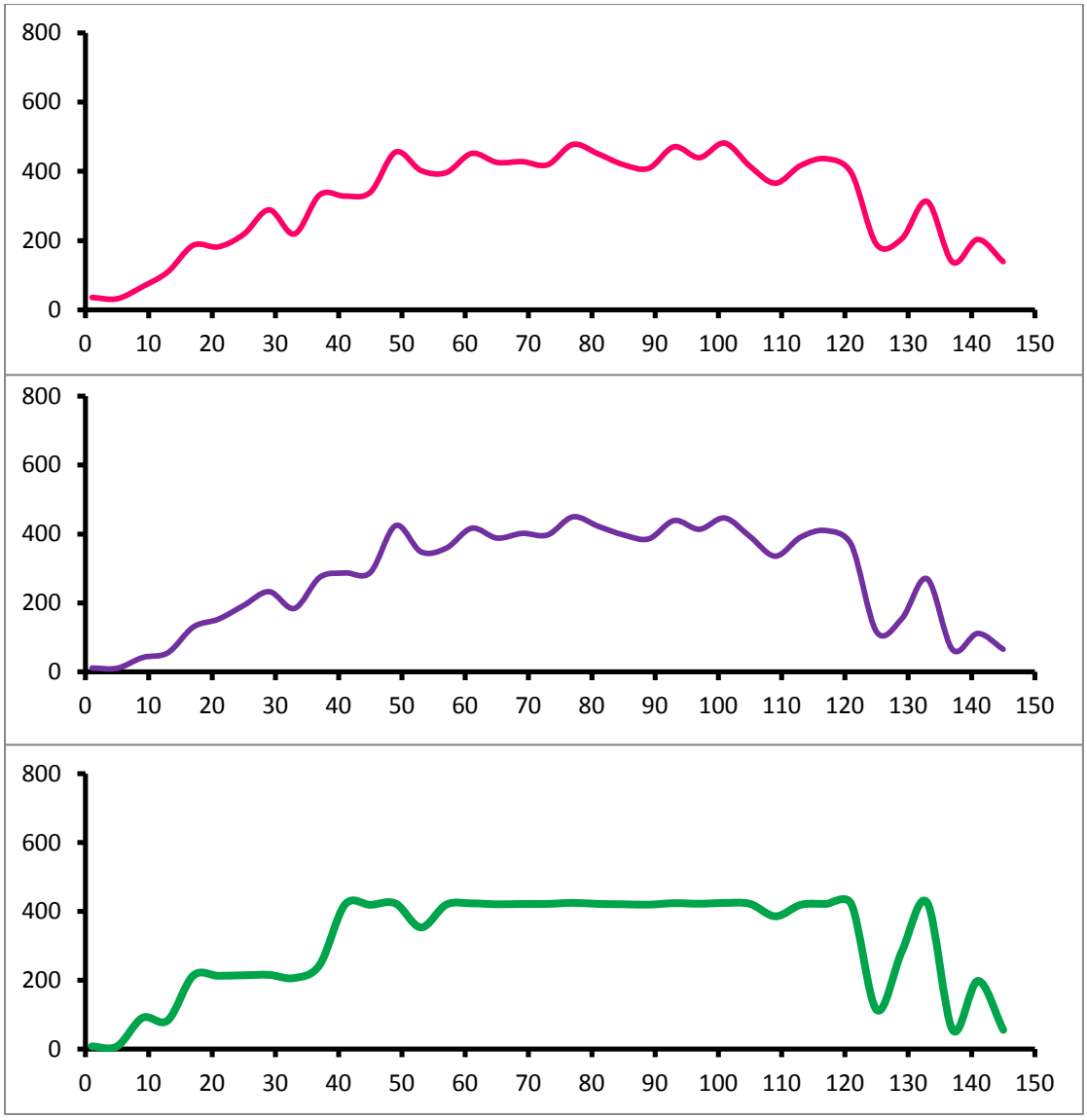

Appendix Figure 6.8: Lano grain size curves: a) mean; b) median; c) mode.

Appendix 6.9: Satupaitea grain size data.

Appendix Table 6.9.1: Satupaitea grain size data obtained using methods described by Dinis and Castilho (2012).

Sub-sample	Depth (cm)	Mean			Average	Median			Average	Mode			Average
		SP - .1	SP - .2	SP - .3		SP - .1	SP - .2	SP - .3		SP - .1	SP - .2	SP - .3	
SP001	1	220.1	454.6	466.4	380.4	208.2	215.6	216.3	213.4	213.0	213.0	213.1	213.1
SP002	4	211.2	211.0	211.8	211.3	202.4	202.7	203.1	202.7	212.3	212.4	212.4	212.3
SP003	7	224.4	223.9	224.0	224.1	211.0	210.9	210.9	210.9	213.6	213.5	213.5	213.5
SP004	10	219.5	218.4	217.5	218.5	209.0	208.3	208.4	208.6	213.5	213.4	213.4	213.5
SP005	13	217.5	212.4	213.4	214.4	204.2	203.9	203.6	203.9	212.2	212.5	212.5	212.4
SP006	16	213.2	214.5	212.4	213.4	202.7	203.9	203.4	203.3	212.6	212.9	212.8	212.7
SP007	19	209.8	209.7	204.5	208.0	201.5	201.0	200.7	201.1	212.5	212.2	212.6	212.4
SP008	22	174.7	185.2	179.9	179.9	180.8	186.1	184.1	183.7	211.8	211.9	211.9	211.9
SP009	25	147.1	146.5	146.5	146.7	151.1	152.4	153.2	152.2	188.9	210.7	189.4	196.3
SP010	28	134.2	135.8	130.0	133.3	137.5	138.9	137.1	137.8	189.1	188.9	212.4	196.8
SP011	31	155.1	151.4	150.8	152.4	157.5	156.8	156.8	157.0	210.5	210.8	210.8	210.7
SP012	34	128.8	130.3	125.9	128.4	132.2	133.7	132.1	132.7	211.3	211.2	212.1	211.5
SP013	37	211.5	425.1	491.7	376.1	206.2	212.5	215.5	211.4	213.6	213.3	213.7	213.5
SP014	40	508.5	604.0	542.2	551.6	216.7	220.3	215.8	217.6	213.1	213.3	213.4	213.2
SP015	43	596.3	689.6	834.4	706.8	212.5	214.5	221.4	216.1	211.0	2779.6	2792.6	1927.7
SP016	46	199.4	198.3	314.9	237.6	194.0	193.2	195.7	194.3	211.3	211.0	211.5	211.3
SP017	49	560.2	801.8	834.3	732.1	200.1	215.7	217.9	211.2	211.9	2734.3	2706.4	1884.2
SP018	52	195.3	194.5	194.6	194.8	191.0	190.7	190.9	190.8	210.8	210.8	210.7	210.8
SP019	55	199.4	793.1	705.3	565.9	193.7	219.2	210.8	207.9	211.4	2734.5	2812.4	1919.4
SP020	58	198.5	349.9	754.8	434.4	193.0	197.9	215.3	202.1	211.1	211.9	2772.0	1065.0
SP021	61	188.1	443.5	553.2	394.9	184.0	191.5	195.9	190.5	188.1	188.3	188.3	188.3

SP022	64	184.2	184.7	183.2	184.1	181.5	182.0	181.9	181.8	187.9	188.0	188.1	188.0
SP023	67	224.9	223.3	388.4	278.9	215.3	214.8	221.6	217.2	215.0	215.1	215.3	215.1
SP024	70	208.4	207.6	208.6	208.2	196.4	195.9	196.6	196.3	210.8	189.1	189.2	196.4
SP025	73	232.0	226.3	255.2	237.8	216.6	214.7	217.1	216.1	214.5	214.6	214.7	214.6
SP026	76	354.4	368.2	362.2	361.6	229.5	231.2	230.2	230.3	214.7	214.8	214.9	214.8
SP027	79	271.8	268.1	441.2	327.0	206.5	203.8	217.0	209.1	214.6	214.5	214.5	214.5
SP028	82	408.9	401.9	449.7	420.1	221.2	220.7	219.0	220.3	215.6	215.7	215.5	215.6
SP029	85	247.1	416.5	248.5	304.0	206.7	224.5	207.2	212.8	216.7	216.6	216.6	216.6
SP030	88	279.1	433.5	332.9	348.5	229.4	243.0	228.1	233.5	216.8	216.7	216.7	216.8
SP031	91	258.1	381.1	442.8	360.6	223.8	231.3	235.2	230.1	216.7	216.7	216.5	216.6
SP032	94	254.8	421.5	248.0	308.1	221.8	229.7	219.7	223.7	215.9	215.8	216.1	215.9
SP033	97	253.4	251.5	250.4	251.8	221.5	221.2	221.3	221.3	215.8	215.8	215.9	215.8
SP034	100	497.8	279.3	518.2	431.8	244.9	229.9	248.5	241.1	215.5	215.6	215.4	215.5

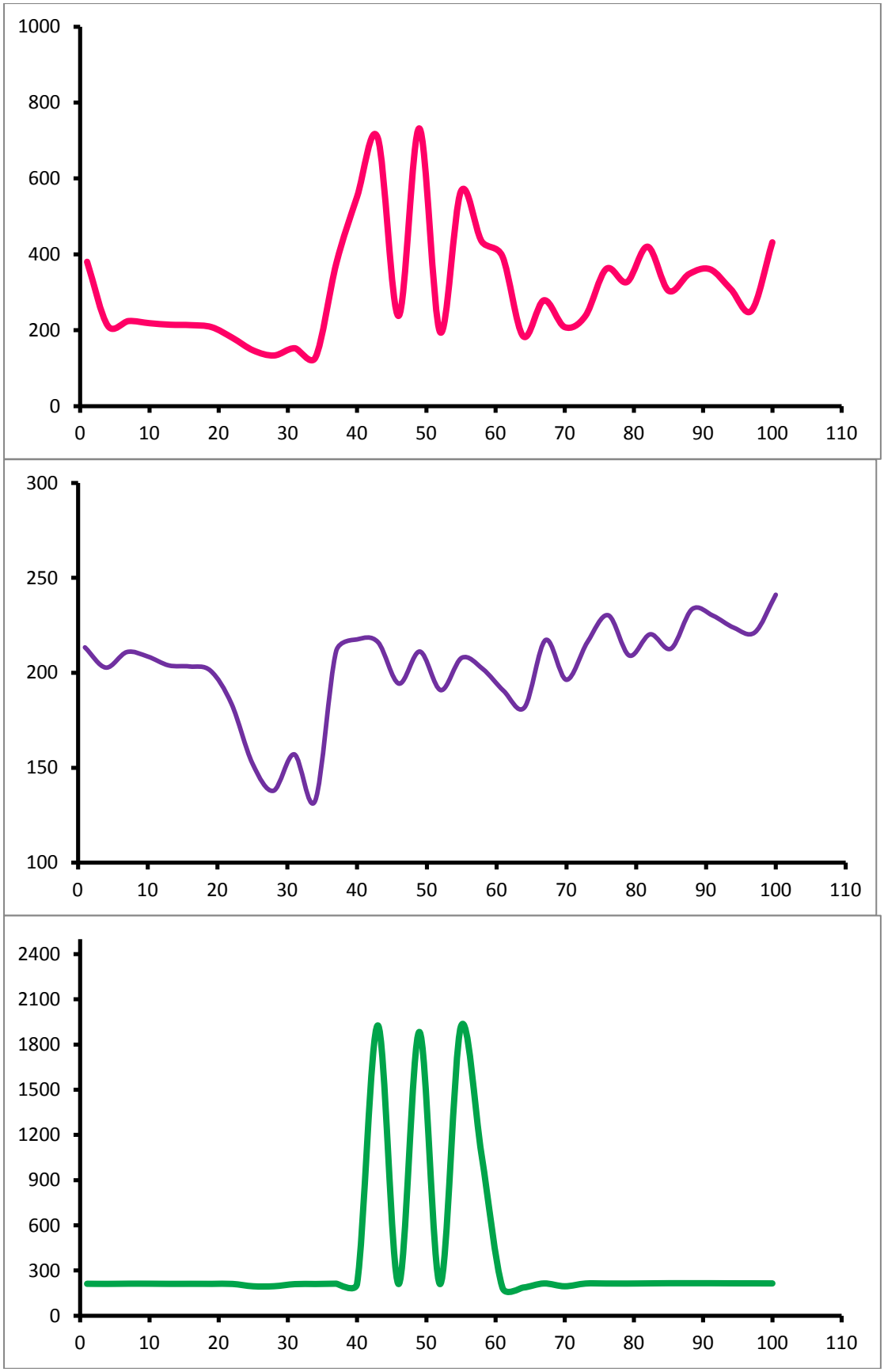

Appendix Figure 6.9: Satupaitea grain size curves: a) mean; b) median; c) mode.

Appendix 6.10: Ta'u grain size data.

Appendix Table 6.10.1: Ta'u grain size data obtained using methods described by Dinis and Castilho (2012).

Sub-sample	Depth (cm)	Mean			Average	Median			Average	Mode			Average
		TA - .1	TA - .2	TA - .3		TA - .1	TA - .2	TA - .3		TA - .1	TA - .2	TA - .3	
TA001	1	279.1	166.1	204.8	216.7	201.4	19.2	32.1	84.2	639.4	428.1	612.0	559.8
TA002	3	359.6	318.1	277.5	318.4	368.1	316.2	262.7	315.6	635.5	631.6	624.2	630.4
TA003	5	443.8	445.2	403.0	430.7	470.1	474.5	437.5	460.7	635.8	632.8	634.2	634.2
TA004	7	321.9	302.7	307.5	310.7	345.5	309.9	315.4	323.6	637.1	638.5	637.2	637.6
TA005	9	465.2	574.2	598.9	546.1	476.7	463.2	466.8	468.9	631.1	626.5	627.8	628.5
TA006	11	403.9	399.7	380.5	394.7	428.3	421.3	407.6	419.1	630.0	637.3	633.4	633.5
TA007	13	425.3	380.8	394.2	400.1	431.2	395.9	402.7	409.9	626.8	625.4	628.3	626.8
TA008	15	310.1	281.9	275.8	289.3	275.8	229.4	204.9	236.7	630.5	628.5	422.1	560.4
TA009	17	316.1	281.8	279.0	292.3	274.8	210.2	194.7	226.6	633.7	629.4	633.6	632.2
TA010	19	364.9	356.2	305.1	342.1	364.4	344.3	286.7	331.8	629.8	635.7	626.3	630.6
TA011	21	390.1	351.5	322.5	354.7	392.5	360.7	319.2	357.5	639.3	640.6	635.8	638.5
TA012	23	408.3	388.1	383.8	393.4	423.3	409.1	409.1	413.9	633.4	632.2	630.2	631.9
TA013	25	399.2	381.9	344.2	375.1	412.5	390.6	352.4	385.2	633.9	636.9	630.5	633.7
TA014	27	249.4	236.7	236.7	240.9	212.6	193.2	192.9	199.6	425.3	425.5	423.9	424.9
TA015	29	402.5	388.5	391.8	394.3	412.7	407.2	414.2	411.4	629.5	630.4	629.9	629.9
TA016	31	366.9	367.5	365.5	366.6	366.9	362.3	358.6	362.6	640.6	645.3	640.3	642.1
TA017	33	253.4	240.4	234.5	242.7	218.5	197.4	189.7	201.9	426.1	482.3	482.4	463.6
TA018	35	292.0	282.6	237.3	270.7	268.4	264.4	238.6	257.1	421.5	421.5	419.0	420.7
TA019	37	182.8	146.3	199.6	176.2	47.8	30.2	36.7	38.2	640.1	0.2	710.9	450.4
TA020	39	213.1	217.1	227.0	219.1	149.0	163.7	164.2	159.0	425.0	425.2	423.9	424.7
TA021	41	370.9	352.6	371.3	365.0	369.7	358.1	366.9	364.9	424.8	424.9	423.8	424.5

TA022	43	358.7	359.2	348.0	355.3	353.7	354.8	350.7	353.1	422.8	421.7	421.4	422.0
TA023	45	367.8	360.5	356.5	361.6	369.5	369.8	367.3	368.9	423.8	424.3	424.5	424.2
TA024	47	232.1	222.8	235.8	230.2	180.6	174.8	181.3	178.9	423.7	420.5	422.4	422.2
TA025	49	304.5	304.3	304.3	304.4	302.0	302.4	303.1	302.5	424.0	424.0	425.4	424.5
TA026	51	526.5	615.6	548.2	563.4	419.7	427.6	418.8	422.1	421.7	423.2	420.8	421.9
TA027	53	538.1	604.2	637.9	593.4	500.6	515.6	494.0	503.4	629.4	632.1	425.0	562.1
TA028	55	510.8	524.7	560.8	532.1	504.1	501.1	522.5	509.2	633.5	628.3	630.3	630.7

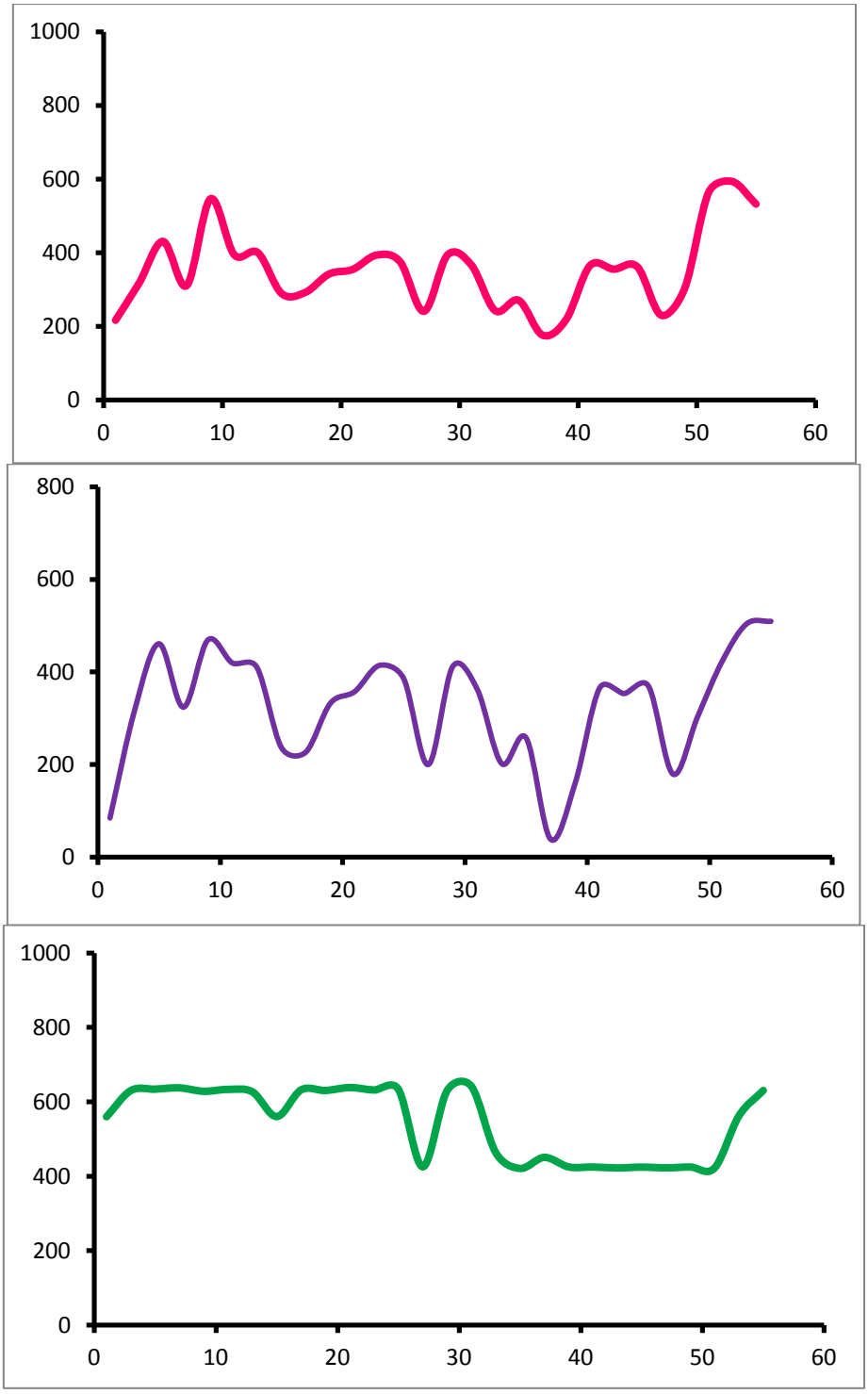

Appendix Figure 6.10: Ta'u grain size curves: a) mean; b) median; c) mode.

APPENDIX 7: pXRF ELEMENT DATA

Overview

Elemental analysis using a portable X-ray Fluorescence Spectrometer (pXRF) was carried out at the University of Canterbury, adapting the methods described by Rothwell (2006), Chagué-Goff (2010), and Chagué-Goff et al. (2011). The Tracer III pXRF obtained from Bruker Elemental Inc. was used (Bruker Inc., 2008).

Relative elemental compositions for each site are provided. Thresh-hold detection is for elements ≥ silicon (Si) in the periodic table.

Contents

Appendix 7.1: Satitoa pXRF data.

Appendix Table 7.1.1: Processed pXRF data of detected elements at Satitoa; processed using ARTAX software developed by Bruker Elemenetal Inc.

Depth (cm)	Ca	Cr	Fe	Mn	Ni	S	Sr	V	Ti
0.5	107790	1336	140229	2175	1473	531	224	714	15127
1.5	94765	1112	127980	1775	1444	330	381	813	12704
2.5	102661	1020	112765	1868	1446	400	59	325	12249
3.5	162910	1038	90261	1603	1666	272	242	353	11001
4.5	208283	841	93523	1829	1437	261	42	209	9950
5.5	189621	975	106460	1518	1661	279	175	449	10879
6.5	134654	1170	99258	1541	1791	226	219	392	12722
7.5	194036	1066	87188	1471	1546	254	221	350	9310
8.5	242844	1067	67671	1059	1598	285	248	468	8367
9.5	378641	518	11042	490	1636	136	11	35	1031
10.5	376860	525	22831	730	1820	173	617	1	2571
11.5	45198	3515	752356	8798	938	215	87	3740	91701
12.5	47768	3278	644410	16101	964	136	209	3371	74249
13.5	44048	3289	671786	12351	935	211	105	3360	81549
14.5	59390	3366	633337	8230	1015	134	258	3351	78523
15.5	52129	3566	646083	10468	1280	85	123	3783	80860
16.5	54659	3781	718028	15850	1011	22	225	3454	89548
17.5	52590	3457	720137	15482	1286	82	88	3826	89833
18.5	66249	3490	676938	11382	1336	1	121	3474	86481
19.5	49249	2993	571967	9222	894	350	143	2818	71511
21	74386	3093	677542	10904	1099	141	165	3374	85664
23	54080	3304	680389	9402	1111	109	159	3377	84588
25	54577	3781	699851	11084	1330	137	111	3565	88212
27	49300	3622	732269	9749	1136	219	145	3666	91608
29	38149	3451	686626	8203	1088	125	195	3442	83334
31	64799	3373	688635	9804	988	75	199	3920	85931
33	50937	3742	815265	15078	1411	95	176	4300	103894
35	67361	3006	697672	13513	1207	38	169	3368	84854
37	47395	3689	739337	10026	1001	2	111	4152	92709
39	51005	3344	755911	17444	1499	119	86	4144	97523
41	32278	4199	799345	11005	1288	166	207	4663	101434
43	57663	3590	766468	10642	1006	72	102	4059	95702
45	65894	3444	701223	24170	1152	130	92	3573	92274
47	51892	3574	766708	17025	1288	101	327	4647	100581
49	52641	3446	709702	27520	1066	269	147	3890	89984
51	28371	4143	880398	14859	1149	0	3	4642	113294
53	27869	3108	658104	7997	1014	98	185	3554	77314
55	47748	3169	659946	7313	1144	239	229	3107	83566
57	74749	3174	650071	8099	1262	262	162	3513	90580
59	48249	2985	650125	7236	929	234	133	3489	80253
61	25303	3106	650274	5898	1157	104	85	3685	77819
63	35817	3210	669095	6187	1367	396	151	3366	84425
65	56670	3244	641736	7633	1136	449	95	3238	82316
67	80322	3405	636632	11849	965	329	275	3365	81673
69	50235	3019	577616	8220	1060	299	43	3019	70555
71	78090	2713	503104	7187	912	294	61	2546	60749

73	32855	3225	663298	7192	1502	367	112	3685	81186
75	130664	2434	511692	7247	1148	769	260	2301	71615
77	167062	2355	440444	6835	945	760	141	2187	60406
79	191220	2154	395977	6167	879	611	231	2021	57436
81	165211	2509	481431	6531	1141	1765	186	2555	63952
83	222195	747	68768	2441	1151	382	253	266	6745
85	240037	856	43424	1387	1183	299	379	163	4894
87	266553	513	37556	1839	1290	487	66	115	2591
89	329920	713	44345	1152	1625	612	422	140	2431

Appendix Table 7.1.2: Satitoa elemental ratios used in this analysis. Ratios are between marine-derived elements relative to terrestrially-dominant iron (Fe), manganese (Mn) and titanium (Ti).

Depth (cm)	Ca/Fe	Ca/Mn	Ca/Ti	Sr/Fe	Sr/Ti	Sr/Mn
0.5	0.769	49.559	7.126	0.002	0.015	0.103
1.5	0.740	53.389	7.459	0.003	0.030	0.215
2.5	0.910	54.958	8.381	0.001	0.005	0.032
3.5	1.805	101.628	14.809	0.003	0.022	0.151
4.5	2.227	113.878	20.933	0.000	0.004	0.023
5.5	1.781	124.915	17.430	0.002	0.016	0.115
6.5	1.357	87.381	10.584	0.002	0.017	0.142
7.5	2.225	131.908	20.842	0.003	0.024	0.150
8.5	3.589	229.314	29.024	0.004	0.030	0.234
9.5	34.291	772.737	367.256	0.001	0.011	0.022
10.5	16.507	516.247	146.581	0.027	0.240	0.845
11.5	0.060	5.137	0.493	0.000	0.001	0.010
12.5	0.074	2.967	0.643	0.000	0.003	0.013
13.5	0.066	3.566	0.540	0.000	0.001	0.009
14.5	0.094	7.216	0.756	0.000	0.003	0.031
15.5	0.081	4.980	0.645	0.000	0.002	0.012
16.5	0.076	3.449	0.610	0.000	0.003	0.014
17.5	0.073	3.397	0.585	0.000	0.001	0.006
18.5	0.098	5.821	0.766	0.000	0.001	0.011
19.5	0.086	5.340	0.689	0.000	0.002	0.016
21	0.110	6.822	0.868	0.000	0.002	0.015
23	0.079	5.752	0.639	0.000	0.002	0.017
25	0.078	4.924	0.619	0.000	0.001	0.010
27	0.067	5.057	0.538	0.000	0.002	0.015
29	0.056	4.651	0.458	0.000	0.002	0.024
31	0.094	6.609	0.754	0.000	0.002	0.020
33	0.062	3.378	0.490	0.000	0.002	0.012
35	0.097	4.985	0.794	0.000	0.002	0.013
37	0.064	4.727	0.511	0.000	0.001	0.011
39	0.067	2.924	0.523	0.000	0.001	0.005
41	0.040	2.933	0.318	0.000	0.002	0.019
43	0.075	5.418	0.603	0.000	0.001	0.010
45	0.094	2.726	0.714	0.000	0.001	0.004
47	0.068	3.048	0.516	0.000	0.003	0.019
49	0.074	1.913	0.585	0.000	0.002	0.005
51	0.032	1.909	0.250	0.000	0.000	0.000
53	0.042	3.485	0.360	0.000	0.002	0.023

55	0.072	6.529	0.571	0.000	0.003	0.031
57	0.115	9.229	0.825	0.000	0.002	0.020
59	0.074	6.668	0.601	0.000	0.002	0.018
61	0.039	4.290	0.325	0.000	0.001	0.014
63	0.054	5.789	0.424	0.000	0.002	0.024
65	0.088	7.424	0.688	0.000	0.001	0.012
67	0.126	6.779	0.983	0.000	0.003	0.023
69	0.087	6.111	0.712	0.000	0.001	0.005
71	0.155	10.865	1.285	0.000	0.001	0.008
73	0.050	4.568	0.405	0.000	0.001	0.016
75	0.255	18.030	1.825	0.001	0.004	0.036
77	0.379	24.442	2.766	0.000	0.002	0.021
79	0.483	31.007	3.329	0.001	0.004	0.037
81	0.343	25.296	2.583	0.000	0.003	0.028
83	3.231	91.026	32.942	0.004	0.038	0.104
85	5.528	173.062	49.047	0.009	0.077	0.273
87	7.097	144.945	102.876	0.002	0.025	0.036
89	7.440	286.389	135.714	0.010	0.174	0.366

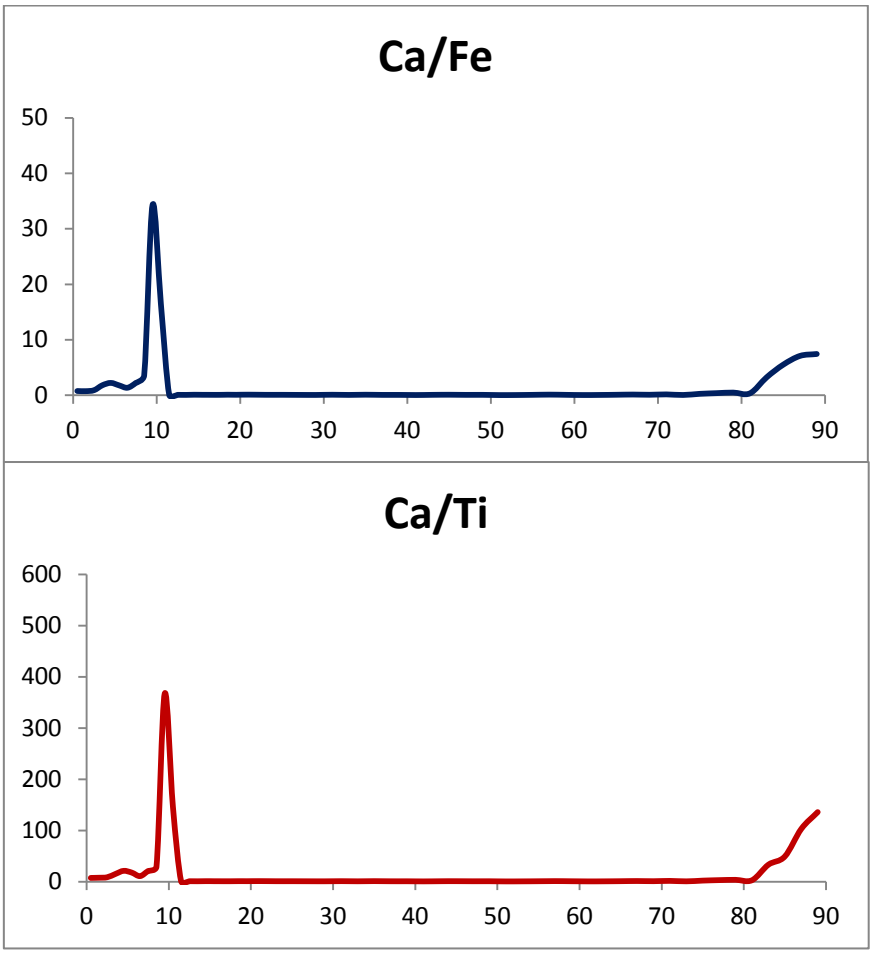

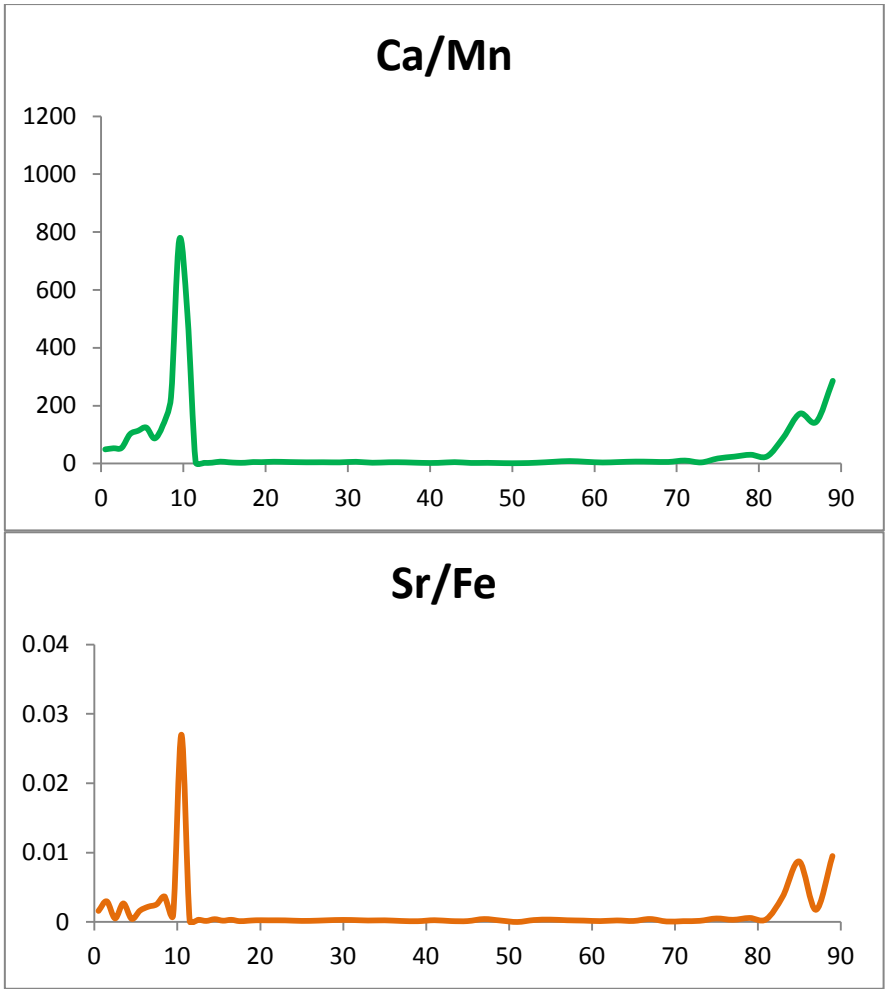
Ca/Mn
1200
1000
800
600
400
200
0
0
10
20
30
40
50
60
70
80
90
Sr/Fe
0.04
0.03
0.02
0.01
0
0
10
20
30
40
50
60
70
80
90

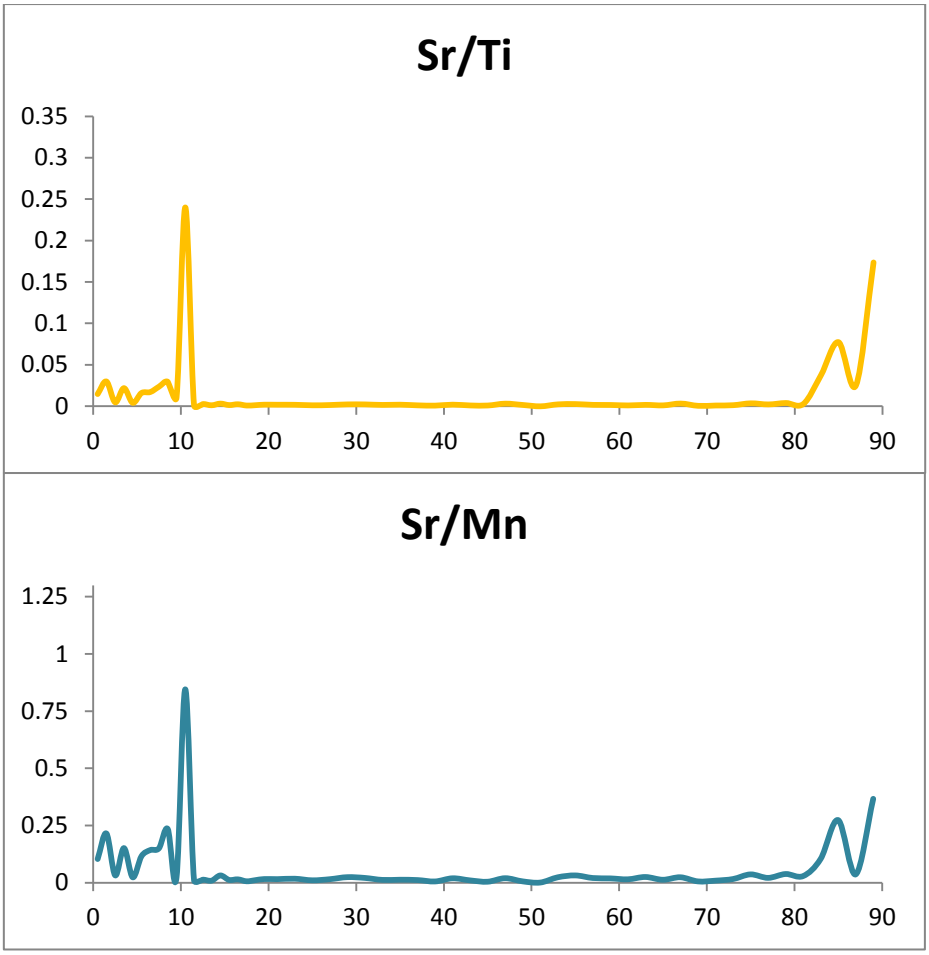

Appendix Figure 7.1: Satitoa pXRF data curves.

Appendix 7.2: Vaovai pXRF data.

Appendix Table 7.2.1: Processed pXRF data of detected elements at Vaovai; processed using ARTAX software developed by Bruker Elemenetal Inc.

Depth (cm)	Ca	Cr	Fe	Mn	Ni	Ti	S	V
0.5	232727	1265	232743	2987	1117	21127	1	830
1.5	145751	1404	280472	3608	1348	26165	1	930
2.5	126733	1429	305078	3651	1255	29598	1	1139
3.5	139409	1385	286988	3757	1405	27018	1	1200
4.5	128714	1353	292205	3740	1149	28456	34	1364
5.5	140600	1404	284630	3734	1186	26406	1	1113
6.5	128844	1273	285562	3667	1170	27039	73	1137
7.5	127730	1530	280211	3120	817	25675	77	1292
8.5	128587	1288	276432	3480	1108	25170	1	1190
9.5	147676	1284	259084	3067	1339	24176	1	904
10.5	174129	1221	225064	2689	1314	19530	1	865
11.5	161376	1547	263816	3190	1289	23465	35	918
12.5	159820	1400	249518	3132	1078	22850	1	1024
13.5	151085	1621	270611	3370	1185	23517	24	1037
14.5	159118	1436	255310	3014	1383	22935	8	1068
15.5	125675	1556	284391	3388	1355	24567	77	1141
16.5	135947	1349	262896	3211	1086	23981	32	1058
17.5	136467	1388	262983	3535	1361	23384	1	1273
18.5	115038	1534	285216	3703	1227	24137	1	1231
19.5	139860	1178	260040	3246	1441	23122	17	859
20.5	179267	1220	232509	3050	1212	19239	8	796
21.5	170905	1243	242191	3130	1183	22532	54	970
22.5	184420	1198	223524	2914	1105	20459	1	912
23.5	161829	1335	248028	2901	1161	22546	1	1237
24.5	152963	1401	232888	2717	1154	20893	88	956
25.5	242310	903	133234	1863	949	10570	94	393
26.5	205838	880	200649	2564	1057	16952	1	743
27.5	130381	1427	287724	3627	1058	26517	1	1362
28.5	144212	1428	247816	3075	1086	21991	1	993
29.5	133258	1042	263857	3402	1084	23553	1	1024
30.5	145608	1377	256529	3173	1153	23626	1	920
31.5	128552	1424	273188	3711	1387	26121	1	1058
32.5	131408	1378	271047	3469	1389	24822	1	1014
33.5	140129	1330	251594	2930	1067	22047	30	780
34.5	132417	1317	269127	3368	1130	24556	1	1125
35.5	140784	1200	252067	2813	1040	21786	26	1004
36.5	127778	1319	272601	3411	1200	25757	1	1136
37.5	138650	1287	257105	3018	1107	23175	146	946
38.5	136619	1507	298355	3619	1448	26712	1	1141
39.5	148295	1434	254725	3162	1185	22722	1	1012
40.5	146071	1474	238541	2921	1241	20640	40	769
41.5	141868	1313	296032	3587	1374	26983	1	952
42.5	156200	1518	279270	3300	1243	25219	1	1163
43.5	140538	1384	292202	3796	1169	25031	33	1319
44.5	154705	1441	257804	3284	1314	23895	1	911
45.5	157492	1431	267601	3161	1373	24294	1	899

46.5	146335	1395	280997	3384	1261	26423	1	1078
47.5	136457	1308	268604	3123	1224	24951	109	1057
48.5	158940	1496	249201	2865	1295	23412	1	1126
49.5	119702	1221	291442	4237	1208	26027	32	1088
50.5	152745	1450	266695	3412	1438	26444	1	950
51.5	125400	1590	327428	4079	1390	31535	1	1413
52.5	133982	1604	323267	3719	1375	31797	1	1449
53.5	146655	1364	264546	3008	1104	23366	68	917
54.5	142245	1519	291772	3395	1098	26620	1	1287
55.5	128394	1594	293552	3258	1164	26896	1	960
56.5	140750	1664	283378	3470	1059	24205	1	1305
57.5	133449	1514	309852	3729	1171	30336	1	1470
58.5	146357	1733	249352	2944	1248	24361	14	1145
59.5	142039	1337	284709	3168	1292	25562	1	1260
60.5	137375	1582	290323	3223	1445	24675	116	988
61.5	151447	1595	285105	3285	1136	24825	1	1053
62.5	135472	1357	282623	3126	1167	26403	20	1019
63.5	134719	1449	292298	3355	1364	27129	1	1140
64.5	153079	1233	241444	2676	1436	21607	1	782
65.5	142696	1274	273760	3672	1109	25647	1	829
66.5	149713	1643	283578	3456	1137	26801	29	1207
67.5	152070	1532	297439	3536	1277	28721	12	1126
68.5	153819	1488	279547	3476	1176	25125	1	1075
69.5	160316	1400	268614	3314	1334	25341	1	1055
70.5	152560	1287	263675	3177	1195	23628	12	861
71.5	158558	1391	282882	3320	1281	27550	1	876

Appendix Table 7.2.2: Vaovai elemental ratios used in this analysis. Ratios are between marine-derived elements relative to terrestrially-dominant iron (Fe), manganese (Mn) and titanium (Ti).

Depth (cm)	Ca/Fe	Ca/Mn	Ca/Ti	S/Fe	S/Mn	S/Ti
0.5	0.99993	77.91329	11.01562	0.00000	0.00033	0.00005
1.5	0.51966	40.39662	5.57046	0.00000	0.00028	0.00004
2.5	0.41541	34.71186	4.28181	0.00000	0.00027	0.00003
3.5	0.48577	37.10647	5.15986	0.00000	0.00027	0.00004
4.5	0.44049	34.41551	4.52326	0.00012	0.00909	0.00119
5.5	0.49397	37.65399	5.32455	0.00000	0.00027	0.00004
6.5	0.45119	35.13608	4.76512	0.00026	0.01991	0.00270
7.5	0.45584	40.93910	4.97488	0.00027	0.02468	0.00300
8.5	0.46517	36.95029	5.10874	0.00000	0.00029	0.00004
9.5	0.56999	48.14998	6.10837	0.00000	0.00033	0.00004
10.5	0.77369	64.75604	8.91598	0.00000	0.00037	0.00005
11.5	0.61170	50.58809	6.87731	0.00013	0.01097	0.00149
12.5	0.64051	51.02810	6.99431	0.00000	0.00032	0.00004
13.5	0.55831	44.83234	6.42450	0.00009	0.00712	0.00102
14.5	0.62323	52.79297	6.93778	0.00003	0.00265	0.00035
15.5	0.44191	37.09416	5.11560	0.00027	0.02273	0.00313
16.5	0.51711	42.33790	5.66895	0.00012	0.00997	0.00133
17.5	0.51892	38.60453	5.83591	0.00000	0.00028	0.00004
18.5	0.40334	31.06616	4.76604	0.00000	0.00027	0.00004
19.5	0.53784	43.08688	6.04878	0.00007	0.00524	0.00074

20.5	0.77101	58.77607	9.31790	0.00003	0.00262	0.00042
21.5	0.70566	54.60224	7.58499	0.00022	0.01725	0.00240
22.5	0.82506	63.28758	9.01413	0.00000	0.00034	0.00005
23.5	0.65246	55.78387	7.17773	0.00000	0.00034	0.00004
24.5	0.65681	56.29849	7.32126	0.00038	0.03239	0.00421
25.5	1.81868	130.06441	22.92431	0.00071	0.05046	0.00889
26.5	1.02586	80.28003	12.14240	0.00000	0.00039	0.00006
27.5	0.45315	35.94734	4.91688	0.00000	0.00028	0.00004
28.5	0.58193	46.89821	6.55777	0.00000	0.00033	0.00005
29.5	0.50504	39.17049	5.65779	0.00000	0.00029	0.00004
30.5	0.56761	45.88969	6.16304	0.00000	0.00032	0.00004
31.5	0.47056	34.64080	4.92140	0.00000	0.00027	0.00004
32.5	0.48482	37.88066	5.29401	0.00000	0.00029	0.00004
33.5	0.55696	47.82560	6.35592	0.00012	0.01024	0.00136
34.5	0.49202	39.31621	5.39245	0.00000	0.00030	0.00004
35.5	0.55852	50.04764	6.46213	0.00010	0.00924	0.00119
36.5	0.46874	37.46057	4.96090	0.00000	0.00029	0.00004
37.5	0.53927	45.94102	5.98274	0.00057	0.04838	0.00630
38.5	0.45791	37.75048	5.11452	0.00000	0.00028	0.00004
39.5	0.58218	46.89911	6.52649	0.00000	0.00032	0.00004
40.5	0.61235	50.00719	7.07708	0.00017	0.01369	0.00194
41.5	0.47923	39.55060	5.25768	0.00000	0.00028	0.00004
42.5	0.55932	47.33333	6.19374	0.00000	0.00030	0.00004
43.5	0.48096	37.02266	5.61456	0.00011	0.00869	0.00132
44.5	0.60009	47.10871	6.47437	0.00000	0.00030	0.00004
45.5	0.58853	49.82347	6.48275	0.00000	0.00032	0.00004
46.5	0.52077	43.24320	5.53817	0.00000	0.00030	0.00004
47.5	0.50802	43.69420	5.46900	0.00041	0.03490	0.00437
48.5	0.63780	55.47644	6.78883	0.00000	0.00035	0.00004
49.5	0.41072	28.25159	4.59915	0.00011	0.00755	0.00123
50.5	0.57273	44.76700	5.77617	0.00000	0.00029	0.00004
51.5	0.38298	30.74283	3.97653	0.00000	0.00025	0.00003
52.5	0.41446	36.02635	4.21367	0.00000	0.00027	0.00003
53.5	0.55436	48.75499	6.27643	0.00026	0.02261	0.00291
54.5	0.48752	41.89838	5.34354	0.00000	0.00029	0.00004
55.5	0.43738	39.40884	4.77372	0.00000	0.00031	0.00004
56.5	0.49669	40.56196	5.81491	0.00000	0.00029	0.00004
57.5	0.43069	35.78681	4.39903	0.00000	0.00027	0.00003
58.5	0.58695	49.71365	6.00784	0.00006	0.00476	0.00057
59.5	0.49889	44.83554	5.55665	0.00000	0.00032	0.00004
60.5	0.47318	42.62333	5.56738	0.00040	0.03599	0.00470
61.5	0.53120	46.10259	6.10058	0.00000	0.00030	0.00004
62.5	0.47934	43.33717	5.13093	0.00007	0.00640	0.00076
63.5	0.46090	40.15469	4.96587	0.00000	0.00030	0.00004
64.5	0.63401	57.20441	7.08469	0.00000	0.00037	0.00005
65.5	0.52124	38.86057	5.56385	0.00000	0.00027	0.00004
66.5	0.52794	43.31973	5.58610	0.00010	0.00839	0.00108
67.5	0.51126	43.00622	5.29473	0.00004	0.00339	0.00042
68.5	0.55024	44.25173	6.12215	0.00000	0.00029	0.00004
69.5	0.59683	48.37538	6.32635	0.00000	0.00030	0.00004
70.5	0.57859	48.02014	6.45675	0.00005	0.00378	0.00051
71.5	0.56051	47.75843	5.75528	0.00000	0.00030	0.00004

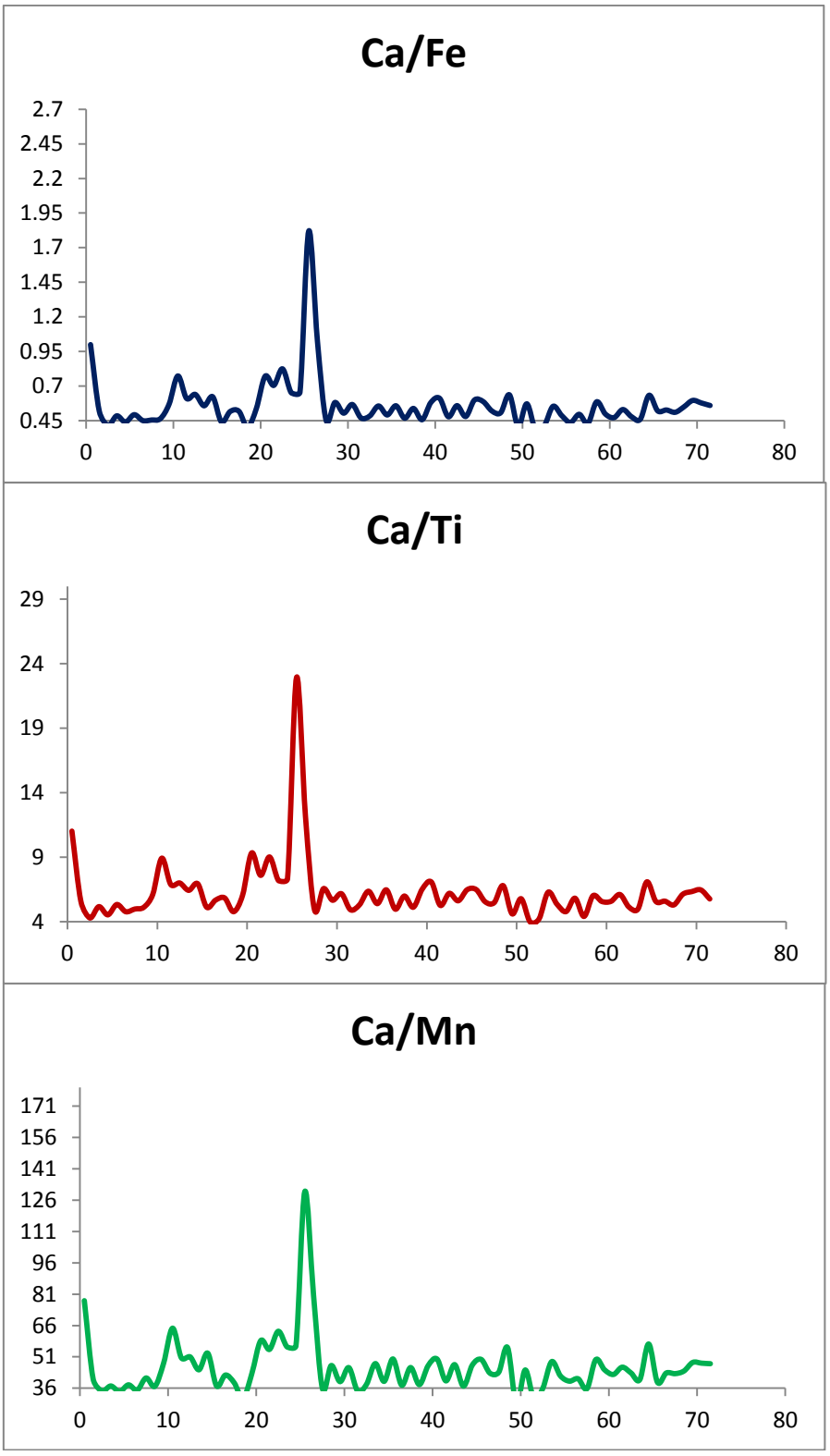
Ca/Fe
2.7
2.45
2.2
1.95
1.7
1.45
1.2
0.95
0.7
0.45
0
10
20
30
40
50
60
70
80
Ca/Ti
29
24
19
14
9
4
0
10
20
30
40
50
60
70
80
Ca/Mn
171
156
141
126
111
96
81
66
51
36
0
10
20
30
40
50
60
70
80

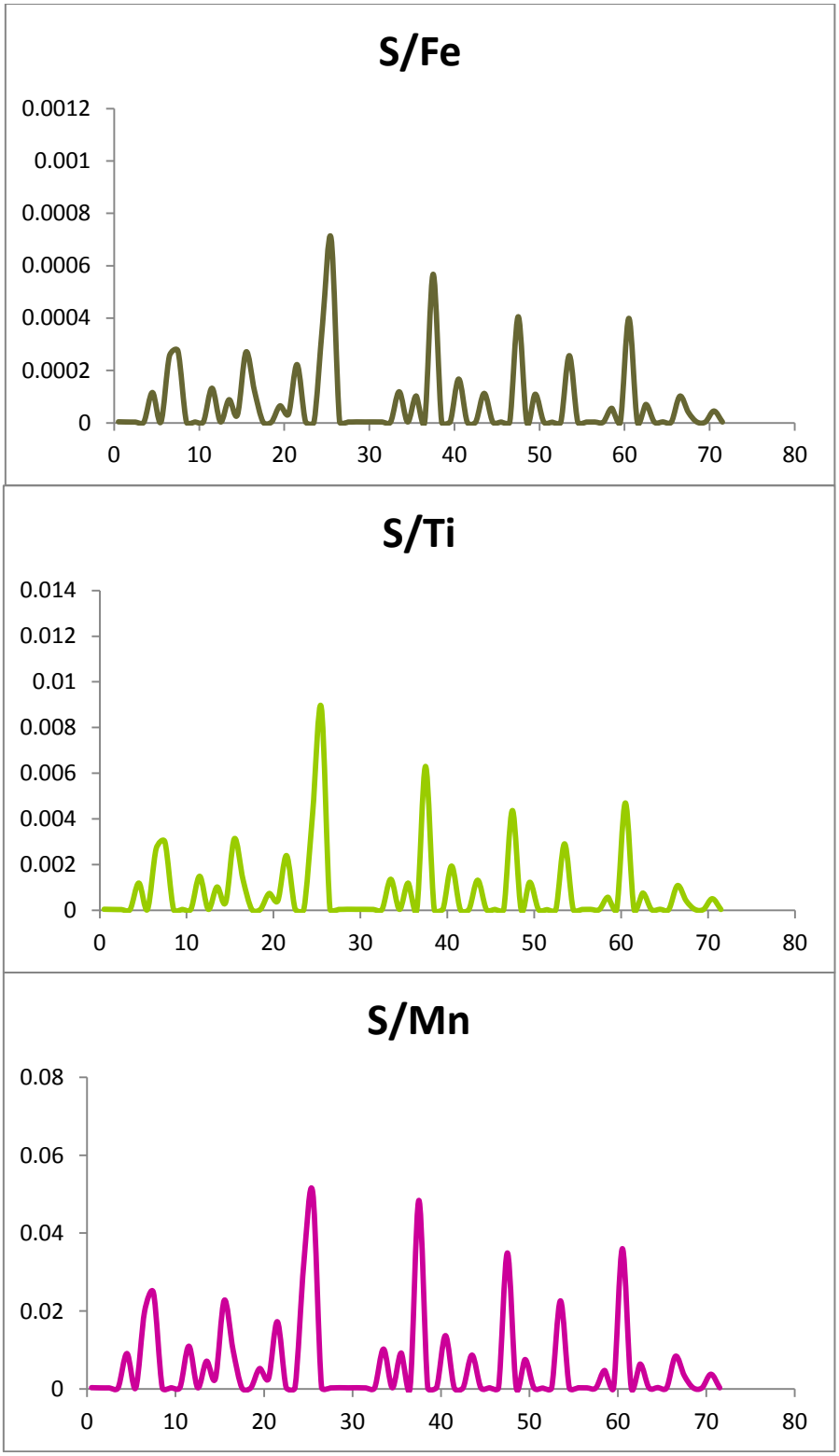

Appendix Figure 7.2: Vaovai pXRF data curves.

Appendix 7.3: Mulivai pXRF data.

Appendix Table 7.3.1: Processed pXRF data of detected elements at Mulivai; processed using ARTAX software developed by Bruker Elemenetal Inc.

Depth (cm)	Ca	Fe	Mn	S	Sr	Ti	V
5	345134	30174	907	249	167	2465	208
17	93519	153421	2591	341	147	13972	725
26	172392	170486	3594	237	202	16629	812
33	352350	37890	877	70	680	2829	120
38	207575	361921	5109	1	408	43545	1459
60	287271	19509	724	11	392	1509	135
83	223196	21565	725	28	278	1659	67
93	22306	75738	1029	955	460	13967	1043
102	356488	44101	784	572	103	4190	171
104	321032	43434	976	205	460	3322	120

Appendix Table 7.3.2: Mulivai elemental ratios used in this analysis. Ratios are between marine-derived elements relative to terrestrially-dominant iron (Fe), manganese (Mn) and titanium (Ti).

Depth (cm)	Ca/Fe	Ca/Mn	Ca/Ti	S/Fe	S/Ti	S/Mn	Sr/Fe	Sr/Ti	Sr/Mn
5	11.438	380.523	140.014	0.008	0.101	0.275	0.006	0.068	0.184
17	0.610	36.094	6.693	0.002	0.024	0.132	0.001	0.011	0.057
26	1.011	47.967	10.367	0.001	0.014	0.066	0.001	0.012	0.056
33	9.299	401.767	124.549	0.002	0.025	0.080	0.018	0.240	0.775
38	0.574	40.629	4.767	0.000	0.000	0.000	0.001	0.009	0.080
60	14.725	396.783	190.372	0.001	0.007	0.015	0.020	0.260	0.541
83	10.350	307.857	134.536	0.001	0.017	0.039	0.013	0.168	0.383
93	0.295	21.677	1.597	0.013	0.068	0.928	0.006	0.033	0.447
102	8.083	454.704	85.081	0.013	0.137	0.730	0.002	0.025	0.131
104	7.391	328.926	96.638	0.005	0.062	0.210	0.011	0.138	0.471

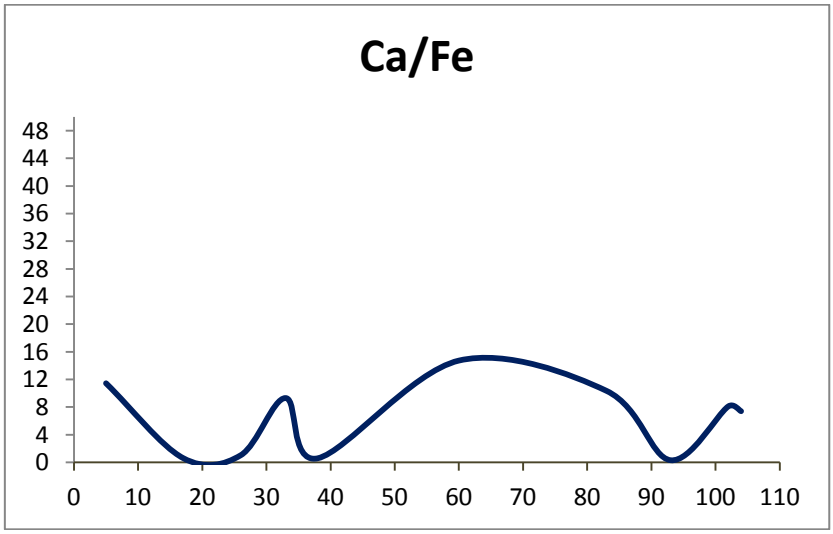

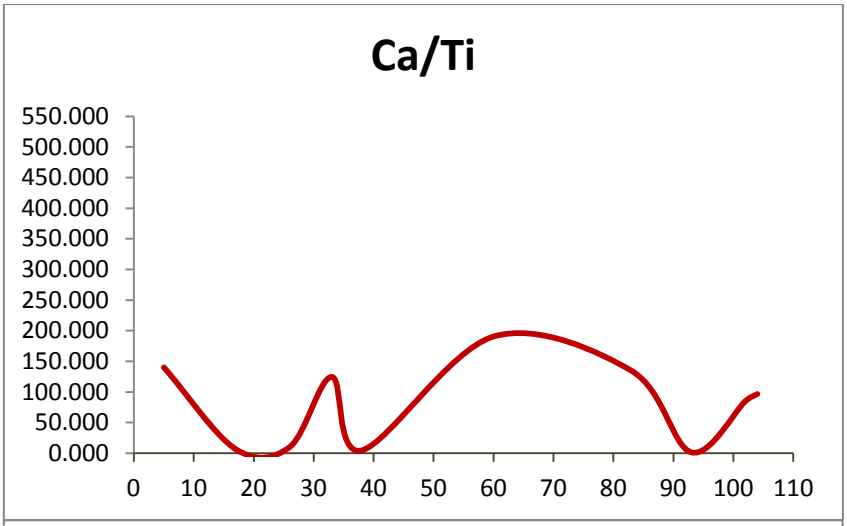
Ca/Ti
550.000
500.000
450.000
400.000
350.000
300.000
250.000
200.000
150.000
100.000
50.000
0.000
0
10
20
30
40
50
60
70
80
90
100
110

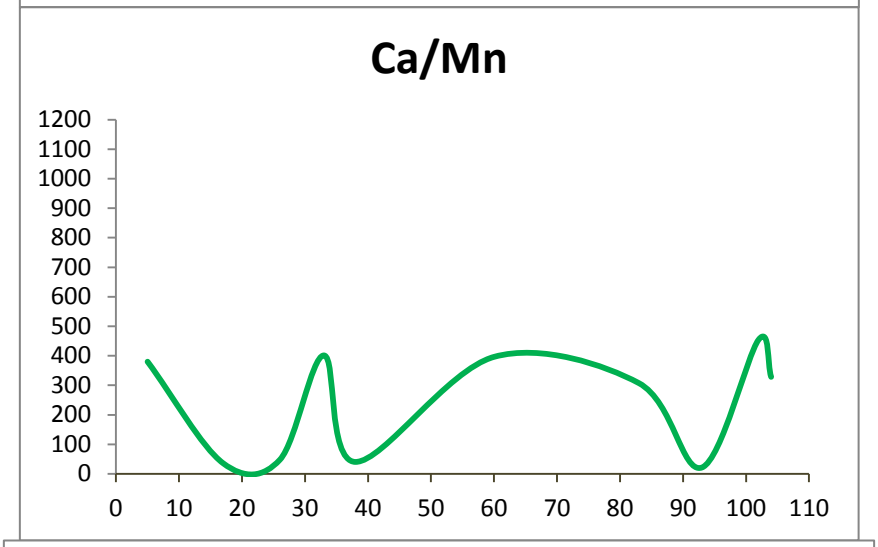
Ca/Mn
1200
1100
1000
900
800
700
600
500
400
300
200
100
0
0
10
20
30
40
50
60
70
80
90
100
110

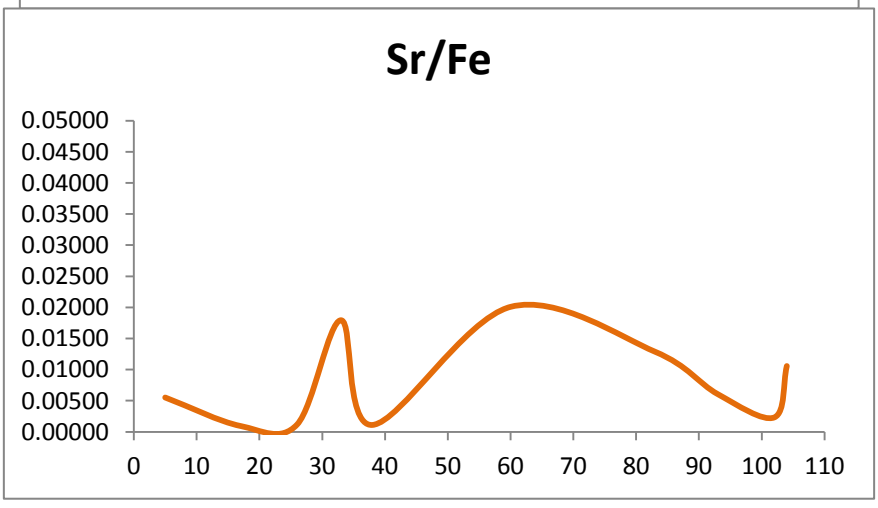
Sr/Fe
0.05000
0.04500
0.04000
0.03500
0.03000
0.02500
0.02000
0.01500
0.01000
0.00500
0.00000
0
10
20
30
40
50
60
70
80
90
100
110

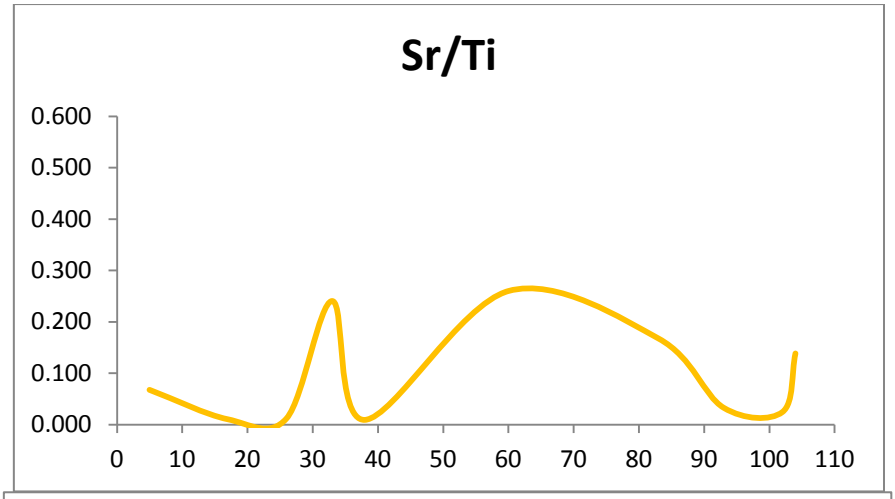
Sr/Ti
0.600
0.500
0.400
0.300
0.200
0.100
0.000
0 10 20 30 40 50 60 70 80 90 100 110

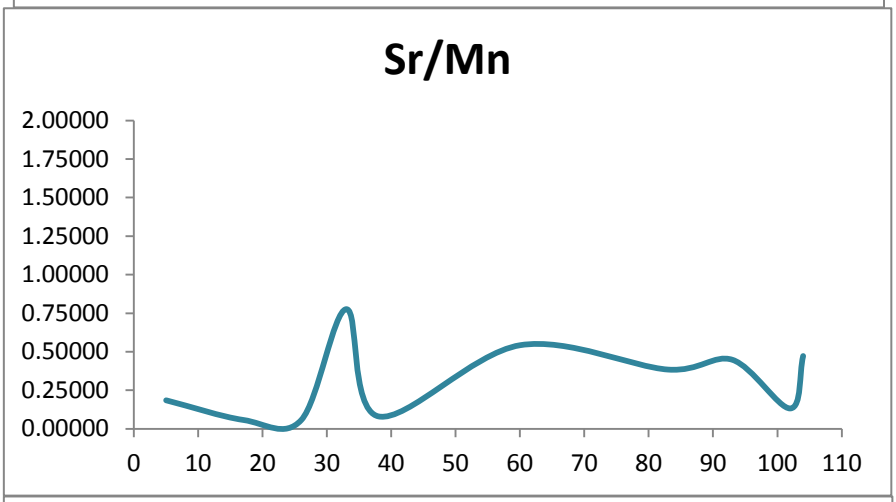
Sr/Mn
2.00000
1.75000
1.50000
1.25000
1.00000
0.75000
0.50000
0.25000
0.00000
0 10 20 30 40 50 60 70 80 90 100 110

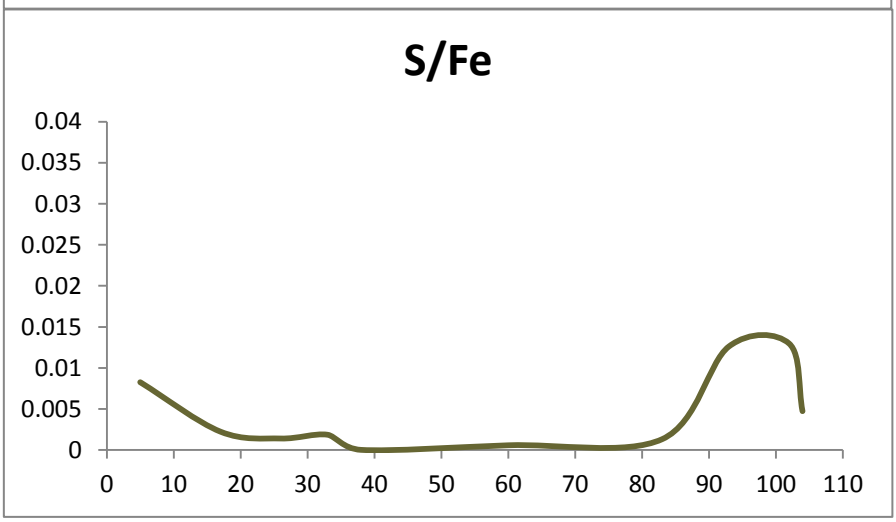
S/Fe
0.04
0.035
0.03
0.025
0.02
0.015
0.01
0.005
0
0 10 20 30 40 50 60 70 80 90 100 110

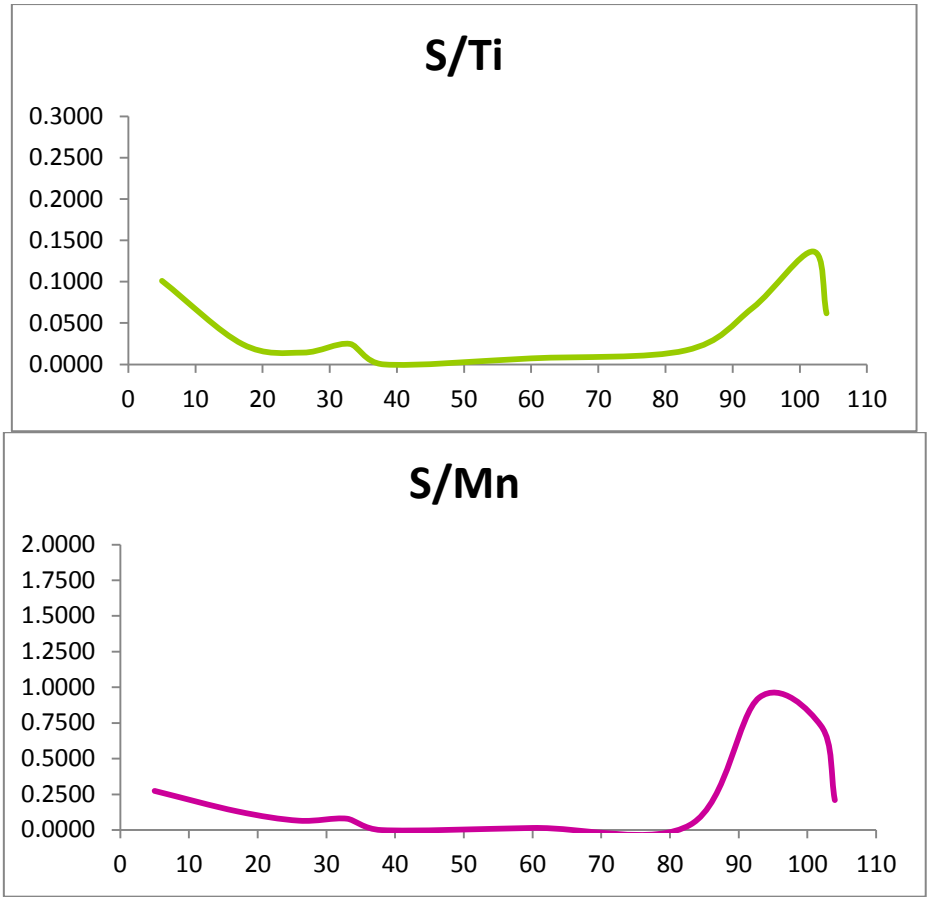

Appendix Figure 7.3: Mulivai pXRF data curves.

Appendix 7.4: Manono pXRF data.

Appendix Table 7.4.1: Processed pXRF data of detected elements at Manono; processed using ARTAX software developed by Bruker Elemenetal Inc.

Depth (cm)	Ca	Cr	Cu	Fe	Mn	Ni	S	Ti	V
1	25980	1567	637	146504	1900	1174	1640	24132	1082
6	4443	1476	371	190942	2176	928	2250	40544	1576
11	3962	1587	869	103863	1487	1463	2433	25553	1286
16	3887	1185	1025	65251	1072	1753	2485	17038	538
21	3244	1157	797	59697	668	1595	2121	8318	387
26	4068	1300	577	61917	1034	1488	2416	17755	598
31	4885	1334	1044	42344	879	2046	2357	13763	405
36	5382	1163	1012	29141	988	1853	2290	9280	329
41	5049	1465	901	52855	937	1632	2011	9062	549
46	7114	1199	940	29494	773	1825	1763	3838	290
51	5571	1090	1013	30938	764	2024	1637	3534	217
56	4691	1243	1327	29547	757	1914	1733	1861	81
61	9212	1435	655	35171	882	1540	2005	6334	265
66	7888	1455	1055	20222	926	1953	663	1769	245
71	6537	1141	949	14849	615	1796	391	731	63
76	7685	1075	986	13982	864	1890	653	856	155
81	8641	1326	1206	14361	743	1989	907	568	60
86	8359	1256	1199	16957	847	2022	1056	690	136
91	7585	867	1104	16183	720	1860	1741	2115	1
96	7980	1405	926	47068	1145	1418	2052	19707	735
101	8018	1269	887	50053	1170	1570	2268	20194	651
106	7063	1076	1161	22532	685	1791	1522	5658	43
111	7415	1037	1215	15853	822	2090	1888	803	36
116	4313	1291	1158	14311	418	2122	1403	750	111
121	5930	1706	855	29508	791	1801	2288	10377	524
126	6216	1196	932	60166	910	1571	3178	13065	347
131	5787	1073	762	39287	924	1835	2363	5136	177
136	7123	1154	795	87128	1135	1406	3483	14473	433
141	9641	1322	792	77650	1206	1732	4248	12830	527
146	6822	975	1190	58125	850	1491	3489	9247	67
151	9827	1251	955	84847	1324	1752	4526	15409	703
156	9434	1228	706	89192	1455	1377	3916	16541	765
161	9696	1316	852	89890	1339	1394	4320	17675	801
166	9622	1221	832	81697	1385	1406	4359	17215	837
171	10031	1541	852	82038	1390	1496	3804	16925	783
176	11879	1324	636	88128	1095	1453	5587	15503	666
181	11093	1538	619	94180	1455	1313	4794	18249	812
186	11627	1207	682	91334	1482	1383	4291	18590	572
191	10917	1341	572	100682	1506	1304	5621	16575	706
196	4756	1401	741	257613	1521	1247	11111	9609	449
201	6787	1156	785	73700	934	1578	5576	7725	463
206	6832	944	860	73323	927	1410	6193	6814	1
211	5603	932	517	147759	1134	997	5235	5032	165
216	11231	1196	495	96268	1174	1293	6923	3448	299
221	8678	846	944	86093	913	1215	6950	2788	1
226	9667	1170	707	109270	1386	1262	6931	6507	325

231	7300	1081	206	184256	1441	860	7796	2239	345
236	9574	1430	599	106906	1260	1462	7000	2532	345
241	8378	1391	830	55457	1248	1761	4739	3677	313
246	7428	2361	509	185237	2440	1007	3645	79259	2962

Appendix Table 7.4.2: Manono elemental ratios used in this analysis. Ratios are between marine-derived elements relative to terrestrially-dominant iron (Fe), manganese (Mn) and titanium (Ti).

Depth (cm)	Ca/Fe	Ca/Mn	Ca/Ti	S/Fe	S/Ti	S/Mn
1	0.177	13.674	1.077	0.011	0.068	0.863
6	0.023	2.042	0.110	0.012	0.055	1.034
11	0.038	2.664	0.155	0.023	0.095	1.636
16	0.060	3.626	0.228	0.038	0.146	2.318
21	0.054	4.856	0.390	0.036	0.255	3.175
26	0.066	3.934	0.229	0.039	0.136	2.337
31	0.115	5.557	0.355	0.056	0.171	2.681
36	0.185	5.447	0.580	0.079	0.247	2.318
41	0.096	5.388	0.557	0.038	0.222	2.146
46	0.241	9.203	1.854	0.060	0.459	2.281
51	0.180	7.292	1.576	0.053	0.463	2.143
56	0.159	6.197	2.521	0.059	0.931	2.289
61	0.262	10.444	1.454	0.057	0.317	2.273
66	0.390	8.518	4.459	0.033	0.375	0.716
71	0.440	10.629	8.943	0.026	0.535	0.636
76	0.550	8.895	8.978	0.047	0.763	0.756
81	0.602	11.630	15.213	0.063	1.597	1.221
86	0.493	9.869	12.114	0.062	1.530	1.247
91	0.469	10.535	3.586	0.108	0.823	2.418
96	0.170	6.969	0.405	0.044	0.104	1.792
101	0.160	6.853	0.397	0.045	0.112	1.938
106	0.313	10.311	1.248	0.068	0.269	2.222
111	0.468	9.021	9.234	0.119	2.351	2.297
116	0.301	10.318	5.751	0.098	1.871	3.356
121	0.201	7.497	0.571	0.078	0.220	2.893
126	0.103	6.831	0.476	0.053	0.243	3.492
131	0.147	6.263	1.127	0.060	0.460	2.557
136	0.082	6.276	0.492	0.040	0.241	3.069
141	0.124	7.994	0.751	0.055	0.331	3.522
146	0.117	8.026	0.738	0.060	0.377	4.105
151	0.116	7.422	0.638	0.053	0.294	3.418
156	0.106	6.484	0.570	0.044	0.237	2.691
161	0.108	7.241	0.549	0.048	0.244	3.226
166	0.118	6.947	0.559	0.053	0.253	3.147
171	0.122	7.217	0.593	0.046	0.225	2.737
176	0.135	10.848	0.766	0.063	0.360	5.102
181	0.118	7.624	0.608	0.051	0.263	3.295
186	0.127	7.845	0.625	0.047	0.231	2.895
191	0.108	7.249	0.659	0.056	0.339	3.732
196	0.018	3.127	0.495	0.043	1.156	7.305
201	0.092	7.267	0.879	0.076	0.722	5.970
206	0.093	7.370	1.003	0.084	0.909	6.681
211	0.038	4.941	1.113	0.035	1.040	4.616

216	0.117	9.566	3.257	0.072	2.008	5.897
221	0.101	9.505	3.113	0.081	2.493	7.612
226	0.088	6.975	1.486	0.063	1.065	5.001
231	0.040	5.066	3.260	0.042	3.482	5.410
236	0.090	7.598	3.781	0.065	2.765	5.556
241	0.151	6.713	2.278	0.085	1.289	3.797
246	0.040	3.044	0.094	0.020	0.046	1.494

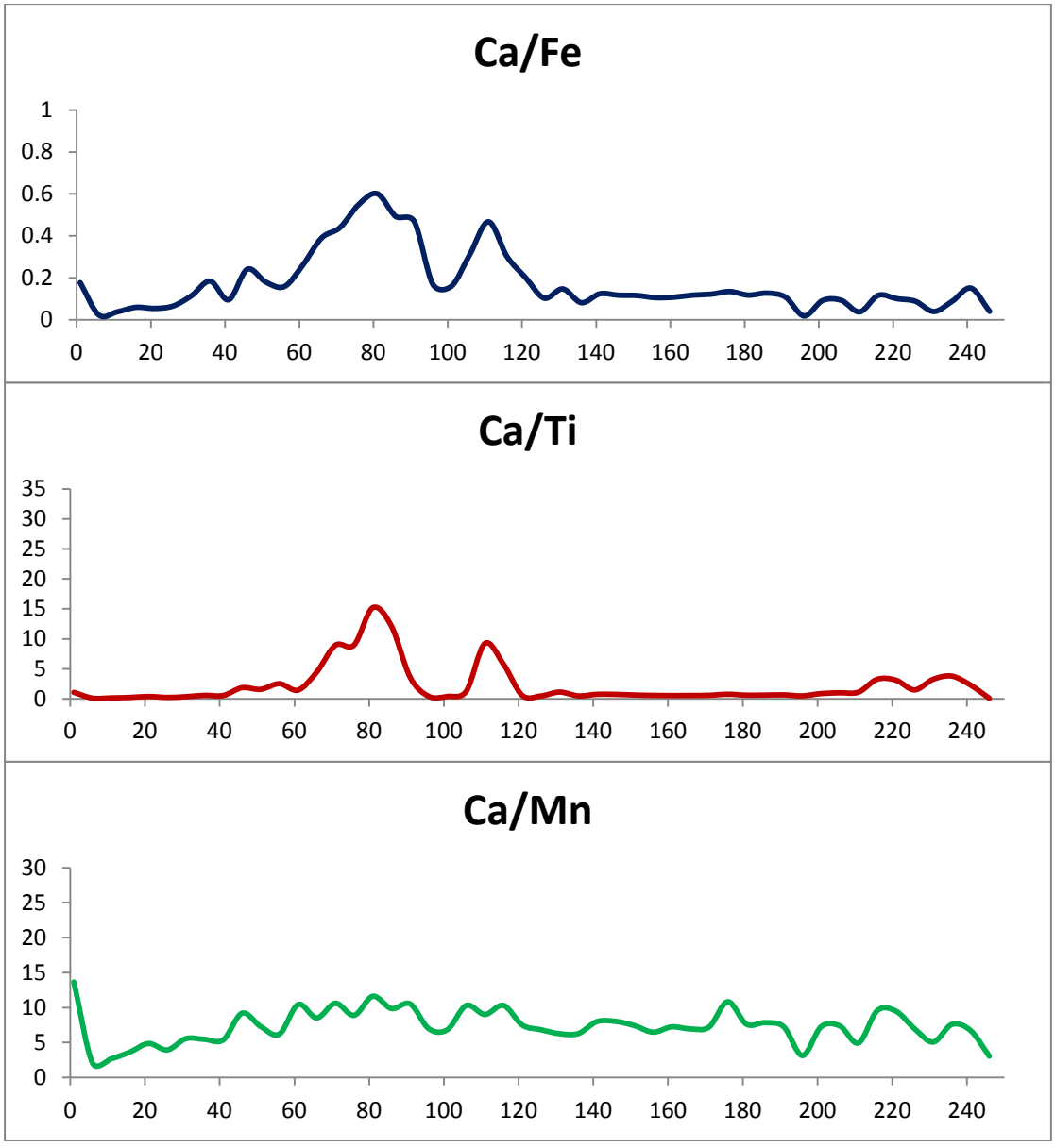

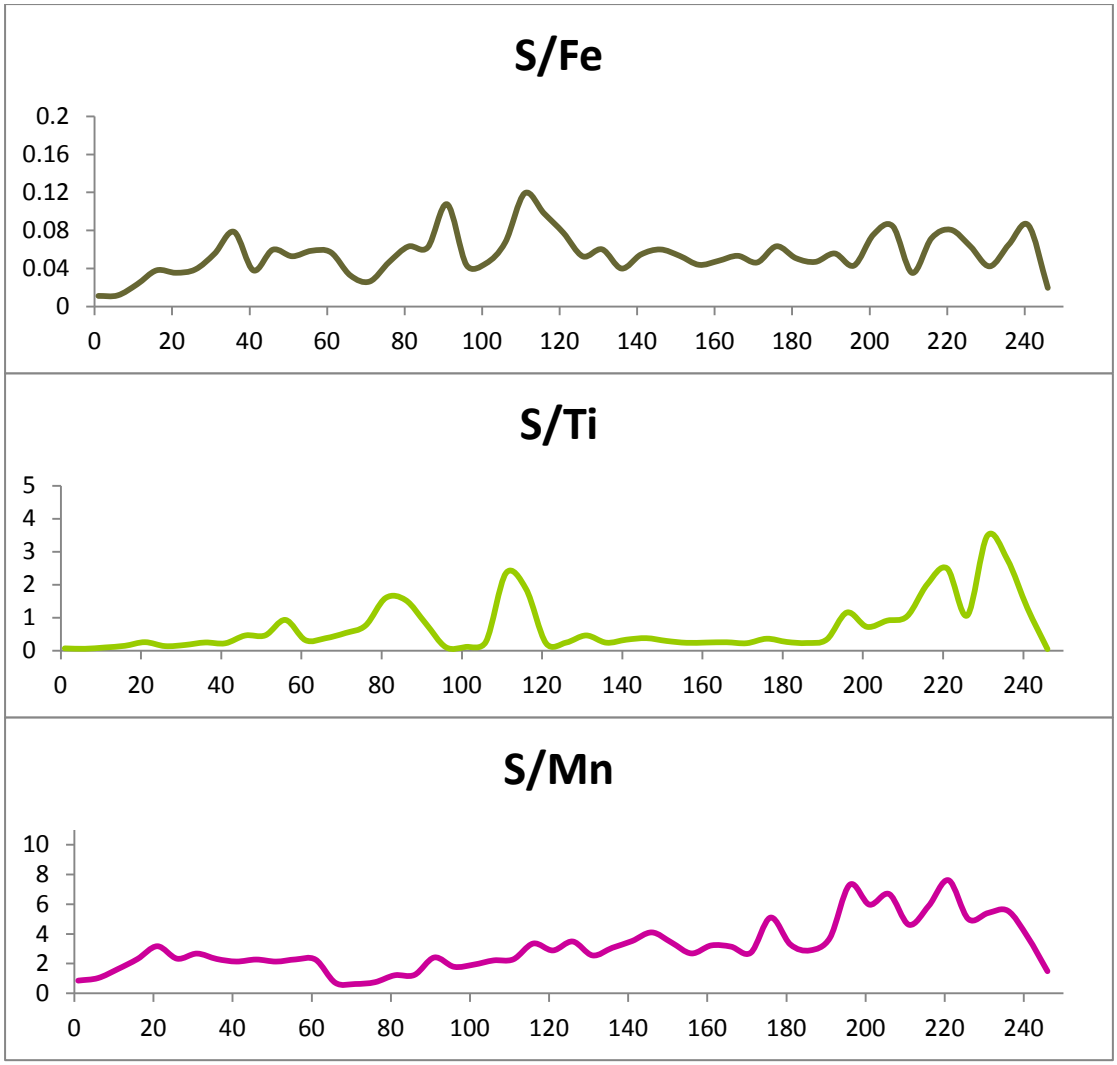

Appendix Figure 7.4: Manono pXRF data curves.

Appendix 7.5: Fagali'i pXRF data.

Appendix Table 7.5.1: Processed pXRF data of detected elements at Fagali'i; processed using ARTAX software developed by Bruker Elemenetal Inc.

Depth (cm)	Ca	Cr	Fe	Ni	S	Si	Ti	V
1	4118	2946	402185	1305	257	578	33279	1326
6	3250	3918	540186	1552	206	745	52233	2701
11	3049	3275	430889	1395	238	630	37360	1806
16	4162	1635	143750	1703	371	380	14933	382
21	3626	1682	104471	2023	389	314	9855	382
26	3428	1474	79389	1923	508	284	8894	210
31	3414	1421	56459	2302	581	322	5726	1
36	3271	1473	76216	2410	429	279	7474	197
41	3387	1425	104665	2384	447	344	9504	255
46	3985	2155	289333	1183	270	398	19725	771
51	3607	5088	709547	1354	238	1376	76427	3127
56	3192	2975	364583	1590	1124	790	33299	1741
61	6236	5628	655505	1740	202	1390	78516	3718
66	3843	4738	522442	1755	1787	1089	65593	2973
71	3392	4764	561051	1463	1830	1169	65544	3189
76	2599	5439	684252	1510	1670	1195	76564	3668
81	3257	5179	764039	1460	819	1066	69026	3226
86	3335	5598	908444	1490	306	1526	78469	3376
91	2361	7429	874807	1754	156	1881	106998	4928
96	2334	6290	874721	1654	173	1978	104166	4147
101	3729	6030	1084388	2571	500	2381	99133	3891
106	2515	6927	902641	1856	420	1771	105231	4627
111	3604	5015	972318	3340	427	2622	84638	2885
116	2074	6118	810542	1991	223	2009	100227	4783
121	2342	5497	761753	2072	162	1595	90335	3680
126	2365	6930	881892	1938	216	2268	111292	4560
131	2708	6329	915387	2000	658	2275	100925	3934
136	3548	5106	933649	2078	2183	2022	80280	3058
141	2564	6052	760131	3769	710	2833	88331	3768
146	4996	5478	966528	1506	289	1012	72230	2970
151	2339	7022	889572	2028	92	2212	110933	4831
156	2231	6405	847817	2295	1	2318	104363	4351
161	2506	6256	850420	2885	1	1607	101738	4260
166	2503	6242	800238	2396	224	2122	95358	3907
171	5670	5125	736220	828	621	1148	63409	3027
176	5658	4826	699942	1426	342	890	61859	2731
181	6287	5536	808638	1564	742	1434	79874	3443
186	7381	5883	961211	1354	217	1350	81711	3531
191	6841	5649	874943	1549	321	1519	72811	2924
196	7161	5669	888013	1425	462	1332	76051	3153
201	7298	5551	854154	1138	383	1400	82103	3245
206	7481	5612	861509	1177	545	1457	80298	3331
211	7590	5414	903471	1040	701	1524	76394	2882
216	6164	5307	821399	1356	660	1593	79783	3463
221	8690	5352	902530	1298	640	1509	70789	2803
226	7277	5017	801563	1405	635	1319	64340	2800

231	7662	5063	748888	1178	684	1615	66687	3078
236	7620	5075	697349	1269	946	1489	68970	2916
241	8840	4981	641239	1525	1157	1374	67080	2552
246	6873	4873	612363	1294	957	1279	66033	2530
251	6055	5895	801279	1574	604	1751	82151	3683
256	5775	6186	837587	1378	767	1803	78582	3799
261	6032	5849	760067	1564	856	1447	72445	3198
266	6052	4642	649962	1567	520	1246	61866	3044
271	6043	7551	782440	1673	625	1574	80661	4024
276	5813	2633	188900	1640	3468	373	15286	2073
281	6701	2499	151848	1867	2689	773	20105	1535
286	4738	1885	87087	1974	1093	626	9737	352
291	7894	2030	197437	2081	4720	209	6050	2182
296	8042	1415	114788	1803	3944	192	1512	1483
299	11143	1253	66408	2166	2282	262	3466	644

Appendix Table 7.5.2: Fagali'i elemental ratios used in this analysis. Ratios are between marine-derived elements relative to terrestrially-dominant iron (Fe), manganese (Mn) and titanium (Ti).

Depth (cm)	Ca/Fe	Ca/Ti	S/Fe	S/Ti	**Si/Fe**	**Si/Ti**
1	0.010	0.124	0.001	0.008	0.001	0.017
6	0.006	0.062	0.000	0.004	0.001	0.014
11	0.007	0.082	0.001	0.006	0.001	0.017
16	0.029	0.279	0.003	0.025	0.003	0.025
21	0.035	0.368	0.004	0.039	0.003	0.032
26	0.043	0.385	0.006	0.057	0.004	0.032
31	0.060	0.596	0.010	0.101	0.006	0.056
36	0.043	0.438	0.006	0.057	0.004	0.037
41	0.032	0.356	0.004	0.047	0.003	0.036
46	0.014	0.202	0.001	0.014	0.001	0.020
51	0.005	0.047	0.000	0.003	0.002	0.018
56	0.009	0.096	0.003	0.034	0.002	0.024
61	0.010	0.079	0.000	0.003	0.002	0.018
66	0.007	0.059	0.003	0.027	0.002	0.017
71	0.006	0.052	0.003	0.028	0.002	0.018
76	0.004	0.034	0.002	0.022	0.002	0.016
81	0.004	0.047	0.001	0.012	0.001	0.015
86	0.004	0.043	0.000	0.004	0.002	0.019
91	0.003	0.022	0.000	0.001	0.002	0.018
96	0.003	0.022	0.000	0.002	0.002	0.019
101	0.003	0.038	0.000	0.005	0.002	0.024
106	0.003	0.024	0.000	0.004	0.002	0.017
111	0.004	0.043	0.000	0.005	0.003	0.031
116	0.003	0.021	0.000	0.002	0.002	0.020
121	0.003	0.026	0.000	0.002	0.002	0.018
126	0.003	0.021	0.000	0.002	0.003	0.020
131	0.003	0.027	0.001	0.007	0.002	0.023
136	0.004	0.044	0.002	0.027	0.002	0.025
141	0.003	0.029	0.001	0.008	0.004	0.032
146	0.005	0.069	0.000	0.004	0.001	0.014
151	0.003	0.021	0.000	0.001	0.002	0.020

156	0.003	0.021	0.000	0.000	0.003	0.022
161	0.003	0.025	0.000	0.000	0.002	0.016
166	0.003	0.026	0.000	0.002	0.003	0.022
171	0.008	0.089	0.001	0.010	0.002	0.018
176	0.008	0.091	0.000	0.006	0.001	0.014
181	0.008	0.079	0.001	0.009	0.002	0.018
186	0.008	0.090	0.000	0.003	0.001	0.017
191	0.008	0.094	0.000	0.004	0.002	0.021
196	0.008	0.094	0.001	0.006	0.001	0.018
201	0.009	0.089	0.000	0.005	0.002	0.017
206	0.009	0.093	0.001	0.007	0.002	0.018
211	0.008	0.099	0.001	0.009	0.002	0.020
216	0.008	0.077	0.001	0.008	0.002	0.020
221	0.010	0.123	0.001	0.009	0.002	0.021
226	0.009	0.113	0.001	0.010	0.002	0.021
231	0.010	0.115	0.001	0.010	0.002	0.024
236	0.011	0.110	0.001	0.014	0.002	0.022
241	0.014	0.132	0.002	0.017	0.002	0.020
246	0.011	0.104	0.002	0.014	0.002	0.019
251	0.008	0.074	0.001	0.007	0.002	0.021
256	0.007	0.073	0.001	0.010	0.002	0.023
261	0.008	0.083	0.001	0.012	0.002	0.020
266	0.009	0.098	0.001	0.008	0.002	0.020
271	0.008	0.075	0.001	0.008	0.002	0.020
276	0.031	0.380	0.018	0.227	0.002	0.024
281	0.044	0.333	0.018	0.134	0.005	0.038
286	0.054	0.487	0.013	0.112	0.007	0.064
291	0.040	1.305	0.024	0.780	0.001	0.035
296	0.070	5.319	0.034	2.608	0.002	0.127
299	0.168	3.215	0.034	0.658	0.004	0.076

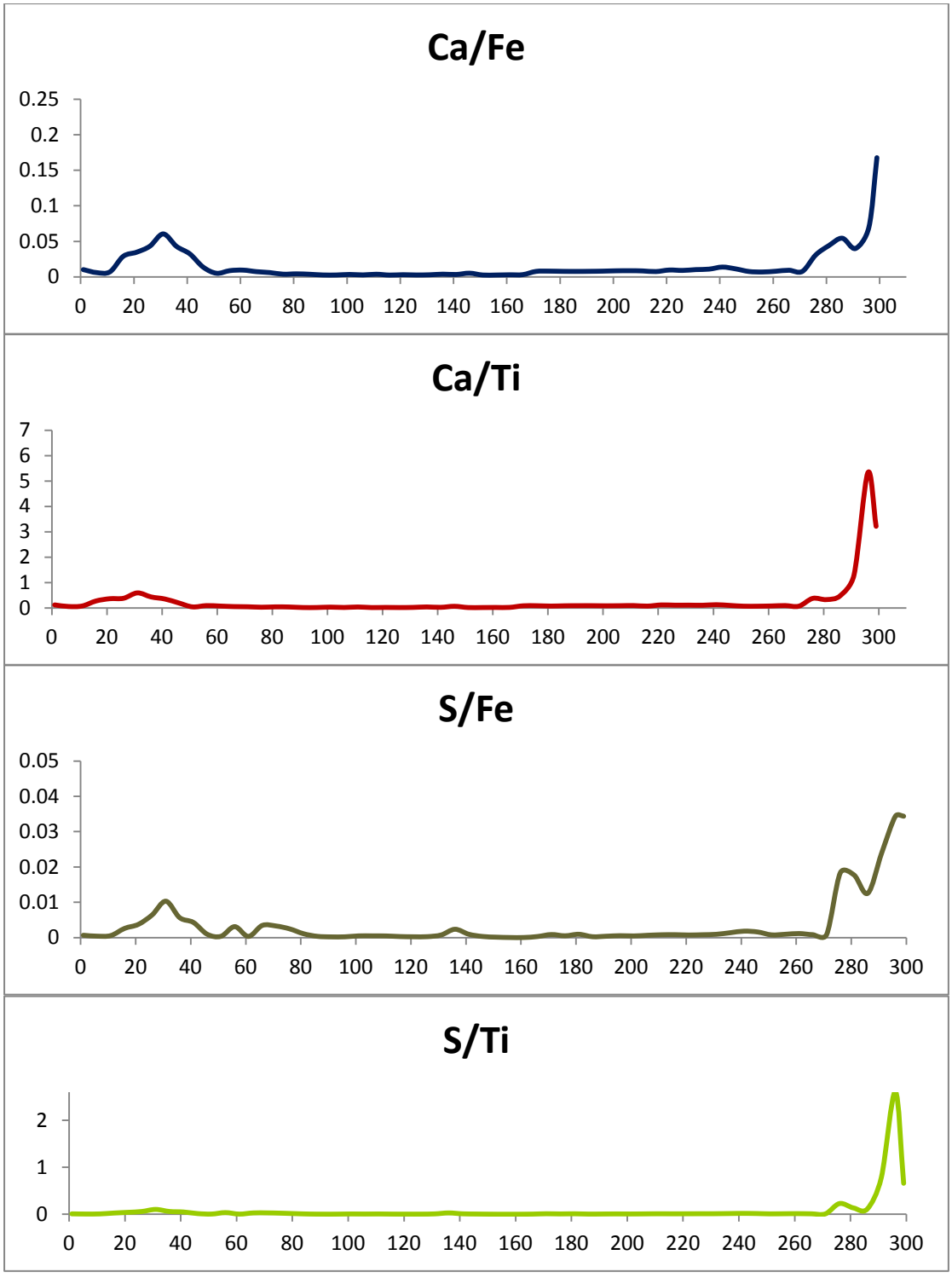
Ca/Fe
0.25
0.2
0.15
0.1
0.05
0
0 20 40 60 80 100 120 140 160 180 200 220 240 260 280 300
Ca/Ti
7
6
5
4
3
2
1
0
0 20 40 60 80 100 120 140 160 180 200 220 240 260 280 300
S/Fe
0.05
0.04
0.03
0.02
0.01
0
0 20 40 60 80 100 120 140 160 180 200 220 240 260 280 300
S/Ti
2
1
0
0 20 40 60 80 100 120 140 160 180 200 220 240 260 280 300

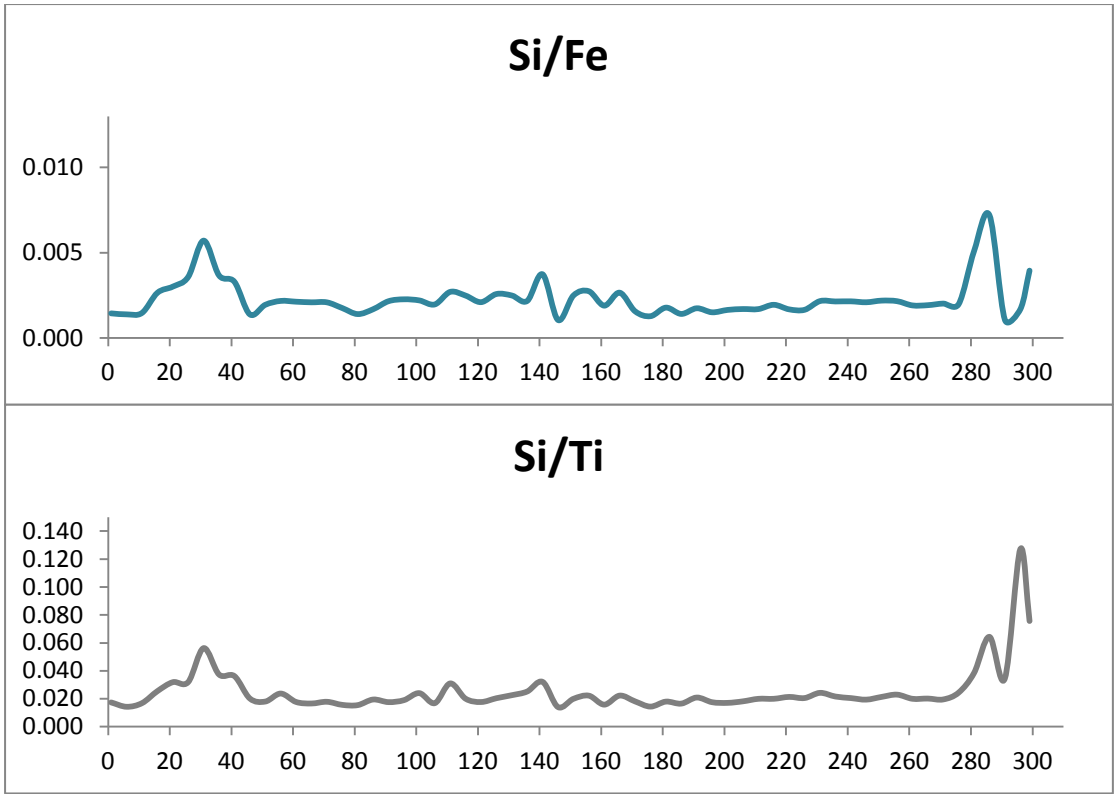

Appendix Figure 7.5: Fagali'i pXRF data curves.

Appendix 7.6: Ma'asina pXRF data.

Appendix Table 7.6.1: Processed pXRF data of detected elements at Ma'asina; processed using ARTAX software developed by Bruker Elemenetal Inc.

Depth (cm)	Ca	Fe	Mn	S	Ti	V
2	73348	1054372	15596	1	89183	9211
8	38990	480454	7003	1454	38618	4162
16	23319	584217	7441	617	51292	4945
29	50604	362224	5189	1644	23106	2746
37	123763	228479	3183	257	14379	1597
41	76329	275383	4323	621	20223	2386
45	161493	147483	3119	775	9790	1175
48	100024	250653	3976	606	16700	2004
50	252666	176474	3173	1	9928	1018
53	146738	334984	6041	234	23632	2605
55	222672	202905	4425	117	11458	1785
58	143711	260602	3992	686	17867	2184
62	123229	310784	4883	2305	23654	2836
68	170357	268134	4453	1	17762	2168
71	78789	403019	5246	849	26788	2998
73	120397	297877	4421	104	21394	2669

Appendix Table 7.6.2: Ma'asina elemental ratios used in this analysis. Ratios are between marine-derived elements relative to terrestrially-dominant iron (Fe), manganese (Mn) and titanium (Ti).

Depth (cm)	Ca/Fe	Ca/Ti	Ca/Mn	S/Fe	S/Ti	S/Mn
2	0.0696	0.8224	4.7030	0.0000	0.0000	0.0001
8	0.0812	1.0096	5.5676	0.0030	0.0377	0.2076
16	0.0399	0.4546	3.1339	0.0011	0.0120	0.0829
29	0.1397	2.1901	9.7522	0.0045	0.0712	0.3168
37	0.5417	8.6072	38.8825	0.0011	0.0179	0.0807
41	0.2772	3.7744	17.6565	0.0023	0.0307	0.1437
45	1.0950	16.4957	51.7772	0.0053	0.0792	0.2485
48	0.3991	5.9895	25.1569	0.0024	0.0363	0.1524
50	1.4317	25.4498	79.6300	0.0000	0.0001	0.0003
53	0.4380	6.2093	24.2903	0.0007	0.0099	0.0387
55	1.0974	19.4338	50.3214	0.0006	0.0102	0.0264
58	0.5515	8.0434	35.9997	0.0026	0.0384	0.1718
62	0.3965	5.2096	25.2363	0.0074	0.0974	0.4720
68	0.6353	9.5911	38.2567	0.0000	0.0001	0.0002
71	0.1955	2.9412	15.0189	0.0021	0.0317	0.1618
73	0.4042	5.6276	27.2330	0.0003	0.0049	0.0235

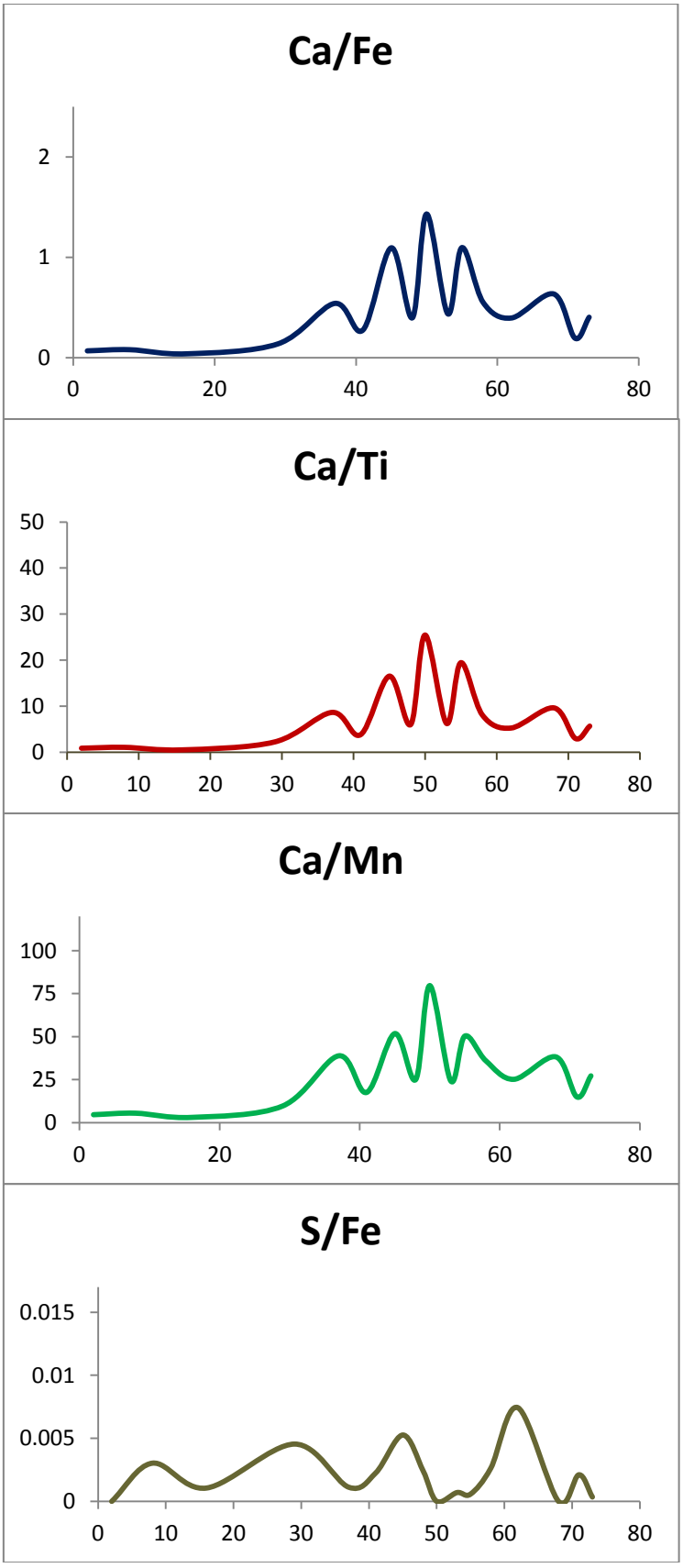
Ca/Fe
2
1
0
0
20
40
60
80
Ca/Ti
50
40
30
20
10
0
0
10
20
30
40
50
60
70
80
Ca/Mn
100
75
50
25
0
0
20
40
60
80
S/Fe
0.015
0.01
0.005
0
0
10
20
30
40
50
60
70
80

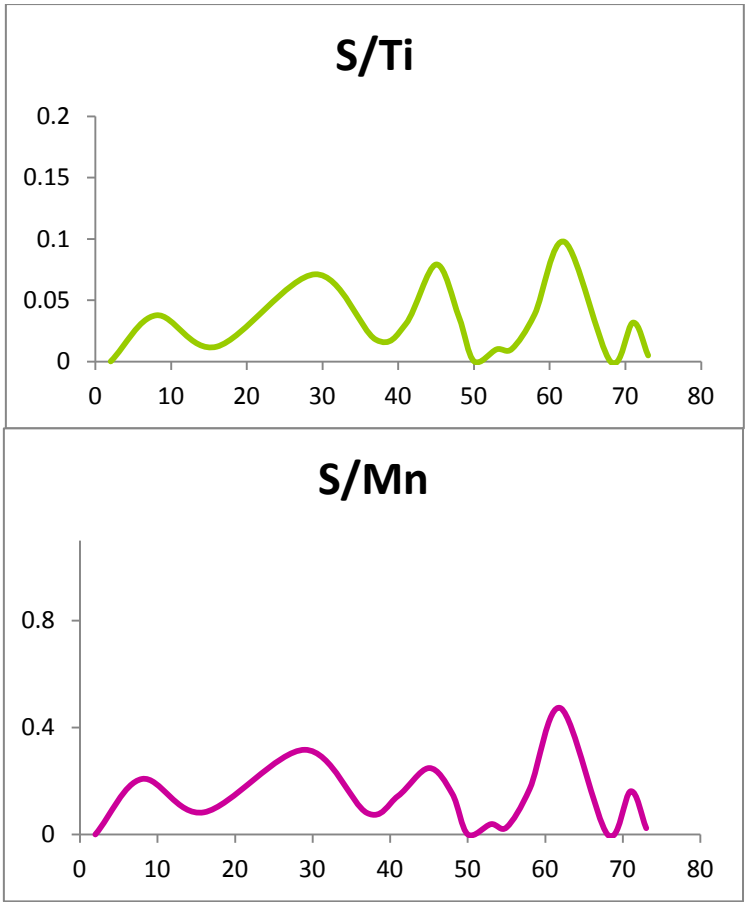

Appendix Figure 7.6: Ma'asina pXRF data curves.

Appendix 7.7: Falealupo pXRF data.

Appendix Table 7.7.1: Processed pXRF data of detected elements at Falealupo; processed using ARTAX software developed by Bruker Elemenetal Inc.

Depth (cm)	Ca	Cr	Cu	Fe	Mn	Ni	S	Si	Ti	V
0.5	184026	870	1067	16121	1018	1814	915	250	472	1
1.5	207379	747	969	13934	841	1882	731	315	593	47
2.5	252035	565	664	16650	800	1657	495	455	836	41
3.5	329890	396	386	9115	612	1559	349	362	557	33
4.5	321021	493	701	9582	610	1785	252	232	455	64
5.5	359049	589	443	7343	599	1747	406	379	376	-79
6.5	322924	646	526	11652	801	1642	197	376	529	205
7.5	359048	448	439	14105	662	1798	148	285	482	15
8.5	220638	753	688	25586	891	1707	1056	271	1364	133
9.5	263100	885	445	17030	1089	1586	704	380	941	1
10.5	315701	616	630	11927	815	1750	357	306	928	61
11.5	306191	561	576	13407	578	1508	470	315	814	101
12.5	322355	554	487	15325	613	1615	493	488	888	1
13.5	331547	653	469	17322	825	1660	565	359	1165	151
14.5	328744	676	476	19929	888	1819	687	386	1149	1
15.5	163349	1577	771	87250	1376	1706	1577	638	8069	411
16.5	131218	1644	891	87577	1421	1855	1385	655	8773	449
17.5	137319	1204	837	83551	1259	1605	1394	784	9063	413
18.5	145694	1581	891	83288	1490	1820	1127	820	8840	493
19.5	100166	1484	995	103789	1514	1632	1802	718	10609	469
21	139052	1557	855	88125	1355	1536	1409	639	10087	182
23	104731	1541	1517	84831	1292	1976	1068	586	9718	405
25	178120	1506	1306	93761	1388	1874	1504	756	9780	334
27	155057	1264	1010	73661	1265	1787	1543	504	8580	375
29	236521	1156	796	36689	854	1774	1122	499	4450	452
31	51683	2152	1436	94333	1310	2505	1697	1342	15055	799
33	28011	1941	1536	92269	893	2520	1376	1023	12446	511
35	27887	2228	1409	86307	1116	2424	1588	936	11504	847
37	29215	1831	1627	93412	1186	2362	1588	1237	14148	540
39	24841	2196	1500	85747	1311	2638	1465	1203	12942	657
41	28410	1945	1396	83068	1162	2346	1526	679	7000	441
43	23978	1828	1333	71906	1067	2523	1672	725	8539	519
45	29267	1815	1685	76794	1014	2298	1784	885	9713	600
47	20570	1801	1750	63416	738	2437	1829	649	7068	531
49	17496	1519	1871	67602	703	2395	1521	676	9123	275

Appendix Table 7.7.2: Falealupo elemental ratios used in this analysis. Ratios are between marine-derived elements relative to terrestrially-dominant iron (Fe), manganese (Mn) and titanium (Ti).

Depth (cm)	Ca/Ti	Ca/Fe	Ca/Mn	Si/Fe	Si/Ti	Si/Mn	S/Fe	S/Ti	S/Mn
0.5	389.886	11.415	180.772	0.016	0.530	0.246	0.057	1.939	0.899
1.5	349.712	14.883	246.586	0.023	0.531	0.375	0.052	1.233	0.869
2.5	301.477	15.137	315.044	0.027	0.544	0.569	0.030	0.592	0.619
3.5	592.262	36.192	539.036	0.040	0.650	0.592	0.038	0.627	0.570
4.5	705.541	33.503	526.264	0.024	0.510	0.380	0.026	0.554	0.413
5.5	954.918	48.897	599.414	0.052	1.008	0.633	0.055	1.080	0.678

6.5	610.442	27.714	403.151	0.032	0.711	0.469	0.017	0.372	0.246
7.5	744.913	25.455	542.369	0.020	0.591	0.431	0.010	0.307	0.224
8.5	161.758	8.623	247.630	0.011	0.199	0.304	0.041	0.774	1.185
9.5	279.596	15.449	241.598	0.022	0.404	0.349	0.041	0.748	0.646
10.5	340.195	26.469	387.363	0.026	0.330	0.375	0.030	0.385	0.438
11.5	376.156	22.838	529.742	0.023	0.387	0.545	0.035	0.577	0.813
12.5	363.012	21.035	525.865	0.032	0.550	0.796	0.032	0.555	0.804
13.5	284.590	19.140	401.875	0.021	0.308	0.435	0.033	0.485	0.685
14.5	286.113	16.496	370.207	0.019	0.336	0.435	0.034	0.598	0.774
15.5	20.244	1.872	118.713	0.007	0.079	0.464	0.018	0.195	1.146
16.5	14.957	1.498	92.342	0.007	0.075	0.461	0.016	0.158	0.975
17.5	15.152	1.644	109.070	0.009	0.087	0.623	0.017	0.154	1.107
18.5	16.481	1.749	97.781	0.010	0.093	0.550	0.014	0.127	0.756
19.5	9.442	0.965	66.160	0.007	0.068	0.474	0.017	0.170	1.190
21	13.785	1.578	102.621	0.007	0.063	0.472	0.016	0.140	1.040
23	10.777	1.235	81.061	0.007	0.060	0.454	0.013	0.110	0.827
25	18.213	1.900	128.329	0.008	0.077	0.545	0.016	0.154	1.084
27	18.072	2.105	122.575	0.007	0.059	0.398	0.021	0.180	1.220
29	53.151	6.447	276.957	0.014	0.112	0.584	0.031	0.252	1.314
31	3.433	0.548	39.453	0.014	0.089	1.024	0.018	0.113	1.295
33	2.251	0.304	31.367	0.011	0.082	1.146	0.015	0.111	1.541
35	2.424	0.323	24.988	0.011	0.081	0.839	0.018	0.138	1.423
37	2.065	0.313	24.633	0.013	0.087	1.043	0.017	0.112	1.339
39	1.919	0.290	18.948	0.014	0.093	0.918	0.017	0.113	1.117
41	4.059	0.342	24.449	0.008	0.097	0.584	0.018	0.218	1.313
43	2.808	0.333	22.472	0.010	0.085	0.679	0.023	0.196	1.567
45	3.013	0.381	28.863	0.012	0.091	0.873	0.023	0.184	1.759
47	2.910	0.324	27.873	0.010	0.092	0.879	0.029	0.259	2.478
49	1.918	0.259	24.888	0.010	0.074	0.962	0.022	0.167	2.164

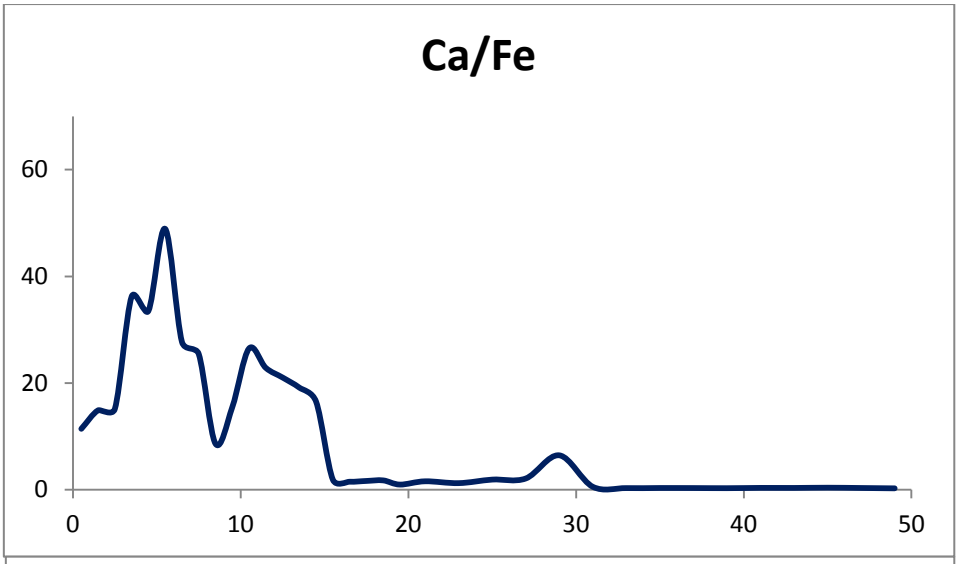
Ca/Fe
60
40
20
0
0
10
20
30
40
50

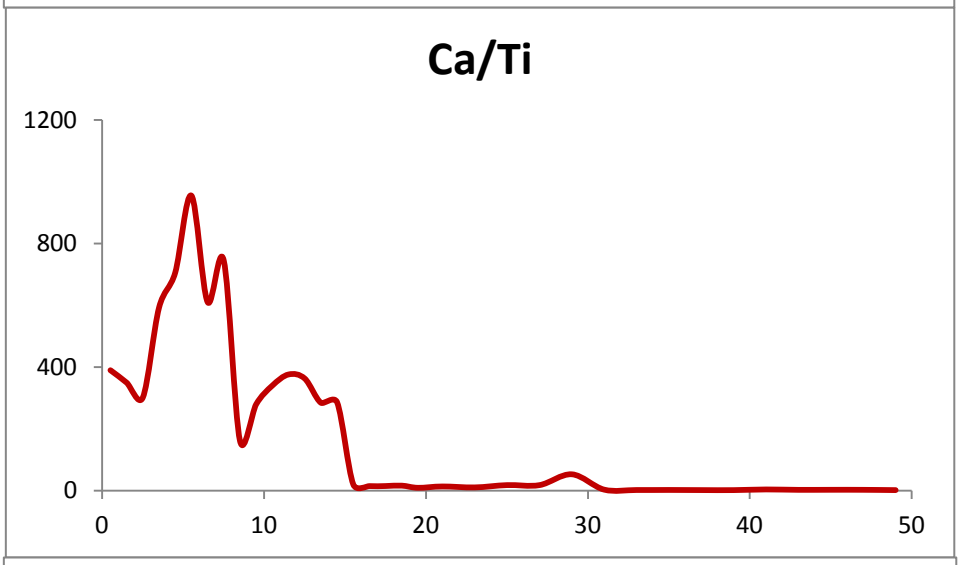
Ca/Ti
1200
800
400
0
0
10
20
30
40
50

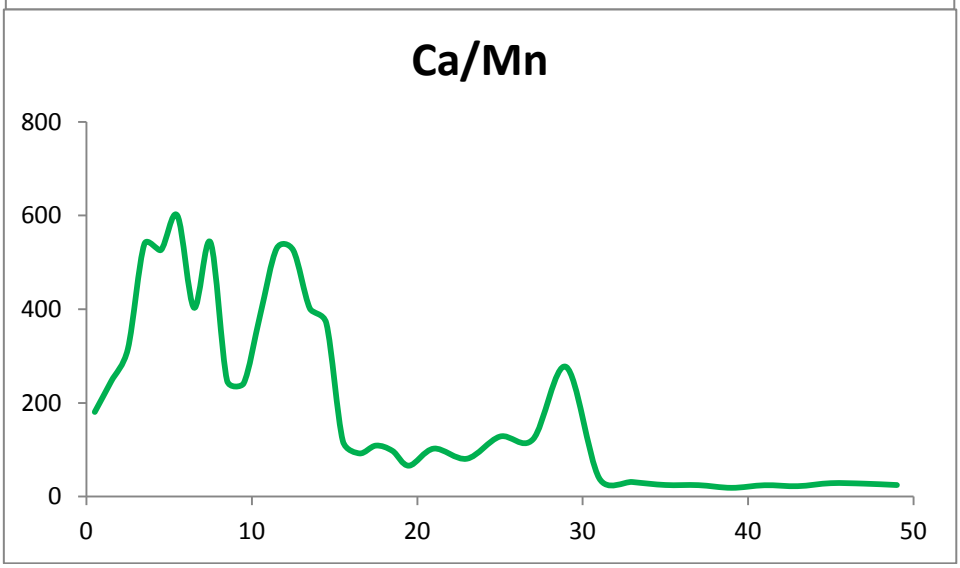
Ca/Mn
800
600
400
200
0
0
10
20
30
40
50

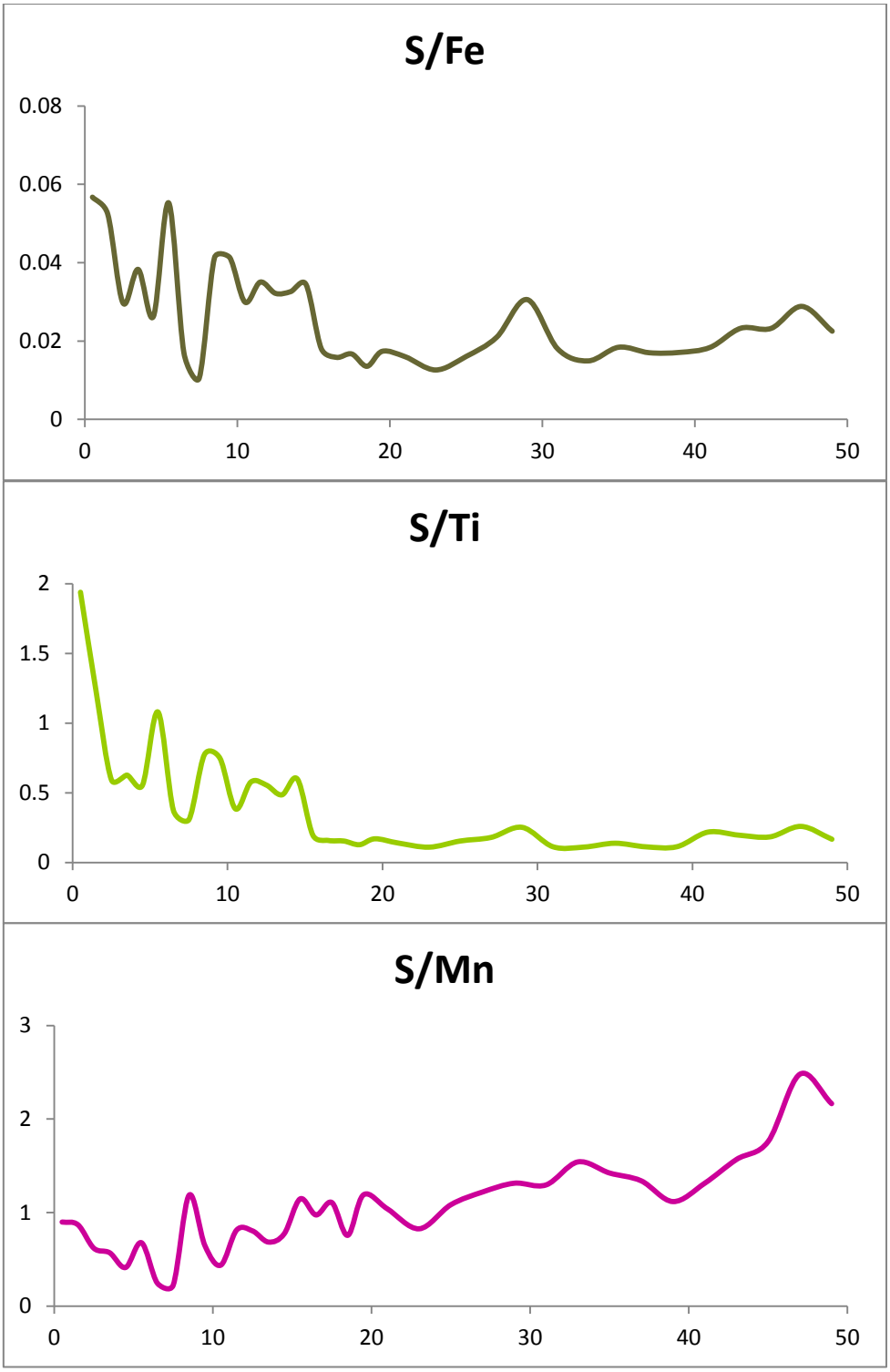
S/Fe
0.08
0.06
0.04
0.02
0
0
10
20
30
40
50
S/Ti
2
1.5
1
0.5
0
0
10
20
30
40
50
S/Mn
3
2
1
0
0
10
20
30
40
50

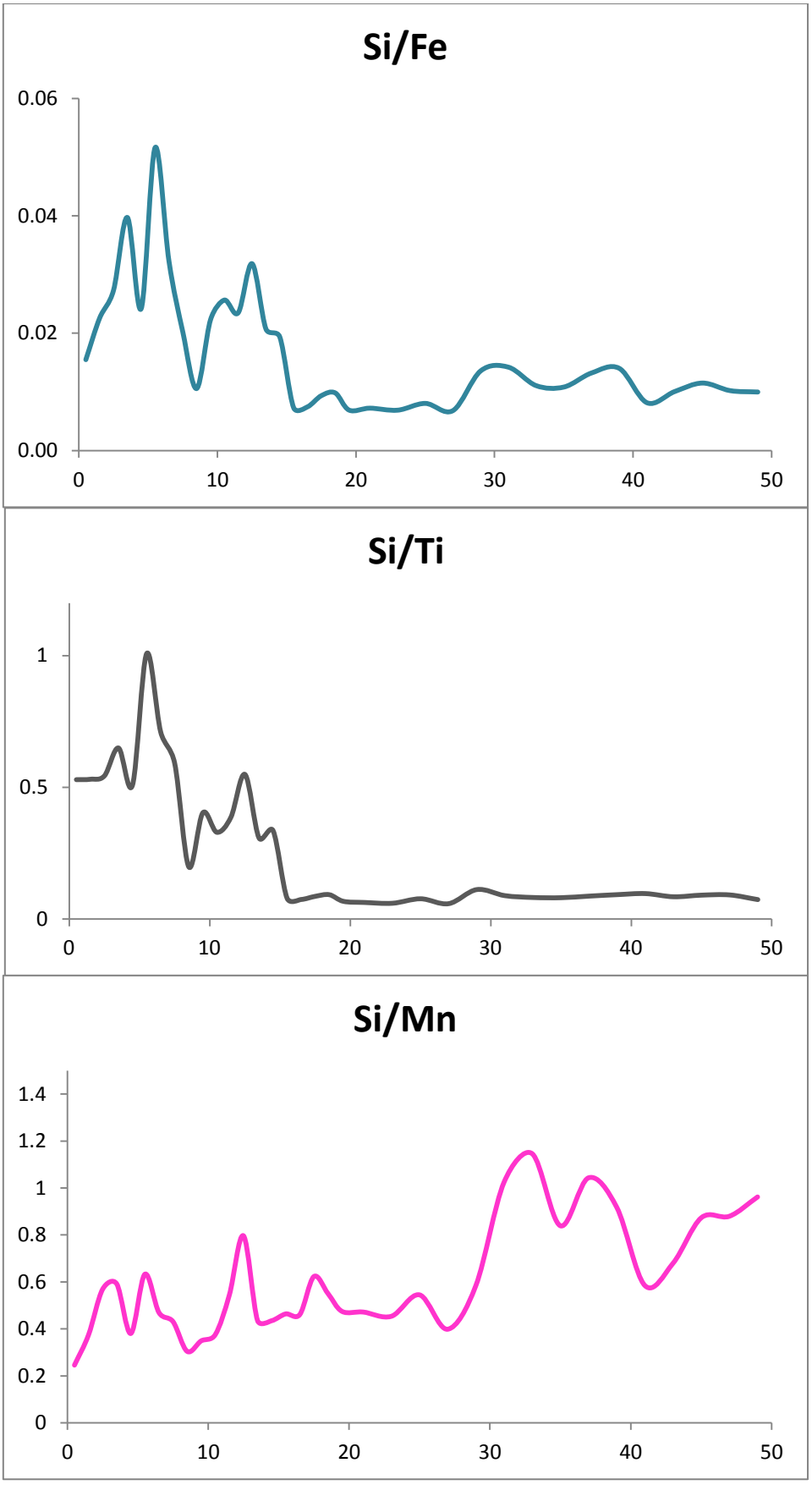

Appendix Figure 7.7: Falealupo pXRF data curves.

Appendix 7.8: Lano pXRF data.

Appendix Table 7.8.1: Processed pXRF data of detected elements at Lano; processed using ARTAX software developed by Bruker Elemenetal Inc.

Depth (cm)	Ca	Cr	Fe	Ni	S	Si	Sr	Ti	V
1	23293	1270	98764	1719	521	273	165	5165	1
5	21539	1743	85564	1794	412	209	169	4847	367
9	37597	1534	90410	1877	573	332	29	8260	241
13	37361	1333	93343	2056	460	389	139	7414	278
17	108831	1089	67675	1618	918	372	269	7422	1
21	158155	1153	56233	1785	812	411	510	5857	290
25	175478	1154	59815	1699	1193	436	388	5305	1
29	146818	1271	88969	1788	1635	535	370	8012	125
33	255358	1091	47938	2104	1518	487	481	5802	181
37	232058	1090	46699	1921	1322	535	419	5090	323
41	113207	1436	97343	1696	3567	302	227	5780	392
45	131252	1370	100837	1688	3306	285	390	5501	403
49	126653	1244	70424	1646	2142	424	-5	4795	228
53	299673	783	42092	1757	1686	418	580	4057	175
57	242509	1036	88607	1467	3713	326	354	4822	164
61	297353	807	43625	1692	2678	427	401	3128	155
65	312871	632	23904	1696	1826	410	379	1741	124
69	348179	674	34640	1686	3455	514	560	1518	292
73	327241	572	37902	1865	3138	356	376	1272	1
77	357935	716	26035	1829	2630	366	98	1155	84
81	351049	649	21068	2035	1936	291	511	1141	62
85	347703	577	21196	1930	2118	189	117	847	226
89	349866	366	22291	1907	2436	380	478	882	35
93	323313	672	24991	1727	2395	300	463	781	1
97	352853	673	32488	1663	2480	256	430	827	95
101	368712	643	25807	1709	2489	366	413	1459	78
105	382073	647	21867	2159	1840	364	550	815	1
109	372047	485	15544	2039	1458	436	493	834	17
113	381723	513	22231	1959	2229	430	525	1256	13
117	335808	530	22991	1928	1569	465	143	1140	29
121	63164	1240	84290	1460	2492	397	157	4427	795
125	107782	1392	64205	1667	2955	557	264	4618	756
129	53703	1993	61498	2069	2586	1184	117	4754	1225
133	136304	1333	46137	1492	2119	874	296	3100	750
137	89164	1543	58545	1847	1998	564	242	4745	709
141	321703	588	51701	1501	2375	402	579	4850	323
145	7378	1037	5924	2560	3627	140	501	65	159
149	8444	1061	76860	1752	2806	187	142	1150	1167

Appendix Table 7.8.2: Lano elemental ratios used in this analysis. Ratios are between marine-derived elements relative to terrestrially-dominant iron (Fe), manganese (Mn) and titanium (Ti).

Depth (cm)	Ca/Fe	Ca/Ti	Si/Fe	Si/Ti	S/Fe	S/Ti	Sr/Fe	Sr/Ti
1	0.236	4.510	0.003	0.053	0.005	0.101	0.002	0.032
5	0.252	4.444	0.002	0.043	0.005	0.085	0.002	0.035
9	0.416	4.552	0.004	0.040	0.006	0.069	0.000	0.004

13	0.400	5.039	0.004	0.052	0.005	0.062	0.001	0.019
17	1.608	14.663	0.005	0.050	0.014	0.124	0.004	0.036
21	2.812	27.003	0.007	0.070	0.014	0.139	0.009	0.087
25	2.934	33.078	0.007	0.082	0.020	0.225	0.006	0.073
29	1.650	18.325	0.006	0.067	0.018	0.204	0.004	0.046
33	5.327	44.012	0.010	0.084	0.032	0.262	0.010	0.083
37	4.969	45.591	0.011	0.105	0.028	0.260	0.009	0.082
41	1.163	19.586	0.003	0.052	0.037	0.617	0.002	0.039
45	1.302	23.860	0.003	0.052	0.033	0.601	0.004	0.071
49	1.798	26.414	0.006	0.088	0.030	0.447	0.000	-0.001
53	7.119	73.866	0.010	0.103	0.040	0.416	0.014	0.143
57	2.737	50.292	0.004	0.068	0.042	0.770	0.004	0.073
61	6.816	95.062	0.010	0.137	0.061	0.856	0.009	0.128
65	13.089	179.708	0.017	0.235	0.076	1.049	0.016	0.218
69	10.051	229.367	0.015	0.339	0.100	2.276	0.016	0.369
73	8.634	257.265	0.009	0.280	0.083	2.467	0.010	0.296
77	13.748	309.900	0.014	0.317	0.101	2.277	0.004	0.085
81	16.663	307.668	0.014	0.255	0.092	1.697	0.024	0.448
85	16.404	410.511	0.009	0.223	0.100	2.501	0.006	0.138
89	15.695	396.673	0.017	0.431	0.109	2.762	0.021	0.542
93	12.937	413.973	0.012	0.384	0.096	3.067	0.019	0.593
97	10.861	426.666	0.008	0.310	0.076	2.999	0.013	0.520
101	14.287	252.716	0.014	0.251	0.096	1.706	0.016	0.283
105	17.473	468.801	0.017	0.447	0.084	2.258	0.025	0.675
109	23.935	446.100	0.028	0.523	0.094	1.748	0.032	0.591
113	17.171	303.920	0.019	0.342	0.100	1.775	0.024	0.418
117	14.606	294.568	0.020	0.408	0.068	1.376	0.006	0.125
121	0.749	14.268	0.005	0.090	0.030	0.563	0.002	0.035
125	1.679	23.340	0.009	0.121	0.046	0.640	0.004	0.057
129	0.873	11.296	0.019	0.249	0.042	0.544	0.002	0.025
133	2.954	43.969	0.019	0.282	0.046	0.684	0.006	0.095
137	1.523	18.791	0.010	0.119	0.034	0.421	0.004	0.051
141	6.222	66.331	0.008	0.083	0.046	0.490	0.011	0.119
145	1.245	113.508	0.024	2.154	0.612	55.800	0.085	7.708
149	0.110	7.343	0.002	0.163	0.037	2.440	0.002	0.123

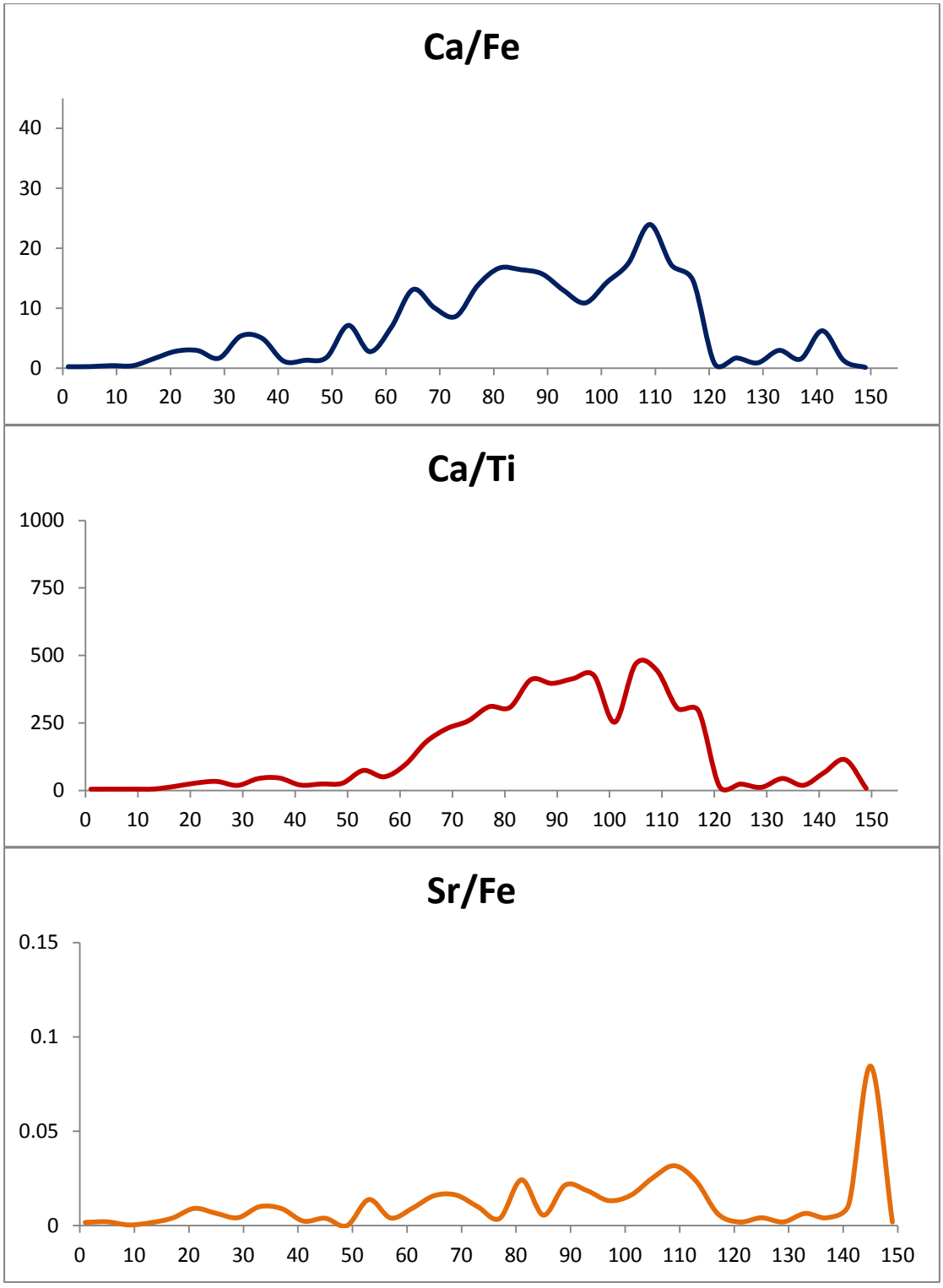
Ca/Fe
40
30
20
10
0
0 10 20 30 40 50 60 70 80 90 100 110 120 130 140 150
Ca/Ti
1000
750
500
250
0
0 10 20 30 40 50 60 70 80 90 100 110 120 130 140 150
Sr/Fe
0.15
0.1
0.05
0
0 10 20 30 40 50 60 70 80 90 100 110 120 130 140 150

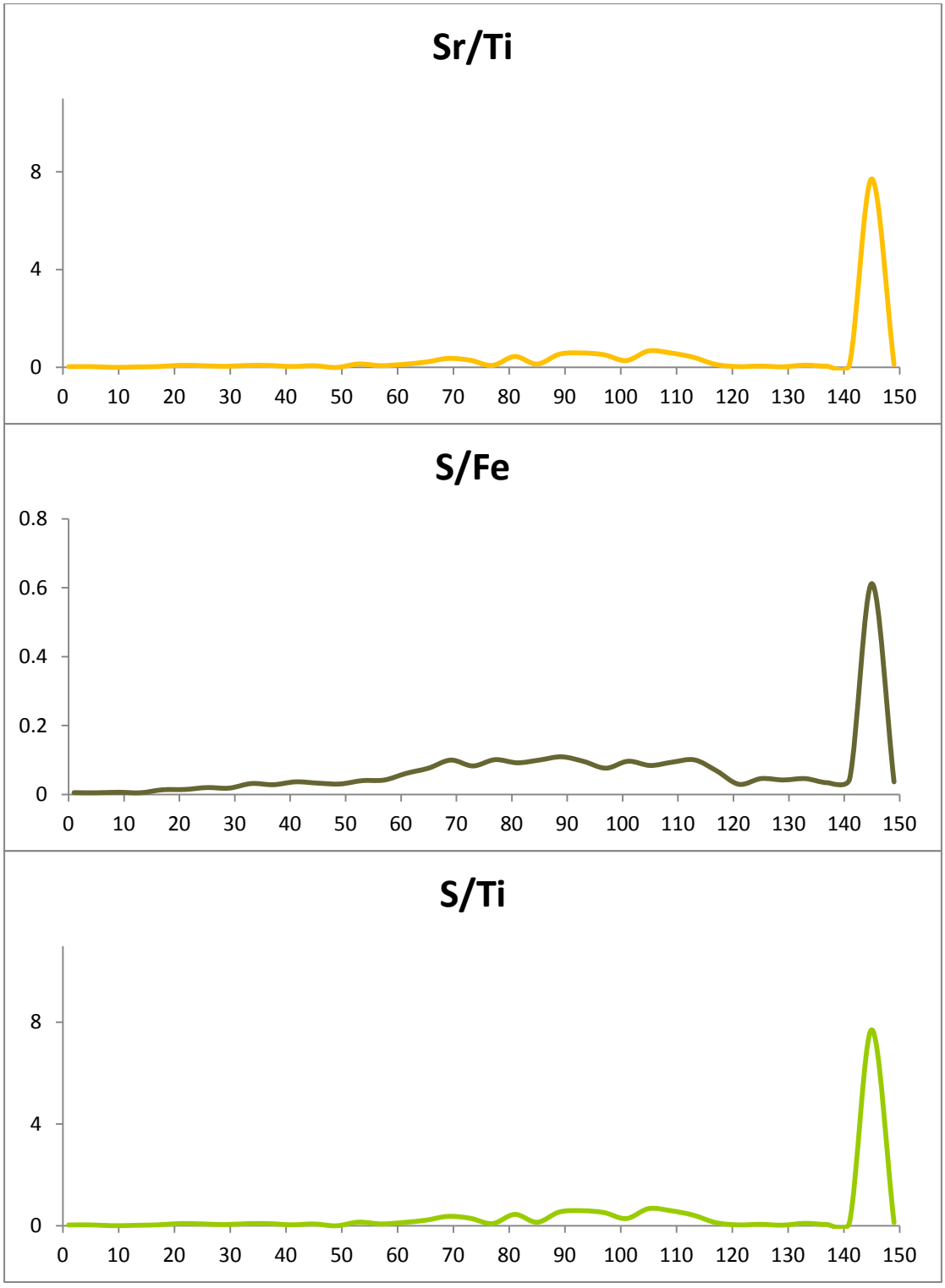
Sr/Ti
8
4
0
0 10 20 30 40 50 60 70 80 90 100 110 120 130 140 150
S/Fe
0.8
0.6
0.4
0.2
0
0 10 20 30 40 50 60 70 80 90 100 110 120 130 140 150
S/Ti
8
4
0
0 10 20 30 40 50 60 70 80 90 100 110 120 130 140 150

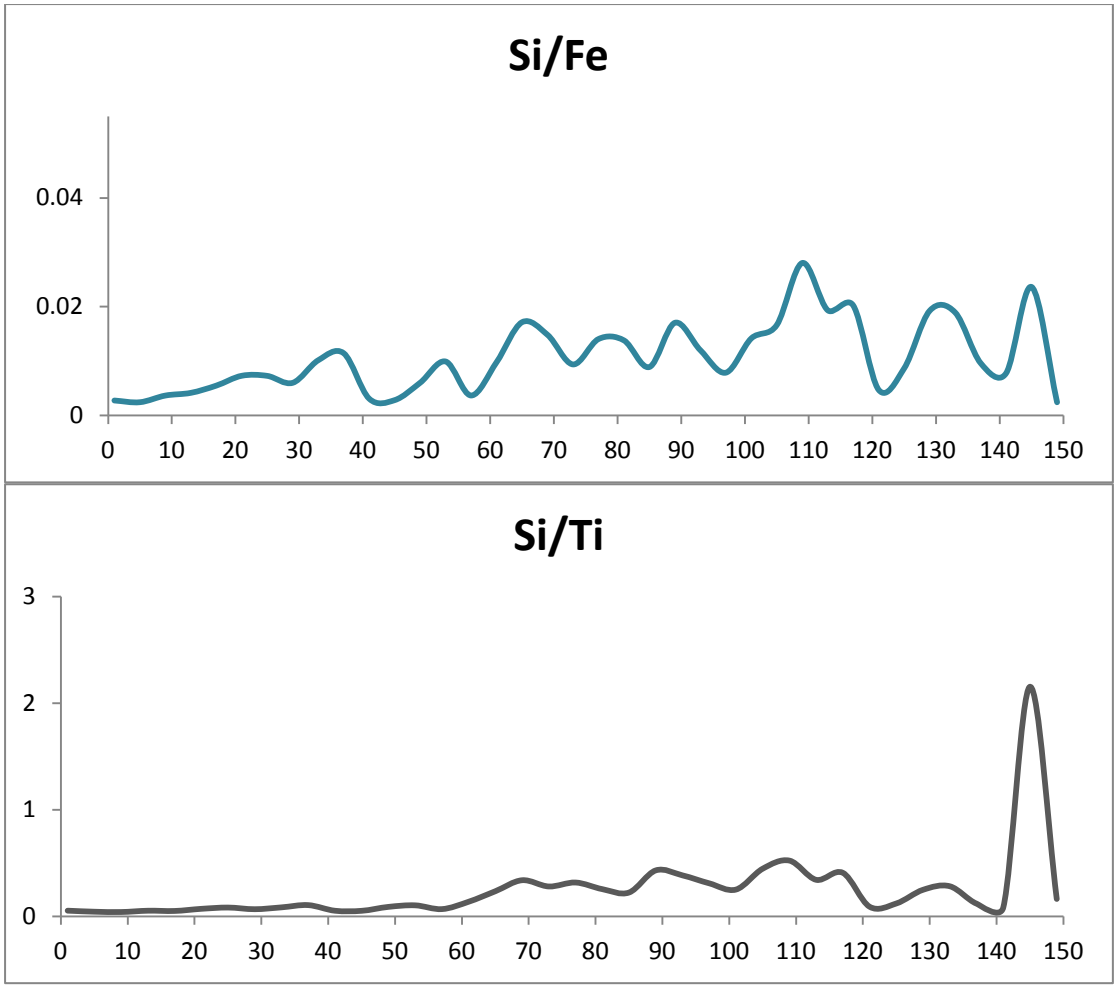

Appendix Figure 7.8: Lano pXRF data curves.

Appendix 7.9: Satupaitea pXRF data.

Appendix Table 7.9.1: Processed pXRF data of detected elements at Satupaitea; processed using ARTAX software developed by Bruker Elemenetal Inc.

Depth (cm)	Ca	Cr	Fe	K	Mn	Ni	Si	Ti	V	Zn
1	26863	2299	348937	5410	4349	1820	2324	20466	1066	677
4	28373	1926	320831	5699	3968	2276	2065	20700	720	878
7	7664	1314	135776	4261	2160	1808	560	4989	182	909
10	16865	1716	211912	4780	2994	2010	1182	12134	459	1052
13	17828	2121	272714	4934	3595	2046	1327	15467	501	651
16	12339	1858	200677	4726	2620	1565	821	11941	541	754
19	13240	2017	219303	4617	3035	1945	908	13775	705	933
21	12135	2128	202599	4676	3023	1911	1158	12765	733	932
22	12150	2275	203376	4392	2867	1757	1071	12296	689	941
25	14518	2144	283073	4742	3523	1833	924	16073	725	719
28	13911	2141	280302	4773	3545	1784	907	14747	621	791
31	17045	2376	312379	4816	3578	1494	1382	15049	604	691
34	13966	2160	368039	4496	4255	1256	1704	29486	1336	641
37	12892	2314	368039	4734	3988	1430	1522	24434	1185	644
40	36379	2800	411417	5915	5184	2428	3175	26236	1352	412
43	31655	2371	377221	5848	4494	2033	2914	24698	1263	632
46	38535	2435	442844	6142	5484	2388	3901	30063	1279	744
49	34477	2580	407999	5923	4869	2413	3775	25585	1169	844
51	32350	2744	370645	5572	4732	1803	2808	23665	1254	551
52	32664	2472	377930	5766	4706	1912	2834	24162	1185	679
55	33061	2735	374147	5668	4802	2105	2614	23004	1515	640
57	31700	2478	380589	5561	4695	2353	2812	22825	1267	627
58	31375	2561	378106	5534	4766	1836	2841	22543	1324	751
61	34849	2904	418880	5722	4648	2240	2887	25632	1099	641
64	30041	2210	381805	5761	4364	1955	2659	22602	1155	802
67	37077	2656	425016	5992	4546	1782	3703	28541	1550	524
70	43836	2475	430556	6435	5083	1778	4574	30231	1342	357
73	43444	2421	443352	6178	4953	1570	3972	29134	1197	540
76	103321	2024	353280	5777	3866	1456	3309	25358	1247	480
79	76114	2904	419899	5345	4336	1827	3322	28830	1444	599
82	49592	2940	478566	5745	4909	1728	4049	32422	1521	588
85	64131	4508	404383	5885	4406	1531	3439	28444	1557	440
88	70167	2694	397236	5519	4549	1714	3402	28264	1357	462
91	47567	2872	454426	6473	5122	2026	3983	32063	1506	526
94	38386	2884	447811	6402	5366	2015	3785	29884	1434	674
97	69174	2133	342413	5507	4113	1851	2961	24905	1270	708
100	72971	3232	429098	5789	5128	2125	3792	31119	1406	655

Appendix Table 7.9.2: Satupaitea elemental ratios used in this analysis. Ratios are between marine-derived elements relative to terrestrially-dominant iron (Fe), manganese (Mn) and titanium (Ti).

Depth (cm)	Ca/Ti	Ca/Fe	Ca/Mn	Si/Ti	Si/Fe	Si/Mn
1	1.313	0.077	6.177	0.114	0.007	0.534
4	1.371	0.088	7.150	0.100	0.006	0.520
7	1.536	0.056	3.548	0.112	0.004	0.259

10	1.390	0.080	5.633	0.097	0.006	0.395
13	1.153	0.065	4.959	0.086	0.005	0.369
16	1.033	0.061	4.710	0.069	0.004	0.313
19	0.961	0.060	4.362	0.066	0.004	0.299
21	0.951	0.060	4.014	0.091	0.006	0.383
22	0.988	0.060	4.238	0.087	0.005	0.374
25	0.903	0.051	4.121	0.057	0.003	0.262
28	0.943	0.050	3.924	0.062	0.003	0.256
31	1.133	0.055	4.764	0.092	0.004	0.386
34	0.474	0.038	3.282	0.058	0.005	0.400
37	0.528	0.035	3.233	0.062	0.004	0.382
40	1.387	0.088	7.018	0.121	0.008	0.612
43	1.282	0.084	7.044	0.118	0.008	0.648
46	1.282	0.087	7.027	0.130	0.009	0.711
49	1.348	0.085	7.081	0.148	0.009	0.775
51	1.367	0.087	6.836	0.119	0.008	0.593
52	1.352	0.086	6.941	0.117	0.007	0.602
55	1.437	0.088	6.885	0.114	0.007	0.544
57	1.389	0.083	6.752	0.123	0.007	0.599
58	1.392	0.083	6.583	0.126	0.008	0.596
61	1.360	0.083	7.498	0.113	0.007	0.621
64	1.329	0.079	6.884	0.118	0.007	0.609
67	1.299	0.087	8.156	0.130	0.009	0.815
70	1.450	0.102	8.624	0.151	0.011	0.900
73	1.491	0.098	8.771	0.136	0.009	0.802
76	4.074	0.292	26.726	0.130	0.009	0.856
79	2.640	0.181	17.554	0.115	0.008	0.766
82	1.530	0.104	10.102	0.125	0.008	0.825
85	2.255	0.159	14.555	0.121	0.009	0.781
88	2.483	0.177	15.425	0.120	0.009	0.748
91	1.484	0.105	9.287	0.124	0.009	0.778
94	1.285	0.086	7.154	0.127	0.008	0.705
97	2.778	0.202	16.818	0.119	0.009	0.720
100	2.345	0.170	14.230	0.122	0.009	0.739

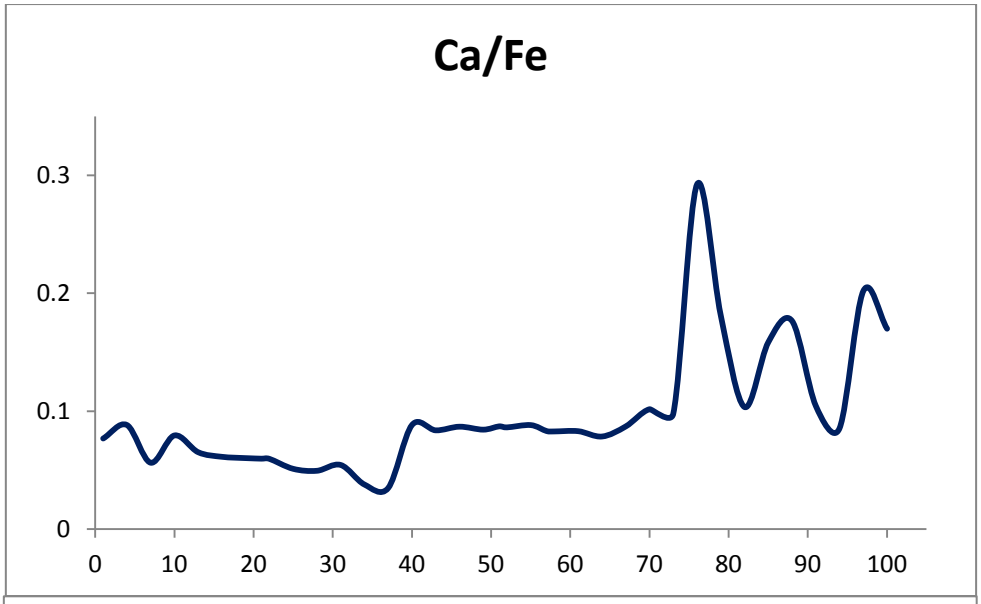
Ca/Fe
0.3
0.2
0.1
0
0 10 20 30 40 50 60 70 80 90 100

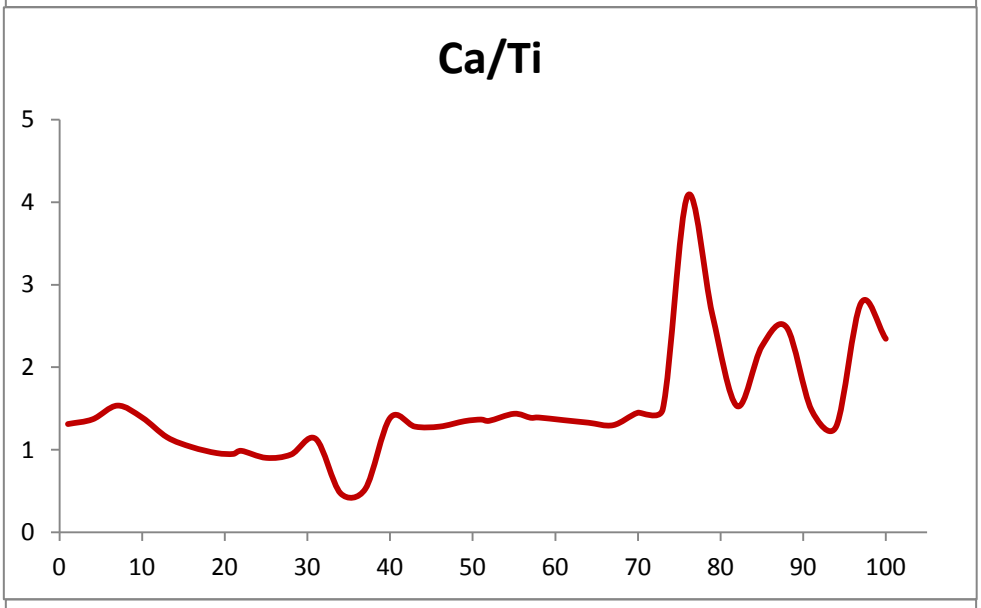
Ca/Ti
5
4
3
2
1
0
0 10 20 30 40 50 60 70 80 90 100

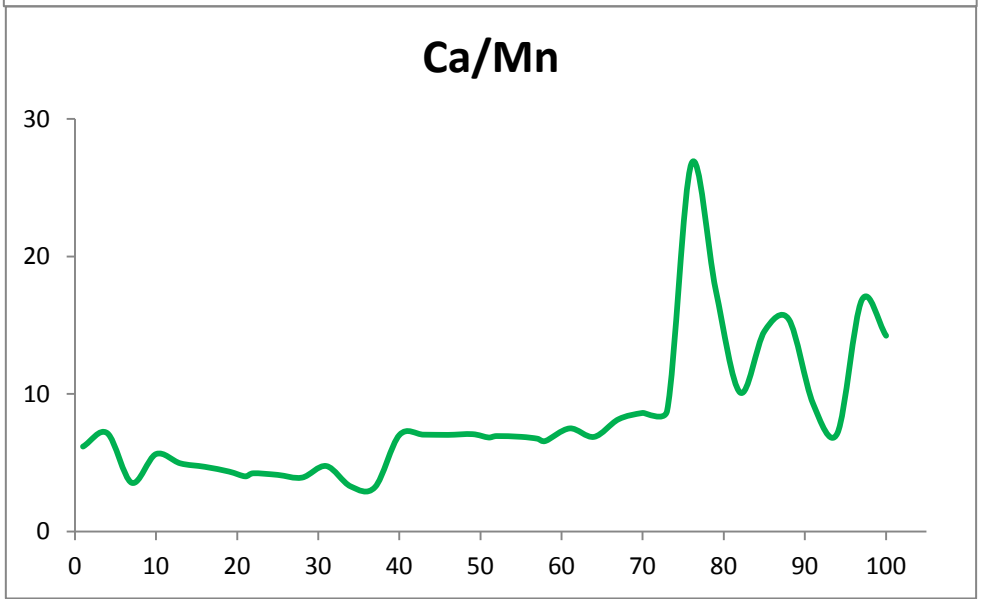
Ca/Mn
30
20
10
0
0 10 20 30 40 50 60 70 80 90 100

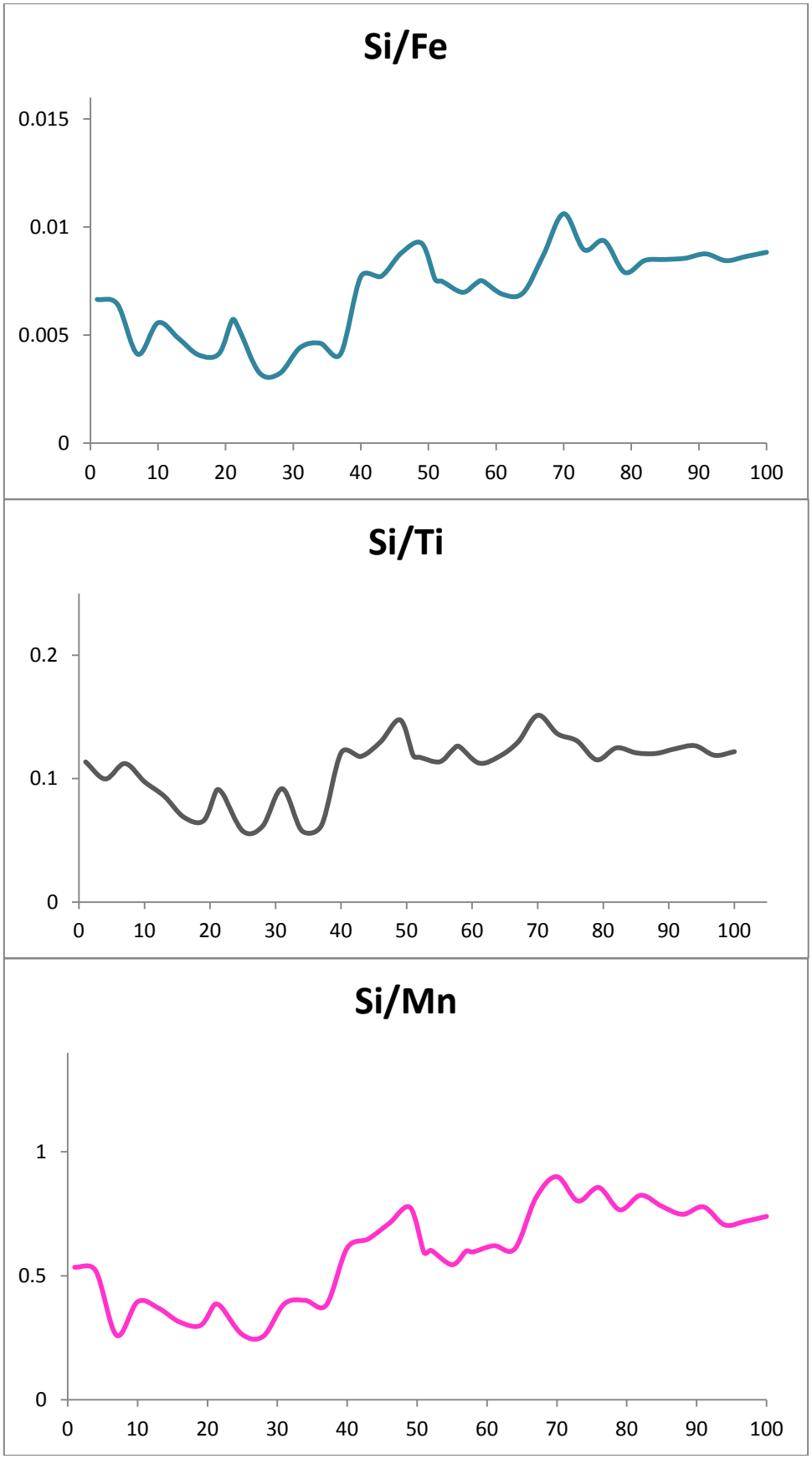

Appendix Figure 7.9: Satupaitea pXRF data curves.

Appendix 7.10: Ta'u pXRF data.

Appendix Table 7.10.1: Processed pXRF data of detected elements at Ta'u; processed using ARTAX software developed by Bruker Elemenetal Inc.

Depth (cm)	Br	Ca	Cr	Fe	S	Sr	Ti	V
1	2978	31801	1731	147845	1005	68	13160	293
3	1150	37552	1895	285965	790	47	26620	584
5	983	47701	1983	315145	775	13	29470	557
7	869	59137	2104	335714	874	-2	31302	748
9	1036	60251	2295	326274	679	80	31541	709
11	985	53104	2965	331228	705	33	39366	1024
13	1130	42669	2573	328698	656	148	33108	869
15	958	70970	2982	379442	735	69	38742	880
17	1028	71362	2940	391731	801	15	43328	1134
19	1048	38287	3005	381554	634	24	41432	1042
21	978	84594	2924	363763	778	23	42513	917
23	889	107495	2957	348888	898	121	40631	769
25	1116	66856	2506	293697	763	48	32885	863
27	789	57870	2849	325634	712	19	35427	1047
29	1409	79664	2431	329488	725	46	31161	764
31	1013	112475	2578	315254	753	60	35077	897
33	1079	91655	3163	404924	726	16	43433	1434
35	876	109870	2883	331249	702	54	39616	979
37	906	57995	2892	353218	725	66	38480	703
39	819	120844	2929	343846	638	22	39494	917
41	619	182279	2133	267057	609	-1	29427	770
43	878	142954	2426	286055	690	-18	34774	563
45	661	141624	2226	276388	623	205	32213	599
47	865	175835	2320	304390	727	140	31794	888
49	892	130245	2454	299409	386	61	33576	705
51	760	260953	1321	114811	615	89	14027	403
53	791	329195	803	60553	660	44	7131	64
55	782	304082	1335	103621	799	52	15021	193

Appendix Table 7.10.2: Ta'u elemental ratios used in this analysis. Ratios are between marine-derived elements relative to terrestrially-dominant iron (Fe), manganese (Mn) and titanium (Ti).

Depth (cm)	Ca/Fe	Ca/Ti	S/Fe	S/Ti	Sr/Fe	Sr/Ti	Br/Fe	Br/Ti
1	0.215	2.416	0.007	0.076	0.000	0.005	0.020	0.226
3	0.131	1.411	0.003	0.032	0.000	0.001	0.007	0.080
5	0.151	1.619	0.003	0.027	0.000	0.002	0.004	0.039
7	0.176	1.889	0.002	0.024	0.000	0.001	0.003	0.032
9	0.185	1.910	0.002	0.025	0.000	0.000	0.003	0.031
11	0.160	1.349	0.003	0.021	0.000	0.000	0.003	0.022
13	0.130	1.289	0.003	0.026	0.000	0.000	0.003	0.026
15	0.187	1.832	0.002	0.019	0.000	0.001	0.002	0.023
17	0.182	1.647	0.002	0.016	0.000	0.002	0.003	0.024
19	0.100	0.924	0.002	0.017	0.000	0.002	0.003	0.027
21	0.233	1.990	0.002	0.017	0.000	0.001	0.003	0.023
23	0.308	2.646	0.002	0.015	0.000	0.002	0.003	0.025

25	0.228	2.033	0.002	0.020	0.001	0.005	0.004	0.034
27	0.178	1.633	0.002	0.023	0.000	0.004	0.003	0.027
29	0.242	2.557	0.002	0.024	0.000	0.002	0.003	0.031
31	0.357	3.207	0.002	0.022	0.000	0.000	0.003	0.030
33	0.226	2.222	0.002	0.019	0.000	0.000	0.003	0.025
35	0.332	2.530	0.002	0.015	0.000	0.001	0.003	0.023
37	0.164	1.464	0.002	0.016	0.000	0.001	0.003	0.026
39	0.351	3.140	0.002	0.018	0.000	0.000	0.003	0.027
41	0.683	4.615	0.003	0.020	0.000	0.001	0.004	0.025
43	0.500	4.858	0.003	0.029	0.000	0.001	0.003	0.031
45	0.512	4.073	0.003	0.026	0.000	0.003	0.003	0.026
47	0.578	5.459	0.003	0.026	0.000	0.004	0.004	0.033
49	0.435	4.097	0.003	0.024	0.000	0.002	0.004	0.035
51	2.273	7.772	0.007	0.024	0.000	0.001	0.008	0.028
53	5.437	23.469	0.012	0.051	0.000	0.001	0.013	0.056
55	2.935	42.642	0.007	0.096	0.000	0.004	0.010	0.143

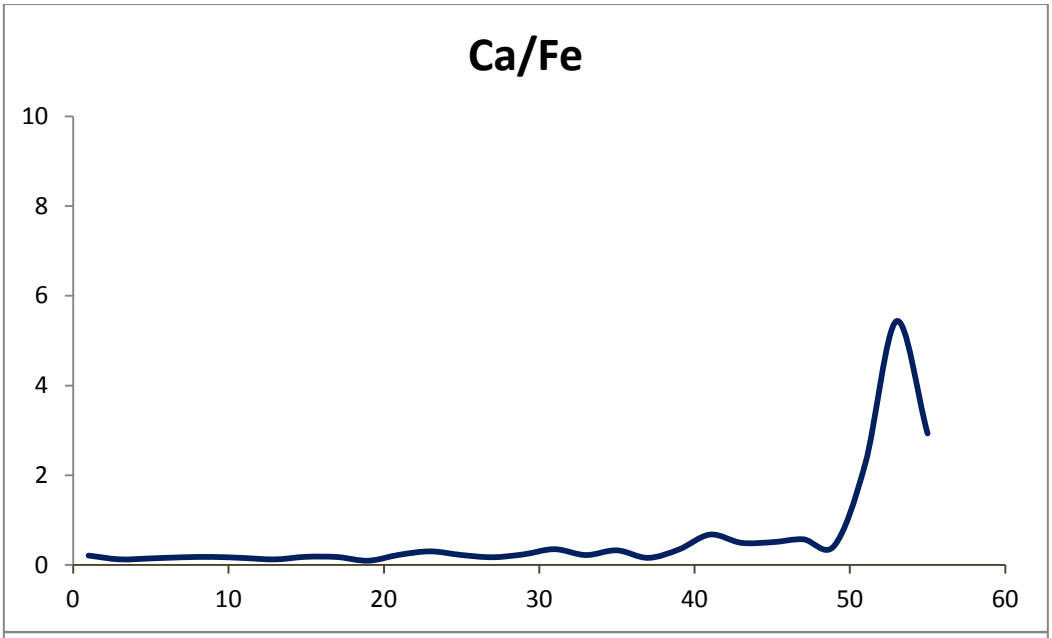
Ca/Fe
10
8
6
4
2
0
0
10
20
30
40
50
60

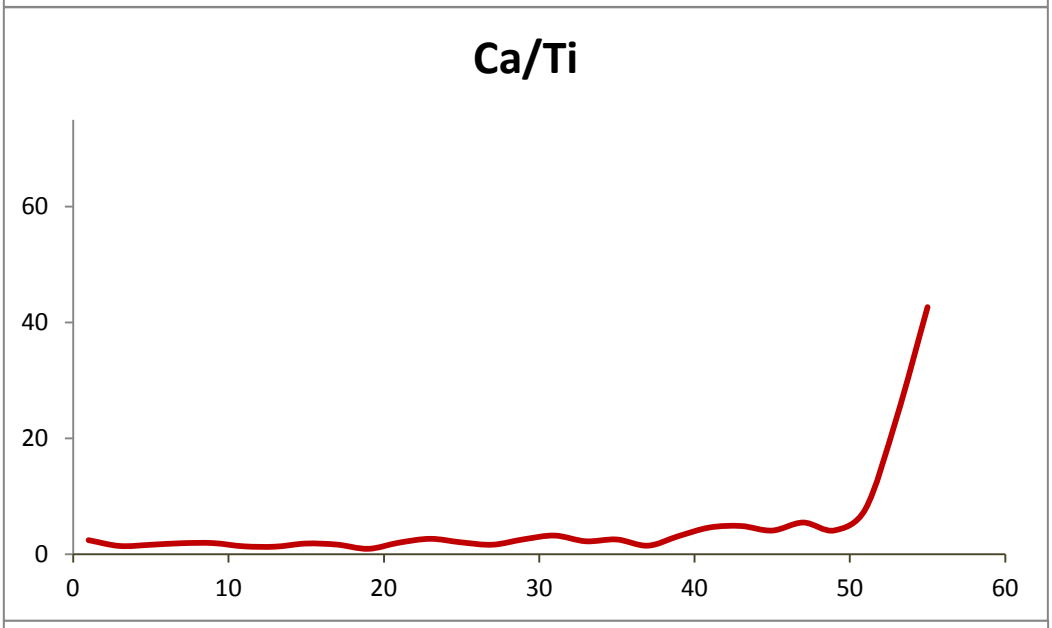
Ca/Ti
60
40
20
0
0
10
20
30
40
50
60

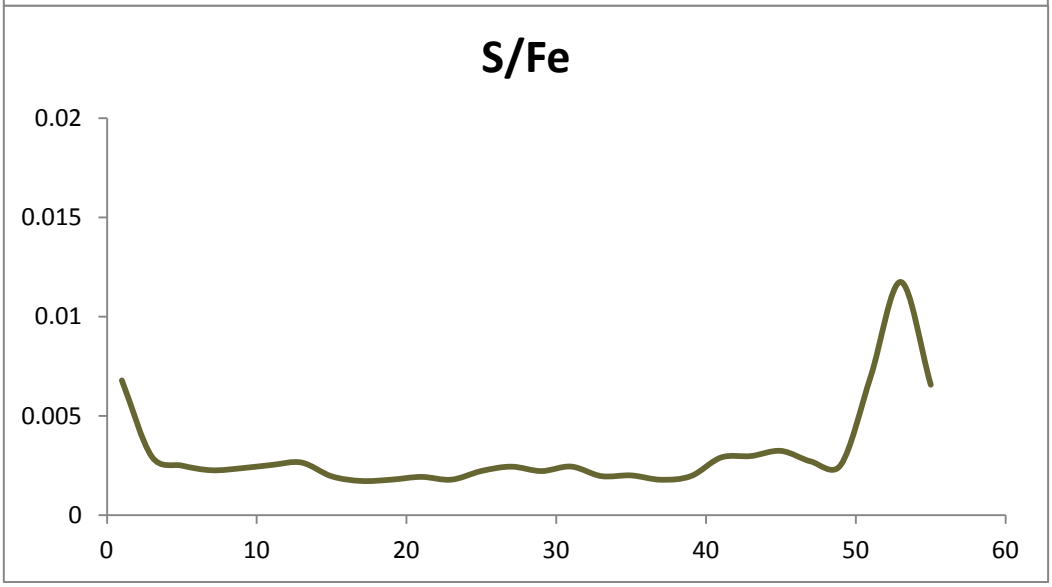
S/Fe
0.02
0.015
0.01
0.005
0
0
10
20
30
40
50
60

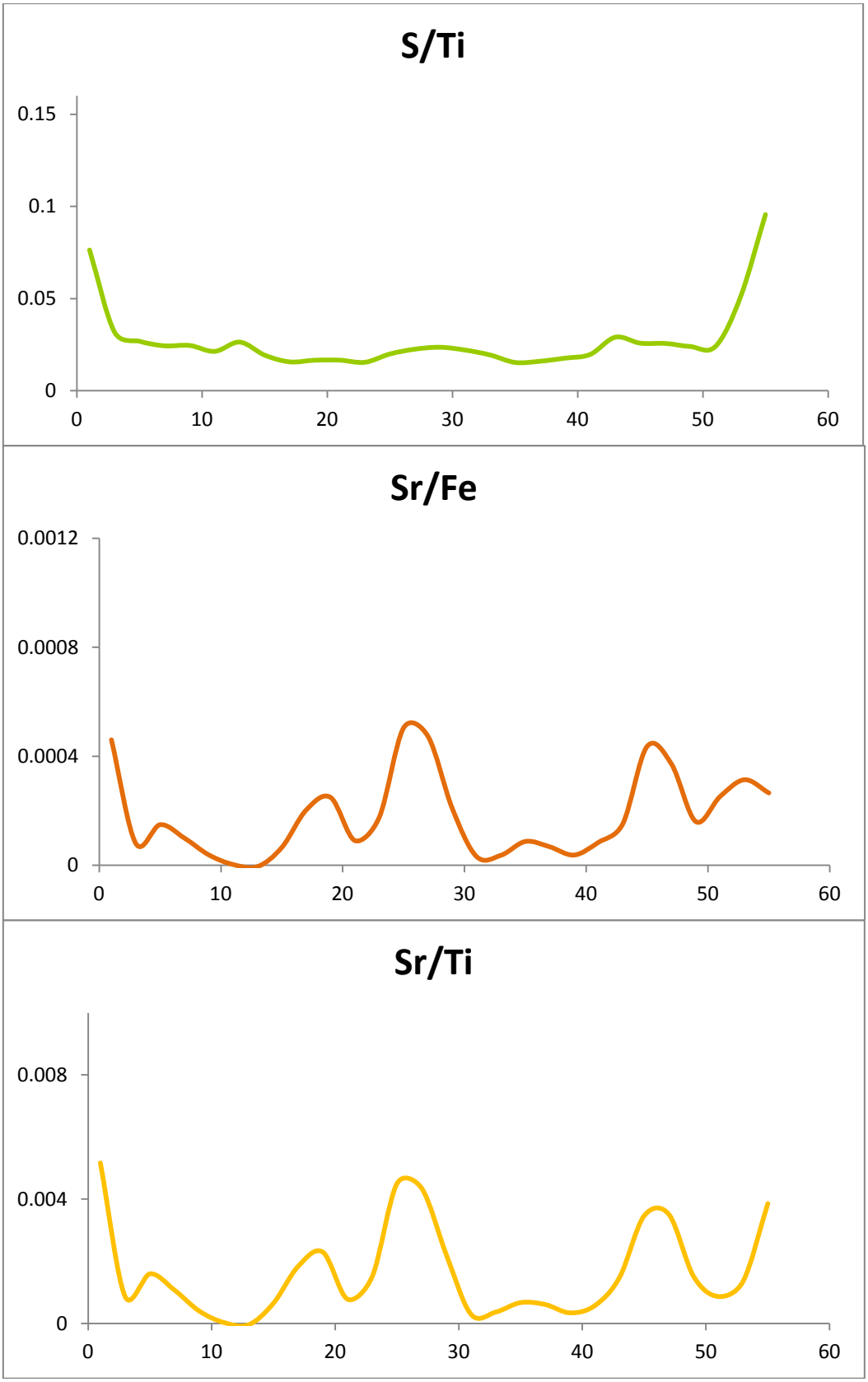
S/Ti
0.15
0.1
0.05
0
0
10
20
30
40
50
60
Sr/Fe
0.0012
0.0008
0.0004
0
0
10
20
30
40
50
60
Sr/Ti
0.008
0.004
0
0
10
20
30
40
50
60

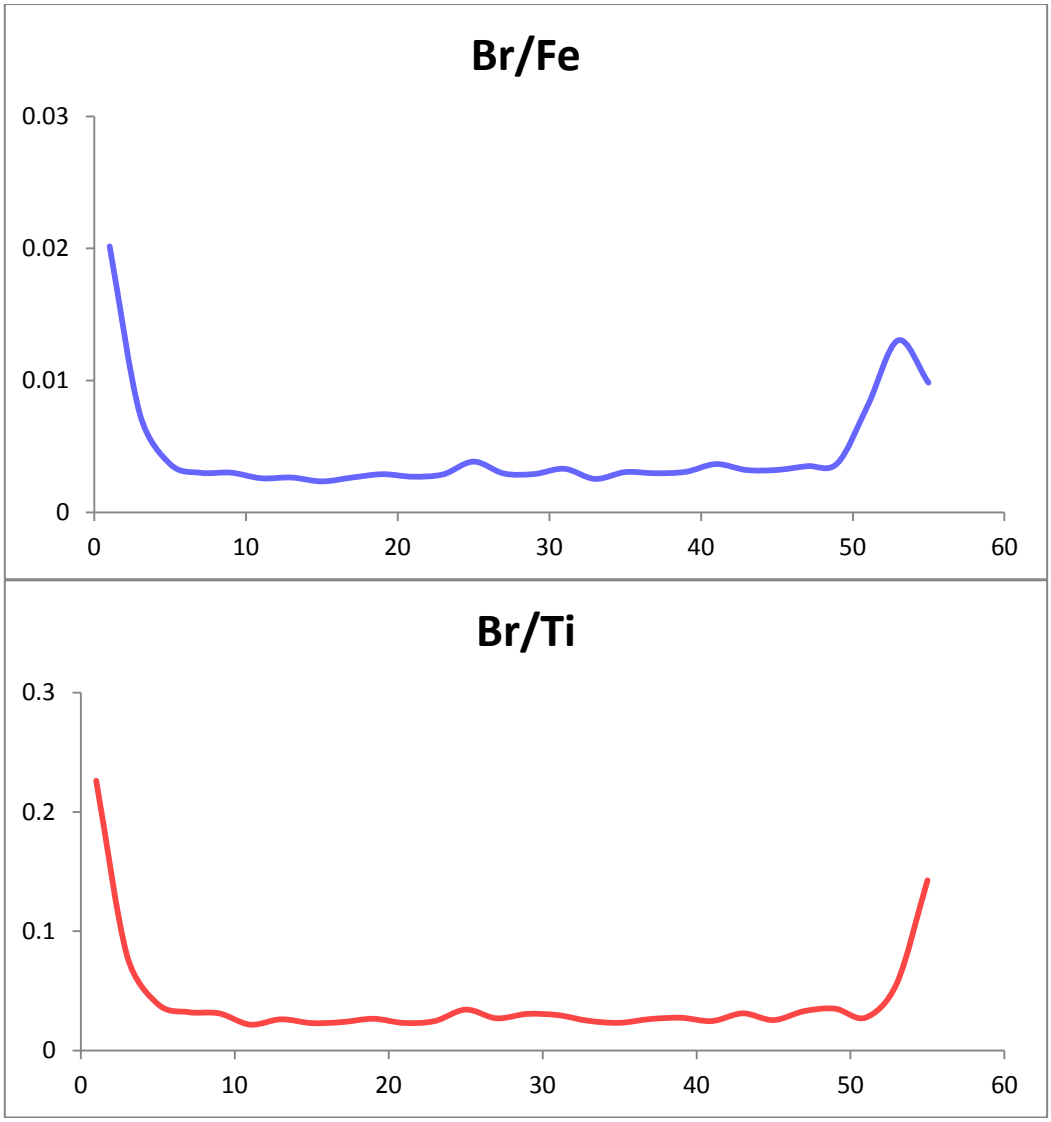

Appendix Figure 7.10: Ta'u pXRF data curves.

APPENDIX 8: ITRAX ELEMENT DATA

Overview

Elmental analysis using the ITRAX core scanner of the Institute for Environmental Research, ANSTO, provded high-resolution (0.5 mm) XRF data for Ma'asina, Manono and Lano. This was implemeneted following methods described in Croudace et al. (2006).

Relative elemental compositions for each site are provided. Thresh-hold detection is for elements ≥ aluminium (Al) in the periodic table.

Elemental ratios used in the thesis are provided for each site. Raw processed data are located in the Department of Geological Sciences data archives, University of Canterbury, and at the Institute for Environmental Research, ANSTO; AINSE Grant 12/119.

Due to the large data quantity in this analysis, sub-appendices containing data for each site are provided in the Data CD accompanying this thesis.

Data CD Contents for Appendix 8

Appendix 8.1: Ma'asina ITRAX element ratio data (Appendix 8.1 in thesis Data CD).

Appendix 8.2: Manono ITRAX element data (Appendix 8.2 in thesis Data CD).

Appendix 8.3: Lano ITRAX element data (Appendix 8.3 in thesis Data CD).

APPENDIX 9: ^{14}C AGE DATA

This Appendix provides radiocarbon data obtained for this research.

Appendix 9.1 provides ages for sample codes OZP, which were obtained from the Institute for Environmental Research, ANSTO, via AINSE Grant 12/119.

Appendix 9.2 provides ages for sample codes WK, which were obtained from the Radiocarbon Dating Laboratory, University of Waikato.

Appendix 9.2 is provided as a digital appendix in the thesis Data CD.

Appendix 9.1: Radiocarbon age data for OZP sample codes.

Obtained via AINSE Grant 12/119.

ANSTO Code	Sample type	Client ID	δ13C (‰) (δ13C ± 1σ)	14C Activity (pMC ± 1σ)	Radiocarbon Age (BP ± 1σ)	Calibrated Age (cal BP), 1σ Range (probability)	Calibrated Age (cal BP), 2σ Range (probability)
OZP113 (Mulivai)	Sediment	MLC-14.002.L6	-25.9 ± 0.3	86.95 ± 0.34	1,125 ± 35	933 – 987 (0.774) 1032 – 1050 (0.226)	928 – 1018 (0.755) 1021 – 1056 (0.245)
OZP114 (Mulivai)	Sediment	MLC-14.003.L4	-27.8 ± 0.1	109.08 ± 0.38	Modern	Modern	Modern
OZP115 (Ta'u)	Sediment	TAC-14.003.50-53	-25.9 ± 0.1	93.54 ± 0.31	535 ± 30	509 – 534 (1.000)	500 – 547 (1.000)
OZP117 (Vaovai)	Unidentified Shell	VVC-14.002.22-24	2.1 ± 0.3	91.42 ± 0.27	720 ± 25	291 – 382 (1.000)	270 – 425 (1.000)
OZP119 (Satitoa)	Shell	STC-14.002.82	0.0*	91.21 ± 0.31	740 ± 30	307 – 403 (1.000)	279 – 445 (1.000)

Calibrated using Calib 6.0 (Stuiver and Reimer, 1993) using the SH Calibration dataset of McCormac et al. (2004) for the sediment samples. Shell samples were calibrated using the Marine09 dataset (Reimer et al. 2009), and a ΔR of 27±25, being the average of 6 values of ΔR determined from shells collected around Samoa (Phelan, 1999; Petchey et al., 2008).

APPENDIX 10: ^{210}Pb AGE DATA

This Appendix provides ^{210}Pb age data obtained from the Institute for Environmental Research, ANSTO, via AINSE Grant 12/119.

Contents

Appendix 10.1: ^{210}Pb ages for Falealupo.

Client Name:	Timothy Davies / Shaun Williams
Client Institution:	University of Canterbury
Project Title:	2012rc0035a
Core Description:	Falealupo

ANSTO ID	Depth (cm)			Dry Bulk Density (g/cm^3)	Cumulative Dry Mass (g/cm^2)			Count Date	Total ^{210}Pb (Bq/kg)			Supported ^{210}Pb (Bq/kg)		
N574	0	-	1	0.98	0.5	±	0.5	17-May-12	20.9	±	0.8	0.4	±	0.1
N575	1	-	2	1.14	1.5	±	0.5	17-May-12	21.1	±	0.9	0.4	±	0.1
N576	2	-	3	0.78	2.5	±	0.5	17-May-12	18.4	±	0.7	0.3	±	0.1
N638	8	-	9	1.30	8.8	±	0.5	11-Jul-12	15.4	±	0.6	0.2	±	0.1
N577	9	-	10	1.03	9.9	±	0.5	17-May-12	12.9	±	0.6	0.4	±	0.1
N578	15	-	16	0.78	15.3	±	0.5	17-May-12	13.9	±	0.6	1.1	±	0.1
N639	18	-	19	0.60	17.4	±	0.5	11-Jul-12	14.7	±	0.6	2.9	±	0.3
N640	22	-	24	0.75	20.5	±	0.9	11-Jul-12	11.8	±	0.5	2.9	±	0.3
N579	28	-	30	0.59	24.5	±	0.8	17-May-12	3.2	±	0.2	0.0	±	0.0

CIC model

Mass Accumulation Rate	0.54 ± 0.11	g/cm2/y
r2 =	0.775253	

Unsupported ^{210}Pb Decay corrected to 11-May-11 (Bq/kg)			Calculated CIC Ages (years)			Calculated CRS Ages (years)			CRS model Mass Accumulation Rates (g/cm^2/year)		
21.1	±	0.9	1	±	1	1	±	1	0.52	±	0.03
21.3	±	0.9	3	±	1	3	±	2	0.48	±	0.03
18.6	±	0.8	5	±	1	5	±	2	0.52	±	0.03
15.8	±	0.7	16	±	3	19	±	4	0.40	±	0.03
12.8	±	0.6	18	±	4	21	±	5	0.45	±	0.04
13.2	±	0.7	28	±	6	36	±	6	0.28	±	0.03
12.2	±	0.7	32	±	7	45	±	7	0.23	±	0.03
9.2	±	0.6	38	±	8	59	±	8	0.20	±	0.03
3.3	±	0.2	45	±	9	75	±	9	0.32	±	0.06

The surface sediment unsuported Pb-210 activity for this core is relatively low, only 21 Bq/kg.

Overall, the unsupported Pb-210 activities for this core exhibit a decay profile with depth (see Figure 3).

The CIC and CRS Pb-210 dating models were used to calculate the sediment ages.
An independent method should be used to validate the calculated ages such as Cs-137, pollen or trace metal records.

Atun Zawadzki - 13 September 2012

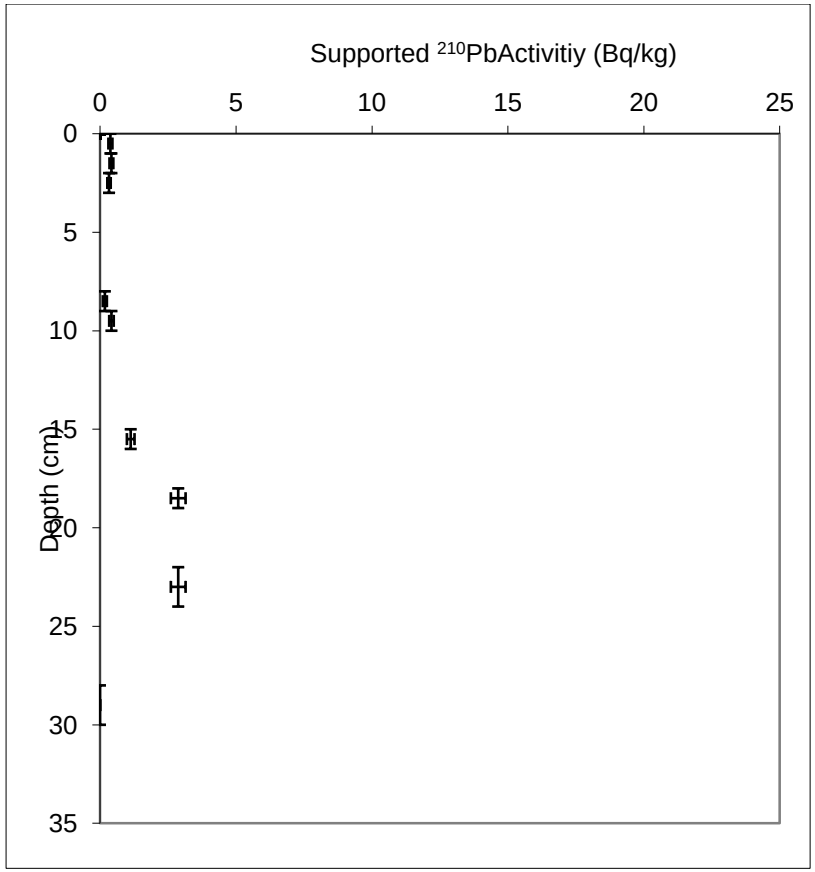
Supported ^{210}PbActivitiy (Bq/kg)
0
5
10
15
20
25
Depth (cm)
0
5
10
15
20
25
30
35

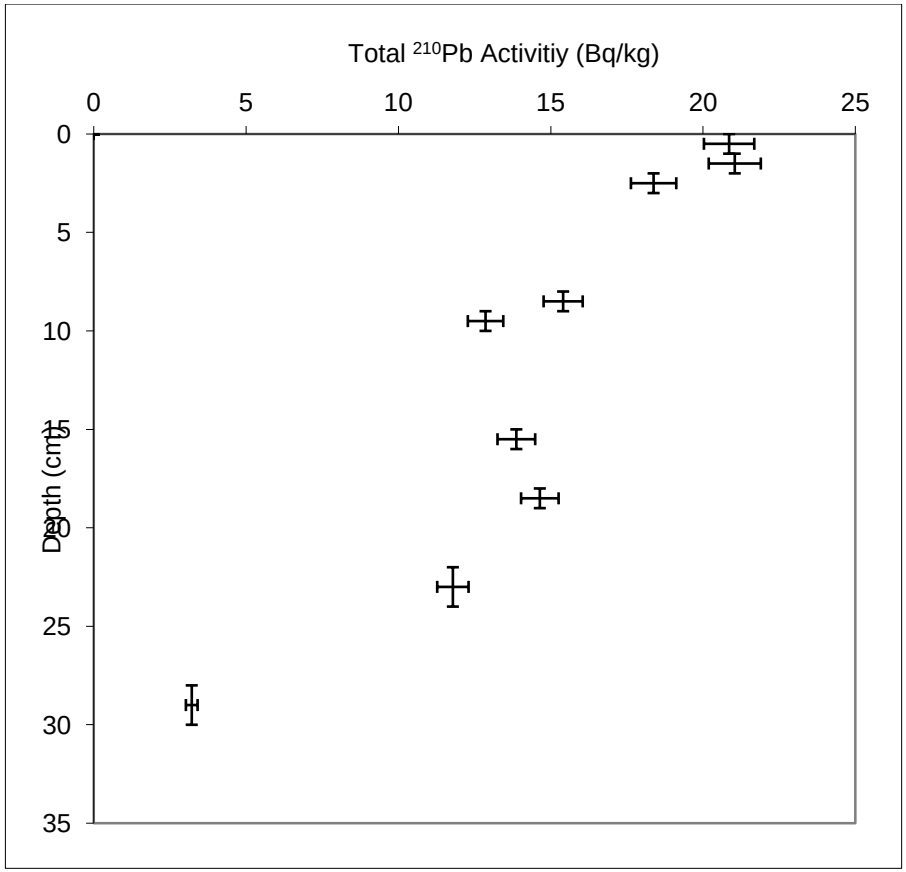
Total ^{210}Pb Activitiy (Bq/kg)
0
5
10
15
20
25
Depth (cm)
0
5
10
15
20
25
30
35

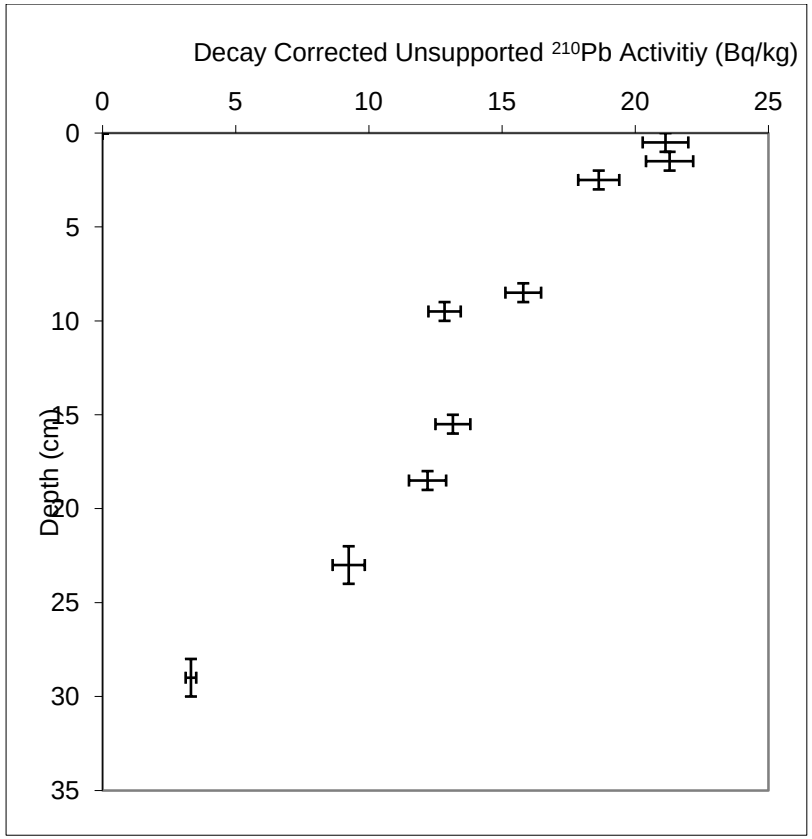
Decay Corrected Unsupported 210Pb Activitiy (Bq/kg)
0
5
10
15
20
25
Depth (cm)
0
5
10
15
20
25
30
35

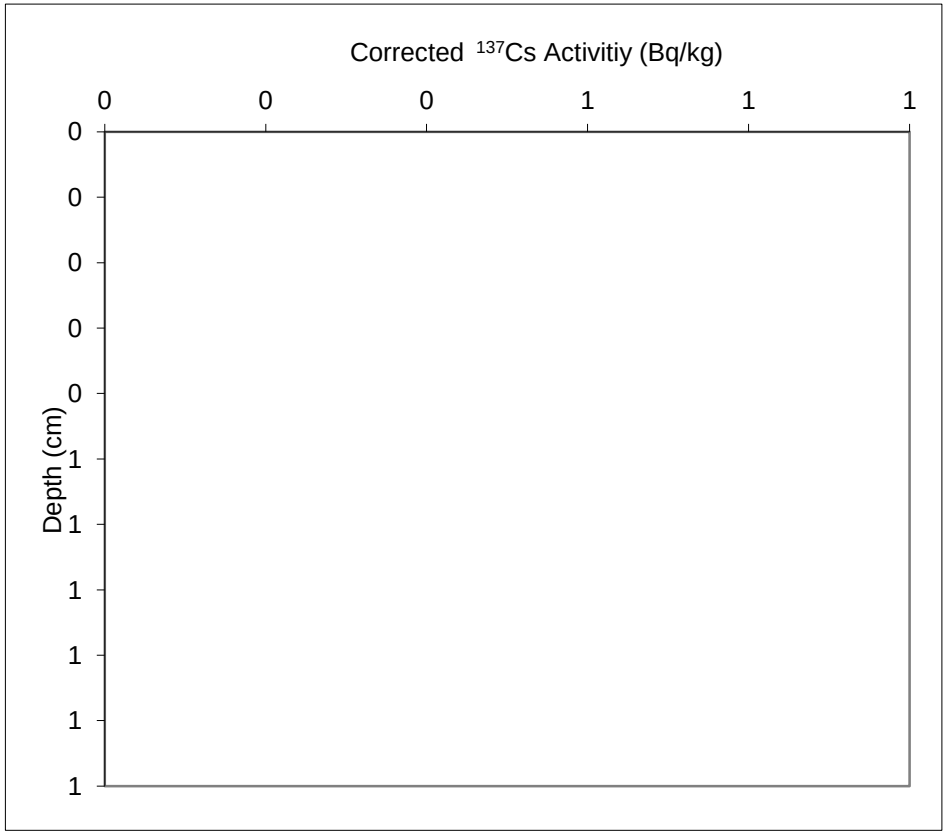
Corrected 137Cs Activitiy (Bq/kg)
0
0
0
1
1
1
Depth (cm)
0
0
0
0
0
1
1
1
1
1
1

Appendix 10.2: Dry bulk density calculations and values used for the Falealupo age determinations.

Sample Site	ANSTO ID	Depth (cm)	Weight of empty beaker (g)	Volume of water added to measuring cyclinder (ml)	Volume in cyclinder after addition of sample (ml)	Quantity of sample added to cyclinder (ml)	Weight of beaker + sample after drying overnight at 105^0C	Weight of dry sample (g)	Dry Bulk Density (g/ml)
Falealupo	N574	0 - 1	27.671	5.0	6.0	1.0	28.656	0.985	0.985
.	N575	1 - 2	27.499	5.0	6.0	1.0	28.643	1.144	1.144
	N576	2 - 3	27.605	5.0	6.5	1.5	28.782	1.177	0.785
	N638	8 - 9	28.666	5.0	6.0	1.0	29.969	1.303	1.303
	N577	9 - 10	28.280	5.0	6.0	1.0	29.306	1.026	1.026
	N578	15 - 16	27.128	5.0	6.0	1.0	27.905	0.777	0.777
	N639	18 - 19	27.672	5.0	6.5	1.5	28.575	0.903	0.602
	N640	22 - 24	29.289	5.0	6.0	1.0	30.042	0.753	0.753
	N579	28 - 30	27.310	5.0	6.5	1.5	28.202	0.892	0.595

Appendix 10.3: ^{210}Pb ages for Ma'asina.

Client Name:	Timothy Davies
Client Institution:	University of Canterbury
Project Title:	2012rc0036a
Core Description:	Maasina

ANSTO ID	Depth (cm)			Dry Bulk Density (g/cm^3)	Cumulative Dry Mass (g/cm^2)			Count Date	Total ^{210}Pb (Bq/kg)			Supported ^{210}Pb (Bq/kg)		
N580	0.0	-	1.5	1.20	0.9	±	0.9	17-May-12	12.9	±	0.6	3.1	±	0.3
N581	3.0	-	4.0	1.69	4.8	±	0.7	17-May-12	10.6	±	0.5	3.2	±	0.3
N583	6.0	-	7.5	2.16	11.1	±	1.2	17-May-12	8.2	±	0.4	3.1	±	0.3
N582	10.0	-	11.0	1.37	17.7	±	0.8	17-May-12	4.8	±	0.3	2.8	±	0.3
N585	16.0	-	17.5	1.93	28.0	±	1.3	17-May-12	9.3	±	0.5	3.7	±	0.3
N584	20.0	-	22.0	1.64	35.6	±	1.7	17-May-12	7.8	±	0.4	2.8	±	0.3

CIC model

Mass Accumulation Rate	0.334 ± 0.051	g/cm2/y
r2 =	0.95542	

Unsupported ^{210}Pb Decay corrected to 11-May-12 (Bq/kg)			Calculated CIC Ages (years)			Calculated CRS Ages (years)			CRS model Mass Accumulation Rates (g/cm^2/year)		
9.9	±	0.7	3	±	3	3	±	1	0.32	±	0.03
7.4	±	0.6	14	±	3	16	±	1	0.29	±	0.04
5.1	±	0.5	33	±	6	43	±	4	0.18	±	0.03
2.0	±	0.4	53	±	8	86	±	11	0.12	±	0.04
5.6	±	0.6									
5.0	±	0.5									

The unsupported Pb-210 activities for this core are relatively low, only 10 Bq/kg at the top of the core. For this reason the calculated ages shown above may not be reliable.
The CIC model calculated ages may be more reliable, assuming the mass accumulation has been constant in the past 50 years.
An independent method should be used to validate the calculated ages such as Cs-137, pollen or trace metal records.

Atun Zawadzki - 12 November 2012

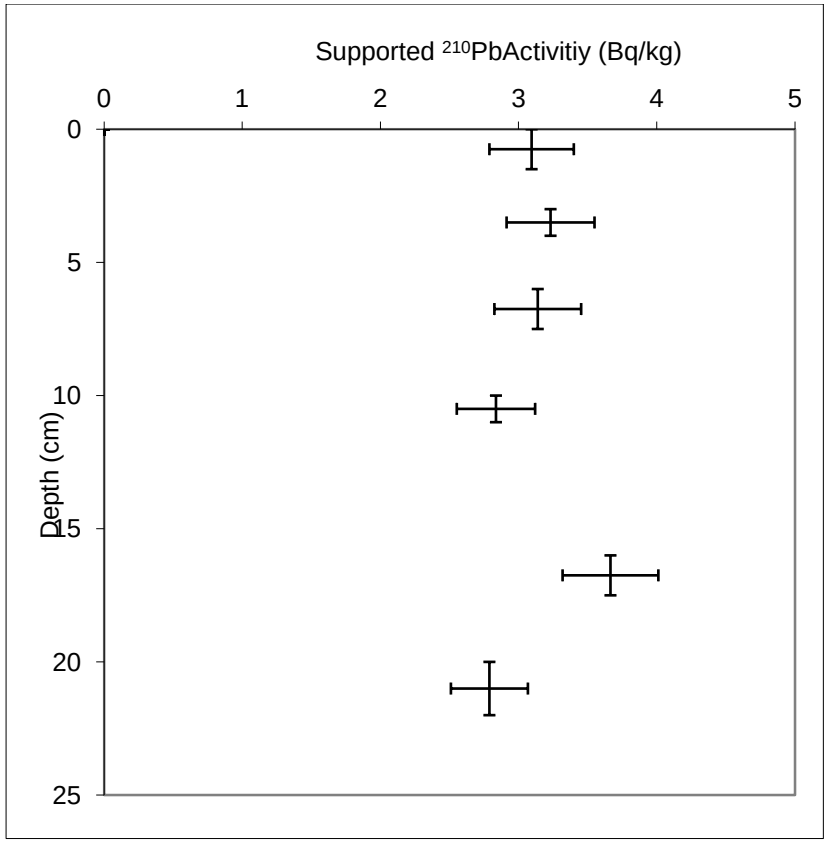
Supported 210PbActivitiy (Bq/kg)
0
1
2
3
4
5
0
5
10
15
20
25
Depth (cm)

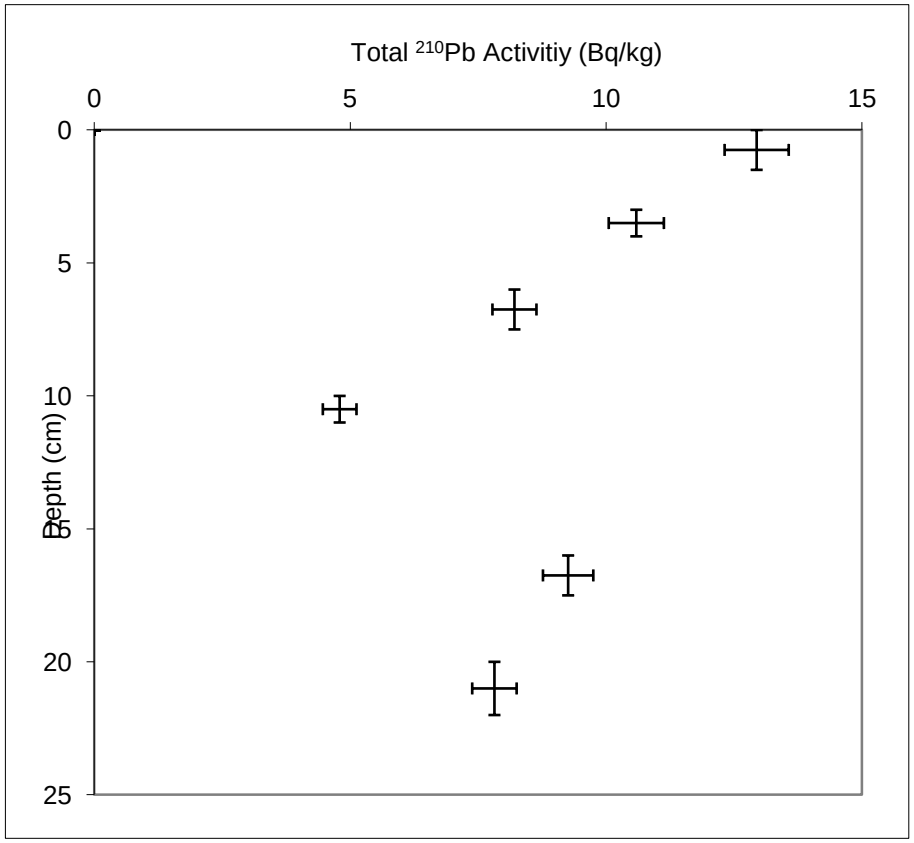
Total 210Pb Activitiy (Bq/kg)
0
5
10
15
0
5
10
15
20
25
Depth (cm)

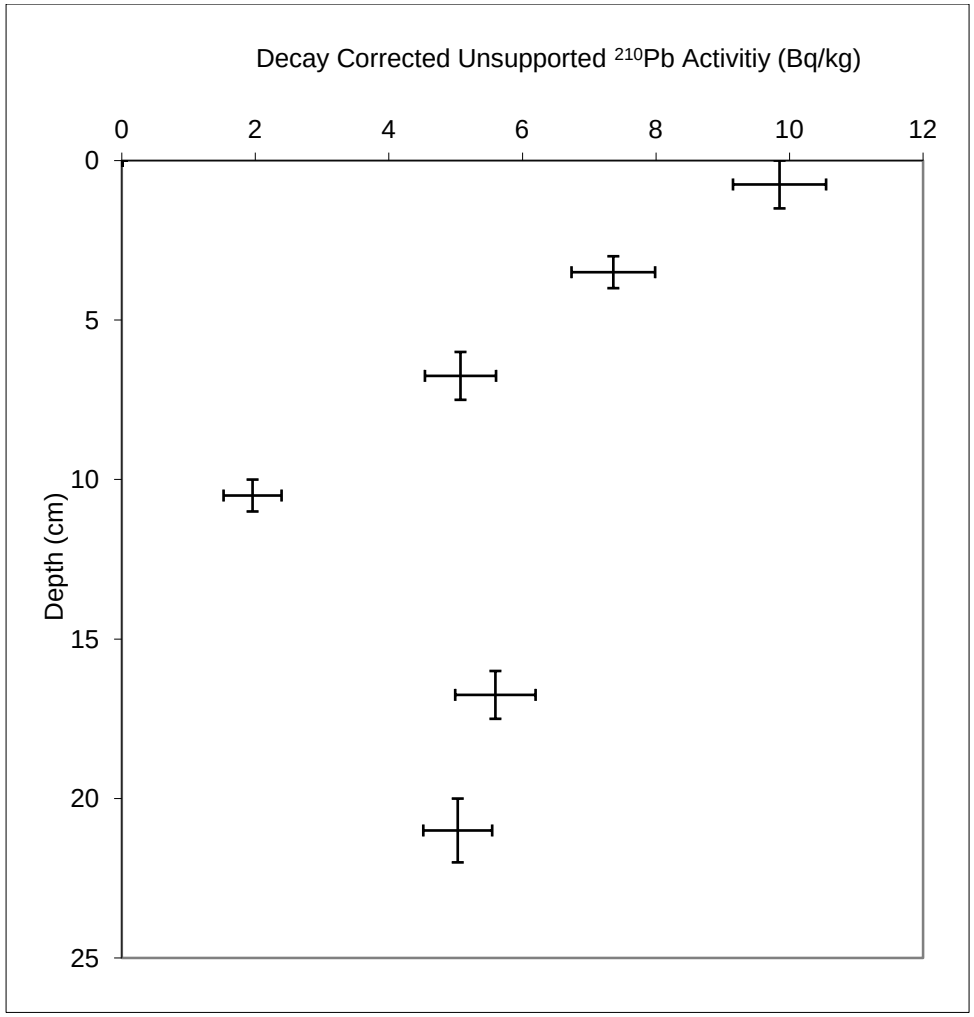
Decay Corrected Unsupported 210Pb Activitiy (Bq/kg)
0
2
4
6
8
10
12
0
5
10
15
20
25
Depth (cm)

Appendix 10.4: Dry bulk density calculations and values used for the Ma'asina age determinations.

Sample Site	ANSTO ID	Depth (cm)	Weight of empty beaker (g)	Volume of water added to measuring cyclinder (ml)	Volume in cyclinder after addition of sample (ml)	Quantity of sample added to cyclinder (ml)	Weight of beaker + sample after drying overnight at 105^0C	Weight of dry sample (g)	Dry Bulk Density (g/ml)
Maasina	N580	0.0 - 1.5	58.959	5.0	6.5	1.5	60.765	1.806	1.204
	N581	3.0 - 4.0	57.632	5.0	6.0	1.0	59.322	1.690	1.69
	N583	6.0 - 7.5	96.907	5.0	6.0	1.0	99.062	2.155	2.155
	N582	10.0 - 11.0	100.931	5.0	6.0	1.0	102.302	1.371	1.371
	N585	16.0 - 17.5	96.318	5.0	7.0	2.0	100.185	3.867	1.9335
	N584	20.0 - 22.0	46.595	5.0	6.5	1.5	49.061	2.466	1.644

APPENDIX 11: RESONANCE DATA

This Appendix provides an overview of the data limitations associated with the resonance modeling in Chapter 4.

The numerical modeling and figures shown were generated by Yoshiki Yamazaki, Volker Roeber, William Templeton, and Kwok Fai Cheung at the University of Hawai'i at Manoa (Ocean and Resources Engineering Department).

Bathymetry data housed at SOPAC (Applied Geosceince Division of the Secretariat of the Pacific Community), was obtained by Shaun Williams via a Memorandum of Understanding with the CEO, Samoan Ministry of Natural Resources and Environment.

Nearshore bathymetry data for east Savai'i was obtained from KIGAM (Korean Institute of Geology and Mines) via collaboration. The data was acquired in 2005 via the 2005 UNDP-KIGAM Project.

Apia and Harbours data shown in the Figures of this Appendix were digitized from nautical charts housed at LINZ (Land Information New Zealand), by Joshua Blackstock and Shaun Williams at the University of Canterbury.

The work associated with this Appendix and Chapter 4, was made possible via a NZ MoRST-Fulbright Graduate Award (IIE Grantee #15101271).

Appendix Discussion

Appendix Figure 11.1 shows the GEBCO 30 sec bathymetry data for Upolu and Savai'i; which was the base modeling domain in this thesis. Appendix Figure 11.2 shows the GEBCO 30 sec data merged with the higher-resolution bathymetry data available for these islands. Even though some nearshore data exists, there are still extensive areas with missing data making it difficult to develop adequate higher-resolution DEM data for modeling tsunamis around Upolu and Savai'i.

Further, a comparison of the merged datasets reveals significant discrepencies between the coastlines depicted by the GEBCO 30 sec, with available nearshore data (Appendix Figures 11.3 – 11.7). Coupled with unrealistic deep water areas in Appendix Figures 11.1, 11.5 and 11.6, further limit the development of a DEM for tsunami modeling.

Hence, the results obtained in Chapter 4 are based on the lower resolution GEBCO 30 sec data, and do not include the nearshore datasets (Appendix Figure 11.2) due to the identified discrepencies. The unrealistic deep water nearshore areas in Figure 11.1 are taken into consideration in the interpretations provided in Chapter 4.

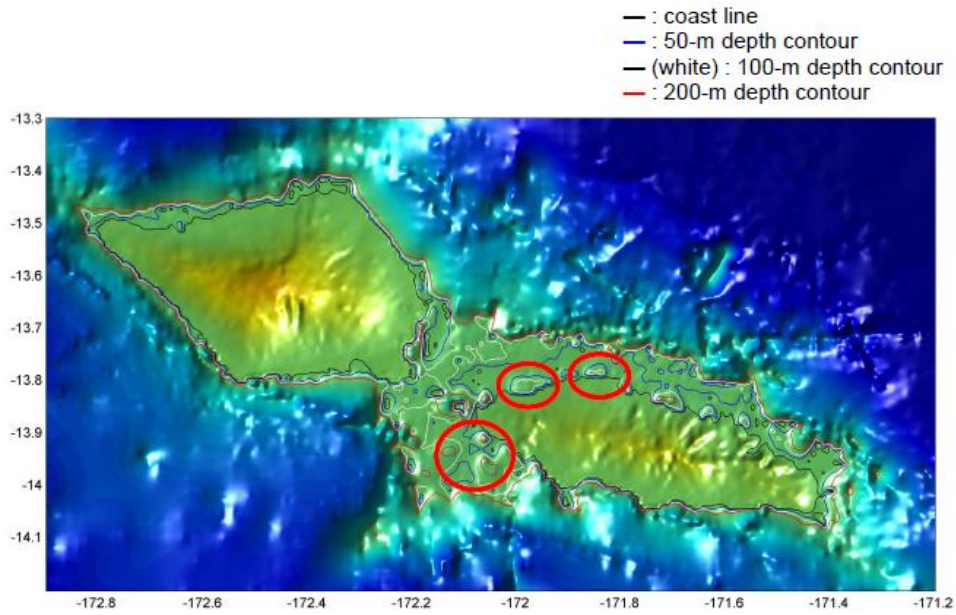

Appendix Figure 11.1: GEBCO 30 sec data for Independent Samoa. Red circles indicate unrealistic deep water nearshore areas.

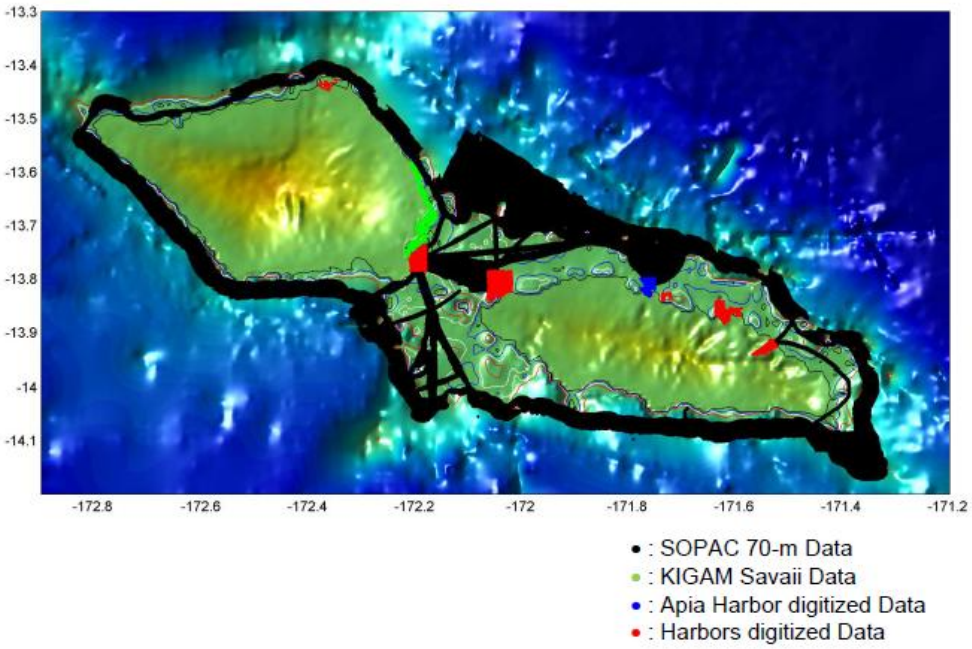

Appendix Figure 11.2: Available bathymetry datasets for Independent Samoa merged with GEBCO 30 sec data.

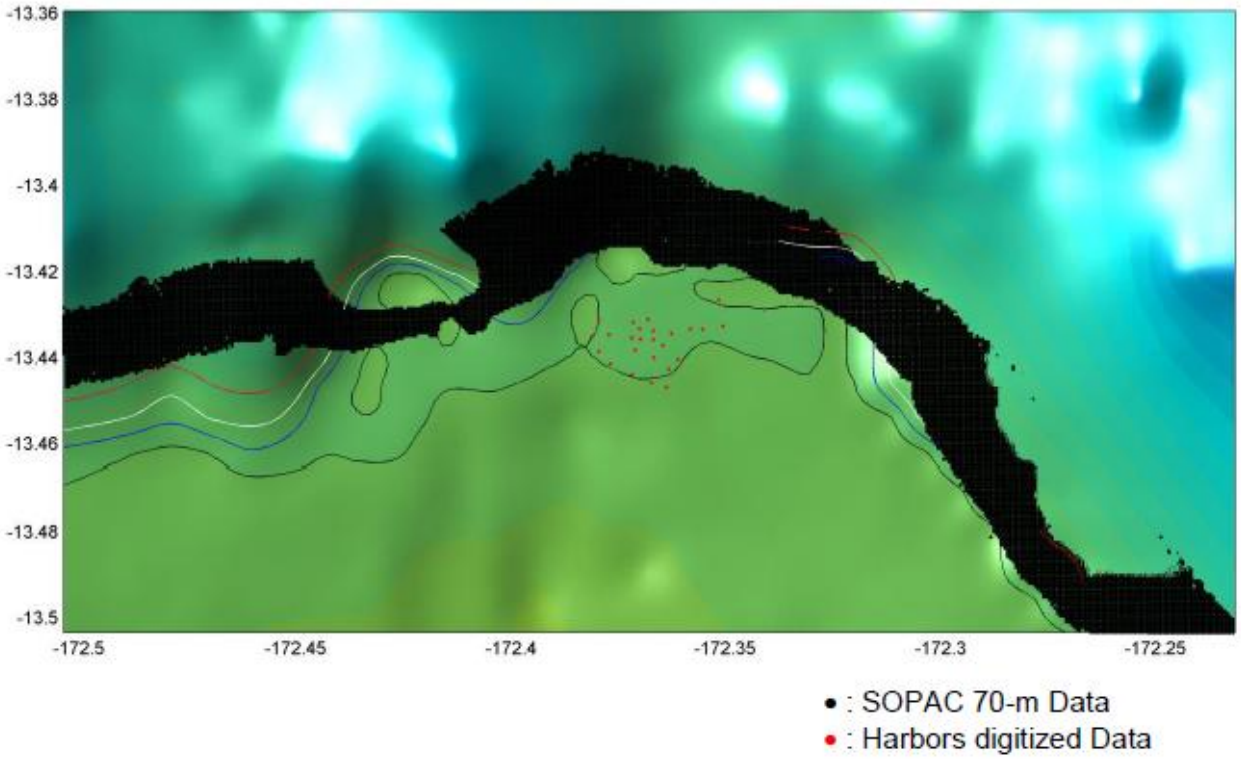

Appendix Figure 11.3: Digitized Mataulu Bay data.

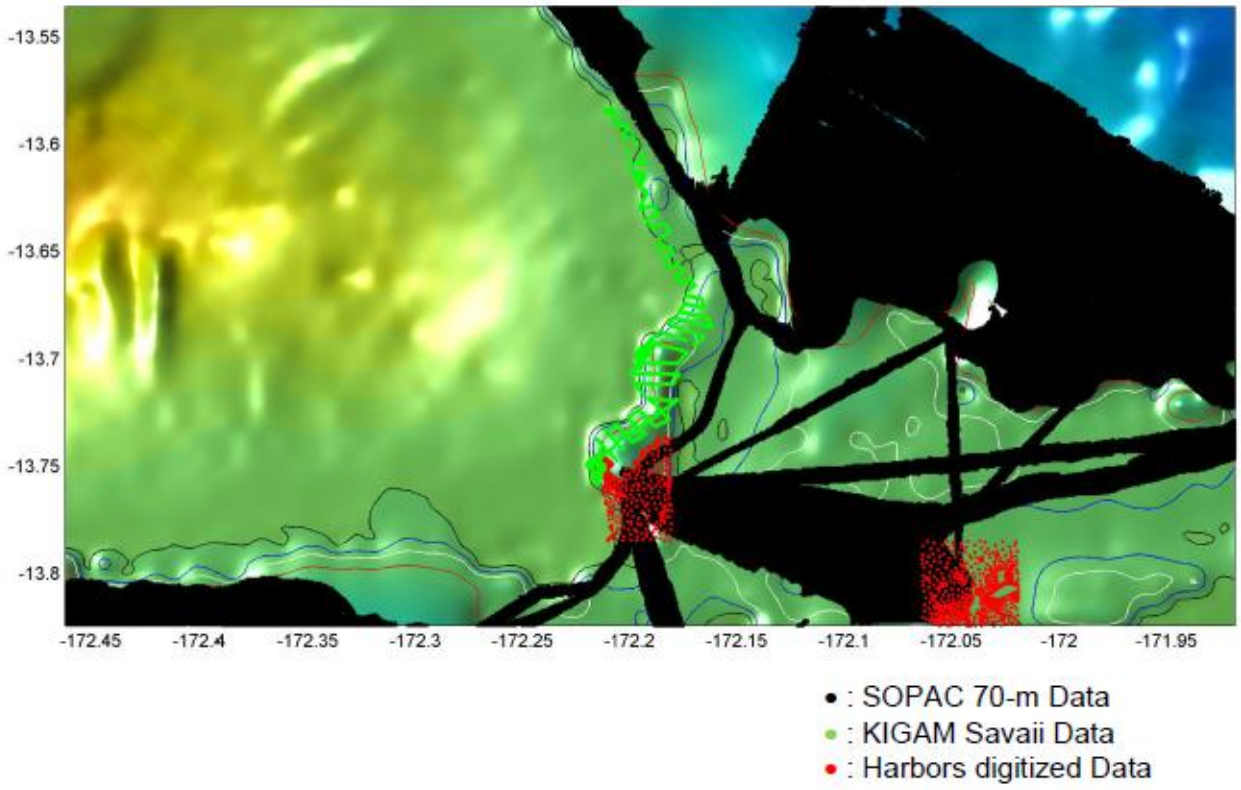

Appendix Figure 11.4: KIGAM data digitized Apolima Strait data.

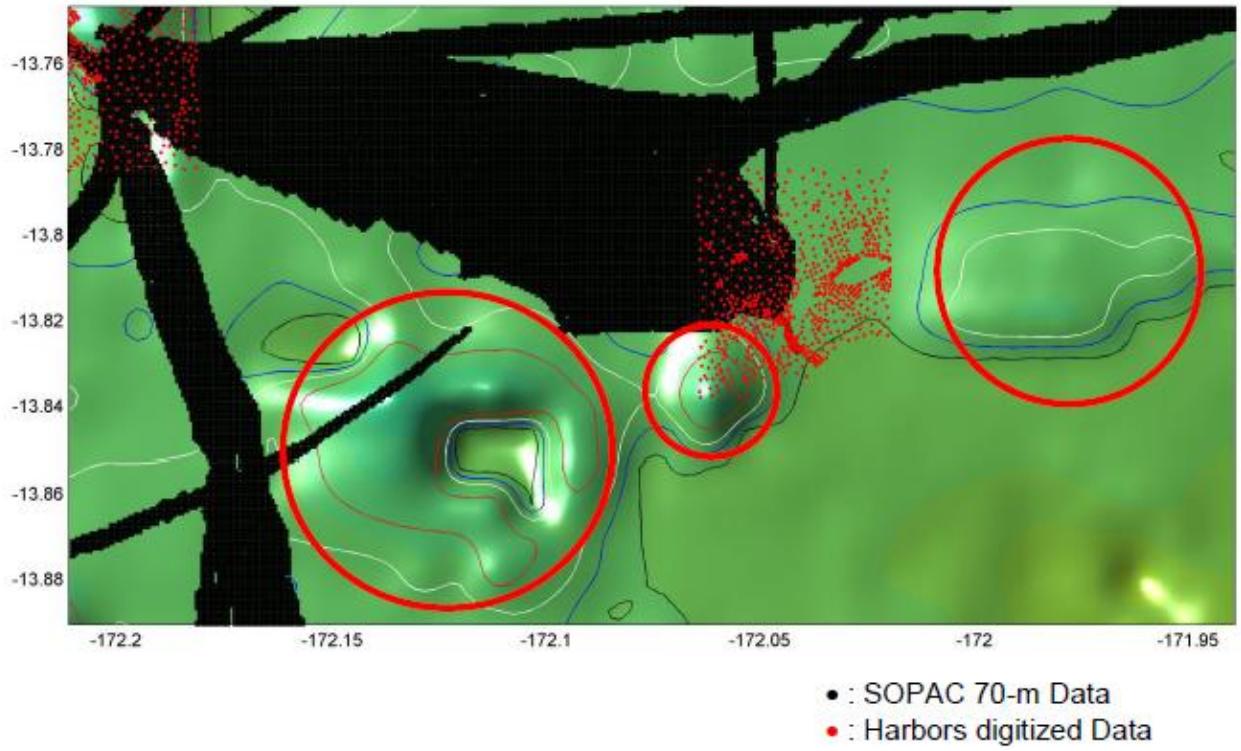

Appendix Figure 11.5: Digitized Mulifanua data

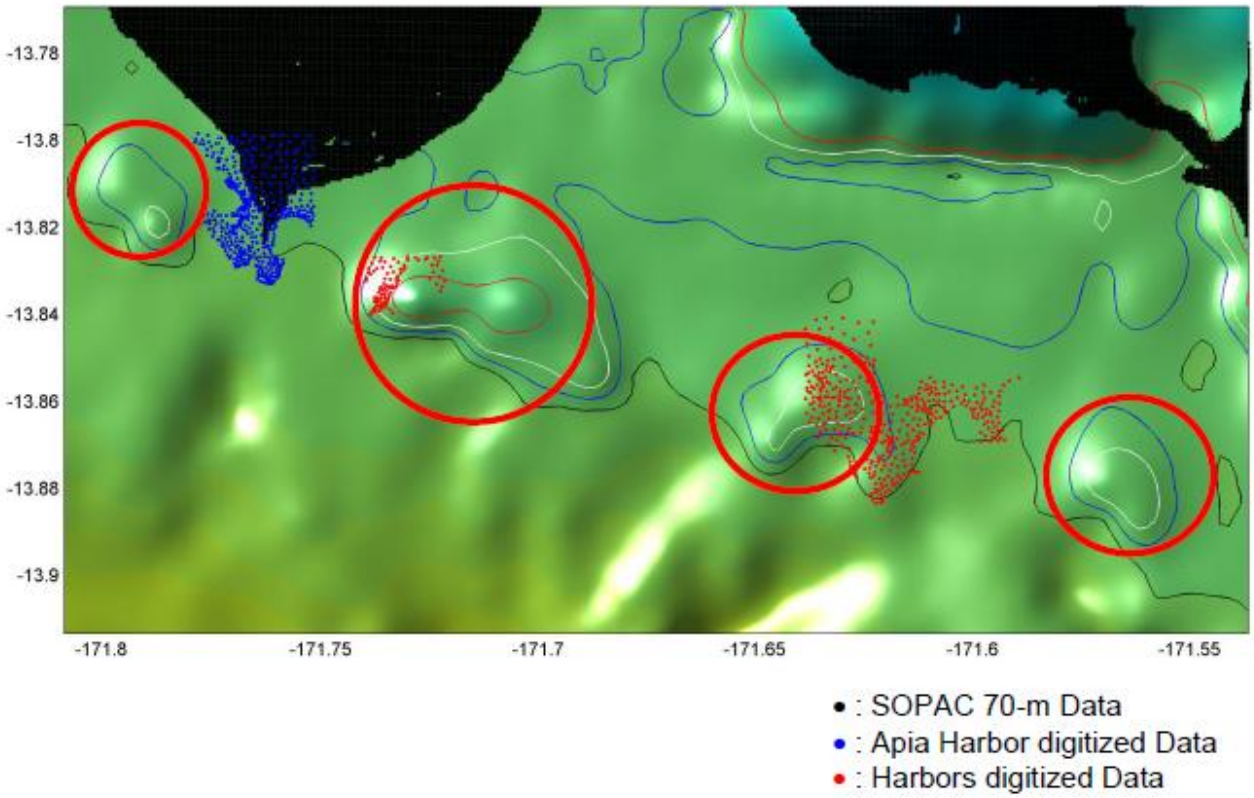

Appendix Figure 11.6: Digitized Apia data

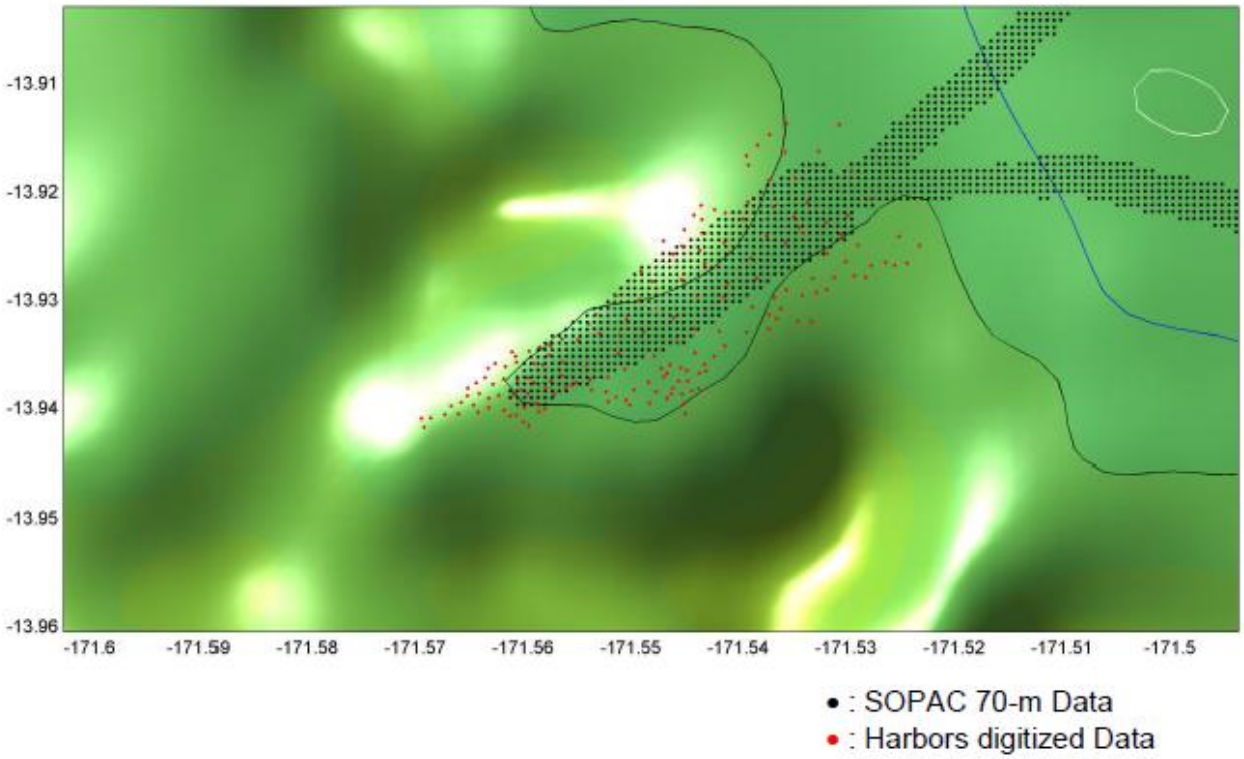

Appendix Figure 11.7: Digitized Fagaloa Bay data